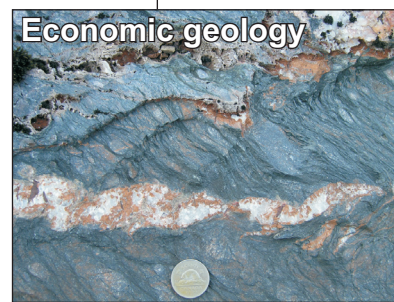
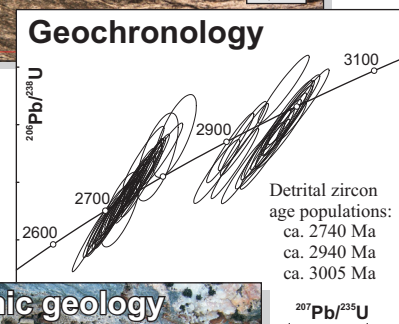
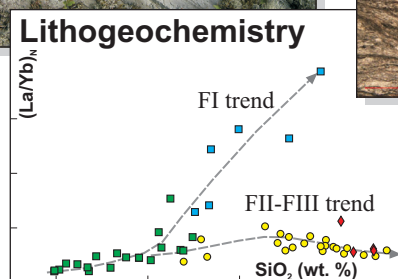
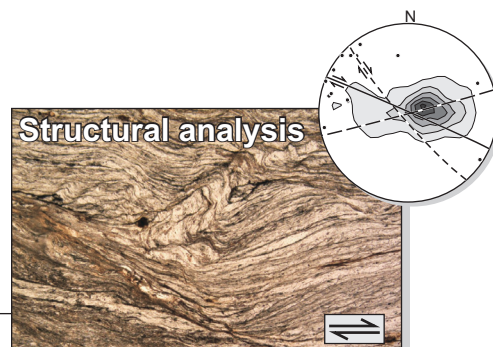
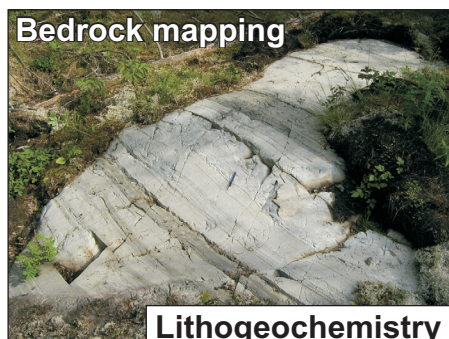




GR2013-1

Geology of the Garner–Gem lakes area, Rice Lake greenstone belt, southeastern Manitoba (parts of NTS 52L11, 14)

GEOSCIENTIFIC REPORT



By
S.D. Anderson



Geoscientific Report GR2013-1

Geology of the Garner–Gem lakes area, Rice Lake greenstone belt, southeastern Manitoba (parts of NTS 52L11, 14)

by S.D. Anderson
Winnipeg, 2013

Mineral Resources

Hon. Dave Chomiak
Minister

Hugh Eliasson
Deputy Minister

John Fox
Assistant Deputy Minister

Manitoba Geological Survey

Christian Böhm
A/Director



Every possible effort is made to ensure the accuracy of the information contained in this report, but Manitoba Mineral Resources does not assume any liability for errors that may occur. Source references are included in the report and users should verify critical information.

Any third party digital data and software accompanying this publication are supplied on the understanding that they are for the sole use of the licensee, and will not be redistributed in any form, in whole or in part. Any references to proprietary software in the documentation and/or any use of proprietary data formats in this release do not constitute endorsement by Manitoba Mineral Resources of any manufacturer's product.

When using information from this publication in other publications or presentations, due acknowledgment should be given to the Manitoba Geological Survey. The following reference format is recommended:

Anderson, S.D. 2013: Geology of the Garner–Gem lakes area, Rice Lake greenstone belt, southeastern Manitoba (parts of NTS 52L11, 14); Manitoba Mineral Resources, Manitoba Geological Survey, Geoscientific Report GR2013-1, 135 p.

NTS grid: 52L11, 52L14

Keywords: Archean; back-arc basins; Bidou assemblage; continental arcs; deformation; Edmunds assemblage; English River basin; Garner assemblage; Garner Lake; Gem assemblage; Gem Lake; geochronology; gold deposits; island arcs; komatiite; lithogeochemistry; magmatism; Manitoba; mapping; massive sulphide deposits; mineral deposits, genesis; North Caribou terrane; Rice Lake belt; rifting; Sm/Nd; stratigraphy; structural analysis; Superior province; U/Pb; Uchi subprovince; volcanics; volcanism

Published by:

Manitoba Mineral Resources
Manitoba Geological Survey
360–1395 Ellice Avenue
Winnipeg, Manitoba
R3G 3P2 Canada

Telephone: (800) 223-5215 (General Enquiry)
(204) 945-4154 (Publication Sales)

Fax: (204) 945-8427

E-mail: minesinfo@gov.mb.ca

Website: manitoba.ca/minerals

This publication is available to download free of charge at manitoba.ca/minerals

Abstract

The Garner–Gem lakes map area is located 160 km north-east of Winnipeg, Manitoba and covers 110 km² at the south-eastern extent of the Archean Rice Lake greenstone belt (RLB). Situated just east of the limit of Paleozoic cover, the RLB represents the westernmost exposure of the volcano-plutonic Uchi subprovince of the western Superior province. It is flanked to the north by the protocontinental North Caribou terrane (NCT) and to the south by the turbiditic English River basin (ERB), with boundaries defined by the crustal-scale Wanipigow and Manigotagan faults, respectively. Spanning the entire width of the RLB, the map area represents an ideal location to evaluate geodynamic and metallogenic models, and to further elucidate the 360 m.y. history (ca. 3.01–2.65 Ga) of crustal growth at the south margin of the NCT.

The bedrock geology of the Garner–Gem lakes area is defined to include four distinct supracrustal assemblages. The crustal-scale Beresford Lake shear zone, representing a major splay of the Wanipigow fault and showing a complex history of movement, separates the ca. 2.89–2.85 Ga Garner assemblage of the NCT on the northeast from the 2.75–2.70 Ga Bidou, Gem and Edmunds assemblages of the Uchi subprovince on the southwest. The Garner assemblage faces northwest and is intruded to the northeast by 2.73–2.72 Ga granitoid rocks of the Wanipigow River plutonic complex, whereas the Neoarchean assemblages face southeast and are juxtaposed to the southwest across the Manigotagan fault and its subsidiary structures with partly equivalent (ca. 2.7 Ga) metasedimentary rocks of the ERB.

Intermediate–felsic volcanoclastic and epiclastic rocks in the Garner assemblage are interpreted to represent a section of continental-arc crust that formed on, or marginal to, the ca. 2.98–2.92 Ga rifted margin of the NCT, and achieved significant thickness prior to emplacement of the 2.87 Ga Garner Lake intrusive complex. Following uplift and erosion, perhaps related to crustal doming above an upwelling mantle plume, these rocks were unconformably overlain by arkosic sandstone (<2.87 Ga), intermediate–felsic volcanic rocks (ca. 2.85 Ga), magnetite-chert iron formation, and subaqueous komatiitic–tholeiitic basalt flows that were deposited in a restricted marine basin and are thought to record extension and rifting of the continental arc. Mafic–ultramafic magmatic rocks in the Garner assemblage have potential for reef-type platinum group element (PGE) and komatiite-hosted Ni sulphide deposits.

Following an extended period (ca. 2.85–2.75 Ga) of magmatic quiescence, renewed subduction beneath the NCT margin is thought to have generated a regionally extensive continental arc, manifest as the ca. 2.75–2.7 Ga Wanipigow River plutonic complex. Outboard of the NCT margin, bimodal subaqueous volcanic rocks of the ca. 2.75–2.73 Ga Bidou assemblage record development of an oceanic arc–back-arc complex, perhaps as a consequence of subduction-zone step-back in response to early accretionary events. Isotopically juvenile, mid-ocean-ridge basalt (MORB)–like tholeiitic basalt flows and basinal marine turbidites (<2.75 Ga) in the lower Bidou assemblage were likely deposited in a mature back-arc basin, and are overlain by 2.73 Ga dacitic volcanoclastic rocks that signal an upward

transition to oceanic-arc magmatism, coeval with emplacement of the 2.73–2.72 Ga Ross River plutonic suite.

Bimodal volcanic rocks of the Gem assemblage (ca. 2.73–2.72 Ga) range in composition from primitive tholeiitic basalt to highly fractionated calcalkalic rhyolite, and are interpreted to record extension and rifting of the arc–back-arc complex, ultimately leading to development of a regionally extensive intra-arc basin. Distinctive volcanic facies, including pumiceous and scoriaceous pyroclastic deposits, welded felsic ignimbrites and high-SiO₂ rhyolite flows, indicate deposition in shallow-subaqueous to subaerial settings. Intermediate–felsic volcanic rocks of the ‘FI suite’ record relatively deep (garnet-present) partial melting of a basaltic source, with minimal fractionation during ascent, whereas the mostly rhyolitic ‘FII–FIII suite’ records shallow (garnet-absent) partial melting followed by fractionation in high-level magma chambers, suggesting an analogy to sites of active extension and rifting in modern arc and back-arc settings, and significant potential for volcanic-hosted base-metal sulphide deposits.

Subsequent to the cessation of major arc volcanism in the RLB and following a short-lived interval of depositional quiescence, basinal marine turbidites of the ca. 2.71–2.7 Ga Edmunds assemblage were deposited conformably over the Gem assemblage in a below-wave-base, progradational submarine fan at the north margin of the ERB. Thin-bedded mudstone-dominated turbidites, intrabasinal conglomerate, massive quartz-lithic sandstone and minor turbiditic iron formations of the lower facies association (LFA) indicate deposition in a channelized, mid- to lower-fan setting. Uranium-lead ages of detrital zircons indicate a maximum depositional age of ca. 2.71 Ga, and suggest a correlation to fluvial-alluvial coarse clastic sedimentary rocks of the San Antonio assemblage, which define a series of fault-bounded, possibly extensional basins along the Wanipigow fault. Lenticular units of tonalite-boulder conglomerate at the base of the upper facies association (UFA) signal a significant change in sediment provenance. Thick-bedded quartz-lithic turbidite and polymictic conglomerate of the UFA, the latter containing abundant tonalite and quartzite clasts, were deposited in a channelized upper-fan setting. Detrital zircons indicate a maximum depositional age of ca. 2.7 Ga, and are dominated by Mesarchean U–Pb ages, indicating uplift and erosional denudation of the NCT. Coeval mafic magmatism was chemically diverse and included MORB-like basalt flows and rare komatiitic basalt sills, suggesting an extensional geodynamic setting and potential for magmatic Ni ($\pm\text{Co}\pm\text{Cu}\pm\text{PGE}$) deposits akin to those at Werner Lake, Ontario.

Regional orogenesis, interpreted to be related to terminal collision of the NCT and the Winnipeg River terrane, is manifest in the study area as multiple generations of ductile and brittle-ductile deformation structures formed under greenschist- to (local) amphibolite-facies metamorphic conditions. Low-angle G_1 structures may result from crustal thickening in the earliest increments of collisional orogenesis. Regionally pervasive G_2 structures record northeast–southwest shortening of the RLB in a kinematic regime of bulk sinistral transpression, contemporaneous with the local metamorphic peak. Overprinting relationships with auriferous, shear-hosted, quartz-carbonate veins indicate that major orogenic Au deposits in the RLB formed

during the late increments of this deformation. Regional constraints suggest that major orogenesis (ca. 2.69–2.66 Ga) in the ERB was coeval with G_2 transpressional deformation in the RLB. The short time interval between sedimentation and peak orogenesis in the ERB appears to require very rapid crustal thickening coupled with significant input of magmatic heat.

The G_3 structures record a transition to a distinctly different kinematic frame under waning metamorphic conditions, and are overprinted by an anastomosed network of brittle-

ductile G_4 shear zones that record progressive, strongly partitioned, dextral transcurrent shear and Z-asymmetric folding in a regional regime of northwest–southeast shortening of the RLB. This ended prior to ca. 2.66 Ga in the Garner Lake area, based on the U-Pb ages of metamorphic rutile in post-shear dikes. Latest deformation (G_5) was associated with conjugate brittle faults that locally served as conduits for large volumes of siliceous hydrothermal fluid, perhaps indicating potential for late-orogenic vein-hosted Au deposits at depth in the orogen.

TABLE OF CONTENTS

	Page
Abstract	iii
Introduction	1
Previous work	1
Methods and scope	2
Acknowledgments	3
Regional setting	3
Stratigraphic and tectonic nomenclature	3
North Caribou terrane	5
Uchi subprovince	6
Bidou and Gem assemblages	7
Edmunds and San Antonio assemblages	7
English River basin	8
Local geology and stratigraphy	8
Lithological nomenclature	8
Garner assemblage	10
Description of rock units	12
Intermediate–felsic volcanoclastic rocks (unit Gn1)	12
Epiclastic rocks (unit Gn2)	12
Intermediate–felsic volcanoclastic rocks (unit Gn3)	13
Garner Lake intrusive complex (unit Gn4)	14
Volcanoclastic and epiclastic rocks (unit Gn5)	15
Komatiite and komatiitic basalt flows (unit Gn6)	18
Basalt, basaltic andesite and andesite flows (unit Gn7)	19
Gabbro, diorite (unit Gn8)	19
Bidou assemblage	19
Description of rock units	20
Basalt flows (unit Bd1; Gunnar formation)	21
Feldspathic greywacke and mudstone (unit Bd2; Stormy Lake formation)	21
Dacitic volcanoclastic rocks (unit Bd3; The Narrows formation; 2730 Ma)	21
Gabbro (unit Bd4)	23
Gem assemblage	23
Description of rock units – West association	25
Basalt and basaltic andesite (unit Gw1)	25
Epiclastic rocks (unit Gw2)	26
Gabbro and diorite (unit Gw3)	29
Dacite and rhyolite (unit Gw4)	29
Rhyolite intrusion breccia (unit Gw5)	36
High-SiO ₂ rhyolite (unit Gw6)	38
Intermediate–felsic crystal-lithic lapilli tuff and tuff (unit Gw7)	40
Description of rock units – East association	41
Intermediate–felsic volcanoclastic and epiclastic rocks (unit Ge1)	41
Pillowed basalt and andesite flows (unit Ge2)	41
Gabbro (unit Ge3)	41
Quartz-feldspar porphyry granite (unit Ge4)	43
Wanipigow River plutonic complex	43

Description of map units.....	44
Hornblende-biotite tonalite and granodiorite (unit Wn1)	44
Biotite granodiorite and granite (unit Wn2).....	44
Orthogneiss (unit Wn3).....	44
Edmunds assemblage	44
Description of rock units.....	46
Greywacke-mudstone turbidite (unit Em1)	46
Polymictic pebble to cobble conglomerate (unit Em2).....	48
Quartz-lithic greywacke (unit Em3)	49
Greywacke–mudstone–iron formation turbidite (unit Em4).....	50
Polymictic cobble to boulder conglomerate (unit Em5)	50
Greywacke-mudstone turbidite (unit Em6)	51
Oligomictic pebble to boulder conglomerate (unit Em7)	52
Basalt, basaltic andesite and andesite flows (unit Em8)	53
Gabbro, diorite and quartz diorite (unit Em9)	53
Quartz-porphyry rhyolite (unit Em10).....	55
Unsubdivided tectonite (precursor uncertain).....	55
Phyllonite, mylonite (unit Us1).....	55
Post-tectonic dikes	55
Gabbro, diorite and quartz diorite (unit Pt1).....	55
Summary of lithostratigraphy and inferred depositional settings.....	56
Lithogeochemistry and Sm-Nd isotope geochemistry	57
Sampling procedures and analytical methods.....	57
Lithogeochemistry	58
Sm-Nd isotope geochemistry	58
Analytical results.....	58
Garner assemblage	62
Mafic rocks.....	63
Komatiitic rocks.....	63
Felsic rocks	65
Bidou assemblage	69
Mafic rocks.....	69
Felsic rocks	71
Gem assemblage	73
Mafic rocks.....	74
FI andesite, dacite and rhyolite	77
FII-FIII andesite and rhyolite.....	77
Felsic intrusion breccia	78
Edmunds assemblage.....	78
Mafic rocks.....	79
Felsic rocks	80
Post-tectonic dikes	80
Summary of geochemical results and inferred geodynamic settings.....	80
Garner assemblage: mature continental arc and plume-influenced arc rift.....	80
Bidou assemblage: mature back-arc basin to immature volcanic arc	80
Gem assemblage: mature volcanic arc to incipient arc rift.....	81
Edmunds assemblage: arc rift to immature intra-arc basin.....	82

U-Pb geochronology	82
Methodology	82
ID-TIMS results	85
Pegmatitic tonalite (unit Gn4d; sample 96-02-1067/CB02-03)	85
Dacitic crystal tuff or coherent flow (unit Gn5c; sample 96-02-1050/CB02-02)	86
Greywacke (Stovel Lake formation; sample 96-05-SLF)	87
Pegmatitic leucogabbro (Tinney Lake formation; sample 96-05-CMG)	87
Greywacke (Stormy Lake formation; unit Bd2a; sample 96-05-SL)	87
Dacitic crystal-lithic lapilli tuff (unit Gw7; sample 96-06-1845)	87
Biotite granite (unit Wn2a; sample 96-03-1116)	88
Feldspar-quartz porphyry (unit Wn2a; sample 96-03-1261/CB02-01)	89
Quartz porphyry (unit Em10; sample 96-07-2150)	89
Post-tectonic diorite (unit Pt1; sample 96-02-1056)	89
LA-MC-ICP-MS results	89
Greywacke (Stovel Lake formation; sample 96-05-SLF)	89
Greywacke (Stormy Lake formation; unit Bd2a; sample 96-05-SL)	90
Volcanic sandstone (unit Gw2a; sample 96-05-MRF)	90
Feldspathic greywacke (unit Em1b; sample 96-02-1004/CB02-05)	90
Quartz-lithic greywacke (unit Em6b; sample 96-06-2059)	90
Interpretation of the U-Pb age data	90
Garner assemblage	90
Bidou assemblage	93
Gem assemblage	93
Wanipigow River plutonic complex	93
Edmunds assemblage	93
Post-tectonic dikes	94
Structural geology	94
Deformation structures	94
G ₁ structures	95
G ₂ structures	95
G ₃ structures	100
G ₄ structures	101
G ₅ structures	109
Structural evolution	112
Economic considerations	113
Magmatic Ni-Cu-PGEs	113
Komatiite-hosted Ni	113
Reef-type PGE	114
Volcanic-associated Zn-Pb-Cu (Ag-Au)	115
Magmatic-hydrothermal Cu-Au-REEs (La, Ce, Nd)	116
Lode Au	116
Shear-hosted quartz-carbonate veins	116
Iron formation-hosted stratabound Au	118
Fault-controlled quartz veins and SiO ₂ replacements	120
Summary and regional implications	122
ca. 3.01–2.92 Ga	122
ca. 2.89–2.85 Ga	123

ca. 2.75–2.73 Ga	123
ca. 2.73–2.71 Ga	125
ca. 2.71–2.69 Ga	126
ca. 2.69–2.64 Ga	127
References.....	128

TABLES

Table 1: Principal supracrustal assemblages at the south margin of the North Caribou terrane.....	5
Table 2: Nomenclature for clastic rocks	10
Table 3: Lithogeochemical data for key map units	59
Table 4: Sm-Nd isotopic data for whole-rock samples	61
Table 5: U-Pb analytical data for zircon and rutile	83
Table 6: Summary of U-Pb zircon and rutile analytical results	85
Table 7: Summary of deformation structures and episodes	94

FIGURES

Figure 1: Regional geological setting of the Rice Lake belt.....	4
Figure 2: Simplified geology of the Rice Lake belt.....	6
Figure 3: Geology of the Garner-Gem lakes area, simplified from the accompanying Map GR2013-1-1	9
Figure 4: Schematic stratigraphic columns for the Garner assemblage.....	11
Figure 5: Outcrop photographs of rocks in units Gn1 and Gn2.....	13
Figure 6: Outcrop photographs of rocks of subunit Gn3b	14
Figure 7: Outcrop photographs of tonalitic segregations in the Garner Lake intrusive complex.....	15
Figure 8: Outcrop photographs of rocks of subunit Gn5a	16
Figure 9: Outcrop photographs of rocks of unit Gn5.....	17
Figure 10: Outcrop and thin-section photographs of rocks from units Gn6 and Gn7	18
Figure 11: Schematic stratigraphic column for the Bidou assemblage.....	20
Figure 12: Outcrop and thin-section photographs of key rocks from the Bidou assemblage.....	22
Figure 13: Schematic stratigraphic columns for the Gem assemblage	24
Figure 14: Outcrop and thin-section photographs of rocks in subunit Gw1a	26
Figure 15: Outcrop and thin-section photographs of rocks in subunit Gw1b.....	27
Figure 16: Outcrop photographs of rocks in unit Gw2	28
Figure 17: Photomicrographs of textures in volcanoclastic turbidites of subunit Gw2a.....	29
Figure 18: Outcrop photographs of gabbro from unit Gw3.....	30
Figure 19: Outcrop and thin-section photographs of rocks from subunit Gw4a	31
Figure 20: Outcrop and thin-section photographs of rocks in subunit Gw4b.....	32
Figure 21: Outcrop photographs of flow-banded dacite of subunit Gw4c.....	33
Figure 22: Outcrop and thin-section photographs of rocks in subunit Gw4d.....	34
Figure 23: Outcrop photographs of interlayered tuff and lapilli tuff at the base of subunit Gw4e.....	35
Figure 24: Outcrop photographs of rocks in subunit Gw4e.....	36
Figure 25: Outcrop photographs of rocks from subunit Gw4f	36
Figure 26: Outcrop photographs of rocks in unit Gw5	37
Figure 27: Volcanic-facies model for a shallow-subaqueous rhyolite flow	38
Figure 28: Outcrop photographs of rocks in unit Gw6	39
Figure 29: Outcrop photographs of rocks in unit Gw7	40
Figure 30: Outcrop and thin-section photographs of rocks in subunit Ge1a	42
Figure 31: Outcrop photographs of rocks in subunit Ge1b.....	42

Figure 32: Outcrop photographs of pillowed andesite and basalt flows of unit Ge2.....	43
Figure 33: Quartz-feldspar porphyry granite of unit Ge4.....	43
Figure 34: Outcrop photographs of gneissic rocks of unit Wn3.....	45
Figure 35: Schematic stratigraphic columns for the Edmunds assemblage.....	46
Figure 36: Outcrop map of the Gem–Edmunds contact	47
Figure 37: Outcrop photographs of rocks of unit Em1	48
Figure 38: Outcrop photographs of rocks in unit Em2	49
Figure 39: Outcrop and thin-section photographs of quartz-lithic greywacke of unit Em3	49
Figure 40: Outcrop photographs of rocks in unit Em4	50
Figure 41: Outcrop photographs of tonalite-clast-bearing conglomerate of unit Em5	51
Figure 42: Outcrop and thin-section photographs of key rocks in unit Em6.....	52
Figure 43: Outcrop photographs of the dacitic conglomerate of unit Em7	53
Figure 44: Outcrop and thin-section photographs of rocks in unit Em8.....	54
Figure 45: Photomicrograph of a rhyolite dike of unit Em10.....	55
Figure 46: Outcrop photographs of post-tectonic dikes cutting tectonite in the Beresford Lake shear zone (BLSZ).....	56
Figure 47: SiO ₂ vs. total alkali plots for the Garner, Bidou, Gem and Edmunds assemblages	62
Figure 48: Nb/Y vs. Zr/TiO ₂ plots for the Garner, Bidou, Gem and Edmunds assemblages.....	63
Figure 49: Al ₂ O ₃ vs. FeO ^t + TiO ₂ vs. MgO plots for the Garner, Bidou, Gem and Edmunds assemblages.....	64
Figure 50: Zr/Y vs. Th/Yb plots for the Garner, Bidou, Gem and Edmunds assemblages.....	65
Figure 51: Trace-element diagrams for mafic volcanic and associated intrusive rocks	66
Figure 52: Discrimination diagrams for mafic volcanic and associated intrusive rocks of the Garner, Bidou, Gem and Edmunds assemblages.....	67
Figure 53: Discrimination diagrams of geochemical values or estimated age versus Sm-Nd isotopic parameters for key map units in the eastern Rice Lake belt.....	68
Figure 54: Discrimination diagrams and primitive-mantle-normalized trace-element diagrams for ultramafic volcanic and intrusive rocks of the Garner assemblage.....	69
Figure 55: Chondrite-normalized rare-earth element diagrams for felsic volcanic and associated intrusive rocks	70
Figure 56: Bivariate plots of element ratios in felsic volcanic and associated intrusive rocks of the Garner, Bidou, Gem and Edmunds assemblages.....	71
Figure 57: Primitive-mantle-normalized trace-element diagrams for felsic volcanic and associated intrusive rocks.....	72
Figure 58: Bivariate plots of Zr vs. selected high-field-strength and rare-earth elements in felsic volcanic rocks of the Garner, Bidou, Gem and Edmunds assemblages	73
Figure 59: Distribution plot of volatile-free SiO ₂ contents of rocks from the West association of the Gem assemblage	74
Figure 60: Harker plots of major-element oxides vs. SiO ₂ for rocks from the West association of the Gem assemblage	75
Figure 61: Plots of selected trace elements and elemental ratios vs. SiO ₂ for rocks from the West association of the Gem assemblage	76
Figure 62: Primitive-mantle-normalized trace-element profiles for representative samples from the West association of the Gem assemblage	77
Figure 63: Primitive-mantle-normalized trace-element plots of Edmunds assemblage dikes.....	79
Figure 64: Plots of major and immobile trace-element data for post-tectonic mafic dikes	81
Figure 65: U-Pb concordia diagrams for igneous zircons from the Garner and Bidou assemblages	86
Figure 66: U-Pb concordia diagrams for igneous zircons from the Gem assemblage and Wanipigow River plutonic complex..	88
Figure 67: U-Pb concordia diagrams for zircons from dikes.....	89
Figure 68: U-Pb concordia diagrams for detrital zircons from the Bidou, Gem and Edmunds assemblages.....	91
Figure 69: Combined frequency histograms and probability-density distribution curves of ²⁰⁷ Pb/ ²⁰⁶ Pb ages for detrital zircons from the Bidou, Gem and Edmunds assemblages.....	92
Figure 70: Simplified geology of the study area, showing major structures, geological contacts, Au occurrences and structural domains.....	96
Figure 71: Stereographic projections of poles to primary layering and bedding.....	97

Figure 72: Outcrop and thin-section photographs of G_1 structures.....	97
Figure 73: Stereographic projections of poles to G_2 planar fabrics	98
Figure 74: Outcrop photographs of G_2 fabrics	99
Figure 75: Stereographic projections of G_2 linear fabrics.....	99
Figure 76: Stereographic projections of F_2 axial planes and axes	100
Figure 77: Outcrop and thin-section photographs of structures in G_2 high-strain zones	101
Figure 78: Outcrop photographs of G_2 structures	102
Figure 79: Stereographic projection of poles to bedding.....	102
Figure 80: Stereographic projections of poles to the S_3 cleavage.....	102
Figure 81: Outcrop photographs of G_3 structures	103
Figure 82: Detailed outcrop map from the narrows in Garner Lake.....	104
Figure 83: Stereographic projections of poles to the mylonitic S_4 foliation	105
Figure 84: Outcrop and thin-section photographs of structures in G_4 mylonite zones	106
Figure 85: Stereographic projections of the L_4 lineation in G_4 mylonite zones.....	106
Figure 86: Outcrop photographs of G_4 shear bands.....	107
Figure 87: Stereographic projections of poles to S_4 shear bands.....	107
Figure 88: Stereographic projections of F_4 axial planes and axes	108
Figure 89: Outcrop photographs of F_4 folds	109
Figure 90: Stereographic projections of the poles to S_4 axial-planar crenulation cleavage.....	109
Figure 91: Outcrop photographs of F_4 folds	110
Figure 92: Stereographic projection of orientation data for G_4 structures	110
Figure 93: Schematic diagram showing the geometry of G_4 structures.....	110
Figure 94: Outcrop photographs of F_4 folds in chloritic G_4 mylonite.....	111
Figure 95: Outcrop photographs of G_4 faults.....	112
Figure 96: Stereographic projection of the poles to G_5 faults in all structural domains	113
Figure 97: Schematic block diagrams illustrating the structural evolution of the Garner–Gem lakes area and the surrounding region	114
Figure 98: Outcrop photographs of alteration and mineralization indicative of seafloor hydrothermal circulation in the Gem assemblage	117
Figure 99: Hand-specimen photographs of mineralization hosted by sheeted veins in intrusion breccia	118
Figure 100: Outcrop photographs of mineralization and alteration associated with shear-hosted quartz-carbonate veins.....	119
Figure 101: Hand specimen of mineralization at the Lily South occurrence	120
Figure 102: Outcrop photographs of quartz veins and alteration associated with G_5 faults	121
Figure 103: Schematic sections illustrating the postulated tectonic evolution of the south margin of the North Caribou terrane.....	124

MAP

GR2013-1-1: Geology and structure of the Garner–Gem lakes area, Rice Lake greenstone belt, southeastern Manitoba (parts of NTS 52L11, 14), 1:20 000 scale..... back pocket

DIGITAL DATA

Data Repository Item DRI2013002: Lithogeochemical database, Sm-Nd isotopic data and U-Pb geochronological data for the eastern Rice Lake greenstone belt, Manitoba (NTS 52L11, 14)¹

¹ MGS Data Repository Item DRI2013002, containing the data or other information sources used to compile this report, is available on the CD-ROM in the back pocket of this report, or online to download free of charge at <http://www2.gov.mb.ca/itm-cat/web/freedownloads.html>, or on request from minesinfo@gov.mb.ca or Mineral Resources Library, Manitoba Mineral Resources, 360–1395 Ellice Avenue, Winnipeg, Manitoba R3G 3P2, Canada.

Introduction

The Garner–Gem lakes area is located 160 km northeast of Winnipeg, Manitoba, at the southeastern extent of the Archean Rice Lake greenstone belt of the western Superior province. The Rice Lake belt (RLB) hosts economically important orogenic Au deposits, most notably the Rice Lake (a.k.a. San Antonio) deposit at Bissett, and shows indications of potential for several other mineral deposit types, including magmatic Ni–Cu–PGE, komatiite-hosted Ni and volcanic-hosted Cu–Zn–Pb–Au–Ag. This report documents the lithology, stratigraphy, depositional setting, geochemistry, geochronology and structural geology of Mesoarchean and Neoarchean supracrustal rocks in the hitherto poorly understood southeastern extent of the RLB, in light of new data collected by the Manitoba Geological Survey (MGS) as part of the Rice Lake Metallogeny Project. Initiated in 2002, the objective of this project was an updated understanding of the geology, tectonic evolution and metallogeny of the RLB (see Anderson, 2002, 2003a, b, 2004, 2005a, b, 2006a, b, 2007, 2008), with the goal of providing an improved geological context and predictive framework for mineral exploration.

Previous work

The earliest reported geological investigation in the Garner–Gem lakes area was conducted in 1912 by E.S. Moore of the Geological Survey of Canada (GSC) as part of a survey to verify reports of the Rice Lake Au discovery in 1911 (Moore, 1913, 1914), and to expand upon the route mapping of the lower Wanipigow and Manigotagan rivers by J.B. Tyrrell and D.B. Dowling (GSC) in 1890 and 1891 (Dowling, 1900). In 1917, the geology of the upper Manigotagan River was investigated by Marshall (1918) as a follow-up to new Au discoveries in the Beresford Lake area. In 1921, Garner and Gem (formerly Island) lakes were examined by the Ontario Department of Mines during the Manitoba–Ontario boundary survey (Burwash, 1923) and, in 1922 and 1923, the most significant Au prospects in the Rice Lake and Beresford Lake map areas were studied by Wright (1924). Wright's map, published at a scale of 1:63 360 (1 inch to 1 mile; Wright, 1927), is the earliest available for the eastern RLB. In 1926, the adjacent Bee Lake area of Ontario was mapped at a reconnaissance scale (1 inch to 4 miles) by Gilbert (1927).

De Lury (1927) provided a good overview of mineral occurrences in the belt and made note of new Au discoveries in the Garner–Gem lakes area in 1925 and 1926, in what was likely the first concerted phase of mineral prospecting. In 1929, the most significant deposits in the district, Central Manitoba and Diana (a.k.a. Gem Lake), were examined by Wright (1930), and the resulting descriptions were incorporated into an early compilation of geology and mineral deposits in south-eastern Manitoba (Wright, 1932a, b). Wright's report includes a 1:24 000 scale map (Map 280A; 1 inch to 2000 feet) that overlaps the northwestern portion of the present study area. In 1936 and 1937, C.H. Stockwell and C.S. Lord (GSC) mapped an area of 65 km² (25 sq. mi.) between Halfway Lake and Beresford Lake, including the then-active Central Manitoba and Gunnar mines. Their report and maps (Stockwell and Lord, 1939; Stockwell, 1940), the latter published at a scale of 1:12 000 (1 inch to 1000 feet), provide particularly valuable descriptions

of these deposits, which remain the largest known in the area. Stockwell (1945a, b) incorporated this work into two regional geological maps for the eastern RLB, which were published at a scale of 1:63 360 (1 inch to 1 mile) and include marginal notes. The area south of Gem Lake was remapped by Russell (1952) at a scale of 1:15 600 (1 inch to 1300 feet), and the Bee Lake area of Ontario was remapped by Shklanka (1967) at a scale of 1:31 680 (1 inch to ½ mile).

Weber (1971b) compiled this early mapping onto a belt-scale geological map (1:63 360 scale or 1 inch to 1 mile) that was released by the Manitoba Mines Branch as part of Project Pioneer (McRitchie and Weber, 1971a), a multidisciplinary study of the Rice Lake region conducted by the Mines Branch and the University of Manitoba from 1966 to 1969. During this project, the Garner–Gem lakes area and the adjacent 'Manigotagan gneissic belt' (English River subprovince) were mapped by Weber (1971a) and McRitchie and Weber (1971b), respectively, at a scale of 1:31 680 (1 inch to ½ mile). Prior to the present study, Weber's map provided the most complete and detailed guide to the geology of the Garner–Gem lakes area. Also included in the Project Pioneer final report, and of pertinence to the present study, are descriptions of the volcanic stratigraphy in the central portion of the RLB (Campbell, 1971), the ultramafic intrusion at Garner Lake (Scoates, 1971) and the structural geology along strike to the northwest at Long Lake (Zwanzig, 1971). Based on these results, Weber (1971c) described the geological evolution of the Rice Lake belt in terms of geosynclinal stages within an Alpine-type orogenic cycle.

Extensive forest fires in 1983 greatly improved the quality of bedrock exposure across the northern and southern portions of the study area, and thereby prompted a renewal of bedrock mapping activity. The Stormy Lake area was mapped at 1:10 000 scale by D.J. Owens and D.M. Seneshen of the University of Manitoba (Owens and Seneshen, 1985; Seneshen and Owens, 1985), and this work was followed up with 1:1000 scale mapping of key stratigraphic sections east (Owens, 1986a, b) and south (Seneshen, 1986) of Stormy Lake. The latter section includes well-preserved pyroclastic deposits that were described in detail by Seneshen (1990). In 1987, Au occurrences south of Gem Lake in the Lily Lake area were investigated by Weber (1987), who noted that the local geology is considerably more complex than indicated on existing maps.

Under the auspices of the 1984–1989 Canada–Manitoba Mineral Development Agreement (MDA), the thoroughly burnt area that extended through Stormy Lake and north of Garner Lake was mapped at 1:2500 scale by R.J. Brommecker of Queen's University during the summers of 1988 and 1989, with the purpose of documenting the structural setting of Au occurrences (Brommecker et al., 1989; Brommecker, 1991, 1996). As a direct result of this study, a previously unrecognized komatiite flow complex was identified north of Garner Lake, further emphasizing the need for new mapping (Brommecker et al., 1993; Poulsen et al., 1993, 1994; Corkery, 1995). Addressing this need was a major objective of the MGS Rice Lake Metallogeny Project in 2002–2007.

Concurrent with the MDA, Manitoba Energy and Mines documented the area's mineral deposits and occurrences

(Theyer and Gaba, 1986; Theyer, 1987, 1994; Theyer and Ferreira, 1990), and several reconnaissance-style geological and geochronological studies were initiated to address belt-scale correlation issues (Turek et al., 1989; Turek and Weber, 1991, 1994; Poulsen et al., 1993, 1994; Davis, 1994; Corkery, 1995). Davis (1994, 1996) reported the results of U-Pb age determinations on zircons from several key map units in the Garner–Gem lakes area, including tonalitic pegmatite in the Garner Lake intrusion and an overlying unit of arkosic sandstone, rhyolitic breccia at Gem Lake, and turbiditic greywacke at Beresford Lake and Gem Lake. Poulsen et al. (1996) reviewed the salient results of the MDA studies.

More recently, the MGS conducted reconnaissance mapping and lithogeochemical sampling in the eastern RLB (Bailes, 1998; Corkery, 1999), and Hollings et al. (1999) examined the geochemistry of the komatiitic flows north of Garner Lake and compared it to those of the Red Lake greenstone belt. As part of the Western Superior NATMAP project, Rogers (2001) re-examined the eastern extension of the RLB in Ontario (the Bee Lake belt) and made minor refinements to Shklanka's map (cf. Shklanka, 1967; Rogers, 2003). Regional compilation maps produced under the auspices of NATMAP include marginal notes on the geology and regional setting of the study area (e.g., Bailes et al., 2003; Lemkow et al., 2006). Results of NATMAP and the concurrent Western Superior LITHOPROBE transects provide regional context for the study area and were presented in a Special Issue of the Canadian Journal of Earth Sciences (Percival and Helmstaedt, 2006).

Methods and scope

The Garner–Gem lakes mapping project was initiated by the MGS in 2002. It was designed to be multidisciplinary in scope and thus involved 1:20 000 scale bedrock mapping, in conjunction with detailed structural analysis, lithogeochemistry, U-Pb geochronology, Sm-Nd isotopic analysis and mineral deposits investigations. The intent was to update the existing map and resolve various geological problems identified by previous workers. Fieldwork in the Garner Lake area took place in 2002 and 2003. Shoreline outcrop on Gem Lake was mapped during parts of the 2003, 2004 and 2005 field seasons, with follow-up traversing campaigns in 2006 and 2007. Laboratory analyses continued until 2010. Preliminary results of fieldwork were published in the MGS *Report of Activities* (Anderson, 2002, 2003a, 2005b, 2006b, 2007) and as MGS preliminary maps (Anderson, 2003b, 2006a). This report and the accompanying 1:20 000 scale map (GR2013-1-1) supersede the preliminary publications.

The study area extends from the south end of Beresford Lake in the north to Slate Lake in the south, and is mostly bounded by the Manitoba-Ontario boundary on the east and Provincial Road (PR) 314 on the west. It is entirely contained within Nopiming Provincial Park, in an area designated to accommodate forestry and mining activities insofar as they do not compromise other park purposes. The mapped area encompasses roughly 110 km² and overlaps portions of the more detailed maps of Stockwell and Lord (1939), Russell (1952), Owens and Seneshen (1985) and Brommecker (1991, 1996), all of which were found to be of good quality. The geology in

the northwest corner of Map GR2013-1-1 is simplified from the 1:10 000 scale preliminary map of Owens and Seneshen (1985). In areas of poor bedrock exposure, these data have been augmented by industry high-resolution aeromagnetic data.

The northern part of the study area is most efficiently accessed from Bissett via PR 304, whereas access to the southern portion is from Lac du Bonnet by way of PR 314. All shoreline outcrops on Garner Lake were accessed by boat, via the Garner River, from the landing at Beresford Lake, whereas those on Gem Lake were accessed by boat from the landing at the terminus of the Gem Lake all-terrain vehicle (ATV) trail. The Manigotagan River system upstream from Gem Lake, which includes Banksian, Lily and Slate lakes, can be reached by boat via a short (150 m) portage from Gem Lake. This area is also accessible via the ATV trail to the abandoned Diana (Gem Lake) mine, from the trail head located opposite the Tooth Lake parking area on PR 314. All inland areas were investigated by traverse, using hand-held GPS and orthorectified aerial photographs for navigation and plotting.

With the exception of the areas between Garner Lake and Gem Lake, east of Beresford Lake and along the wide valley of the Garner River, bedrock exposures are generally abundant in the study area and are particularly extensive around Stormy Lake and Gem Lake; however, the quality of these exposures is generally poor for geological mapping purposes. In those areas that burned in 1983, the exposures remain largely free of vegetation but are mostly covered by a film of black lichen that significantly obscures textural features. Extensive blowdown and dense regrowth make for exceedingly arduous traversing in low-lying areas of the burn. Areas of exceptionally thick regrowth include crowded thickets of immature spruce trees that appear to have supported a thick blanket of snow or ice at some point in time but were reduced to a chaotically broken jumble under the accumulated weight; these areas are all but impassable. The area bounded by Garner Lake, Gem Lake and the Manigotagan River was mostly spared from the fire and thus included large tracts of mature boreal forest. Here, bedrock exposures are generally covered by lichen and moss, the latter of which was peeled to facilitate examination. Most of the timber in this area was harvested between 1995 and 2002, resulting in significantly improved access and scattered clean exposures along logging roads. Drift cover is generally thin and discontinuous in the study area; roches moutonnées and glacial striae indicate ice flow primarily from the east-northeast (~060°).

During the mapping, mesoscopic petrological and structural features in bedrock were examined, described in detail, measured and photographed, and a suite of grab and oriented rock samples was collected to obtain thin sections for petrographic and microstructural examination. A representative suite of 112 least-altered rock samples was collected and submitted to Activation Laboratories Ltd. (Ancaster, Ontario) to obtain major- and trace-element data by high-precision inductively coupled plasma–emission spectrometry (ICP-ES) and –mass spectrometry (ICP-MS) on whole rocks. A subset of 19 samples, selected to include key units from each tectonostratigraphic assemblage, was submitted to R.A. Creaser at the University of Alberta Radiogenic Isotope Facility for Sm-Nd isotope analysis. In addition, 13 samples were submitted for U-Pb dating to

L.M. Heaman at the University of Alberta Radiogenic Isotope Facility; these included 8 samples of volcanic and plutonic rock for isotope dilution–thermal ionization mass spectrometry (ID-TIMS) on igneous zircon, and 5 samples of sandstone for laser-ablation, multicollector, inductively coupled plasma–mass spectrometry (LA-MC-ICP-MS) on detrital zircon populations. All of these data are presented herein.

Acknowledgments

Assistance during fieldwork was provided by P. Kremer, A. Carlson and C. Chamale of the University of Manitoba, and K. Reid and R. Moody of Brandon University. Discussions with A. Bailes and T. Corkery helped clarify some of the ideas presented in this report. C. Böhm and T. Corkery assisted with the collection of geochronological samples in 2002, and C. Böhm performed some of the subsequent U-Pb isotope analyses. L. Chackowsky, P. Lenton, M. McFarlane and M. Pacey provided GIS and digital cartographic expertise, and B. Lenton drafted many of the figures. R. Boulay, B. Kuran, T. Lewis, P. Sargeant, P. Theyer, T. Tuba and M. Tuchscherer are acknowledged for providing fruitful discussion, as well as free access to mineral properties and proprietary data. Logistical support was provided by D. Binne and N. Brandon. Thin sections and rock powders were prepared by G. Bengert, R. Unruh and V. Varga in the MGS Rock Preparation Laboratory, under the direction of D. Berk and D. Snuggs. Particular thanks are extended to K. Freisen of Inner City Youth Alive Inc. for facilitating access to accommodations at Gem Lake. This report was improved through review by E. Syme.

Regional setting

The Rice Lake greenstone belt (RLB) is one of several strands of Neoproterozoic and Mesoproterozoic supracrustal rocks that, along with the Red Lake and Birch-Uchi belts in Ontario, define the western segment of the volcano-plutonic Uchi subprovince² (Card and Ciesielski, 1986; Stott and Corfu, 1991) of the western Superior province (Figure 1). The Uchi subprovince is flanked to the north by the mainly metaplutonic Berens River subprovince and to the south by metasedimentary rocks and derived gneiss, migmatite and granitoid plutonic rocks of the English River subprovince (Card and Ciesielski, 1986). Thurston et al. (1991) included the Berens River subprovince and the Mesoproterozoic portions of the Uchi subprovince in the continental ‘North Caribou terrane’ (NCT), which has come to be regarded as the protocratonic nucleus of the western Superior province (e.g., Stott and Corfu, 1991; Williams et al., 1992; Corfu et al., 1998; Skulski et al., 2000; Percival et al., 2002, 2006b; Whalen et al., 2003). Accordingly, the Mesoproterozoic portions of the Uchi subprovince in Manitoba are described herein as part of the NCT. Using the revised terminology of Stott et al. (2010), the English River subprovince is herein referred to as the English River basin (ERB). The Garner–Gem lakes area spans the RLB (Figure 1) and adjacent portions of the NCT and ERB, and thus represents an ideal location to evaluate geodynamic models for the western Superior province.

Stratigraphic and tectonic nomenclature

Supracrustal rocks in the RLB were assigned to the Rice Lake group and the unconformably overlying San Antonio formation by Stockwell (1945a, b). A revised stratigraphic scheme developed during Project Pioneer had the Rice Lake group divided into the mainly metavolcanic Wallace Lake, Bidou Lake and Gem Lake subgroups (each with two or more formations) and the metasedimentary Edmunds Lake formation (see Campbell, 1971; McRitchie, 1971; Weber, 1971a, b). Subsequent reconnaissance mapping and geochronology at Garner Lake (e.g., Brommecker et al., 1993; Poulsen et al., 1993, 1994; Davis, 1994) prompted Poulsen et al. (1996) to propose one additional unit, the mainly metavolcanic Garner Lake subgroup (see also Corkery, 1995, Figure GS-26-2), parts of which had previously been assigned to the Gem Lake subgroup and Edmunds Lake formation of Weber (1971a, b).

Poulsen et al. (1996) also proposed an alternative tectonostratigraphic nomenclature, wherein the supracrustal components of the RLB were subdivided into distinct ‘assemblages’ in the sense proposed by Thurston et al. (1991) for the north-western Superior province in Ontario (i.e., distinct associations of stratified rocks deposited in a common setting in a discrete interval of time; see also Williams et al., 1992). Poulsen et al. (1996) identified six assemblages on the basis of U-Pb age determinations and stratigraphic and structural relationships: the Mesoproterozoic Wallace Lake assemblage; the Mesoproterozoic–Neoproterozoic Garner Lake assemblage; and the Neoproterozoic Bidou Lake, Gem Lake, Edmunds Lake and San Antonio assemblages (Table 1; Figure 2). This nomenclature was subsequently adopted and expanded by Bailes et al. (2003), who defined 15 assemblages in the western Uchi subprovince and assigned to them tectonic affinities on the basis of their overall lithological character, augmented by whole-rock geochemical and Sm–Nd isotopic data. In accordance with the nomenclature of Bailes et al. (2003), ‘Lake’ has been dropped from the assemblage names used in this report. Broadly comparable assemblages are recognized from widely separated areas along the south margin of the NCT, thereby providing a basis for regional tectonostratigraphic correlations (e.g., Percival et al., 2006b).

Although the application of plate-tectonic theory to studies of Archean lithospheric evolution remains the subject of considerable debate (e.g., Chardon et al., 1998; de Wit, 1998; Hamilton, 1998, 2003, 2007; Bédard et al., 2003, 2012; McCall, 2003; Stern, 2005; Brown, 2006; Cawood et al., 2006; Kerrich and Polat, 2006; Furnes et al., 2007; Rollinson, 2007; Condie and Pease, 2008; Wyman, 2012), the weight of evidence pertaining to the assembly of the Superior province prior to cratonization at ca. 2.6 Ga strongly implicates subduction-accretion processes and the collisional interactions of disparate oceanic and continental terranes (e.g., Langford and Morin, 1976; Blackburn, 1980; Hoffman, 1989; Percival and Williams, 1989; Card, 1990; Williams, 1990; Williams et al., 1992). This evidence is particularly compelling in the western Superior province, where the plate-tectonic paradigm appears to offer a cohesive explanation for the linear arrangement of volcanic-plutonic,

² For the sake of consistency, the Manitoba Geological Survey has opted to make a universal change from capitalized to noncapitalized for the generic part of lithostructural feature names (formal stratigraphic and biostratigraphic nomenclature being the exceptions).

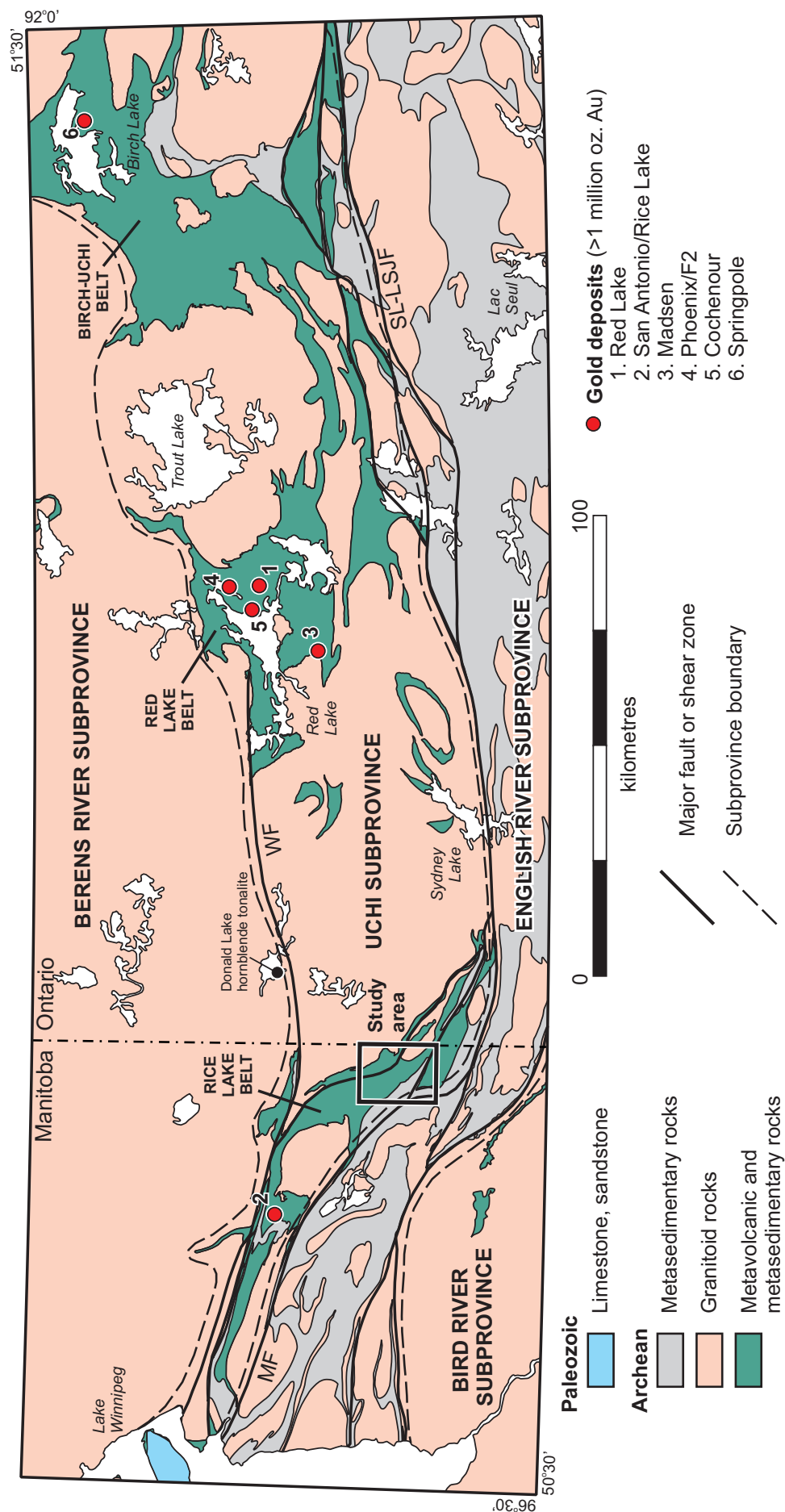


Figure 1: Regional geological setting of the Rice Lake Belt in the western Uchi subprovince (after Lemkow et al., 2006), showing the location of the study area and major Au deposits. Abbreviations: MF, Manigotagan fault; SL-LSJF, Sydney Lake–Lake St. Joseph fault; WF, Wanipigow fault.

Table 1: Principal supracrustal assemblages at the south margin of the North Caribou terrane, Manitoba (after Poulsen et al., 1996; Bailes et al., 2003).

Assemblage name	Age constraints	Equivalent units (Manitoba)	Equivalent units (Ontario)	Key rock types and chemical affinity	Depositional setting	Tectonic significance
San Antonio	<2.705 Ga	Guano Island; Hole River; Manigotagan; Siderock	None known	Quartz greywacke, conglomerate, turbiditic greywacke	Subaerial fault-bounded fluvial basin; basal angular unconformity	Post-accretion, pre-orogenic; denudation of NCT margin
Edmunds	<2.72 Ga (lower); <2.71 Ga (upper); >2.70 Ga	English River	Bee Lake (Kangaroo formation)	Turbiditic greywacke, mudstone, conglomerate, iron formation; minor TH to CA basalt, basaltic andesite and gabbro	Submarine fan; mature arc-rift basin; basal conformity	Regionally extensive intra-arc basin; uplift and denudation of NCT margin
Gem	<2.73 Ga; ca. 2.72 Ga	Black Island; Rainy Lake Road, Townsite and Round Lake units	Bee Lake (Odd and Anderson formations); St. Joseph	TH to CA basalt, basaltic andesite; CA ADR; hypabyssal intrusions; epiclastic rocks	Subaerial to shallow subaqueous arc-rift basin	Restricted extensional basin in Bidou arc; slab rollback?
Bidou	<2.75 Ga (lower); 2.73 Ga (upper)	Black Island (part of); Independence Lake unit	Confederation	TH basalt and gabbro; CA dacite, rhyolite; turbiditic greywacke and conglomerate	Mature back-arc basin (lower); subaqueous volcanic arc (upper)	Oceanic or marginal arc-back-arc complex; northward subduction
Garner	>2.87 Ga (lower); 2.87 Ga (GLIC); ca. 2.85 Ga (upper)	None known	Bruce Channel and Trout Bay	CA ADR; peridotite, pyroxenite; arkose; iron formation; komatiite-KB; TH basalt and gabbro	Subaqueous volcanic arc (lower); intra-arc rift (upper)	Continental arc
Wallace	<2.99 Ga; >2.92 Ga	Lewis-Story; Wanipigow North; Little Beaver; Big Island	Balmer (\pm Ball)	Arkosic 'grit'; quartzite; iron formation; carbonate; komatiite-KB; TH basalt and gabbro	Shallow marine continental platform and restricted rift basins	Stabilization of NCT; initial rifting

Abbreviations: ADR, andesite-dacite-rhyolite; CA, calcalkalic; GLIC, Garner Lake intrusive complex; KB, komatiitic basalt; NCT, North Caribou Terrane; TH, tholeiitic

plutonic and sedimentary subprovinces over distances of more than 1000 km, as well as for geological relationships observed at local scales (e.g., Stott and Corfu, 1991; White et al., 2003; Percival et al., 2006a, b). Plate tectonics is therefore utilized as the descriptive context for this report, with the caveat that several key hallmarks of subduction, such as blueschist, mélangé and classical ophiolite (i.e., mid-ocean-ridge-type; Dilek and Furnes, 2011) have not been documented in the region.

North Caribou terrane

In Manitoba, the south margin of the NCT includes three main components: 1) dominantly tonalitic plutonic complexes (3.01–2.99 Ga); 2) nonconformably overlying platform-rift sequences (2.99–2.92 Ga); and 3) Mesoarchean (2.94–2.90 Ga) and Neoarchean (2.75–2.70 Ga) continental-arc plutons (Bailes and Percival, 2000, 2005a; Percival et al., 2002, 2006a, b; Bailes et al., 2003; Whalen et al., 2003; Sasseville et al., 2006). The platform-rift sequences are best preserved along the east shore of Lake Winnipeg (Lewis-Story assemblage), north of Rice Lake (Little Beaver and Wanipigow North assemblages) and at Wallace Lake (Wallace assemblage; herein defined to include fault-bounded panels of tholeiitic basalt and diabase, which were referred to as the 'Big Island assemblage' by Sasseville

et al., 2006). Continental-platform quartz arenite and pebble conglomerate in the Wallace and Lewis-Story assemblages contain single age-populations of ca. 2.99 Ga detrital zircons (Davis, 1994; Percival et al., 2006a) and are overlain by komatiite-tholeiite flow complexes, with minor intercalated iron formation, that are thought to record ca. 2.99–2.92 Ga plume-related magmatism associated with rifting of the NCT (Percival et al., 2002, 2006a). The Little Beaver assemblage consists of strongly transposed psammitic and semipelitic schist, with minor iron formation and gabbro sills (Anderson, 2008), that contain a single age-population of ca. 2.99 Ga detrital zircons (McNicoll and Percival, unpublished data, 2001) and perhaps represent a distal facies of the Mesoarchean rift sequence.

In the western and central portions of the RLB, the south boundary of the NCT is sharply defined by the Wanipigow fault, which is one of the principal structures of the region (Figure 2) and is interpreted to represent a long-lived crustal-scale structure of the type associated with major terrane boundaries and orogenic Au districts in other Archean greenstone belts. It trends east-southeast and, though poorly exposed, is delineated by fault-bounded basins of fluvial-alluvial siliciclastic rocks and a pronounced topographic lineament. It is characterized by a steeply dipping zone of interleaved tectonite, mylonite and

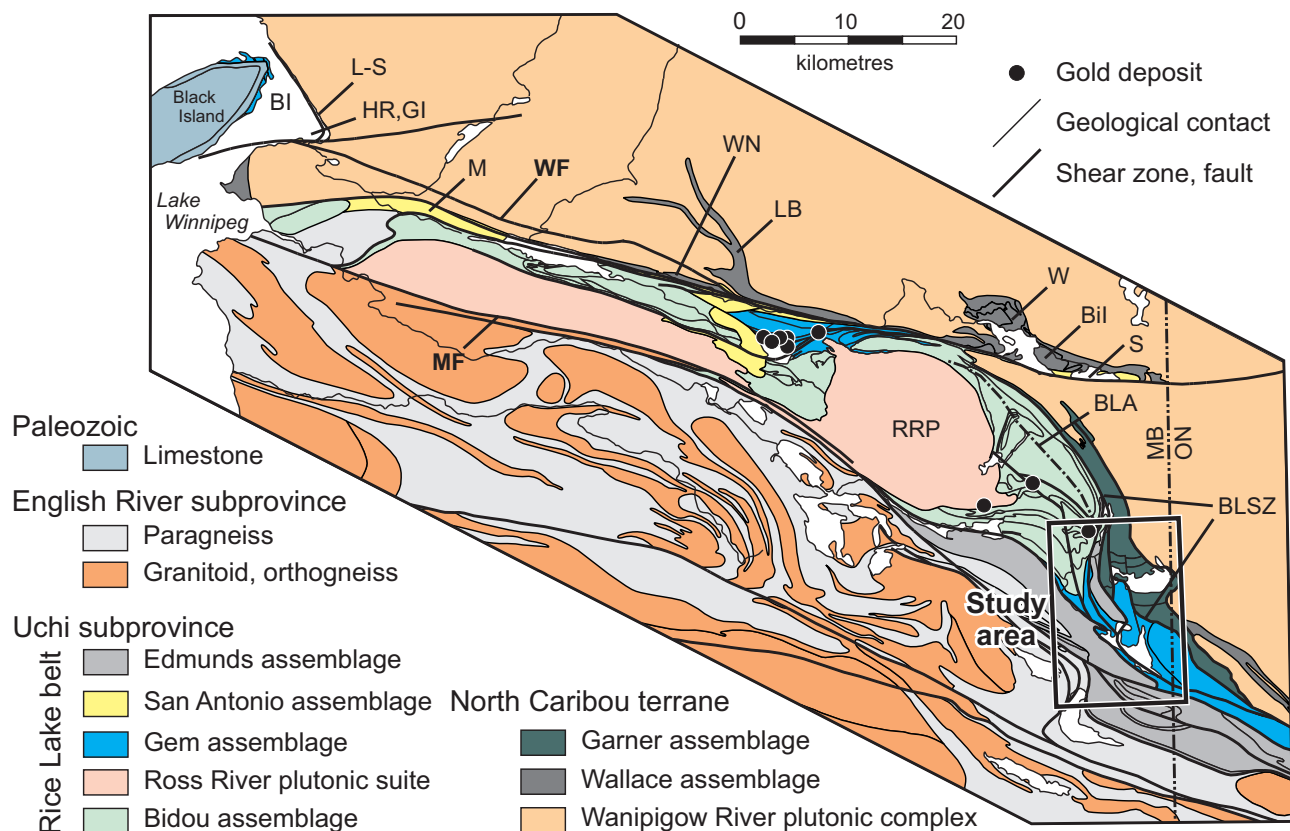


Figure 2: Simplified geology of the Rice Lake belt, showing the principal lithotectonic assemblages, major Au deposits and location of the study area. Abbreviations: Bil, Big Island assemblage; BI, Black Island assemblage; BLA, Beresford Lake anticline; BLSZ, Beresford Lake shear zone; GI, Guano Island assemblage; HR, Hole River assemblage; LB, Little Beaver assemblage; L-S, Lewis-Storey assemblage; M, Manigotagan assemblage; MF, Manigotagan fault; RRP, Ross River pluton; S, Siderock assemblage; W, Wallace assemblage; WF, Wanipigow fault; WN, Wanipigow North assemblage. Refer to Table 1 for descriptions of each assemblage.

phyllonite that ranges up to 1.5 km wide and, north of Rice Lake, contains kinematic evidence of an early episode of sinistral-reverse oblique-slip shear, followed by a protracted episode of dextral transcurrent-shear deformation (Anderson, 2008). The strike-slip component of movement was likely dominant, as indicated by the fact that there is no significant change in crustal level across the zone.

The Wanipigow fault appears to bifurcate toward the east at Wallace Lake, where a northern splay is traced eastward as a prominent topographic lineament that extends through Siderock Lake and continues along strike for approximately 90 km to Red Lake, Ontario (Figure 1). In a drillhole intercept between Wallace and Siderock lakes (Assessment File 74224, Manitoba Mineral Resources, Winnipeg), the structure is defined by a 10 cm thick seam of fault gouge that separates foliated supracrustal rocks on the north from fault breccia and cataclasite derived from granite on the south, suggesting the northern splay represents a relatively late and mostly brittle structure. Offset of the greenstone-granitoid contact indicates approximately 20 km of dextral displacement (Figure 2). The southern splay, known as the Beresford Lake shear zone (BLSZ; corresponds to the 'Beresford Lake deformation zone' of Brommecker et al., 1989), trends southeast through the Garner-Gem lakes area (Figure 2) and merges with the Sydney Lake-Lake St. Joseph fault farther along strike in Ontario. As described below, the

BLSZ separates Mesoarchean and Neoarchean assemblages in the study area and thus represents the interface between the NCT and Uchi subprovince. Here, the south margin of the NCT is occupied by the Wanipigow River plutonic complex and Garner assemblage, the latter of which is formally described for the first time in this report.

Uchi subprovince

The Uchi subprovince in Manitoba consists of subaqueously deposited volcanic and derived epiclastic rocks, syn-volcanic gabbro sills and tonalite-granodiorite plutons, and unconformably overlying terrestrial and marine siliciclastic rocks, which collectively define the RLB south of the Wanipigow fault. The exposed portion of the belt trends southeast for a distance of 145 km from the eastern extent of Paleozoic cover at Lake Winnipeg to just east of the Manitoba-Ontario border, and ranges up to 15 km wide (Figure 2). Regional aeromagnetic data indicate that the belt extends at least 150 km to the west beneath Paleozoic cover, where it widens considerably. The eastern extent of the RLB in Ontario, referred to as the Bee Lake belt, was mapped in detail by Shklanka (1967) and was recently revisited by Rogers (2001, 2003).

Uranium-lead zircon geochronological data indicate that major volcanism in the Manitoba segment of the Uchi subprovince spanned roughly 30 m.y., between 2745 and 2715 Ma,

whereas overlying sedimentary successions were deposited shortly after cessation of major volcanism, within a roughly 20 m.y. time interval between 2715 and 2695 Ma (Krogh et al., 1974; Ermanovics and Wanless, 1983; Turek et al., 1989; Turek and Weber, 1991; Davis, 1994, 1996; Percival et al., 2006a; Sasseville et al., 2006; Anderson, 2008). Following the terminology of Poulsen et al. (1996), volcanic rocks south of the Wanipigow fault are subdivided into the Bidou and Gem assemblages, whereas the younger sedimentary successions are subdivided into the Edmunds and San Antonio assemblages (Figure 2). Each displays significant differences in constituent rock types and inferred depositional settings; the volcanic assemblages are also differentiated by geochemical signatures and U-Pb ages. Only the San Antonio assemblage is not present in the Garner–Gem lakes area. As outlined below, these Neoproterozoic assemblages are interpreted to record back-arc, arc and arc-rift magmatism and synorogenic sedimentation within a north-verging subduction-accretion complex that developed over a span of roughly 50 m.y. along the NCT margin (e.g., Stott and Corfu, 1991; Poulsen et al., 1996; Sanborn-Barrie et al., 2001; Percival et al., 2002, 2006a, b; Bailes et al., 2003; Bailes and Percival, 2005a; Anderson, 2008).

Bidou and Gem assemblages

The Bidou assemblage consists of intercalated tholeiitic basalt flows, gabbro sills and basinal marine sedimentary rocks, which are overlain by a thick accumulation of calcalkalic felsic volcanoclastic rocks. The basalt and gabbro are chemically analogous to mid-ocean-ridge and back-arc-basin basalt (MORB and BABB, respectively), and the Bidou assemblage is therefore interpreted to record a transition from back-arc to arc magmatism (e.g., Poulsen et al., 1996; Bailes et al., 2003; Bailes and Percival, 2005a; Percival et al., 2006a). Uranium-lead zircon ages from the volcanic rocks and overlying sedimentary successions constrain this magmatism to ca. 2745–2730 Ma (Bailes et al., 2003; Percival et al., 2006a; Anderson, 2008). The thickest and most complete section of the Bidou assemblage, the stratigraphy of which was formally defined by Campbell (1971), defines a map-scale anticline in the core of the RLB east of the Ross River tonalite pluton (Figure 2). Possible local correlatives include >2724 Ma felsic–intermediate volcanoclastic rocks west of the Ross River pluton (the Independence Lake unit of Anderson, 2008) and ca. 2730 Ma (Ermanovics and Wanless, 1983) rhyolitic volcanoclastic rocks at Black Island (part of the Black Island assemblage of Bailes and Percival, 2005a).

The Gem assemblage is systematically described for the first time in this report. It consists of volcanic, subvolcanic intrusive and derived epiclastic rocks of mostly transitional tholeiitic–calcalkalic affinity that overlie the Bidou assemblage in apparent conformity at Gem Lake. Volcanic rocks in the Gem assemblage show a much wider range of compositions (basalt to high-SiO₂ rhyolite) than the underlying Bidou assemblage (basalt to dacite), and locally include distinctive high-SiO₂ rhyolite flows and pyroclastic rocks that show a chemical affinity to intra-arc rifts. Uranium-lead zircon ages from volcanic and overlying sedimentary rocks at the Gem Lake type locality constrain volcanism to ca. 2730–2715 Ma (Turek et al., 1989;

Davis, 1994, 1996). Age-equivalent rocks are documented at Rice Lake (the Rainy Lake Road, Townsite and Round Lake units of Anderson, 2008) and at Black Island on Lake Winnipeg (the Gray Point and Drumming Point sequences of Bailes and Percival, 2005a), in sections that have traditionally been included in the Bidou assemblage. However, in contrast to the chemically uniform flows of MORB-like tholeiitic basalt that characterize the Bidou assemblage type section east of the Ross River pluton, subaqueous basaltic flows in the Gem-equivalent sections at Gem Lake, Rice Lake and Black Island show much greater chemical variability, from tholeiitic (MORB-like) to calcalkalic (arc-like). The ca. 2724 Ma Ross River pluton (Anderson, 2008) intrudes the Bidou assemblage in the core of the RLB and is part of a voluminous tonalite–granodiorite–granite suite emplaced coeval with the youngest (2730–2715 Ma) volcanic assemblages. Age-equivalent rocks also occur in the Bee Lake belt in Ontario (ca. 2718 Ma Anderson Lake formation; Rogers, 2001; Lemkow et al., 2006).

Edmunds and San Antonio assemblages

The Edmunds and San Antonio assemblages consist of basinal marine and terrestrial siliciclastic rocks, respectively, that unconformably overlie the Bidou and Gem assemblages in several locations. The Edmunds assemblage consists of greywacke-mudstone turbidite, with minor conglomerate, chert and iron formation, deposited in a submarine fan system within a regionally extensive basin along the south flank of the Rice Lake belt. It is systematically described for the first time in this report. A locally thick basal unit of siliceous mudstone indicates that major sedimentation was preceded by a period of relative quiescence. As described by Weber (1971c), lenses of tonalite-boulder conglomerate in the medial portion of the assemblage mark an abrupt change in facies association and indicate a rapid change in sediment source and supply rate, perhaps in response to a sudden change in base level related to tectonic activity. Detrital zircon U-Pb analyses (Davis, 1996) indicate that deposition of the lower facies association occurred sometime after 2725 Ma, whereas the upper facies association includes detrital zircons as young as 2705 Ma. In the adjacent Bee Lake belt, probable equivalents to the upper facies association include a thick unit of tonalite-boulder conglomerate with a maximum depositional age of 2703 Ma (Rogers and McNicoll, unpublished, cited by Lemkow et al., 2006). Equivalent, though higher grade, rocks to the south are intruded by a 2696 Ma granodiorite pluton (Rogers and McNicoll, unpublished, cited by Lemkow et al., 2006), thereby constraining sedimentation to ca. 2700 Ma.

The fluvial-alluvial San Antonio assemblage consists of pebbly crossbedded arenite, polymictic conglomerate and planar-bedded greywacke that are disposed in a series of areally restricted, probably fault-bounded, subaerial basins along the NCT-Uchi interface (Figure 2). Weber (1971c) interpreted these rocks as continental-delta deposits and noted their similarity to classical synorogenic molasse sequences. At Rice Lake, the basal contact is a sharp angular unconformity, suggesting early accretion-related deformation of the underlying volcanic assemblages (e.g., Anderson, 2008) and thus a broadly synorogenic timing for sedimentation; these rocks may be proximal

equivalents to the lower facies association of the Edmunds assemblage. Uranium-lead ages from detrital zircons in arenite just above the unconformity indicate a maximum depositional age of 2705 Ma (Percival et al., 2006a). Probable local equivalents are also found in the Hole River (<2708 Ma) and Guano Island (<2728 Ma) assemblages at Lake Winnipeg (Percival et al., 2006a), the Manigotagan assemblage west of Wanipigow Lake (e.g., Lemkow et al., 2006) and the Siderock Lake assemblage (<2709 Ma) at Siderock Lake (Sasseville et al., 2006), all of which apparently postdate major arc magmatism, as suggested by the absence of crosscutting intrusions. Abundant Mesoarchean (3.0–2.9 Ga) detrital zircons in both the Edmunds and San Antonio assemblages (Davis, 1996; Percival et al., 2006a) point to the uplifted NCT margin as a major source of detritus, and distinguish them from superficially similar rocks in the underlying volcanic assemblages (see below).

English River basin

The English River basin is an east-trending belt of medium- to high-grade metasedimentary rocks and associated granitoid plutonic rocks that ranges up to 50 km wide and flanks the Uchi subprovince to the south over a strike length of more than 700 km. Referred to as the Manigotagan gneissic belt in Manitoba (McRitchie and Weber, 1971b), this belt ranges from 15 to 40 km wide and is bounded to the north by the Manigotagan fault, a subvertical mylonite that is traced for more than 100 km along strike in Manitoba and is continuous with the Sydney Lake–Lake St. Joseph fault in Ontario (Figure 1). The metasedimentary rocks consist mainly of greywacke turbidite and mudstone that were deposited in a submarine fan (or fans) after cessation of major volcanism in adjacent terranes (Davis, 1996). Detrital zircon ages span a range from 3080 to 2704 Ma, indicating that the sediment was largely derived from the NCT and Uchi subprovince, and was at least locally deposited after 2704 Ma (Corfu et al., 1995; Davis, 1996); regional constraints require sedimentation mainly between 2715 and 2700 Ma. These rocks, which were referred to as the Manigotagan and English River assemblages by Bailes et al. (2003), are thought to represent higher grade equivalents to the Edmunds assemblage in the adjacent Uchi subprovince. Various tectonic scenarios have been postulated for the English River basin, including fore-arc (Langford and Morin, 1976; Breaks, 1991; Hrabí and Cruden, 2006), back-arc (Pan et al., 1998) or syncollisional foreland (Davis, 1998) basins. Hoffman (1989) interpreted the English River basin as an accretionary prism (see also Card, 1990), which incorporated a precursor fore-arc basin adjacent to a volcanic arc represented by the Uchi subprovince.

The sedimentary succession was intruded by voluminous diorite–tonalite–granodiorite plutons at ca. 2698 Ma, prior to regional deformation and high-T–low-P metamorphism at ca. 2691 Ma (Corfu et al., 1995) that were related to terminal collision of the North Caribou and Winnipeg River terranes (Percival et al., 2006a, b). Metamorphic mineral assemblages indicate that peak metamorphism varied from middle greenschist facies in the north to localized granulite facies, accompanied by partial melting and migmatization, in the south (e.g., McRitchie and Weber, 1971b; Breaks, 1991). Late-tectonic granite plutonism at ca. 2663 Ma (Turek et al., 1989) and ca. 2660 Ma

titanite ages (Corfu et al., 1995) record the waning stages of thermotectonism at the present level of exposure. South and west of the Garner–Gem lakes area, medium- to high-grade metasedimentary rocks are juxtaposed with low-grade rocks of the Uchi subprovince along a greenschist-facies high-strain zone that trends through Flintstone Lake, roughly parallel to the Moose River, and appears to represent the main strand of the Manigotagan fault.

Local geology and stratigraphy

Supracrustal rocks in the Garner–Gem lakes area are here divided into the Mesoarchean–Neoarchean Garner assemblage and the Neoarchean Bidou, Gem and Edmunds assemblages (Figure 3), in keeping with the terminology of Poulsen et al. (1996). The Garner assemblage is intruded to the east by variably gneissic granitoid rocks of the Wanipigow River plutonic complex of the NCT, and is juxtaposed to the west with Neoarchean supracrustal rocks of the Bidou, Gem and Edmunds assemblages across the Beresford Lake shear zone (BLSZ). West of the BLSZ, the Neoarchean assemblages define the regional-scale Beresford Lake anticline (BLA), the hinge of which is truncated west of Beresford Lake by the Moore Lake shear zone (MLSZ; Figure 3). East-younging supracrustal rocks between the MLSZ and BLSZ define the strongly transposed eastern limb of the BLA. The essentially intact western limb includes a major parasitic fold referred to as the Manigotagan River anticline (MRA; Figure 3). Southwest of the study area, the Neoarchean assemblages are juxtaposed with metasedimentary rocks of the English River basin across the Manigotagan fault (MF).

All of these units are described in detail below, in order of decreasing known or apparent age; unit and subunit codes correspond to those on the accompanying Map GR2013-1-1. Some of the subunits described in the text and legend are too small to depict at 1:20 000 scale and therefore do not appear as unique polygons on the map. Descriptions of supracrustal units in the Garner, Bidou and Edmunds assemblages are presented in stratigraphic order; however, no stratigraphic order is implied by the organization of unit descriptions for the Gem assemblage, except where specified. For each assemblage, detailed descriptions of map units are preceded by a general overview of key features, with emphasis on salient contributions of previous workers. As noted above, this report provides the first formal descriptions of the Garner, Gem and Edmunds assemblages.

Lithological nomenclature

Regional metamorphic grade in the study area generally increases toward the English River basin in the southwest and the Wanipigow River plutonic complex in the northeast. In detail however, abrupt changes in metamorphic mineral assemblage across the BLSZ and MF indicate the presence of fault-controlled metamorphic discontinuities. Southwest of the MF, metasedimentary rocks of the English River basin contain upper-greenschist- to lower-amphibolite-facies mineral assemblages (biotite=andalusite or hornblende; McRitchie and Weber, 1971b; Weber, 1971a) and are intruded by swarms of variably deformed granitoid and granitic pegmatite dikes. These dikes are absent between the MF and the BLSZ, and

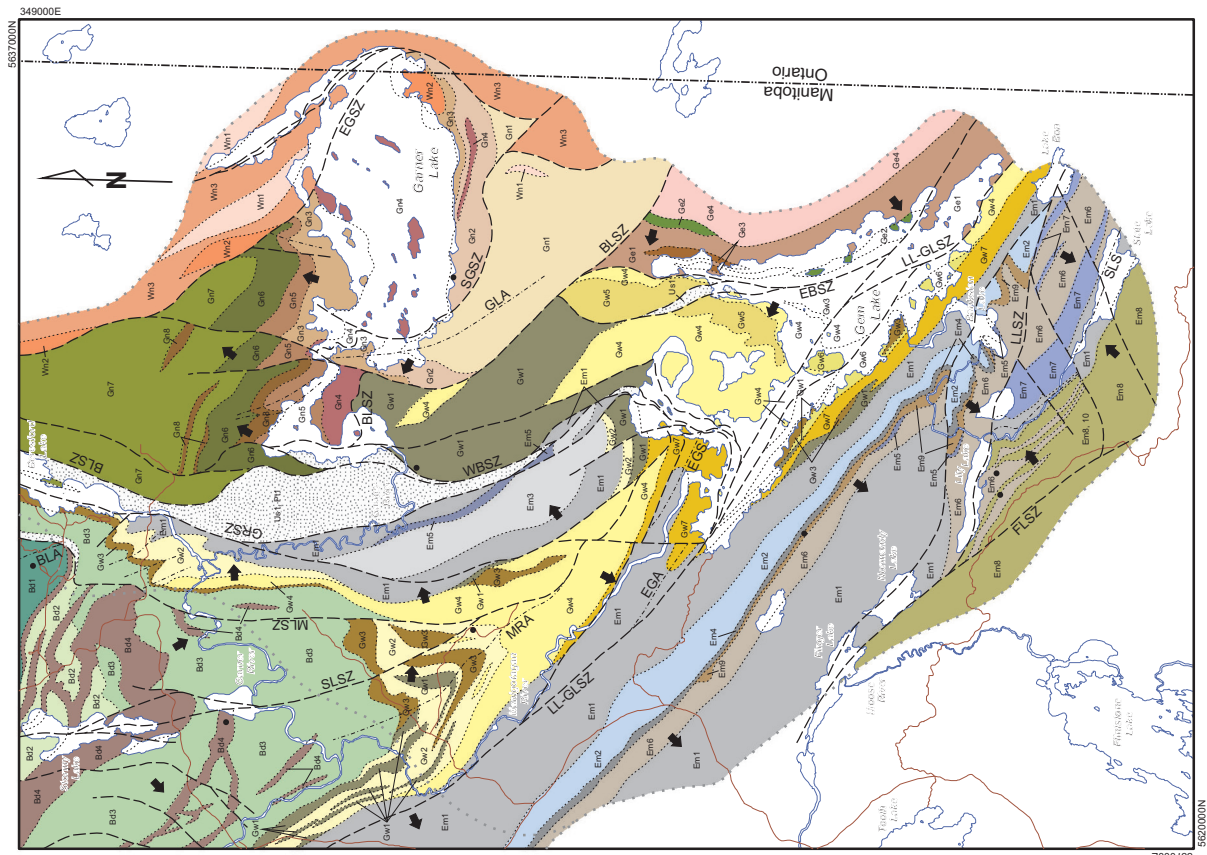
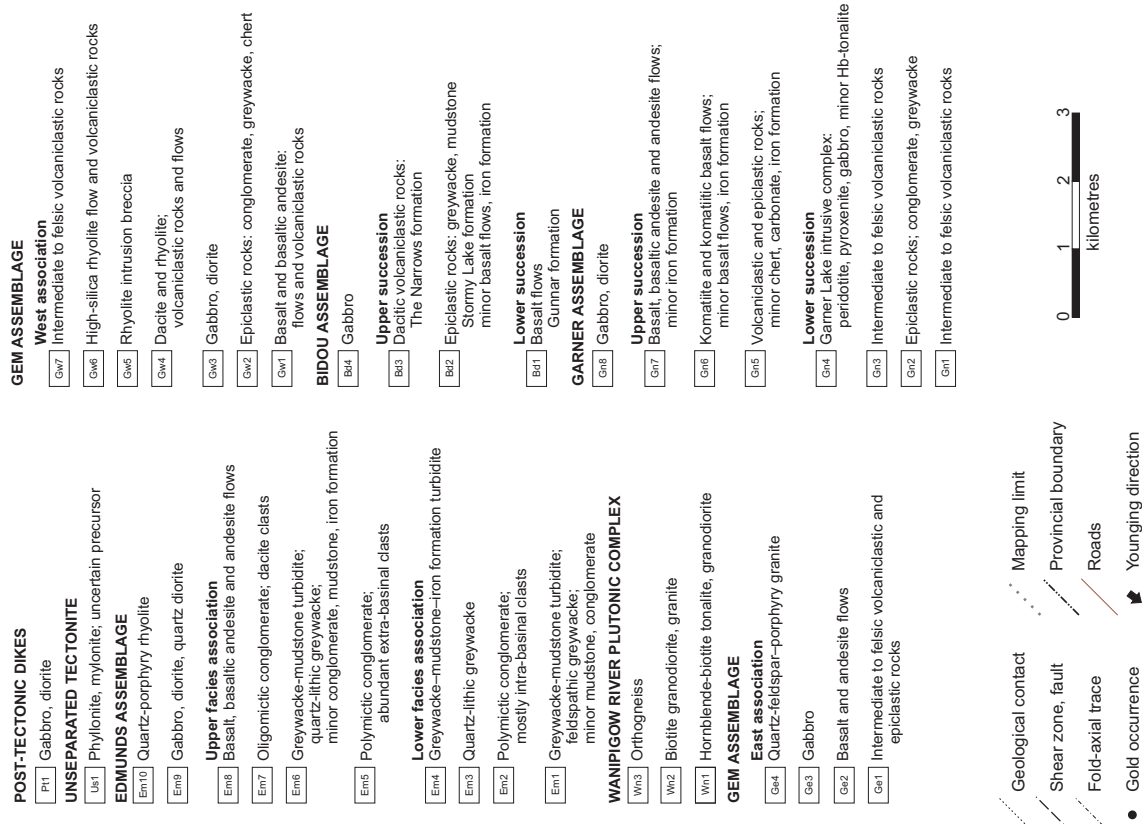


Figure 3. Geology of the Garner-Gem lakes area, simplified from the accompanying Map GR2013-1-1 (refer to this map for detailed geology and subunit descriptions). The grey dotted line shows the outline of the area mapped as part of this study. Abbreviations: BLA, Beresford Lake anticline; BLSZ, Beresford Lake shear zone; EBSZ, East Bay shear zone; EGSZ, East Garner shear zone; EGA, East Gem anticline; EGS, East Gem syncline; FLSZ, Finger Lake shear zone; GLA, Garner Lake anticline; GRSZ, Garner River shear zone; LLSZ, Lily Lake shear zone; LL-GLSZ, Long Lake-Gem Lake shear zone; MRA, Manigotagan River anticline; MGSZ, Moore Lake shear zone; SLSZ, Slate Lake syncline; WBSZ, Stormy Lake shear zone; WBSZ, West Bay shear zone.



mineral assemblages (chlorite±biotite±white mica±actinolite) indicate regional metamorphism in the low- to middle-greenschist facies. Northeast of the BLSZ, rocks of the Garner assemblage record peak metamorphism in the upper-greenschist to amphibolite facies (biotite±garnet±hornblende). Weber (1971a) interpreted this metamorphic zonation to be related to emplacement of the Wanipigow River plutonic complex. Despite the locally significant metamorphic overprint, the prefix ‘meta’ is not utilized in this report, and the rocks are described and classified throughout in terms of known or inferred protolith. Primary structures and textures are generally well preserved outside of the major high-strain corridors.

Volcanic rock types in the study area are further classified on the basis of bulk chemistry, utilizing SiO₂ content (recalculated to 100% volatile free), as follows: basalt (46–53 wt. %), basaltic andesite (53–57 wt. %), andesite (57–63 wt. %), dacite (63–69 wt. %), rhyolite (69–75 wt. %) and high-SiO₂ rhyolite (>75 wt. %). The MgO content, recalculated to 100% volatile free, is utilized to classify mafic and ultramafic volcanic rocks as follows: basalt (<12 wt. %), komatiitic basalt (12–18 wt. %) and komatiite (>18 wt. %). Magmatic rock types are also classified according to chemical affinity or series (i.e., calcalkalic, transitional calcalkalic–tholeiitic or tholeiitic) using Zr/Y and Th/Yb ratios and the methodology of Ross and Bédard (2009).

Clastic rock types in the study area are classified into two end members: volcanoclastic and epiclastic (Table 2). The term ‘volcanoclastic’ is used in a descriptive sense to denote rocks that are exclusively composed of texturally immature volcanic-rock fragments, and are therefore inferred to be products of volcanic eruptions. However, no specific fragmentation process, transport mechanism or depositional site is implied. These rocks are described using the standard granulometric terms of Fisher (1966), specifically breccia, tuff breccia, lapilli tuff, lapillistone and tuff, but in the nongenetic sense advocated by Gibson et al. (1999); that is, the terms are not strictly applied to lithified primary pyroclastic deposits (e.g., Fisher, 1966; Cas and Wright, 1987). Rocks that are interpreted to be of primary volcanoclastic origin (i.e., pyroclastic, autoclastic, hyaloclastic or peperitic; White and Houghton, 2006) are described using the appropriate

genetic modifier (e.g., pyroclastic breccia), whereas rocks interpreted to be resedimented syneruptive equivalents (see McPhie et al., 1993) are denoted with ‘reworked’ as a genetic modifier (e.g., reworked pyroclastic breccia). Epiclastic rocks exhibit textural evidence of deposition by ‘normal’ sedimentary processes and are described using the standard granulometric terms for sedimentary particles (Wentworth, 1922). These rocks are subdivided into two end members depending on the provenance of the constituent clasts (Table 1). Those composed exclusively of volcanic-rock clasts are referred to as ‘volcanic’ conglomerate, sandstone or mudstone, whereas those of mixed provenance are referred to by the same terms but without the ‘volcanic’ modifier.

Garner assemblage

As originally defined by Poulsen et al. (1996), the Garner assemblage consists of a north-younging succession of supracrustal and intrusive rocks that extends north and south of Garner Lake along the eastern margin of the Rice Lake belt (Figure 3). Weber (1971a, b) included these rocks in the Gem Lake subgroup and Edmunds Lake formation of the Rice Lake group. However, most were subsequently shown to be part of a geologically distinct and significantly older succession (Brommecker et al., 1993; Poulsen et al., 1993, 1994) that was referred to as the Garner Lake subgroup by Corkery (1995). Poulsen et al. (1996) defined the Garner assemblage to include 1) a lower succession of sedimentary and/or volcanic rocks; 2) the Garner Lake layered ultramafic intrusion; and 3) an upper succession of gabbro, felsic volcanoclastic rocks, iron formation, and intercalated komatiitic and basaltic flows. At Garner Lake, this assemblage has a maximum strike length of approximately 5 km and a stratigraphic thickness of at least 8 km, and is bounded to the west by the BLSZ. To the east, the assemblage is intruded by granitoid rocks of the Wanipigow River plutonic complex.

The lower succession of the Garner assemblage is defined herein to consist of intermediate–felsic volcanoclastic and epiclastic rocks, which are intruded by peridotite, pyroxenite and gabbro of the Garner Lake intrusive complex (GLIC; Figure 4).

Table 2: Nomenclature for clastic rocks (after Fisher, 1966; Cas and Wright, 1987; McPhie et al., 1993; Gibson et al., 1999; White and Houghton, 2006).

Volcanoclastic ¹					Epiclastic	
Nongenetic	Primary ²				Volcanic provenance ³	Mixed provenance ⁴
	Pyroclastic	Autoclastic	Hyaloclastic	Peperitic		
Breccia, tuff breccia	Pyroclastic breccia, tuff breccia	Autoclastic breccia, tuff breccia	Hyaloclastic breccia, tuff breccia	Peperitic breccia, tuff breccia	Volcanic boulder or cobble conglomerate	Boulder or cobble conglomerate
Lapillistone	Pyroclastic lapillistone	Autoclastic lapillistone	Hyaloclastic lapillistone	Peperitic lapillistone	Volcanic pebble conglomerate	Pebble conglomerate
Lapilli tuff	Pyroclastic lapilli tuff	Autoclastic lapilli tuff	Hyaloclastic lapilli tuff	Peperitic lapilli tuff	Volcanic pebbly sandstone	Pebbly sandstone
Tuff	Pyroclastic tuff	Autoclastic tuff	Hyaloclastic tuff	Peperitic tuff	Volcanic sandstone or mudstone	Sandstone or mudstone

¹ Composed of texturally immature volcanic-rock clasts; no evidence of significant reworking
² Composed of primary volcanic clasts; transport and final deposition by volcanic or syneruptive processes
³ Composed of volcanic-rock clasts; transport and final deposition by sedimentary processes
⁴ Polymictic; transport and final deposition by sedimentary processes

These data indicate a minimum age of 2871 Ma for the volcaniclastic hostrocks of the GLIC.

In the western narrows of Garner Lake, the base of the upper succession of the Garner assemblage is defined by a thin unit of arkosic sandstone and pebble conglomerate that lies in sharp depositional contact with differentiated rocks at the north margin of the GLIC. Davis (1994) reported a U-Pb age of 2871 ± 2 Ma from four analyses of single zircons from the arkosic sandstone, which is identical to the interpreted emplacement age of the GLIC and thereby indicates the presence of an erosional unconformity within the Garner assemblage. To the north, the arkosic sandstone is overlain by intermediate-felsic volcaniclastic rocks, iron formation and a thick pile of subaqueous flows that range in composition from komatiite to calcalkalic basaltic andesite (Brommecker et al., 1993). Although a comagmatic relationship between the komatiitic flows and underlying GLIC was inferred initially by Brommecker et al. (1993), the field relationships and U-Pb zircon ages described herein appear to preclude this possibility (see also Poulsen et al., 1994). Hollings et al. (1999) attributed the komatiitic flows to plume-related magmatism within a volcanic-arc formed on, or marginal to, the NCT.

Description of rock units

Intermediate-felsic volcaniclastic rocks (unit Gn1)

Volcaniclastic rocks of unit Gn1 are exposed in widely scattered outcrops south of Garner Lake, at the southern extent of the generally north-younging stratigraphic succession that constitutes the Garner assemblage (Figure 3). Although field relationships are ambiguous and reliable younging criteria are absent, unit Gn1 is thought to define the stratigraphic base of the assemblage, in keeping with the original definition of Poulsen et al. (1996); however, the external contacts of this unit mostly coincide with high-strain zones. To the west, amphibolite-facies volcaniclastic rocks of unit Gn1 are juxtaposed across the BLSZ with greenschist-facies rocks of the Gem assemblage. The Wanipigow River plutonic complex intrudes unit Gn1 from the east and this contact is overprinted by the East Garner shear zone. To the north, the contact with unit Gn2 is overprinted by the South Garner shear zone, which is marked by a 5–10 m thick zone of mylonite and ultramylonite. The constituent rock types of this unit are strongly deformed and recrystallized, with most containing a penetrative shape-fabric defined by deformed clasts or aligned hornblende porphyroblasts.

Heterolithic to monolithic breccia and tuff breccia of subunit Gn1a dominate in the western portion of the unit and appear to be at least 800 m thick. These rocks typically weather buff to light grey and are poorly sorted, matrix to clast supported and crudely stratified. Where less deformed, the clasts are typically angular to subangular and equant, and range up to 50 cm across. The dominant clast type is a light grey to green, aphanitic to fine-grained dacite that contains variable proportions of plagioclase and/or hornblende phenocrysts. Rare exposures of monolithic breccia and tuff breccia that show jigsaw-fit textures and consist almost exclusively of angular blocks of porphyritic dacite are suggestive of primary autoclastic deposits

(Figure 5a). Heterolithic variants contain abundant clasts of aphanitic dacite, coarsely plagioclase-phyric andesite, aphyric basalt and quartz-phyric rhyolite, and were most likely deposited as debris flows. The apparent absence of interstratified mudstone suggests a subaerial to shallow marine depositional site, or very rapid accumulation of the volcaniclastic pile. The northeast portion of unit Gn1 includes very thick (>100 m) homogeneous intervals of buff to light grey, crystal-lithic tuff (Figure 5b), which has a rhyolitic bulk composition (subunit Gn1b). These rocks contain up to 5% angular crystals of plagioclase, quartz and hornblende (0.5–5 mm) in a recrystallized groundmass of fine- to medium-grained plagioclase, quartz and biotite, with accessory garnet, white mica and apatite. They locally also contain angular lithic clasts (1–2%; <1 cm), which vary from equant to elongate and wispy. The clasts are scattered throughout the rock or, very rarely, are concentrated into diffuse layers up to 10 cm thick. Crystal-lithic tuff also forms diffuse 1–2 m thick beds in association with the breccia and tuff breccia of subunit Gn1a. The massive character, fragmental texture and felsic composition of subunit Gn1b are suggestive of rhyolitic ignimbrites (i.e., pyroclastic-flow deposits); however, no evidence was found to firmly establish a primary pyroclastic origin.

Epiclastic rocks (unit Gn2)

Unit Gn2 is exposed along the south and west shorelines of the main basin of Garner Lake and consists of interstratified pebble to cobble volcanic conglomerate, feldspathic greywacke and mudstone. Most of these rocks are very strongly recrystallized and deformed, likely as a consequence of contact metamorphism and subsequent strain partitioning along the south contact of the GLIC. The conglomerate (subunit Gn2a) is polymictic, poorly sorted and matrix supported, and dominates in the eastern portion of this unit, where it is locally up to 500 m thick. The conglomerate is nonstratified in most locations. Angular to well-rounded clasts of mafic, intermediate and felsic volcanic rocks range up to 50 cm across and are supported in a pebbly mudstone matrix (Figure 5c). Well-rounded boulder-sized clasts indicate significant subaerial transport of detritus prior to final deposition in a marine setting, likely via debris flows. Subunit Gn2b consists of thinly interbedded feldspathic greywacke and mudstone, and ranges from 300 to 400 m thick in the western portion of this unit. The greywacke is buff to light grey and very fine to medium grained, and forms planar beds from 1 to 3 cm thick (Figure 5d). Medium-grained greywacke contains 25–30% rounded to angular plagioclase grains up to 3 mm across, with less than 10% detrital quartz. In thin section, these rocks consist of recrystallized quartz and feldspar, with subordinate biotite, muscovite, garnet and opaque minerals. Minor interbeds of dark grey or brown mudstone range up to 2 cm thick, but most are less than 1 cm. The greywacke beds are massive to normally graded, with scoured bases and locally well-developed load structures, indicating deposition from turbidity currents in a subaqueous fan setting. One outcrop contains several fining and thinning upward cycles from 3 to 5 m thick, perhaps representing channel-fill deposits in a suprafan lobe. Unit Gn2 records erosional denudation of a nearby

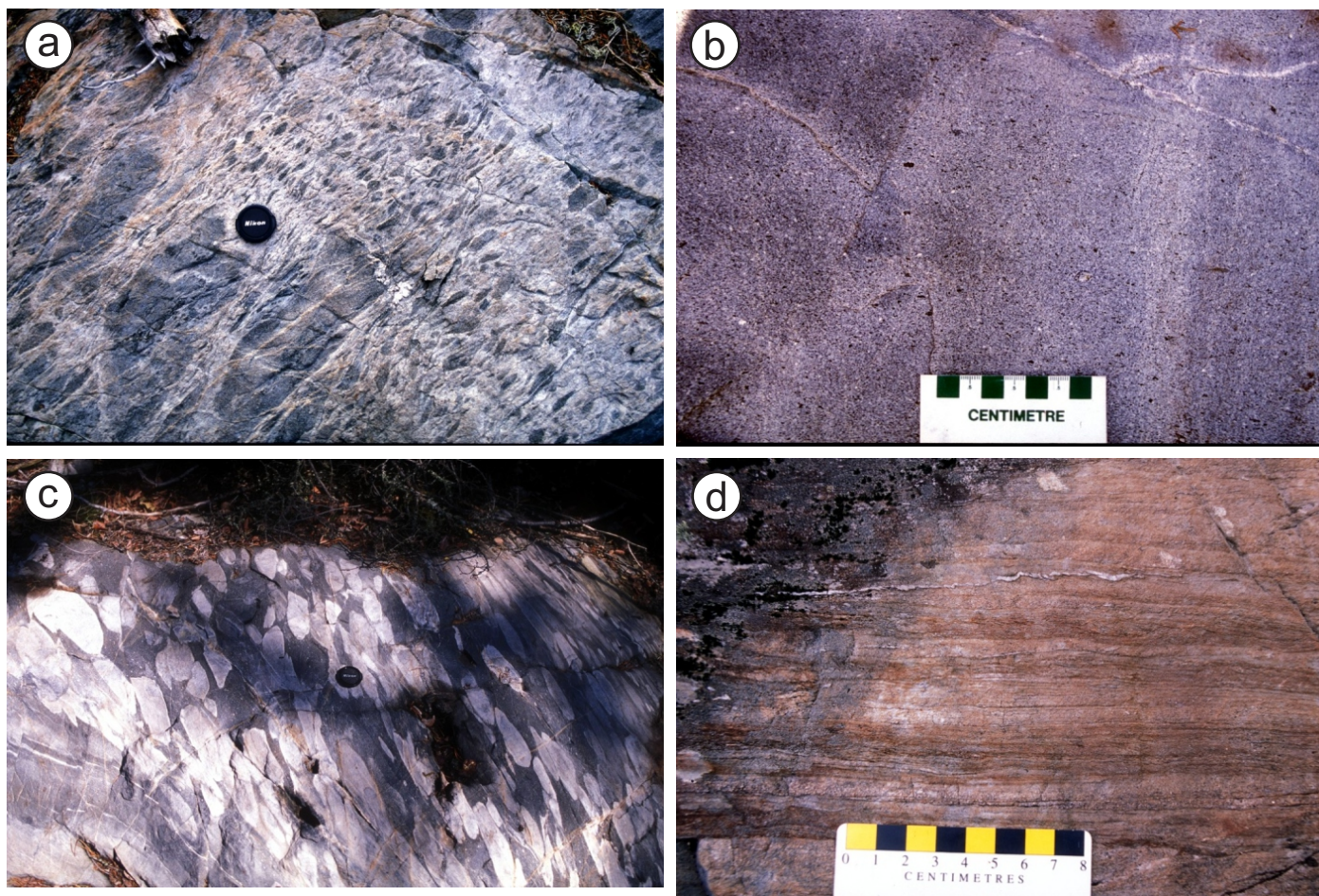


Figure 5: Outcrop photographs of rocks in units Gn1 and Gn2: **a)** monolithic dacite breccia (subunit Gn1a; note jigsaw-fit texture of clasts in lower left of photo), south of Garner Lake; **b)** massive crystal-lithic tuff (subunit Gn1b), south of Garner Lake; **c)** crudely stratified volcanic conglomerate (subunit Gn2a) with minor interlayers of thin-bedded volcanic sandstone (lower left), southeast of Garner Lake; **d)** thin-bedded volcanic greywacke and mudstone (subunit Gn2b), western shoreline of Garner Lake.

intermediate–felsic volcanic edifice, possibly during a relatively quiescent phase of the volcanic arc.

Intermediate–felsic volcanoclastic rocks (unit Gn3)

Intermediate–felsic volcanoclastic rocks of unit Gn3 crop out along the north, west and southeast margins of the GLIC, and are best exposed in shoreline outcrops in the northwest portion of the main basin of Garner Lake. These rocks are intruded by dikes of pyroxenite and melagabbro that are inferred to be related to the GLIC. Adjacent to the contacts, the volcanoclastic rocks consist of strongly recrystallized biotite schist, characterized by medium-grained foliated biotite and granoblastic feldspar and quartz. Along the northern contact, they locally contain concentrically zoned spots of epidote, quartz, feldspar and amphibole (Figure 6a) and large porphyroblasts of inclusion-poor garnet (\pm staurolite \pm cordierite; Weber, 1971a) that are unique to this locality and are interpreted to represent a contact metamorphic effect related to emplacement of the GLIC. Despite the intense recrystallization, mesoscopic primary textures are generally well preserved in these outcrops. The original stratigraphic thickness of unit Gn3 has been considerably inflated by younger intrusions, but is estimated to be approximately 1200 m.

Monolithic breccia and tuff breccia are the dominant rock types, and are interstratified with minor lapilli tuff and possible coherent flows. Whole-rock geochemical data indicate that the southeastern portion of this unit is mostly of andesitic bulk composition (subunit Gn3a), whereas the northern and western portions are dacitic and rhyolitic (subunit Gn3b). Despite these differences, the field characteristics are quite uniform and the rocks characteristically weather light grey and are dark grey on fresh surfaces. Most specimens contain sparse ($<10\%$) plagioclase and/or ferromagnesian (hornblende \pm pyroxene) phenocrysts in a recrystallized groundmass of plagioclase, quartz and biotite (\pm muscovite \pm chlorite), with accessory epidote-clinzoisite, pyrite, rutile, apatite and zircon. Secondary biotite, chlorite, actinolite and epidote form pseudomorphs after the ferromagnesian phenocrysts. Breccia, tuff breccia and lapilli tuff of unit Gn3 are monolithic, poorly sorted and clast supported. Variations in the size and proportion of clasts define a crude stratification in some locations, but these rocks are mostly unstratified. The clasts range up to 25 cm in maximum dimension and are typically very angular, equant and blocky (Figure 6b). Many clasts have curvilinear or cusped margins, indicating that they may have been generated by autoclastic or hyaloclastic fragmentation of coherent lava flows or domes.

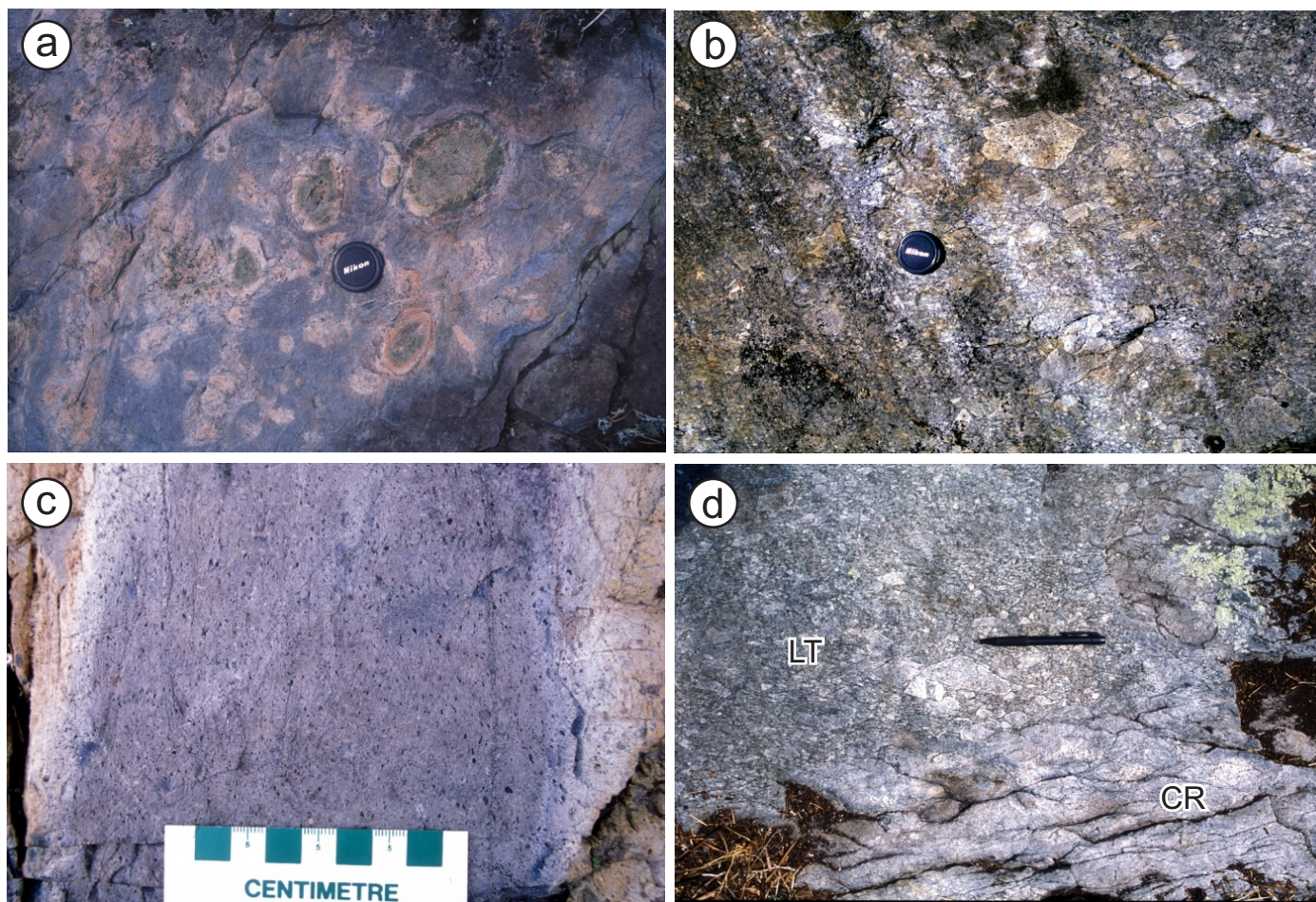


Figure 6: Outcrop photographs of rocks of subunit Gn3b from the northwest shoreline of Garner Lake: **a)** concentric spots composed of feldspar, epidote, quartz and actinolite in rhyolitic volcaniclastic rocks at the north margin of the Garner Lake intrusive complex; **b)** rhyolitic tuff breccia; note polygonal, partially joint-bounded rhyolite clast to the upper right of the lens cap; **c)** coherent rhyolite with sparse feldspar and ferromagnesian phenocrysts; **d)** irregular brecciated contact between coherent rhyolite (CR) and rhyolitic lapilli tuff (LT).

Rare examples of polygonal rhyolite clasts indicate derivation from columnar-jointed flows, domes or high-level sills. Small bodies of aphyric to sparsely porphyritic dacite and rhyolite with irregular brecciated contacts are locally exposed on the north shore of Garner Lake (Figure 6c, d) and are interpreted to represent coherent flow lobes. These rocks were most likely deposited on the proximal flank of an effusive, intermediate–felsic volcanic edifice.

Garner Lake intrusive complex (unit Gn4)

The Garner Lake intrusive complex (GLIC) crops out as islands and in small shoreline exposures in the main basin and western narrows of Garner Lake. Crosscutting relationships indicate an intrusive relationship between the GLIC and adjacent intermediate–felsic volcaniclastic rocks of unit Gn3. Given that layered ultramafic and gabbroic complexes tend to characterize the roots of volcanic arcs (Hamilton, 1988), it is likely that the volcanic arc (as represented by the lower succession of the Garner assemblage) had achieved a substantial crustal thickness prior to emplacement of the GLIC. As described in detail below, the erosional unconformity that defines the upper

contact of the GLIC in western Garner Lake requires a major episode of uplift and erosional denudation subsequent to its emplacement.

Although Scoates (1971) inferred a late-tectonic relative age for the GLIC, deformation structures and overprinting relationships indicate that it was emplaced prior to most, if not all, ductile deformation recorded in the country rocks. Macroscopic igneous layering in the GLIC trends generally west-southwest and is overprinted by northwest- and northeast-trending open folds that mimic the geometry of folds observed in the country rocks. To the east, the intrusive contact with younger granitoid rocks of the Wanipigow River plutonic complex (WRPC) is strongly overprinted by the East Garner shear zone. Bodies of serpentinized peridotite and pyroxenite within the WRPC on the west side of the northeast arm of Garner Lake are interpreted to represent large rafts or fault-bounded slices of the GLIC. The South Garner shear zone cuts progressively upsection from southeast to northwest along the western limit of the GLIC, such that the total exposed width decreases from 2 km in the east to approximately 400 m in the west.

Island exposures of the GLIC were mapped and described in detail by Scoates (1971) and consequently received only

cursory examination during the present study. As described by Scoates (1971), the thickest and most continuous portion of the GLIC underlies most of the main basin of Garner Lake and consists of alternating layers of serpentinized peridotite and pyroxenite that range from 100 to 400 m thick. The serpentinized peridotite (subunit Gn4a) weathers orange-brown and is typically massive and homogeneous, except for irregular veinlets of fibrous serpentine. Most rocks contain 5–10% disseminated magnetite and are consequently moderately to strongly magnetic. Scoates (1971) described evidence of gradational contacts with adjacent layers of dark green, fine- to medium-grained clinopyroxenite (subunit Gn4b), which contains less than 10% plagioclase as very fine laths. This rock type is only weakly magnetic and is thus clearly distinguished from serpentinized peridotite in areas of nonexposure using high-resolution aeromagnetic data. In conjunction with the mapping of Scoates (1971), these data indicate the presence of five major peridotite layers in the main body of the GLIC, which alternate with four pyroxenite layers (Figures 3, 4) and appear to be less continuous and of less uniform thickness than shown on previous maps (e.g., Scoates, 1971; Weber, 1971a).

The northernmost pyroxenite layer is exposed on the north shore of the main basin and south shore of the narrows in Garner Lake, and contains significant volumes of melagabbro, leucogabbro and hornblende tonalite. The melagabbro (subunit Gn4c) is dark green-grey and fine to medium grained, containing 10–50% plagioclase, whereas the leucogabbro (subunit Gn4d) is light green to grey and medium to coarse grained, containing 50–75% plagioclase, typically with 1–5% quartz and magnetite. Primary ferromagnesian minerals are completely replaced by actinolite, chlorite and carbonate. Both rock types locally include patches or irregular dikes (<2 m) of medium-grained to pegmatitic tonalite (Figure 7a, b), which typically contains 20–25% hornblende, 10–20% blue quartz, 5–10% K-feldspar and up to 10% magnetite in a groundmass of coarse-grained plagioclase. Irregular shapes and generally diffuse contacts indicate that these bodies formed as a result of late-stage segregation during in situ differentiation of the gabbro. One outcrop on the north shore of Garner Lake shows a fairly continuous northwestward progression (over 40–50 m) from pyroxenite to melagabbro to leucogabbro, all of which contain irregular patches of hornblende tonalite, suggesting that the roof of the complex lies along the north margin, as inferred by Scoates (1971). An irregular patch of pegmatitic hornblende tonalite hosted by melagabbro at the top of the GLIC on the south shore of the narrows was collected for U-Pb geochronological analysis and yielded an approximate emplacement age 2870 ± 0.5 Ma (sample 96-02-1067/CB02-03; see ‘U-Pb geochronology’ section).

Volcaniclastic and epiclastic rocks (unit Gn5)

Unit Gn5 is exposed on both shores of the narrows in the northwest portion of Garner Lake and consists of arkosic sandstone and pebble conglomerate; intermediate-felsic volcaniclastic rocks with minor chert, carbonate and ferruginous mudstone; and iron formation. Here, this unit unconformably overlies pyroxenite and gabbro of unit Gn4 to the south, and is overlain to the north by komatiitic flows of unit Gn6. The

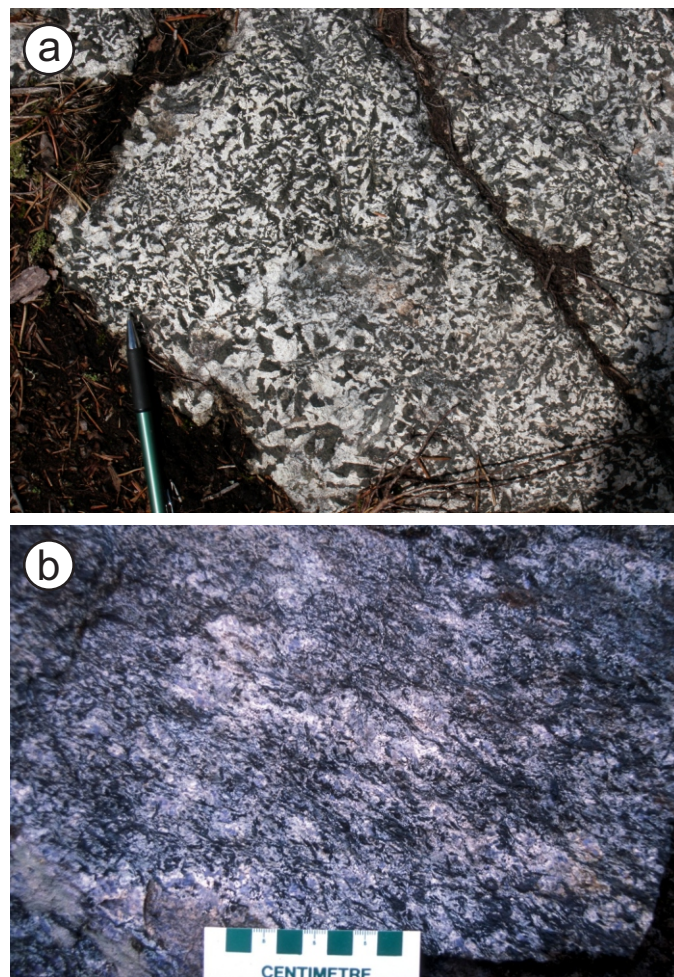


Figure 7: Outcrop photographs of tonalitic segregations near the north margin of the Garner Lake intrusive complex: **a)** pegmatitic hornblende tonalite in pyroxenite, eastern Garner Lake; **b)** blue-quartz-bearing, hornblende-biotite tonalite in melagabbro, south shoreline of the narrows in Garner Lake.

maximum stratigraphic thickness is approximately 600 m near the western extent of this unit at the BLSZ. Toward the south-east, unit Gn5 is traced in outcrop for approximately 2 km along strike to the east end of the narrows, where it is tightly folded and offset by a north-trending fault. The stratigraphic thickness of the unit at this locality is less than 20 m. East of this fault, it was identified in a single outcrop at the interface between units Gn3 and Gn6 north of the main basin of Garner Lake, and is therefore delineated mostly on the basis of aeromagnetic data. The distinct thinning of this unit toward to east may be indicative of significant topographic relief on the unconformity, or is perhaps due to later structural attenuation. Unit Gn5 is analogous in many respects to the ‘sedimentary interface zones’ described by Thurston et al. (2008) in the Abitibi greenstone belt, which likewise contain chemical and coarse-clastic sedimentary rocks and mark significant depositional gaps or geochemical transitions between major stratigraphic units. It is also comparable to platform-rift sequences documented in other Archean cratons (e.g., Thurston and Chivers, 1990; Hunter et al., 1998; Bleeker et al., 1999; Thurston and Kozhevnikov, 2000; Hartlaub et al., 2004; Percival et al., 2006a; Sasseville et al., 2006).

The base of unit Gn5 is marked by a crudely stratified unit of arkosic sandstone and tonalite-pebble conglomerate (subunit Gn5a) that is traced along strike for a distance of 1.2 km along the south shore of the narrows, and ranges from approximately 150 m thick in the west to 7 m thick in the east. This subunit is also exposed on the north shore of the narrows, near the eastern end, where it is 2–3 m thick. The basal contact with pyroxenite, gabbro and pegmatitic hornblende tonalite of the GLIC is either sharp or gradational over 1–3 m, whereas the upper contact with overlying volcanoclastic rocks of subunit Gn5b is sharp (Figure 8a). The arkosic sandstone weathers light pinkish-grey to medium grey or green and is medium to coarse grained, with scattered pebbles of blue quartz, feldspar and tonalite (Figure 8b); Davis (1994) referred to this rock type as ‘quartz-rich grit’. Most specimens contain angular to subrounded grains of blue quartz (2–25%) and up to 15% fine-grained magnetite. In thin section, this rock consists of angular to rounded grains of quartz and minor plagioclase in a fine-grained matrix of quartz, feldspar, chlorite, sericite, carbonate and magnetite, with accessory epidote-clinozoisite, apatite and tourmaline. Diffuse pebble lags, faint laminae of chloritic mudstone and subtle variations in the proportion of quartz grains and matrix define planar beds in some outcrops. These beds have scoured, normally graded bases and massive tops. Trough crossbedding is present in one

location within a 70 cm thick bed of quartz-rich arkose at the contact with underlying pyroxenite of the GLIC (Figure 8c).

Interbeds of matrix- or clast-supported pebble conglomerate range up to 2 m thick and generally have diffuse contacts. These beds vary from massive to normally or reversely graded and contain poorly sorted, subangular to subrounded clasts of tonalite up to 12 cm across in a matrix of fine- to medium-grained chloritic sandstone (Figure 8d). These features indicate that subunit Gn5a was likely deposited in a fluvial-alluvial setting, in proximity to a source of tonalitic detritus. Detrital zircon geochronology by Davis (1994) indicates that the tonalite was likely similar to the late-stage segregations in the underlying GLIC. In particular, detrital zircons in the arkose yielded an age (2871 ± 2 Ma) that is identical to the age of igneous zircons in the GLIC (2871 ± 1 Ma), and have similar Th/U ratios (Davis, 1994). Coupled with the field relationships, these data establish the presence of a significant erosional unconformity at the base of unit Gn5.

Subunit Gn5a is overlain by 200–300 m of andesitic volcanoclastic rocks, with minor interlayers of thinly interbedded chert, carbonate and ferruginous argillite (subunit Gn5b). The andesitic rocks weather pale green or grey and are dark green on fresh surfaces. The dominant rock type is a monolithic

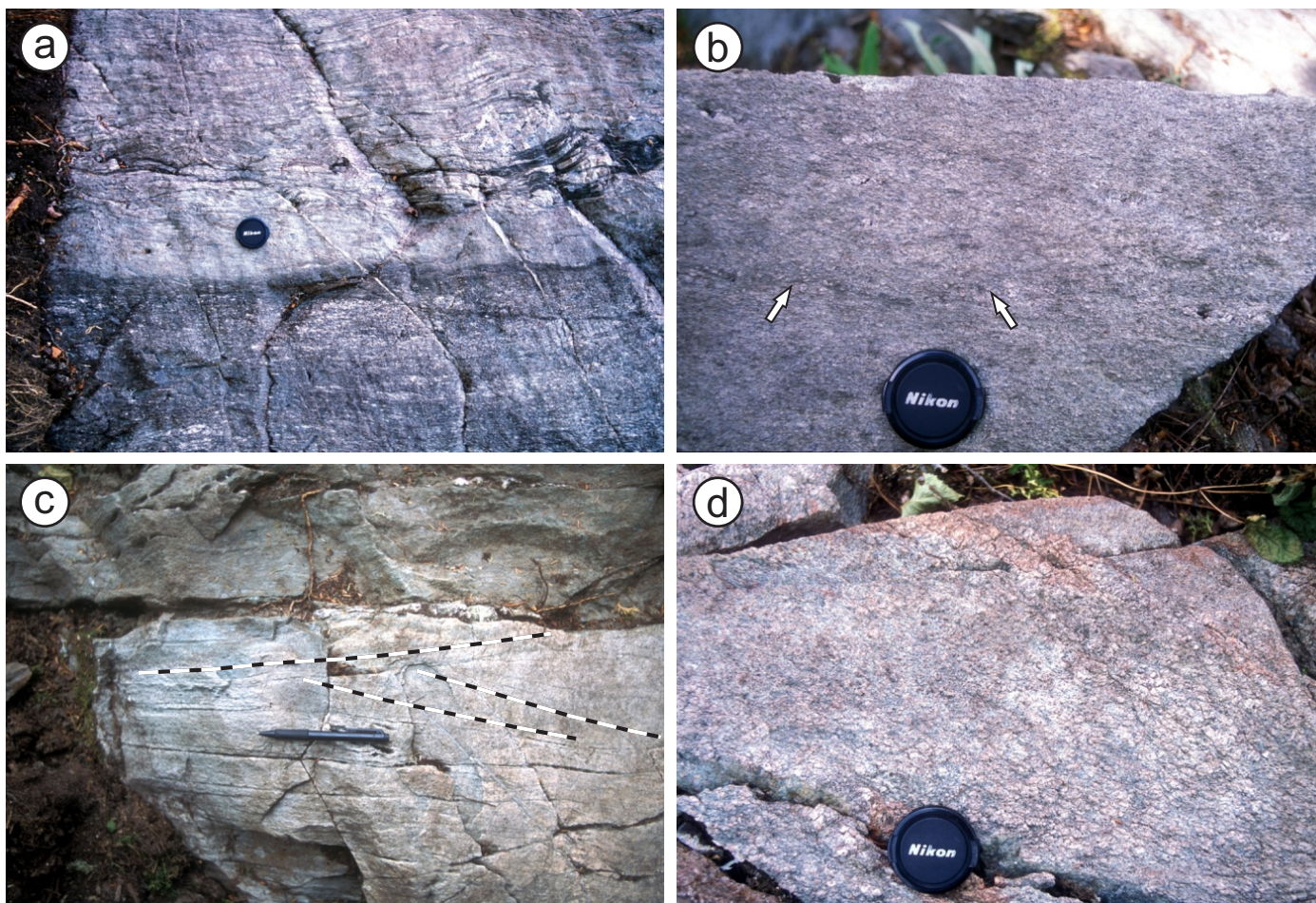


Figure 8: Outcrop photographs of rocks of subunit Gn5a from the narrows in Garner Lake: **a)** sharp depositional contact between arkosic sandstone (bottom) and overlying andesitic volcanoclastic rocks of subunit Gn5b (top), north shore of narrows near the eastern end; **b)** faintly stratified, pebbly arkosic sandstone (diffuse pebble lag indicated by arrows), south shore of narrows at the western end; **c)** crossbedded quartz-rich arkose near the base of subunit Gn5a (younging direction is toward the top of the photo; crossbeds indicated by dashed lines), south-central portion of the narrows; **d)** tonalite-pebble conglomerate, same location as Figure 8b.

tuff breccia that is poorly sorted, matrix to clast supported and massive to crudely stratified (Figure 9a). Angular to subangular (to rarely well-rounded) clasts of andesite range up to 20 cm in maximum dimension and contain up to 15% plagioclase phenocrysts (0.5–1.0 mm). The tuffaceous matrix consists of microgranular feldspar, quartz, chlorite, actinolite, epidote and opaque minerals, and contains slightly smaller and fewer phenocrysts. One outcrop near the base of this unit includes several distinct layers, from 10 to 20 cm thick, that contain a high proportion (~20%) of possible scoriaceous pyroclasts. These clasts are very angular or wispy (<10 cm) and consist of light green aphanitic andesite that contains abundant (50–60%) round quartz amygdulites from 0.5 to 1.0 mm in diameter. Farther upsection, the andesitic volcanoclastic rocks are interstratified with one or more 10–25 m thick horizons of thinly interbedded chert, carbonate and ferruginous mudstone (Figure 9b), which place the depositional site below wave base in a marine setting. The chert weathers light grey to white and forms laminated beds up to 30 cm thick. In thin section, the chert consists almost exclusively of fine-grained granoblastic quartz, with accessory hornblende, biotite, garnet and carbonate. The mudstone consists of thinly layered chlorite-biotite schist that contains coarse porphyroblasts of garnet and hornblende, and is strongly sulphidic in places, with disseminated to local fracture-controlled pyrite or layers of solid to semisolid pyrite up to 20 cm thick.

Subunit Gn5b is overlain, in turn, by 100–200 m of very homogeneous dacite (subunit Gn5c), which crops out in two locations in the northwest end of Garner Lake and appears to represent either a massive crystal tuff or a coherent flow. The dacite weathers buff to light grey, is dark grey on fresh surfaces and varies from aphanitic to very sparsely plagioclase phyric (2–5%; <2 mm), but is otherwise nondescript (Figure 9c). In thin section, this rock has a seriate-porphyrific texture defined by euhedral plagioclase laths in a microgranular groundmass of feldspar, quartz, sericite, chlorite and carbonate. A sample (96-02-1050/CB02-02) of this material was collected for U-Pb zircon geochronological analysis to constrain the age of felsic volcanism in the upper succession of the Garner assemblage. It yielded an approximate emplacement age of 2851 ± 1 Ma (see ‘U-Pb geochronology’ section).

To the north, the dacite is overlain by 40–80 m of banded iron formation (subunit Gn5d) that is delineated by detailed aeromagnetic data over a strike length of 3.5 km at the interface between units Gn5 and Gn6. This subunit consists of thin (1–10 cm), rhythmically alternating layers of magnetite and light grey chert (Figure 9d), indicating deposition below wave base in a quiescent marine basin prior to the major subaqueous effusions of komatiitic and basaltic lava that constitute the upper portion of the assemblage.

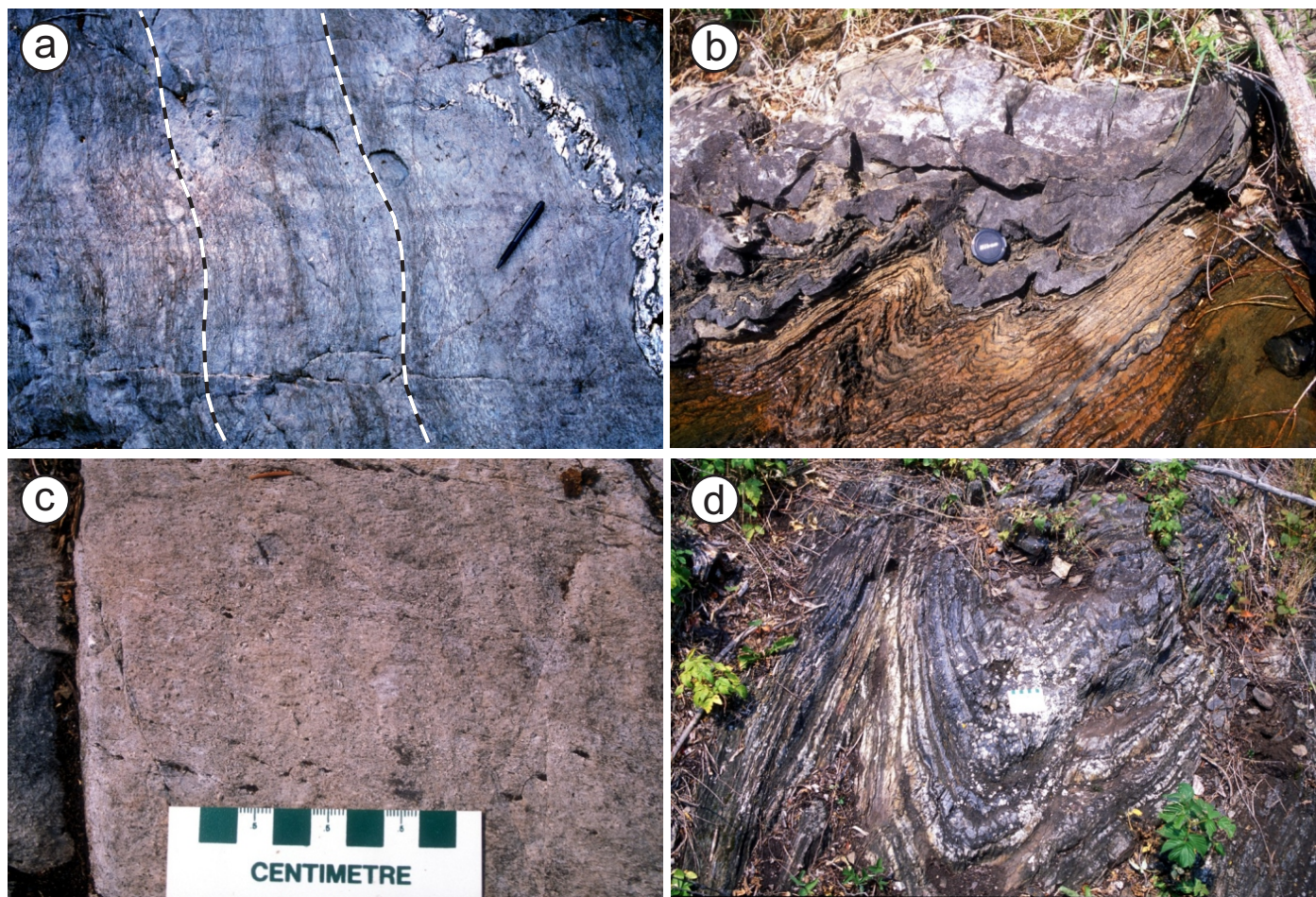


Figure 9: Outcrop photographs of rocks of unit Gn5 from the narrows in Garner Lake: **a)** stratified andesitic volcanoclastic rocks of subunit Gn5b (dashed lines indicate the trace of bedding; horizontal features in outcrop are glacial striations), north shore of narrows; **b)** thin-bedded chert (grey) and carbonate (brown) of subunit Gn5b, north shore of narrows; **c)** massive dacite of subunit Gn5c, island outcrop northwest of the narrows; **d)** thin-bedded magnetite-chert iron formation of subunit Gn5d, northwest corner of Garner Lake.

Komatiite and komatiitic basalt flows (unit Gn6)

Komatiite and komatiitic basalt of unit Gn6 have been identified on the basis of textural criteria and lithogeochemistry within a 600 m stratigraphic interval near the base of the very thick (>2.5 km) succession of subaqueous effusive rocks that define the top of the Garner assemblage. The komatiitic rocks concordantly overlie magnetite-chert iron formation of subunit Gn5d, and are traced along strike for approximately 4 km between the BLSZ and the East Garner shear zone. Brommecker et al. (1993) reported MgO contents of 21–25 wt. % (recalculated to 100% volatile free) from komatiite flows near the northwest extent of this unit, and described well-preserved examples of spinifex texture, polyhedral joints and breccia that confirm an extrusive origin. As described below, these characteristics are not typical outside of this ‘type’ locality.

The komatiitic rocks (subunit Gn6a) weather emerald green, dark green-grey or rusty brown, and are typically non-descript in outcrop. They form low-lying, lichen-covered outcrops that contain at least one moderate to strong foliation and variable Fe-Mg carbonate alteration, all of which significantly

obscure or destroy primary features. In thin section, they consist mostly of felty colourless tremolite, with subordinate clinozoisite, actinolite, chlorite and carbonate. The dominance of tremolite over actinolite distinguishes these rocks from the basaltic flows of unit Gn7. Spinifex texture was observed in three locations and consists of closely packed radiating clusters of tremolite (\pm actinolite), which represent pseudomorphic replacements after primary acicular pyroxene or olivine crystals up to 5 cm in length (Figure 10a, b). These textures occur in otherwise featureless rocks that are thought to represent massive flows; however, the outcrop is generally not suitable for determining flow organization. A high-Mg (~31 wt. % MgO) specimen of this rock contains cumulate olivine (Figure 10c), which likely accumulated at the base of a massive flow or subvolcanic sill. Pillowed flows identified in two locations are characterized by bun-shaped pillows up to 1.0 m across, with 1–3 cm thick selvages and up to 5% interpillow carbonate. Whole-rock geochemical analyses of the spinifex-textured and pillowed flows indicate that they are mostly komatiitic basalt (see also Poulsen et al., 1996; Hollings et al., 1999) rather than komatiite, with

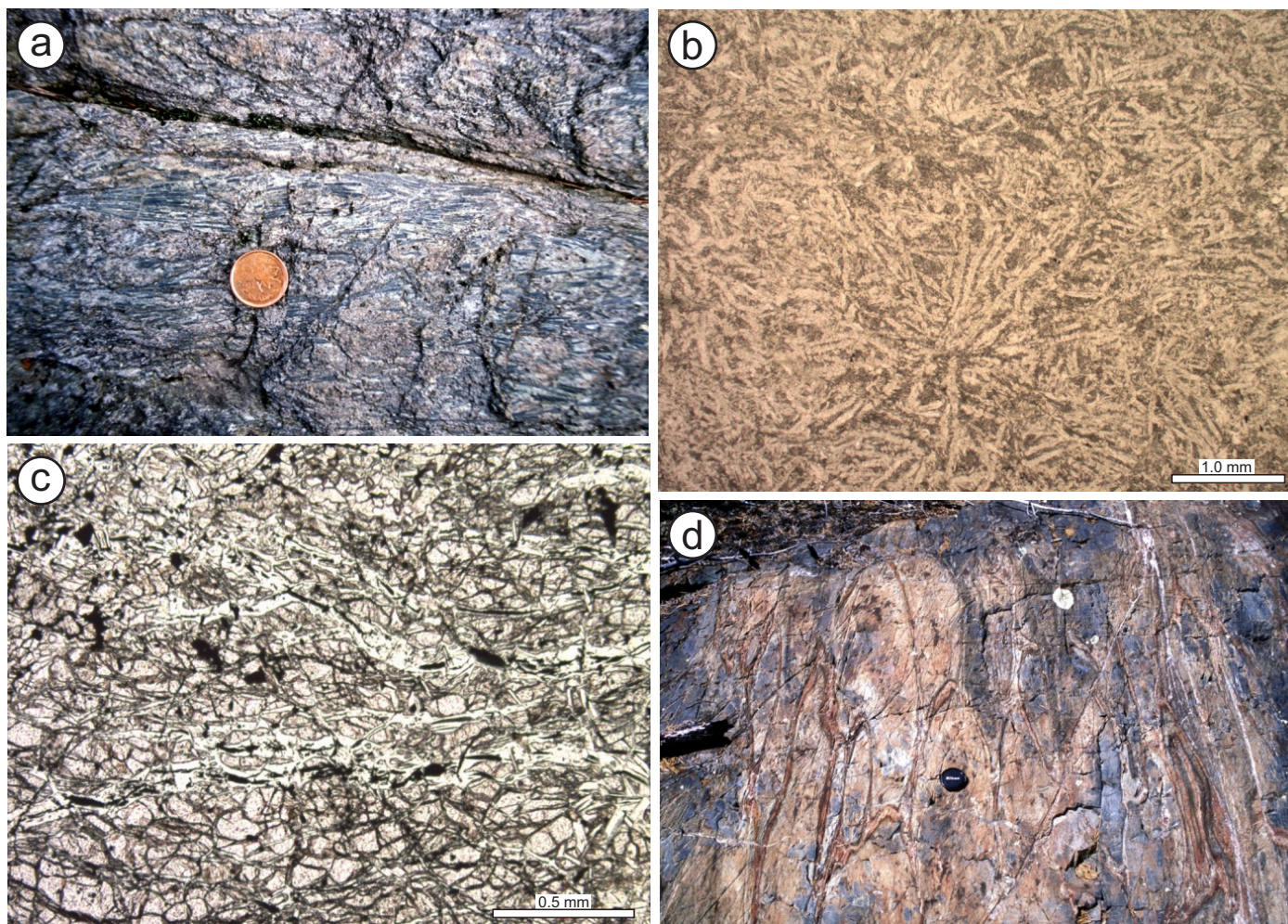


Figure 10: Outcrop and thin-section photographs of rocks from units Gn6 and Gn7 north of Garner Lake: **a)** spinifex texture in komatiitic basalt from the west-central portion of unit Gn6, defined by radiating aggregates of acicular pyroxene or olivine that are pseudomorphically replaced by tremolite-actinolite; **b)** photomicrograph of spinifex texture in komatiitic basalt, showing radiating clusters of fibrous tremolite after primary acicular pyroxene or olivine (plane-polarized light); **c)** cumulate-textured olivine and fracture-controlled serpentine and magnetite from a massive ultramafic flow or sill in the eastern portion of unit Gn6 (plane-polarized light); **d)** strongly flattened pillows in a tholeiitic basalt flow from the southeast portion of unit Gn7 (younging direction is toward the top of the photo; photo taken facing north).

MgO contents between 12 and 17 wt. % (recalculated to 100% volatile free) and strongly enriched Cr (871–2080 ppm) and Ni (151–919 ppm). Flow contacts are locally marked by magnetite-chert iron formations (subunit Gn6b) up to 1.5 m thick. In outcrop, these iron formations are discontinuous along strike, perhaps as a consequence of topographic relief on the depositional substrate, thermal erosion by overriding flows or post-depositional structural disruption.

Basalt, basaltic andesite and andesite flows (unit Gn7)

Basalt, basaltic andesite and andesite flows of map unit Gn7 crop out sporadically east of Beresford Lake, at the top of the upper succession of the Garner assemblage, and have a stratigraphic thickness of at least 2 km. Most of this unit consists of massive and pillowed flows of Fe- and Mg-tholeiitic basalt (subunit Gn7a), which are intercalated with subordinate flows of transitional tholeiitic–calcalkalic basaltic andesite and andesite. Near the base, tholeiitic basalt flows are locally intercalated with komatiitic flows of unit Gn6 (Brommecker et al., 1993; Hollings et al., 1999). The basalt weathers light grey or green or buff and is dark green on fresh surfaces. Most flows are aphyric and nonamygdaloidal, with a fine- to medium-grained, subophitic texture. Some contain sparse (2–3%) plagioclase phenocrysts up to 1.5 mm in length. In thin section, these rocks consist of fine-grained actinolite, plagioclase, epidote-clinozoisite, chlorite, carbonate, titanite and opaque minerals. In some, the relict subophitic texture is defined by pseudomorphic aggregates of epidote-clinozoisite after primary plagioclase laths. Pillowed flows appear to predominate over massive in most localities, and consist of strongly flattened, bun-shaped pillows ranging from 0.1 to 1.5 m in maximum dimension, with 0.5–5 cm thick aphanitic selvages (Figure 10d). Pillow cores commonly contain light grey to pink variolites up to 3 cm across, which are a characteristic feature of this unit. Epidote is also locally abundant in pillow cores, as well as in the interstices. Flow contacts are marked by discontinuous layers of brecciated basalt, thin (<10 cm) seams of interflow chert or thin (0.5–1.5 m) units of magnetite-chert iron formation (subunit Gn7b). Gabbro dikes and sills form a significant component of most outcrops and are described below.

Gabbro, diorite (unit Gn8)

Sill-like intrusions of gabbro and diorite are particularly abundant in the lower portions of map units Gn6 and Gn7, where they range up to 250 m thick, and are also a minor component of unit Gn5. Gabbro predominates over diorite and is chemically similar to the tholeiitic basalt flows of unit Gn7. The gabbro typically weathers light green-grey and is fine to medium grained, with an equigranular, subophitic to ophitic texture (subunit Gn8a). Plagioclase content varies widely (30–70%) and most specimens are nonmagnetic. Glomeroporphyritic gabbro (subunit Gn8b) has a distinctive spotted appearance, characterized by equant clots of actinolite and chlorite up to 10 mm across that likely represent pseudomorphic replacements after primary pyroxene glomerocrysts. Some specimens also contain sparse (2–3%) plagioclase phenocrysts up to 2.5 cm in maximum dimension. In contrast to the gabbroic portions of the GLIC, the gabbro of unit Gn8 tends to be very

homogeneous on the scale of individual outcrops and lacks pegmatitic segregations.

Bidou assemblage

The Bidou assemblage defines the map-scale Beresford Lake anticline in the core of the RLB and is intruded by synvolcanic tonalite and granodiorite plutons, of which the Ross River pluton is the most prominent example (Figure 2). East of the pluton, the Bidou assemblage is approximately 6–7 km thick and includes seven conformable and laterally extensive map units (Figure 11), which were formally defined as formations by Campbell (1971) based in part on the mapping of Stockwell and Lord (1939) and Stockwell (1945a). These seven units constitute the Bidou Lake subgroup of Weber (1971a, b) and have been interpreted to record an upward transition from back-arc to arc magmatism (Bailes et al., 2003; Bailes and Percival, 2005a). Voluminous sills of tholeiitic gabbro intrude all these units.

In the core of the anticline, the back-arc succession consists of laterally continuous units of massive and pillowed, mid-ocean-ridge- or back-arc basin-like (Bailes and Percival, 2005a) tholeiitic basalt flows (the Unnamed basalt and the Tinney Lake and Gunnar formations), which alternate with stratified units of turbiditic feldspathic greywacke and mudstone containing minor intercalations of laminated chert and heterolithic volcanic conglomerate (the Stovel Lake and Dove Lake formations). This succession is interpreted to have been deposited in a relatively quiescent marine basin, which received alternating influxes of effusive basalt and arc-derived detritus; the base is not exposed. Two samples were collected for U-Pb zircon geochronological analysis to constrain the age of this succession: 1) a lithic greywacke from the base of the Stovel Lake formation, just above the Unnamed basalt (sample 96-05-SLF), and; 2) a pegmatitic segregation in a thick gabbro sill near the upper contact of the Tinney Lake formation at the site of the past-producing Central Manitoba mine (sample 96-05-CMG). The greywacke sample yielded a maximum depositional age of ca. 2745 Ma, whereas the pegmatitic gabbro did not yield useful results (see ‘U-Pb geochronology’ section).

The overlying Stormy Lake formation marks the first appearance of quartz as a significant detrital component, and consists mainly of immature feldspathic greywacke and mudstone, with subordinate volcanic conglomerate, dacitic volcanoclastic rocks, iron formation and pillowed basalt. A discontinuous conglomerate at the base of the Stormy Lake formation contains boulders of tonalite, suggesting significant uplift and erosion in the source area (Campbell, 1971). The overlying arc succession, referred to as The Narrows formation, ranges up to 2.4 km in thickness and consists of coarse volcanoclastic rocks derived from calcalkalic porphyritic dacite. As suggested by Weber (1971a), these rocks were likely deposited as subaqueous debris flows in proximity to an active volcanic centre. Turek et al. (1989) reported a U-Pb zircon age of 2731 ± 3 Ma for The Narrows formation, which represents the minimum age for the Bidou assemblage as a whole, as well as overlapping ages of 2728 ± 8 and 2731 ± 13 Ma for porphyry dikes that intrude the back-arc succession. Turek and Weber (1991)

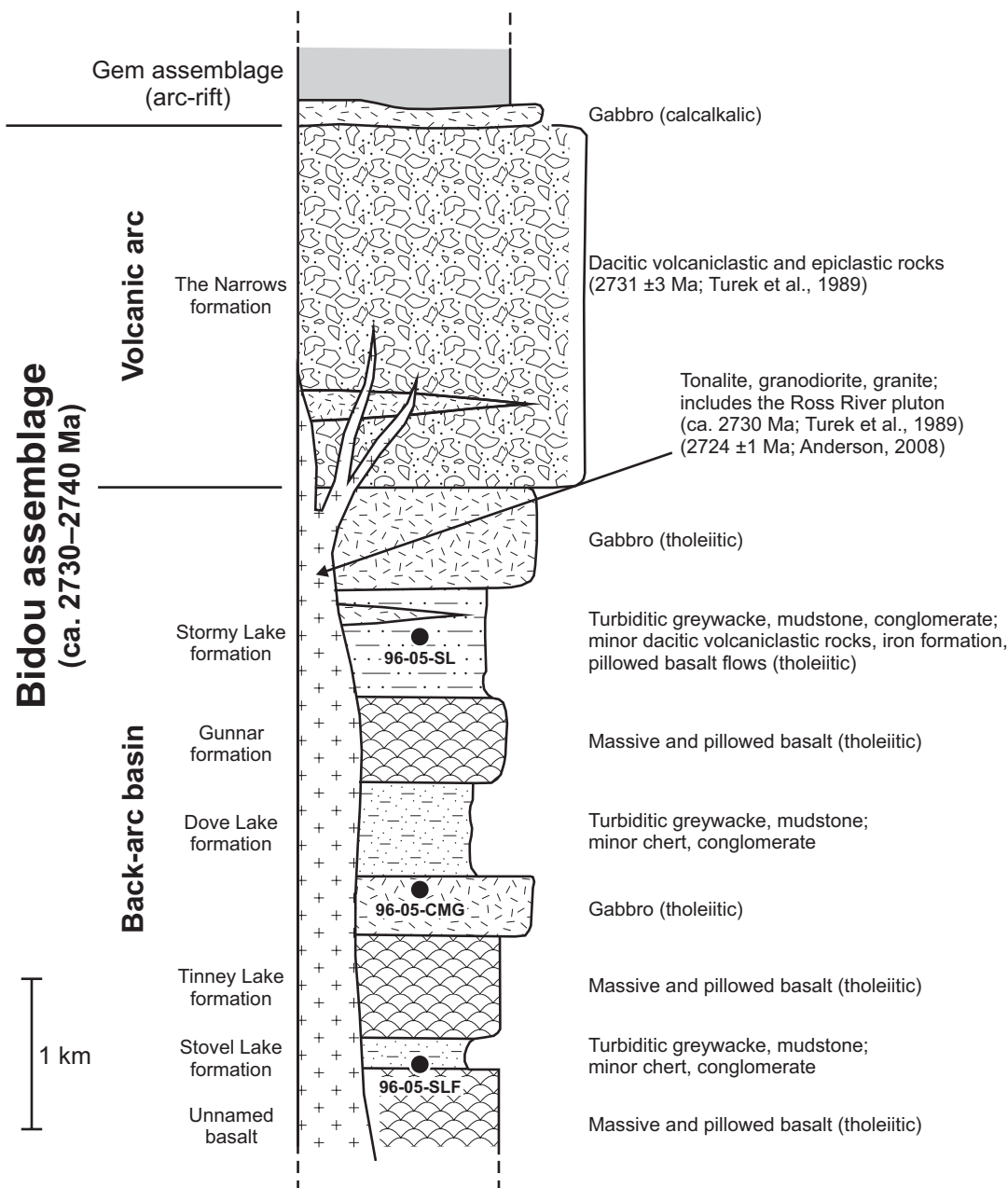


Figure 11: Schematic stratigraphic column for the Bidou assemblage (after Stockwell, 1945a; Campbell, 1971). Unit codes correspond to those in the text and on the accompanying Map GR2013-1-1. Black circles indicate the approximate stratigraphic location of the U-Pb geochronology samples.

reported an age of 2733 ± 6 Ma for a texturally similar porphyry dike that cuts The Narrows formation.

In the stratigraphic scheme of Campbell (1971), The Narrows formation was thought to be conformably overlain by greywacke-mudstone turbidite of the Edmunds Lake formation. Subsequently, however, Owens and Seneshen (1985) described a distinctive association of felsic volcanoclastic turbidite, mafic pyroclastic rocks, amygdaloidal mafic flows and hypabyssal gabbro sills at this contact (see also Seneshen and Owens, 1985; Seneshen, 1986), which they assigned to the 'Manigotagan River formation' of the Bidou Lake subgroup. Although not cited by these authors, this distinctive unit is also indicated on the maps of Wright (1932), Stockwell (1945b) and Weber (1971b). Crossbedded sandstone in pillow interstices suggests

a shallow-subaqueous depositional setting (Seneshen and Owens, 1985) during a transition from arc volcanism (upper Bidou assemblage) to basinal marine sedimentation (Edmunds assemblage). On the basis of new lithogeochemical and geochronological data (this report), these rocks are included in the Gem assemblage, a correlation also suggested by Seneshen (1990) and Poulsen et al. (1996). Hence, The Narrows formation is considered herein to define the top of the Bidou assemblage (Figure 11).

Description of rock units

Only the upper three formations of the Bidou assemblage (Gunnar, Stormy Lake and The Narrows) are exposed in the

study area (Figure 3). Of these, only The Narrows formation was examined in any detail by the author. For the sake of completeness, however, brief descriptions of each of these units are provided below. Details regarding the nature and distribution of these units on a regional scale were provided by Stockwell and Lord (1939) and Campbell (1971).

Basalt flows (unit Bd1; Gunnar formation)

Tholeiitic basalt flows of the Gunnar formation (unit Bd1) received only cursory examination during this study, but crop out extensively in the hinge of the Beresford Lake anticline at the northern limit of the map area. Campbell (1971) estimated the thickness of this formation at between 300 and 600 m. In the vicinity of the Gunnar mine, the basalt weathers light green to buff and is dark green on fresh surfaces, with a fine- to medium-grained subophitic texture and sparse plagioclase phenocrysts (≤ 2 mm). Pillowed flows predominate and consist of bun-shaped pillows up to 1.5 m across with only minor ($< 5\%$) interpillow material. The pillows have thin (< 2 cm) selvages and contain sparse quartz (\pm epidote \pm calcite) amygdules that vary from round to tubular and are concentrated along the upper margins (Figure 12a). Stockwell and Lord (1939) described gradational contacts with subordinate flows of massive and brecciated basalt, as well as thin horizons of laminated chert at flow contacts. At the mine, the pillowed flows contain patchy to semipervasive epidote alteration and are intruded by plagioclase (\pm quartz)–porphyry dikes.

Feldspathic greywacke and mudstone (unit Bd2; Stormy Lake formation)

The Stormy Lake formation concordantly overlies basalt flows of the Gunnar formation and likewise received only cursory examination during this study. Considerable variations in the thickness of this unit appear to correlate with structural position with respect to the macroscopic Beresford Lake anticline: the formation is approximately 600–700 m thick on the west limb, thickens considerably in the hinge and is highly attenuated and thinned on the transposed east limb. Extensive exposures of this unit in the Stormy Lake area consist mostly of interbedded feldspathic greywacke and mudstone, with minor interlayers of heterolithic volcanic conglomerate, dacitic tuff breccia and lapilli tuff, and laminated chert and oxide-facies iron formation, all of which are included in subunit Bd2a. Voluminous gabbro sills account for approximately 50% of the stratigraphic section and range up to several hundreds of metres thick (Owens and Seneshen, 1985). As described by Campbell (1971) and Brommecker (1991), the base of this formation is marked by lenses of polymictic conglomerate that contain rare boulders of tonalite and gabbro, indicating significant uplift and erosion in the source area.

The greywacke is typically fine to medium grained and weathers buff to light greenish-grey, with medium grey to green fresh surfaces. In thin section, it consists of angular to subrounded crystal (plagioclase \gg quartz) and lithic grains in a fine-grained groundmass of feldspar, chlorite, sericite, carbonate, quartz and epidote-clinzoisite (Figure 12b). Individual beds are tabular-planar and massive or normally graded, and

range up to 3 m thick (typically 30–60 cm), with sharp scoured bases (Figure 12c). Slump folds and mudstone rip-ups are common; the overall features of these beds indicate deposition below storm-wave base via turbulent density currents, likely in a submarine fan setting. Although Campbell (1971) described progressive upward increase in the percentage of detrital quartz in the greywacke, most beds observed by the author contain only minor (1–3%) coarse detrital quartz, which is concentrated along the scoured basal contacts. Weber (1971a) and Brommecker (1991) described abundant pea-like aggregates of epidote and carbonate in thick beds of ‘pisolitic sandstone’, and noted that they locally overprint bedding and therefore must have formed by secondary processes, such as contact metamorphism or hydrothermal alteration.

The greywacke is interstratified on several scales with a variety of different rocks, suggesting a very dynamic, near-slope depositional setting in the upper channelled portion of the submarine fan. Rare horizons of laminated to thin-bedded graphitic mudstone, magnetite iron formation and/or chert are typically less than 1 m thick and indicate intervals of depositional quiescence, with coeval exhalative activity. Crudely stratified units of heterolithic cobble to boulder conglomerate range up to 20 m thick and contain mostly subangular to rounded clasts of intermediate–felsic volcanic material; these units are massive to normally graded and likely represent upper-fan channel-fill deposits. Subordinate interlayers of dacitic tuff breccia and lapilli tuff closely resemble those in the overlying The Narrows formation (described in detail below) and indicate influxes of volcanic-arc detritus, likely transported as subaqueous debris flows. Local flows of pillowed and brecciated basalt (subunit Bd2b) are similar in appearance to those in the underlying Gunnar formation (Weber, 1971a), and likewise consist of Mg-tholeiitic basalt (Brommecker, 1991). In this regard, the Stormy Lake formation appears to record the transition from a basalt-dominated back-arc basin to dacite-dominated volcanic arc. A greywacke sample (96-05-SL) collected from near the middle of the formation southwest of the Gunnar mine for U-Pb geochronological analysis of detrital zircons yielded a maximum depositional age of ca. 2734 Ma (see ‘U-Pb geochronology’ section).

Dacitic volcanoclastic rocks (unit Bd3; The Narrows formation; 2730 Ma)

The Narrows formation defines the top of the Bidou assemblage in the southeastern Rice Lake belt. As described by Weber (1971a) and Owens and Seneshen (1985), this formation consists predominantly of dacitic volcanoclastic rocks and is divided on the basis of clast size into two subunits: crystal tuff and lapilli tuff (subunit Bd3a), and breccia and tuff breccia (subunit Bd3b). Stockwell and Lord (1939) referred to these subunits as ‘porphyritic trachyte’ and ‘porphyritic trachyte breccia’, respectively. Contacts between these subunits are irregular and gradational (Weber, 1971a; Owens and Seneshen, 1985), and both contain minor intercalations of re-worked volcanic sandstone and conglomerate. Sills of tholeiitic melagabbro and leucogabbro account for 30–40% of the section on the west limb of the Beresford Lake anticline, where the formation varies up to 2.4 km thick. As noted by Stockwell

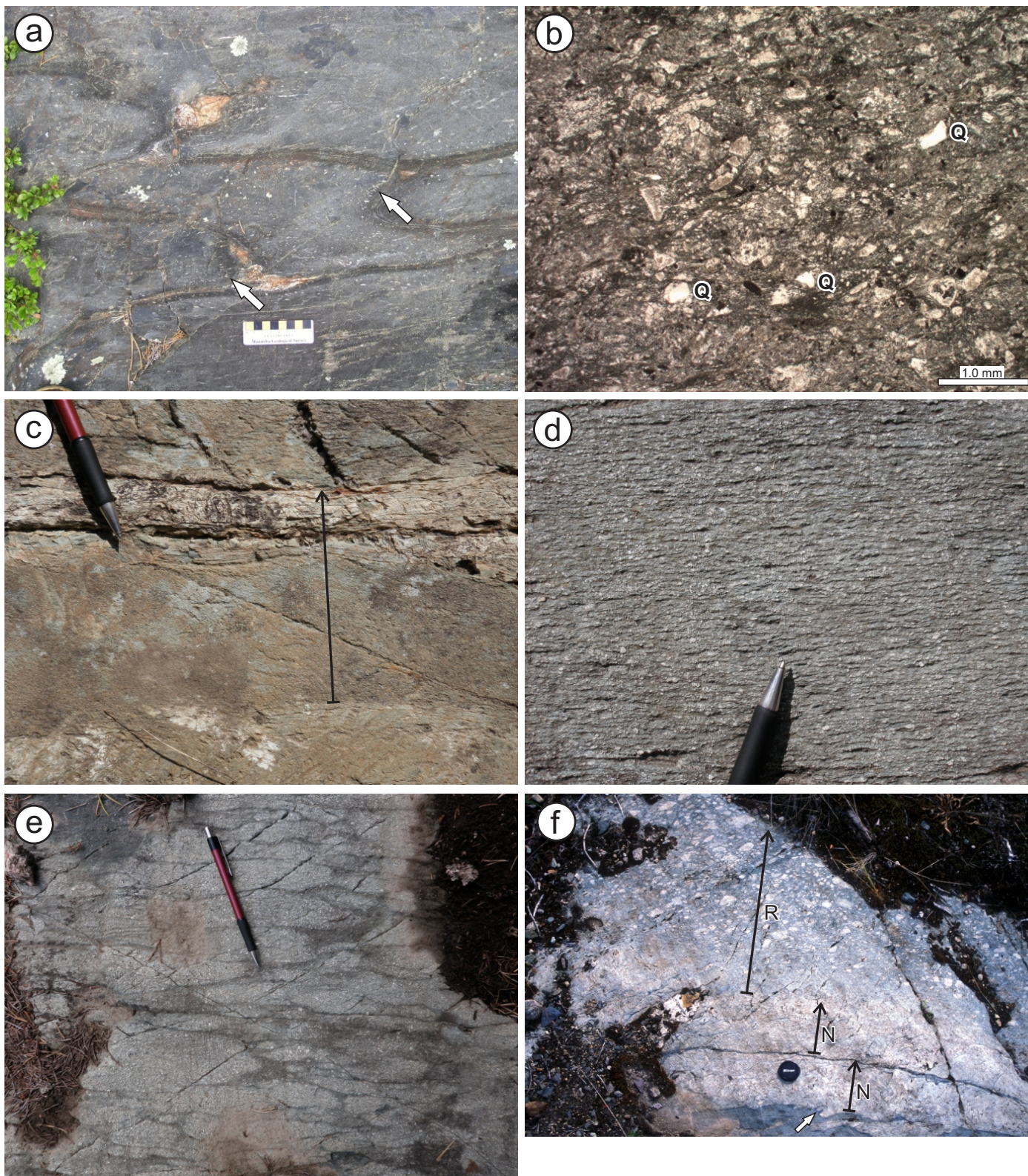


Figure 12: Outcrop and thin-section photographs of key rocks from the Bidou assemblage: **a)** pillowed plagioclase-phyric basalt of unit Bd1, with quartz amygdules along pillow margins (arrows), Halfway Lake; dark grey colour of the flows in this location results from contact metamorphism in the aureole of the Ross River pluton; **b)** photomicrograph (plane-polarized light) of feldspathic greywacke in unit Bd2, with detrital quartz indicated (Q), southwest of Gunnar mine; this sample was processed for U-Pb geochronological analysis of detrital zircons; **c)** turbidite in unit Bd2, composed of normally graded feldspathic greywacke and rippled to planar-laminated mudstone, southwest of Gunnar mine; black arrow(s) indicate graded beds; **d)** crystal tuff of subunit Bd3a, northwest of Grassy Rice Bay (Garner River); **e)** monolithic dacite breccia of unit Bd3b, northwest of Grassy Rice Bay (Garner River); **f)** normal (N) and reverse (R) size-grading in bedded volcanic sandstone and conglomerate of subunit Bd3b, south of Grassy Rice Bay (Garner River); younging direction in this outcrop is indicated by load structures (white arrow).

and Lord (1939) and Weber (1971a), The Narrows formation is similar in most respects to porphyritic volcanoclastic rocks north of Rice Lake (i.e., the 'Townsite dacite' of Poulsen et al., 1996); however, age constraints preclude a direct correlation (see Anderson, 2008).

Crystal tuff and crystal-lithic tuff of subunit Bd3a crop out most extensively in the lower portion of the unit, west of Stormy Lake. These rocks weather light greenish grey to buff and are massive to very crudely stratified. Most of the crystal tuff is seriate porphyritic, with subangular to angular (euhedral or broken) plagioclase crystals (20–40%; 0.5–5 mm) set in a fine-grained groundmass of feldspar, quartz, chlorite, sericite, epidote-clinzoisite and carbonate (Figure 12d). Most specimens also contain less than 1% quartz crystals (<5 mm). Lithic lapilli consist mostly of plagioclase (\pm quartz \pm hornblende)-phyric dacite and are difficult to distinguish from the crystal-tuff matrix in hand specimen. In thin section, the lapilli tend to be more equigranular and porphyritic than the crystal tuff, and contain a higher proportion of intact euhedral phenocrysts with a much finer grained (microgranular) groundmass. Some specimens contain rare lapilli of dark green basalt and white quartz-phyric rhyolite. Breccia and tuff breccia of subunit Bd3b dominate in the hinge of the Beresford Lake anticline and the upper portion of the formation west of Stormy Lake. These rocks weather light grey-green to buff and are dark green on fresh surfaces. Most outcrops are monolithic to slightly heterolithic, poorly sorted, matrix supported and massive to very crudely stratified. Angular to rounded clasts of light green-grey plagioclase-phyric dacite dominate and generally range up to 50 cm across (Figure 12e). Other clast types include basalt and rhyolite; exotic or resedimented clasts are absent. The crystal-tuff matrix contains slightly smaller and fewer plagioclase phenocrysts and is slightly more chloritic.

There is no evidence (e.g., pumice, gas segregation pipes, columnar joints, etc.) to suggest that unit Bd3 was deposited by primary pyroclastic processes. The breccia and tuff breccia are thickly interstratified in places with well-bedded intervals of volcanic sandstone and polymictic volcanic conglomerate, the latter of which locally contain well-rounded boulders up to 2 m across. Beds in these intervals range up to several metres thick and vary from massive to normally or reversely graded (Figure 12f). Rare scours and load structures provide reliable younging criteria. The rounded shapes and coarsely porphyritic textures of the dacite clasts are suggestive of reworked autoclastic detritus, which was likely redeposited below wave base in a shallow-subaqueous setting by syneruptive high-density grain and debris flows.

Gabbro (unit Bd4)

Regionally extensive gabbro sills are a characteristic feature of the Bidou assemblage, and constitute a significant proportion of the overall stratigraphic thickness of each of the constituent formations. The gabbro is chemically indistinguishable from associated flows of Fe- or Mg-tholeiitic basalt. The sills range up to several hundreds of metres in thickness; dikes are comparatively rare and generally less than 20 m thick. The gabbro weathers from dark green to light green or grey and varies from fine to coarse grained, typically with a well-preserved

ophitic to subophitic texture. Porphyritic varieties contain sparse plagioclase phenocrysts up to 3 cm. Thicker sills tend to be coarser grained and show evidence of in situ differentiation in the form of locally developed magmatic layering, upward increases in plagioclase (\pm quartz \pm magnetite) content or the presence of irregular patches or dikes of pegmatitic leucogabbro, quartz diorite or anorthosite near upper contacts (Stockwell and Lord, 1939; Brommecker, 1991). Contacts with the country rock tend to be sharp, planar and concordant to very slightly discordant, with well-developed chilled margins. Contact-metamorphic effects are limited to narrow bleached zones in sedimentary rocks within a metre or so of the contacts (Stockwell and Lord, 1939), consistent with relatively high-level emplacement. A sample of pegmatitic leucogabbro (96-05-CMG) was collected from the thick gabbro sill at the Central Manitoba mine for U-Pb geochronological analysis, but did not yield useful results (see 'U-Pb geochronology' section).

Gem assemblage

The Gem assemblage crops out extensively in the Gem Lake area and consists of subaqueous to subaerial effusive volcanic rocks and related hypabyssal intrusions that range in composition from basalt to high-SiO₂ rhyolite and are intercalated with primary and variably reworked volcanoclastic rocks, and minor epiclastic rocks. The Gem assemblage, as defined herein, corresponds to the Banksian Lake formation of the Gem Lake subgroup (Weber, 1971a) and, in the northwest, includes rocks that were assigned to the Manigotagan River formation of the Bidou Lake subgroup by Seneshen and Owens (1985). As noted by Weber (1971a), the Gem assemblage appears to record a nearly complete (basalt to rhyolite) differentiation cycle, in contrast to the essentially bimodal (basalt and dacite) Bidou assemblage. At Gem Lake, the Gem assemblage is disposed as a series of structural panels separated by high-strain zones (Figure 3), which are correlated on the basis of geochemical attributes and U-Pb ages of the constituent rocks. Two litho-geochemical associations are apparent, and are described below as the 'East' and 'West' associations (Figure 13). These chemical associations are mutually distinct, and are also distinct from rocks of similar bulk composition in the Garner and Bidou assemblages. Within each association, felsic volcanic units are further distinguished by unique combinations of weathering colour, primary texture and phenocryst population.

The West association is well exposed on the western limb of the BLA, where it defines the hinge of the parasitic MRA, and is also well exposed on the strongly transposed eastern limb, between the MLSZ and GRSZ (Figure 3). It concordantly overlies The Narrows formation of the Bidou assemblage on both limbs of the BLA and is likewise overlain by mudstone-dominated turbidites of the Edmunds assemblage. Grey to black, aphyric to sparsely plagioclase-phyric dacite and rhyolite are characteristic and include coherent flows and associated pumiceous pyroclastic rocks that are unique to this portion of the Rice Lake belt. The stratigraphic thickness of the association varies between 400 and 800 m on the limbs of the BLA, but ranges up to 3000 m in the structurally thickened hinge of the fold. Abundant turbidite bedforms and pillowed flows indicate a subaqueous depositional setting for this portion of the

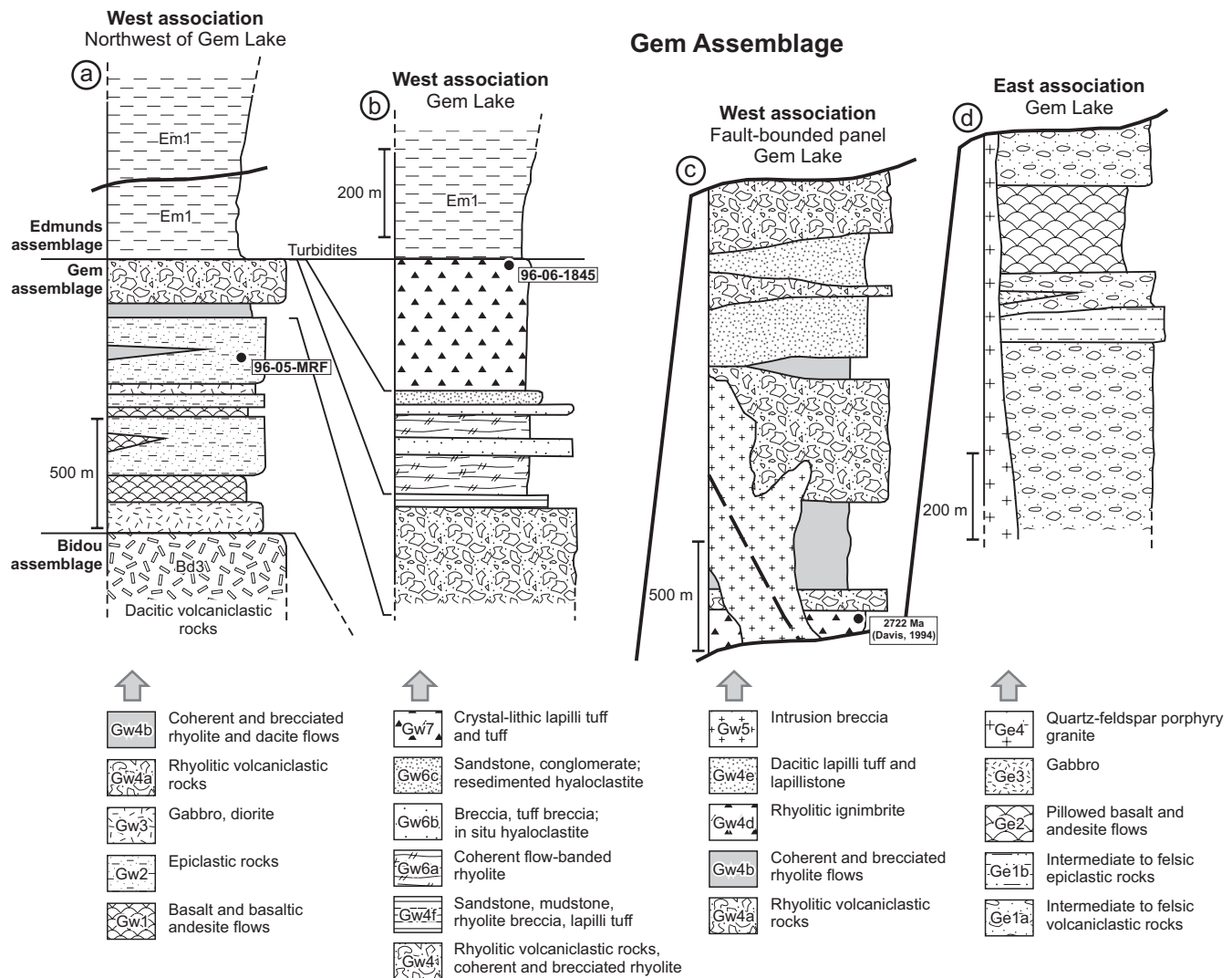


Figure 13: Schematic stratigraphic columns for the Gem assemblage: **a)** West association, west limb of the Beresford Lake anticline (BLA), northwest of Gem Lake; **b)** West association, west limb of the BLA, south-central Gem Lake; **c)** West association, fault-bounded panel, central peninsula in Gem Lake; **d)** East association, east-central Gem Lake. Unit codes correspond to those in the text and on the accompanying Map GR2013-1-1. Black circles indicate the approximate stratigraphic location of the U-Pb geochronology samples.

association. The West association is also disposed in a fault-bounded panel that extends north from the central peninsula in Gem Lake to the western basin of Garner Lake. Here, the association is locally disrupted by faults, but appears to be at least 2000 m thick, with a westerly younging direction. In this panel, the association lacks turbidite bedforms and pillowed flows, but includes well-preserved examples of welded rhyolitic ignimbrites that are interpreted to indicate a subaerial or very shallow subaqueous depositional setting. Davis (1994) obtained a U-Pb zircon age of 2722 ± 2 Ma from a quartz-phyric ignimbrite on the central peninsula in Gem Lake, indicating that at least this portion of the association is 5–10 m.y. younger than the Bidou assemblage. This age overlaps within error the best-estimate age of 2724 ± 1 Ma reported by Anderson (2008) for biotite granodiorite of the Ross River pluton, which intrudes the Bidou assemblage in the core of the Rice Lake belt. In the West association, basalt and basaltic andesite flows of tholeiitic–calcalkalic affinity are intercalated with calcalkalic rhyolite

and high-SiO₂ rhyolite flows. A similar lithogeochemical association is documented in the ca. 2723 Ma Gray Point sequence at Lake Winnipeg and is interpreted to record extension and localized rifting of the arc–back-arc complex represented by the Bidou assemblage (e.g., Bailes and Percival, 2005a; Percival et al., 2006a).

The East association of the Gem assemblage is at least 1.2 km thick and consists of a homoclinal, westerly younging panel exposed along the eastern shoreline of Gem Lake. Volcanoclastic and epiclastic rocks derived from coarsely porphyritic dacite and andesite are characteristic and are intruded from the east by a large pluton of quartz- and feldspar-porphyritic granite. This association extends to the east into Ontario, where Rogers and McNicoll (unpublished, cited by Lemkow et al., 2006) obtained a U-Pb zircon age of $2718 +3/-2$ Ma from a ‘felsic tuff’ at Bee Lake, which is located 5.5 km to the east along strike. This age overlaps within error the probable age of the West association and suggests a possible correlation with

ca. 2720 Ma (Anderson, 2008) volcanoclastic rocks north of Rice Lake, which similarly consist of porphyritic andesite and dacite (i.e., the 'Townsite dacite' of Poulsen et al., 1996).

Description of rock units – West association

Seven distinct lithological units are recognized in the West association of the Gem assemblage and are described below in general order of their stratigraphic position on the west limb of the Beresford Lake anticline (BLA). Unlike map units in the Bidou and Edmunds assemblages, those in the Gem assemblage tend to be markedly lenticular and do not define a consistent stratigraphic order. Abrupt lateral and vertical facies variations are in keeping with a dynamic depositional setting. Basaltic volcanic and intrusive rocks of map units Gw1 and Gw3, respectively, occur at various stratigraphic levels and are intercalated with felsic coherent flows and volcanoclastic rocks of unit Gw4. Epiclastic rocks of unit Gw2 crop out on both limbs of the BLA in the northwestern portion of the study area and appear to represent a relatively distal facies of the assemblage. Unit Gw5 is a hypabyssal intrusion breccia of rhyolitic bulk composition that was emplaced into volcanoclastic rocks of unit Gw4 and is restricted to the fault-bounded panel on the central peninsula in Gem Lake. A distinctive rhyolite flow (unit Gw6) and possible dacitic ignimbrite (unit Gw7) define the top of the assemblage along the southwest shore of Gem Lake.

Basalt and basaltic andesite (unit Gw1)

Effusive flows and volcanoclastic rocks of unit Gw1 consist of basalt and basaltic andesite, with minor andesite, and are identified at several stratigraphic levels in the Gem assemblage. They tend to form prominently lenticular map units that range up to several hundreds of metres in thickness over relatively short (<2 km) strike lengths. Subunit Gw1a is identified on both limbs of the BLA and consists of pillowed, massive and brecciated flows, and associated volcanoclastic rocks, that characteristically contain quartz amygdulites. Pillowed flows, at least locally, define the upper and lower contacts of the assemblage on both limbs of the BLA, indicating that effusive basaltic volcanism spanned the entire depositional history. Thin flows are particularly abundant on the west limb, but are only locally mappable at 1:20 000 scale. Subunit Gw1b is chemically indistinguishable from subunit Gw1a, but typically lacks quartz amygdulites and is dominated by coarse volcanoclastic rocks. It is only identified in the fault-bounded panel that extends north from the central peninsula in Gem Lake to the western basin of Garner Lake. As described below, textural features indicate significant differences in eruptive setting for the two subunits.

Pillowed, massive and brecciated flows, and associated volcanoclastic rocks, of subunit Gw1a are composed of amygdaloidal basalt and basaltic andesite, with lesser andesite. These rocks weather light green or grey and are dark green on fresh surfaces. They vary in places from aphyric to coarsely plagioclase phyric, but typically exhibit a seriate-porphyritic texture defined by tabular phenocrysts of plagioclase (<20%; 1–5 mm) in a felted groundmass of fine-grained plagioclase, chlorite, actinolite, epidote-clinzoisite, carbonate, white mica, titanite and opaque minerals (Figure 14a). The characteristic feature of

these rocks is the presence of quartz (\pm carbonate \pm white mica) amygdulites, which are sparsely (<5%) distributed throughout or are concentrated along the inner margins of pillow selvages or flow contacts. The amygdulites are typically round and 0.1–1.5 cm in diameter. Several flows contain amygdulites up to 8 cm in diameter (Figure 14b), perhaps indicating a shallow-water eruptive setting. In continuous exposures, massive amygdaloidal flows varying from several metres to several decametres in thickness locally grade upsection or laterally into pillowed or brecciated flows. The pillowed flows consist of bun-shaped to amoeboid pillows up to 1.5 m in maximum dimension, with minor (<15%) interpillow hyaloclastite (Figure 14c). Pillow selvages are 1–3 cm thick and are typically amygdaloidal along their inner margins.

Associated intervals of breccia, tuff breccia and lapilli tuff are monolithic, unsorted, nonstratified and typically clast supported. They consist of very angular to subangular, blocky to amoeboid or wispy clasts (<25 cm) of variably amygdaloidal and plagioclase-phyric basalt. Curvilinear and cusped margins and local jigsaw-fit texture indicate autoclastic or hyaloclastic processes as the mechanism of fragmentation for most of these rocks. Included in this unit are the basaltic lava flows, peperite and tephra-fall deposits described by Seneshen (1990) from the west limb of the BLA. In this location, thin (<20 m) flows of massive, pillowed and brecciated amygdaloidal basalt and basaltic andesite are interstratified with turbiditic volcanic sandstone of unit Gw2 (Figure 14d). Seneshen (1986, 1990) described pillowed flows and thick accumulations of basaltic scoria that are indicative of Strombolian-type eruptions in a shallow-water setting. These rocks are locally cut by irregular dikes or lobes of amygdaloidal basalt that have particularly thick (3–5 cm) chilled margins.

Breccia, tuff breccia and lapilli tuff of subunit Gw1b are restricted to the fault-bounded panel that extends north from the central peninsula in Gem Lake to the western basin of Garner Lake. These rocks are similar in many respects to the volcanoclastic rocks in subunit Gw1a, but differ in that they only rarely contain amygdulites (Figure 15a) and do not appear to be associated with pillowed flows. They also tend to contain slightly coarser and more crowded plagioclase phenocrysts. Monolithic breccia and tuff breccia dominate and consist of angular to subangular, blocky or wispy clasts of basalt and basaltic andesite. Some clasts have ragged fluidal rinds suggestive of basaltic spatter (Figure 15b). Coarse fragmental rock types are generally unsorted, matrix to clast supported and nonstratified, although subtle variations in the size and proportion of clasts define a crude stratification in some localities (Figure 15c). Heterolithic variants consist of slightly less angular basaltic clasts that contain highly variable proportions of plagioclase phenocrysts and also locally contain a small proportion (<10%) of light grey dacite clasts. Possible coherent flows of porphyritic basaltic andesite are exposed in two locations and show irregular gradational contacts with fragmental (blocky) basaltic andesite. Associated jigsaw-fit breccia with less than 5% matrix is interpreted to result from autoclastic fragmentation of lava-flow lobes or cryptodomes (Figure 15d). The fluidal clasts, coupled with the apparent absence of pillowed flows, suggest that subunit Gw1b may have been erupted in a subaerial setting.

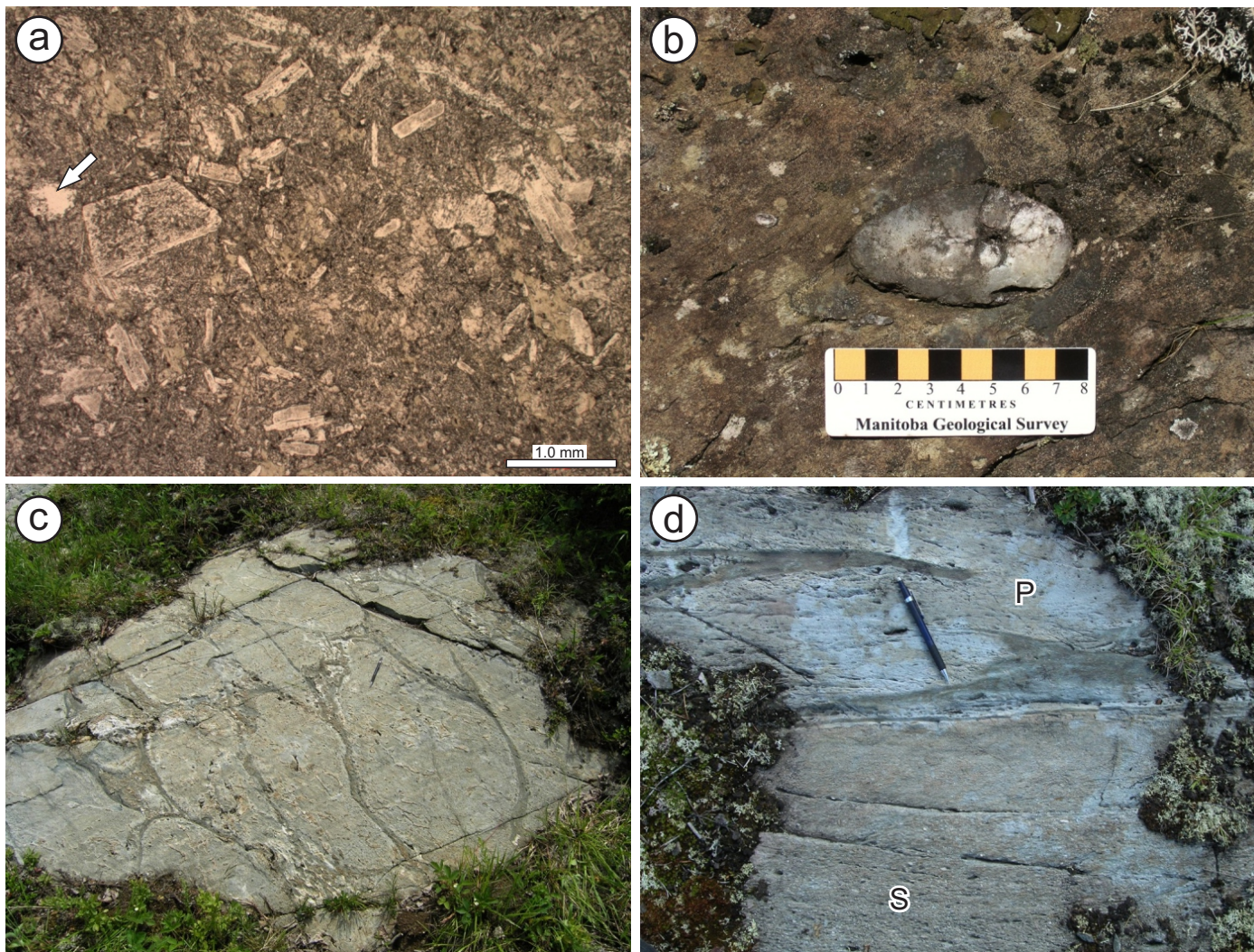


Figure 14: Outcrop and thin-section photographs of rocks in subunit Gw1a: **a)** photomicrograph (plane-polarized light) of basaltic andesite from the east limb of the Beresford Lake anticline (BLA); seriate-porphyritic texture is defined by euhedral phenocrysts of plagioclase; quartz-calcite amygdule indicated by arrow; **b)** large quartz amygdule in pillowed flow on east limb of the BLA; **c)** pillowed basaltic andesite (same location as 14a), showing relatively intact pillow shapes and minor interpillow hyaloclastite (pencil for scale on the largest pillow); **d)** sharp depositional contact between graded volcanic sandstone (S) and pillowed basaltic andesite (P) on the west limb of the BLA (younging direction is toward the top of the photo).

Epiclastic rocks (unit Gw2)

Well-stratified volcanic conglomerate, sandstone, mudstone and chert of unit Gw2 define thick and continuous map units on both limbs of the BLA in the northwestern portion of the map area (Figure 3). At its lateral extents, unit Gw2 appears to record a relatively continuous transition from active arc volcanism (Bidou) to basinal marine sedimentation (Edmunds), and is interpreted to constitute a distal facies of the Gem assemblage. In the hinge and west limb of the BLA, the sedimentary rocks of unit Gw2 are intercalated with basalt and basaltic andesite flows and associated volcanoclastic rocks (unit Gw1), and are intruded by abundant sills and dikes of gabbro and diorite (unit Gw3). Here, unit Gw2 corresponds to the Manigotagan River formation of Seneshen and Owens (1985), and thus includes the felsic volcanoclastic turbidite and mass-flow deposits described in detail by Seneshen (1990). As described by Seneshen (1990), abundant juvenile pyroclasts (i.e., pumice) in the felsic volcanoclastic turbidite, thick accumulations

of subaqueously deposited basaltic tephra, and local pillowed, massive and brecciated basaltic flows and associated peperite all indicate coeval volcanism and sedimentation in a subaqueous-fan depositional setting. Deep erosional scours and local crossbedded sandstone in pillow interstices indicate a relatively shallow-water setting.

On the east limb of the BLA, the thickest and most continuous section of unit Gw2 is exposed at the confluence of Beresford Creek and the Garner River, and ranges up to 500 m thick over a mapped strike length of 3.5 km. Here, unit Gw2 lies in gradational contact to the east with overlying thin-bedded turbidites of the Edmunds assemblage (unit Em1). Although similar in some respects, these units are distinguished on the basis of the following field criteria in this location: 1) turbidites in unit Gw2 tend to be thicker and coarser than those in unit Em1, and are composed of relatively immature detritus; 2) conglomerate interbeds in unit Gw2 are abundant and thick, and are composed of angular volcanic clasts, whereas those in unit Em1 are

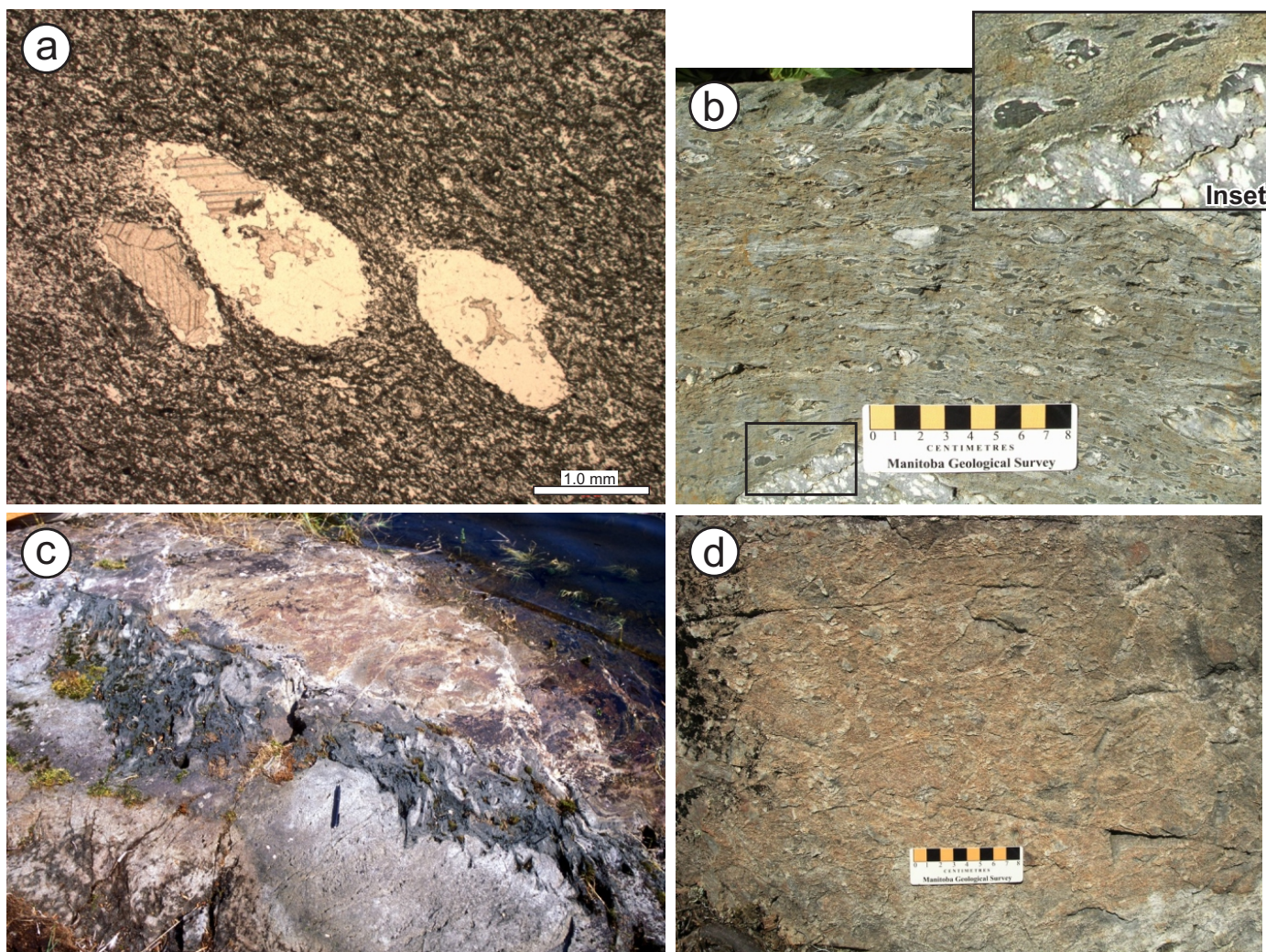


Figure 15: Outcrop and thin-section photographs of rocks in subunit Gw1b: **a)** quartz-calcite amygdules in massive basaltic andesite flow (plane-polarized light), roughly midway between Gem and Garner lakes; **b)** heterolithic lapilli tuff composed of aphyric and coarsely plagioclase-phyric basaltic andesite clasts in a chloritic tuff matrix, same location as previous photo; inset shows detail of quenched fluidal margin on the large clast in the lower left of the photo; **c)** stratified tuff breccia and breccia composed of plagioclase-phyric basaltic andesite, western portion of Garner Lake; **d)** jigsaw-fit texture of closely packed angular blocks in otherwise massive basaltic andesite, northwest of Gem Lake.

comparatively minor and thin, and include a significant component of well-rounded ‘exotic’ (e.g., tonalite, quartzite) clasts (U-Pb analyses of detrital zircons also indicate significant differences in provenance; see ‘U-Pb geochronology’ section), and; 3) hypabyssal gabbro sills are common in unit Gw2 but are not observed near the base of unit Em1.

The characteristic rock types of unit Gw2 are volcanic sandstone and mudstone with interbeds of laminated black chert and volcanic pebble conglomerate (subunit Gw2a), and polymictic pebble to boulder volcanic conglomerate with minor interbeds of pebbly volcanic sandstone (subunit Gw2b). The volcanic sandstone is typically a fine- to medium-grained feldspathic greywacke that weathers buff to light grey to white and is dark grey on fresh surfaces. It consists of angular to subrounded crystal (plagioclase>quartz) and lithic grains in a fine-grained matrix of feldspar, quartz, chlorite, sericite and carbonate. Beds are planar, normally graded or less commonly massive, and range up to 1.5 m thick (typically <30 cm), with

sharp scoured bases (Figure 16a). Some beds are reversely graded near the base. Coarse (>0.5 mm) detrital quartz is generally absent, although some beds contain up to 5% quartz in basal lag deposits. Subordinate interbeds (<5 cm) of laminated light grey mudstone represent the upper division of Bouma AE turbidites. Bed contacts are sharp and planar. Interbeds of laminated chert up to 30 cm thick indicate periodic episodes of sediment starvation. Although most of these beds were likely deposited from turbidity currents in a relatively quiescent (i.e., below wave base) marine setting, local trough crossbedding and deep erosional scours in thin (<2 m) intervals of lenticular-bedded volcanic sandstone and mudstone (Figure 16b) indicate a more dynamic setting, such as the channelled or shoaling portion of a submarine fan. Seneshen and Owens (1985, Figure GS-23-6) described pillow interstices infilled with trough-crossbedded sandstone, suggesting that deposition at least locally occurred in a shoaling, shallow-subaqueous to subaerial setting, with coeval effusive volcanism. Conglomerate beds in subunit Gw2a

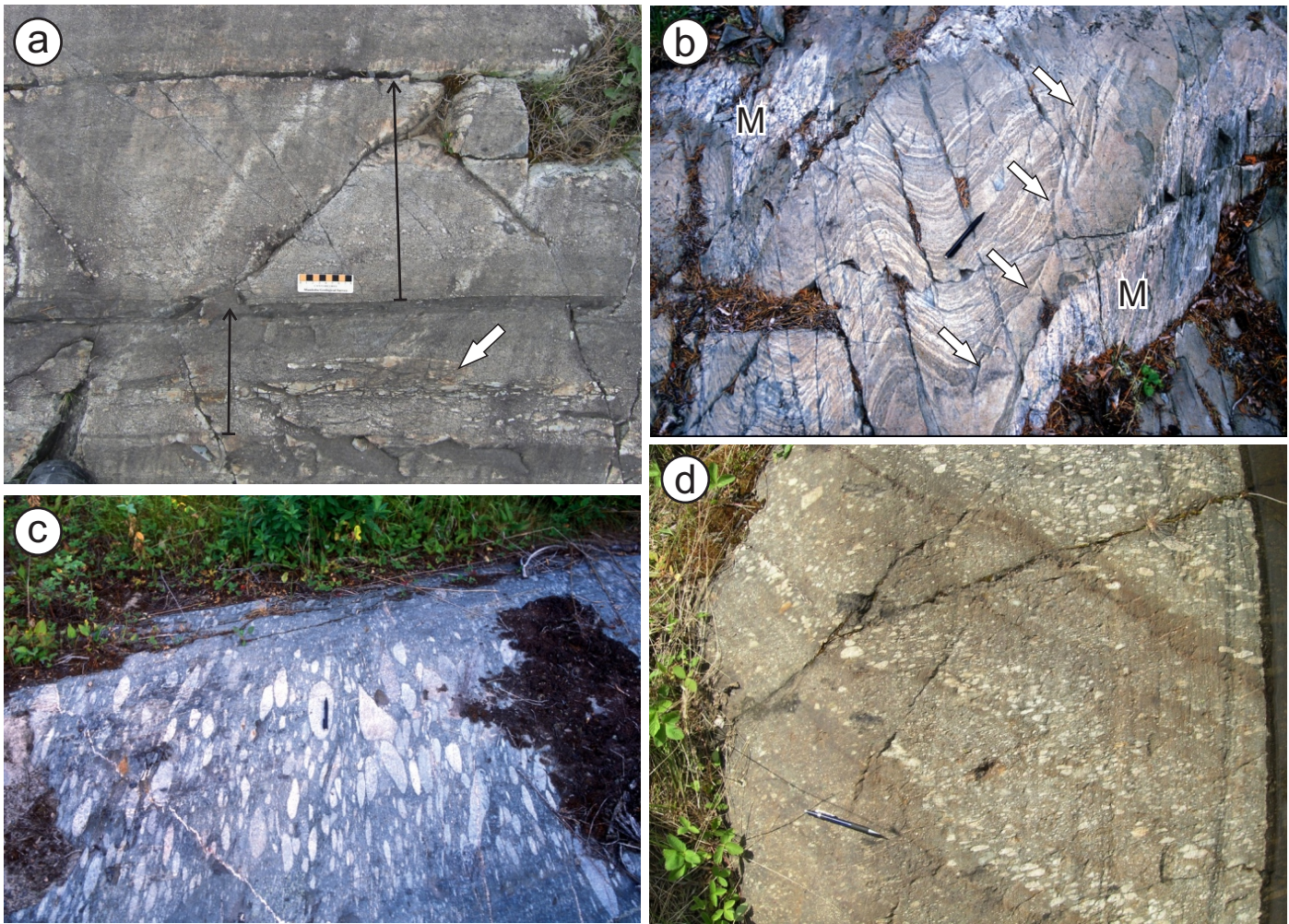


Figure 16: Outcrop photographs of rocks in unit Gw2 from the west limb of the Beresford Lake anticline (BLA): **a)** turbiditic bedforms in volcanic sandstone and mudstone of subunit Gw2a (younging direction is toward the top of the photograph; black arrows indicate graded beds); lower bed is normally graded and contains large mudstone rip-up clasts (arrow); upper bed is reversely graded at the base and normally graded at the top; **b)** lenticular-bedded volcanic sandstone and laminated mudstone (M) of subunit Gw2a, showing local crossbedding and deep erosional scour (arrows); **c)** stratified pebble and cobble conglomerate of subunit Gw2b; rounded clasts indicate significant subaerial transport; outcrop is situated near the hinge of a macroscopic F_2 fold, as indicated by the near-orthogonal relationship between bedding and the flattened clasts (S_2 planar shape-fabric); **d)** stratified pebble conglomerate; note high degree of clast rounding.

are poorly sorted, matrix to clast supported and massive to normally graded, and locally define the base of 4–5 m thick fining- and thinning-upward cycles; deeply scoured basal contacts are consistent with upper-fan channel-fill deposits. A sample of the volcanic sandstone (96-05-MRF), collected for U-Pb geochronological analysis of the detrital zircon population, yielded a maximum emplacement age of ca. 2724 Ma (see ‘U-Pb geochronology’ section).

Polymictic volcanic conglomerate of subunit Gw2b is poorly sorted, matrix supported and crudely stratified, and typically consists of rounded to subrounded, pebble- to cobble-sized clasts (<25 cm) in a matrix of pebbly mudstone or feldspathic greywacke (Figure 16c, d). One outsized boulder measures at least 2 m across. The clasts consist mainly of pale green, feldspar-phyric andesite and dacite, with lesser aphyric to quartz-phyric grey dacite, amygdaloidal basalt, quartz-phyric white rhyolite and aphyric dark grey rhyolite. Some beds contain abundant clasts of reworked volcanoclastic rock

and, concentrated near the base, laminated to thin-bedded mudstone rip-ups. Individual beds range up to 10 m thick. The very coarse matrix-supported clast population and immature mud-rich matrix indicate that these rocks were most likely deposited as high-density debris flows. The generally high degree of clast rounding suggests significant subaerial transport. Well-stratified portions of this subunit consist of diffuse, normally or reversely graded conglomerate beds up to 1 m thick, with abundant examples of composite (reverse to normal) size-grading. Bed contacts vary from planar to deeply scoured. As noted above, the volcanic conglomerate beds locally occur at the base of fining- and thinning-upward cycles that likely represent channel-fill deposits; such features are characteristic of conglomerate deposited in upper-fan feeder channels (Walker 1978, 1984).

On the west limb of the BLA, subunit Gw2a includes two intervals of distinctive pyroclast-rich felsic volcanoclastic turbidites, which were identified by Seneshen and Owens (1985) and described in detail by Seneshen (1986, 1990). As described

by Seneshen (1990), these intervals range between 6 and 50 m thick and are composed of several discrete ‘flow units’ ranging from 0.7 to 17 m in thickness. Contacts between flow units vary from planar to scoured and are typically sharp. Internally, each flow unit consists of a lower bed of nonstratified ‘lapilli tuff’ and an upper layer of laminated to thick-bedded ‘tuff’. The lapilli-tuff beds are normally graded, with sharp to gradational contacts and locally scoured bases, whereas the tuff beds are planar and massive to normally graded with sharp contacts. As suggested by Seneshen (1990), these features indicate that the beds were emplaced as subaqueous high- and low-density turbidites, respectively. The high-density turbidites include up to 35% collapsed pumice, in addition to crystal and lithic clasts (Figure 17a, b). The pumice clasts are typically reversely graded with respect to abundance, and locally also size, whereas lithic clasts are normally graded. In thin section, many of the quartz grains in these rocks exhibit cusped margins and shard-like shapes, which are indicative of primary pyroclastic fragmentation (Figure 17b).

Based on the high abundance of juvenile pyroclasts, Seneshen (1990) proposed that the high-density turbidites were the direct products of subaerially erupted pyroclastic flows that entered seawater, whereas the low-density turbidites were deposited later by normal sedimentary processes acting on unconsolidated pyroclastic deposits. However, as noted by McPhie et al. (1993, p. 107–108), pyroclast-rich submarine gravity-flow deposits can also be generated by other means, such as subaqueous explosive eruptions or entirely post-eruptive sedimentary processes, and the resulting deposits can be difficult to distinguish even in modern settings. Hence, these deposits are herein included with the turbiditic volcanic sandstone, mudstone and conglomerate of subunit Gw2a, with no inferences drawn with respect to the original eruptive setting of the pyroclastic detritus.

Gabbro and diorite (unit Gw3)

Gabbro and diorite form sill-like intrusions and dikes at various stratigraphic levels in the Gem assemblage, most of which are not mappable at 1:20 000 scale. The largest sills range up to 200 m thick and are traced along strike for up to 2.0 km. Dikes vary from planar to highly irregular and are typically less than 2 m thick. The thickest sills and areas of most intense diking are spatially associated with pillowed basalt and basaltic andesite flows of subunit Gw1a. Gabbro predominates over diorite and is chemically similar to the associated flows, consistent with a comagmatic relationship. The gabbro typically weathers light grey-green and is dark green on fresh surfaces, with fine- to medium-grained, equigranular (subunit Gw3a) or seriate-porphyritic (subunit Gw3b) textures. Most specimens contain 50–75% plagioclase laths (<2 mm) in a fine-grained felted groundmass of actinolite, biotite, plagioclase, chlorite, epidote, titanite and opaque minerals (Figure 18a). Porphyritic gabbro contains up to 30% tabular plagioclase phenocrysts up to 4 mm in length (Figure 18b). Leucocratic specimens also locally contain up to 5% magnetite, and are thus strongly magnetic. Contacts with the country rock vary from planar to highly irregular, and typically exhibit fairly thick (2–5 cm) chilled margins. In some of these intrusions, round quartz amygdulites (1–2%; 1.5–5 mm) are concentrated along the inside of the chilled margin, indicating hypabyssal emplacement.

Dacite and rhyolite (unit Gw4)

Unit Gw4 consists of a heterogeneous association of volcanoclastic rocks, with minor effusive flows and derived epiclastic rocks, that mostly correspond to rocks described by Weber (1971a) as dacite flows, dacitic to rhyodacitic crystal tuff and lapilli tuff, and rhyodacitic tuff breccia. This unit includes six texturally distinct subunits that are grouped together on the

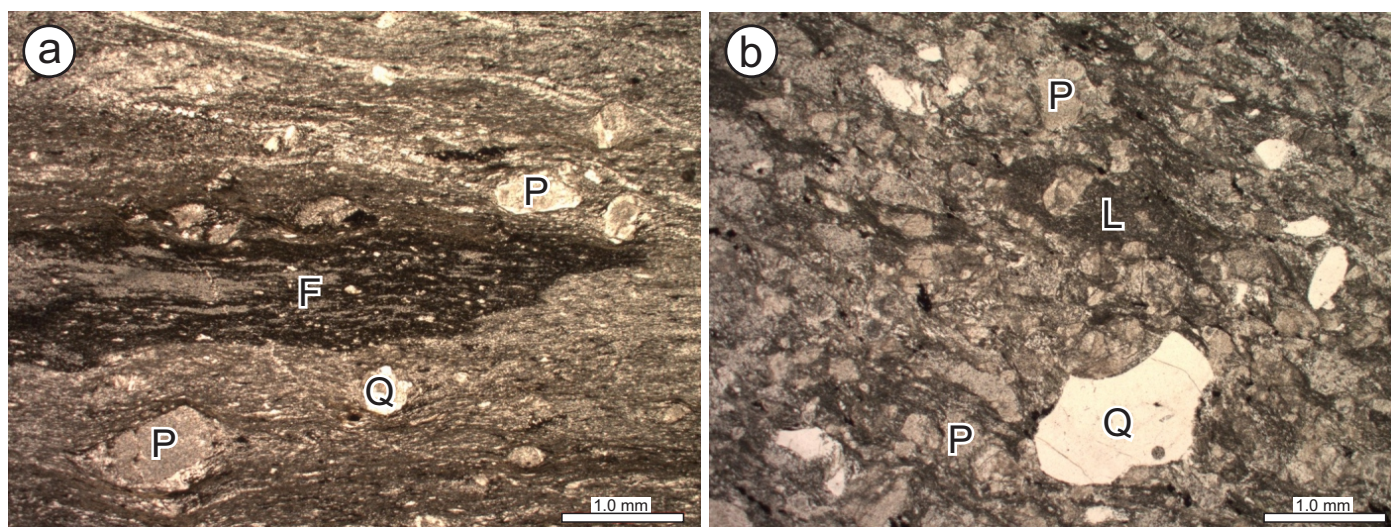


Figure 17: Photomicrographs (plane-polarized light) of textures in volcanoclastic turbidites of subunit Gw2a on the west limb of the Beresford Lake anticline: **a)** angular to subrounded plagioclase (P) and quartz (Q) crystals and fiamme (F) in pebbly volcanic sandstone; the internal texture of the fiamme is interpreted to represent relict vesicles; **b)** angular plagioclase (P), quartz (Q) and porphyritic lithic (L) grains in pebbly volcanic sandstone; the very angular cusped shapes of quartz grains in this sample are indicative of pyroclastic fragmentation.

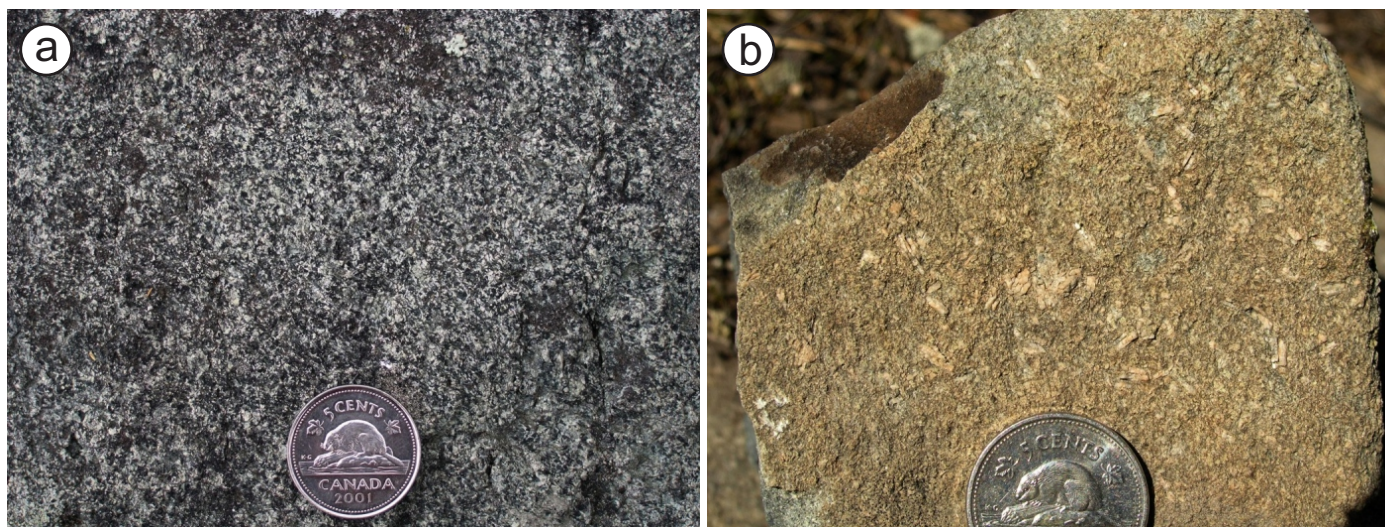


Figure 18: Outcrop photographs of gabbro from unit Gw3: **a)** equigranular gabbro (subunit Gw3a), central portion of Gem Lake; **b)** plagioclase-porphyritic gabbro (subunit Gw3b), east limb of the Beresford Lake anticline.

basis of their close spatial association and very uniform trace-element geochemical signatures. Bulk compositions are dominantly rhyolite, with subordinate dacite, high-SiO₂ rhyolite and andesite. Unit Gw4 is exposed on both limbs of the BLA and dominates the southern portion of the fault-bounded panel that extends north from the central peninsula in Gem Lake toward the west end of Garner Lake. It ranges up to 700 m thick near the hinge of the MRA and tapers out along strike on both limbs. Unit Gw4 is between 500 and 900 m thick in the fault-bounded panel and is structurally truncated to the north and south. Subunits Gw4a and Gw4b account for most of the unit on both limbs of the BLA, as well as in the fault-bounded panel on the central peninsula in Gem Lake. The remaining four subunits (Gw4c–f) are only observed on islands and the central peninsula in Gem Lake.

Rhyolitic volcanoclastic rocks of subunit Gw4a weather light greenish grey to buff (or rarely white) and are dark grey on fresh surfaces. They consist mostly of crystal-lithic lapilli tuff and lapillistone (Figure 19a), which are thickly interstratified with subordinate crystal tuff, tuff breccia and breccia. These rock types are typically monolithic, poorly sorted and nonstratified to crudely stratified. Lithic clasts are very angular to subrounded and equant (<35 cm), and consist mostly of aphyric to very sparsely plagioclase (±quartz)-phyric rhyolite and dacite. In some specimens, these clasts are distinctly shard like. In places, these rocks also contain a subordinate population (<20%) of dark grey to olive-green or brown plagioclase (±quartz)-phyric fiamme, which are highly elongate (up to 10 cm) and wispy with ragged terminations, and are interpreted to represent collapsed pumice (Figure 19b). In thin section, possible examples of previously glassy shards are completely replaced by fine-grained white mica, yet locally retain primary shapes (Figure 19c). Variations in the size and proportion of clasts locally define a diffuse stratification in otherwise massive outcrops.

The lapilli tuff and tuff breccia are generally matrix supported, with between 5 and 30% lithic clasts, whereas the lapillistone and breccia tend to be clast supported. Crystal tuff

forms the matrix and also occurs as massive layers up to several metres thick. It contains euhedral to subhedral phenocrysts of plagioclase (5–20%; <4 mm) and rare anhedral crystals of quartz (<2%; <2 mm) in a microgranular groundmass of quartz, feldspar, sericite, biotite, chlorite and carbonate. Massive layers of lapilli tuff and lapillistone range up to 10 m thick in continuous exposures and are locally separated by thin (<1 m) intervals of stratified tuff and lapilli tuff (Figure 19d). Layer contacts are sharp and planar. These stratified intervals locally contain low-angle crossbeds and are thus suggestive of pyroclastic surge deposits. In one of these intervals, the strata are defined by variations in the size and proportion of spheroidal aggregates of fine-grained siliceous material (Figure 19e, f). The aggregates range from 2 to 10 mm in diameter and exhibit a concentric internal structure, suggesting they likely represent accretionary lapilli. This locality is situated on the small island adjacent to the west shoreline of the central peninsula in Gem Lake; the presence of accretionary lapilli would imply a sub-aerial eruptive setting for at least parts of unit Gw4. The overall characteristics of subunit Gw4a are indicative of rhyolitic ignimbrites generated by gravitational or explosive collapse of the associated rhyolite and dacite lava flows or domes, which are described in the following paragraph.

Coherent and brecciated flows or domes of subunit Gw4b are composed of aphyric to sparsely plagioclase-phyric rhyolite and dacite. These rocks account for a significant portion of the section in the hinge and west limb of the MRA and are also abundant on the central peninsula in Gem Lake. Contact relationships are not well defined, but the flows or domes appear to grade, at least locally, into adjacent coarse volcanoclastic rocks of subunit Gw4a. The rhyolite and dacite typically weather light grey to greenish grey and are light grey to black on fresh surfaces, with a conchoidal fracture habit (Figure 20a, b). In thin section, they contain sparse (3–5%, <3 mm) euhedral to subhedral phenocrysts of plagioclase (±quartz) in a microgranular groundmass of feldspar, quartz, sericite, biotite and carbonate (Figure 20c). The southeasternmost portion of this subunit is dominated high-SiO₂ rhyolite flows that weather a distinctive pale greyish-white to yellowish-white. Coherent flows or

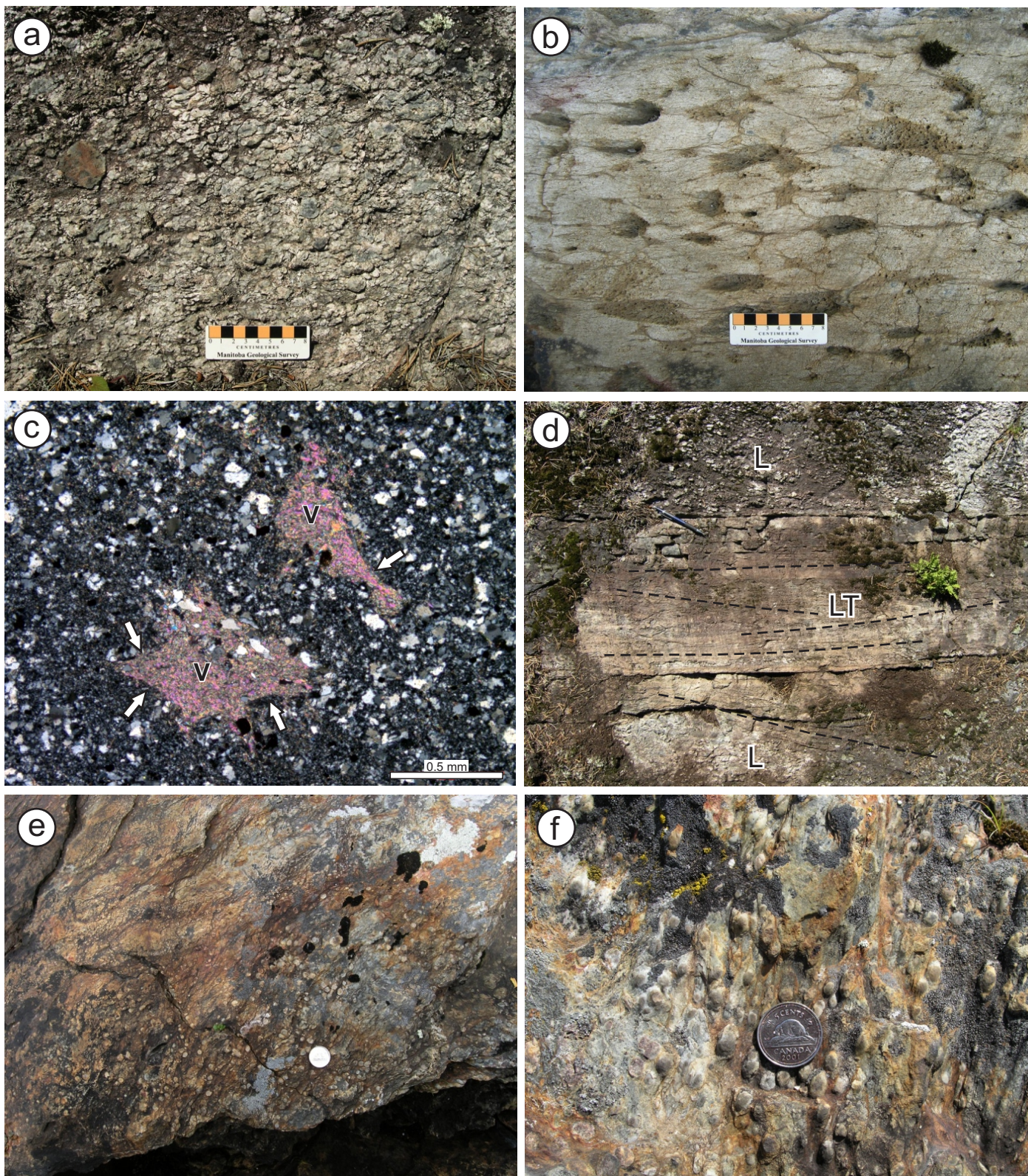


Figure 19: Outcrop and thin-section photographs of rocks from subunit Gw4a: **a)** rhyolitic lapillistone, with minor clasts of dark green-brown aphyric andesite or basalt, central peninsula in Gem Lake; **b)** rhyolitic lapilli tuff with partially collapsed pumice lapilli, southeastern Gem Lake; **c)** photomicrograph (cross-polarized light) of ash-sized juvenile vitriclasts (V), replaced by white mica, in rhyolitic tuff, southeastern Gem Lake; note well-preserved cusped margins (arrows); **d)** interlayered rhyolitic lapillistone (L) and thin-bedded lapilli tuff (LT), central peninsula in Gem Lake; faint low-angle crossbeds (dashed lines) in the lapilli tuff layer are suggestive of pyroclastic surge deposits; **e)** possible accretionary lapilli (light-coloured nodules) in bedded rhyolitic tuff and lapilli tuff, small island on west side of central peninsula in Gem Lake; **f)** detail of Figure 19e.

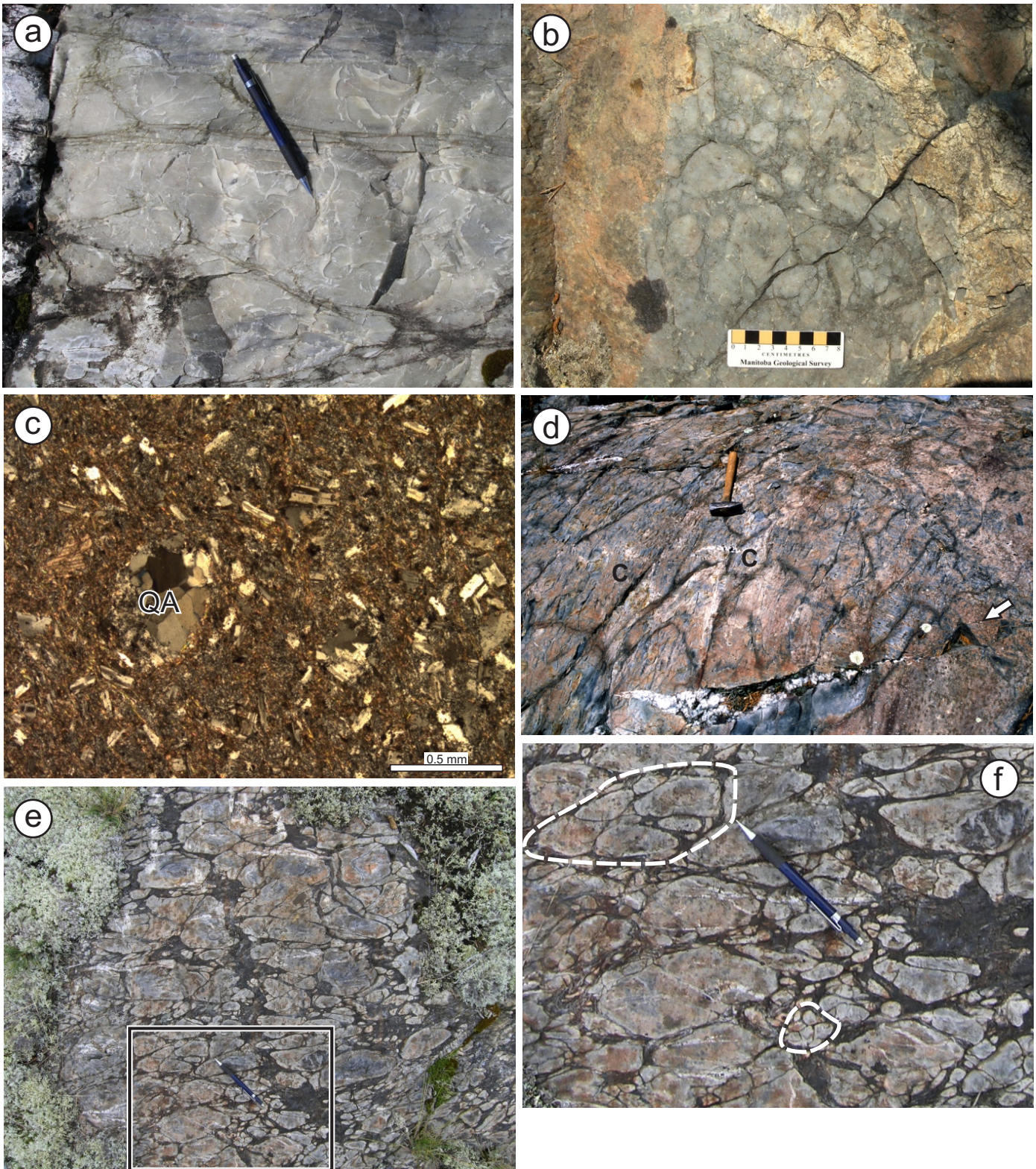


Figure 20: Outcrop and thin-section photographs of rocks in subunit Gw4b: **a)** coherent, faintly flow-banded rhyolite with prominent conchoidal fracture, central Gem Lake; **b)** brecciated rhyolite, central peninsula in Gem Lake; **c)** photomicrograph (cross-polarized light) of coherent rhyolite with well-preserved primary texture defined by feldspar microlites and round quartz amygdules (QA), east limb of Beresford Lake anticline (BLA); **d)** weakly deformed columnar jointing in amygdaloidal rhyolite flow (polygonal columns indicated by C; quartz amygdule indicated by arrow), same location as previous photo; **e)** pseudobreccia texture produced by fracture-controlled sericite alteration (greenish brown) of coherent rhyolite, west limb of BLA; note rounded yet interlocking aspect of the pseudoclasts, which can only result from in situ alteration along fractures; **f)** detail of previous photo, showing rounded pseudoclasts (outlined) with internal jigsaw fit texture.

domes are massive to very faintly flow banded, whereas brecciated flows or domes consist of closely packed, locally interlocking blocks of coherent rhyolite and dacite; some contain sparse (<5%) round quartz amygdules (Figure 20c). A distinctive flow of amygdaloidal rhyolite on the east limb of the BLA contains well-developed columnar jointing (Figure 20d). The flows are commonly associated with disseminated to fracture-controlled sericite±pyrite alteration that is evidenced by patchy gossan on outcrop surfaces and local false-fragmental (Allen, 1988) or pseudobreccia textures (Figure 20e, f).

On the central peninsula in Gem Lake, the fault-bounded panel of the West association includes a distinctive flow-banded dacite that is described as subunit Gw4c. This flow is at least 100 m thick; external contacts are not exposed. The dacite is light grey to buff on weathered surfaces and dark grey on fresh surfaces (Figure 21a, b). It contains sparse (<5%) euhedral phenocrysts of plagioclase and amphibole up to 4 mm in length. The amphibole phenocrysts are replaced by carbonate and thus form recessive pits on weathered outcrop surfaces. The flow banding is defined by light grey siliceous bands less than 10 cm in thickness that alternate with dark greenish-grey or brown sericitic bands typically less than 1.5 cm in thickness. In thin section, the sericitic bands contain isolated to coalesced spheroidal patches of microgranular quartz, feldspar and opaque minerals that possibly represent recrystallized spherulites. Contacts between the bands are gradational over 1–5 mm. The flow bands are locally very planar and laterally continuous in individual outcrops, and thus superficially resemble sedimentary beds. However, these rocks lack any other indication of a sedimentary origin, such as size-grading, and the flow banding is contorted in places. Flow-banded clasts are not observed in the adjacent volcanoclastic rocks of unit Gw4e, perhaps indicating that this dacite was emplaced as a very high level intrusion or cryptodome.

Subunit Gw4d consists of a thickly layered succession of rhyolitic crystal-lithic tuff and lapilli tuff, with minor tuff breccia and breccia, which are readily distinguished from adjacent rocks by their high abundance of quartz phenocrysts. These

rocks are the source of the 2722 ± 2 Ma U-Pb zircon age reported by Davis (1994). This subunit trends north-northeast along the eastern shoreline of the central peninsula in Gem Lake and has an exposed thickness of approximately 150 m. It is at least partially structurally bounded to the east and is overlain to the west by heterolithic lapilli tuff and lapillistone of subunit Gw4e. The internal layering dips steeply west and is defined by variations in the content and size of quartz phenocrysts, lithic clasts and fiamme (Figure 22a). Individual layers range up to 5 m thick and are monolithic, poorly sorted, matrix to clast supported, and nonstratified to very crudely stratified. Layer contacts vary from sharp to gradational and are planar to deeply scoured. The rocks weather buff to grey-white and are dark grey on fresh surfaces. They contain subhedral to anhedral phenocrysts (1–3 mm) of quartz (up to 15%) and plagioclase (up to 3%) in a microgranular groundmass of quartz, plagioclase, biotite, chlorite and carbonate (Figure 22b). In thin section, lithic clasts are slightly coarser grained than the matrix, but contain fewer and smaller phenocrysts. These clasts are angular to subrounded and range up to 25 cm across. The fiamme are dark grey to brown, highly elongate (up to 5 cm) and wispy, with ragged terminations, and are aligned subparallel to layer contacts. They appear to be concentrated (up to 45%) near the upper contacts of some layers and are partially coalesced in these locations (Figure 22a, c). In other layers, the fiamme are isolated and evenly distributed. In thin section, they consist of very fine grained sericite, chlorite and biotite, with minor quartz and plagioclase, and rare feldspar spherulites (<1 mm; Figure 22b, d). The fiamme are interpreted to represent welded, devitrified and recrystallized pumice; the partially coalesced fiamme are interpreted to result from the fusing together of pumice during welding. In the southernmost exposure of this subunit, the crystal-lithic lapilli tuff also contains rare lithophysae and partially coalesced spherulitic aggregates (Figure 22e, f). The lithophysae range up to 3 cm across and have well-preserved internal structures that include concentric banding and central vugs lined with fibrous crystals (Figure 22e). Lithophysae only form during high-temperature devitrification of coherent glass and are thus a reliable indicator

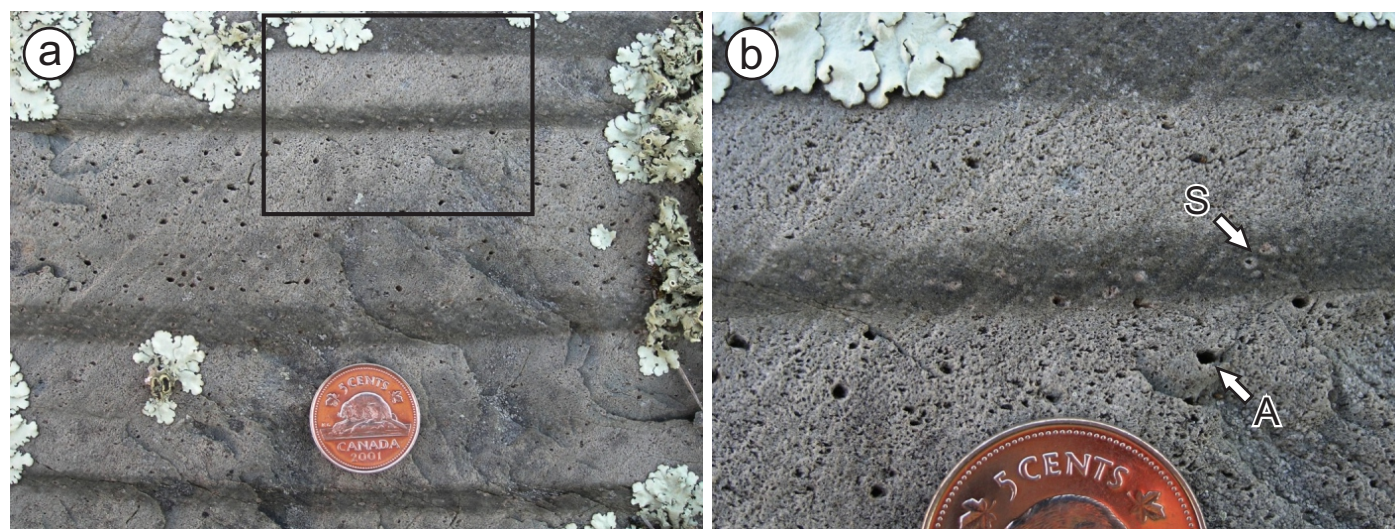


Figure 21: Outcrop photographs of flow-banded dacite of subunit Gw4c from the southern tip of the central peninsula in Gem Lake: **a)** alternating siliceous (light grey) and sericitic (darker greenish-grey) bands; note gradational contacts between bands; **b)** detail of Figure 21a, showing spheroidal patches (S) in the sericitic bands and recessively weathered amphibole phenocrysts (A) in the siliceous bands.

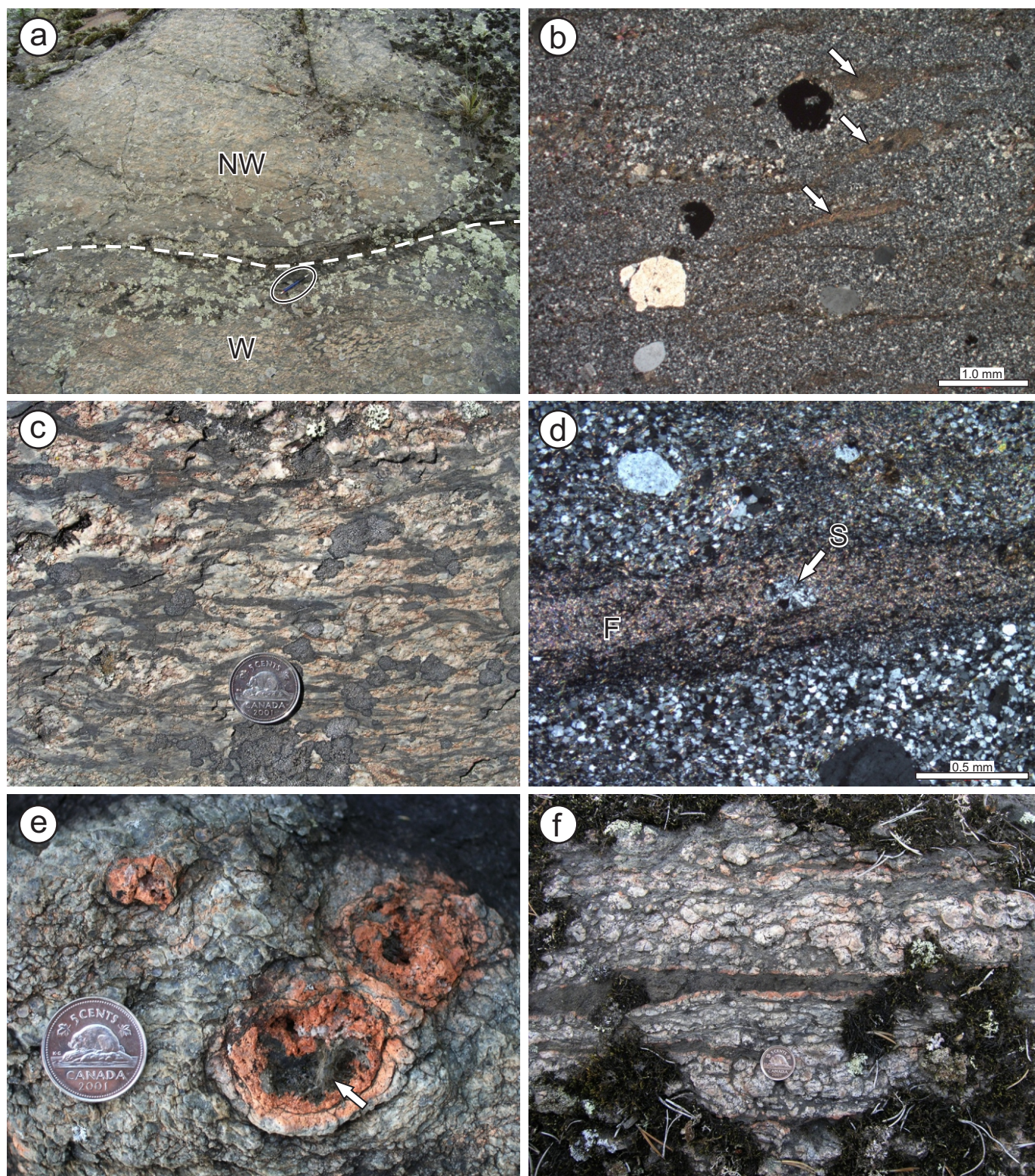


Figure 22: Outcrop and thin-section photographs of rocks in subunit Gw4d, southeastern shoreline of the central peninsula in Gem Lake: **a)** sharp depositional contact (dashed line) between welded (W) and nonwelded (NW) ignimbrite (see text for discussion); younging direction is toward the top of the photo; pencil for scale (circled); **b)** photomicrograph of crystal-lithic lapilli tuff showing anhedral, partially resorbed phenocrysts of quartz in a recrystallized groundmass of feldspar, quartz and phyllosilicate minerals; fiamme (indicated by arrows) consist of very fine grained sericite, chlorite and biotite (cross-polarized light); **c)** welded ignimbrite composed of dark grey-brown, partially coalesced fiamme in a matrix of crystal-lithic lapilli tuff, same outcrop as shown in Figure 22a; fiamme are aligned parallel to layer contacts; **d)** photomicrograph (cross-polarized light) of a fiamme (F) composed of very fine-grained phyllosilicate minerals and rare feldspar spherulites (S); **e)** lithophysae in quartz-phyric lapilli tuff; the central vug in the largest lithophysis is lined by pale green fibrous crystals (arrow) of an unidentified mineral; pink colouration may be due to thermal oxidation, which would provide further evidence for high-temperature emplacement; **f)** partially coalesced spherulitic aggregates (white) and fiamme (dark brown) in quartz-phyric lapilli tuff; note patchy pink colouration of the spherulitic aggregates.

of welding in primary pyroclastic deposits (McPhie et al., 1993). On this basis, subunit Gw4d is interpreted to represent a partially welded rhyolitic ignimbrite and was therefore most likely emplaced in a subaerial setting.

The welded ignimbrite of subunit Gw4d is overlain to the west by a thick succession of heterolithic to monolithic lapilli tuff and lapillistone of subunit Gw4e. The contact is exposed in two locations and is marked by a 5–10 m thick interval of planar-bedded or diffusely layered tuff and lapilli tuff (Figure 23a). Scours, compound (reverse to normal) size-grading and a local abundance of accretionary lapilli (Figure 23b) in this interval are suggestive of pyroclastic surge deposits. Subunit Gw4e is best exposed along the southern and western shorelines of the central peninsula in Gem Lake, where it appears to be 400–500 m thick. It is locally interstratified with rhyolitic volcanoclastic rocks of subunit Gw4a and flows/domes of subunit Gw4b, and is intruded by the rhyolite intrusion breccia of unit Gw5. It is distinguished from similar volcanoclastic rocks in subunit Gw4a on the basis of its more diverse clast populations, distinctly chloritic matrix and the apparent absence of fiamme. The lapilli tuff and lapillistone weather greenish grey to brown and are dark green-grey on fresh surfaces; they are typically poorly sorted, clast supported and nonstratified. The monolithic variants consist mostly of light greenish-grey, aphyric to sparsely plagioclase- or quartz-phyric dacite clasts (Figure 24a), whereas the heterolithic variants include clasts of aphyric basalt, with or without subordinate clasts of black or white aphyric rhyolite, quartz-phyric rhyolite, plagioclase-phyric andesite or leucogabbro (Figure 24b). The clasts (<3 cm) are equant and typically subangular to subrounded. The matrix consists of fine-grained feldspar, quartz, chlorite, sericite, carbonate and opaque minerals (pyrite, rutile), and contains up to 40% subhedral crystals of plagioclase (<3 mm). On the basis of the heterolithic clast population, slightly higher degree of clast

rounding and nonstratified aspect, this subunit is interpreted to represent subaerial, high-density, mass-flow deposits.

Well-stratified epiclastic and volcanoclastic rocks of subunit Gw4f are exposed on three islands in the central portion of Gem Lake. In each of these localities, the subunit includes intervals of thin-bedded, buff to light grey volcanic sandstone and siliceous mudstone, and is situated in the immediate stratigraphic footwall of the rhyolite lava flow of unit Gw6. It also contains, and is underlain by, zones of weak to moderate sericite±pyrite alteration, which locally intensify into 4–5 m thick zones of strongly gossanous quartz-sericite-pyrite phyllonite.

In the easternmost locality, this subunit is approximately 35–40 m in thickness and separates pale greyish-white coherent rhyolite of subunit Gw4b on the northeast from dark grey flow-banded rhyolite of subunit Gw6a on the southwest. Here, the base of the subunit is marked by a 1.5 m thick interval of thin-bedded siliceous sandstone and mudstone, which dips steeply to the southwest. This interval is overlain, in turn, by 4 m of crudely stratified lapilli tuff and 15–20 m of monolithic rhyolite breccia that appears to have been derived from the underlying coherent rhyolite. The base of the lapilli tuff contains angular rip-up clasts of the underlying mudstone and is deeply scoured (Figure 25a).

In the central locality, this subunit is at least 40 m in thickness and overlies coherent rhyolite of subunit Gw4b; the upper contact is not exposed. Here, the subunit appears to consist of two coarsening-upward cycles. The base of each cycle consists of thinly interbedded siliceous mudstone and fine-grained volcanic sandstone (Figure 25b), whereas the top is composed of medium- to coarse-grained, pebbly volcanic sandstone with minor interbeds of siliceous mudstone. Bed contacts are locally disrupted by load structures, but are typically sharp and planar. Normally graded sandstone beds up to 50 cm in thickness have

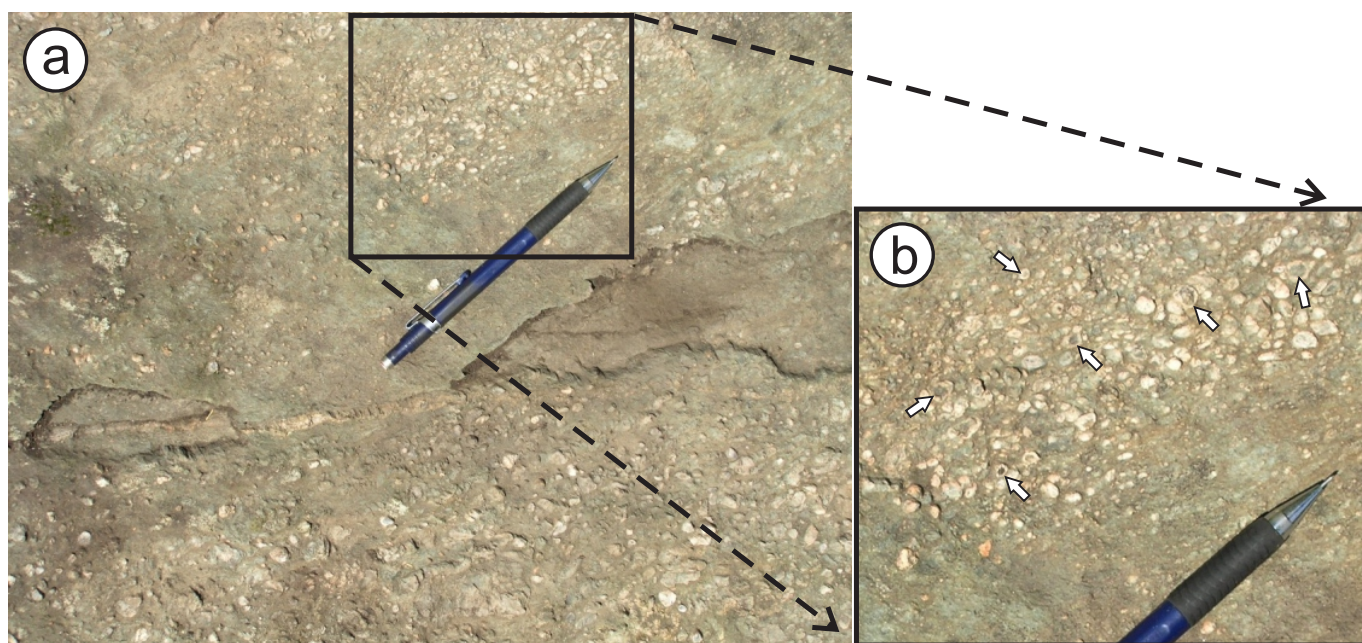


Figure 23: Outcrop photographs of interlayered tuff and lapilli tuff at the base of subunit Gw4e, southeast shoreline of the central peninsula in Gem Lake: **a)** crudely bedded heterolithic lapilli tuff and chloritic tuff; **b)** detail of Figure 23a, showing abundant cored lapilli (indicated by arrows).

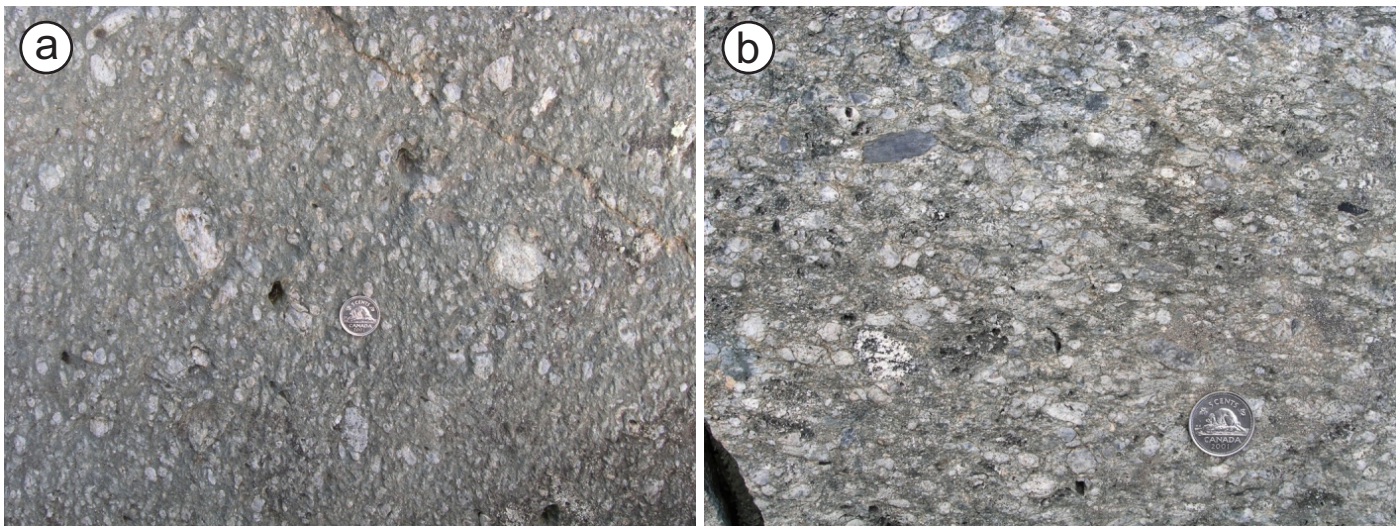


Figure 24: Outcrop photographs of rocks in subunit Gw4e: **a)** monolithic lapilli tuff composed of aphyric to sparsely plagioclase-phyric clasts of dacite or rhyolite in a chloritic tuff matrix, south end of the central peninsula in Gem Lake; **b)** heterolithic lapillistone, west side of the central peninsula in Gem Lake.

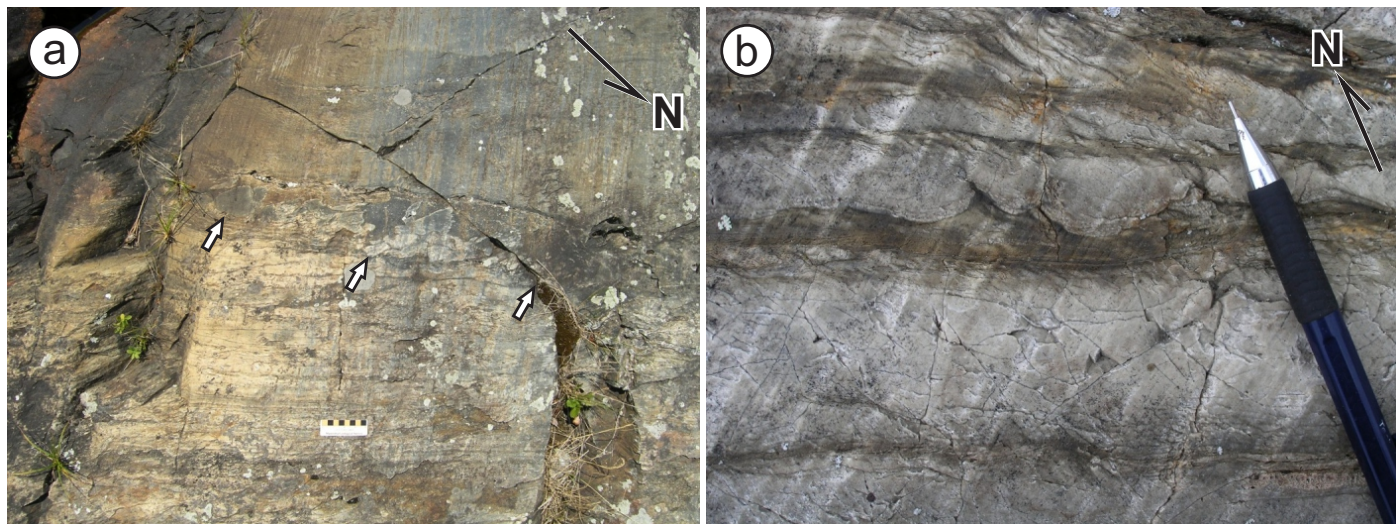


Figure 25: Outcrop photographs of rocks from subunit Gw4f, central Gem Lake: **a)** thin-bedded siliceous sandstone and mudstone (bottom) overlain by crudely stratified lapilli tuff (top), eastern locality; scoured contact (arrows) is marked by large rip-ups of the underlying sedimentary rocks; younging direction is toward the southwest; **b)** normal size-grading and load structures in thin-bedded siliceous sandstone and mudstone, central locality; younging direction is toward the northeast; see text for discussion.

scoured basal contacts and locally contain large mudstone rip-ups, indicating that they were deposited from turbidity currents. Laminated interbeds (<50 cm) of black siliceous mudstone in the upper cycle indicate periodic intervals of sediment starvation in a marine setting. Bedding in this locality generally trends west-northwest, dips steeply to the north and is overprinted by tight S-folds. Abundant younging criteria establish tops to the north. Hence, the central and eastern localities are situated on opposite limbs of a tight macroscopic anticline that trends parallel to the southwest shoreline of Gem Lake (Figure 3).

The western locality consists of similar rock types, but is intensely transposed on the west limb of the anticline. Subunit Gw4f was likely deposited in a relatively quiescent marine setting, during a hiatus in rhyolitic volcanism. The associated sericite-pyrite alteration indicates that deposition may have been

accompanied by seafloor hydrothermal circulation, and thus suggests potential for volcanic-associated base-metal sulphide deposits in this subunit.

Rhyolite intrusion breccia (unit Gw5)

Rhyolite intrusion breccia of unit Gw5 is restricted to the large peninsula in central Gem Lake, where it is traced in a northerly direction along strike for a distance of 3 km and ranges up to approximately 400 m thick. The unit is truncated to the north by the Beresford Lake shear zone and is bisected into northern and southern portions by a subsidiary splay of this structure. Included in this unit are rocks described by Weber (1971a) as rhyodacitic tuff breccia, rhyolite agglomerate and felsite of the Banksian Lake formation of the Gem Lake subgroup, and a small stock of differentiated and altered quartz diorite;

these were collectively interpreted to represent a ‘volcanic vent’ complex. The intrusion breccia is defined herein to include two components, aphanitic rhyolite and biotite leucogranite, that are not divisible at 1:20 000 scale. External contacts are irregular and generally discordant to stratification in the volcanoclastic country rocks (unit Gw4), indicating emplacement as a hypabyssal intrusion or cryptodome(s).

The rhyolite (Figure 26a) weathers light pinkish or greyish white and is light grey on fresh surfaces. It contains sparse subhedral phenocrysts of pinkish-white feldspar and blue quartz (1–4%; <2 mm) in a microgranular groundmass of quartz, feldspar and minor biotite. Some specimens also contain blocky inclusions or very coarse phenocrysts (up to 10 cm) of opalescent blue quartz. The rhyolite has a jigsaw-fit breccia texture that appears to grade locally into irregular bodies of massive to faintly flow-banded coherent rhyolite. The associated biotite leucogranite (Figure 26b) weathers light greyish pink and is pinkish grey on fresh surfaces, with a fine- to medium-grained equigranular texture defined by interlocking crystals of pinkish-white feldspar (65–85%), blue quartz (10–20%), biotite (5–10%) and accessory magnetite (1–3%). Opalescent quartz

locally forms irregular veinlets or blebs up to 10 cm in the longest dimension. In most outcrops, the biotite leucogranite and aphanitic rhyolite constitute an intrusion breccia, with blocky jigsaw-fit inclusions of rhyolite in a leucogranite matrix (Figure 26c); this rock type corresponds to the ‘rhyolite agglomerate and felsite’ of Weber (1971a). In others, the leucogranite contains subordinate, though still abundant, blocky inclusions of the aphanitic rhyolite, with minor inclusions of dark green aphyric basalt.

In its central portion, the intrusion breccia is locally characterized by high-temperature alteration assemblages of the type associated with some intrusion-related (e.g., porphyry or epithermal) mineral systems. This alteration consists of patchy zones of weak to moderate sericite-pyrite, K-feldspar or biotite-magnetite±epidote alteration, with or without sheeted quartz±magnetite±actinolite±epidote±K-feldspar±chlorite±pyrite±chalcopyrite veins (Figure 26d). The magnetite-rich alteration is unique to unit Gw5 and is clearly delineated by high-resolution aeromagnetic data. Trace-element profiles for representative samples of altered rhyolite and leucogranite are likewise unique in that they vary from relatively flat to markedly concave

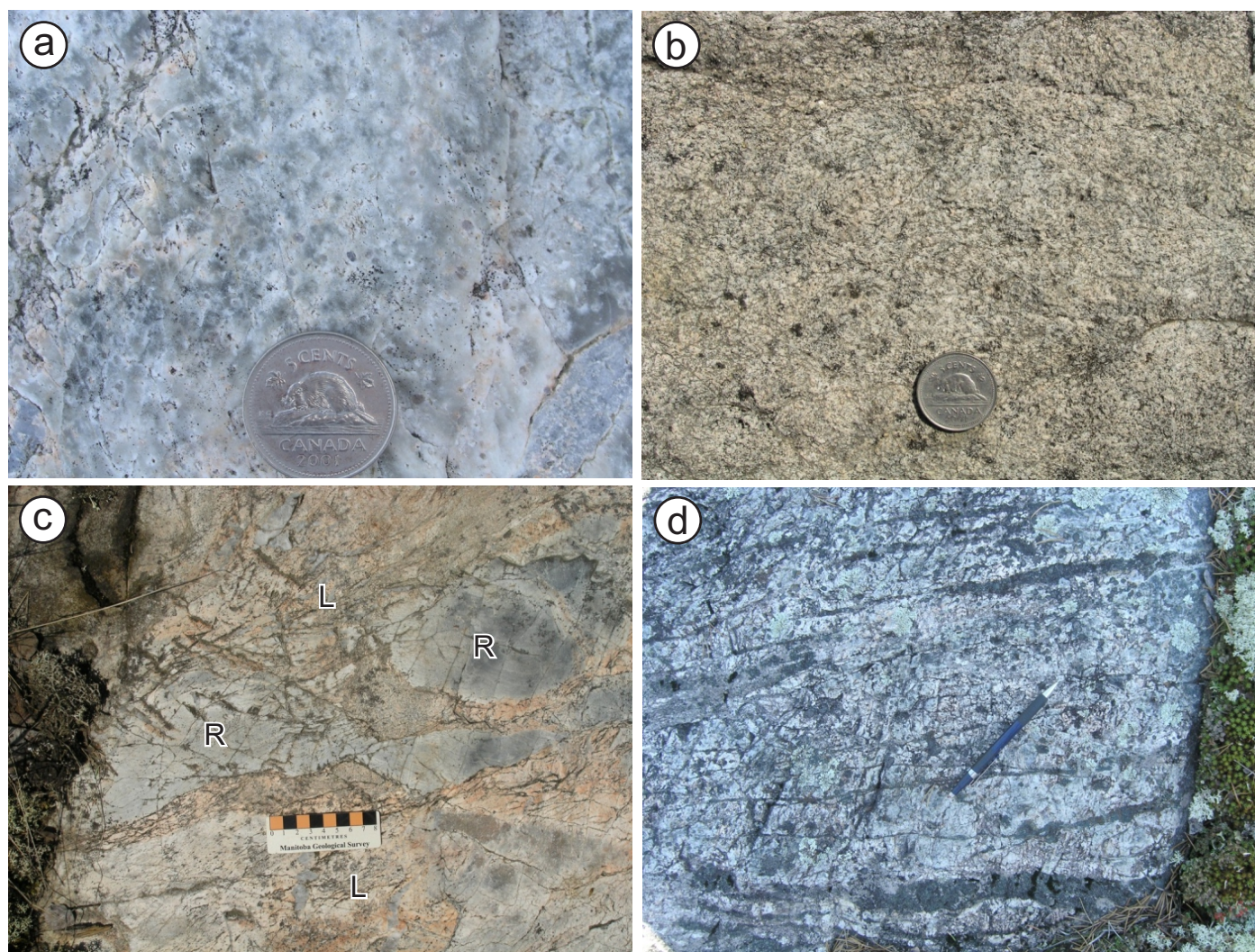


Figure 26: Outcrop photographs of rocks in unit Gw5, central peninsula in Gem Lake (Figure 26a, b and c are from the central portion of the northern body of the intrusion, whereas Figure 26d is from the central portion of the southern body): **a)** quartz-feldspar-phyric rhyolite; **b)** leucogranite; **c)** intrusion breccia of rhyolite (R) in leucogranite (L); **d)** sheeted actinolite veins and patchy actinolite-epidote-magnetite alteration in rhyolite.

upward, and show evidence of significant decoupling of the high-field-strength elements from the light rare-earth (LREE) and middle rare-earth (MREE) elements. As described in the 'Lithogeochemistry' section, this decoupling is interpreted to result from selective removal of LREE and MREE during a transient episode of high-temperature hydrothermal alteration, which most likely accompanied emplacement of the hypabyssal intrusion or cryptodome.

High-SiO₂ rhyolite (unit Gw6)

Unit Gw6 is exposed along the southwest shore of Gem Lake and on adjacent small islands, where it was mapped over a strike length of 4 km (Figure 3). It defines a prominent lenticular body that ranges up to 400 m thick in its central portion and grades outward from coherent flow-banded rhyolite in the interior (subunit Gw6a), through an inner margin of rhyolitic breccia, tuff breccia and lapilli tuff (subunit Gw6b), to a relatively thin outer margin of derived volcanic conglomerate, sandstone and mudstone (subunit Gw6c). A fault-bounded section of this unit is also exposed on the large island in the central portion of the lake. The character and arrangement of the subunits in the main body indicate an analogy to the characteristic volcanic facies of silicic lava flows or domes emplaced in shallow-subaqueous settings (Figure 27), which ideally progress outward from proximal coherent lava, through a medial carapace of viscous flow breccia and quench-fragmented in situ hyaloclastite, to a distal apron of resedimented hyaloclastite (e.g., McPhie and Allen, 1992; McPhie et al., 1993; Stewart and McPhie, 2006). Comparable facies have been described for subaqueous rhyolite flows and domes in Archean (de Rosen-Spence et al., 1980; Lafrance et al., 2000) and Paleoproterozoic (Ayres and Pelouin, 2000) greenstone belts.

Subunit Gw6a defines the proximal interior facies of the lava flow and consists mostly of coherent flow-banded high-SiO₂ rhyolite (75–78 wt. % SiO₂), which is traced along strike for 2 km and ranges up to 200 m thick. The coherent rhyolite weathers light grey and is dark grey to black on fresh surfaces, with a prominent conchoidal fracture (Figure 28a). It is typically aphanitic and aphyric, although some specimens contain very sparse (<1%) feldspar and quartz phenocrysts up to 2 mm. Flow banding is ubiquitous and varies from relatively regular to highly contorted. A lobe of coherent flow-banded rhyolite at least 30 m in thickness also occurs stratigraphically above the main flow within rhyolitic breccia, tuff breccia and lapilli tuff of the in situ hyaloclastite facies; this lobe is exposed on the south tip of the large island near the southeast end of the main flow. High-SiO₂ rhyolite lavas of the type described here are a good indication of proximity to the source vent, in that they are generally of small volume and are unlikely to travel more than 3–4 km (Cas and Wright, 1987).

Although contact relationships are obscured by overburden, the coherent lava facies is presumed to grade outward into breccia, tuff breccia and lapilli tuff of the in situ hyaloclastite facies (subunit Gw6b). These coarse volcanoclastic rocks are unsorted, matrix to clast supported and nonstratified, and range up to 50 m thick in continuous exposures. The breccia and tuff breccia consist almost exclusively of very angular to subangular blocky fragments of aphyric flow-banded rhyolite in a matrix of greenish-grey to brown siliceous tuff (Figure 28b). The clasts typically range up to 40 cm across, but outsized clasts up to 1.5 m are present locally. In one outcrop, the size and proportion of clasts progressively decrease upsection (toward the southwest) over 40–50 m. Curviplanar and cusped clast margins and local jigsaw-fit textures in matrix-poor breccias (Figure 28b, c) indicate proximity to flow margins and establish quench

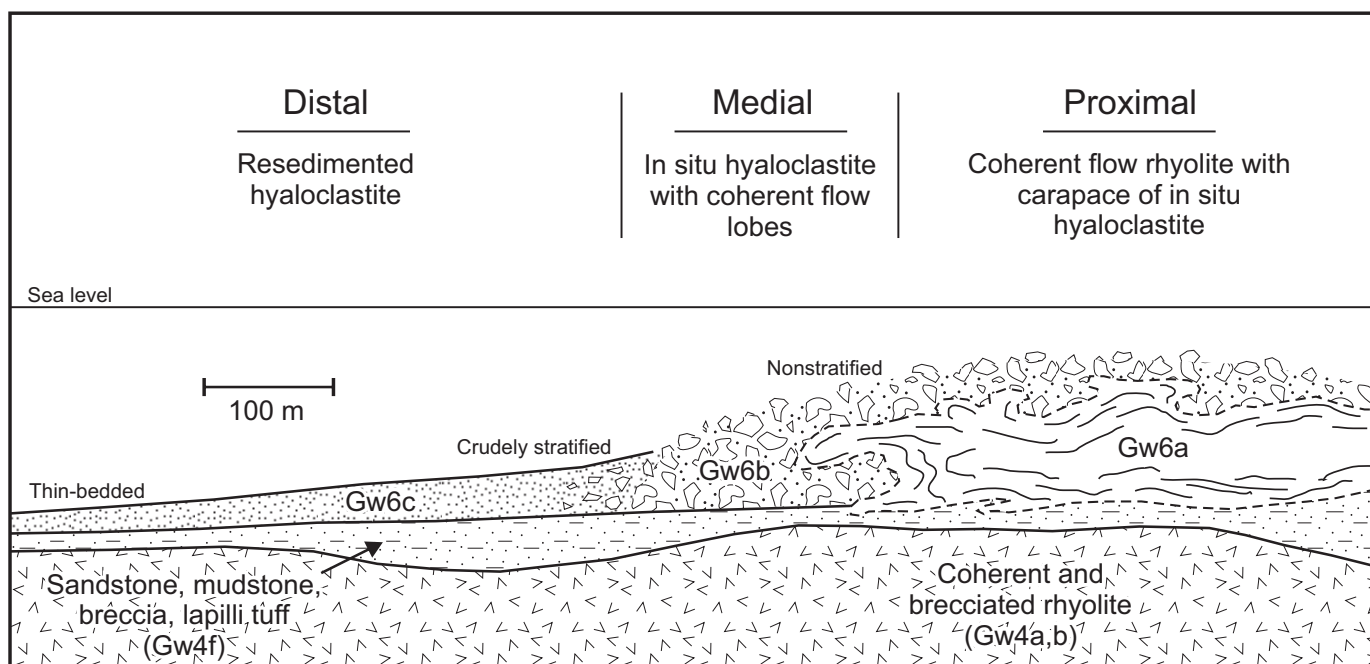


Figure 27: Volcanic-facies model for a shallow-subaqueous rhyolite flow (after McPhie et al., 1993; Stewart and McPhie, 2006), showing the character and arrangement of the constituent rocks and their interpreted correspondence to the various subunits of unit Gw6 in the West association of the Gem assemblage.

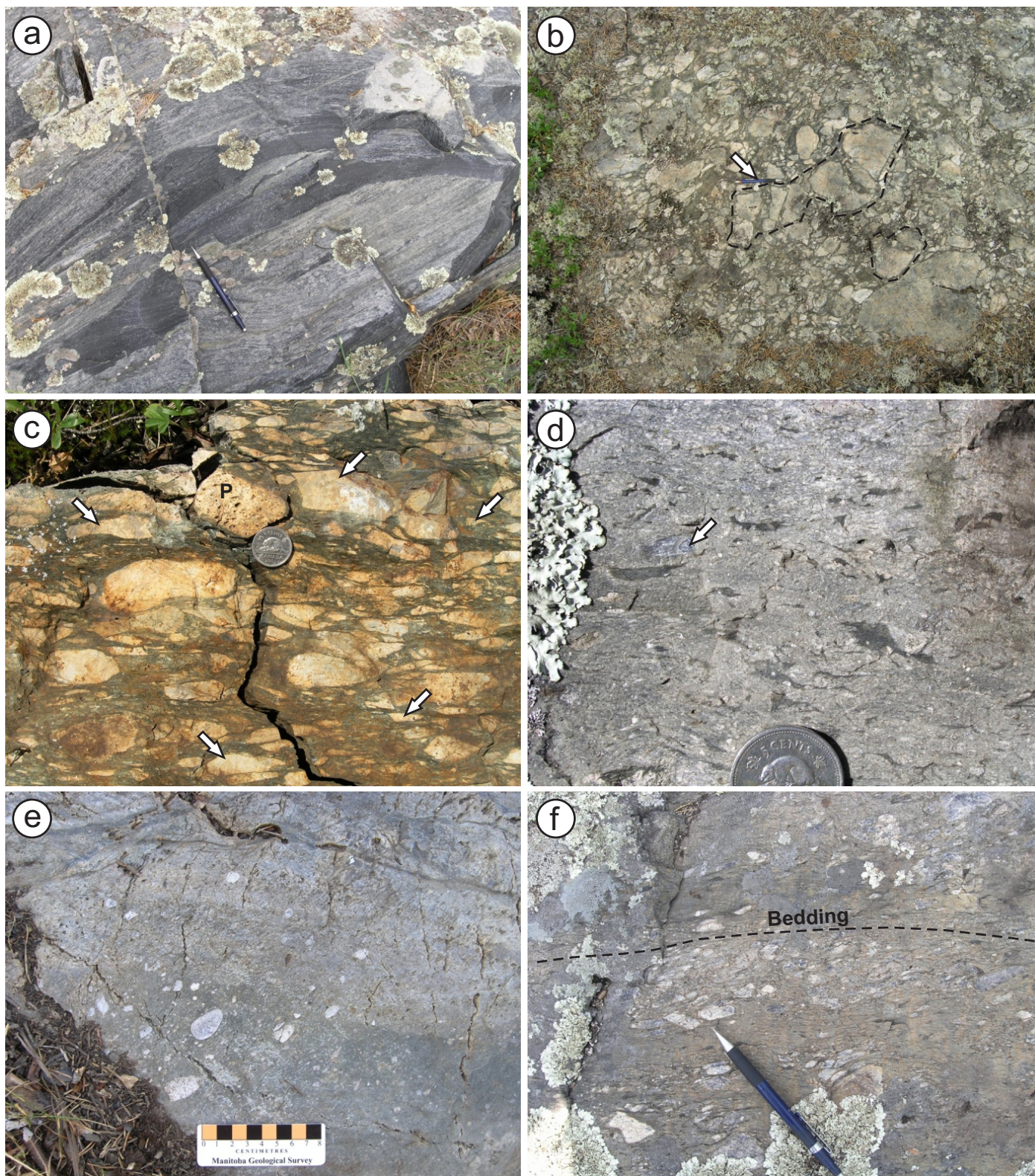


Figure 28: Outcrop photographs of rocks in unit Gw6: **a)** coherent flow-banded rhyolite of the proximal facies, south shoreline of Gem Lake; **b)** nonstratified monolithic breccia of the medial (in situ hyaloclastite) facies, large island in central Gem Lake; jigsaw-fit clasts of flow-banded rhyolite are outlined (pencil for scale indicated by arrow); **c)** lapilli tuff near the top of the medial facies, south shoreline of Gem Lake; note cusped rhyolite clasts (arrows) and intact pumice lapilli (P); **d)** lapilli tuff near the top of the medial facies, small island at south shoreline of Gem Lake; eutaxitic texture defined by abundant grey-brown fiamme (collapsed pumice); includes minor lapilli of flow-banded rhyolite (arrow); **e)** pebbly sandstone of the distal (resedimented hyaloclastite) facies, large island in central Gem Lake; note well-rounded rhyolite clasts; **f)** bedded pebble conglomerate, sandstone and mudstone of the distal facies, small island near south shoreline of Gem Lake; pebbles consist exclusively of flow-banded rhyolite.

fragmentation (\pm autobrecciation) as the dominant mechanism of clast formation. Although completely recrystallized, the tuffaceous matrix is interpreted to represent in situ hyaloclastite, based on the juvenile morphology of the contained lava blocks. Highly elongate to irregular fiamme of dark grey or brown feldspar and quartz-phyric material are a minor component ($<10\%$) of the breccia and tuff breccia, and are interpreted to represent collapsed pumice (Figure 28d). Significant volume loss during compaction is evidenced by the generally higher proportion of phenocrysts in the fiamme as compared to the flow-banded rhyolite clasts. Locally, uncompacted blocks (<40 cm) of pumice contain round quartz or carbonate-filled vesicles up to 3 cm across (Figure 28c); hydrothermal infilling of vesicles shortly after deposition may account for the relatively intact shapes of these blocks.

Lapilli tuff of the in situ hyaloclastite facies consists of shard-like clasts of flow-banded rhyolite, collapsed pumice and scattered crystals of quartz and feldspar in a matrix of fine-grained, light grey to green hyaloclastite tuff. It forms massive layers up to 20 m thick or, more rarely, is crudely stratified. Locally, a well-preserved eutaxitic texture is defined by dark grey fiamme (compacted pumice) that vary in abundance up to 40% and in length up to 15 cm. The fiamme are elongate to irregular and wispy, with ragged terminations. The high abundance of pumice establishes coeval explosive activity, perhaps at the source vent, and is compatible with a shallow-subaqueous eruptive setting.

The in situ hyaloclastite facies grades outward into, and is locally interstratified with, a well-bedded apron of volcanic conglomerate, sandstone and mudstone of the resedimented hyaloclastite facies (subunit Gw6c). This apron of sedimentary rocks ranges up to 50 or 60 m thick in its proximal portions and tapers out along strike to the southeast over 800–1000 m; this unit is thin and discontinuous to the northwest along strike from the coherent rhyolite. The volcanic conglomerate is poorly sorted and matrix to clast supported, and forms diffuse beds up to several metres thick that vary from massive to normally or reversely graded and likely represent debris flows. Pebble- to boulder-sized clasts of flow-banded rhyolite exhibit a higher

degree of rounding than clasts in the in situ hyaloclastite facies. A small proportion of well-rounded and subspherical clasts indicates significant reworking in a subaerial to shallow-subaqueous setting (Figure 28e). Scattered fiamme in these rocks may be the products of coeval explosive (i.e., hydroclastic or pyroclastic) eruptions. Subordinate interlayers of bedded volcanic sandstone and mudstone range up to several metres thick. The sandstone is pebbly and medium to very coarse grained, and forms massive to normally graded beds up to 30 cm thick, with minor ($<10\%$) interbeds of laminated mudstone up to 4 cm thick (Figure 28f). Bed contacts vary from diffuse to sharp and scoured, and are locally disrupted by sediment fluidization structures; these features indicate deposition below wave base via turbidity currents.

Intermediate-felsic crystal-lithic lapilli tuff and tuff (unit Gw7)

Unit Gw7 consists of crystal-lithic lapilli tuff and tuff, with minor tuff breccia, which range in composition from andesite to rhyolite (62–73 wt. % SiO_2). This unit was mapped continuously along strike for 7.0 km adjacent and roughly parallel to the southwest shoreline of Gem Lake, and corresponds to ‘dacitic to rhyodacitic crystal tuff’ on the map of Weber (1971a). Over most of this distance, it ranges from 200 to 350 m thick and defines the top of the Gem assemblage. At the outlet of the Manigotagan River on Gem Lake, this unit is tightly folded by an anticline-syncline fold pair and is disrupted by several high-strain zones; it is approximately 800 m thick in the structurally thickened hinge of the syncline (Figure 3). Unit Gw7 pinches out along strike to the northwest and continues beyond the limit of the mapped area to the southeast. The upper contact is well exposed in several locations and shows a fairly continuous transition over 10–15 m from massive crystal-lithic lapilli tuff to thin-bedded greywacke, mudstone and chert of the Edmunds assemblage.

The crystal-lithic lapilli tuff and tuff weather light green or grey or buff and are darker grey-green on fresh surfaces (Figure 29a). The crystal component consists of sparse ($<15\%$)

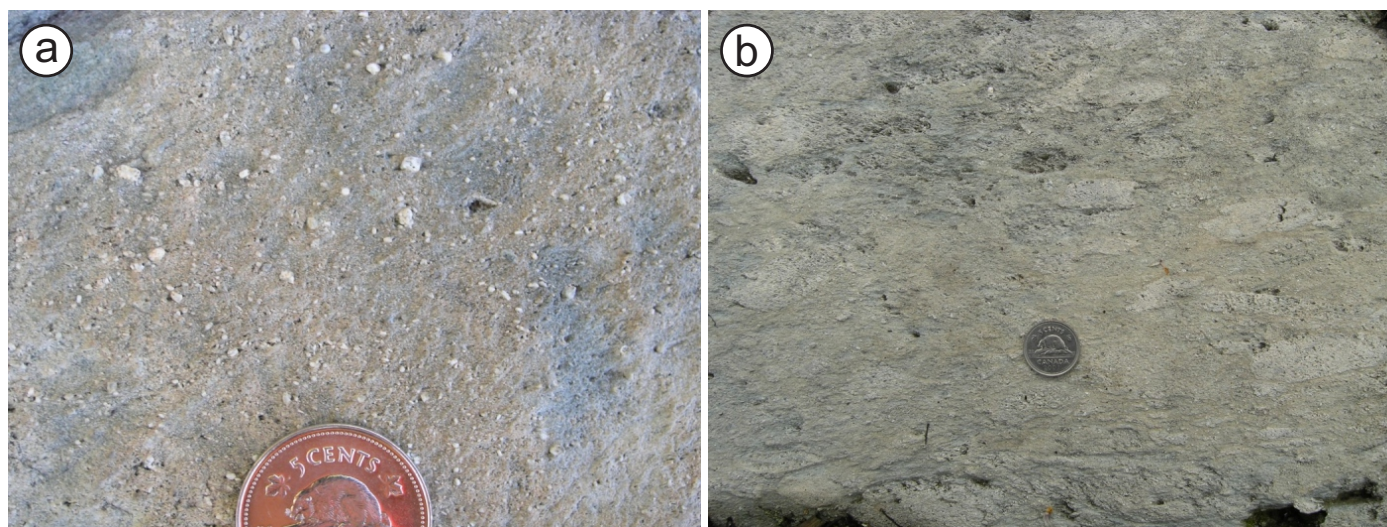


Figure 29: Outcrop photographs of rocks in unit Gw7: **a)** dacitic crystal-lithic lapilli tuff, southern shoreline of Gem Lake; **b)** dacitic tuff breccia, western shoreline of Gem Lake.

phenocrysts of feldspar and quartz that vary in size up to 5 mm and in shape from euhedral to anhedral. Quartz phenocrysts are typically subordinate (1–3%) to feldspar and are finer grained (1–2 mm). The groundmass consists of fine-grained plagioclase, white mica, chlorite, carbonate and epidote-clinozoisite. Lithic clasts (<20 cm) are angular to subrounded, unsorted and matrix supported, and generally account for less than 20% of the rock. The clasts consist mostly of light green-grey feldspar-phyric dacite that is similar in texture to the crystal-tuff matrix, with lesser clasts of dark grey aphyric rhyolite. Some outcrops contain diffuse layers of lapilli tuff or tuff breccia up to 1 m thick (Figure 29b); however, most appear to be very homogeneous and nonstratified. The massive and fragmental aspects of this unit are suggestive of a felsic ignimbrite, in which case the apparent absence of welding or gas segregation features may relate to the subaqueous depositional setting. A sample (96-06-1845) of the crystal-lithic lapilli tuff from the western extent of this unit yielded a U-Pb zircon age of 2727 ± 2 Ma, which is interpreted to approximate the timing of emplacement (see ‘U-Pb geochronology’ section).

Description of rock units – East association

Intermediate–felsic volcanoclastic and epiclastic rocks (unit Ge1)

Intermediate–felsic volcanoclastic and epiclastic rocks of unit Ge1 are the characteristic rocks of the East association of the Gem assemblage. These rocks form a well-stratified succession at least 1000 m thick that includes minor pillowed flows (unit Ge2) and gabbro sills (unit Ge3). Two subunits are recognized. Subunit Ge1a consists of interstratified breccia, tuff breccia and lapilli tuff that appear to represent first-cycle volcanoclastic debris deposited in proximity to an intermediate–felsic volcanic centre. Volcanic conglomerate, sandstone and mudstone of subunit Ge1b reflect variable degrees of reworking of this debris in a subaerial to shallow-subaqueous setting. These subunits are locally interstratified on a scale of metres or tens of metres, and are at least partly gradational. Subunit Ge1b is thickest and most abundant in the southern portion of the unit.

Coarse volcanoclastic rocks (breccia and tuff breccia) in subunit Ge1a are monolithic to slightly heterolithic, unsorted and generally matrix supported, and form diffuse beds up to several metres thick that are massive to crudely stratified (Figure 30a). Very angular to subrounded blocks of light green to grey andesite or dacite dominate and range up to 50 cm across. Most blocks contain 20–30% euhedral phenocrysts of plagioclase (1–5 mm in the longest dimension), although the size and proportion of plagioclase phenocrysts are quite variable from clast to clast and outcrop to outcrop. Heterolithic breccia and tuff breccia contain minor (<5%) fragments of light grey-white, aphyric to sparsely porphyritic (plagioclase±quartz) rhyolite and aphyric amygdaloidal basalt. Some of the rhyolite clasts also contain spherulites up to 2 cm across (Figure 30b). The matrix consists of crystal-lapilli tuff that contains 10–20% subhedral plagioclase crystals in a groundmass of fine-grained feldspar, chlorite, carbonate, epidote-clinozoisite and opaque minerals. Massive interlayers of light green-grey crystal-lapilli tuff range up to several metres thick and contain euhedral to

subhedral, evenly distributed plagioclase crystals (20–75%; 0.5–7.0 mm) in a chloritic tuff matrix, with minor lithic lapilli (<5%; <15 cm; Figure 30c, d). In two locations, these layers are overprinted by fracture-controlled chlorite (±garnet) alteration.

Subunit Ge1b is dominated by pebble to boulder volcanic conglomerate, which is heterolithic and poorly sorted, and varies from matrix to clast supported. Individual beds are typically massive and structureless, with diffuse contacts. The clasts are well rounded to subangular and up to 60 cm across (typically 5–15 cm), and consist of variably plagioclase-phyric dacite and andesite, with minor rhyolite and basalt (Figure 31a). Some beds contain abundant examples of resedimented clasts; however, ‘exotic’ clasts are absent. The conglomerate is thickly interstratified with intervals of thin- to thick-bedded, medium- to coarse-grained, pebbly volcanic sandstone, with minor interbeds of light grey-green volcanic mudstone. The volcanic sandstone contains subhedral plagioclase (5–10%) and quartz (<2%) grains up to 3 mm and forms tabular-planar beds up to 50 cm thick that have sharp scoured bases and show consistent normal size-grading (Figure 31b). The overall features of unit Ge1 are indicative of deposition via debris flows and low-density turbidity currents in the channelled upper portion of a volcanoclastic submarine fan.

Pillowed basalt and andesite flows (unit Ge2)

Pillowed flows composed of calcalkalic amygdaloidal basalt and andesite define lenticular map units up to 100 m thick in the central and northern portions of the East association. The upper and lower contacts of the flow units are nowhere exposed, but are presumed to be depositional, based on the common occurrence of amygdaloidal basalt clasts in the adjacent volcanoclastic and epiclastic rocks of unit Ge1. The basalt and andesite weather light grey to green and are dark green on fresh surfaces. They are typically fine grained and aphyric, with up to 20% round epidote and quartz amygdules (1–10 mm; Figure 32a); some are nonamygdaloidal and/or contain sparse plagioclase phenocrysts (2–3%; <1.5 mm). In thin section, these rocks are composed of fine-grained plagioclase, actinolite, chlorite, epidote-clinozoisite, carbonate, titanite and opaque minerals. The pillows are bun shaped to amoeboid and generally less than 1.5 m in maximum dimension (moderately to strongly flattened), with thin (<1.5 cm) chloritic selvages. One outcrop near the southern extent of this unit contains very large pillows or flow lobes up to 4.5 m long by 1.5 m thick. Most outcrops contain less than 10% interpillow hyaloclastite and patchy zones of moderate to strong epidote alteration (Figure 32b). The pillowed flows are locally intercalated with 1–3 m thick layers of flow breccia or bedded hyaloclastite. Massive flows are apparently lacking.

Gabbro (unit Ge3)

Dikes and sills of gabbro are a common component of outcrops of unit Ge1 in the northern and southern portions of the East association. The dikes are typically less than 1.5 m thick and composed of dark green melanocratic gabbro with a fine- to medium-grained, equigranular subophitic texture defined by plagioclase laths (45–60%; <1.5 mm) in a groundmass of actinolite, chlorite, plagioclase, epidote, carbonate and opaque

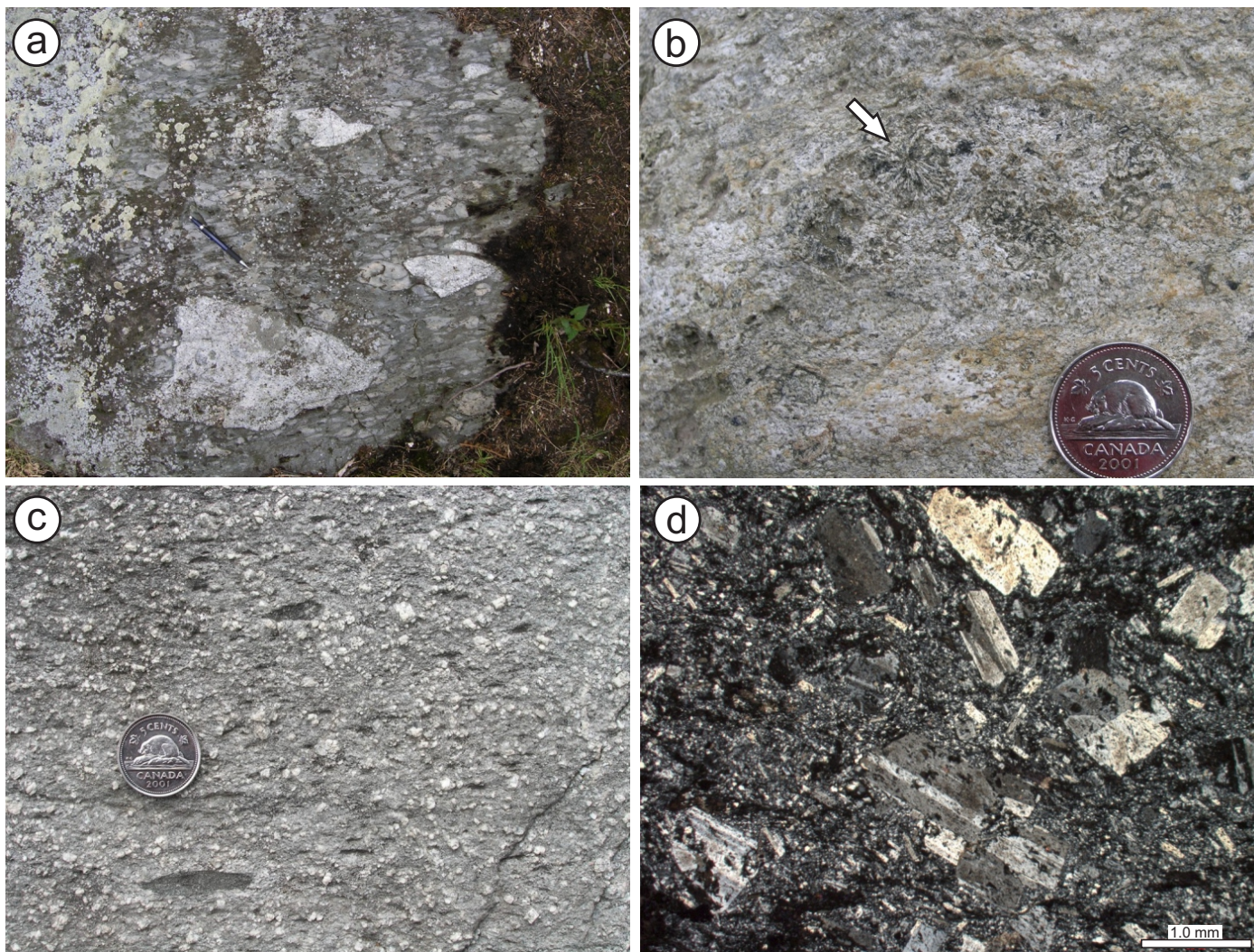


Figure 30: Outcrop and thin-section photographs of rocks in subunit Ge1a, eastern shoreline of Gem Lake: **a)** heterolithic tuff breccia, showing outsized angular clasts of light grey porphyritic andesite (pencil for scale just above large clast); **b)** spherulitic rhyolite clast in heterolithic tuff breccia; **c)** crystal-lithic lapilli tuff composed of blocky plagioclase crystals and dark grey lithic clasts in a crystal-tuff matrix; **d)** photomicrograph (cross-polarized light) of the crystal-lithic lapilli tuff in Figure 30c, showing coarse euhedral plagioclase phenocrysts in finer grained crystal-tuff matrix.

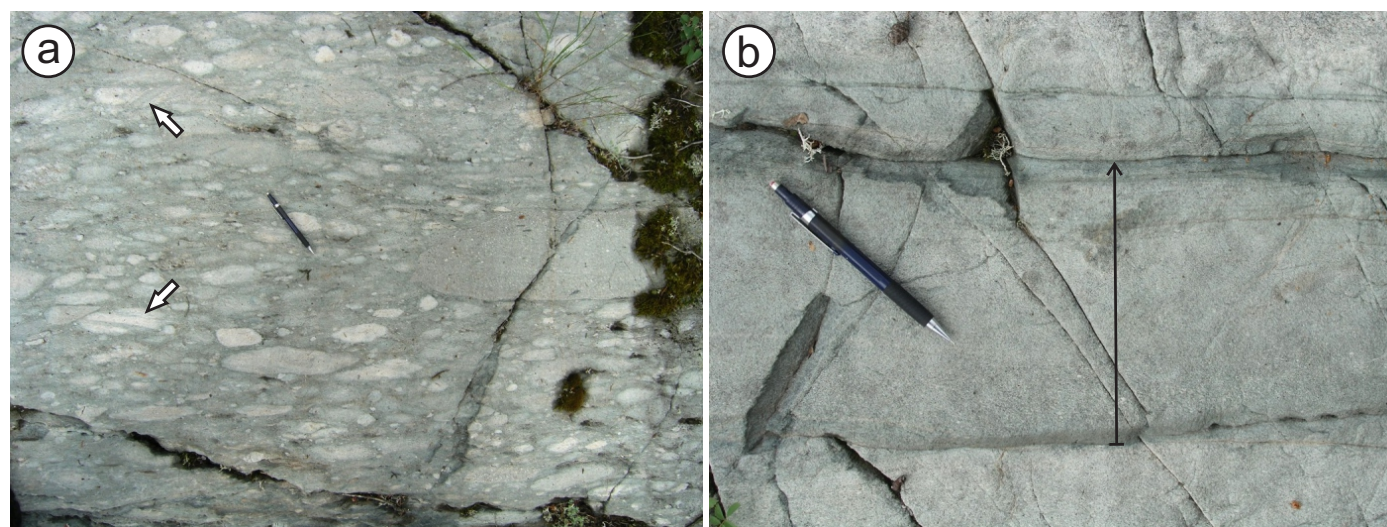


Figure 31: Outcrop photographs of rocks in subunit Ge1b, eastern shoreline of Gem Lake: **a)** heterolithic volcanic conglomerate; note high proportion of rounded clasts and resedimented clasts (arrows); **b)** normally graded bed of volcanic sandstone (indicated by black arrow); younging direction is toward the top of the photo.

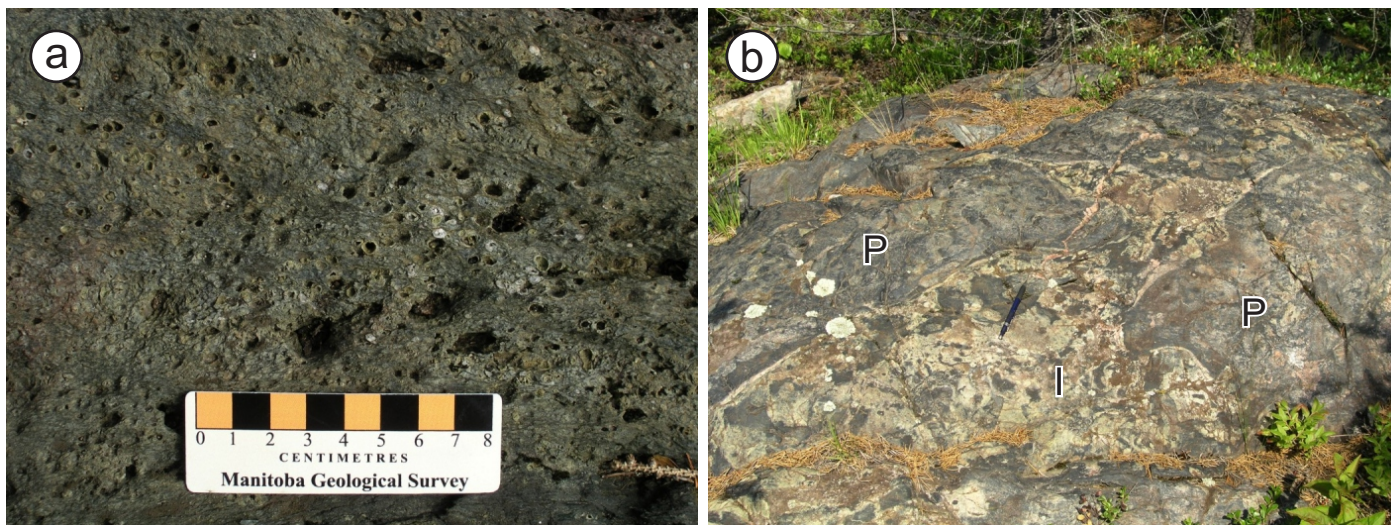


Figure 32: Outcrop photographs of pillowed andesite and basalt flows of unit Ge2: **a)** abundant quartz-epidote amygdules in andesite pillow core, large island in the central portion of the East association; **b)** epidotized hyaloclastite in the interstices (I) between large basalt pillows (P), inland outcrop near the northern extent of the East association.

minerals; this gabbro is typically strongly magnetic. The sills range up to approximately 100 m thick and tend to be internally heterogeneous, with irregular zones and patches of medium- to coarse-grained pyroxenite or ophitic-textured leucogabbro (60–75% plagioclase; 2–3% quartz). Most outcrops contain patchy epidote alteration. One outcrop on the north shoreline of the eastern bay of Gem Lake is an intrusion breccia composed of angular fragments of leucogabbro in a matrix of melanocratic gabbro and pyroxenite.

Quartz-feldspar porphyry granite (unit Ge4)

Unit Ge4 consists of a large pluton of quartz- and feldspar-phryic granite that crops out extensively in the area east of Gem Lake. The contact is not exposed; however, a 40–50 m wide aureole of hornfels in adjacent volcanoclastic and epiclastic rocks of unit Ge1 indicates an intrusive relationship. This pluton is truncated to the northeast by the Beresford Lake shear zone and is thus structurally separated from adjacent granitoid intrusive rocks of the Wanipigow River plutonic complex. Litho-geochemical data indicate a close affinity to rhyolite flows of units Gw4 and Gw6 in the West association of the Gem assemblage. Hence, this pluton is described here as part of the volcanic stratigraphy, rather than as part of the Wanipigow River plutonic complex (see below).

The granite weathers light grey to pink and is greenish grey to pink on fresh surfaces (Figure 33). It is typically characterized by a seriate-porphyrific texture defined by subhedral phenocrysts (20–45%; 2–5 mm) of blue-grey quartz in a fine- to medium-grained groundmass of K-feldspar, plagioclase and quartz, with accessory (<5%) biotite, magnetite, chlorite, epidote, white mica and rutile. The K-feldspar and quartz commonly display myrmekitic textures; some specimens also contain pink K-feldspar phenocrysts (10–15%; 2–5 mm). Most outcrops are very homogeneous and massive; crosscutting dikes are absent in the pluton.

Wanipigow River plutonic complex

The Wanipigow River plutonic complex (WRPC) received only limited examination in the present study, but it is exposed extensively along the northeastern limit of the map area. The WRPC represents the Manitoba segment of a vast batholithic domain that extends for several hundred kilometres to the north and east of the study area as part of the Berens River sub-province (Card and Ciesielski, 1986). Corfu and Stone (1998) described the WRPC as including several distinct suites of calcalkalic granitoid rocks that were emplaced between 2.75 and 2.69 Ga into older (ca. 3.0 Ga) tonalitic crust of the continental North Caribou terrane. Most of the complex consists of voluminous suites of hornblende±biotite tonalite–granodiorite–granite and biotite granite–granodiorite, with lesser suites of biotite tonalite–granodiorite, gneissic tonalite–granodiorite, peraluminous granite and sanukitoid (Corfu and Stone, 1998).

As described in detail below, the WRPC in the study area is subdivided into three units or suites (Wn1, hornblende-biotite



Figure 33: Quartz-feldspar porphyry granite of unit Ge4, east of Gem Lake.

tonalite and granodiorite; Wn2, biotite granodiorite and granite; Wn3, orthogneiss) that may correspond, respectively, to the 'hornblende tonalite', 'biotite granite' and 'gneiss' suites of Corfu and Stone (1998). Along the southwest margin of the complex at Garner Lake, the granitoid rocks intrude the ca. 2.87 Ga Garner Lake intrusive complex, which thus indicates their maximum emplacement age. Dikes of tonalite and granodiorite are common, though minor, components of the Garner assemblage and the lower Bidou assemblage, but are nowhere observed to cut the overlying Gem or Edmunds assemblages in the study area, indicating that much of this magmatism likely occurred prior to ca. 2.72 Ga. Field relationships and geochemical data indicate a broadly synvolcanic timing for the rhyolite intrusion breccia (unit Gw5) and quartz-feldspar porphyry granite (unit Ge4) in the Gem assemblage. For this reason, they are described as part of the volcanic stratigraphy.

Direct U-Pb age constraints on the WRPC come from the Ontario portion, where a biotite granodiorite at Eagle Lake (located 25 km southeast of Garner Lake) yielded an age of 2720 ± 5 Ma (Rogers and McNicoll, unpublished, cited by Lemkow et al., 2006) and a hornblende tonalite at Donald Lake (located 28 km northeast of Garner Lake) returned an age of $2736 +3/-2$ Ma (Corfu and Stone, 1998). Turek et al. (1989) reported an age of 2731 ± 10 Ma for a foliated quartz diorite in granitoid gneiss of the WRPC at Wallace Lake.

Description of map units

Hornblende-biotite tonalite and granodiorite (unit Wn1)

Hornblende-biotite tonalite and granodiorite of map unit Wn1 dominate the WRPC northeast of Garner Lake and appear to represent the main precursor for the gneissic rocks of unit Wn3. Included in this unit are rare dikes of tonalite and granodiorite (<5 m thick) that intrude the Garner assemblage, as well as texturally similar tonalite and granodiorite plutons and dikes that intrude the lower Bidou assemblage in the central portion of the Rice Lake belt. The latter intrusions have yielded ages of ca. 2.73–2.72 Ga (Turek et al., 1989; Anderson, 2008) and are referred to as the Ross River plutonic suite. These rocks weather light grey to buff and are dark grey on fresh surfaces, with a fine- to medium-grained, equigranular (subunit Wn1a) or porphyritic (subunit Wn1b) texture. The latter varieties contain up to 15% subhedral K-feldspar phenocrysts (≤ 1.0 cm) in a fine-grained groundmass of plagioclase, K-feldspar and quartz. Hornblende contents vary from 5 to 25% and most specimens contain 5–10% biotite and 2–5% magnetite. Most outcrops are quite homogeneous, with only minor xenoliths of mafic intrusive or extrusive material. Hornblende phenocrysts define a pervasive and penetrative S-L fabric in most localities east of the BLSZ.

Biotite granodiorite and granite (unit Wn2)

Biotite granite of unit Wn2 is only a minor component of the WRPC in the study area, and also forms narrow dikes and a small (0.4 by 1.1 km) pluton that intrude the Garner assemblage. The granite weathers light pinkish grey to white and is characterized by a fine- to medium-grained equigranular texture

(subunit Wn2a). It contains 15–20% quartz, 10–15% K-feldspar and 60% plagioclase, with less than 10% fine-grained biotite. Porphyritic varieties contain up to 5% euhedral to subhedral K-feldspar phenocrysts up to 3.0 cm (subunit Wn2b). Most outcrops display a moderate to strong S-L fabric and are fairly homogeneous, with only minor mafic inclusions and rare dikes or patches of aplitic granite. A sample (96-03-1116) of biotite granite from the small pluton in the southeast corner of Garner Lake yielded a U-Pb zircon age of 2726 ± 1 Ma, which is interpreted to represent the best estimate of the emplacement age. Also collected for analysis was a sample (96-03-1261/CB02-01) of a narrow (2–3 m) dike of feldspar-quartz–phyric biotite granite that intrudes komatiitic flows north of Garner Lake, at the type locality of unit Gn6, which yielded a maximum emplacement age of ca. 2747 Ma (see 'U-Pb geochronology' section).

Orthogneiss (unit Wn3)

Orthogneiss of map unit Wn3 is developed along the contact between the WRPC and the Garner assemblage, where it varies from 200 to 300 m thick. Another unit of orthogneiss trends away from this contact toward the north-northwest along the northeast arm of Garner Lake and is of unknown thickness. In most localities, the orthogneiss is heterogeneous, well layered and strongly foliated, and includes multiple components (Figure 34a). Subunit Wn3a is mostly granitic orthogneiss derived from hornblende-biotite tonalite–granodiorite–quartz diorite that are similar in most respects to unit Wn1, with subordinate enclaves of quartzofeldspathic gneiss and gabbroic orthogneiss. Subunit Wn3b is mostly a gabbroic orthogneiss that appears to have been derived from the Garner Lake intrusive complex (unit Gn4) and contains subordinate enclaves of granitic orthogneiss, quartzofeldspathic gneiss, pyroxenite and serpentinized peridotite. Crosscutting relationships observed along the west margin of subunit Wn3b at the north shore of Garner Lake indicate that the quartzofeldspathic gneiss is derived, at least in part, from felsic volcanoclastic rocks of the Garner assemblage, which were successively intruded by pyroxenite, gabbro and granitoid dikes. Unit Wn3 also includes unseparated domains of garnet-biotite-hornblende straight gneiss of uncertain precursor (Figure 34b). Most of the orthogneiss contains a penetrative planar fabric defined by the gneissic layering and aligned hornblende and biotite; hornblende also locally defines a down-dip mineral lineation. Thin zones of retrograde mylonite and cataclastite locally overprint these fabrics and contain shallowly plunging quartz ribbon and slickenline lineations.

Edmunds assemblage

The Edmunds assemblage is the youngest supracrustal succession in the southeastern Rice Lake belt and mostly corresponds to the Edmunds Lake formation of Campbell (1971) and Weber (1971a). It is at least 2.5 km thick on the west limb of the Beresford Lake anticline (BLA), where it concordantly overlies the Gem assemblage along the Manigotagan River. Here, a locally thick basal unit of laminated mudstone indicates a period of depositional quiescence prior to major sedimentation. Greywacke-mudstone turbidite is the characteristic lithology and was deposited below wave base in a submarine-fan setting

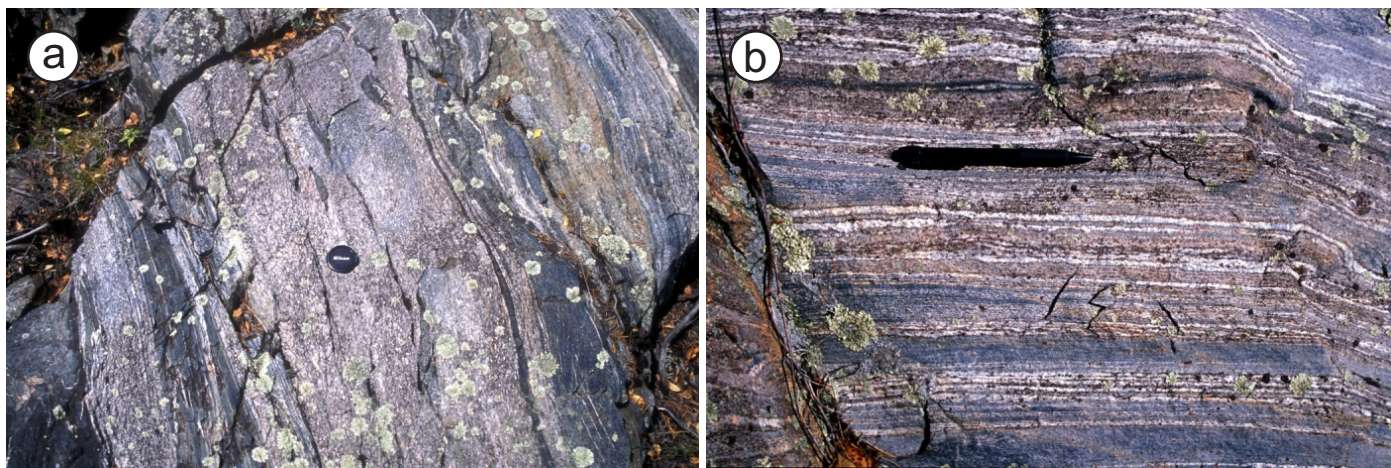


Figure 34: Outcrop photographs of gneissic rocks of unit Wn3 from the large island near the eastern shoreline of Garner Lake: **a)** multicomponent gneiss derived from granitic and gabbroic precursors; note angular inclusions of gabbro in the central granitic layer; **b)** garnet-biotite-hornblende straight gneiss; rhythmic interlayering of garnet-rich and garnet-poor layers may indicate a metasedimentary precursor.

(Campbell, 1971; Weber, 1971a, c) after cessation of major volcanism in the RLB (Davis, 1996). The internal stratigraphy of the turbiditic rocks (Figure 35) corresponds closely to classical models for progradational submarine fans (e.g., Walker, 1978, 1984) and includes representatives of each of the key sedimentary facies (i.e., classic turbidites, massive sandstone, pebbly sandstone, clast-supported conglomerate and matrix-supported debris flows; Walker, 1978).

As described by Weber (1971c), an abrupt internal change in facies association indicates a profound shift in sediment source and supply rate, perhaps in response to a change in base level related to regional tectonism. In general, turbidites in the lower facies association (LFA) are thin bedded and mudstone dominated, and contain fine- to medium-grained feldspathic greywacke, whereas those in the upper facies association (UFA) are thick bedded and dominated by coarse-grained, quartz-lithic greywacke; these correspond respectively to ‘distal’ and ‘proximal’ turbidites in the scheme of Walker (1978). Conglomerate beds in the LFA contain mostly intrabasinal clasts, whereas those in the UFA contain abundant clasts of tonalite and quartzite from an extrabasinal source.

South of Gem Lake, the UFA includes thick, laterally continuous units of effusive mafic volcanic rocks and dacitic volcanic conglomerate that were previously considered part of the Banksian Lake formation of the Gem Lake subgroup (Weber, 1971b). These units are referred to as ‘interlayers’ by Weber (1971a) and were interpreted to represent “...the crests of anticlinal zones of underlying volcanic rocks.” As described in this report, however, they are interstratified on a variety of scales with turbidite and polymictic conglomerate of the Edmunds assemblage, and younging criteria do not support the existence of anticlinal culminations of the type suggested by Weber (1971a). These units are herein interpreted to represent primary stratigraphic interlayers within the Edmunds assemblage, as was suggested by Shklanka (1967) for equivalent rocks in the Bee Lake area, and subsequently by Weber (1987) based on his follow-up reconnaissance of the Lily Lake area. These interlayers indicate that the later stages of basin infilling were

accompanied by major basalt effusions and erosional denudation of the adjacent volcanic arc, and are interpreted in terms of an extensional geodynamic setting. Weber (1971a) assigned the thicker siliciclastic interlayers within the mafic volcanic units to the Rathall Lake formation of the Gem Lake subgroup, but these are also considered herein as part of the Edmunds assemblage, for the reasons described below.

Published analyses of detrital zircons in three samples of greywacke from the Edmunds assemblage in the study area indicate two broad age groupings at 2705–2728 Ma and 2997–3014 Ma, within which three distinct, reproducible ages are apparent: 3009 ± 2 Ma, 2998 ± 2 Ma and 2727 ± 2 Ma (Davis, 1996). The older ages implicate the Mesoarchean NCT as a significant source of detritus. The youngest data points indicate maximum depositional ages of 2725 Ma and 2705 Ma for strata in the LFA and UFA, respectively (Davis, 1996; sample locations are from unpublished data provided by H. Poulsen; see Figure 35). In Ontario, correlative rocks of the Kangaroo Lake formation in the Bee Lake belt (Rogers, 2003) contain tonalite boulders dated at 2703 ± 2 Ma and are intruded by the $2696 +3/-2$ Ma Wingiskis Lake pluton (Rogers and McNicoll, unpublished, cited by Lemkow et al., 2006), thereby constraining the latest stages of deposition to ca. 2700 Ma, roughly coeval with the onset of collisional orogenesis. Subaerial sedimentary rocks of the <2705 Ma (Percival et al., 2006a) San Antonio assemblage are exposed in several locations along the south margin of the NCT and likely represent proximal equivalents to the LFA of the Edmunds assemblage.

Map patterns and younging criteria south of Gem Lake define an early generation of macroscopic, tight to isoclinal, upright folds, which are extensively overprinted and disrupted by dextral shear zones and Z-asymmetric folds that developed late in the deformation history, during progressive transcurrent shear along the south margin of the RLB. The overprinting structures are pervasive and intense within a 0.5–1.0 km wide zone that trends in an easterly direction through Lily Lake and is referred to as the Lily Lake shear zone (Figure 3). North of the shear zone, the Edmunds assemblage consists of a generally

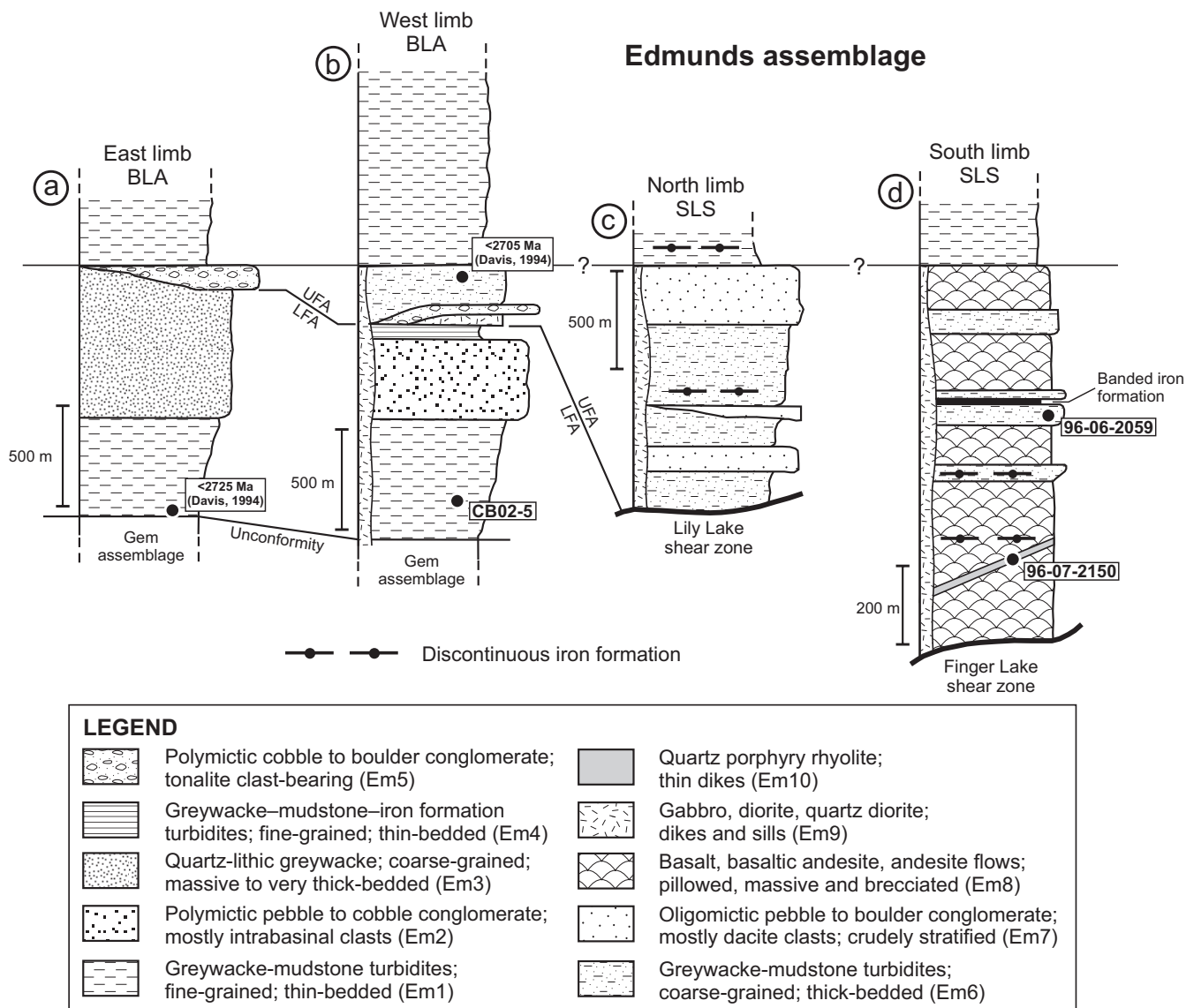


Figure 35: Schematic stratigraphic columns for the Edmunds assemblage: **a)** east limb of the Beresford Lake anticline (BLA), north-west of Gem Lake; **b)** west limb of the BLA, southwest of Gem Lake; **c)** north limb of the Slate Lake syncline (SLS), north of Slate Lake; **d)** south limb of the SLS, south of Lily Lake. Unit codes in legend correspond to those in the text and on Map GR2013-1-1. Black circles indicate the approximate stratigraphic location of the U-Pb geochronology samples. Abbreviations: LFA, lower facies association; UFA, upper facies association.

southwest-younging succession on the west limb of the BLA and is dominated by the LFA. South of the shear zone, the assemblage is dominated by the UFA and younging criteria define the axial trace of a macroscopic isoclinal fold that trends along the Manigotagan River from Lily Lake to Slate Lake and is referred to as the Slate Lake syncline.

Description of rock units

Greywacke-mudstone turbidite (unit Em1)

Unit Em1 defines the base of the Edmunds assemblage in the study area and consists of a thick succession of monotonously interbedded mudstone and greywacke, with minor interbeds of siliceous mudstone and polymictic pebble conglomerate. This unit is best exposed on the west limb of the

BLA, where it ranges between 200 and 1000 m thick. On the east limb, this unit is strongly transposed and truncated by the Garner River shear zone, and is approximately 500 m thick. Abundant younging reversals on both limbs of the anticline indicate that the succession is tightly folded. The basal contact with underlying volcanic rocks of the Gem assemblage is exposed in several locations and is clearly depositional. In three locations where it is observed to overlie pillowed and brecciated basaltic flows, the basal contact is sharp and marked by a 1–5 m thick interval of laminated to very thin bedded siliceous mudstone (Figures 36, 37a), suggesting deposition below wave base during a period of relative quiescence in a sediment-starved marine setting. Where it overlies a volcanoclastic substrate, the basal section includes thickly stratified intervals in which layers of thin-bedded mudstone and greywacke alternate with 1–3 m thick, normally graded beds of locally derived

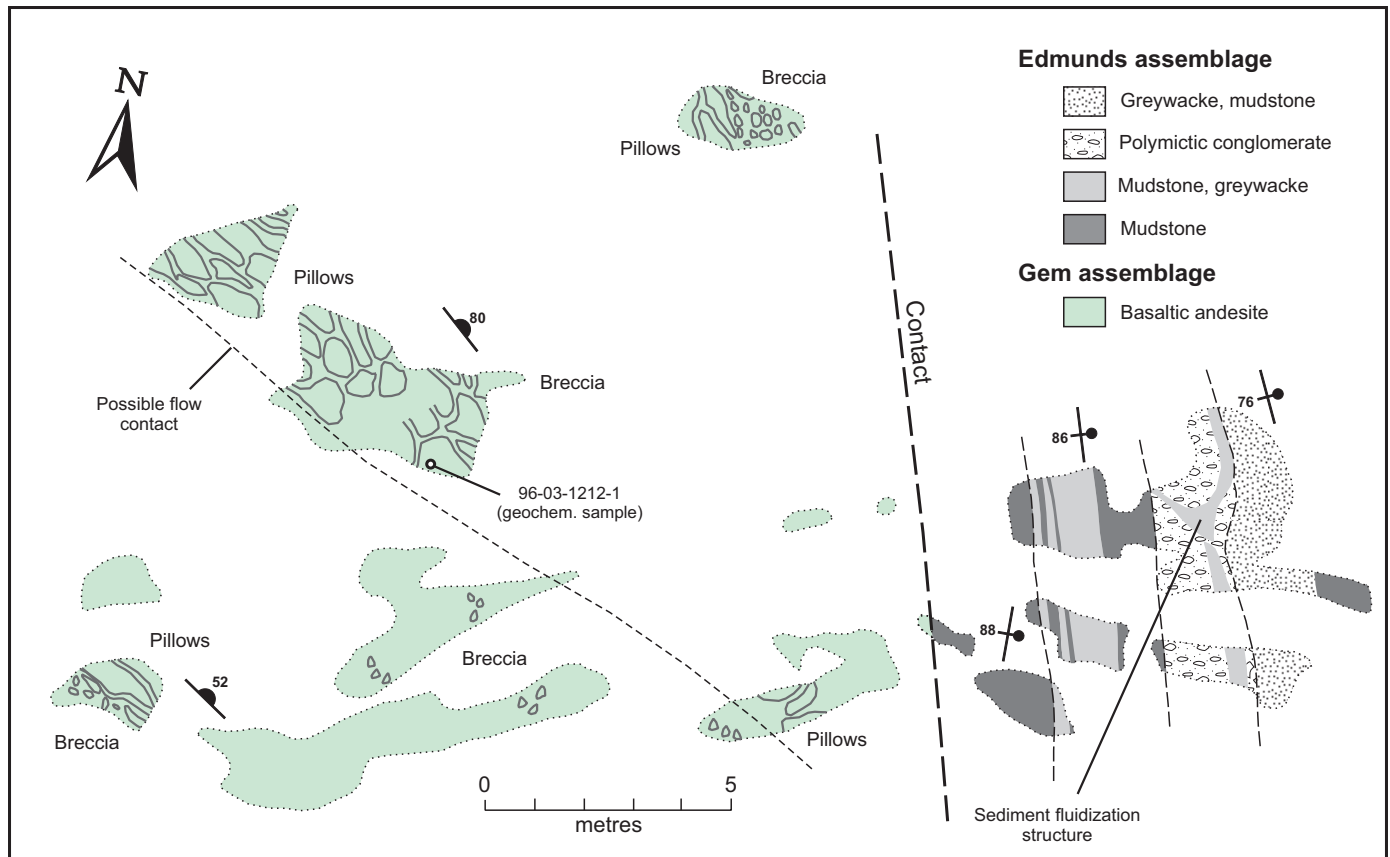


Figure 36: Outcrop map of the Gem–Edmunds contact, located on the east limb of the Beresford Lake anticline, 2 km southwest of Garner Lake (UTM Zone 15, 341104E, 5630189N, NAD 83). Pillowed and brecciated basaltic andesite flows (unit Gw1) of the Gem assemblage are overlain by mudstone, greywacke and polymictic conglomerate (unit Em1) of the Edmunds assemblage. A depositional (as opposed to wholly structural) contact relationship is indicated by the high proportion of locally derived clasts in the polymictic conglomerate bed. The angular discordance exhibited by primary structures on either side of the contact in this location may relate to 1) the existence of significant paleotopography during eruption of the basaltic flows; 2) local tilting or block faulting of the Gem assemblage prior to the onset of turbiditic sedimentation; or 3) structural modification during regional folding or late-orogenic faulting. Unadorned areas of the outcrop polygons indicate locations where primary textures are completely obscured by lichen.

volcaniclastic material, the latter decreasing in thickness and abundance upsection over 20–30 m. Bedding above and below the contact is subconcordant to concordant, except at the locality shown in Figure 36.

Subunit Em1a consists of very thin to medium-bedded mudstone and greywacke, with minor interbeds of siliceous mudstone. The mudstone weathers light brown, grey or pale yellowish green, and forms laminated to very thin bedded layers up to 30 cm thick. Near the base of the unit, layers of laminated, dark grey to black siliceous mudstone locally range up to 2.5 m thick (Figure 37a) and are weakly magnetic and/or graphitic. Fine- to medium-grained feldspathic greywacke typically constitutes less than 30% of this subunit and weathers light grey or brown. The greywacke beds are planar and generally less than 10 cm thick, and show normal size-grading with sharp bases (Figure 37b). Basal lag deposits contain up to 10% quartz, feldspar and lithic grains (0.5–2.0 mm). Some beds contain abundant mudstone rip-up clasts and slump folds (Figure 37c). Graded beds, load casts and scours provide reliable younging criteria in most outcrops. These features indicate deposition via turbidity currents in a submarine-fan setting. Some of these turbidites exhibit the classical Bouma sequence

(‘ABCDE’; Figure 37d), although most are ‘ABE’ or ‘AE’ turbidites, characteristic of deposition in a lower- to mid-fan setting (Walker, 1978, 1984). Thicker greywacke beds (up to 50 cm) have deeply scoured bases with well-developed pebble lags (up to 20%, 0.5–5 cm clasts) and typically define the base of 0.5–1.5 m thick fining-upward cycles that likely represent channel fills. A sample (96-02-1004/CB02-5) from one of these beds near the base of unit Em1, collected for U-Pb analysis of detrital zircons, yielded a maximum depositional age of 2738 Ma and contained a significant population of Mesoarchean zircons (see ‘U-Pb geochronology’ section).

Subunit Em1b is characterized by generally thicker (5–30 cm) and more abundant greywacke beds (up to 80% in some outcrops), and rare interbeds of pebble to cobble conglomerate up to 1.5 m thick. The latter beds are massive to normally graded, poorly sorted and matrix or clast supported, and contain well-rounded to angular clasts up to 15 cm across. Most clasts consist of variably feldspar-phyric volcanic material or mudstone rip-ups of apparently local derivation, although some beds also contain rare clasts of tonalite. Subunit Em1b was likely deposited in a channelized suprafan lobe.

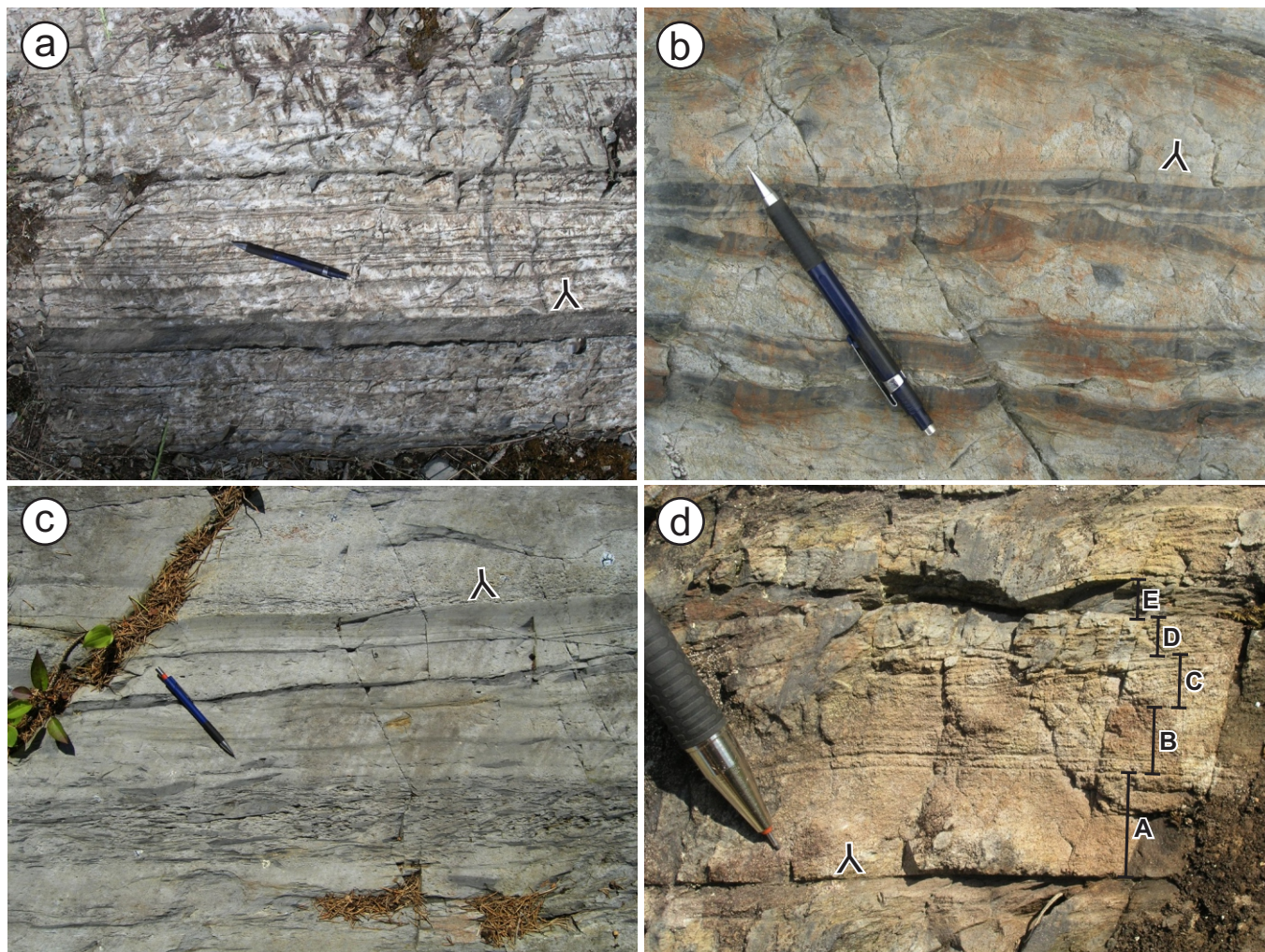


Figure 37: Outcrop photographs of rocks of unit Em1 of the Edmunds assemblage (younging directions indicated): **a)** laminated to thin-bedded siliceous mudstone at the base of the assemblage, east limb of the Beresford Lake anticline (BLA), same locality as shown in Figure 36 (pencil points north); **b)** normal size-grading and load structures in thin-bedded greywacke-mudstone turbidites, east limb of the BLA, northwest of Gem Lake (pencil points north); **c)** abundant mudstone rip-ups in thin-bedded turbidites, west limb of the BLA, south shoreline of Gem Lake (pencil points north); **d)** thin (~5 cm) turbidite showing the complete (ABCDE) Bouma sequence, west limb of the BLA, south of Gem Lake.

Thin-bedded greywacke-mudstone turbidites also define the top of the Edmunds assemblage in the study area and are included in unit Em1 solely on the basis of their similar field characteristics. These turbidites overlie the upper facies association along the western limb of the BLA and in the core of the Slate Lake syncline, and appear to record the onset of a second major cycle of basin subsidence and sedimentation in an overlapping submarine-fan system. No direct stratigraphic correlation with turbidites at the base of the assemblage is implied.

Polymictic pebble to cobble conglomerate (unit Em2)

Unit Em2 consists of polymictic pebble to cobble conglomerate, with minor interbeds of greywacke and mudstone (Figure 38a). This unit is best exposed on the west limb of the BLA, where it has been mapped continuously over a strike length of 8 km (Figure 3). From northwest to southeast along strike, it varies from 650 to 150 m in thickness. Similar conglomerate on the east limb of the BLA forms comparatively thin beds (<2 m) that are not mappable at 1:20 000 scale. In most

exposures, the conglomerate is poorly sorted and matrix to clast supported, and contains mostly rounded to subangular clasts (≤ 20 cm) in a matrix of medium- to coarse-grained feldspathic greywacke. Clasts of variably feldspar (\pm quartz)-phyric, intermediate-felsic volcanic rock dominate in most localities and are representative of the underlying Gem assemblage (clasts of flow-banded aphyric rhyolite and plagioclase-phyric basaltic andesite are particularly diagnostic; Figure 38b). In some outcrops, the conglomerate consists mostly of locally derived rip-ups of thin-bedded mudstone and greywacke. Variations in the size and proportion of clasts define a crude stratification in some locations, whereas the conglomerate in other locations is well stratified with diffuse interbeds (30–50 cm) of medium- to coarse-grained greywacke or interlayers of greywacke-mudstone turbidite. Intervals of unstratified conglomerate range up to at least 25 m thick locally. Individual conglomerate beds vary from massive to normally graded and, in some outcrops, show a consistent pattern of decreasing clast size and bed thickness upsection (i.e., fining- and thinning-upward sequences), which

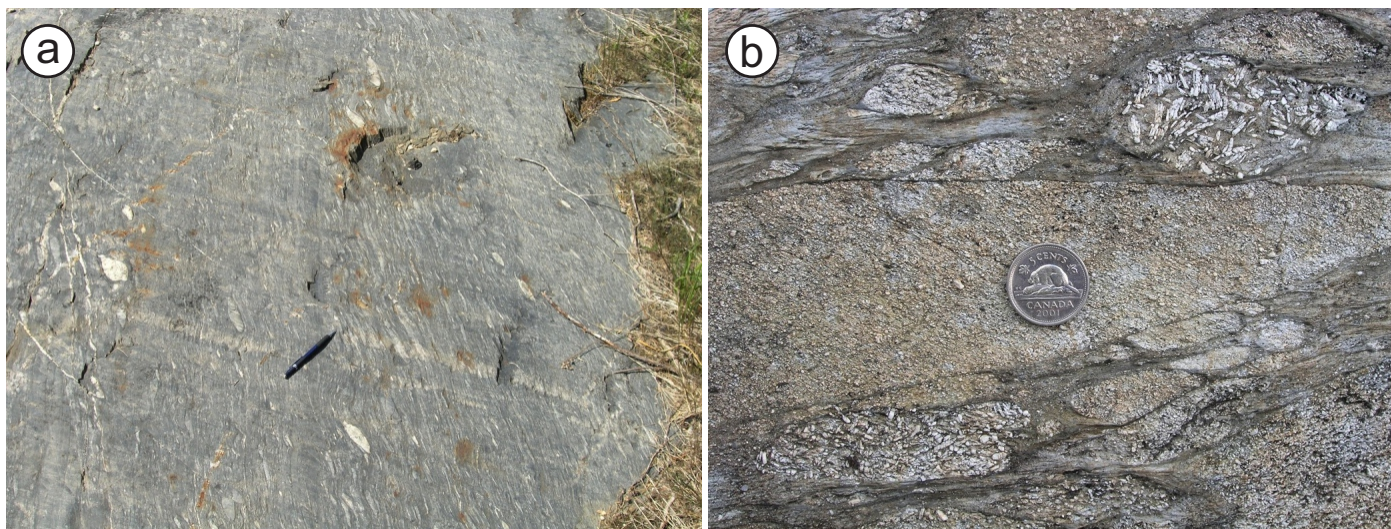


Figure 38: Outcrop photographs of rocks in unit Em2: **a)** crudely stratified pebble conglomerate, west limb of the BLA, west of Gem Lake along the access trail; strongly flattened clasts define a shape-fabric that is discordant to bedding in this outcrop; **b)** plagioclase-phyric basaltic andesite clasts (upper right and lower left) derived from unit Gw1 of the Gem assemblage, east limb of the BLA, northwest of Gem Lake.

is indicative of channel-fill deposits and waning flow conditions in a mid- to upper-fan setting (Walker, 1978).

Quartz-lithic greywacke (unit Em3)

Unit Em3 is only exposed on the east limb of the BLA, where it varies from 450 to 850 m in thickness and is truncated to the north and south by shear zones. Internal younging reversals indicate the presence of macroscopic isoclinal folds that are parasitic to the BLA; hence, the stratigraphic thickness is considerably less than indicated above. The characteristic rock is a light grey- to buff-weathering, medium- to coarse-grained, pebbly quartz-lithic greywacke (Figure 39a, b) that contains angular to subrounded grains (1–5 mm) of quartz (10–40%) and feldspar ($\leq 5\%$). This greywacke forms very thick and mas-

sive beds (>2 m), such that only a crude stratification is apparent in most outcrops. Mudstone rip-up clasts up to 30 cm in their longest dimension are scattered throughout (up to 5%) or are concentrated (up to 30%) into diffuse basal lags. Bed tops are defined by discontinuous (scoured) beds of darker grey or brown mudstone, or very fine grained greywacke, that are generally less than 5 cm thick. Rare intervals of interbedded greywacke and mudstone contain greywacke beds up to 2 m thick that show consistent normal size-grading. Near the base of this unit, the greywacke contains beds of polymictic pebble to cobble conglomerate up to 2 m thick. These characteristics indicate that unit Em3 corresponds to the ‘massive sandstone facies’ of Walker (1978), which is thought to represent channel-fill deposits in braided suprafan-lobe settings.

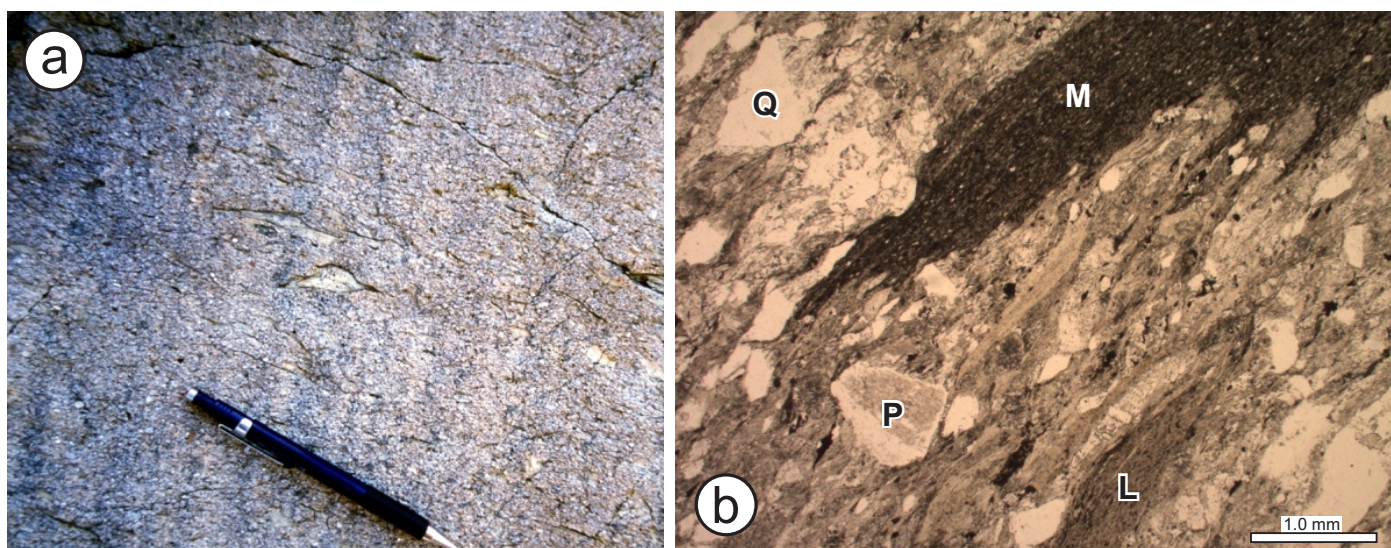


Figure 39: Outcrop and thin-section photographs of quartz-lithic greywacke of unit Em3 on the east limb of the BLA, northwest of Gem Lake: **a)** coarse-grained quartz-lithic greywacke with abundant mudstone rip-ups; **b)** photomicrograph (plane-polarized light) of quartz-lithic greywacke showing angular quartz (Q), plagioclase (P) and lithic (L) grains, and wispy mudstone rip-ups (M).

Greywacke–mudstone–iron formation turbidite (unit Em4)

Unit Em4 defines a laterally extensive marker horizon that is clearly delineated by aeromagnetic data over a strike length of 11 km on the west limb of the BLA, and here marks the top of the lower facies association of the Edmunds assemblage (Figure 3). Along much of the defined strike length, the upper contact of unit Em4 coincides with a gabbro sill. This unit is truncated southeast of Banksian Lake by the Lily Lake shear zone and continues to the northwest beyond the western limit of the study area. It is not present on the east limb of the BLA.

Unit Em4 ranges from 40 to 100 m thick and consists of monotonously interbedded greywacke, mudstone and oxide-facies iron formation. The greywacke weathers light grey to reddish brown and is very fine to medium grained and feldspathic. Individual beds are planar and less than 20 cm thick (generally 1–5 cm), and grade upward into thin layers (<5 cm) of very thin bedded to laminated, dark grey-brown mudstone and magnetite (Figure 40a). These beds are typical of ‘ABE’ turbidites deposited in a mid-fan setting; the laminated mudstone-magnetite layers suggest the presence of coeval exhalative activity. Some of the iron formation layers contain low-angle crossbeds (Figure 40b), which indicate deposition via turbidity currents as opposed to pelagic settling. In one location, systematic variations in bed thickness define thinning-upward cycles, ranging from 0.5 to 1.0 m thick, within larger thinning-upward sequences on a scale of 5–10 m. As described by Walker (1984), such features might be related to lateral shifting of a suprafan lobe. Barrett and Fralick (1989) described similar rocks in a submarine-fan succession along the south margin of the Beardmore–Geraldton belt in Ontario, which they interpreted as deposits from turbidity currents in either the inter-channel areas of the mid to upper fan or in the distal areas of the lower fan. In the present case, the contact with underlying conglomerate of unit Em2 varies from sharp to diffuse, with the latter type marked by 20–40 m of interbedded pebble conglomerate, greywacke and mudstone, without oxide-facies iron

formation; this association is suggestive of channel-fill deposits and thus favours an interchannel, rather than lower-fan, setting for unit Em4.

Polymictic cobble to boulder conglomerate (unit Em5)

Unit Em5 consists of a distinctive tonalite-clast-bearing pebble to boulder conglomerate that is identified in three locations on the west limb of the BLA, where it defines the base of the upper facies association of the Edmunds assemblage. Here, the conglomerate ranges up to 60 m thick and is markedly lenticular. Unit Em5 is also identified on the east limb of the BLA, where it is traced along strike for at least 1.5 km at the upper contact of unit Em3 and varies up to 100 m thick (Figure 3). The conglomerate is polymictic and poorly sorted, and varies from clast to matrix supported (Figure 41a). Individual exposures vary from massive to crudely stratified, with bedding in the latter defined by variations in the size and proportion of clasts, or by diffuse beds of pebbly greywacke. The clasts range up to 50 cm in size and vary from well rounded to subangular (typically rounded to subrounded), indicating that they underwent significant subaerial transport in a high-energy fluvial system. Though highly variable, the clast population characteristically includes a significant proportion of well-rounded tonalite or granodiorite clasts, and thus signals the arrival of detritus from a more deeply eroded source. Most outcrops are dominated by clasts derived from underlying sedimentary and volcanic units, but also include a subordinate population of extrabasinal clasts (e.g., quartzite and vein quartz). The matrix typically consists of medium- to coarse-grained pebbly greywacke and locally contains up to 30% coarse detrital quartz. At one locality on the west limb of the BLA, well-rounded (in many cases nearly spherical) to subrounded boulders of tonalite are supported in a distinctly ‘muddy’ matrix of pebbly greywacke (Figure 41b); these features indicate deposition via low-density debris flows. In submarine-fan systems, such deposits characterize upper-fan feeder channels situated near the foot of the slope into the basin (e.g., Walker, 1978, 1984).

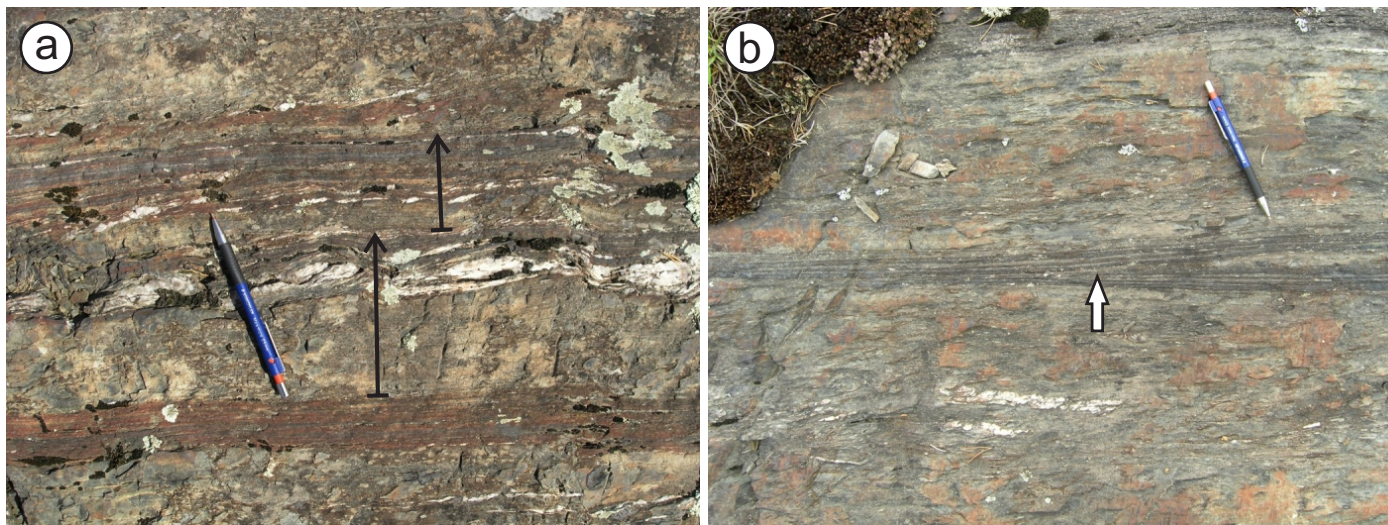


Figure 40: Outcrop photographs of rocks in unit Em4 on the west limb of the Beresford Lake anticline (BLA), southwest of Gem Lake (pencil points north on both photos): **a)** thin-bedded turbidites composed of greywacke, mudstone and magnetite iron formation; attenuated and back-rotated quartz veins (white) tend to mark the contacts between beds (black arrows indicate individual turbidites); **b)** low-angle crossbedding (arrow) in magnetite iron formation.

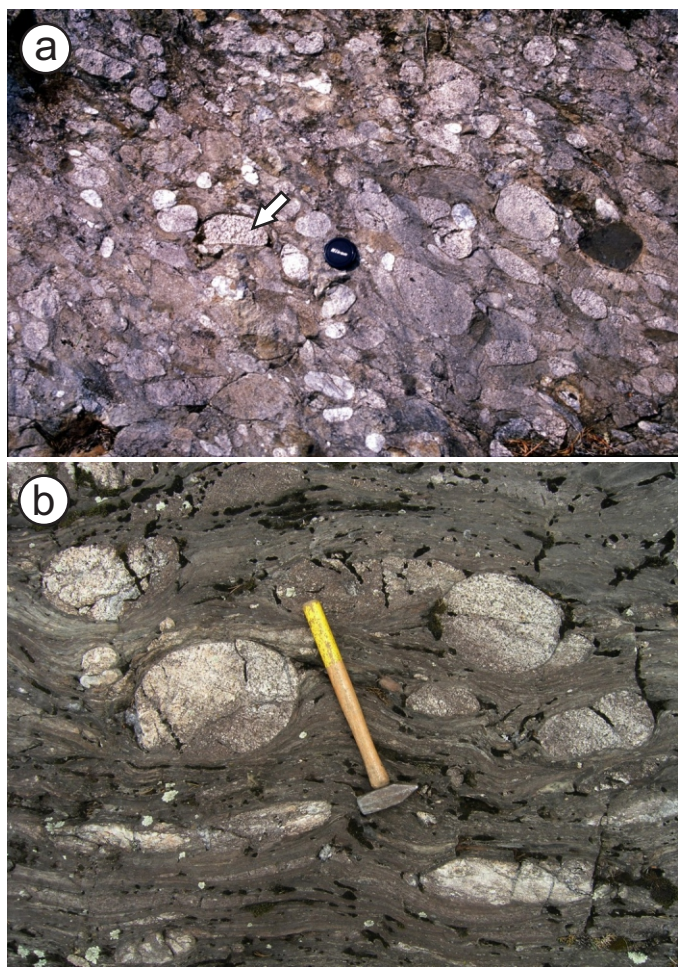


Figure 41: Outcrop photographs of tonalite-clast-bearing conglomerate of unit Em5: **a)** clast-supported cobble conglomerate on the east limb of the Beresford Lake anticline (BLA), southwest of Garner Lake; tonalite cobble indicated by arrow; lens cap in centre of photograph for scale; **b)** matrix-supported conglomerate on the west limb of the BLA, showing nearly spherical boulders of tonalite, northeast of Lily Lake.

Greywacke-mudstone turbidite (unit Em6)

Unit Em6 consists mostly of quartz-lithic greywacke and mudstone turbidite, and is divided into two subunits (Em6a and Em6b), which are separated by the Lily Lake shear zone. Subunit Em6a occurs northwest of the shear zone and is traced for 8 km along strike as a relatively homogeneous, 100–300 m thick succession of thick-bedded turbidites (Figure 3). It appears to be analogous to the ‘proximal turbidite facies’ of Walker (1978), indicating that deposition likely occurred in a nonchannelled suprafan lobe. Over much of this strike length, the basal contact is marked by a gabbro sill. This subunit contains minor thin (≤ 0.5 m) interbeds of polymictic pebble conglomerate, and rare layers (≤ 1.5 m thick) of black siliceous mudstone, iron formation and thinly interbedded graphitic mudstone and feldspathic greywacke.

Southeast of the Lily Lake shear zone, subunit Em6b defines a series of lenticular map units that vary up to 400 m thick on both limbs of the Slate Lake syncline. This subunit contains the same association of rock types as subunit Em6a, but is characterized by more abundant and thicker interbeds of

polymictic pebble to cobble conglomerate and thicker, more continuous layers of laminated magnetite-chert iron formation. These rocks were likely deposited within the channelled portion of the suprafan lobe. The most significant layer of iron formation (Figure 42a) extends along strike in a southeasterly direction for 1.2 km from Lily Lake (Figure 3), ranges up to 20–30 m thick, and is spatially associated with several significant Au showings, which are collectively referred to as the ‘Beaver Gold’ occurrence. Subunit Em6b is also interstratified on a variety of scales with oligomictic (dacite) conglomerate and effusive mafic volcanic rocks, which likely indicate proximity to a fault-controlled margin of the basin. The latter two rock types locally attain significant thicknesses and are therefore described as separate map units below.

The typical quartz-lithic greywacke of unit Em6 is light grey to buff to pink and medium to very coarse grained, and contains up to 40% granules and pebbles (2–5 mm) of quartz, feldspar and lithic material (Figure 42b, c). The quartz grains tend to be very angular to subangular, with only a small proportion showing subrounded shapes. The matrix consists of fine- to medium-grained quartz, feldspar, sericite, chlorite, carbonate and pyrite. The greywacke forms tabular-planar beds up to 1.5 m thick (typically 30–50 cm) that have sharp scoured bases and consistent normal size-grading; crossbedding is absent. Thicker beds have well-developed basal lag deposits that contain angular mudstone rip-ups and rounded pebbles of quartz and lithic material. In some outcrops, medium- to coarse-grained greywacke forms massive beds up to 5 m thick. Most beds are capped by layers of light brown to grey, sericitic or graphitic mudstone, which are generally less than 15 cm thick and account for less than 10% of the section. As noted above, these rocks are interpreted to represent proximal (i.e., upper-fan) turbidites.

Interbeds of polymictic pebble to cobble conglomerate in subunit Em6b range up to several metres thick (≤ 4 m) and are typically massive, poorly sorted and matrix supported. Bed contacts vary from sharp to diffuse (Figure 42d). Intervals of stratified conglomerate with only minor ($< 20\%$) discontinuous and diffuse interbeds of coarse-grained quartz-lithic greywacke locally range up to 25 m thick. Crossbedding is absent from these intervals and the conglomerate beds show both normal and reverse size-grading, which is indicative of channel-fill deposits in an upper-fan setting. Subangular to very well rounded clasts range in size up to 30 cm (typically 5–10 cm) and are supported in a matrix of light grey to buff, medium- to very coarse grained, pebbly quartz-lithic greywacke. Clast types include porphyritic and aphyric grey-green dacite, mudstone, aphyric black rhyolite (commonly flow-banded), quartz-phyric white rhyolite, tonalite–granodiorite, quartz-feldspar porphyry, vein quartz, magnetite-chert iron formation, orthoquartzite, gabbro and basalt. The heterogeneous clast population and high degree of rounding establish significant subaerial transport of detritus. Well-rounded boulders of tonalite up to 50 cm across are abundant in some of the thicker conglomerate beds, and tend to be associated with very well rounded, high-sphericity clasts of grey to white orthoquartzite, indicating a significant influx of extrabasinal detritus, which was likely sourced from deeply eroded portions of the North Caribou terrane (i.e., the Wallace assemblage). A sample (96-06-2059) of very coarse

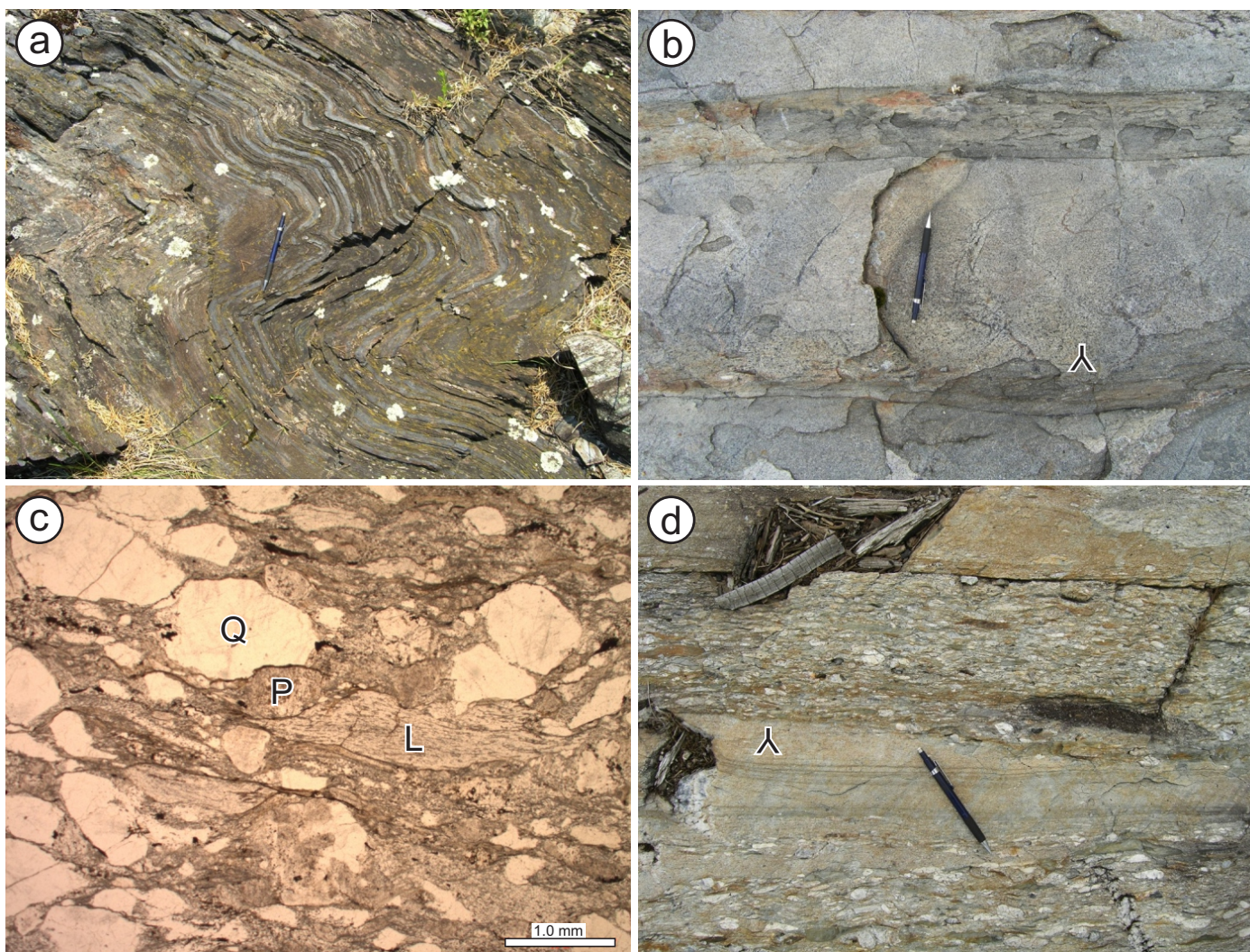


Figure 42: Outcrop and thin-section photographs of key rocks in unit Em6: **a)** thin-bedded magnetite-chert iron formation, south limb of the Slate Lake syncline, south of Lily Lake; **b)** thick-bedded quartz-lithic greywacke of subunit Em6a, north shore of Lily Lake; note normal size-grading and thin interbeds of sericitic mudstone; younging direction indicated; **c)** photomicrograph (plane-polarized light) of quartz-lithic greywacke of subunit Em6a, showing angular quartz (Q), plagioclase (P) and lithic (L) grains, west limb of the Beresford Lake anticline, north of Lily Lake; **d)** interbedded polymictic conglomerate and quartz-lithic greywacke of subunit Em6b, north limb of the Slate Lake syncline, north of Slate Lake (pencil points north); younging direction indicated by scoured base of the upper conglomerate bed.

grained, pebbly, quartz-lithic greywacke from an interval of polymictic conglomerate south of Lily Lake, collected for detrital zircon U-Pb analysis, yielded a maximum depositional age of 2732 Ma and, significantly, contained mostly Mesoproterozoic zircons (see ‘U-Pb geochronology’ section).

Oligomictic pebble to boulder conglomerate (unit Em7)

Oligomictic (dacite) conglomerate of unit Em7 is exposed at three stratigraphic levels on the north limb of the Slate Lake syncline. The lower unit is approximately 120 m thick and is well exposed along the south shoreline of Lake Bon. The middle unit is less well exposed, but appears to form a lenticular body that ranges up to 50 m thick over a strike length of 800 m. The upper unit underlies the prominent outcrop ridge that extends southeast from the unnamed lake immediately east of Lily Lake to the eastern limit of the mapped area. Over

this distance (~3.0 km along strike), the upper unit decreases in thickness from just over 500 m in the northwest to approximately 50 m in the southeast. The Lily Lake shear zone defines the northwestern extent of the upper and lower units; the middle unit is truncated to the northwest by a later fault. On the south limb of the syncline, dacitic conglomerate layers up to 10 m thick are interstratified with quartz-lithic greywacke and polymictic conglomerate of subunit Em6b, but are not mappable at 1:20 000 scale.

Conglomerate of unit Em7 is unsorted, matrix supported and massive to very diffusely stratified (Figure 43a). The clast population consists almost exclusively of buff to light green plagioclase-phyric dacite, with rare clasts of slightly darker green, more coarsely and densely plagioclase-phyric andesite. The clasts vary from well rounded to subangular and range up to 1.5 m across (typically <25 cm). The matrix is a medium- to coarse-grained feldspathic greywacke that contains up to

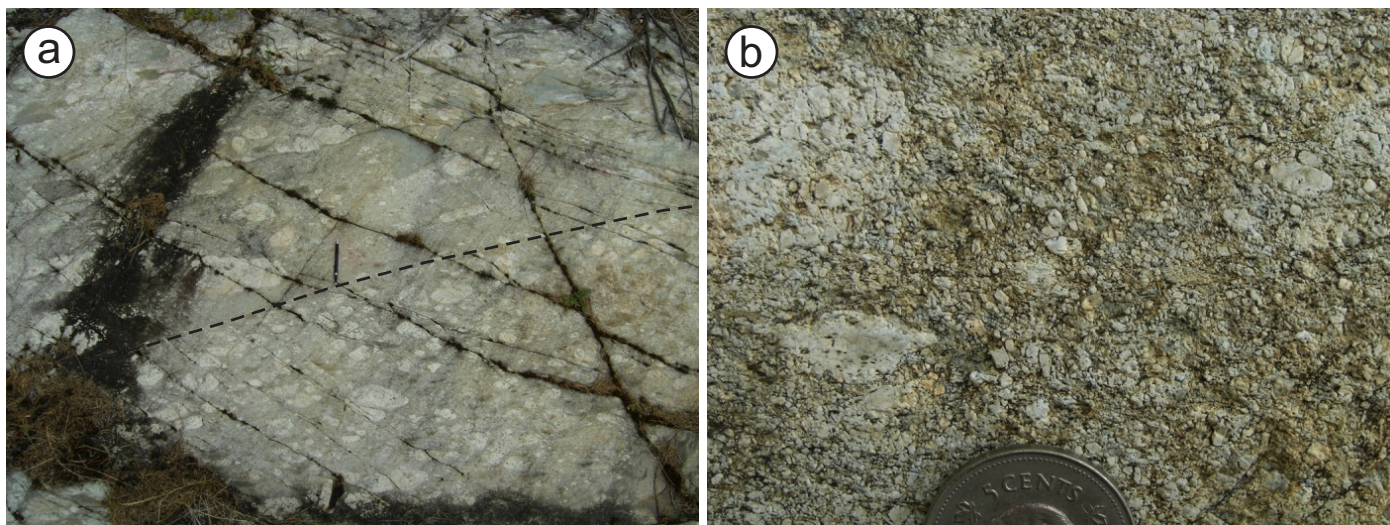


Figure 43: Outcrop photographs of the dacitic conglomerate of unit Em7 on the north limb of the Slate Lake syncline: **a)** matrix-supported and crudely stratified conglomerate; bed contact indicated by the dashed line; **b)** detail of the feldspathic matrix to the conglomerate in Figure 43a.

70% feldspar crystals (≤ 2.0 mm) and usually accounts for 80% of the rock (Figure 43b). Coarse detrital quartz is generally absent from the matrix, except on the south limb of the syncline, where the dacitic conglomerate beds contain up to 40% quartz (1–5 mm) in the matrix. Along the upper and lower contacts of the thicker units, the dacitic conglomerate contains a slightly more diverse clast population and is interstratified with polymictic pebble conglomerate, coarse-grained greywacke and graphitic mudstone of subunit Em6b, the latter of which establishes deposition in a marine environment. Coupled with the significant thicknesses of dacitic conglomerate, these characteristics indicate deposition via a series of large-volume subaqueous debris flows or avalanches within the proximal feeder channel to the submarine fan.

Basalt, basaltic andesite and andesite flows (unit Em8)

Effusive mafic–intermediate volcanic rocks of unit Em8 are only exposed on the south limb of the Slate Lake syncline, south of the Lily Lake shear zone. Pillowed, massive and brecciated flows (subunit Em8a) and derived tectonite (subunit Em8b) define a thick (>1 km) succession along the southern limit of the mapped area and, to the north, are interstratified on a variety of scales with well-bedded clastic and chemical sedimentary rocks of unit Em6 (Figure 3). Whole-rock geochemical data indicate that the flows are of transitional tholeiitic–calcalkalic affinity and range in composition from basalt to andesite. Basalt and basaltic andesite dominate and weather buff to pale green to rusty brown, with dark grey or green fresh surfaces. Most specimens are fine grained, aphyric and nonamygdaloidal, although some locally contain sparse plagioclase phenocrysts (1–5%; 0.5–10 mm) and round quartz amygdules (1–3%; 1–5 mm). In thin section, they consist of fine-grained plagioclase, chlorite, actinolite, epidote-clinzoisite and carbonate, with accessory titanite, quartz and opaque minerals. The andesitic samples contain closely packed plagioclase laths up to 0.5 mm in length (Figure 44a). Chlorite and carbonate replace actinolite in strongly altered specimens, and the mafic

teconite consists of chlorite-carbonate phyllonite that is anastomosed around relatively low-strain enclaves in which primary textures and structures are preserved (Figure 44b). Pillows in these enclaves are amoeboid to bun shaped and less than 2 m in maximum dimension, with chloritic selvages (<2 cm thick) and less than 5% interpillow material (mainly carbonate). Individual flows range up to at least 10 m thick and are capped by 0.5–3 m thick layers of flow-top breccia. Where they can be conclusively identified, the massive flows range up to 5 m thick and locally transition upward into pillowed and/or brecciated flow tops, which thus provide reliable younging criteria (Figure 44c, d). In these locations, it is apparent that strain was strongly partitioned into the layers of flow-top breccia, which were presumably less competent than the associated massive or pillowed flows owing to the high proportion of matrix material (carbonatized hyaloclastite).

Individual flows or flow units are also locally separated by intervals (up to 30 m thick) of interbedded feldspathic greywacke, quartz-lithic greywacke, polymictic pebble conglomerate, graphitic mudstone and/or iron formation (unit Em6b), which correspond to the ‘Rathall Lake formation’ of Weber (1971a). Fine-grained mafic dikes and sills form a significant component (5–10%) of some flows, and are also observed to cut adjacent clastic sedimentary rocks. The association of subaqueous basalt flows with resedimented coarse-clastic rocks and chemical sedimentary rocks on the south limb of the Slate Lake syncline indicates deposition in an upper-fan setting, perhaps in proximity to a basin-bounding fault that channelled mafic magmas and hydrothermal fluids.

Gabbro, diorite and quartz diorite (unit Em9)

Unit 9 consists of mafic–intermediate dikes and sills that intrude all units of the Edmunds assemblage, but are most abundant south of the Lily Lake shear zone, where they are spatially associated with mafic–intermediate flows of unit Em8. Only the sills define mappable units at 1:20 000 scale; the most

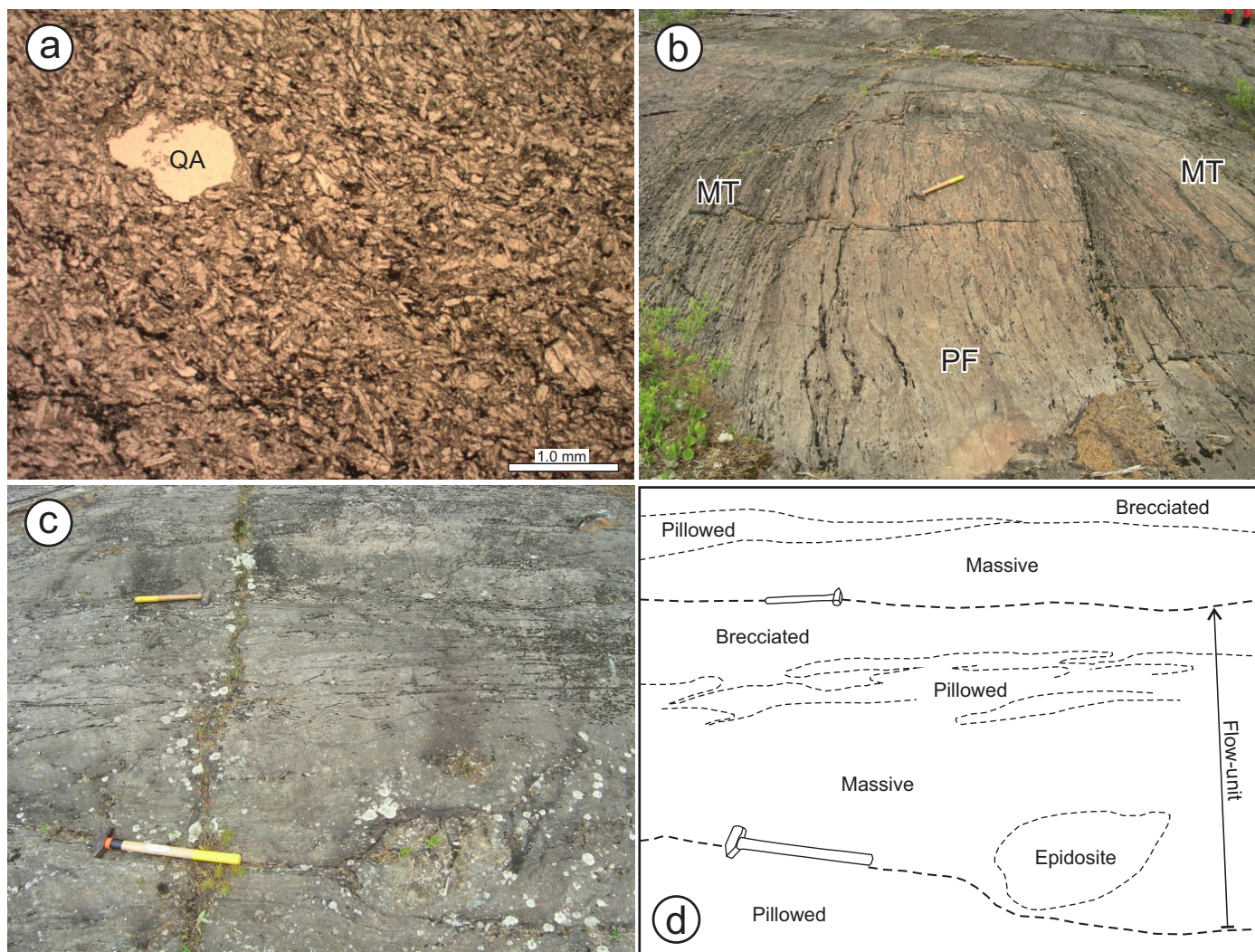


Figure 44: Outcrop and thin-section photographs of rocks in unit Em8 on the south limb of the Slate Lake syncline, southeast of Lily Lake: **a)** photomicrograph (plane-polarized light) of massive andesite flow; note well-preserved plagioclase laths and subrounded quartz amygdule (QA); **b)** pillowed basalt flow (PF) preserved as low-strain enclave in mafic tectonite (MT) derived from flow breccia; **c)** and **d)** outcrop photograph and corresponding sketch showing an upward transition from massive to pillowed to brecciated basalt in a single 1.5 m thick flow unit; upper and lower contacts of the flow unit are marked by hammers; younging direction is toward the top of the photo, which was taken facing northeast.

prominent of these ranges up to 150 m thick and is traced along strike for a distance of approximately 7 km at the upper contact of unit Em4. Gabbro sills up to at least 50 m thick also intrude the thick succession of flows along the southern limit of the mapped area. Whole-rock geochemical data indicate that these intrusions range in composition from gabbro to quartz diorite, and include three chemical suites (tholeiitic, transitional tholeiitic–calcalkalic and calcalkalic) that are readily distinguished by their distinctive immobile trace-element signatures (see ‘Lithochemistry’ section). Hence, the intrusions appear to be more chemically diverse than the associated flows of transitional tholeiitic–calcalkalic basalt, basaltic andesite and andesite. In general, these rocks weather dark brown to light green or buff and are dark green on fresh surfaces, with fairly uniform field characteristics. Most are quite strongly altered and foliated, particularly where hosted by siliciclastic rocks. Primary subophitic textures are defined by fine plagioclase laths (30–70%; 0.5–1.5 mm) in a groundmass of felty chlorite, actinolite,

epidote-clinozoisite and carbonate, with accessory titanite and opaque minerals. Leucocratic examples tend to contain sparse (5–15%) plagioclase phenocrysts up to 5 mm. These intrusions are typically less than 3 m thick and have sharp parallel contacts, with locally preserved chilled margins up to 2 cm in thickness.

The thick sill that defines the upper contact of unit Em4 throughout much of the map area is typically 60–80 m thick, and is bounded above and below by zones of strongly foliated mafic tectonite. In most outcrops, the sill consists of dark green to brown, fine- to medium-grained gabbro that has an equigranular, subophitic to ophitic texture defined by blocky to tabular plagioclase crystals (30–40%; 0.5–1.5 mm) in a groundmass of actinolite, chlorite, epidote-clinozoisite and opaque minerals. This rock also generally contains 1–3% finely disseminated pyrrhotite (±chalcopyrite) and is strongly magnetic. Where strongly altered, the actinolite is replaced by chlorite and carbonate. In other outcrops, the sill consists of light green to grey

porphyritic diorite, which contains subhedral phenocrysts of plagioclase (10–20%) that range up to 5 mm in length. In one location, the sill shows a continuous variation upsection from melanocratic equigranular gabbro on the northeast to leucocratic porphyritic diorite on the southwest, perhaps as a result of in situ magmatic differentiation.

Quartz-porphyry rhyolite (unit Em10)

South of Lily Lake, the thick basal section of map unit Em8 is intruded in several locations by narrow (≤ 1.2 m) dikes of quartz-phyric rhyolite. This rock weathers pale grey to buff-pink and is dark grey on fresh surfaces; it contains sparse euhedral to subhedral quartz phenocrysts (1–3%; 0.5–2.0 mm) that are evenly distributed in an aphanitic to very fine grained groundmass of quartz, feldspar, sericite, carbonate, chlorite and opaque minerals (Figure 45). Some of the quartz phenocrysts have irregular embayed margins. The dikes have sharp parallel contacts and are transposed into parallelism with the tectonite fabric in the country rock. Clasts of texturally similar quartz-phyric rhyolite are present in beds of polymictic conglomerate farther upsection. Hence, a sample of a rhyolite dike (96-07-2150) was collected for U-Pb zircon geochronological analysis in an attempt to constrain the age of volcanism and sedimentation in the upper facies association of the Edmunds assemblage. This sample yielded a poorly constrained maximum emplacement age of ca. 2727 Ma (see ‘U-Pb geochronology’ section).

Unsubdivided tectonite (precursor uncertain)

Phyllonite, mylonite (unit Us1)

Unsubdivided tectonite of map unit Us1 is mostly restricted to the panel of rocks bounded by the Beresford Lake and Garner River shear zones and the proximal segments of their major splays. The thickest, most continuous zone of tectonite extends along strike over a distance of 12 km from the south end of Beresford Lake to Gem Lake, and ranges up to 1.4 km thick west of Garner Lake in an area of particularly poor-quality

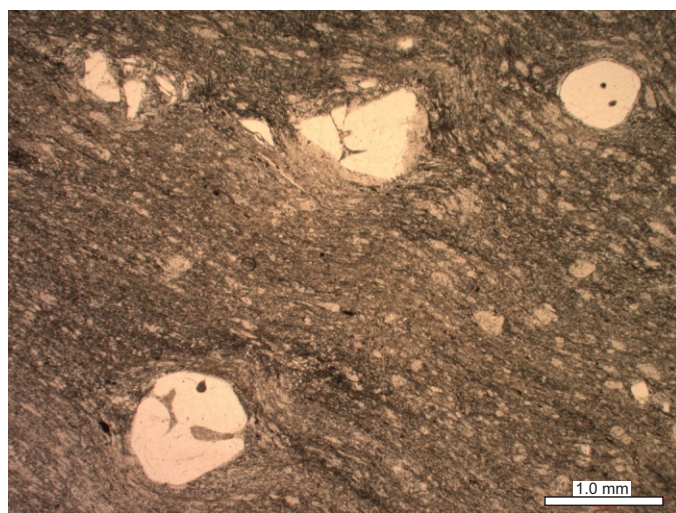


Figure 45: Photomicrograph of a quartz-porphyry rhyolite dike of unit Em10 that cuts basalt flows southeast of Lily Lake. Note subhedral and variably embayed quartz phenocrysts.

bedrock exposure. It is bounded on the west by the Garner River shear zone and on the east by the main strand of the Beresford Lake shear zone (BLSZ). In most exposures, the tectonite is characterized by an intense centimetre- to metre-scale compositional layering defined by strongly attenuated and transposed primary features and/or alternating domains of chlorite-sericite phyllonite and quartzofeldspathic mylonite. A penetrative and pervasive shape-fabric defined by flattened primary features and foliated chlorite-sericite is oriented parallel to the layering and locally includes a linear shape-fabric that varies in orientation from down-dip to subhorizontal. Along the margins, the tectonite grades outward over 10–100 m into rocks with clearly recognizable primary features. Rare enclaves of lower finite strain are also preserved within the tectonite. From these, it appears likely that intermediate volcanic rocks of the Gem assemblage were the main precursor to the tectonite west and southwest of Garner Lake. Northwest of Garner Lake, the tectonite contains strongly transposed layers of magnetite-chert iron formation and enclaves of komatiitic basalt, indicating derivation from the adjacent Garner assemblage.

Outcrops of the tectonite along the main strand of the BLSZ are characterized by deeply pitted surfaces that result from preferential weathering and erosion of disseminated to fracture-controlled Fe-carbonate alteration. Most outcrops also contain strongly attenuated and folded quartz veins, at least some of which are auriferous (e.g., the Marlin-Swordfish showing; Assessment File 74298). Overprinting relationships indicate as many as five generations of deformation structure, which include an early differentiated crenulation cleavage that is overprinted by at least two generations of asymmetric, tight to isoclinal folds and late kink folds (the structural aspects of this tectonite are described in detail in the ‘Structural geology’ section). All of these fabrics are crosscut by post-tectonic mafic dikes, as described below.

Post-tectonic dikes

Gabbro, diorite and quartz diorite (unit Pt1)

Post-tectonic dikes of calcalkalic gabbro, diorite and quartz diorite (unit Pt1) are spatially associated with the BLSZ, and are particularly abundant in the thick zone of tectonite west of Garner Lake. These dikes weather light green or grey and are dark green on fresh surfaces, with a fine- to medium-grained equigranular texture. They are typically leucocratic, with 50–70% plagioclase, 30–50% ferromagnesian minerals and up to 5% quartz. In thin section, the plagioclase is moderately to strongly saussuritized and the ferromagnesian minerals are completely replaced by chlorite and rutile. Some dikes also contain tabular phenocrysts of plagioclase (~5%; 2–5 mm) or pseudomorphic replacements (chlorite-rutile) after acicular phenocrysts of amphibole (5–10%; ≤ 3 mm), which tend to be concentrated in their central portions; the latter rock type may correspond to the ‘hornblende lamprophyre’ dikes described by Stockwell and Lord (1939) from the vicinity of the Central Manitoba mine. The dikes range up to 1.5 m thick (typically 20–50 cm) and have sharp (planar to irregular) contacts, with well-developed chilled margins up to 3 cm thick (Figure 46a). One of these

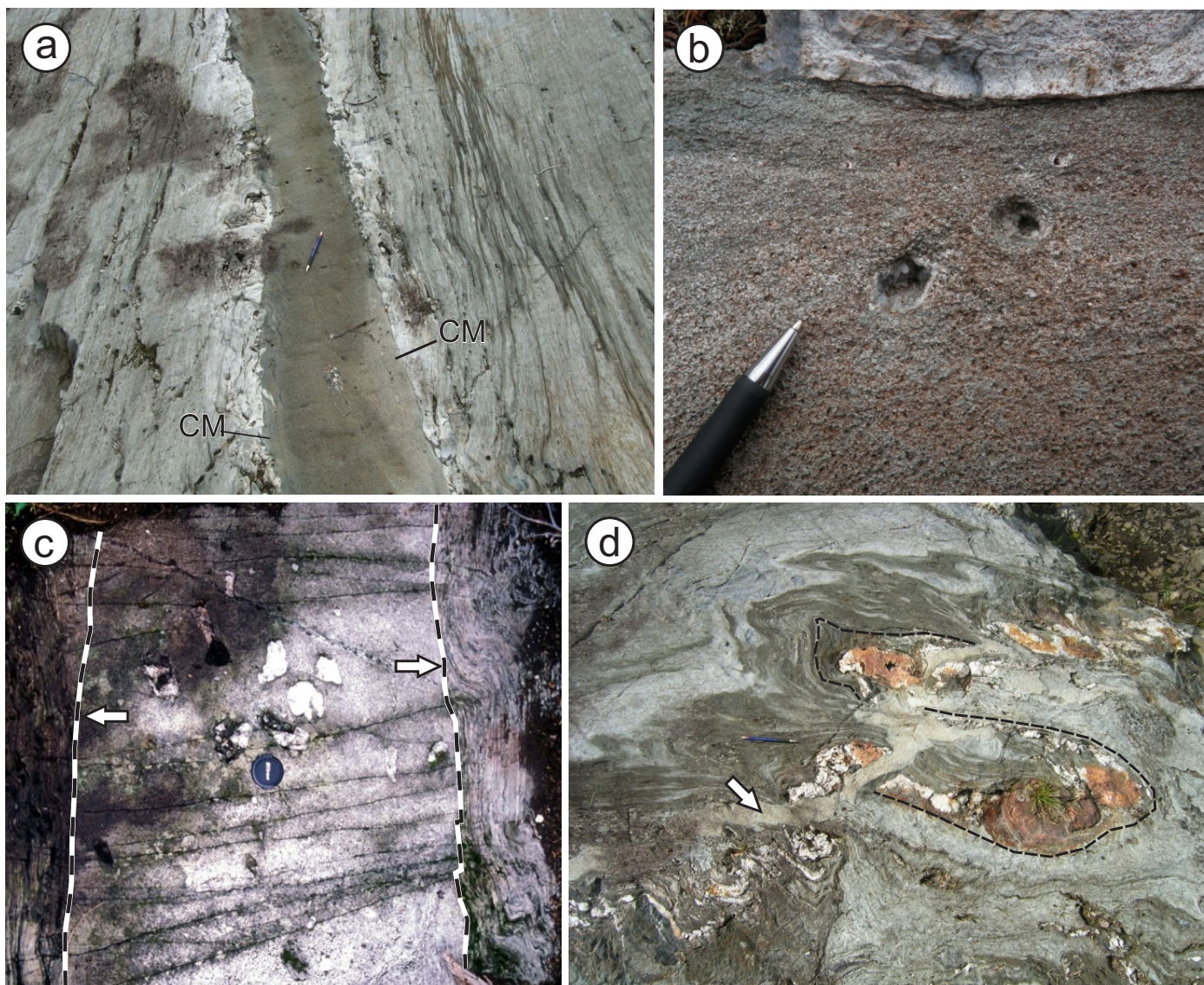


Figure 46: Outcrop photographs of post-tectonic dikes cutting tectonite in the Beresford Lake shear zone (BLSZ), southwest of Garner Lake: **a)** gabbro dike with well-developed chilled margins (CM) and slightly irregular contacts; dike crosscuts strongly deformed andesitic volcanic rocks; the 'bleaching' of the country rocks along the margins of the dike may be the result of hydrothermal alteration along a precursor fracture; **b)** partially filled vesicles in gabbro dike (same locality as Figure 46a); **c)** quartz xenoliths in the core of a diorite dike (contacts indicated by dashed lines) that sharply crosscuts high-strain fabrics in the country rocks (arrows); **d)** narrow, irregular gabbro dike (arrow), showing crosscutting relationship to isoclinal folds (indicated by dashed lines) and highly attenuated quartz veins in tectonite; quartz veins are auriferous in this outcrop; pencil for scale just above arrow.

dikes contains vesicles up to 1 cm in diameter that are partially filled by drusy quartz (Figure 46b).

In all locations, the dikes discordantly cut penetrative deformation fabrics in the wallrocks and appear to be massive (i.e., nonfoliated), although some contain a weak chlorite foliation that is only apparent in thin section. In the BLSZ southwest of the Garner Lake outlet, these dikes also cut across tightly folded auriferous quartz veins and contain xenoliths of vein quartz (Figure 46c, d). A sample (96-02-1056) of a quartz diorite dike from the east margin of the BLSZ at Garner Lake was collected for U-Pb geochronological analysis to constrain the emplacement age and the minimum age of penetrative ductile deformation. Secondary rutile in this sample yielded a poorly constrained age of ca. 2665 Ma (see 'U-Pb geochronology'

section), which is taken to indicate the minimum age of dike emplacement.

Summary of lithostratigraphy and inferred depositional settings

The Garner assemblage includes two distinct successions of supracrustal rocks. The lower succession consists mainly of coarse intermediate-felsic volcanoclastic and derived epiclastic rocks, and was likely deposited in a shallow-marine setting on the proximal flank of a subaerially exposed volcanic arc. Layered peridotite, pyroxenite and gabbro of the Garner Lake intrusive complex were emplaced into this succession at ca. 2870 Ma (Davis, 1994), indicating that the volcanic arc had achieved significant thickness by that time. The pronounced

erosional unconformity at the top of the lower succession indicates uplift and erosional denudation of the volcanic arc, perhaps in response to accretionary tectonic processes or thermal doming above an ascending mantle plume. Arkosic sandstone, tonalite-pebble conglomerate, intermediate–felsic volcanoclastic rocks with minor interlayers of chert, carbonate and argillite, and a thick unit of magnetite–chert iron formation at the base of the upper succession record deposition in a restricted marine basin, prior to the major effusions of subaqueous komatiitic and basaltic lavas that constitute the top of the succession. These features are indicative of an extensional geodynamic setting, possibly related to impingement of a mantle plume and consequent uplift and rifting of the volcanic arc. The upper succession is analogous to Archean rift sequences documented elsewhere, which are generally thought to be ‘plume influenced’.

The Bidou assemblage also includes two distinct successions of supracrustal rocks. The lower succession consists of laterally continuous formations of subaqueous basalt flows, which alternate with well-stratified formations of basinal marine turbidites and are intruded by thick gabbro sills. The basalt and gabbro are chemically analogous to back-arc basin basalt (Bailes and Percival, 2005a), indicating that this succession was likely deposited in a relatively quiescent back-arc basin, which received alternating influxes of spreading-centre basalt and arc-derived detritus. Tonalite boulders in volcanic conglomerate and the appearance of quartz as a significant detrital component in volcanoclastic turbidites of the Stormy Lake formation signal a transition from back-arc to arc volcanism near the top of this succession. The upper succession consists of a thick accumulation of coarse volcanoclastic rocks derived from ca. 2730 Ma (Turek et al., 1989) porphyritic dacite, which were deposited as subaqueous debris and grain flows in proximity to an active volcanic centre. Arc magmatism culminated with emplacement of synvolcanic (ca. 2730–2720 Ma; Turek et al., 1989; Anderson, 2008) tonalite and granodiorite plutons of the Ross River plutonic suite into the back-arc succession.

Effusive volcanic rocks and related hypabyssal intrusions in the Gem assemblage range in composition from basalt to high-SiO₂ rhyolite, and are intercalated with thick accumulations of primary and variably reworked volcanoclastic rocks, and minor epiclastic rocks. Turbidite bedforms and pillowed flows indicate a subaqueous depositional setting for most of the assemblage. Thick beds of basaltic scoria and crossbedded sandstone in the interstices of associated pillowed flows (Seneshen, 1990) are suggestive of Strombolian-type eruptions in shallow-water settings, whereas well-preserved examples of welded felsic ignimbrites (2722 Ma; Davis, 1994) and accretionary lapilli indicate local subaerial or very shallow subaqueous Plinian-type eruptions. Abundant felsic pyroclastic rocks were likely generated by gravitational or explosive collapse of associated high-SiO₂ rhyolite, rhyolite and dacite lava flows or domes; these rocks are characteristic of the Gem assemblage. Rapid lateral and vertical facies variations, coupled with the wide compositional range of effusive flows, indicate proximal deposition in a composite volcano made up of multiple eruptive centres. Taken together, these characteristics are compatible with a dynamic volcanic-arc or arc-rift setting.

The base of the Edmunds assemblage is marked by a locally thick laminated mudstone, indicating a period of depositional quiescence prior to major sedimentation. Greywacke-mudstone turbidites dominate and were deposited below wave base in a progradational submarine fan that formed after cessation of arc volcanism. An abrupt internal change in facies association signals a profound shift in sediment source and supply rate, perhaps in response to a change in base level related to regional tectonism. The lower facies association (<2725 Ma; Davis, 1996) consists of distal greywacke-mudstone turbidites, polymictic conglomerate (mostly intrabasinal clasts), massive quartz-lithic greywacke, and greywacke–mudstone–iron formation turbidites, which were likely deposited in a channelized lower- to mid-fan setting. In contrast, the upper facies association (<2705 Ma; Davis, 1996) includes polymictic conglomerate with abundant extrabasinal clasts, proximal greywacke-mudstone turbidites, dacitic volcanic conglomerate (debris flows) and massive to pillowed basaltic flows, which were deposited in a channelized upper-fan to feeder-channel setting, likely in proximity to a basin-bounding fault scarp that may have served as the conduit for the basaltic flows. The later stages of submarine-fan sedimentation were accompanied by major basalt effusions and erosional denudation of the adjacent volcanic arc, suggesting an extensional geodynamic setting.

Lithogeochemistry and Sm-Nd isotope geochemistry

In order to characterize the geochemistry and chemical stratigraphy of volcanic and associated intrusive rock types in the Garner–Gem lakes area, a suite of representative rock samples, encompassing most of the principal map units, was collected for lithogeochemical analysis. In this section, the geochemical attributes of these samples are described and the variations in major- and trace-element chemistry and Sm-Nd isotopic compositions are examined in detail. These data indicate the chemically distinct nature of basaltic magmatism in each supracrustal assemblage and lend considerable support to the interpretations described in the preceding text. The data also provide insight into the potential sources and geodynamic settings of magmatic rocks in the southeastern Rice Lake belt, and thus constrain regional-scale tectonic and metallogenic models.

Sampling procedures and analytical methods

A suite of 112 rock samples was collected for geochemical analysis during the bedrock mapping program. Samples of volcanic and associated intrusive rocks were obtained from each major map unit in each supracrustal assemblage, with care taken to ensure a wide spatial distribution of sample sites and representation of the full diversity of rock types. Each sample consisted of 2–5 kg of least altered homogeneous rock collected by hammer from bedrock and manually trimmed at the sample site to remove all weathered surfaces, veins, altered fractures or other inhomogeneities. Samples of pillowed flows were obtained from the cores of single pillows. Volcanoclastic samples were monolithic and characterized by textural similarity of clasts and matrix. In the MGS rock-preparation facility, the clean rock chips were crushed in a steel jaw-crusher and pulverized in a steel swing-mill. The powders were homogenized

by rolling and split to obtain approximately 55 g of analytical material.

Lithogeochemistry

The whole-rock powders were submitted to Activation Laboratories Ltd. (Ancaster, Ontario) and analyzed using the '4Litho' analytical package, which employs a lithium metaborate-tetraborate fusion technique, followed by nitric-acid digestion and analysis by inductively coupled plasma–emission spectrometry (ICP-ES) for the major elements and selected trace elements (Ba, Sc, Sr, V, Y, Zr), and by inductively coupled plasma–mass spectrometry (ICP-MS) for trace and rare-earth elements. Each sample batch included a minimum of one internal standard and one blind duplicate for analytical quality control. The resulting geochemical data exhibit very systematic intra- and intersample elemental behaviour, particularly for the high-field-strength elements (Ti, Y, Zr, Nb, Hf, Ta) and rare-earth elements. Totals for the major-element oxides range from 98.55 to 100.89 wt. %. Despite regional metamorphic recrystallization in the greenschist to lower amphibolite facies and evidence of secondary chemical modification of some samples in the form of visible alteration, higher loss-on-ignition values (>4 wt. %) and/or depleted Na ($\text{Al}_2\text{O}_3/\text{Na}_2\text{O} > 10$; Spitz and Darling, 1978), the systematic behaviour of the high-field-strength elements and rare-earth elements is taken to indicate that they were largely immobile during alteration and metamorphism. Variations in these elements are therefore thought to reflect primary igneous processes.

For completeness, this report includes an analysis of ICP whole-rock geochemical data for a suite of 23 samples collected in the area by A.H. Bailes of the Manitoba Geological Survey (MGS) under the auspices of the Western Superior NATMAP project (Bailes, 1998). These data were released as part of Data Repository Item DRI2005004 (Bailes and Percival, 2005b), which was published in conjunction with Geoscientific Report GR2005-2 (Bailes and Percival, 2005a). Also included in this report are previously unreleased ICP whole-rock data for a suite of 29 samples collected in 1995 and 1999 by M.T. Corkery (MGS); sampling procedures and analytical methods were the same as those described above.

Representative analyses of key map units are presented in Table 3. All major-, trace- and rare-earth element data are included in Data Repository Item DRI2013002 (on CD-ROM in back pocket). For plotting purposes, major-element values were recalculated to 100% volatile free and analytical results below detection limits were arbitrarily assigned a value of 50% of the detection limit.

Sm-Nd isotope geochemistry

A subset of 19 least altered samples, selected to include key map units from each of the supracrustal assemblages, was submitted for Sm-Nd isotope geochemical analysis to the University of Alberta Radiogenic Isotope Facility (Edmonton, Alberta). Sampling and initial processing procedures were the same as those for the lithogeochemical samples. Processing and analysis for $^{143}\text{Nd}/^{144}\text{Nd}$ and $^{147}\text{Sm}/^{144}\text{Nd}$ isotopic ratios followed the chromatographic and mass-spectrometry procedures

described by Unterschutz et al. (2002) and Schmidberger et al. (2007). Samarium and neodymium isotopic compositions were determined by multicollector ICP-MS using an in-house Nd isotope standard (Schmidberger et al., 2007). Chemical-processing blanks were <200 pg for Nd and Sm. Neodymium isotope data are presented relative to a $^{143}\text{Nd}/^{144}\text{Nd}$ value of 0.511850 for the La Jolla standard. Neodymium depleted-mantle model ages (T_{DM}) were calculated for samples with $^{147}\text{Sm}/^{144}\text{Nd} < 0.14$ using the model of DePaolo (1981), and present-day depleted-mantle values of $^{147}\text{Sm}/^{144}\text{Nd} = 0.2137$ and $^{143}\text{Nd}/^{144}\text{Nd} = 0.513163$. All epsilon Nd values (ϵ_{Nd}) were calculated at the known or inferred age of crystallization (i.e., they are initial ϵ_{Nd} values). They are reported relative to a chondritic uniform reservoir (CHUR) with present-day values of $^{147}\text{Sm}/^{144}\text{Nd} = 0.1967$ (Jacobsen, 1980) and $^{143}\text{Nd}/^{144}\text{Nd} = 0.512638$ (Goldstein et al., 1984). The resulting Sm-Nd isotopic data (Table 4) provide insight into the possible contributions of crust and mantle during magma petrogenesis. These data are also included in Data Repository Item DRI2013002.

Included in this analysis are Sm-Nd isotopic data for 12 samples collected by A.H. Bailes and M.T. Corkery (MGS) under the auspices of the Western Superior NATMAP project, and analyzed by K. Tomlinson at the Geological Survey of Canada (GSC; Ottawa, Ontario). These data were released as part of Data Repository Item DRI2005004 (Bailes and Percival, 2005b), which was published in conjunction with Geoscientific Report GR2005-2 (Bailes and Percival, 2005a), but have not previously been described. Three samples in the GSC dataset are essentially duplicates of samples in the University of Alberta dataset (i.e., they were collected in proximity from the same geological unit) and returned similar model ages and epsilon Nd values (relative ϵ_{Nd} differences are 0.3–0.5 for the three 'duplicate' sets).

Samples with 1000- and 2000-series numbers were collected by the author. Samples collected by A.H. Bailes are indicated by 10-series numbers, whereas those collected by M.T. Corkery are indicated by 100-series numbers. Samples DM-1 and DM-2 (both gabbro) were collected from the waste dump and a surface outcrop, respectively, at the Diana (Gem Lake) mine. Samples collected outside the mapped area for U-Pb geochronology are indicated by letter codes, as follows: CMG, Central Manitoba mine (gabbro); MRF, Manigotagan River formation (greywacke); SL, Stormy Lake formation (greywacke); SLF, Stovel Lake formation (greywacke). Universal Transverse Mercator (UTM) co-ordinates (NAD 83, Zone 15) obtained onsite by GPS are provided for all samples in Data Repository Item DRI2013002.

Analytical results

Geochemical attributes of volcanic and associated intrusive rocks in the Garner–Gem lakes area are described below in order of decreasing known or apparent age of the host lithotectonic assemblage. Discrimination diagrams in Figures 47–50 show geochemical data for the entire sample suite, separated according to assemblage and map unit. Subsequent diagrams show subsets of these data, separated according to lithological and/or geochemical criteria, as described in the text and figure captions. Detailed geochemical descriptions are provided for

Table 3: Lithogeochemical data for representative samples of key map units in the Garner–Gem lakes area.

Sample	1133-1	1033-1	173-1	1053-1	1254-2	1173-1	39-1	50-1	212-1	1866-1	201-1	1816-1	1871-1	1871-2	1717-1	1289-1	1557-1	1971-1	1959-1	1139-1	1116-1	2142-1	2081-1	2235-1	1056-1
Unit	Gn1b	Gn3b	Gn4b	Gn5c	Gn6a	Gn7a	Bd1	Bd3a	Bd4	Gw1a	Gw3a	Gw4b	Gw5	Gw5	Gw6a	Gw7	Ge1a	Ge2	Ge4	Wn1a	Wn2a	Em8	Em9	Em9	Pt1
Rock type (wt. %)	Rhy	Dac	Pyx	Dac	Kom bsit	Bsit	Bsit	Dac	Gab	Bsit and	Dio	Rhy	Rhy	Lgmt	Rhy	Dac	Dac	Bsit	Gmt	Grdi	Grnt	Bsit	Dio	Gab	Dio
SiO ₂	69.73	65.86	50.20	64.81	50.20	48.93	49.73	64.09	44.68	55.23	52.40	71.90	74.83	70.09	76.85	67.61	65.18	48.66	77.04	69.22	73.77	50.39	52.81	47.92	53.66
Al ₂ O ₃	15.74	14.23	2.81	15.13	9.25	14.16	13.66	15.78	20.48	15.82	14.53	12.47	13.32	14.37	11.73	15.22	15.56	13.69	11.39	15.59	13.82	14.95	14.54	13.72	16.03
Fe ₂ O ₃	3.67	5.46	8.75	4.72	11.01	13.46	13.07	5.27	8.28	11.69	11.73	4.84	0.81	3.39	2.23	2.66	4.63	12.65	3.02	3.26	1.87	12.94	9.19	17.98	8.74
MnO	0.07	0.07	0.20	0.06	0.21	0.21	0.21	0.06	0.11	0.22	0.18	0.11	0.03	0.08	0.04	0.04	0.09	0.18	0.06	0.05	0.04	0.16	0.15	0.24	0.14
MgO	1.41	3.38	17.77	1.98	13.09	7.56	7.30	2.26	6.74	2.97	5.28	0.68	0.15	0.76	0.17	0.57	2.41	6.51	0.08	1.29	0.39	6.18	7.91	4.26	4.12
CaO	3.37	3.12	16.12	2.39	12.52	10.75	10.68	2.43	11.38	7.29	7.61	1.29	1.79	2.10	0.25	3.42	5.11	13.98	0.53	3.38	1.17	8.97	7.15	7.08	5.66
Na ₂ O	3.93	3.43	0.32	5.01	1.10	2.05	2.40	6.07	1.69	3.64	3.56	4.01	5.42	3.74	4.54	4.76	3.24	2.13	4.41	4.56	4.00	1.96	2.90	3.93	1.63
K ₂ O	1.58	2.36	0.05	1.46	0.13	0.29	0.10	0.66	0.05	0.89	0.31	3.15	0.95	2.30	3.16	1.37	1.10	0.35	3.00	1.58	4.01	0.19	0.80	0.09	1.67
TiO ₂	0.36	0.50	0.30	0.60	0.30	0.77	0.88	0.47	0.63	1.58	1.13	0.38	0.28	0.60	0.17	0.59	0.54	1.04	0.17	0.34	0.15	1.53	0.73	1.92	0.75
P ₂ O ₅	0.10	0.14	0.01	0.16	0.03	0.06	0.08	0.16	0.05	0.27	0.16	0.04	0.02	0.02	0.01	0.16	0.10	0.21	0.03	0.09	0.04	0.28	0.43	0.17	0.33
LOI	0.42	0.76	2.46	3.29	1.54	0.85	2.10	2.72	4.89	0.62	1.87	1.66	0.94	1.52	0.65	2.71	1.83	0.76	0.64	0.69	0.88	2.69	3.79	2.28	7.39
TOTAL	100.37	99.30	99.48	99.60	99.35	99.07	100.20	99.97	98.98	100.20	98.74	100.50	98.55	98.97	99.81	99.10	99.79	100.20	100.40	100.06	100.15	100.20	100.40	99.58	100.12
Mg# (ppm)	43.2	55.1	80.1	45.4	70.2	52.7	52.5	45.9	61.7	33.5	47.1	21.8	26.8	30.8	13.1	29.8	50.8	50.5	5.0	44.0	29.2	48.6	63.1	31.9	48.3
Y	6	15	7	19	6	16	18	13	13	27	33	50	3	8	59	9	9	35	73	6	18	23	24	38	19
Sc	5	10	54	8	42	40	47	11	20	22	30	4	1	22	1	10	9	24	1	5	3	33	20	42	15
Zr	98	171	24	162	16	36	53	129	41	128	127	331	384	386	365	147	102	84	310	94	100	111	130	110	124
V	42	64	195	76	183	283	290	77	141	158	199	3	3	22	3	76	77	215	3	48	17	249	171	463	151
Nb	5.9	10.7	0.4	9.7	2.7	1.6	2.3	4.7	1.9	8.0	5.5	26.0	13.0	12.0	25.0	8.3	3.9	11.0	17.0	4.9	8.4	7.0	7.0	5.0	6.3
Hf	2.9	5.0	4.6	4.6	0.4	1.2	1.3	3.2	1.2	3.6	3.9	8.4	9.9	9.4	10.4	3.8	2.9	2.2	9.1	2.8	3.7	2.8	3.6	3.5	3.7
Ta	0.4	0.9	0.9	0.9	0.0	0.1	0.2	0.4	0.1	0.5	0.4	1.5	3.1	1.1	1.5	0.9	0.4	0.4	1.5	0.4	1.5	0.5	0.5	0.3	0.3
Th	2.3	7.5	0.1	7.2	0.1	0.2	0.4	3.1	0.3	1.9	1.4	6.7	2.4	4.1	7.8	4.6	2.3	2.4	8.0	3.3	14.2	0.7	8.4	0.6	5.5
Cr	10	125	2620	10	1320	245	33	10	345	10	89	10	10	10	10	45	31	250	10	10	10	110	390	20	75
Co	6	16	66	9	60	54	59	15	39	21	34	1	1	4	1	17	12	43	1	8	3	37	31	54	24
Ni	10	95	409	10	402	158	40	8	171	10	56	10	10	10	10	37	36	450	10	10	10	70	190	40	33
Cu	5	45	40	21	142	216	133	5	73	30	64	10	5	20	5	41	16	5	5	20	5	80	40	90	20
Zn	102	78	67	82	70	120	39	56	33	110	94	140	15	15	50	37	72	70	70	56	39	100	110	130	83
Ga	18	19	4	19	11	16	17	19	18	18	18	21	15	16	24	22	20	18	20	18	17	20	19	25	22
Ba	514	662	18	259	54	62	22	258	9	196	83	528	336	158	628	425	261	65	642	459	392	60	197	32	499
Sr	304	204	17	168	147	88	117	378	140	374	197	34	166	49	51	325	368	336	44	373	106	209	630	174	332
La	13.9	30.9	0.8	30.1	0.9	1.5	3.4	20.2	2.6	17.9	11.9	52.7	3.5	4.1	50.6	30.9	14.1	26.5	55.4	17.4	23.0	8.5	36.3	5.0	34.5
Ce	28.2	55.8	1.9	53.5	2.5	4.9	8.7	40.3	6.7	41.2	30.4	112.0	5.2	6.4	114.0	61.6	28.3	78.4	116.0	31.8	42.9	21.3	76.4	13.8	69.7
Pr	2.71	6.17	0.29	5.90	0.39	0.84	1.16	4.39	0.93	5.55	3.94	14.10	0.52	0.65	14.60	6.49	3.19	12.30	15.30	3.15	4.03	3.11	10.10	2.27	8.78
Nd	10.3	22.0	1.5	21.0	2.2	4.9	6.2	17.3	5.0	21.8	18.3	48.8	1.6	2.2	55.8	23.8	12.6	51.2	59.3	12.1	15.3	12.1	38.4	11.9	35.4
Sm	1.9	4.4	0.6	4.0	0.8	1.8	2.1	2.9	1.5	4.9	4.4	9.1	0.2	0.5	11.1	4.0	2.5	10.1	12.8	2.1	3.4	3.1	7.7	3.4	7.4
Eu	0.60	1.09	0.19	1.08	0.31	0.75	0.78	0.87	0.66	1.72	1.42	1.83	0.90	1.01	1.75	1.03	0.75	2.13	1.75	0.63	0.43	1.07	2.04	1.17	1.87

Table 3: Lithochemical data for representative samples of key map units in the Garner–Gem lakes area. (continued)

Sample	1133-1	1033-1	173-1	1053-1	1254-2	1173-1	39-1	50-1	212-1	1866-1	201-1	1816-1	1871-1	1871-2	1717-1	1289-1	1557-1	1971-1	1959-1	1139-1	1116-1	2142-1	2081-1	2235-1	1056-1
Unit	Gn1b	Gn3b	Gn4b	Gn5c	Gn6a	Gn7a	Bd1	Bd3a	Bd4	Gw1a	Gw3a	Gw4b	Gw5	Gw5	Gw6a	Gw7	Ge1a	Ge2	Ge4	Wn1a	Wn2a	Em8	Em9	Em9	Pt1
Rock type	Rhy	Dac	Pyx	Dac	Kom bsit	Bsit	Bsit	Dac	Gab	Bsit and	Dio	Rhy	Rhy	Lgrmt	Rhy	Dac	Dac	Bsit	Grt	Grt	Grt	Bsit	Dio	Gab	Dio
Gd	1.5	3.7	0.8	3.6	1.0	2.7	2.5	2.9	2.1	4.8	5.2	8.0	0.2	0.6	10.6	2.9	2.2	7.7	11.0	1.6	3.2	3.5	6.0	4.3	6.0
Tb	0.2	0.6	0.2	0.6	0.2	0.5	0.5	0.4	0.4	0.8	0.9	1.5	0.1	0.1	1.7	0.4	0.3	1.3	2.2	0.2	0.6	0.7	0.9	1.0	0.8
Dy	1.3	3.3	1.2	3.2	1.4	3.4	3.1	2.2	2.3	5.1	5.4	8.9	0.4	1.1	10.0	2.2	1.9	7.2	13.1	1.2	3.2	4.0	4.5	6.8	4.0
Ho	0.3	0.7	0.2	0.6	0.3	0.7	0.7	0.4	0.5	1.0	1.2	1.8	0.1	0.3	2.0	0.4	0.3	1.3	2.6	0.2	0.7	0.7	0.8	1.3	0.7
Er	0.8	2.0	0.6	1.8	1.0	2.3	2.0	1.2	1.4	3.0	3.4	5.7	0.4	1.1	6.2	1.0	0.9	3.6	7.9	0.6	2.0	2.1	2.3	4.0	2.0
Tm	0.12	0.30	0.10	0.27	0.15	0.33	0.32	0.20	0.22	0.44	0.52	0.89	0.08	0.19	0.95	0.13	0.13	0.50	1.21	0.08	0.30	0.31	0.33	0.62	0.27
Yb	0.7	1.9	0.7	1.7	0.9	2.2	1.9	1.1	1.4	2.8	3.2	5.7	0.7	1.5	5.9	0.8	0.9	3.0	7.7	0.5	1.8	2.0	2.1	4.1	1.7
Lu	0.12	0.29	0.10	0.25	0.14	0.31	0.29	0.17	0.20	0.42	0.49	0.87	0.14	0.27	0.83	0.13	0.14	0.39	1.09	0.08	0.28	0.31	0.31	0.63	0.24
Sr/Y	50.7	13.6	2.5	8.8	24.5	5.5	6.5	29.1	10.8	13.9	6.0	0.7	55.3	6.1	0.9	36.1	40.9	9.6	0.6	62.2	5.9	9.1	26.3	4.6	17.5
Zr/Y	16.3	11.4	3.5	8.5	2.7	2.3	2.9	9.9	3.2	4.7	3.8	6.6	128.0	48.3	6.2	16.3	11.3	2.4	4.2	15.7	5.6	4.8	5.4	2.9	6.5
Eu/Eu*	1.1	0.8	0.9	0.9	1.1	1.1	1.0	0.9	1.1	1.1	0.9	0.7	13.8	5.6	0.5	0.9	1.0	0.7	0.5	1.0	0.4	1.0	0.9	0.9	0.9
(La/Yb) _{CN}	13.3	11.6	0.8	12.8	0.7	0.5	1.3	12.7	1.4	4.6	2.7	6.6	3.6	2.0	6.2	26.4	11.2	6.3	5.2	23.1	9.2	3.0	12.4	0.9	14.2
(La/Sm) _{CN}	4.6	4.6	0.9	4.9	0.8	0.5	1.1	4.4	1.1	2.4	1.7	3.7	11.3	5.3	2.9	5.0	3.6	1.7	2.8	5.3	4.4	1.8	3.0	0.9	3.0
(Gd/Yb) _{CN}	1.6	1.6	1.0	1.8	0.9	1.0	1.1	2.1	1.3	1.4	1.4	1.2	0.2	0.3	1.5	2.8	2.0	2.1	1.2	2.5	1.5	1.4	2.4	0.9	2.9
(La/Yb) _{MN}	22.6	19.7	1.4	21.7	1.2	0.8	2.2	21.7	2.4	7.8	4.6	11.3	6.1	3.3	10.5	44.9	19.1	10.8	8.8	39.4	15.6	5.2	21.1	1.5	24.2
(La/Sm) _{MN}	7.5	7.4	1.5	7.9	1.3	0.9	1.7	7.2	1.8	3.8	2.8	6.1	18.4	8.6	4.8	8.2	5.9	2.8	4.6	8.6	7.2	2.9	5.0	1.5	4.9
(Gd/Yb) _{MN}	1.6	1.6	1.0	1.8	0.9	1.0	1.1	2.1	1.3	1.4	1.4	1.2	0.2	0.3	1.5	2.8	2.0	2.1	1.2	2.5	1.5	1.5	2.4	0.9	2.9

Abbreviations: Bsit, basalt; Bsit and, basaltic andesite; CN, chondrite normalized; Dac, dacite; Dio, diorite; Gab, gabbro; Gmt, granite; Grd, granodiorite; Kom bsit, komatiitic basalt; Lgrmt, leucogranite; MN, mid-ocean-ridge basalt normalized; Pyx, pyroxenite; Rhy, rhyolite

Table 4: Sm-Nd isotopic data for whole-rock samples from the eastern Rice Lake belt.

Sample number ⁽¹⁾	UTM Zone 15, NAD 83		Rock type (unit)	Sm (ppm)	Nd (ppm)	¹⁴⁷ Sm/ ¹⁴⁴ Nd ⁽²⁾	¹⁴³ Nd/ ¹⁴⁴ Nd ⁽³⁾	Err. ⁽⁴⁾ (2σ)	T _{DM} ⁽⁵⁾ (Ga)	T ⁽⁶⁾ (Ga)	εNdT ⁽⁷⁾
	Easting	Northing									
Garner assemblage											
96-02-1091	345769	5632160	Rhyolitic tuff (Gn3b)	4.11	20.99	0.11850	0.51118	6	3.16	2.900	0.8
36-99-235-1	345264	5632210	Dacitic tuff (Gn3b)	3.80	20.48	0.11710	0.51113	4	3.05	2.900	0.3
36-95-173-1	344725	5631950	Pyroxenite (Gn4b)	0.55	1.50	0.22268	0.51345	62		2.870	6.3
CB02-03	343748	5632463	Pegmatitic tonalite (Gn4d)	3.28	11.92	0.16617	0.51201	10		2.870	-1.0
CB02-04	342925	5632607	Arkositic sandstone (Gn5a)	5.36	20.12	0.16105	0.51203	4		2.850	1.2
CB02-02	343545	5633064	Dacitic tuff or dacite (Gn5c)	4.38	23.58	0.11222	0.51104	5	3.17	2.850	-0.2
96-03-1254-2	343262	5634079	Komatiitic basalt (Gn6)	0.67	2.01	0.20001	0.51286	9		2.850	3.1
36-98-186-2	342602	5634261	Komatiite (Gn6)	2.39	10.10	0.13524	0.51162	17	2.79	2.850	2.7
96-03-1181-1	344772	5633449	Basaltic andesite (Gn7)	1.77	6.51	0.16424	0.51206	6		2.850	0.6
36-98-184-1	342534	5634117	Basalt (Gn7)	1.73	4.85	0.21260	0.51300	5		2.850	1.2
Bidou assemblage											
07-98-43-1	340768	5639275	Basalt (Unnamed basalt)	2.86	9.13	0.18923	0.51264	7		2.730	2.7
07-98-046-1	762549	5643862	Basalt (Unnamed basalt)	2.64	8.02	0.19280	0.51268	4		2.730	2.2
07-98-041-1	758100	5643865	Greywacke (Dove Fm.)	3.03	15.70	0.11913	0.51119	20	3.03	2.730	-1.0
07-98-040-1	758048	5643765	Basalt (Bd1)	2.14	6.40	0.18941	0.51253	20		2.730	0.5
07-98-050-1	762389	5639148	Dacitic tuff breccia (Bd3b)	2.94	17.32	0.10681	0.51107	19	2.84	2.730	1.0
Gem assemblage											
96-04-1569-2	343432	5625521	Basalt (Gw1a)	2.43	8.13	0.18037	0.51233	8		2.725	-0.3
36-99-197-1	339387	5630929	Basalt (Gw1a)	3.02	12.57	0.15794	0.51201	6		2.725	1.4
07-98-047-1	759667	5636873	Basaltic andesite (Gw1a)	6.76	29.31	0.13622	0.51156	8	2.95	2.725	0.2
07-98-048-1	759660	5636980	Greywacke (Gw2a)	1.83	9.16	0.11412	0.51125	6	2.77	2.725	1.9
36-99-220-1	340410	5632262	Rhyolite (Gw4a)	8.90	47.29	0.11461	0.51126	11	2.76	2.725	1.9
96-04-1547-1	345031	5626599	Rhyolite tuff (Gw4d)	5.27	27.61	0.11542	0.51122	7	2.99	2.725	0.9
96-05-1722-1	344942	5624070	Rhyolite (Gw6a)	10.67	54.95	0.11737	0.51124	6	3.02	2.725	0.6
96-03-1287-2	342287	5627163	Rhyolitic tuff (Gw7)	3.44	20.64	0.10085	0.51095	6	2.97	2.725	0.7
96-04-1557-1	345494	5626322	Dacitic tuff (Ge1a)	2.47	12.74	0.11733	0.51125	6	3.01	2.725	0.8
96-06-1971-1	345991	5627538	Basalt (Ge2)	9.38	48.78	0.11622	0.51122	8	3.02	2.725	0.6
Wanipigow River plutonic complex											
96-03-1116	347679	5630991	Biotite granite (Wn2a)	2.85	13.08	0.13172	0.51148	10	3.10	2.725	0.2
Edmunds assemblage											
CB02-05	338030	5630272	Greywacke (Em1b)	2.95	17.22	0.10351	0.51100	8	2.98	2.700	0.4
96-07-2151-1	342452	5621780	Basalt flow (Em8)	3.93	13.96	0.17022	0.51224	7		2.700	1.4
96-06-2081-1	345200	5621569	Diorite (Em9)	7.51	37.53	0.12097	0.51131	8	3.03	2.700	0.4
96-07-2235-1	341121	5625957	Gabbro (Em9)	3.32	9.84	0.20419	0.51286	8		2.700	1.7
96-07-2150-1	342576	5621962	QFP (Em10)	10.78	45.02	0.14477	0.51179	6		2.700	1.5

⁽¹⁾ First two digits indicate geologist (CB, C. Böhm; 07, A. Bailes; 36, T. Corkery; 96, S. Anderson); second two digits indicate year of collection

⁽²⁾ estimated error is better than 0.5%

⁽³⁾ normalized to ¹⁴⁶Nd/¹⁴⁴Nd = 0.7219; external precision based on repeat La Jolla Nd standard runs

⁽⁴⁾ analytical uncertainty; x 10⁻⁶

⁽⁵⁾ depleted-mantle Nd model ages calculated according to the model of DePaolo (1981)

⁽⁶⁾ known or inferred age

⁽⁷⁾ ε_{Nd} values at the known or inferred age (T) calculated using present-day chondritic ratios of ¹⁴³Nd/¹⁴⁴Nd = 0.512638 and ¹⁴⁷Sm/¹⁴⁴Nd = 0.1967

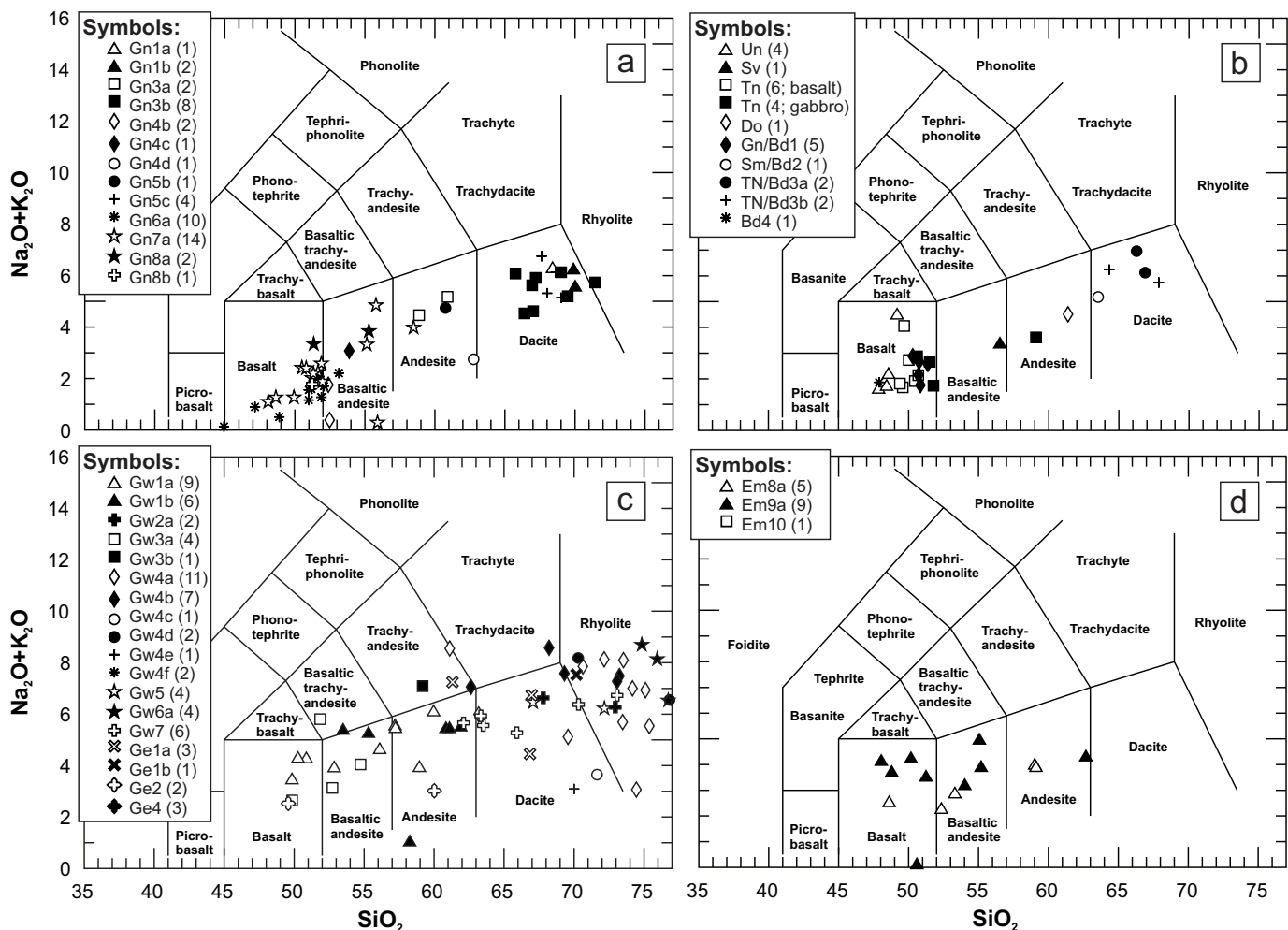


Figure 47: SiO_2 vs. total alkali plots (Le Bas et al., 1986): **a)** Garner assemblage ($n = 49$); **b)** Bidou assemblage ($n = 27$); **c)** Gem assemblage ($n = 69$); **d)** Edmunds assemblage ($n = 15$). Unit codes in the symbol legends correspond to those from the preceding text and accompanying Map GR2013-1-1. Numbers in parentheses indicate the number of analyses from each unit (note that some high- SiO_2 samples from the Gem and Edmunds assemblages plot off the right margin of this diagram). Abbreviations for the formations of the Bidou assemblage (Campbell, 1971) in Figure 47b: Do, Dove Lake formation; Gn, Gunnar formation; Sm, Stormy Lake formation; Sv, Stovel Lake formation; TN, The Narrows formation; Tn, Tinney Lake formation; Un, Unnamed basalt.

mafic and felsic rocks from each assemblage, separated on the basis of SiO_2 content (recalculated to 100% volatile free) as follows: mafic, $\text{SiO}_2 < 57$ wt. % ($n = 60$); felsic, $\text{SiO}_2 > 63$ wt. % ($n = 62$). Chemically primitive (i.e., mafic) rocks from each assemblage are described first, since these provide the clearest insight into source characteristics and possible tectonic settings. The chemistry of ultramafic ($\text{SiO}_2 < 53$ wt. %, $\text{MgO} > 12$ wt. %; $n = 12$) volcanic rocks from the Garner assemblage is also described in detail. Epiclastic rocks and samples of andesitic composition (SiO_2 57–63 wt. %; $n = 20$) are mostly excluded from consideration, but are included for reference in Data Repository Item DRI2013002.

The following abbreviations are used throughout: BABB, back-arc-basin basalt; CAB, calcalkalic basalt; DL, detection limit; E-MORB, enriched mid-ocean-ridge basalt; HFSE, high-field-strength elements (Hf, Nb, Ta, Ti, Y, Zr); HREE, heavy rare-earth elements (Er to Lu); LREE, light rare-earth elements (La to Sm); MREE, middle rare-earth elements (Eu to Ho); N-MORB, normal mid-ocean-ridge basalt; VAT, volcanic-arc

tholeiite (basalt). Normalizing values are from Sun and McDonough (1989), abbreviated as follows: CN, chondrite normalized; PM, primitive-mantle normalized; MN, MORB normalized (using N-MORB values).

Garner assemblage

Major-element and immobile trace-element discrimination diagrams indicate a subalkaline affinity and bimodal distribution of volcanic and associated intrusive rock compositions in the Garner assemblage (Figures 47a, 48a). Four samples of dacitic volcanoclastic rocks near the base of the assemblage (units Gn1b, Gn3b) show slightly elevated Nb/Y, suggestive of a mildly alkaline affinity (Figure 48a). On the Jensen (1976) diagram, the basaltic rocks define a discontinuous trend from calcalkalic basalt, through Fe- and Mg-tholeiitic basalt, to komatiitic basalt and komatiite (Figure 49a). Immobile trace-element ratios indicate that the dacitic rocks are calcalkalic, whereas the basaltic rocks are mostly tholeiitic, with some samples showing transitional tholeiitic–calcalkalic affinity (Figure 50a).

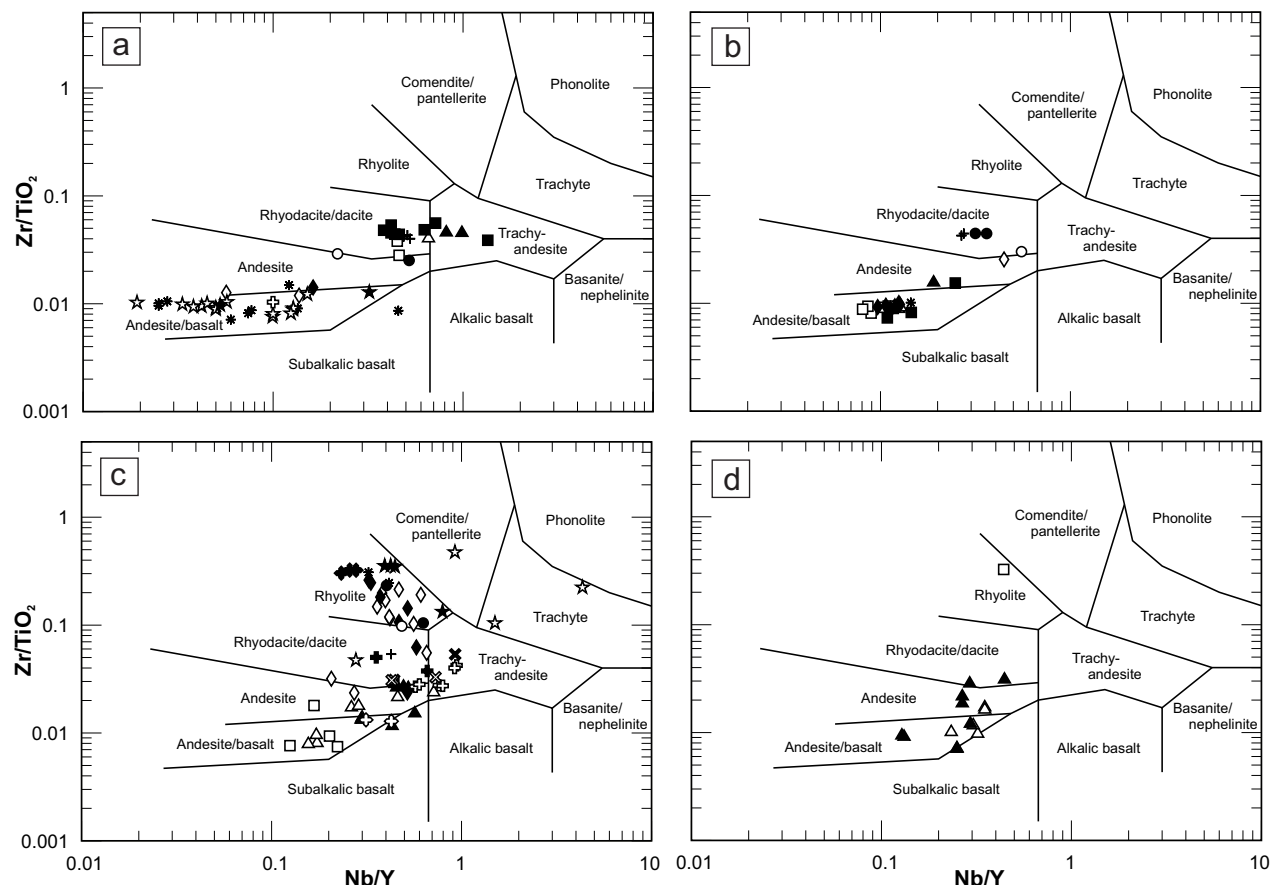


Figure 48: Nb/Y vs. Zr/TiO_2 plots (Winchester and Floyd, 1977): **a)** Garner assemblage; **b)** Bidou assemblage; **c)** Gem assemblage; **d)** Edmunds assemblage. Symbols as in Figure 47.

Mafic rocks

Basalt and basaltic andesite flows (unit Gn7) and associated sills (unit Gn8) in the Garner assemblage have SiO_2 contents of 48–56 wt. %, TiO_2 of 0.5–1.1 wt. % and FeO^+ of 9–12 wt. %, with Mg numbers from 45 to 63. Chromium values range from 54 to 523 ppm (average 260 ppm) and Ni values from 96 to 265 ppm (average 149 ppm). These rocks have relatively flat profiles on an N-MORB-normalized trace-element plot, with unfractionated to weakly fractionated LREE, unfractionated HREE and variable negative Nb anomalies. The HREE and LREE are mostly depleted in relation to N-MORB (Figure 51a). Thorium, Nb, Ti and Yb define linear trends when plotted against Ce or Zr as indices of fractionation (not shown), suggesting that these variations may be, at least in part, controlled by fractional crystallization.

Strongly depleted Nb, coupled with weak depletions of Zr and Ti, are suggestive of basalts erupted in volcanic arc or back-arc settings (Perfit et al., 1980; Saunders and Tarney, 1984; Kelemen et al., 1990; Saunders et al., 1991). On ternary plots of Th–Hf–Ta (Wood, 1980) and La–Y–Nb (Cabanis and Lecolle, 1989), the samples plot mostly in the fields for volcanic-arc basalt (VAT), although some trend toward mildly enriched N-MORB compositions (Figure 52a, b) and are thus chemically similar to BABB (Saunders and Tarney, 1984; Sinton and Fryer, 1987; Volpe et al., 1987; Stern et al., 1990; Ewart et al., 1994; Pearce and Stern, 2006). On the Nb/Yb versus Th/Yb diagram of Pearce and Peate (1995), most of the data points

scatter well above the MORB array (Figure 52c), suggesting a significant input of a high Th/Yb crustal component. Mostly low (but variable) Nb/Yb ratios indicate a strongly depleted mantle source, which would favour an oceanic rather than continental-arc setting (Pearce and Peate, 1995; Pearce 2008). A near-vertical trend of data points on a plot of La/Sm versus Th/Nb (Figure 52d) is indicative of a significant input of subduction-related (i.e., high Th/Nb) crustal material, as is typical of volcanic-arc settings (e.g., Pearce and Peate, 1995). Initial ϵ_{Nd} values of 1.2 and 0.6 (at 2.85 Ga) for samples of basalt (184-1) and andesite (1181-1), respectively, co-vary with chemical proxies for crustal contamination (Figure 53a, b), thus confirming some interaction with older, isotopically evolved crustal materials. The petrogenesis of these rocks may have involved partial melting of mantle-wedge peridotite in an intraoceanic setting, and some interaction with crustal materials. Alternatively, taking into account their close spatial and temporal association with komatiitic volcanism, the tholeiitic basalt could also have been generated by partial melting in the head of a mantle plume (Campbell et al., 1989) that impinged on, and was contaminated by, pre-existing arc crust (e.g., Dostal and Mueller, 1997; Hollings et al., 1999).

Komatiitic rocks

Subordinate flows of komatiitic basalt (unit Gn6; Figure 54a) near the base of the tholeiitic basalt succession have

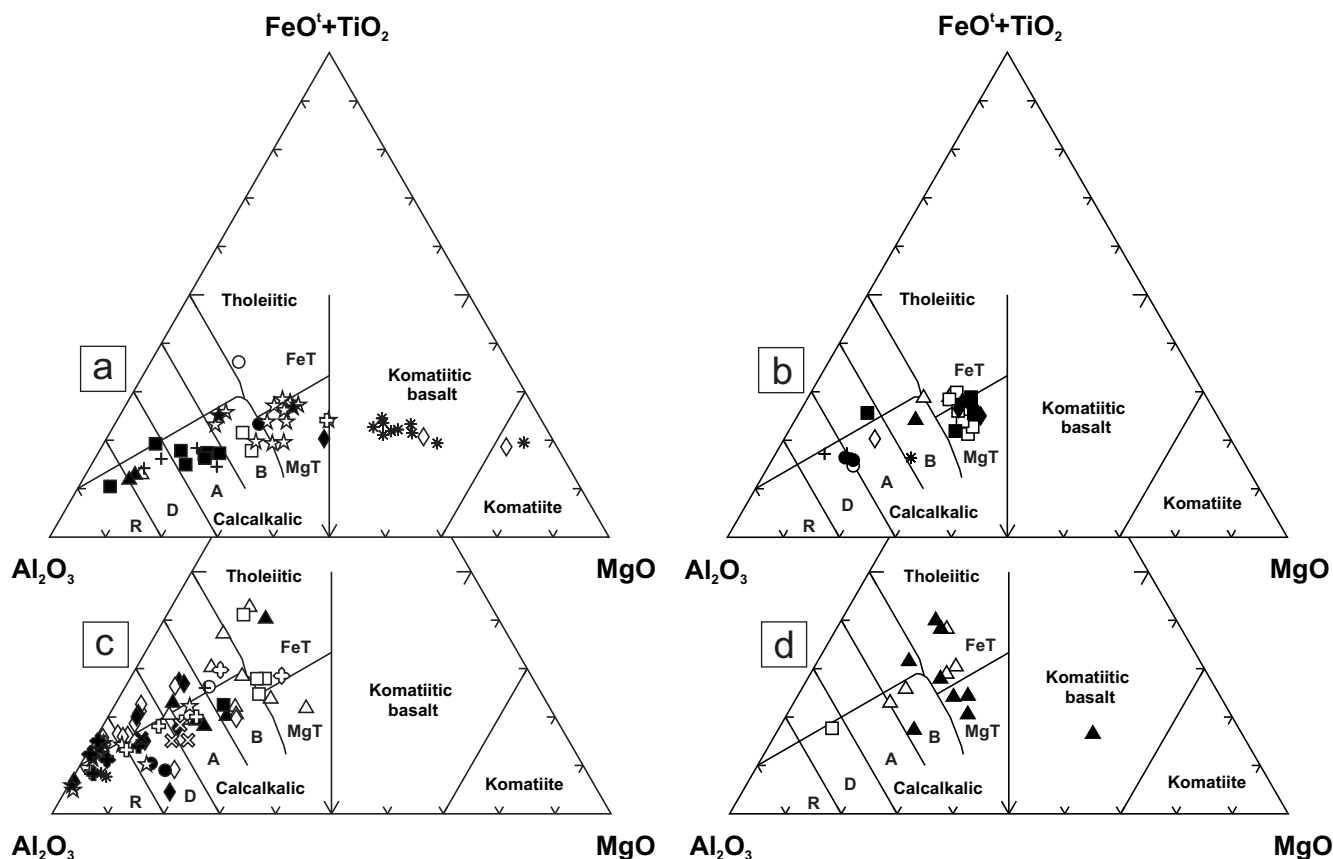


Figure 49: Al_2O_3 vs. $\text{FeO}^t + \text{TiO}_2$ vs. MgO plots (Jensen, 1976; FeO^t = total Fe expressed as FeO): **a)** Garner assemblage; **b)** Bidou assemblage; **c)** Gem assemblage; **d)** Edmunds assemblage. Symbols as in Figure 47. Abbreviations: A, andesite; B, basalt; D, dacite; FeT, Fe-tholeiite; MgT, Mg-tholeiite; R, rhyolite.

SiO_2 contents of 47–53 wt. %, TiO_2 of 0.3–0.6 wt. %, FeO^t of 10–13 wt. % and MgO of 12–17 wt. %, with Mg numbers from 67 to 72. Chromium values range from 871 to 2080 ppm (average 1564 ppm) and Ni values from 151 to 919 ppm (average 428 ppm), as is typical of highly primitive melts. These rocks mostly plot as Ti-depleted komatiite on the MgO versus $\text{Al}_2\text{O}_3/\text{TiO}_2$ plot (Figure 54b) of Sproule et al. (2002). N-MORB-normalized trace-element profiles are flat and strongly depleted, with unfractionated LREE and HREE, negative Nb anomalies and positive Th anomalies (Figure 51b). Primitive-mantle-normalized profiles likewise show depleted LREE, unfractionated HREE, negative Nb anomalies and weak positive Th anomalies (Figure 54c), and accord well with those presented by Hollings et al. (1999, Figure 4e) for komatiitic basalt from the same unit. A komatiitic basalt flow in the upper portion of the complex has an initial ϵ_{Nd} value of 3.1 (at 2.85 Ga; Figure 53a, b) and plots along the depleted-mantle evolution curve (Figure 53c); hence, any interaction with isotopically evolved crust (as suggested by the Th-Nb anomalies) must have been minor.

Ultramafic komatiite has been identified in two locations and thus appears to represent a minor component of the komatiite-tholeiite flow complex, although the possibility that it is under-represented in outcrop due to preferential weathering and erosion cannot be ruled out. In the east, an ultramafic komatiite flow (30.9 wt. % MgO , 1660 ppm Cr, 1780 ppm Ni) at the base of the complex lies in sharp contact with underlying

sedimentary and volcanoclastic rocks of unit Gn5. In contrast to the overlying komatiitic basalts, this flow has a gently sloped PM profile, with weakly fractionated LREE and HREE (Figure 54c, sample 1185-2). Weak negative Nb, Zr and Ti anomalies, coupled with the weak enrichment of highly incompatible trace elements, suggest minor contamination by crustal material. Another ultramafic komatiite (19.6 wt. % MgO , 1450 ppm Cr and 695 ppm Ni) higher up in the stratigraphy near the western extent of the complex shows a comparatively steep profile, with fractionated LREE and HREE, a pronounced negative Nb anomaly and a positive Th anomaly (Figure 54c, sample 186-2). Coupled with increases in $\text{La}/\text{Sm}_{\text{PM}}$ and $\text{Th}/\text{La}_{\text{PM}}$ ratios and SiO_2 content (45–49 wt. %), the more pronounced negative Nb anomaly is indicative of significant contamination of the western flow by crustal material; the fact that these attributes are exhibited by only this flow suggests assimilation of a local source during emplacement. This sample has an initial ϵ_{Nd} value of 2.7 (at 2.85 Ga) and plots slightly above the depleted-mantle evolution curve (Figure 53c); hence, it appears likely that the contaminant was also isotopically juvenile.

Shown for comparison in Figure 54c are two profiles for pyroxenite from the east (173-1) and west (154-1) portions of the Garner Lake intrusive complex (unit Gn4b) that also show evidence of crustal contamination (i.e., fractionated LREE and positive Th anomaly), which likewise appears to be more significant in the west. Sample 173-1 has an initial ϵ_{Nd} value of 6.3

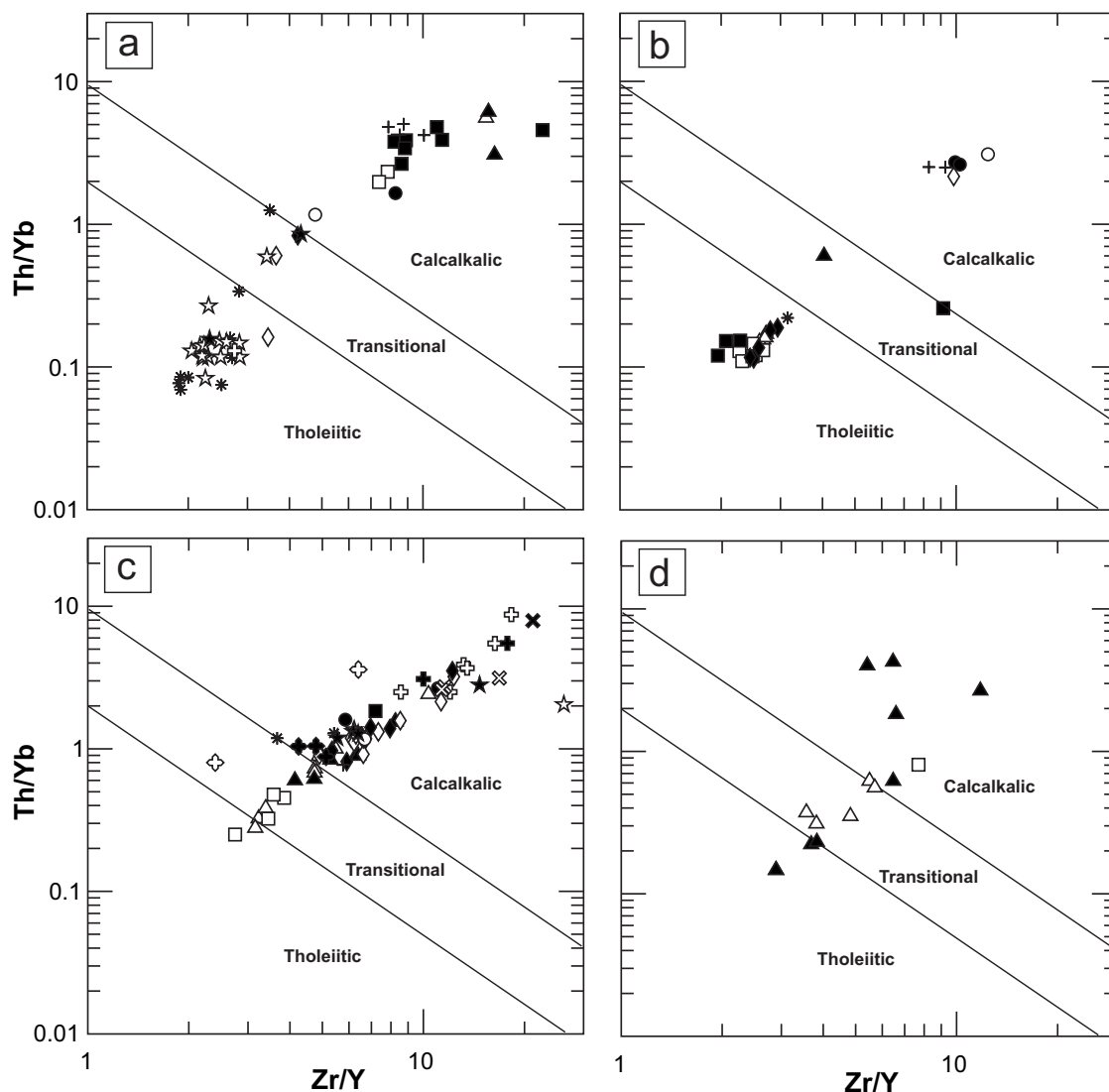


Figure 50: Zr/Y vs. Th/Yb plots (Ross and Bédard, 2009): **a)** Garner assemblage; **b)** Bidou assemblage; **c)** Gem assemblage; **d)** Edmunds assemblage. Symbols as in Figure 47.

(at 2.87 Ga; Figure 53c), which is probably spurious given the very low Sm and Nd contents of this sample and the very large analytical uncertainty (Table 4).

Low abundances of highly incompatible trace elements ($\text{La}/\text{Sm}_{\text{PM}} < 1$), coupled with high Mg contents and initial ϵ_{Nd} values, indicate derivation of the komatiitic basalt flows from a strongly depleted mantle source. Negative Nb and positive Th anomalies (relative to La) likely reflect crustal contamination, although the strongly depleted LREE require that any crustal component is minor. As described by Nesbitt et al. (1979) and Campbell et al. (1989), the high eruption temperatures required for komatiitic flows imply derivation from anomalously hot mantle, which is most plausibly attributed to upwelling thermal plumes. Campbell et al. (1989) noted the common association of komatiitic and tholeiitic basalt flows in Archean greenstone belts, which they attributed to melting in different thermal regions of mantle plumes: komatiite from the hotter plume axes and basalt from the cooler plume heads. Similar models have been proposed for komatiite–tholeiite associations in the Superior province (e.g., Dostal and Mueller, 1997; Polat et al.,

1999), including those of the Balmer assemblage in the Red Lake greenstone belt (Tomlinson et al., 1998). In a study that included samples from the Garner assemblage, Hollings et al. (1999) noted the presence of arc-like felsic volcanic rocks in these associations, which they attributed to interaction between mantle plumes and volcanic arcs.

Felsic rocks

Two distinct chemical types of felsic (66–72 wt. % SiO_2) volcanoclastic rocks are distinguished in the Garner assemblage. Samples from unit Gn1 near the base of the assemblage are characterized by smooth, listric-shaped profiles on a CN trace-element plot (Figure 55a), with enriched and fractionated LREE, weakly fractionated HREE and negligible Eu anomalies (Figure 56a, b). The Zr/Y ratios are relatively high (15–16; Figure 56c) and Cr and Ni contents are at or below detection limits. In contrast, overlying volcanoclastic rocks of units Gn3 and Gn5 are characterized by slightly ‘kinked’ profiles (Figure 55a, b) that show higher overall REE contents and significantly enriched HREE, generally with correspondingly lower

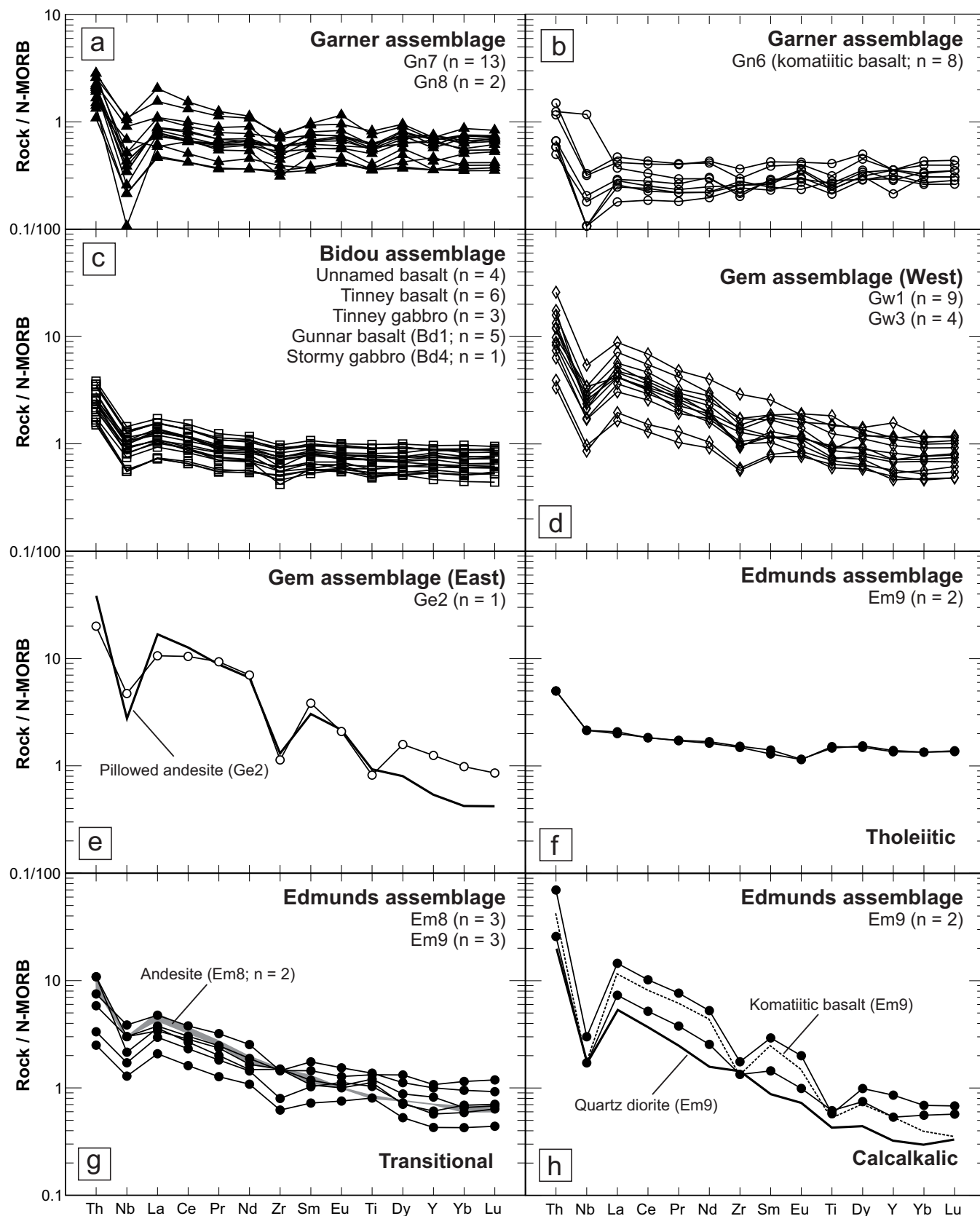


Figure 51: N-MORB-normalized trace-element diagrams for mafic ($\text{SiO}_2 < 57$ wt. % and $\text{MgO} < 12$ wt. %, volatile free) volcanic and associated intrusive rocks: **a**) Garner assemblage; **b**) Garner assemblage komatiitic basalt (MgO 12–18 wt. %, volatile free; included for comparison purposes); **c**) Bidou assemblage; **d**) Gem assemblage (West association); **e**) Gem assemblage (East association); includes an analysis of pillowed andesite from the same flow unit (Ge2); **f**), **g**) and **h**) Edmunds assemblage; includes analyses of associated andesite, quartz diorite and komatiitic basalt for comparison purposes. Normalizing values and order from Sun and McDonough (1989). Abbreviation: N-MORB, normal mid-ocean-ridge basalt.

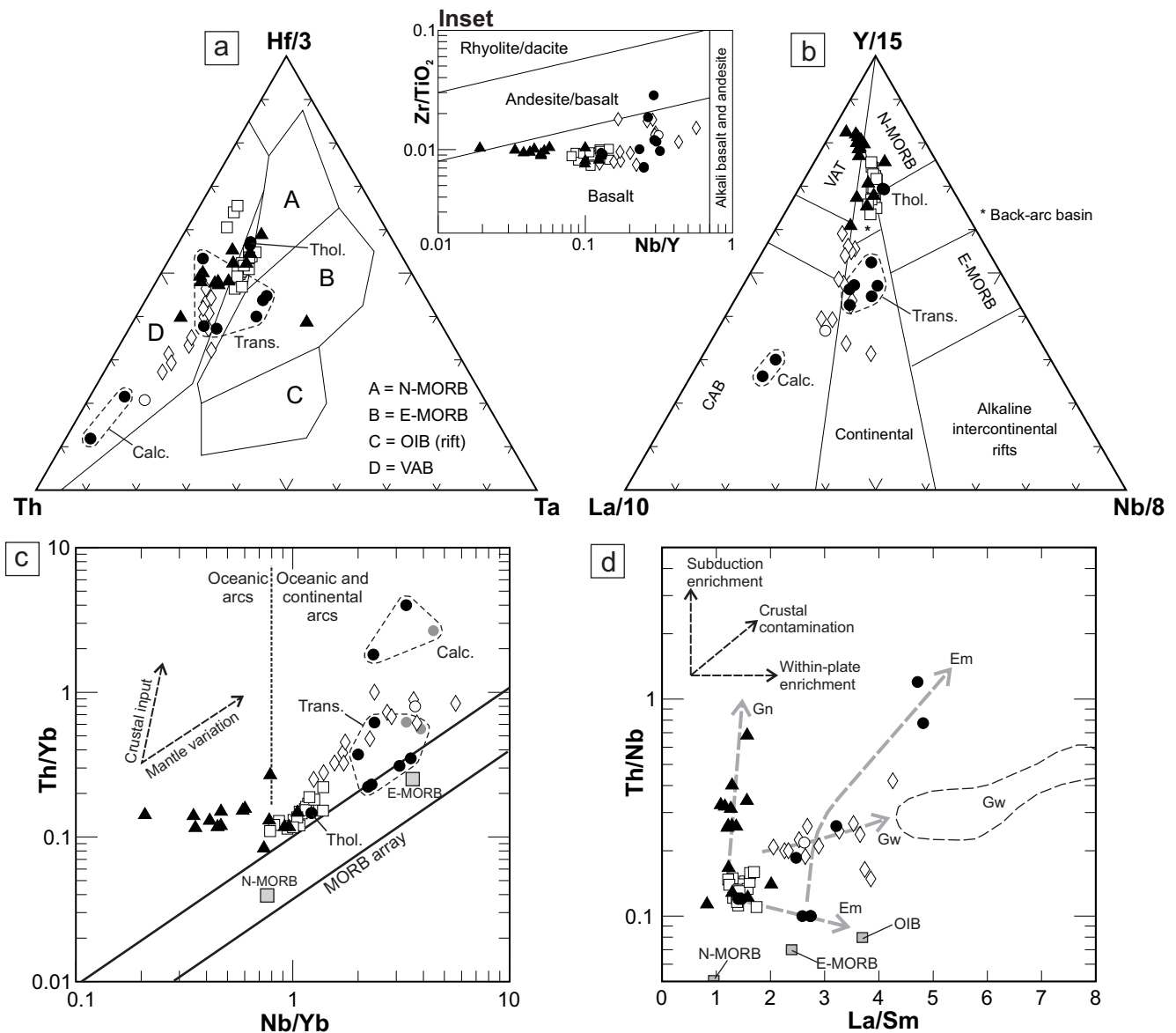


Figure 52: Discrimination diagrams for mafic volcanic and associated intrusive rocks of the Garner (filled triangles, $n = 15$), Bidou (open squares, $n = 19$), Gem (West association, open diamonds, $n = 13$; East association, open circle, $n = 1$) and Edmunds (filled circles, $n = 10$; fields for the three distinct chemical types are indicated by dashed outlines and labels; see text) assemblages: **a)** Th vs. Hf/3 vs. Ta diagram (Wood, 1980); inset Nb/Y vs. Zr/TiO₂ diagram (modified from Winchester and Floyd, 1977; Pearce, 1996); **b)** La/10 vs. Y/15 vs. Nb/8 diagram (Cabanis and Lecolle, 1989); **c)** Nb/Yb vs. Th/Yb diagram (Pearce and Peate, 1995); **d)** La/Sm vs. Th/Nb diagram; heavy dashed arrows show the apparent evolutionary trends of mafic magmatism in the Garner (Gn), Gem (Gw), and Edmunds (Em) assemblages; dashed outline indicates the typical compositions of felsic volcanic rocks in the West association of the Gem assemblage (Gw). Abbreviations: CAB, calcalkalic basalt; Calc., calcalkalic; E-MORB, enriched mid-ocean-ridge basalt; N-MORB, normal mid-ocean-ridge basalt; OIB, ocean-island basalt; Thol., tholeiitic; Trans., transitional tholeiitic–calcalkalic; VAB, volcanic-arc basalt; VAT, volcanic-arc tholeiite (basalt). N-MORB, E-MORB and OIB values from Sun and McDonough (1989).

La/Yb_{CN} ratios. Aside from single outlier values, these samples also have less fractionated LREE and HREE, and weak negative Eu anomalies (Figure 56a, b). The Zr/Y ratios are comparatively low (8–11; Figure 56c) and the majority of samples (9 of 12) have very high concentrations of Cr (74–168 ppm; average 131 ppm) and Ni (57–160 ppm, average 103 ppm). Both suites show negative Nb and Ti anomalies and weak positive Zr anomalies on PM plots (Figure 57a, b). However, samples from unit Gn1 are distinguished by consistently lower contents of Th, HFSE and REE, and relatively depleted HREE (see also Figure 58a–f), resulting in less pronounced negative Ti anomalies.

The relatively high Zr/Y and La/Yb ratios, low Y and Yb values and negligible Eu anomalies that characterize the felsic volcanoclastic rocks of the Garner assemblage (Figure 56c, d) indicate their affinity to ‘FI’ felsic volcanic rocks in the scheme of Leshner et al. (1986), which are thought to be derived by low-degree partial melting of mafic sources under high pressures (i.e., in the field of garnet stability), with minimal fractionation during ascent (Leshner et al., 1986; Hart et al., 2004). Very low Y (6.0–6.4 ppm) and Yb (0.54–0.75 ppm) contents and high La/Yb (19–32) and Sr/Y (51–62) ratios of samples from unit Gn1 indicate their close affinity to ‘adakitic’ rocks in volcanic arcs,

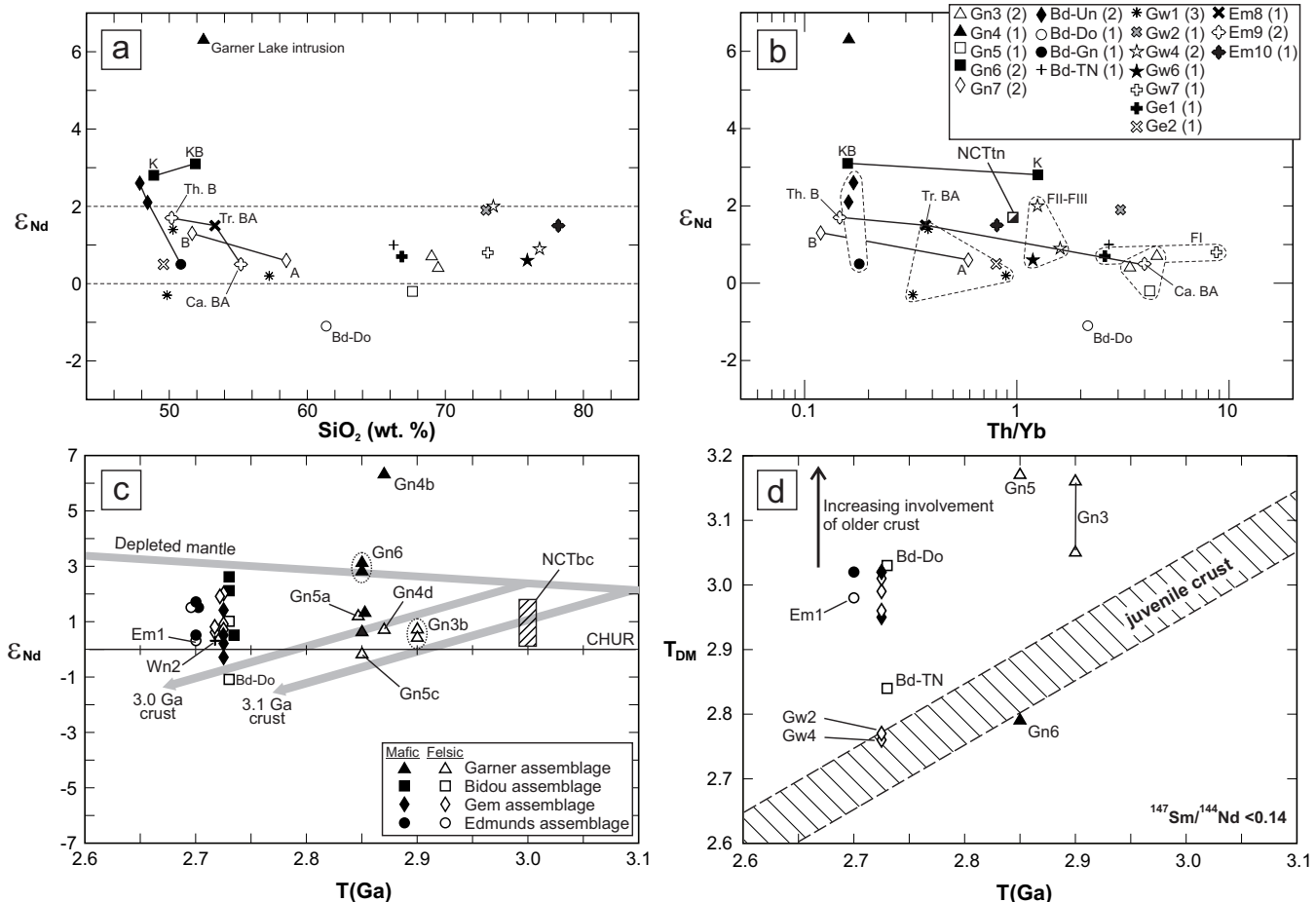


Figure 53: Discrimination diagrams of geochemical values or estimated age (T) versus Sm-Nd isotopic parameters for key map units in the eastern Rice Lake belt: **a)** SiO_2 (wt. %, recalculated to 100% volatile free) vs. ϵ_{Nd} ; tie-lines join mafic samples from the various assemblages; symbols as in Figure 53b; **b)** Th/Yb vs. ϵ_{Nd} ; tie lines join mafic samples from the various assemblages; plotted for comparison is a representative analysis of 3007 Ma tonalite from the south margin of the North Caribou terrane (NCTtn; data from Whalen et al., 2003); **c)** T (Ga) vs. ϵ_{Nd} ; depleted-mantle evolution trend is from Henry et al. (1998, 2000); arrows indicate the isotopic evolution of felsic crust that separated from the depleted mantle at 3.0 and 3.1 Ga (after Henry et al., 2000); hatched box indicates the range of values for ca. 3.0 Ga basement complexes at the south margin of the North Caribou terrane (NCTbc; data from Whalen et al., 2003); the sample suite for each assemblage defines a vertical array on this diagram; where necessary, overlapping samples in the arrays were separated slightly in a lateral direction to reduce clutter; **d)** T (Ga) vs. T_{DM} ; symbols as in Figure 53c; field for juvenile crust ($T_{DM} \approx T$) indicated by hatched pattern. Abbreviations: A, andesite; B, basalt; BA, basaltic andesite; Ca, calcalkalic; CHUR, chondritic uniform reservoir; K, komatiite; KB, komatiitic basalt; T, known or inferred age of emplacement (Ga); T_{DM} , depleted-mantle model age; Th, tholeiitic; Tr, transitional tholeiitic-calcalkalic. Sample 'Bd-Do' represents greywacke of the Dove Lake formation. All epsilon Nd values (ϵ_{Nd}) were calculated at the known or inferred age of crystallization (i.e., they are 'initial' ϵ_{Nd} values).

which are restricted to supra-subduction settings where young, hot, oceanic lithosphere is being subducted (e.g., Defant and Drummond, 1990; Martin, 1999; Moyen, 2009). These rocks have been interpreted as low-degree partial melts of the subducting slab (e.g., Defant and Drummond, 1990; Martin, 1999; Martin et al., 2005) or the metasomatized mantle wedge (e.g., Castillo et al., 1999; Garrison and Davidson, 2003; Macpherson et al., 2006; Richards and Kerrich, 2007; Chiaradia et al., 2009; Moyen, 2009), with or without modification/hybridization of the primary basaltic melt by 'normal' arc-magmatic processes, such as assimilation-fractional crystallization (AFC) or melting-assimilation-storage-homogenization (MASH; Hildreth and Moorbath, 1988), in the mantle or lower crust.

In the case of unit Gn1, the high La/Yb ratios and depleted and fractionated HREE are consistent with garnet fractionation

or partial melting in the presence of residual garnet (which partitions Y and HREE over LREE), suggesting that the magma differentiated in the mantle or lower crust (Leshner et al., 1986; Hart et al., 2004; Macpherson et al., 2006; Davidson et al., 2007; Richards and Kerrich, 2007). Chromium and Ni contents at or below detection limits suggest minimal interaction with mantle-wedge peridotite (Martin, 1999). In contrast, the lower La/Yb (~13–18) ratios, slightly depleted MREE (as indicated by the 'kinked' REE profiles) and enriched and less fractionated HREE of samples from units Gn3 and Gn5 appear to implicate amphibole as a residual or fractionating phase (which partitions MREE over HREE), and may thus reflect fractionation at shallower depths (e.g., Davidson et al., 2007; Bachmann and Bergantz, 2008). Nevertheless, the much higher Cr and Ni contents of these rocks suggest derivation from a parent melt that had

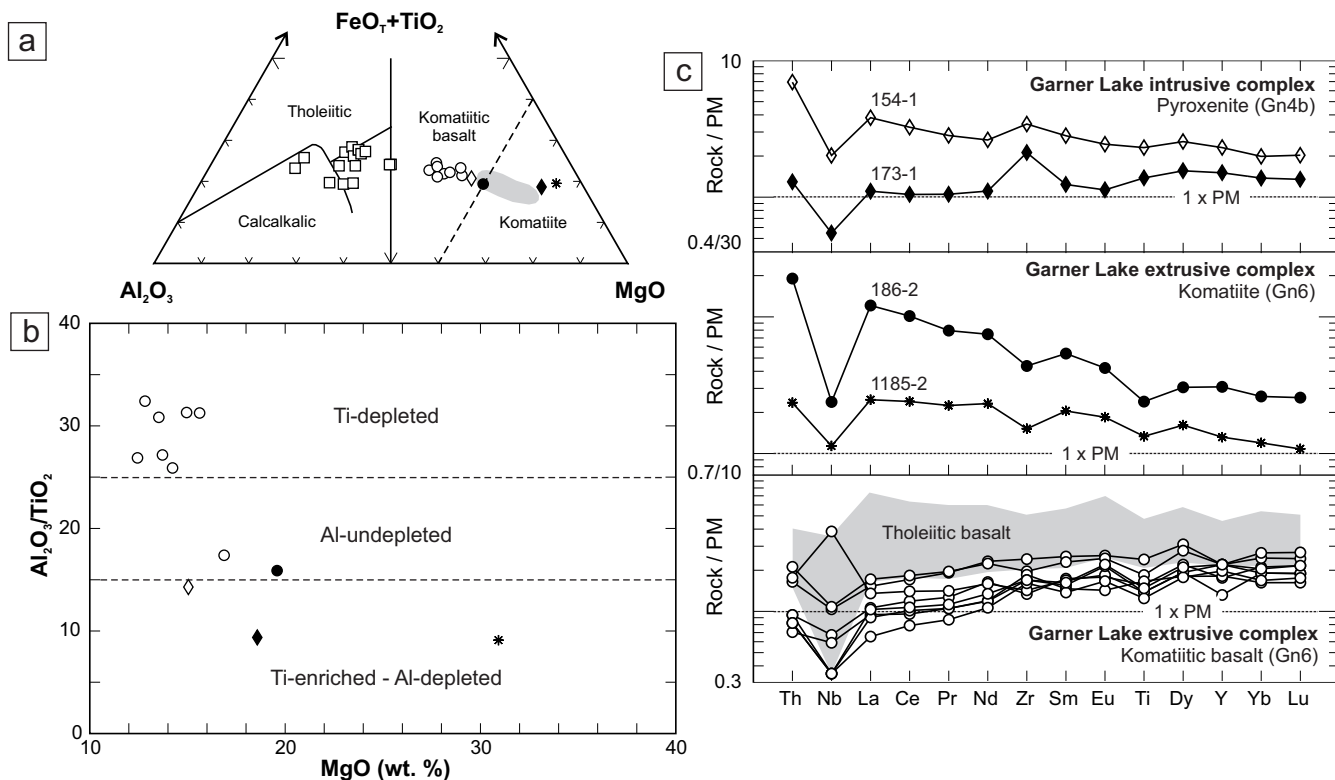


Figure 54: Discrimination diagrams and primitive-mantle-normalized (PM) trace-element diagrams for ultramafic volcanic and intrusive rocks of the Garner assemblage: **a)** Al_2O_3 vs. $\text{FeO}^t + \text{TiO}_2$ vs. MgO diagram (Jensen, 1976), shaded field showing the composition of komatiite from the locality described by Brommecker et al. (1993); data from Brommecker (1991); symbols as in Figure 54c; open squares show compositions of associated basalt flows ($n = 16$); **b)** MgO vs. $\text{Al}_2\text{O}_3/\text{TiO}_2$ diagram, showing the fields for the various compositional types of komatiitic rocks identified by Sproule et al. (2002); symbols as in Figure 54c; **c)** top panel, pyroxenite from the east (173-1; filled diamonds) and west (154-1; open diamonds) portions of the Garner Lake intrusive complex; middle panel, komatiite from the east (1185-2; stars) and west (186-2; filled circles) portions of the komatiite flow complex; bottom panel, komatiitic basalt (open circles; $n = 8$) from various locations in the flow complex; shaded field shows the pattern for associated tholeiitic basalt ($n = 13$); normalizing values and order from Sun and McDonough (1989).

undergone significant interaction with mantle-wedge peridotite. Initial ϵ_{Nd} values (0.8 to -0.2 , $n = 3$) and depleted-mantle model ages (3.17–3.05 Ga, $n = 3$) of felsic volcanoclastic rocks from units Gn3 and Gn5 also indicate significant interaction with isotopically evolved, older crustal material (Figure 53c, d; Table 4). Such features are fully in keeping with a supra-subduction setting for felsic volcanism in the Garner assemblage and may reflect variable interactions between partial melts of the mantle wedge and lower crust, as is thought to occur by MASH processes at the crust–mantle transition beneath volcanic arcs (e.g., Hildreth and Moorbath, 1988).

Bidou assemblage

Major-element and immobile trace-element discrimination diagrams indicate a subalkaline affinity and distinctly bimodal (basalt and dacite) distribution for volcanic and associated intrusive rock compositions in the Bidou assemblage (Figures 47b, 48b). Samples of intermediate composition include volcanic sandstone from the Dove and Stovel formations and a quartz diorite segregation in gabbro of the Tinney formation, and thus represent ‘hybrid’ rock types that are not considered further. The basaltic rocks cluster tightly at the boundary between Fe- and Mg-tholeiitic basalt on the Jensen (1976)

diagram (Figure 49b), and immobile trace-element ratios likewise indicate their tholeiitic affinity; the dacitic rocks are calcalkalic (Figure 50b).

Mafic rocks

Basalt flows and associated gabbro sills in the Bidou assemblage (units Un, Tn, Gn/Bd1 and Bd4; Figure 47b) have SiO_2 contents of 48–52 wt. %, TiO_2 of 0.6–1.4 wt. % and FeO^t of 8–13 wt. % over a range of Mg numbers from 44 to 62. The basalts have relatively flat profiles on an N-MORB-normalized trace-element plot, with weakly fractionated LREE and HREE, and weak negative Nb anomalies (Figure 51c). In relation to N-MORB, the HREE are depleted and the LREE are depleted or weakly enriched; most samples exhibit very weak Zr depletion. Chromium values range from 33 to 345 ppm (average 146 ppm) and Ni values from 40 to 171 ppm (average 77 ppm). Thorium, Nb, Ti and Yb plot along well-defined linear trends against Ce or Zr as indices of fractionation (not shown), suggesting a fractionation control.

Ternary plots of Th–Hf–Ta (Wood, 1980) and La–Y–Nb (Cabanis and Lecolle, 1989) indicate that the basalt is transitional between VAT and mildly enriched N-MORB (Figure

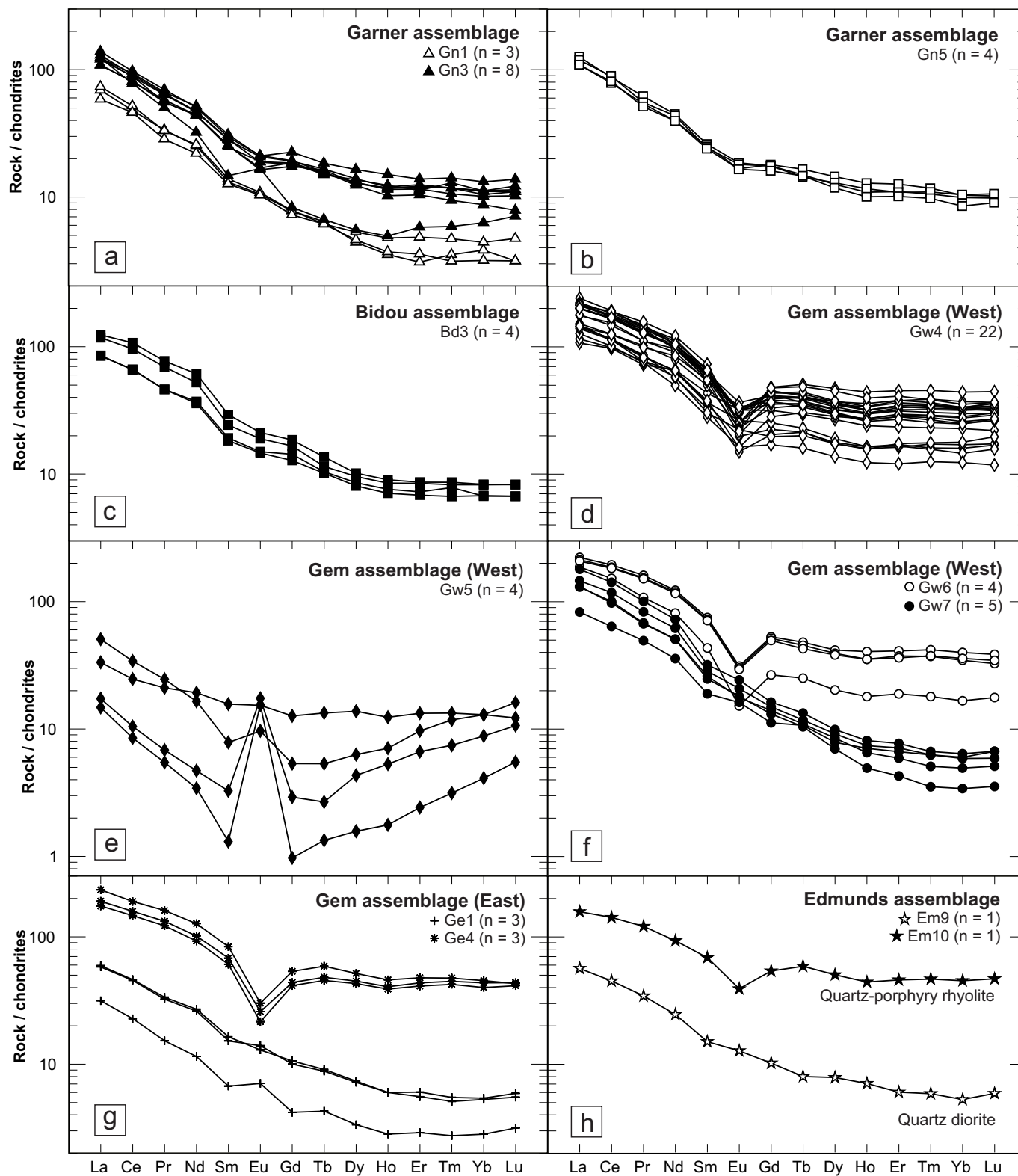


Figure 55: Chondrite-normalized rare-earth element diagrams for felsic ($\text{SiO}_2 \geq 63$ wt. %, volatile free) volcanic and associated intrusive rocks: **a)** and **b)** Garner assemblage; **c)** Bidou assemblage; **d), e)** and **f)** Gem assemblage (West association); **g)** Gem assemblage (East association); **h)** Edmunds assemblage. Normalizing values and order from Sun and McDonough (1989).

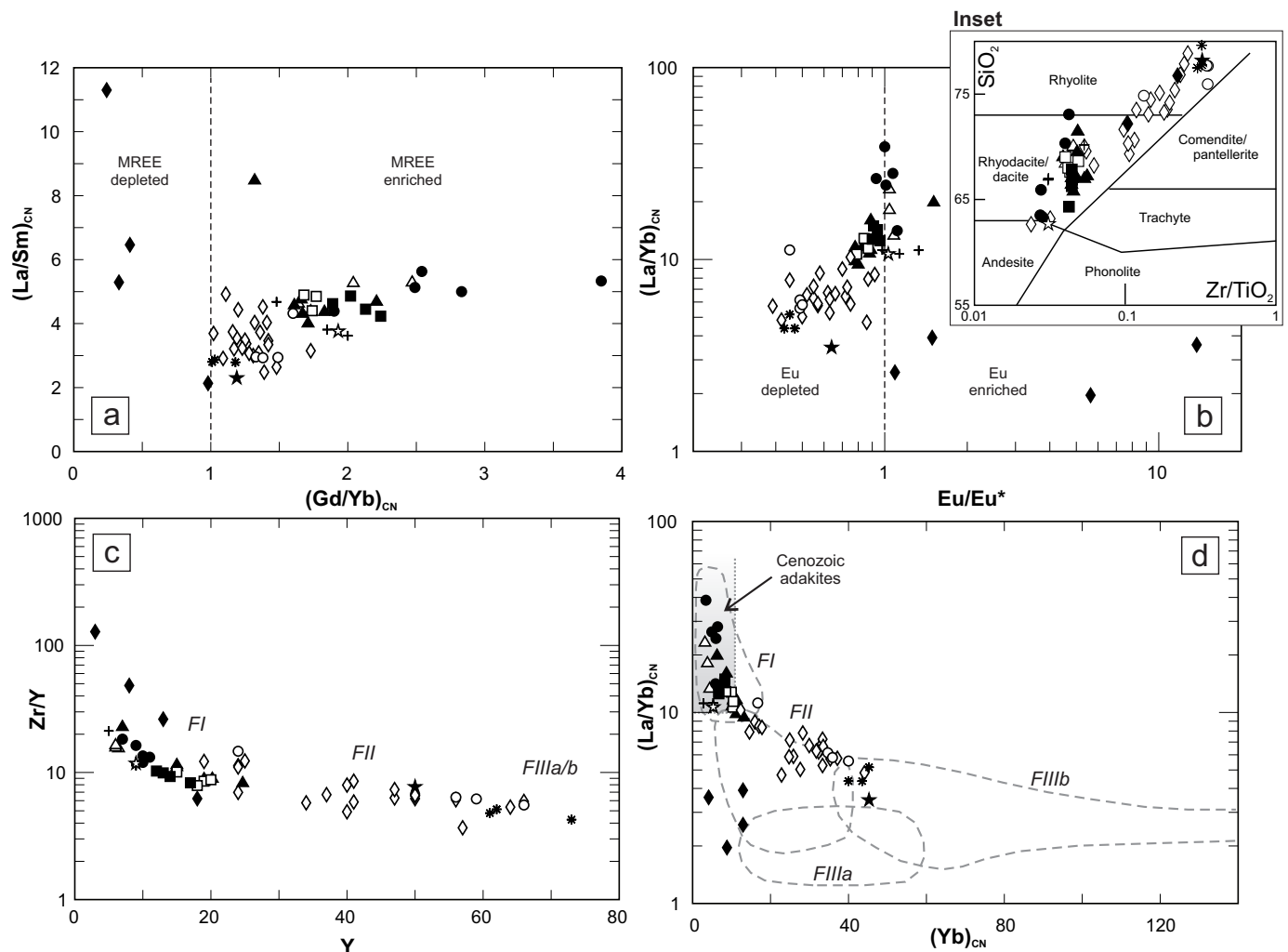


Figure 56: Bivariate plots of rare-earth element and trace-element ratios in felsic volcanic and associated intrusive rocks of the Garner, Bidou, Gem and Edmunds assemblages (symbols as in Figure 55): **a)** Gd/Yb_{CN} vs. La/Sm_{CN} ; **b)** Eu/Eu^* vs. La/Yb_{CN} , where $\text{Eu}^* = 0.5 (\text{Sm}_{\text{CN}} + \text{Gd}_{\text{CN}})$; inset Zr/TiO_2 vs. SiO_2 diagram (modified from Winchester and Floyd, 1977); **c)** Y vs. Zr/Y diagram, showing the general compositions of FI, FII and FIIIa/b felsic volcanic rocks (after Leshner et al., 1986); **d)** Yb_{CN} vs. La/Yb_{CN} diagram, showing the fields for FI, FII, FIIIa and FIIIb felsic volcanic rocks (from Leshner et al., 1986; Hart et al., 2004); field for Cenozoic adakite is from Martin et al. (2005). Normalizing values from Sun and McDonough (1989). Abbreviation: MREE, middle rare-earth element.

52a, b), and is thus chemically similar to basalt associated with seafloor-spreading centres in back-arc basins (e.g., Saunders and Tarney, 1984; Sinton and Fryer, 1987; Volpe et al., 1987; Stern et al., 1990; Ewart et al., 1994; Pearce and Stern, 2006), including particularly those documented from the Mariana Trough (Gribble et al., 1998), East Scotia Ridge (Fretzdorff et al., 2002) and Manus Basin (Sinton et al., 2003). On the Nb/Yb versus Th/Yb diagram of Pearce and Peate (1995), the data points define a trend slightly above and parallel to the MORB array (Figure 52c), suggesting a minor input of high Th/Yb crustal material and a variably enriched mantle source and/or variable degrees of partial melting. The data points define a relatively tight cluster on a plot of La/Sm versus Th/Nb (Figure 52d), suggesting negligible variation in mantle-source composition or crustal input over the eruptive history represented by the sample suite. Compositionally similar basalts in modern settings characterize steady-state seafloor-spreading centres in relatively mature (>100 km wide) back-arc basins,

where they are thought to result from decompression-induced partial melting of upwelling mantle (e.g., Price et al., 1990; Stern et al., 1990; Gribble et al., 1998). Initial ϵ_{Nd} values appear to decrease stratigraphically upward from the Unnamed basalt (2.7–2.2) to the Gunnar formation basalt (0.5; Figure 53a), perhaps on account of contamination of the latter by intervening sedimentary rocks of the Dove Lake formation, which contain a significant component of older, isotopically evolved, crustal material (initial $\epsilon_{\text{Nd}} = -1$; depleted-mantle model age = 3.03 Ga; Figure 53a, d).

Felsic rocks

Dacitic volcanoclastic rocks (64–68 wt. % SiO_2 , $\text{Zr/Y} = 8.3\text{--}10.3$) of The Narrows formation at the top of the Bidou assemblage (unit Bd3) are characterized by listric-shaped REE profiles on a CN trace-element plot (Figure 55c), with enriched and fractionated LREE, fractionated HREE and negligible Eu anomalies (Figure 56a, b). On a PM plot, these samples show

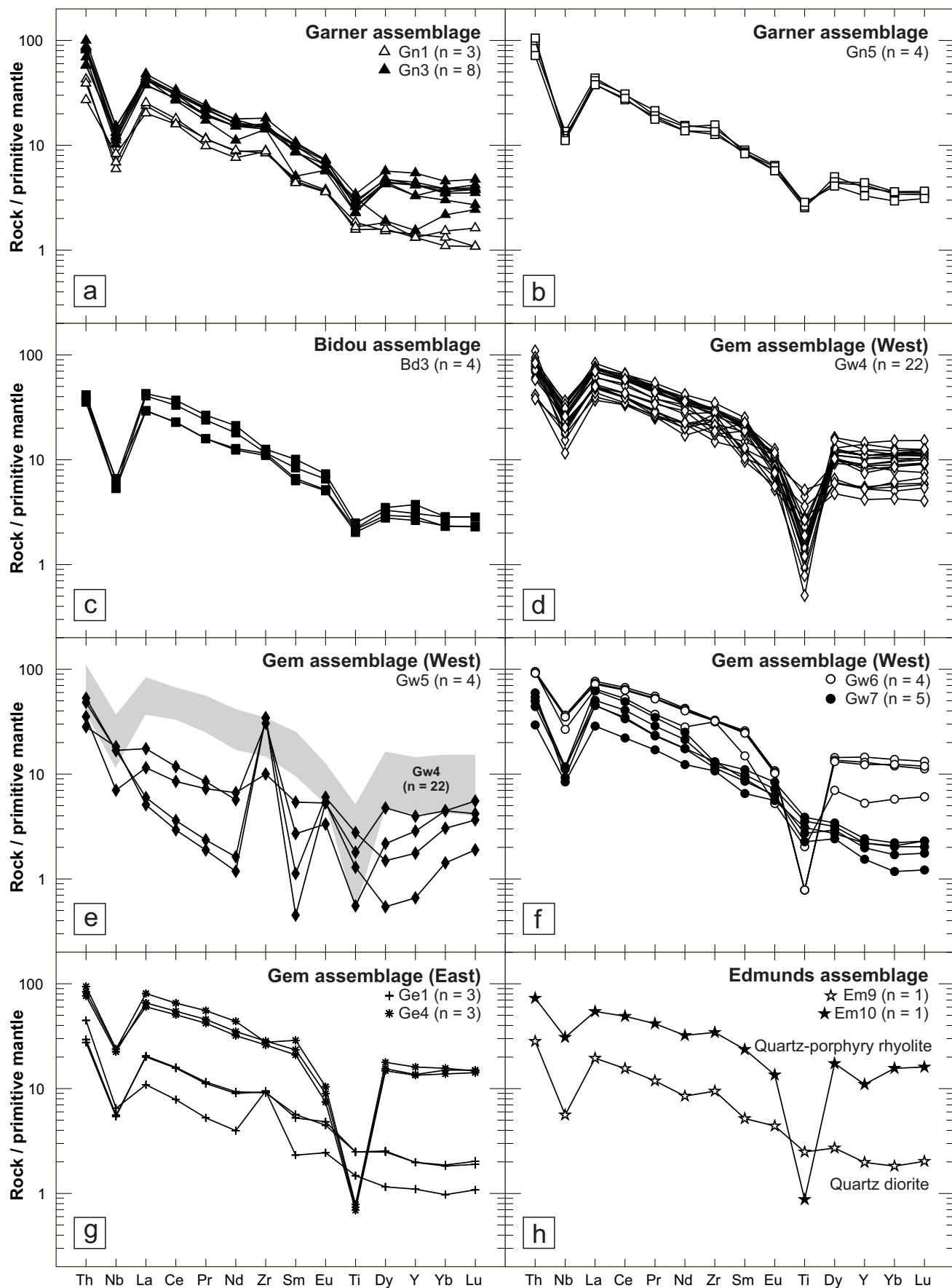


Figure 57: Primitive-mantle-normalized trace-element diagrams for felsic volcanic and associated intrusive rocks (symbols as in Figure 55): **a)** and **b)** Garner assemblage; **c)** Bidou assemblage; **d), e)** and **f)** Gem assemblage (West association); **g)** Gem assemblage (East association); **h)** Edmunds assemblage. Normalizing values and order from Sun and McDonough (1989).

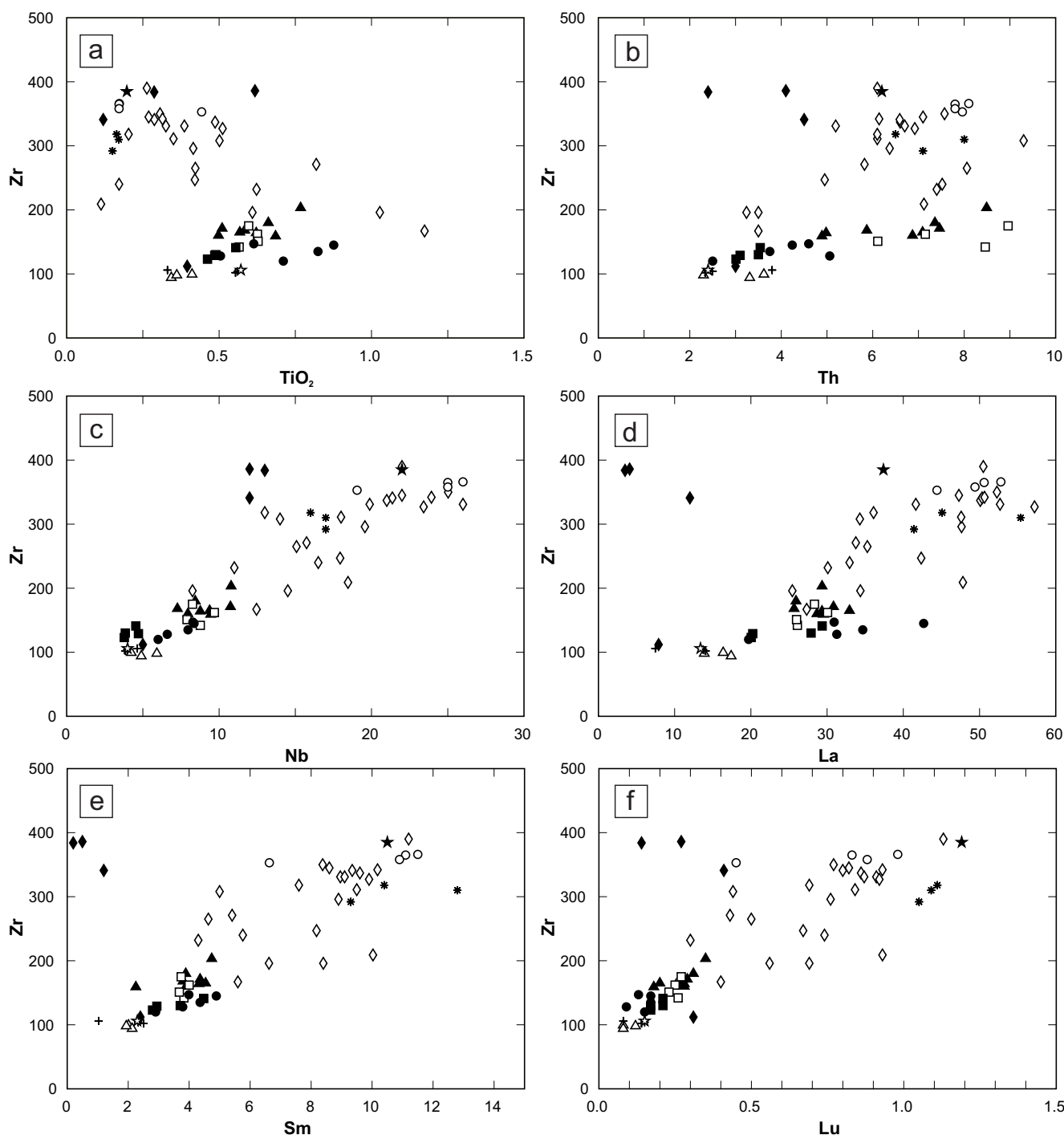


Figure 58: Bivariate plots of Zr vs. selected high-field-strength and rare-earth elements in felsic volcanic and associated intrusive rocks of the Garner, Bidou, Gem and Edmunds assemblages (symbols as in Figure 55): **a)** TiO_2 vs. Zr; **b)** Th vs. Zr; **c)** Nb vs. Zr; **d)** La vs. Zr; **e)** Sm vs. Zr; **f)** Lu vs. Zr.

pronounced negative Nb anomalies and moderate negative Ti (Figure 57c). Chromium and Ni contents of these samples are low (≤ 25 ppm and 29 ppm, respectively). Relatively high La/Yb (17–21) and Zr/Y (8–10) ratios, low Yb (1.1–1.4 ppm) and Y (12–17 ppm) values, and negligible Eu anomalies (Figure 56c, d) indicate an affinity to FI felsic volcanic rocks in the scheme of Leshner et al. (1986) and are broadly comparable to adakitic rocks in supra-subduction settings. A sample of unit Bd3 has an initial ϵ_{Nd} value of 1 and a model age of 2.84 Ga,

indicating minor interaction with slightly older isotopically evolved crust (Figure 53c, d, Table 4).

Gem assemblage

Compared to the Garner and Bidou assemblages, geochemical values for volcanic and associated intrusive rocks in the Gem assemblage show significant scatter on both major-element and immobile trace-element discrimination diagrams

(Figures 47c, 48c), indicating a comparatively complex petrogenesis. Rhyolite and high-SiO₂ rhyolite constitute a significant portion of the association. Most samples are subalkaline, although some show higher alkali contents and/or Nb/Y that are suggestive of mildly alkaline affinity (Figures 47c, 48c). The basaltic rocks mostly show transitional tholeiitic–calcalkalic affinities, whereas the felsic rocks are calcalkalic (Figures 49c, 50c).

In the West association of the Gem assemblage, volcanic and associated intrusive rocks vary in composition from primitive basalt (10.5 wt. % MgO, 343 ppm Cr, 261 ppm Ni, Mg# 63) to high-SiO₂ rhyolite (79 wt. % SiO₂) and are distinctly bimodal, with a well-defined Daly gap between 64 and 69 wt. % SiO₂ (Figure 59). Harker-type plots of major-element oxides show well-defined fractionation trends with increasing SiO₂ (Figure 60a–h), as is typical of magmatic suites in volcanic arcs (e.g., McBirney, 1984; Plank and Langmuir, 1988; Hunter, 1998; Castillo et al., 1999; Eichelberger et al., 2006; Jicha et al., 2009). Hence, these trends are interpreted in terms of ‘normal’ volcanic-arc petrogenetic processes (i.e., crystal fractionation, magma mixing or wallrock assimilation). With increasing SiO₂, the contents of FeO^t, MgO, Al₂O₃, CaO and TiO₂ generally decrease; Na₂O and K₂O increase; and P₂O₅ values increase up to about 62 wt. % SiO₂ and decrease thereafter. Trace-element data (e.g., Figure 61a–d) generally show single continuous trends up to about 62 wt. % SiO₂, which suggests a common petrogenetic path for the basaltic and andesitic lavas. Trends for Al₂O₃, P₂O₅ and TiO₂ show inflections at about 62 wt. % SiO₂ (Figure 60c, g, h), likely signalling the onset of amphibole, apatite and magnetite fractionation, respectively. As described in detail below, divergent trends in the trace-element data at SiO₂ contents above 62 wt. % indicate two distinct petrogenetic paths for felsic volcanic rocks in the Gem assemblage (Figure 61e–h), which are referred to below as ‘FI’ and ‘FII-FIII’ suites using the terminology of Leshner et al. (1986). Similar geochemical ranges and trends are also apparent in the much smaller sample suite (n = 9) from the East association of the assemblage.

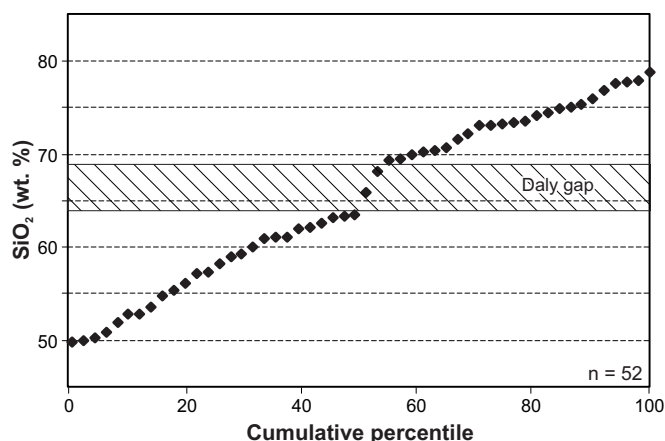


Figure 59: Distribution plot of volatile-free SiO₂ contents of volcanic and associated intrusive rocks from the West association of the Gem assemblage, showing the near absence of dacitic rocks (~64–69 wt. % SiO₂), thus indicating the existence of a ‘Daly gap’.

Mafic rocks

Basalt and basaltic andesite (unit Gw1), and associated intrusive rocks (unit Gw3) in the West association of the Gem assemblage have SiO₂ contents of 50–57 wt. %, TiO₂ of 0.8–2.5 wt. % and FeO^t of 7–16 wt. % over a large range of Mg numbers (27–63). These rocks have moderately to steeply inclined profiles on a trace-element plot normalized to N-MORB, with fractionated LREE and HREE, and variable negative Nb anomalies (Figure 51d). In relation to N-MORB, the HREE are mostly depleted and the LREE are moderately to strongly enriched. Chromium values range from less than detection limit (DL) to 360 ppm, and Ni values from less than DL to 261 ppm.

In the East association of the Gem assemblage, pillowed flows in map unit Ge2 are composed of calcalkalic basalt and andesite (Figure 50c). The basalt (49.6 wt. % SiO₂, 1.1 wt. % TiO₂, 11.6 wt. % FeO^t, Mg# 51) has a steeply sloped N-MORB–normalized trace-element profile, with enriched and fractionated LREE, fractionated HREE and pronounced negative Nb, Zr and Ti anomalies (Figure 51e). The trace-element profile for the andesite (60 wt. % SiO₂, 1.3 wt. % TiO₂, 9.4 wt. % FeO^t, Mg# 37) is much more steeply sloped and shows strongly enriched and fractionated LREE, strongly depleted and fractionated HREE and prominent negative Nb and Zr anomalies (Figure 51e). Chromium and Ni values for the basalt are 250 and 450 ppm, respectively, and for the andesite 242 and 126 ppm, respectively.

The strongly enriched LREE and Th in relation to Nb and Zr in the basaltic rocks of the Gem assemblage indicate a chemical affinity to volcanic-arc basalts (Perfit et al., 1980; Kelemen et al., 1990; Saunders et al., 1991). Accordingly, most of the basaltic rocks from the Gem assemblage plot in the ‘volcanic-arc basalt’ fields on ternary plots of Th–Hf–Ta (Figure 52a; Wood, 1980) and La–Y–Nb (Figure 52b; Cabanis and Lecolle, 1989), although the latter diagram shows evidence of weak Nb enrichment relative to typical CAB, which causes the data points to straddle the boundary with continental basalts (Figure 52b). On both diagrams, the most primitive basalt sample (sample 1569-2: 10.5 wt. % MgO, 343 ppm Cr, 261 ppm Ni, Mg# 63) is compositionally similar to VAT and BABB, and the remainder of the data points define trends that extend toward the higher La and Th contents typical of CAB. On the Nb/Yb versus Th/Yb diagram of Pearce and Peate (1995), the data points define a continuation of the trend delineated by the back-arc-like tholeiitic basalts of the Bidou assemblage. This trend is well above and roughly parallel to the MORB array (Figure 52c), indicating a significant input of high-Th/Yb crustal material and a variably enriched mantle source and/or variable degrees of partial melting (Pearce and Peate, 1995; Pearce, 2008). The data points define a moderately sloped trend on a plot of La/Sm versus Th/Nb (Figure 52d), which implicates crustal contamination in their petrogenesis.

Fractionated HREE (Gd/Yb_{MN} > 1.2) and the trend of increasing La/Yb_{CN} and Gd/Yb_{CN} ratios with increasing SiO₂ contents (Figure 61f, h) indicate the presence of garnet (which partitions HREE over MREE) as either a residual phase during partial melting or a fractionation product (e.g., Macpherson et al., 2006; Davidson et al., 2007; Pearce, 2008). Coupled with the depleted HFSE and enriched LREE and Th, these attributes

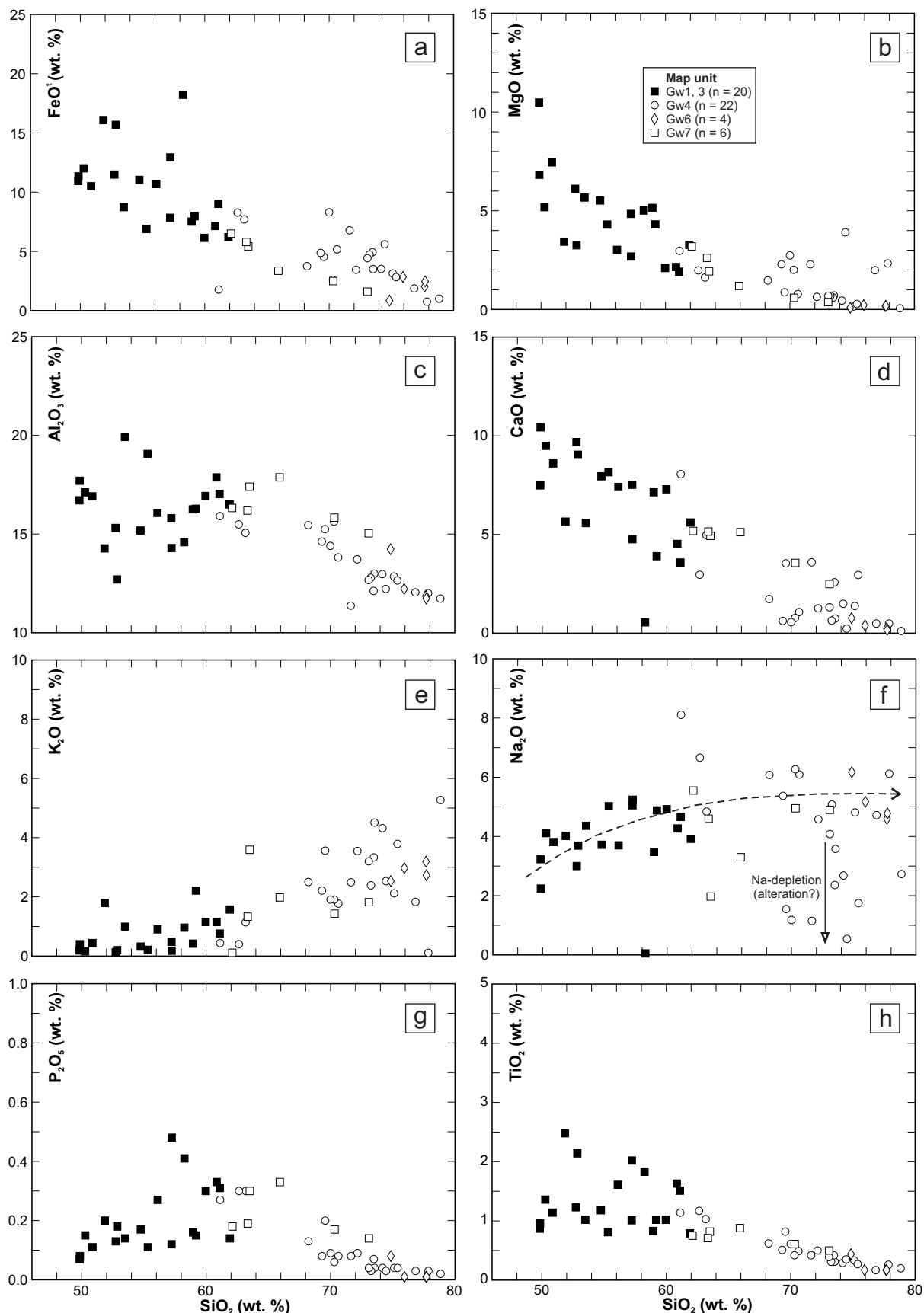


Figure 60: Harker plots of major-element oxides vs. SiO_2 for volcanic and associated intrusive rocks from the West association of the Gem assemblage, separated according to map unit as shown in the legend (upper right): **a)** SiO_2 vs. FeO' ; **b)** SiO_2 vs. MgO ; **c)** SiO_2 vs. Al_2O_3 ; **d)** SiO_2 vs. CaO ; **e)** SiO_2 vs. K_2O ; **f)** SiO_2 vs. Na_2O ; **g)** SiO_2 vs. P_2O_5 ; **h)** SiO_2 vs. TiO_2 . Epiclastic rocks and samples of altered rhyolite from unit Gw5 (see text) are omitted.

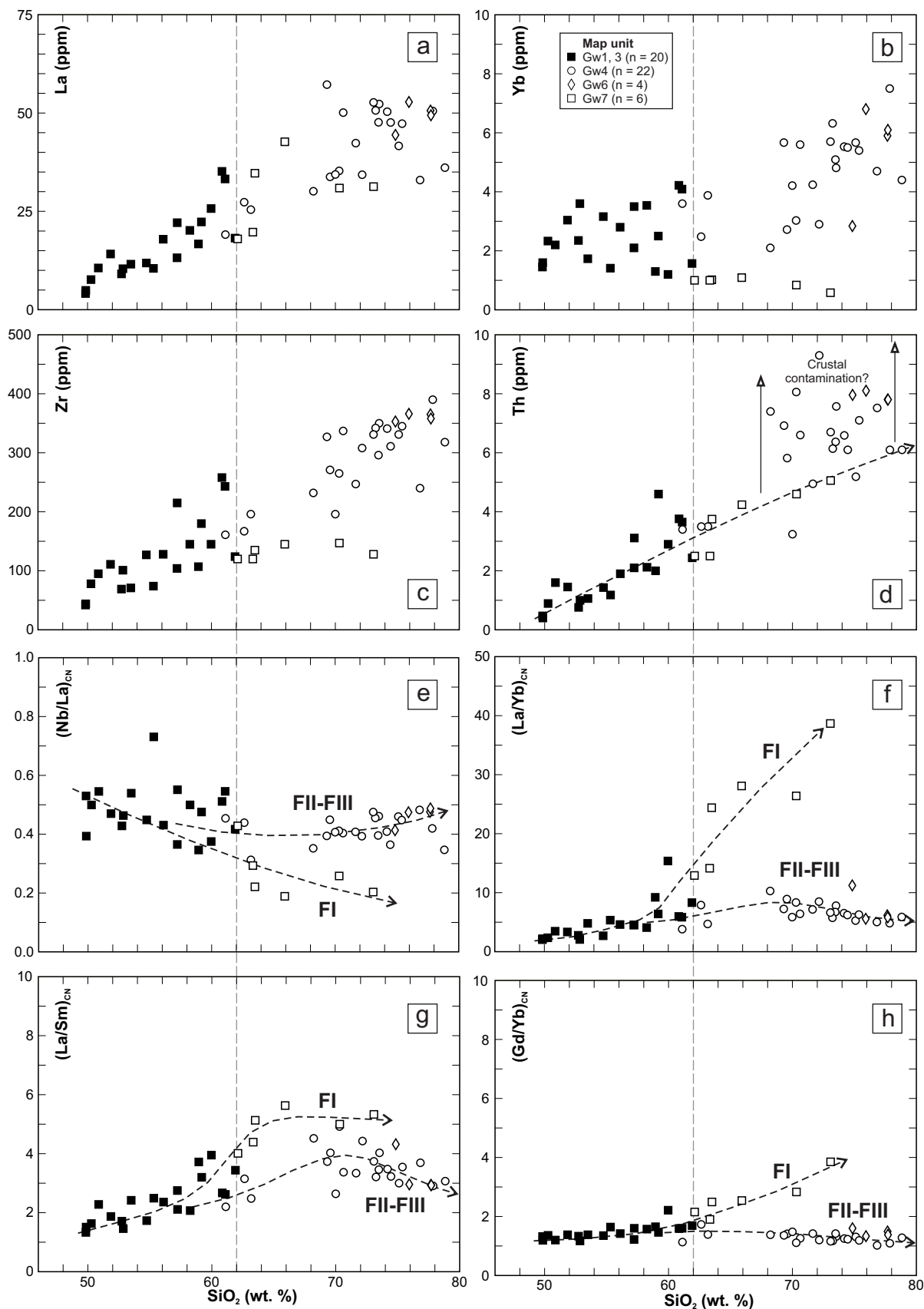


Figure 61: Plots of selected trace elements and elemental ratios vs. SiO_2 for volcanic and associated intrusive rocks from the West association of the Gem assemblage: **a)** SiO_2 vs. La; **b)** SiO_2 vs. Yb; **c)** SiO_2 vs. Zr; **d)** SiO_2 vs. Th; **e)** SiO_2 vs. $(\text{Nb/La})_{\text{CN}}$; **f)** SiO_2 vs. $(\text{La/Yb})_{\text{CN}}$; **g)** SiO_2 vs. $(\text{La/Sm})_{\text{CN}}$; **h)** SiO_2 vs. $(\text{Gd/Yb})_{\text{CN}}$. Dashed arrows show compositional trends defined by variations with increasing SiO_2 content, which become pronounced at SiO_2 contents above 62 wt. % (dashed vertical line) and define two distinct chemical suites (FI and FII-FIII; see text).

indicate a petrogenetic affinity to volcanic-arc basalt, which is interpreted to result from relatively deep partial melting of mantle-wedge peridotite that has been metasomatized by fluids derived from downgoing slabs (e.g., Perfit et al., 1980; Tatsumi, 1986; Plank and Langmuir, 1988; Saunders et al., 1991; Hawkesworth et al., 1993; Pearce and Peate, 1995). Initial ε_{Nd} values range from 1.4 to -0.3 ($n = 4$), with model ages of 3.02 and 2.95 Ga that are consistent with variable interaction with older, isotopically evolved, crustal material (Figure 53).

FI andesite, dacite and rhyolite

Intermediate–felsic volcanic rocks of the FI suite define major volcanoclastic map units in both the East (Ge1) and West (Gw7) associations of the Gem assemblage, and consist mainly of feldspar-phyric dacite and low- SiO_2 rhyolite, with minor andesite. Felsic volcanoclastic rocks from unit Gw7 (63–73 wt. % SiO_2 , $\text{Zr/Y} = 12.0\text{--}18.3$) are characterized by steep, listric-shaped profiles on a CN trace-element plot (Figure 55f), with enriched and fractionated LREE, fractionated HREE and negligible Eu anomalies (Figure 56a, b). On a PM plot, these samples show pronounced negative Nb anomalies and very weak negative Ti (Figure 57f). Chromium and Ni contents vary from less than DL up to 83 ppm and 42 ppm, respectively. Felsic volcanoclastic rocks from unit Ge1 (67–70 wt. % SiO_2 , $\text{Zr/Y} = 11.3\text{--}21.2$) are characterized by less enriched and fractionated LREE, less fractionated HREE and variable positive Eu anomalies (Figures 55g, 56a, b). On a PM-normalized plot, these samples show variable negative Nb, variable positive Zr and very weak negative Ti (Figure 57g). Chromium and Ni contents are low (≤ 34 ppm and ≤ 36 ppm, respectively).

The high Zr/Y and La/Yb ratios, low Y and Yb contents and negligible Eu anomalies of the felsic volcanoclastic rocks of units Gw7 and Ge1 indicate their correspondence to ‘FI’ felsic volcanic rocks in the scheme of Leshner et al. (1986; Figure 56c, d), which are thought to be derived by low-degree partial melting of mafic sources at high pressure (i.e., in the garnet stability field), with minimal fractionation during ascent (Leshner et al., 1986; Hart et al., 2004). Coupled with elevated Sr/Y ratios (22–41), these attributes are also comparable to adakite-like rocks in supra-subduction settings. Steep REE patterns (Figure 55f), fractionated HREE (Figure 56a) and prominent trends of increasing La/Yb_{CN} , La/Sm_{CN} and Gd/Yb_{CN} with increasing SiO_2 content (Figures 16, 61f–h) indicate the presence of garnet as either a residual phase during partial melting or as a fractionation product, and thus suggest that the magma(s) differentiated at significant depth (e.g., Hart et al., 2004; Macpherson et al., 2006; Davidson et al., 2007). Indeed, the absence of Eu or Ti anomalies precludes the possibility of significant plagioclase or Fe–Ti–oxide fractionation, respectively, as might be expected had the melt evolved in a mid- to upper-crustal magma chamber. Minor contamination by isotopically enriched and slightly older crustal material is compatible with the initial ε_{Nd} values (0.7 and 0.8) and model ages (3.01 and 2.97 Ga) of the FI suite (Figure 53b), and may account for the progressive enrichment of Th and LREE, and consequent increase in the magnitude of the negative Nb anomaly, with increasing SiO_2 content (Figures 61e, 62).

FII–FIII andesite and rhyolite

Intermediate and felsic rocks of the FII–FIII suite define major volcanoclastic and effusive units (Gw4, Gw6) in the West association of the Gem assemblage, and the large quartz-feldspar porphyry granite (Ge4) intrusion in the East association. In the West association, the FII–FIII suite consists mostly of aphyric to sparsely feldspar (\pm quartz)–phyric rhyolite (68–79 wt. % SiO_2 , $\text{Zr/Y} = 5.3\text{--}14.7$) and minor andesite; dacitic compositions are conspicuously rare (Figures 59, 60). The rhyolite is characterized by sharply kinked profiles on CN trace-element plots (Figure 55d, f). The LREE are uniformly enriched and strongly fractionated, whereas the HREE are variably enriched and only weakly fractionated; all samples show negative Eu anomalies (Figure 56a, b). On PM plots, these samples show negative Nb anomalies and very pronounced negative Ti (Figure 57d, f). Chromium and Ni contents are generally below detection limit.

Samples of the quartz-feldspar porphyry granite (unit Ge4) in the East association of the assemblage are characterized by very high SiO_2 contents (78–80 wt. %) and relatively flat trace-element profiles. Chondrite-normalized profiles are sharply kinked (Figure 55g), with enriched and fractionated LREE, strongly enriched and unfractionated HREE and strong negative Eu anomalies (Figure 56a, b). Downward ‘kinks’ at Sm–Gd and Ho (Figure 55g) are indicative of the ‘lanthanide tetrad effect’, which is common in rocks from highly evolved felsic magmatic systems and is generally thought to result from chemical complexation in late-stage, volatile-rich silicate melts (e.g., Bau, 1996; Irber, 1999; Jahn et al., 2001; see discussion by Bau, 1997; Pan, 1997). Primitive-mantle-normalized profiles (Figure 57g) show very pronounced negative Ti anomalies and strong negative Nb anomalies. Chromium and Ni contents are below detection limit.

Moderate to low Zr/Y and La/Yb ratios, coupled with negative Eu anomalies and enriched Yb and Y contents, in samples

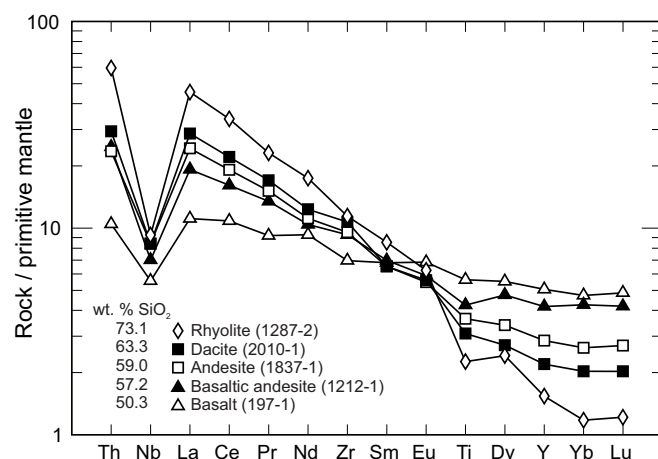


Figure 62: Primitive-mantle-normalized trace-element profiles for representative samples of basalt, basaltic andesite, andesite, FI dacite and FI rhyolite from the West association of the Gem assemblage (normalizing values and order from Sun and McDonough, 1989). With increasing SiO_2 content, the samples show progressive depletion of HREE (+Ti+Y), enrichment of LREE (+Th+Nb+Zr) and deeper negative Nb anomalies, at near-constant Sm–Eu concentrations, suggesting that they result from variable degrees of partial melting (perhaps of a common mafic source) in the presence of residual garnet, with minor crustal contamination.

from units Gw4, Gw6 and Ge4 indicate their correspondence to 'FII' and 'FIII' felsic volcanic rocks in the scheme of Leshner et al. (1986; Figure 56c, d). Uniformly low Gd/Yb_{CN} ratios (Figure 61h) and strongly enriched HREE (Figure 57d, f) preclude garnet as a fractionation product or residual phase during partial melting, and therefore suggest that the magma(s) differentiated in the middle to upper crust (e.g., Macpherson et al., 2006; Davidson et al., 2007). With increasing SiO₂ content, La/Sm_{CN} ratios increase from about 2.5 in the andesite (~62 wt. % SiO₂) to a maximum of about 5 in the rhyolite (~70 wt. % SiO₂) and thereafter decrease sharply, whereas Gd/Yb_{CN} ratios remain constant or decrease slightly across the entire compositional range of the FII-FIII suite (Figure 61g, h). Coupled with the deep negative Eu and Ti anomalies (Figure 57d, f, g), such trends are consistent with plagioclase, Fe-Ti oxide and hornblende (which partitions the MREE over HREE) as the principal fractionation products or residual phases (e.g., Hart et al., 2004; Davidson et al., 2007; Richards and Kerrich, 2007; Bachmann and Bergantz, 2008).

Leshner et al. (1986) interpreted similar attributes to indicate either high-degree partial melting of a crustal source or plagioclase-dominated fractionation of an intermediate parent in high-level magma chambers. Given that the FII-FIII suite does not define a continuous chemical trend on Harker-type plots, but instead shows a significant Daly gap between the andesitic and rhyolitic members (63–68 wt. % SiO₂), straightforward fractional crystallization from an intermediate melt is considered unlikely (e.g., Eichelberger et al., 2006). Although some authors have suggested that the paucity of intermediate lavas at Cenozoic volcanic centres may relate to the poor 'eruptibility' of viscous crystal-rich magmas produced via fractional crystallization (e.g., Geist et al., 1995), such arguments are unconvincing when dealing with a subvertical volcanic succession that is well-exposed across several kilometres of stratigraphic thickness (as at Gem Lake) yet shows no evidence of a high-level crystal-rich magma chamber. It therefore seems likely that the FII-FIII suite was derived by high-degree partial melting of a mafic source under low-P–high-T conditions in the middle to upper crust, with only minor fractionation during ascent, as has been proposed for chemically similar rocks elsewhere (e.g., Barrie et al., 1993; Hart et al., 2004). Such rocks are thought to be characteristic of corridors of extensional faulting and high heat flow in arc-rift settings (e.g., Syme, 1998; Hart et al., 2004), and a similar scenario is envisioned for the Gem assemblage.

The FII-FIII suite shows a large range of initial ϵ_{Nd} values (1.9–0.6; $n = 3$) and model ages (3.02–2.76 Ga, $n = 3$; Table 4) and a significant scatter toward higher Th values (Figure 61d), which indicates significant contamination by crustal material. Sharp decreases in La/Sm_{CN} ratios at SiO₂ contents above ~70 wt. % may indicate late-stage fractionation of an accessory mineral phase that strongly partitioned the LREE, such as monazite, allanite or apatite (Watson and Capobianco, 1981; Miller and Mittlefehldt, 1982; Rapp and Watson, 1986).

Felsic intrusion breccia

Rhyolite and high-SiO₂ rhyolite (67–81 wt. % SiO₂) from the intrusion breccia (unit Gw5) on the central peninsula in Gem

Lake are chemically distinct from all other felsic rock types in the study area. The sample suite consists of three samples of rhyolite and one sample of leucogranite, all of which exhibit uniformly low CN La/Yb ratios (2.0–3.9; Figure 56b), and Cr and Ni contents below DL. Chondrite-normalized REE profiles (Figure 55e) vary from relatively flat with a negligible Eu anomaly, to markedly concave-upward with strongly depleted MREE and a very pronounced positive Eu anomaly (Figure 56a, b). The Eu/Eu* ratio does not co-vary with chemical proxies for plagioclase accumulation (i.e., Al, Ca or Sr), which rules out the possibility of significant cumulate plagioclase in these samples. Primitive-mantle-normalized profiles are also concave-upward and indicate significant decoupling of the HFSE and REE, with strongly enriched Zr in relation to Nd and Sm, and variably enriched or depleted Nb and Ti in relation to La and Dy, respectively (Figure 57e). This plot also shows that the HFSE (Nb, Ti, Zr), Th, Eu and the least incompatible REE (Lu) mostly overlap the ranges defined by the host felsic volcanic rocks (unit Gw4; Figure 57e), whereas the LREE and more incompatible MREE are generally depleted (see also Figure 58).

Campbell et al. (1984) described similar 'concave-upward' patterns (Tb/Yb_{CN} ratios <1) for strongly altered rocks beneath massive-sulphide deposits in the Superior province, which they interpreted in terms of selective hydrothermal mobilization of LREE, MREE and Y in relation to HREE and HFSE. As described by these authors (also Terakado and Fujitani, 1998), the HFSE, HREE and Th remain largely immobile under all but the most intense alteration conditions, which can lead to a marked decoupling from the more mobile LREE and MREE. Fluid-rock interaction under high-temperature conditions can also lead to decoupling of Eu from the MREE (e.g., Bau, 1991), which, in the present case, is evidenced by the pronounced positive Eu anomalies in those samples most depleted in MREE. Similar patterns are reported from high-SiO₂ rhyolite and leucogranite, where they are attributed to fractional crystallization of accessory minerals, or to chemical complexation with B, Cl, F, O and/or P in highly evolved magmatic systems that are transitional between silicate melts and aqueous hydrothermal fluids (e.g., Bau, 1996; Irber, 1999; Jahn et al., 2001). Given the association with high-temperature alteration assemblages, it appears likely that the unusual trace-element systematics of the intrusion breccia likewise result from late-stage magmatic-hydrothermal processes; for this reason, these samples are excluded from petrogenetic considerations. These rocks are further described in the 'Economic considerations' section.

Edmunds assemblage

Major-element and immobile trace-element discrimination diagrams indicate that volcanic and intrusive rocks in the Edmunds assemblage are of subalkaline affinity and mostly mafic to intermediate composition (Figures 47d, 48d). Basalt, basaltic andesite and andesite occur as pillowed and massive flows (unit Em8) and subvolcanic dikes and sills (unit Em9). The flows show transitional tholeiitic–calcalkalic affinity, whereas the dikes and sills show a large variation from tholeiitic to calcalkalic (Figure 50d). A sample of one of the sills shows a very primitive chemistry (17.5 wt. % MgO, 770 ppm Cr, 560 ppm Ni, Mg# 79) and plots as komatiitic basalt on the

Jensen (1976) diagram (Figure 49d). The sample suite also includes a calcalkalic high-SiO₂ rhyolite (Figures 48d, 50d) from a quartz porphyry dike (Em10). As shown in Figure 63, intermediate and felsic dikes in the Edmunds assemblage show a close chemical similarity to extrusive and intrusive rocks in the East association of the Gem assemblage, perhaps indicating a similar eruptive setting.

Mafic rocks

Basaltic rocks in the Edmunds assemblage are characterized by highly variable SiO₂ (48–55 wt. %), TiO₂ (0.8–2.0 wt. %) and FeO^t (9–17 wt. %) contents, with a correspondingly wide range of Mg numbers (32–63). Major- and trace-element geochemical signatures indicate three distinct suites: tholeiitic basalt, transitional tholeiitic–calcalkalic basalt and basaltic andesite, and calcalkalic basaltic andesite. The transitional tholeiitic–calcalkalic suite is the most abundant and forms the thick succession of pillowed and massive flows and associated sill-like subvolcanic intrusions south of Lily Lake, as well as thin dikes and sills that intrude the intercalated clastic rocks. The tholeiitic suite is restricted to the laterally extensive sill that caps the turbiditic iron formation of unit Em4, whereas the calcalkalic suite is made up of dikes and sills that intrude clastic rocks at several stratigraphic levels.

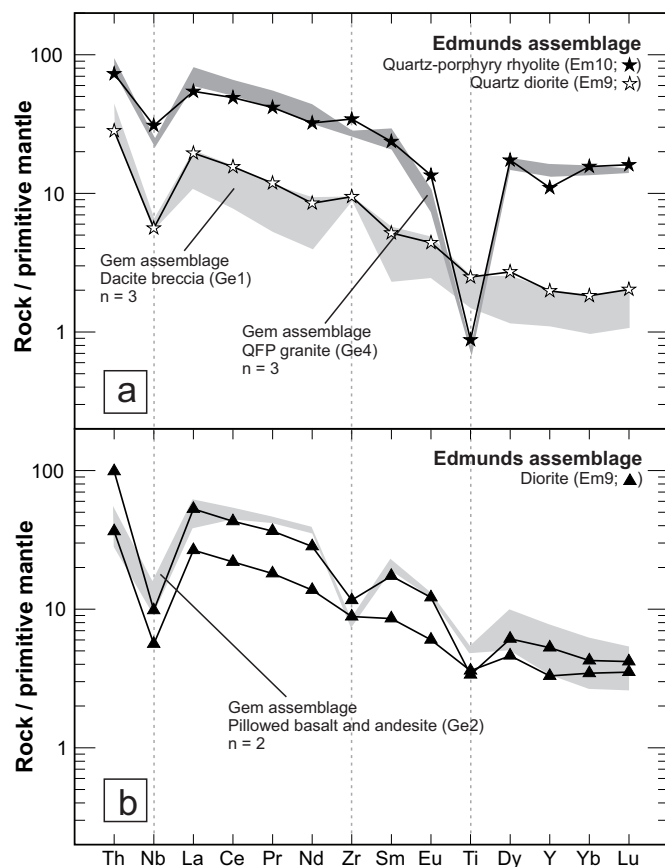


Figure 63: Primitive-mantle–normalized trace-element plots of Edmunds assemblage dikes, with fields for chemically similar extrusive and intrusive rocks from the East association of the Gem assemblage shown for comparison (grey shading): **a)** quartz-porphyry rhyolite (Em10) and quartz diorite (Em9); **b)** diorite (Em9). Normalizing values and order from Sun and McDonough (1989). Abbreviation: QFP, quartz-feldspar porphyry.

The tholeiitic suite ($n = 2$) has weakly enriched and essentially flat N-MORB–normalized trace-element profiles, with weakly fractionated LREE, unfractionated HREE, negligible Nb anomalies and positive Th anomalies (Figure 51f). Chromium and Ni values are ~30 and ~35 ppm, respectively. The transitional tholeiitic–calcalkalic suite ($n = 6$) is characterized by moderately sloped profiles, with enriched and fractionated LREE, mostly depleted and weakly fractionated HREE, weak negative Nb anomalies and variable positive Th anomalies (Figure 51g). Chromium values for the transitional tholeiitic–calcalkalic suite range from 40 to 110 ppm (average 75 ppm) and Ni values from 30 to 210 ppm (average 97 ppm). Intercalated flows of pillowed andesite have similar profiles and are shown for comparison on Figure 51g. The calcalkalic suite ($n = 2$) has very steep profiles, with enriched and fractionated LREE, weakly depleted and fractionated HREE, negative Nb anomalies, and strong positive Th anomalies (Figure 51h). Chromium and Ni values for the two basaltic andesite samples average 350 and 110 ppm, respectively. Similar profiles are exhibited by samples of komatiitic basalt and quartz diorite (shown for comparison on Figure 51h), and are similar to basalt and andesite flows (unit Ge2) in the East association of the Gem assemblage. The komatiitic basalt has a very steep profile, with strongly enriched and fractionated LREE, strongly depleted and fractionated HREE, and deep negative Nb, Zr and Ti anomalies.

The transitional tholeiitic–calcalkalic samples plot within or between the fields for E-MORB and primitive-arc basalt on plots of Th–Hf–Ta (Figure 52a; Wood, 1980) and La–Y–Nb (Figure 52b; Cabanis and Lecolle, 1989), and are chemically similar in most respects to enriched (‘E-MORB-like’) basalt associated with spreading centres and arc-rift settings in back-arc basins (e.g., Volpe et al., 1988; Hochstaedter et al., 1990; Price et al., 1990; Falloon et al., 1992; Fretzdorff et al., 2002; Pearce and Stern, 2006). In keeping with their flat N-MORB–normalized trace-element profiles, the tholeiitic samples overlap each other and plot as mildly enriched N-MORB on the La–Y–Nb diagram (Figure 52b; Cabanis and Lecolle, 1989). On account of their elevated Th contents, these samples plot between the fields for volcanic-arc tholeiite and mildly enriched N-MORB on the Th–Hf–Ta diagram of Wood (1980), and are comparable to enriched basalt found in mature spreading centres in the Mariana Trough (Gribble et al., 1998) and East Scotia Ridge (Fretzdorff et al., 2002), as well as rifts and spreading centres in the Manus Basin (Sinton et al., 2003). Thorium- and La-enriched, Nb-depleted calcalkaline samples plot well within the field for typical CAB (Figure 52a, b) from arc volcanoes.

On the Nb/Yb versus Th/Yb diagram of Pearce and Peate (1995), the data points appear to define two distinct variation trends: 1) a ‘mantle variation’ trend that straddles the upper boundary of the MORB array and is defined by the tholeiitic and low-Th/Yb transitional tholeiitic–calcalkalic samples; and 2) a ‘crustal input’ trend that is steeply inclined to the MORB array and is defined by the high-Th/Yb transitional tholeiitic–calcalkalic and calcalkalic samples (Figure 52c; also apparent on Figure 52d). Similar variations in arc–back-arc systems (e.g., Fretzdorff et al., 2002, Figure 13a) are thought to reflect mantle heterogeneity and the complex interplay between decompression-induced partial melting of depleted or

enriched MORB-like mantle versus volatile-fluxed partial melting of mantle-wedge peridotite contaminated by hydrous fluids derived from downgoing slabs (e.g., Pearce and Stern, 2006). In this regard, the superimposition of N-MORB-, E-MORB- and arc-like basaltic magmatism in the Edmunds assemblage may indicate an analogy to regions of active extension and insipient rifting in volcanic arcs (e.g., Hochstaedter et al., 1990; Gribble et al., 1998). Localized emplacement of mantle-derived melts, as represented by the komatiitic basalt, may indicate that initial extension was accompanied by upwelling mantle, perhaps associated with slab roll-back or far-field mantle-plume activity. Initial ϵ_{Nd} values (at 2.7 Ga) of representative samples of mafic–intermediate volcanic and intrusive rocks in the Edmunds assemblage (tholeiitic ϵ_{Nd} = 1.7, transitional ϵ_{Nd} = 1.4, calcalkalic ϵ_{Nd} = 0.4) co-vary with proxies for crustal contamination (Figure 53a, b).

Felsic rocks

A sample from a quartz diorite dike (Em9; 63 wt. % SiO_2 , $\text{Zr/Y} = 11.8$) that intrudes unit Em8 is characterized by a smoothly sloped profile on a CN trace-element plot (Figure 55h), with enriched and fractionated LREE, fractionated HREE and no Eu anomaly (Figure 56a, b). The PM profile shows strongly negative Nb, weak positive Zr and weak negative Ti (Figure 57h). Chromium and Ni contents are high (190 and 100 ppm, respectively) relative to other felsic samples in the study area. Relatively high La/Yb and Zr/Y ratios, low Yb and Y values, and negligible Eu anomalies (Figure 56c, d) indicate an affinity to FI felsic volcanic rocks in the scheme of Leshner et al. (1986); this sample is chemically indistinguishable from FI suite dacite (unit Ge1) in the East association of the Gem assemblage (Figure 63).

A sample from a quartz-phyric dike (Em10) composed of high- SiO_2 rhyolite (78 wt. % SiO_2 , $\text{Zr/Y} = 7.7$) that intrudes unit Em8 exhibits a comparatively flat profile on a CN trace-element plot (Figure 55h), with enriched and fractionated LREE, unfractionated and strongly enriched HREE, and a negative Eu anomaly (Figure 56a, b). The PM profile shows a moderate negative Nb anomaly and pronounced negative Ti (Figure 57h). Chromium and Ni contents are below DL. These geochemical attributes indicate a chemical affinity to FII or FIII felsic volcanic rocks (Figure 56c, d) in the scheme of Leshner et al. (1986); this sample is chemically indistinguishable from the quartz-feldspar porphyry granite intrusion (unit Ge4) in the East association of the Gem assemblage (Figure 63).

Post-tectonic dikes

Major-element and immobile trace-element discrimination diagrams indicate that post-tectonic dikes intruding the major high-strain zones in the study area are of subalkaline affinity and mafic–intermediate composition (Figure 64a). These rocks have SiO_2 contents of 44–58 wt. %, TiO_2 of 0.5–1.6 wt. % and FeO^* of 6–11 wt. %, with moderate Mg numbers (47–48). High Th/Yb and Zr/Y (5.1–7.6) ratios indicate these rocks are of calcalkalic affinity (Figure 64b). Trace-element profiles normalized to N-MORB (Figure 64c) are steeply inclined, with fractionated LREE and HREE, and strong negative Nb anomalies.

In relation to N-MORB, the HREE are mostly depleted and the LREE are strongly enriched. Chromium values range from 24 to 112 ppm and Ni values from 33 to 102 ppm. The strongly enriched LREE and Th in relation to Nb, Zr and Ti in the post-tectonic mafic dikes indicate a chemical affinity to volcanic-arc basalt (Perfit et al., 1980; Kelemen et al., 1990; Saunders et al., 1991). Accordingly, these rocks plot in the ‘volcanic-arc basalt’ (VAB) field on the Zr/Y vs. Th/Yb diagram (Figure 64d; Wood, 1980).

Summary of geochemical results and inferred geodynamic settings

Garner assemblage: mature continental arc and plume-influenced arc rift

Coarse volcanoclastic rocks in the lower and upper successions of the Garner assemblage consist mostly of calcalkalic dacite and rhyolite, which are chemically similar to felsic volcanic rocks in modern oceanic or continental-arc settings. A subset of these rocks near the base of the assemblage exhibits a close chemical affinity to adakite, perhaps indicating that their petrogenesis involved partial melting of subducted oceanic crust. Initial ϵ_{Nd} values (0.8 to –0.2) indicate significant interaction with isotopically evolved crust, and may therefore favour a continental-arc setting. Following uplift and erosional denudation of the volcanic arc (as evidenced by the erosional unconformity at the base of the upper succession), a relatively quiescent marine basin formed and was subsequently filled by komatiitic and tholeiitic basalt flows that show chemical evidence of derivation from a strongly depleted mantle source. Komatiitic basalt (initial ϵ_{Nd} values of 3.1 and 2.7, respectively) shows evidence of little or no contamination by isotopically juvenile crustal material and could be attributed to an upwelling mantle plume that impinged on the base of the volcanic arc. Thermal doming above this plume may account for erosional denudation of the arc, with consequent extension and rifting to form the marine basin. The tholeiitic basalt is comparable to oceanic-arc or back-arc basin basalt and shows evidence of crustal contamination (initial ϵ_{Nd} values are 1.2 and 0.6). Its petrogenesis may have involved partial melting of metasomatized mantle-wedge peridotite or, given the spatial and temporal association with komatiitic basalt, partial melting in the head of a mantle plume (e.g., Campbell et al., 1989) that was contaminated by mantle-wedge peridotite or arc crust (e.g., Dostal and Mueller, 1997; Tomlinson et al., 1998; Hollings et al., 1999).

Bidou assemblage: mature back-arc basin to immature volcanic arc

Gabbro sills and laterally continuous formations of subaqueous basalt flows in the lower succession of the Bidou assemblage consist of Fe- and Mg-tholeiitic basalt, and are chemically similar to basalt erupted at steady-state seafloor-spreading centres in relatively mature (>100 km wide) back-arc basins. At the base of the succession, the basalt shows evidence of only minor crustal contamination (initial ϵ_{Nd} values of 2.7 and 2.2) and was likely derived from decompression-induced partial melting of upwelling mantle peridotite. Intervening

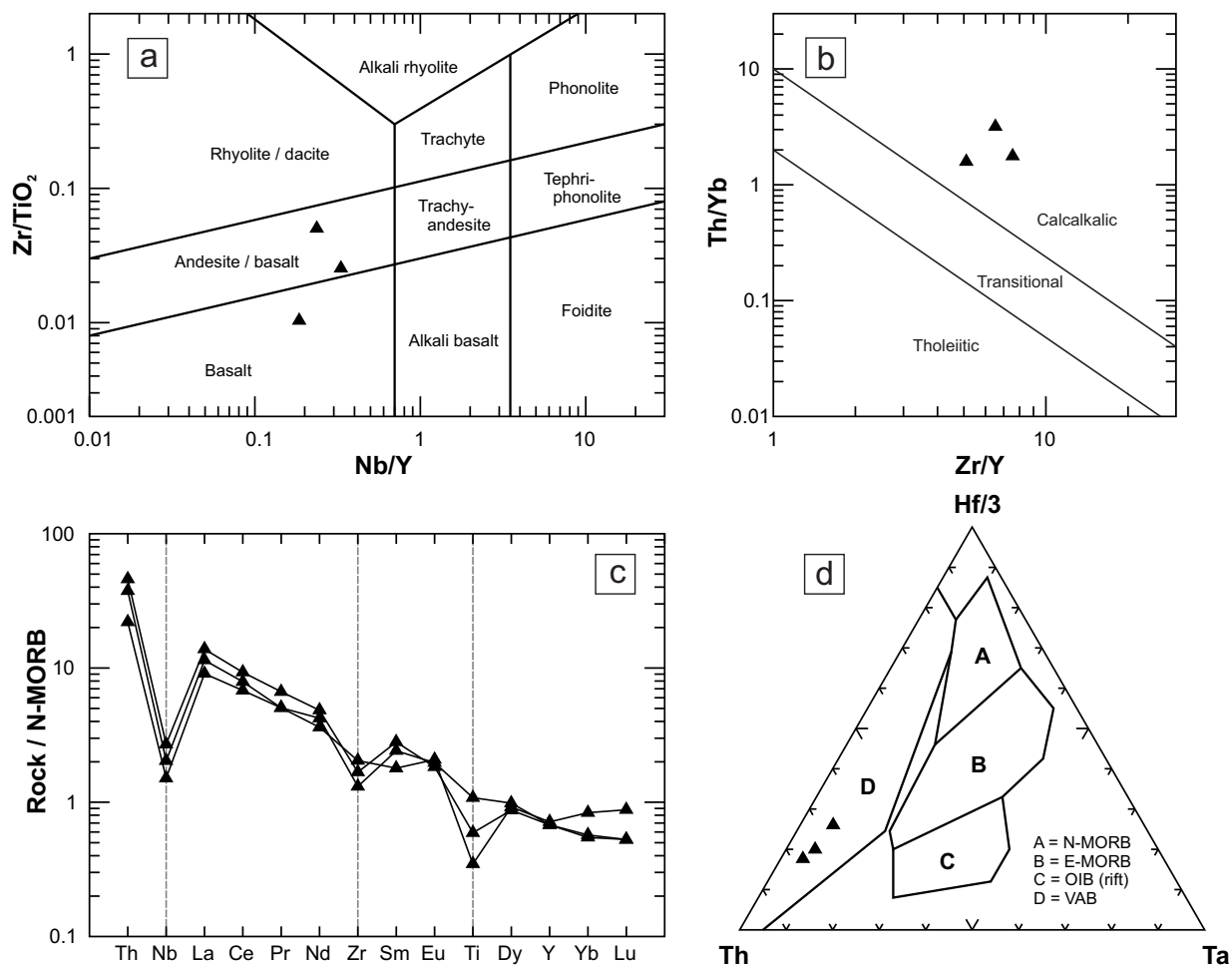


Figure 64: Plots of major- and immobile trace-element data for post-tectonic mafic dikes ($n = 3$) from high-strain zones at Beresford, Garner and Gem lakes: **a)** Nb/Y vs. Zr/TiO₂ diagram (Pearce, 1996; modified from Winchester and Floyd, 1977); **b)** Zr/Y vs. Th/Yb diagram (Ross and Bédard, 2009); **c)** multi-element plot normalized to N-MORB (normalizing values and order from Sun and McDonough, 1989); **d)** Th vs. Hf/3 vs. Ta diagram (Wood, 1980). Abbreviations: E-MORB, enriched mid-ocean-ridge basalt; N-MORB, normal mid-ocean-ridge basalt; OIB, ocean-island basalt; VAB, volcanic-arc basalt.

formations of basinal marine turbidites record influxes of arc-derived detritus, which culminated with deposition of a thick accumulation of coarse volcanoclastic rocks derived from calcalkalic dacite. This dacite is broadly comparable to adakite and shows evidence (initial ϵ_{Nd} value of 1.0 and model age of 2.84 Ga) of minor interaction with slightly older, isotopically evolved crustal material, indicating an upward transition from back-arc to volcanic-arc magmatism, probably in an intraoceanic setting.

Gem assemblage: mature volcanic arc to incipient arc rift

Effusive flows, primary volcanoclastic rocks and related hypabyssal intrusions in the Gem assemblage were deposited in shallow-subaqueous to subaerial settings and vary in composition from primitive basalt to high-SiO₂ rhyolite. These rocks define a single compositional trend up to approximately 62 wt. % SiO₂, as is typical of magmatic suites in volcanic arcs. The basaltic rocks show a continuous variation in chemical affinity from back-arc or primitive-arc tholeiite to evolved calcalkalic (arc) basalt, with evidence of variable contamination by

crustal materials (initial ϵ_{Nd} values range from 1.4 to -0.3), and are interpreted to result from relatively deep partial melting of mantle-wedge peridotite that has been metasomatized by fluids derived from a downgoing slab. Andesite, dacite and rhyolite of the FI suite are comparable to adakitic rocks in supra-subduction settings and were likely derived by low-degree partial melting of mafic sources in the mantle or lower crust, with variable contamination by crustal materials (initial ϵ_{Nd} values of 0.7–0.8), and minimal fractionation during ascent. Andesite and rhyolite of the FII-FIII suite are comparable to volcanic rocks in modern and ancient rifts, which are interpreted to result from high heat flows and consequent low-degree partial melting in the mid to upper crust. The chemistry of these rocks provides evidence of variable contamination by crustal materials (initial ϵ_{Nd} values of 1.9–0.6), with a trend toward highly evolved compositions via late-stage fractionation and locally intense alteration by magmatic-hydrothermal fluids. The common association of FII- and especially FIII-type rhyolite with volcanic-hosted massive-sulphide deposits in the Superior province (e.g., Leshner et al., 1986; Barrie et al., 1993; Hart et al., 2004; Gaboury and Pearson, 2008) and elsewhere (e.g., Lentz, 1998; Syme, 1998) indicates a link between rhyolite petrogenesis and the high heat

flows and structural permeability required for deposit genesis, and has been specifically attributed to high-level partial melting in active rift environments (Hart et al., 2004).

Edmunds assemblage: arc rift to immature intra-arc basin

Sedimentation in the Edmunds assemblage is interpreted to have taken place in a progradational submarine fan that formed after cessation of major volcanism and a short-lived period of depositional quiescence. The lower facies association (LFA) represents the channelized lower- to mid-fan portions of the submarine fan. An abrupt change in facies association signals a profound shift in sedimentation, accompanied by major erosional denudation of the adjacent volcanic arc and locally voluminous effusions of basalt, perhaps in response to a sudden change in base level related to renewed extension of the arc-rift basin. The upper facies association (UFA) represents the channelized upper-fan to feeder-channel portions of the submarine fan, and was likely deposited in proximity to a basin-bounding fault that served as a conduit for hydrothermal fluids and basaltic magmas.

Magmatic rocks in the UFA range in composition from tholeiitic basalt to calcalkalic andesite, and include minor dikes or sills of komatiitic basalt and calcalkalic high-SiO₂ rhyolite. Three chemical suites of basaltic rocks are distinguished: 1) tholeiitic basalt, 2) transitional tholeiitic–calcalkalic basalt and basaltic andesite, and 3) calcalkalic basaltic andesite. The transitional tholeiitic–calcalkalic suite (initial ϵ_{Nd} of 1.4) is most abundant and consists of flows and associated intrusions that are chemically similar to enriched (E-MORB–like) basalts associated with spreading centres or rifts in back-arc basins. The tholeiitic suite (initial ϵ_{Nd} of 1.7) is confined to the laterally extensive sill at the basal contact of the UFA and is comparable to mildly enriched (N-MORB–like) basalts found at mature spreading centres in back-arc basins, whereas the calcalkalic suite (initial ϵ_{Nd} of 0.4) consists of comparatively minor dikes and sills that are chemically analogous to typical volcanic-arc (CAB-like) basalts. This chemical diversity is similar to that documented in back-arc basins, where it is generally thought to reflect some combination of mantle heterogeneity, variable degrees of partial melting and the complex interplay between decompression-induced partial melting of depleted mantle versus volatile-fluxed partial melting of mantle-wedge peridotite. In the case of the Edmunds assemblage, the superimposition of N-MORB–, E-MORB– and CAB-like magmatism may reflect a geodynamic evolution from arc rift to immature intra-arc basin.

U-Pb geochronology

In order to better constrain the ages of volcanism, plutonism and sedimentation in the southeastern portion of the Rice Lake belt, thirteen key map units were sampled for U-Pb geochronological analysis. Eight samples of volcanic or intrusive rocks were submitted for conventional U-Pb dating of igneous zircons by isotope dilution–thermal ionization mass spectrometry (ID-TIMS), whereas detrital zircons from five samples of clastic rocks were submitted for U-Pb dating by laser ablation, multicollector, inductively coupled plasma–mass spectrometry (LA-MC-ICP-MS). Selected zircons from

two samples of greywacke were also analyzed by ID-TIMS to better constrain the maximum age of deposition. As described in detail below, the ID-TIMS dataset includes a large number of highly discordant analyses, which, in some cases, precluded unambiguous interpretation of the data.

Methodology

Each sample consisted of 10–15 kg of least altered representative rock that was collected by hammer or rock saw from bedrock and was manually trimmed at the sample site to remove all weathered surfaces, veins, altered fractures or other inhomogeneities. The resulting ‘clean’ rock chips were triple bagged, sealed in plastic rock pails and shipped to the University of Alberta Radiogenic Isotope Facility (Edmonton, Alberta) for mineral separation, processing and analysis. Heavy minerals were separated using standard crushing, pulverizing and heavy liquid techniques, followed by sorting of the concentrates using a Frantz isodynamic separator. Final selection of mineral separates was done by hand under a binocular microscope.

Zircon and rutile separates underwent conventional U-Pb dating by isotope dilution–thermal ionization mass spectrometry (ID-TIMS), which generally followed the procedures outlined in Heaman et al. (2002). Exterior surfaces of intact zircon crystals were generally removed by air abrasion, whereas crystal fragments were mostly unabraded. Two single-grain zircon fractions from sample 96-03-1116 were further processed using the thermal annealing–chemical abrasion technique of Mattinson (2005). All analyses were performed on a VG354 mass spectrometer operated in single Faraday or Daly (analogue) collector peak-hopping mode, and were corrected for mass discrimination based on replicate measurement of the NBS981 and U500 standards. In addition, all measurements obtained with the Daly photomultiplier detector were adjusted for detector bias. The isotopic composition of common Pb in excess of analytical blank (2 pg of Pb) was calculated using the two-stage model of Stacey and Kramers (1975). The resulting U-Pb isotopic data are listed in Table 5 and are also presented as concordia diagrams. All errors reported in Table 5 are quoted at 1 σ and were calculated by numerical propagation of all known sources of uncertainty. Regression calculations and age uncertainties were determined using the Isoplot version 3.0 application of Ludwig (2003). This program was also used to generate the concordia diagrams; error ellipses on these diagrams are shown at 2 σ .

Detrital zircons underwent U-Pb dating by laser-ablation, multicollector, inductively coupled plasma–mass spectrometry (LA-MC-ICP-MS), which generally followed the procedures outlined by Simonetti et al. (2005). Mineral-separation techniques were identical to those for the ID-TIMS samples, and the resulting zircons were hand-picked, mounted in epoxy and polished to half-section thickness for analysis. All analyses were performed on a Nu Plasma MC-ICP-MS coupled to a frequency-quintupled Nd:YAG laser-ablation system. Ion-counting detectors were used to measure ²⁰⁷Pb, ²⁰⁶Pb and ²⁰⁴Pb, whereas U was measured on Faraday collectors. The procedures for determining the Faraday ion-counter factor and the Faraday multiplier calibration, and for correcting the measured Pb isotope ratios for instrumental mass bias, have been described

Table 5: U-Pb isotope dilution–thermal ionization mass spectrometry (ID-TIMS) analytical data for zircon and rutile from bedrock samples in the eastern Rice Lake belt. Also provided in Data Repository Item DR12013002.

Sample/ fraction	Description ⁽¹⁾	Weight (μg)	U (ppm)	Th (ppm)	Pb (ppm)	Model Th/U ⁽⁵⁾	²⁰⁶ Pb (pg)	Isotopic ratios ⁽²⁾			Age (Ma) ⁽²⁾		Disc. (%) ⁽⁴⁾	
								²⁰⁶ Pb/ ²³⁸ U	²⁰⁷ Pb/ ²³⁵ U	²⁰⁷ Pb/ ²⁰⁶ Pb	²⁰⁶ Pb/ ²³⁸ U	²⁰⁷ Pb/ ²³⁵ U		
96-02-1067 (CB02-03); Garner Lake; Pegmatitic tonalite; UTM 343748 mE, 5632463 mN (Zone 15, NAD 83)														
1z	euh lt tan nabr frag; (1)	3.5	1245.4		809.3	0.85	3.7	0.52272 ±0.00067	14.7635 ±0.0192	0.20484 ±0.00003	2710.7 ±2.8	2865.2 ±0.2	6.6	
2z	subh pr lt tan abr; (1)	3.4	1957.1		1439.0	1.10	2.9	0.56620 ±0.00094	15.9078 ±0.0264	0.20377 ±0.00006	2892.2 ±3.9	2856.6 ±0.5	-1.6	
3z	subh platy ltan abr; (1)	2.0	2112.4		1488.0	1.08	8.4	0.54296 ±0.00071	15.2422 ±0.0200	0.20360 ±0.00004	2795.8 ±3.0	2855.3 ±0.3	2.6	
4z	subh pr abr frag; (1)	3.0	270.1		176.7	0.59	2.2	0.55401 ±0.00080	15.6924 ±0.0226	0.20543 ±0.00006	2841.8 ±3.3	2869.9 ±0.5	1.2	
5z	euh pr tan abr; (1)	6.0	693.2		431.4	1.05	1.4	0.47926 ±0.00066	13.5363 ±0.0181	0.20485 ±0.00008	2524.0 ±2.9	2865.2 ±0.6	14.4	
96-02-1050 (CB02-02); Garner Lake; Dacitic crystal tuff or coherent flow; UTM 343545 mE, 5633064 mN (Zone 15, NAD 83)														
1z	subh pr-stubby tan-brown abr; (2)	1.0	795.8		439.9	0.47	3.5	0.48359 ±0.00112	12.9225 ±0.0300	0.19381 ±0.00008	2542.9 ±4.9	2774.7 ±0.6	10.1	
2z	euh-subh pr col abr; (1)	2.8	199.6		39.1	0.82	2.3	0.17149 ±0.00029	1.7245 ±0.0051	0.07293 ±0.00017	1020.3 ±1.6	1012.1 ±4.7	-0.9	
3z	euh-subh pr tan-brown abr; (2)	1.3	674.4		434.1	0.64	28.8	0.54023 ±0.00079	15.1793 ±0.0235	0.20379 ±0.00011	2784.4 ±3.3	2856.8 ±0.9	3.1	
4z	euh-subh pr brown abr; (1)	2.4	702.7		398.7	0.51	9.9	0.49058 ±0.00066	13.3989 ±0.0181	0.19809 ±0.00005	2573.2 ±2.8	2810.5 ±0.4	10.2	
5z	subh pr tan abr; (1)	1.0	527.7		343.4	0.56	3.8	0.55404 ±0.00080	15.8390 ±0.0234	0.20734 ±0.00006	2842.0 ±3.3	2884.9 ±0.5	1.8	
6z	pink subh frags; (6)	5.0	255.3		149.9	0.59	111.0	0.54176 ±0.00069	15.2756 ±0.0312	0.20450 ±0.00028	2790.8 ±2.9	2862.4 ±2.2	3.1	
7z	pink euh frags; (6)	2.0	199.9		106.1	0.53	8.2	0.55683 ±0.00072	15.5939 ±0.0226	0.20311 ±0.00013	2853.5 ±3.0	2851.4 ±1.0	-0.1	
8z	tiny pink euh pr; M; (6)	2.6	500.2		259.6	0.52	33.5	0.50172 ±0.00070	13.8256 ±0.0222	0.19986 ±0.00014	2621.2 ±3.0	2825.0 ±1.2	8.8	
9z	larger pink broken pr; M; (1)	2.7	145.1		90.2	0.62	12.3	0.52213 ±0.00072	14.9320 ±0.0273	0.20742 ±0.00020	2708.2 ±3.0	2885.5 ±1.5	7.5	
96-05-SLF; Tinney Lake (Stovel Lake Formation); Greywacke; UTM 340948 mE, 5638862 mN (Zone 15, NAD 83)														
1z	grain 1-1 from LA mount	6.9	38.8		17.3	25.5	473	0.52813 ±0.00130	13.8590 ±0.0581	0.19032 ±0.00054	2733.6 ±5.5	2744.9 ±4.7	0.5	
2z	grain 1-23 from LA mount	4.3	223.8		75.9	32.8	2.9	0.14165 ±0.00023	1.4715 ±0.0053	0.07534 ±0.00024	853.9 ±1.3	1077.6 ±6.3	22.2	
3z	grain 1-12 from LA mount	2.1	67.7		71.4	154.4	37	0.63100 ±0.00835	17.1518 ±0.7596	0.19714 ±0.00515	3153.5 ±32.9	2802.7 ±42.1	-15.9	
96-05-CMG; Central Manitoba mine; Pegmatitic leucogabbro; UTM 335242 mE, 5641742 mN (Zone 15, NAD 83)														
1z	pink to tan frags; 15NM; (8)	18.7	138.9		391.0	111.6	2.82	4.1	0.46541 ±0.00049	12.0987 ±0.0130	0.18854 ±0.00004	2463.4 ±2.2	2729.5 ±0.4	11.7
2z	lt tan best frags; 15NM; (8)	13.8	213.3		904.2	189.4	4.24	9.1	0.42204 ±0.00051	10.6875 ±0.0130	0.18366 ±0.00005	2269.7 ±2.3	2686.2 ±0.5	18.4
3z	lt tan parts of euh pr; 15NM; (4)	6.3	242.6		608.3	132.4	2.51	5.6	0.30744 ±0.00038	7.9750 ±0.01050	0.18813 ±0.00008	1728.1 ±1.9	2725.9 ±0.7	41.6
4z	col frags; (10)	8.2	64.1		213.9	69.6	3.34	182.5	0.42114 ±0.00177	10.3947 ±0.1152	0.17902 ±0.00156	2265.6 ±8.0	2643.8 ±14.4	16.9
5z	best tan frags; (7)	3.3	188.1		855.5	231.3	4.55	167.7	0.46458 ±0.00177	11.2528 ±0.1479	0.17567 ±0.00186	2459.7 ±7.8	2612.4 ±17.5	7.0
6z	lt tan; 15NM; (6)	5.3	132.2		473.4	138.3	3.58	18.8	0.53846 ±0.00084	13.9374 ±0.0369	0.18773 ±0.00036	2777.0 ±3.5	2722.4 ±3.2	-2.5
96-05-SL; Beresford Lake (Stormy Lake Formation); Greywacke; UTM 340817 mE, 5636142 mN (Zone 15, NAD 83)														
1z	grain 1-7 from LA mount	2.1	54.0		44.5	40.7	0.82	51.8	7.2185 ±0.1071	0.18173 ±0.00234	1631.9 ±11.6	2668.8 ±21.2	43.8	

Table 5: U-Pb isotope dilution–thermal ionization mass spectrometry (ID-TIMS) analytical data for zircon and rutile from bedrock samples in the eastern Rice Lake belt. Also provided in Data Repository Item DRI2013002. (continued)

Sample/ fraction	Description ⁽¹⁾	Weight (µg)	U (ppm)	Th (ppm)	Pb (ppm)	Model Th/U ⁽³⁾	²⁰⁶ Pb (pg)	Isotopic ratios ⁽²⁾			Age (Ma) ⁽²⁾		Disc. (%) ⁽⁴⁾		
								²⁰⁶ Pb/ ²³⁸ U	²⁰⁷ Pb/ ²³⁵ U	²⁰⁶ Pb/ ²³⁸ U	²⁰⁷ Pb/ ²³⁵ U	²⁰⁷ Pb/ ²⁰⁶ Pb			
3z	grain 1-42 from LA mount	4.6	34.6	17.2	21.1	0.50	5.7	914	0.51141 ±0.00123	13.3276 ±0.0360	0.18901 ±0.00025	2662.7 ±5.3	2703.1 ±2.5	2733.5 ±2.2	3.2
96-06-1845; Gem Lake; Crystal-lithic lapilli-tuff; UTM 341735 mE, 5627494 mN (Zone 15, NAD 83)															
1z	large dark pink pr; 10NM; (1)	7.1	154.2	85.8	95.2	0.56	15.5	2333	0.52304 ±0.00060	13.5758 ±0.0167	0.18825 ±0.00008	2712.1 ±2.5	2720.6 ±1.2	2726.9 ±0.7	0.7
2z	small pr; 10NM; (7)	8.9	249.7	163.3	156.6	0.65	74.9	953	0.50586 ±0.00064	13.1314 ±0.0202	0.18827 ±0.00013	2638.9 ±2.7	2689.1 ±1.5	2727.1 ±1.2	3.9
3z	largest pink pr; 2NM; (1)	7.2	72.6	34.5	44.0	0.48	16.6	1019	0.51051 ±0.00088	13.2289 ±0.0290	0.18794 ±0.00025	2658.8 ±3.7	2696.1 ±2.1	2724.2 ±2.1	2.9
96-03-1116; Garnier Lake; Biotite granite; UTM 347679 mE, 5630991 mN (Zone 15, NAD 83)															
1z	lt tan stubby euh pr; (3)	2.0	380.0	130.5	219.6	0.34	7.2	4086	0.51650 ±0.00098	13.5330 ±0.0260	0.19004 ±0.00010	2684.2 ±4.2	2717.6 ±1.9	2742.5 ±0.8	2.6
2z	lt tan euh pr-needle frags; (3)	2.0	793.1	380.5	444.3	0.48	27.0	1322	0.47490 ±0.00072	12.2660 ±0.0190	0.18734 ±0.00011	2504.8 ±3.1	2624.9 ±1.6	2718.9 ±1.0	9.5
3z	lt tan pr euh-subh abr; (1)	3.0	118.7	68.9	57.0	0.48	3.0	4179	0.50570 ±0.00089	13.0820 ±0.0240	0.18761 ±0.00008	2638.3 ±3.7	2685.6 ±1.7	2721.3 ±0.7	3.7
4z	short pr platy lt tan abr; (1)	1.5	470.4	281.2	281.2	0.55	3.8		0.51636 ±0.00074	13.3993 ±0.0199	0.18820 ±0.00006	2683.7 ±3.1	2708.2 ±1.4	2726.5 ±0.5	1.9
5z	large pink abr; 2M; (1)	12.8	204.7	102.1	113.7	0.50	13.2	6508	0.48090 ±0.00050	12.6054 ±0.0133	0.19011 ±0.00004	2531.2 ±2.2	2650.6 ±1.0	2743.1 ±0.4	9.3
6z	col el, TA-CA (6hr); (1)	2.4	163.1	62.2	83.7	0.38	15.3	702	0.43075 ±0.00082	11.1869 ±0.0288	0.18836 ±0.00027	2309.1 ±3.7	2538.8 ±2.4	2727.9 ±2.4	18.2
7z	col eq, TA-CA (6hr); (1)	5.4	40.4	19.7	26.9	0.49	39.9	167	0.44657 ±0.00169	11.6110 ±0.0838	0.18857 ±0.00093	2380.0 ±7.5	2573.6 ±6.7	2729.8 ±8.1	15.3
96-03-1261 (CB02-01); Garnier Lake; Feldspar-quartz porphyry dike; UTM 342817 mE, 5634198 mN (Zone 15, NAD 83)															
1z	1 pink zircon sm prism	1.5	238.6	151.6	156.1	0.64	19.7	601	0.51737 ±0.00189	13.3382 ±0.1428	0.18698 ±0.00163	2688.0 ±8.0	2703.9 ±10.1	2715.8 ±14.3	1.2
2z	1 tan broken zircon prism	1.5	203.0	124.3	124.0	0.61	3.3	3030	0.51475 ±0.00082	13.5216 ±0.0288	0.19052 ±0.00025	2676.9 ±3.5	2716.8 ±2.0	2746.6 ±2.2	3.1
3z	1 tan zircon	1.2	223.6	145.4	125.7	0.65	3.3	2372	0.46792 ±0.00075	12.2944 ±0.0242	0.19056 ±0.00020	2474.4 ±3.3	2627.1 ±1.9	2747.0 ±1.7	11.9
96-07-2150; Lily Lake; Quartz porphyry dike; UTM 342576 mE, 5621962 mN (Zone 15, NAD 83)															
1z	broken col pr; 5NM; (7)	23.7	49.8	25.2	29.6	0.51	10.6	3599	0.51259 ±0.00066	13.3066 ±0.0166	0.18827 ±0.00010	2667.7 ±2.8	2701.7 ±1.2	2727.1 ±0.9	2.7
2z	col pr; 5NM; (4)	8.1	57.8	30.4	34.0	0.53	5.1	2898	0.50428 ±0.00077	13.0022 ±0.0226	0.18700 ±0.00017	2632.2 ±3.3	2679.8 ±1.6	2716.0 ±1.5	3.8
3z	small col pr; 5NM; (8)	7.1	60.5	32.5	35.5	0.54	5.3	2569	0.50204 ±0.00096	12.9867 ±0.0362	0.18761 ±0.00033	2622.6 ±4.1	2678.7 ±2.6	2721.3 ±2.9	4.4
4z	col pr; 5NM; (3)	9.1	20.5	11.0	12.3	0.54	6.6	893	0.49571 ±0.00126	12.8676 ±0.0653	0.18827 ±0.00073	2595.3 ±5.4	2670.0 ±4.8	2727.1 ±6.4	5.9
5z	small col round 5NM Abr (1)	0.8	38.4	45.9	132.9	1.20	90.9	28	0.68987 ±0.04125	18.8521 ±4.7505	0.19820 ±0.03982	3382.1 ±155.5	3034.3 ±217.8	2811.4 ±295.3	-26.2
6z	small col oval 5NM Abr (1)	0.8	48.6	26.3	39.7	0.54	15.1	84	0.43578 ±0.00373	11.2675 ±0.1711	0.18753 ±0.00193	2331.7 ±16.7	2545.5 ±14.1	2720.6 ±16.8	17.0
96-02-1056; Garnier Lake; Post-tectonic diorite dike; UTM 342744 mE, 5632856 mN (Zone 15, NAD 83)															
1r	milky frags; M; (39)	90.0	5.4	2.9	6.2	0.53	310.1	65	0.52067 ±0.00245	13.0140 ±0.1480	0.18128 ±0.00171	2702.0 ±10.4	2680.7 ±13.4	2664.6 ±15.5	-1.7
2r	milky frags; M; (50)	103.4	5.4	2.7	5.8	0.49	327.4	66	0.48979 ±0.00278	12.0348 ±0.1704	0.17821 ±0.00175	2569.8 ±12.0	2607.1 ±13.2	2636.3 ±16.2	3.1

⁽¹⁾ magnetic susceptibility is indicated by M (magnetic) or NM (non-magnetic), prefaced by the inclination of the Frantz isodynamic separator; number in parentheses indicates number of grains included in analysis

⁽²⁾ isotopic ratios and ages are corrected for fractionation, blank (5pg Pb; 1pg U), spike and initial common lead (Stacey and Kramers, 1975)

⁽³⁾ Th concentration estimated from the amount of ²⁰⁶Pb present in the analysis and the ²⁰⁷Pb/²⁰⁶Pb age

⁽⁴⁾ amount of discordance along a reference line to zero age

All errors in this table are reported at 1σ

Abbreviations: abr, abraded; col, colourless; el, elongate; eq, equant; euh, euhedral; frag(s), fragment(s); LA, laser ablation; lt, light; nabr, non-abraded; pr, prism; subh, subhedral; TA-CA, thermal annealing and chemical abrasion

by Simonetti et al. (2005). Common Pb corrections utilized the projected age of the zircon and the corresponding initial Pb isotopic compositions from the two-stage evolution model of Stacey and Kramers (1975). The resulting U-Pb isotopic data are listed in Appendix 1 and plotted on concordia diagrams. All errors reported Appendix 1 are quoted at 1σ and were calculated by numerical propagation of all known sources of uncertainty. The concordia diagrams were generated using the Isoplot version 3.0 application of Ludwig (2003), and the error ellipses are shown at 2σ . The detrital zircon data are also presented on diagrams that combine binned frequency histograms and probability distribution curves, which were generated using the Age-Display application of Sircombe (2004). For the purposes of interpretation, the results were filtered to include only the most concordant ($\geq 90\%$) and precise (1σ analytical errors ≤ 20 Ma) $^{207}\text{Pb}/^{206}\text{Pb}$ ages. Table 6 summarizes the results and preferred interpretation of the U-Pb analyses.

ID-TIMS results

Pegmatitic tonalite (unit Gn4d; sample 96-02-1067/CB02-03)

This sample was collected from an outcrop on the south shoreline of the narrows in Garner Lake, roughly midway between the east and west basins. It consists of pegmatitic hornblende tonalite from an irregular segregation in melagabbro at the north margin of the Garner Lake intrusive complex, approximately 5 m beneath the unconformity at the base of unit Gn5. Similar material near the north margin of the complex in eastern Garner Lake returned a U-Pb zircon age of 2871 ± 1 Ma (Davis, 1994). Sample 96-02-1067/CB02-03 was analyzed to test the correlation of the eastern and western portions of the complex. This sample contained euhedral to subhedral, prismatic to tabular, light tan zircons with moderate to high U concentrations. Five single-grain zircon fractions were analyzed,

Table 6: Summary of the preferred interpretation and geological significance of the results of U-Pb zircon and rutile analyses of bedrock samples in the eastern Rice Lake belt.

Sample ¹	Assemblage	Map unit ²	Rock type	Salient results ³	Interpretation
U-Pb ID-TIMS					
96-02-1067 (CB02-03)	Garner	Gn4d	Pegmatitic tonalite	2869.9 ± 0.5 Ma (1.2)	Approx. emplacement age
96-02-1050 (CB02-02)	Garner	Gn5c	Dacitic crystal tuff or coherent flow	2851.4 ± 1.0 Ma (-0.1)	Approx. emplacement age?
96-05-SLF ⁴	Bidou		Greywacke; Stovel Lake Fm.	2744.9 ± 4.7 Ma (0.5)	Maximum age of deposition
96-05-CMG	Bidou		Pegmatitic leucogabbro	2722.4 ± 3.2 Ma (-2.5)	None
96-05-SL ⁴	Bidou	Bd2a	Greywacke; Stormy Lake Fm.	2733.5 ± 2.2 Ma (3.2)	Maximum age of deposition
96-06-1845	Gem	Gw7	Dacitic crystal-lithic lapilli tuff	2727 ± 2 Ma	Depositional age
96-03-1116	WRPC	Wn2a	Biotite granite	2726 ± 1 Ma	Emplacement age
96-03-1261 (CB02-01)	WRPC	Wn2a	Feldspar-quartz porphyry dike	2746.6 ± 2.2 Ma (3.1)	Maximum emplacement age
96-07-2150	Edmunds	Em10	Quartz porphyry dike	2727.1 ± 0.9 Ma (2.7)	Maximum emplacement age
96-02-1056		Pt1	Post-tectonic diorite dike; metamorphic rutile	2664.6 ± 15.5 Ma (-1.7)	Minimum emplacement age; minimum age of ductile deformation
U-Pb LA-MC-ICPMS⁵					
96-05-SLF	Bidou		Greywacke; Stovel Lake Fm.	2736 Ma	Approximate age of deposition
96-05-SL	Bidou	Bd2a	Greywacke; Stormy Lake Fm.	2719 , 2630 Ma	Hydrothermal reset?
96-05-MRF	Gem	Gw2a	Volcanic sandstone	2724 Ma	Approximate age of deposition
96-02-1004 (CB02-05)	Edmunds	Em1b	Feldspathic greywacke	3007, 2938, 2738 Ma	Main sources of detritus;
96-06-2059	Edmunds	Em6b	Quartz-lithic greywacke	2997 , 2927, 2732 Ma	Main sources of detritus; maximum age of deposition (2732 Ma)

¹ Mineral separates from sample 96-02-1056 consisted of rutile; all other separates were zircon

² Unit codes correspond to those on Map GR2013-1-1; samples without unit codes were collected outside of the map area

³ Numbers in parentheses indicate discordance (in percent) along a reference line to zero age; bold numbers indicate the dominant mode in the detrital zircon population

⁴ Analysis performed on single zircon grains plucked from the corresponding laser ablation mount

⁵ Listed results correspond to maxima in the probability distribution curves

Abbreviation: WRPC, Wanipigow River plutonic complex

all of which yielded discordant results ranging in age between 2855 and 2870 Ma (Table 5). A linear regression using all the data points indicates an upper-intercept age of 2861 Ma, with 0% probability of fit (Figure 65a). Two of the fractions have $^{207}\text{Pb}/^{206}\text{Pb}$ ages that are identical at 2865.2 Ma, whereas the least discordant fraction (fraction 4; 1.2% discordant) yielded a $^{207}\text{Pb}/^{206}\text{Pb}$ age of 2869.9 ± 0.5 Ma. This single-grain fraction was abraded and had the lowest U and Pb concentrations of all the analyses. The $^{207}\text{Pb}/^{206}\text{Pb}$ age is identical within error to the best-estimate emplacement age of 2871 ± 1 Ma from pegmatite in the eastern portion of the complex, and also overlaps within error the 2871 ± 2 Ma age obtained from detrital zircons in the unconformably overlying arkosic sandstone of unit Gn5 (Davis, 1994). For these reasons, the 2870 Ma age is interpreted to closely approximate the emplacement age of the pegmatitic tonalite segregation.

Dacitic crystal tuff or coherent flow (unit Gn5c; sample 96-02-1050/CB02-02)

This sample was collected from an outcrop of feldsparphyric dacite north of the narrows in Garner Lake, which is interpreted to represent either a massive crystal tuff or coherent flow. Sample 96-02-1050/CB02-02 contained euhedral to subhedral, prismatic zircon crystals and crystal fragments, which are colourless, pink, tan or brown. Single-grain fractions of each of the four colour types and five multigrain fractions (three pink; two tan-brown) were analyzed, and these yielded variably discordant results and a wide range of $^{207}\text{Pb}/^{206}\text{Pb}$ ages (Table 5). One single-grain abraded fraction (fraction 2) of colourless zircon yielded an anomalously young, near-concordant $^{207}\text{Pb}/^{206}\text{Pb}$ age of 1012.1 ± 4.7 Ma, whereas the remainder of the fractions yielded $^{207}\text{Pb}/^{206}\text{Pb}$ ages ranging between 2775 and 2886 Ma. A linear regression using all the data points indicates upper- and

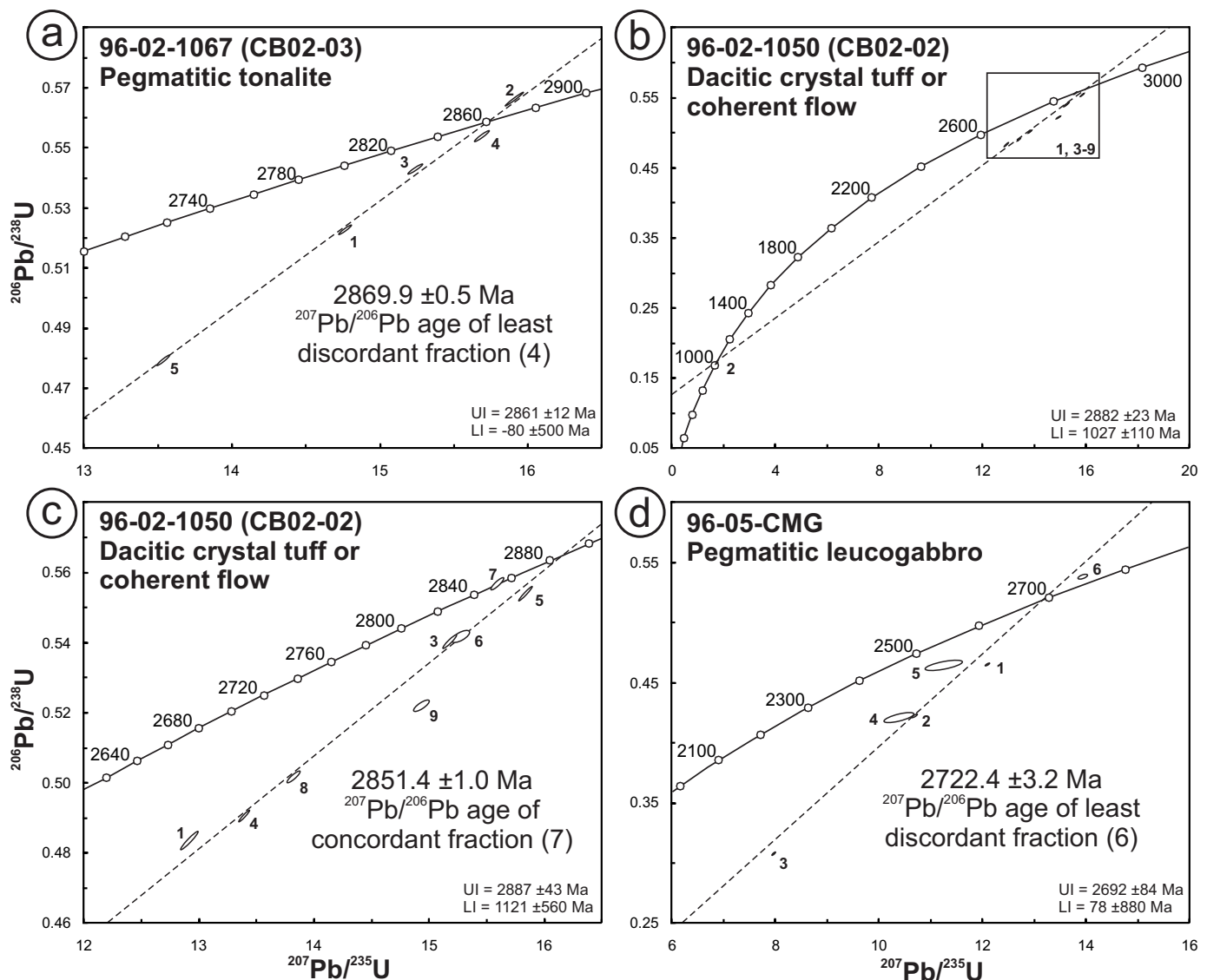


Figure 65: U-Pb concordia diagrams for igneous zircons from plutonic and volcanic rocks in the Garner and Bidou assemblages: **a)** pegmatitic tonalite of the Garner Lake intrusive complex (sample 96-02-1067/CB02-03); **b)** dacitic crystal tuff or coherent flow of the Garner assemblage (sample 96-02-1050/CB02-02), showing all data; inset indicates location of Figure 65c; **c)** sample 96-02-1050/CB02-02, showing only the analytical results with Archean ages; **d)** pegmatitic leucogabbro in the Bidou assemblage (sample 96-05-CMG). Numbers adjacent to the data points correspond to those of the various fractions in Table 5. Abbreviations: LI, lower intercept; UI, upper intercept.

lower-intercept ages of 2882 and 1027 Ma, with 0% probability of fit (Figure 65b). Similar upper- and lower-intercept ages (2887 and 1121 Ma, respectively; probability of fit = 0%) are obtained by a regression of just the Archean data points (Figure 65c), possibly indicating that the discordant results stem from significant Pb loss during a thermal event at ca. 1000–1100 Ma, with minor growth of new zircon (see below). Two single-grain fractions yielded $^{207}\text{Pb}/^{206}\text{Pb}$ ages that are identical within error at 2885 Ma and could perhaps represent zircons that were inherited from felsic volcanic rocks in the lower succession of the Garner assemblage, the minimum age of which is indicated by the ca. 2870 Ma age (Davis, 1994) of the Garner Lake intrusive complex. A multigrain fraction (fraction 7) of pink zircon fragments returned an essentially concordant $^{207}\text{Pb}/^{206}\text{Pb}$ age of 2851.4 ± 1 Ma, which may indicate the approximate emplacement age of the crystal tuff or coherent flow.

Greywacke (Stovel Lake formation; sample 96-05-SLF)

This sample was collected from an outcrop on the southwest shoreline of Tinney Lake near the hinge of the Beresford Lake anticline, and consists of pebbly feldspathic greywacke from a very thick (3–5 m), normally graded bed at the base of the Stovel Lake formation. The sample has a bulk composition of basaltic andesite and was collected approximately 2.5 m above the upper contact of the Unnamed basalt; the contact in this location is marked by a 1–3 m thick bed of heterolithic volcanic conglomerate. Sample 96-05-SLF was processed for LA-MC-ICP-MS analysis of detrital zircons, and the resulting data (see below) show significant discordance and include a number of analyses with anomalously young (560–1110 Ma) $^{207}\text{Pb}/^{206}\text{Pb}$ ages. Three grains were plucked from the mount for follow-up ID-TIMS analysis in an attempt to constrain the age of deposition and confirm the young ages. Fraction 1 yielded a near-concordant $^{207}\text{Pb}/^{206}\text{Pb}$ age of 2745 Ma (Table 5), which is taken to indicate the maximum depositional age of the Stovel Lake formation. Fraction 2 yielded a strongly discordant age of 1078 Ma, which appears to confirm the anomalously young ages indicated by the laser-ablation analyses. The U and Pb concentrations of this grain are comparable to those for the single-grain fraction (fraction 2) from sample 96-02-1050/CB02-02, which also returned an anomalously young age (Table 5). Fraction 3 yielded a strongly reverse-discordant age of 2803 Ma with an unacceptably high analytical error and is therefore not considered further.

Pegmatitic leucogabbro (Tinney Lake formation; sample 96-05-CMG)

This sample was collected from a thick gabbro sill at the site of the past-producing Central Manitoba mine. It consists of very coarse grained to locally pegmatitic leucogabbro from an irregular, subconcordant patch (1 m by 10 m) in the upper portion of the sill. Multi-element profiles indicate that the pegmatitic leucogabbro is chemically similar to the host gabbro sill and the tholeiitic-basalt country rocks but characterized by strongly elevated Zr, Ti and Eu, in keeping with a higher degree of fractionation. Based on the field relationships and geochemistry,

the patch is interpreted to result from in situ magmatic differentiation of the sill, and a sample of this material was collected to constrain the age of mafic magmatism in the lower portion of the Bidou assemblage. The separate from sample 96-05-CMG contained fragments of light tan to pink or colourless zircon. Six multigrain fractions were selected for analysis, and these yielded variably discordant results, with $^{207}\text{Pb}/^{206}\text{Pb}$ ages ranging between 2612 and 2730 Ma (Table 5; Figure 65d). Five of the fractions yielded results that are greater than 10% discordant and/or had high analytical errors. The least discordant (–2.5%) fraction has a $^{207}\text{Pb}/^{206}\text{Pb}$ age of 2722.4 ± 3.2 Ma, which could be taken to approximate the emplacement age. However, if the leucogabbro did indeed result from in situ differentiation of the gabbro sill, as appears likely, this result suggests that the sill is unrelated to the host tholeiitic basalt flows, which must be older than the overlying dacitic volcanoclastic rocks (ca. 2730 Ma; Turek et al., 1989) of The Narrows formation. This result therefore provides no new constraints on the age of mafic magmatism in the lower Bidou assemblage. Given the scatter in the data, no additional significance is assigned to the results from this sample.

Greywacke (Stormy Lake formation; unit Bd2a; sample 96-05-SL)

This sample was collected from an outcrop approximately 500 m south-southwest of the past-producing Gunnar mine in the central portion of the Stormy Lake formation. It consists of medium-grained feldspathic greywacke from the normally graded base of a relatively thick (0.5 m) turbidite that has a dacitic bulk composition. It was processed for LA-MC-ICP-MS analysis of detrital zircons, and the resulting data (see below) show significant discordance. Three grains were plucked from the mount for follow-up ID-TIMS analysis in an attempt to constrain the age of deposition. Fraction 1 yielded a strongly discordant $^{207}\text{Pb}/^{206}\text{Pb}$ age of 2669 Ma (44% discordant; Table 5), whereas fraction 2 failed during the analysis and is therefore not reported. Fraction 3 yielded a slightly discordant age of 2734 Ma, which is taken to indicate the maximum depositional age of the Stormy Lake formation.

Dacitic crystal-lithic lapilli tuff (unit Gw7; sample 96-06-1845)

This sample was collected near the northwestern extent of unit Gw7, on the south bank of the Manigotagan River approximately 600 m downstream from Gem Lake. It consists of unstratified, light grey, crystal-lithic lapilli tuff of dacitic bulk composition that is situated approximately 15 m stratigraphically below the basal contact of the overlying Edmunds assemblage. Sample 96-06-1845 contained prismatic pink zircons of various sizes. Two single-grain fractions of large pink prisms and a multigrain fraction of small prisms were selected for analysis, and all three yielded slightly discordant results and $^{207}\text{Pb}/^{206}\text{Pb}$ ages that overlap within error. A linear regression of the data points defines a Pb-loss line with an upper-intercept age of 2727 ± 2 Ma (22% probability of fit) and a lower-intercept age of 20 Ma (Figure 66a); the upper-intercept age is taken to approximate the emplacement age of the lapilli tuff.

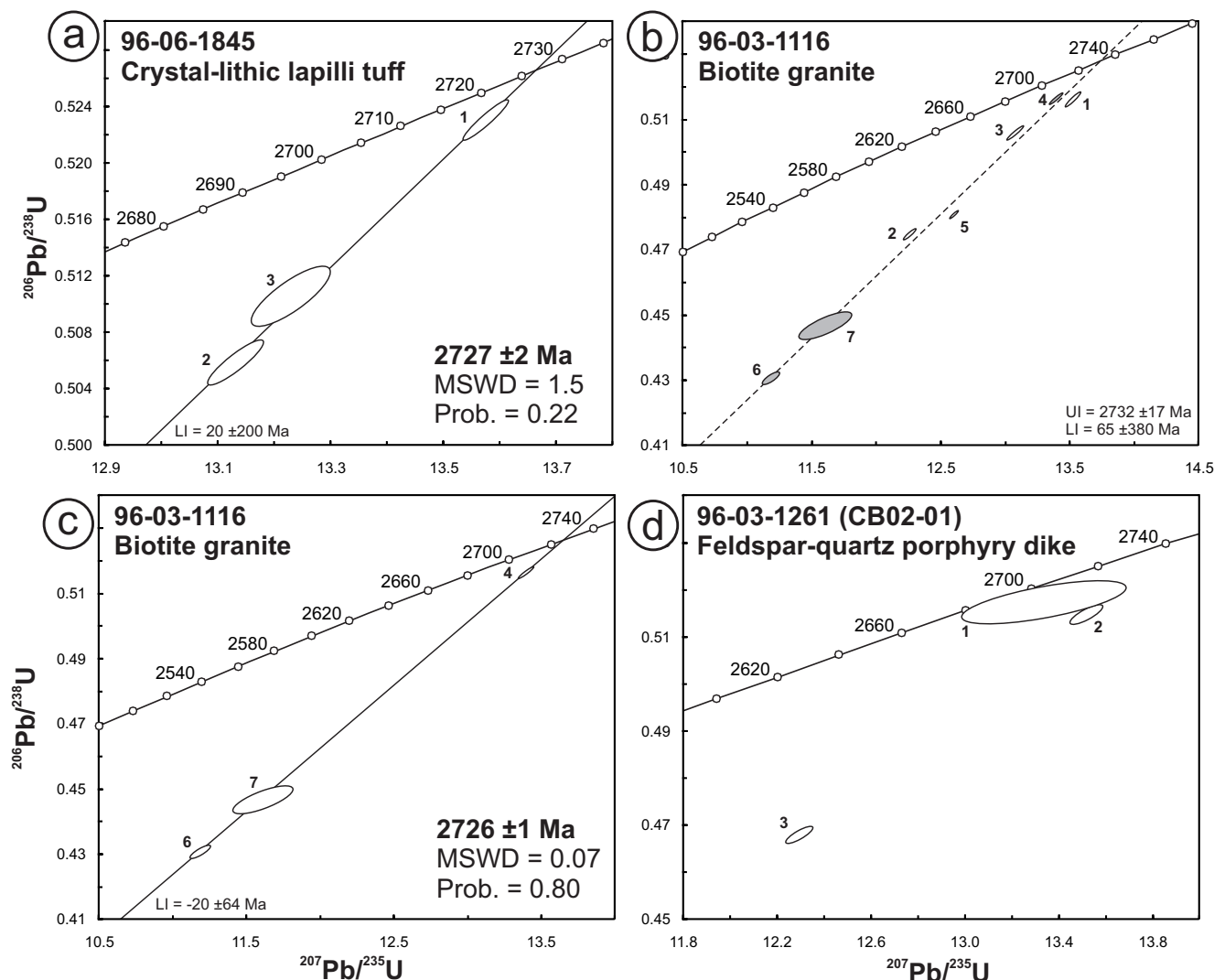


Figure 66: U-Pb concordia diagrams for igneous zircons from volcanic and plutonic rocks of the Gem assemblage and Wanipigow River plutonic complex: **a)** crystal-lithic lapilli tuff of unit Gw7 (sample 96-06-1845); **b)** biotite granite of unit Wn2a (sample 96-03-1116), showing all data; **c)** sample 96-03-1116, showing the three fractions used to calculate the probable emplacement age; **d)** feldspar-quartz porphyry dike of unit Wn2a (sample 96-03-1261/CB02-01). Numbers adjacent to the data points correspond to those of the various fractions in Table 5. Abbreviations: LI, lower intercept; MSWD, mean square of weighted deviates; Prob., probability; UI, upper intercept.

Biotite granite (unit Wn2a; sample 96-03-1116)

This sample consists of equigranular biotite granite from the small pluton that intrudes intermediate volcanoclastic rocks (unit Gn3) of the Garner assemblage in the southeastern portion of Garner Lake. Contact relationships are well exposed along the southeastern margin of the pluton, and clearly indicate the relative ages of the country rock, granite emplacement and penetrative ductile deformation. The granite was therefore selected for analysis to constrain the absolute age of emplacement, and to place minimum and maximum age constraints, respectively, on volcanism (unit Gn3) and ductile deformation. Sample 96-03-1116 contained a heterogeneous population of light tan to pink or colourless prismatic zircons, which vary in morphology from stubby to platy or needle like. Three single-grain fractions and two multigrain fractions were selected initially for analysis, and yielded variably discordant results (1.9–9.5%), with $^{207}\text{Pb}/^{206}\text{Pb}$ ages ranging between 2719 and 2743 Ma (Table 5). Two of these fractions overlap within error at 2743 Ma. In an

attempt to obtain less discordant data, two additional single-grain fractions (fractions 6, 7) were selected for analysis and were processed using the thermal annealing–chemical abrasion (TA-CA) method of Mattinson (2005). These fractions yielded $^{207}\text{Pb}/^{206}\text{Pb}$ ages that overlap within error (2727.9 ± 2.4 and 2729.8 ± 8.1 Ma) but are more strongly discordant (15–18%) than the initial analyses. A linear regression using all data points yields an upper-intercept age of 2732 Ma (0% probability of fit) and a lower-intercept age of 65 Ma (Figure 66b). The least discordant fraction from the initial analyses (fraction 4; 1.9% discordant), which consisted of a single platy prismatic zircon, yielded a $^{207}\text{Pb}/^{206}\text{Pb}$ age of 2726.5 ± 0.5 Ma that overlaps within error the ages of the two single-grain fractions processed using the TA-CA method. A linear regression using only these data points defines a Pb-loss line with an upper-intercept age of 2726 ± 1 Ma (80% probability of fit) and a lower-intercept age of -20 Ma (Figure 66c); the upper-intercept age is taken as the best estimate of the age of the granite pluton. The complex

systematics in this sample may be the result of zircon inheritance, coupled with Archean Pb loss.

Feldspar-quartz porphyry (unit Wn2a; sample 96-03-1261/CB02-01)

This sample was collected from an outcrop located approximately 700 m north of the western basin of Garner Lake. It consists of feldspar-quartz porphyritic granite from a 5 m thick dike that intrudes komatiite flows at the type locality described by Brommecker et al. (1993). Sample 96-03-1261/CB02-01) was selected for analysis to provide a minimum age on the host komatiitic flows (unit Gn6) of the Garner assemblage. This sample contained light tan to pink, prismatic zircons. Three single-grain fractions were selected for analysis and yielded variably discordant results (Table 5). The least discordant fraction yielded a $^{207}\text{Pb}/^{206}\text{Pb}$ age of 2716 Ma, with a large analytical error, whereas the remaining two fractions yielded ages that overlap within error at 2747 Ma (Figure 66d). The overlapping $^{207}\text{Pb}/^{206}\text{Pb}$ ages are taken to indicate the maximum emplacement age of the dike.

Quartz porphyry (unit Em10; sample 96-07-2150)

This sample was collected approximately 1 km south of Lily Lake on the south limb of the Slate Lake syncline. It consists of quartz-phyrlic rhyolite from a 0.5–1.0 m thick dike that intrudes pillowed and massive basalt flows of unit Em8. Clasts of texturally similar rhyolite are present in polymictic conglomerate farther upsection from the sample site; hence, this sample was selected for analysis in an effort to constrain the age of volcanism and sedimentation in the upper facies association of the Edmunds assemblage. Sample 96-07-2150 contained colourless zircons that vary in morphology from euhedral (prismatic) to anhedral (subspherical). Two single-grain fractions and four multigrain fractions were selected for analysis and yielded variably discordant results (2.7–17.0%), with one spurious result

(fraction 5; Table 5). Two fractions returned identical $^{207}\text{Pb}/^{206}\text{Pb}$ ages of 2727.1 Ma, whereas two other fractions yielded ages that overlap within error at 2721 Ma. A linear regression of all the data points (excluding the spurious analysis) indicates an upper-intercept age of 2724 Ma (0% probability of fit) and a lower-intercept age of 42 Ma (Figure 67a). Given the scatter in the data, the 2727 Ma $^{207}\text{Pb}/^{206}\text{Pb}$ ages are taken as a rough estimate of the maximum emplacement age of the dike.

Post-tectonic diorite (unit Pt1; sample 96-02-1056)

This sample was collected from an outcrop on the western shoreline of the west basin of Garner Lake. It consists of fine-grained equigranular diorite from a post-tectonic dike that cuts unseparated tectonite near the eastern margin of the Beresford Lake shear zone. It was selected for analysis to constrain the age of dike emplacement and thus provide a minimum age for penetrative ductile deformation in the host shear zone. Although sample 96-02-1056 did not contain any zircon, it was found to contain abundant rutile. In thin section, the rutile is mostly contained within clots of chlorite and carbonate that appear to represent replacement products after primary ferromagnesian phenocrysts. Two fractions of rutile were selected for analysis and returned slightly discordant $^{207}\text{Pb}/^{206}\text{Pb}$ ages of 2665 Ma and 2636 Ma (Table 5; Figure 67b). The 2665 Ma age of the least discordant fraction (fraction 1; –1.7% discordant) is interpreted to provide a minimum age constraint on dike emplacement, and would therefore also indicate the minimum age of penetrative ductile deformation in the Beresford Lake shear zone.

LA-MC-ICP-MS results

Greywacke (Stovel Lake formation; sample 96-05-SLF)

As described above, this sample consists of pebbly greywacke from the base of the Stovel Lake formation, collected

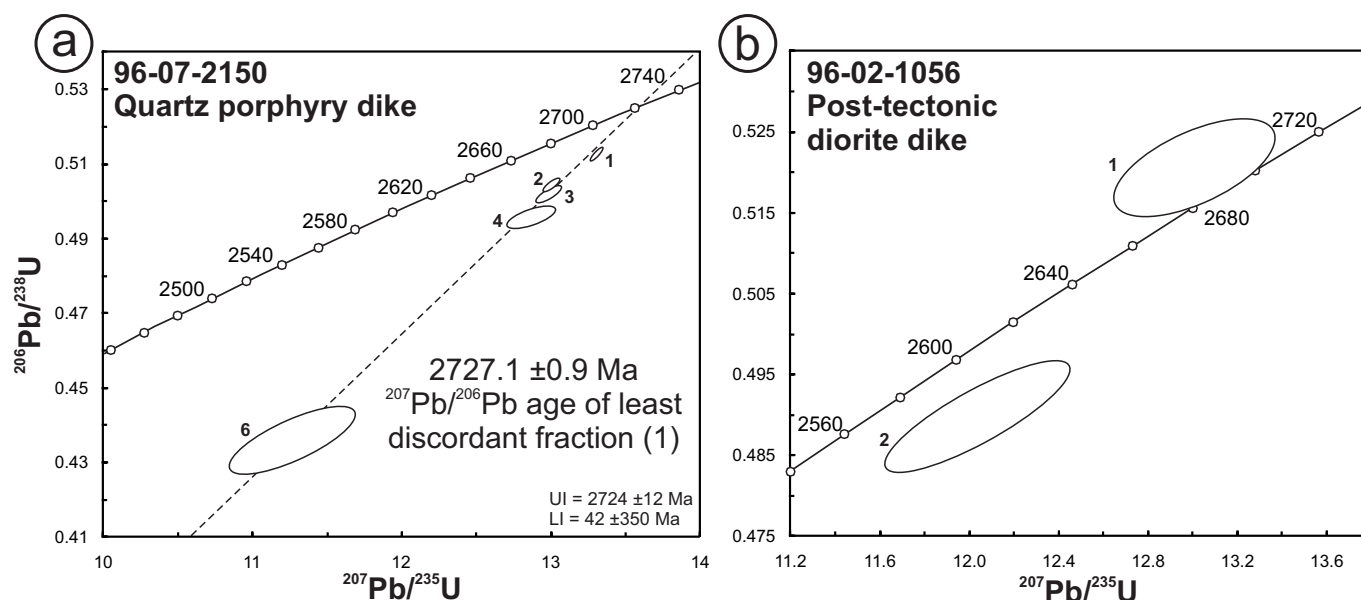


Figure 67: U-Pb concordia diagrams for zircons from: **a)** quartz porphyry dike of unit Em10 (sample 96-07-2150); **b)** post-tectonic diorite dike (unit Pt1; sample 96-02-1056). Abbreviations: LI, lower intercept; UI, upper intercept.

from an outcrop on the southwest shoreline of Tinney Lake. Forty detrital zircons were analyzed and define two distinct populations with $^{207}\text{Pb}/^{206}\text{Pb}$ ages of ca. 560–1110 Ma ($n = 7$) and 2670–2780 Ma ($n = 31$); both populations show significant discordance (Figure 68a; two spurious analyses are excluded). The younger population includes an analysis with a near-concordant $^{207}\text{Pb}/^{206}\text{Pb}$ age of 1016 Ma, which may indicate ‘new’ zircon growth during a Proterozoic thermal event (see below). The older population defines an essentially unimodal distribution with a probability maximum at 2736 Ma (Figure 69a), consistent with a local source dominated by ca. 2730–2740 Ma detritus.

Greywacke (Stormy Lake formation; unit Bd2a; sample 96-05-SL)

As described above, this sample consists of medium-grained greywacke that was collected from an outcrop approximately 500 m south-southwest of the past-producing Gunnar mine in the central portion of the Stormy Lake formation. Forty-eight detrital zircons were analyzed and, in common with sample 96-05-SLF, show significant discordance, with a number of seemingly spurious results (Figure 68b). The distribution profile for the filtered dataset shows a slightly wider range of ages compared to sample 96-05-SLF, with a prominent mode centred at 2719 Ma and a subsidiary mode at ca. 2630 Ma (Figure 69b). As described previously, the Stormy Lake formation is stratigraphically overlain by ca. 2730 Ma (Turek et al., 1989) dacitic volcanoclastic rocks of The Narrows formation, and both are intruded along strike to the northwest by the ca. 2724 Ma (Anderson, 2008) Ross River pluton. Hence, most of the $^{207}\text{Pb}/^{206}\text{Pb}$ ages in sample 96-05-SL are too young to be primary and are interpreted to indicate significant Pb loss.

Volcanic sandstone (unit Gw2a; sample 96-05-MRF)

This sample was collected from an outcrop on the west shoulder of Provincial Road 314, approximately 900 m south of the Manigotagan River. It consists of coarse-grained volcanic sandstone from a 35 cm thick, doubly graded bed (Figure 16a) in an interval of volcanoclastic turbidites near the top of unit Gw2, on the west limb of the Beresford Lake anticline. This locality corresponds to the ‘progradational fan succession’ described by Seneshen (1990). The sample has a dacitic bulk composition and contains abundant juvenile pyroclasts, which include cusped quartz shards and possible collapsed pumice. The 56 zircons analyzed yielded mostly Neoproterozoic $^{207}\text{Pb}/^{206}\text{Pb}$ ages. One slightly discordant analysis returned an age of 1200 Ma (Figure 68c). The distribution profile for the filtered dataset indicates an essentially unimodal population of $^{207}\text{Pb}/^{206}\text{Pb}$ ages with a prominent mode at 2724 Ma (Figure 69c), consistent with a local source dominated by ca. 2720–2730 Ma detritus.

Feldspathic greywacke (unit Em1b; sample 96-02-1004/CB02-05)

This sample was collected from an outcrop on the Gem Lake logging road (now closed), approximately 300 m south of the bridge over the Manigotagan River. It consists of medium-grained feldspathic greywacke from a 45 cm thick, normally

graded turbidite that is part of the lower facies association of the Edmunds assemblage (the sample site is located approximately 250 m stratigraphically above the basal contact). The 49 zircons analyzed define three distinct populations (Figure 68d). The distribution profile includes a prominent mode at 2738 Ma and subsidiary modes at 2938 Ma and 3007 Ma (Figure 69d; note that none of the analyses were removed from the dataset by the filtering process). In keeping with the detrital zircon results from the underlying Bidou and Gem assemblages, the dominant mode is taken to indicate a mostly local source dominated by ca. 2730–2740 Ma detritus, whereas the older modes signal the arrival of ‘exotic’ detritus from a presumably more distant source.

Quartz-lithic greywacke (unit Em6b; sample 96-06-2059)

This sample was collected from an outcrop approximately 500 m southeast of Lily Lake along the Beaver Gold trend. It consists of very coarse grained greywacke that contains up to 40% quartz granules and abundant pebbles of feldspar-phyric dacite. The greywacke is interbedded with polymictic conglomerate and magnetite-chert iron formation of subunit Em6b on the south limb of the Slate Lake syncline, and is part of the upper facies association of the Edmunds assemblage. It is also interlayered with pillowed basalt flows of unit Em8 and dacitic volcanic conglomerate of unit Em7. The 60 zircons analyzed define three distinct populations (Figure 68e) of similar age to those of sample 96-02-1004/CB02-05. However, the distribution profile for the filtered dataset is significantly skewed toward older ages, with a prominent mode at 2997 Ma and subsidiary modes at 2927 Ma and 2732 Ma (Figure 69e). The dominance of ca. 3.0 Ga zircons is consistent with the high abundance of exotic clasts in adjacent conglomerate beds and points to an extrabasinal source for much of the detritus.

Interpretation of the U-Pb age data

Garner assemblage

The new U-Pb age data presented above do not provide significant new insights into the age of the Garner assemblage, but do lend support to inferences drawn previously by Davis (1994) and Poulsen et al. (1996). As described above, intermediate-felsic volcanic, volcanoclastic and epiclastic rocks in the lower succession of the assemblage are intruded by layered peridotite, pyroxenite and gabbro of the Garner Lake intrusive complex (GLIC). Davis (1994) reported a U-Pb zircon age of 2871 ± 1 Ma for pegmatitic segregations near the north margin of the complex in eastern Garner Lake, which is taken to closely approximate the emplacement age of the GLIC as a whole. A similar emplacement age is inferred for segregations in the western portion of the complex, based on the $^{207}\text{Pb}/^{206}\text{Pb}$ age of ca. 2870 Ma for the least discordant analysis from the sample of pegmatitic tonalite (96-02-1067/CB02-03) analyzed as part of this study. These data provide a minimum age constraint for the lower succession of the assemblage and lend support to the correlation of the eastern and western portions of the GLIC. Distinctly older (ca. 2885 Ma) zircons in the sample of dacitic crystal tuff or coherent flow (unit Gn5c; sample 96-02-

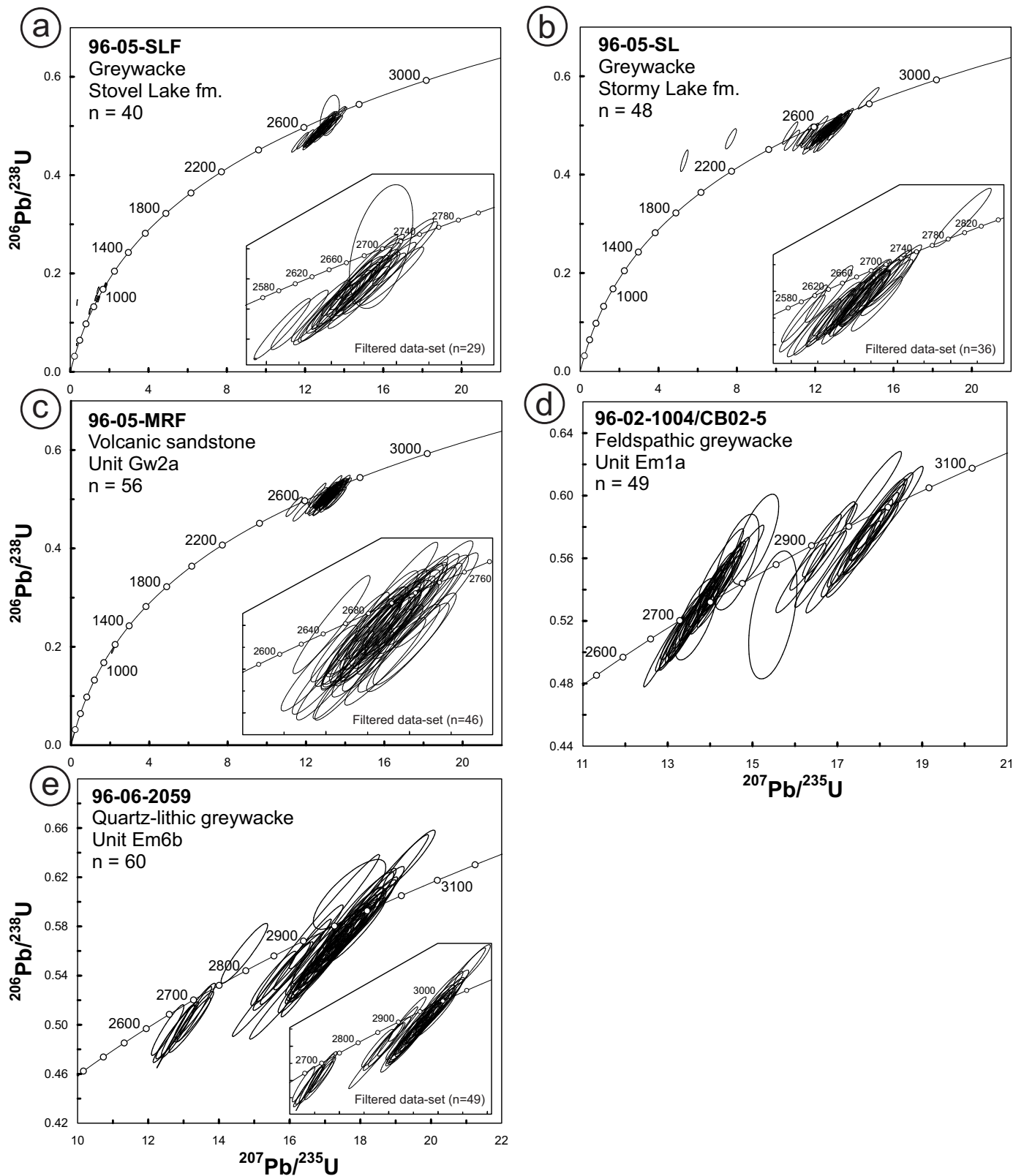


Figure 68: U-Pb concordia diagrams for detrital zircons from sedimentary rocks in the Bidou, Gem and Edmunds assemblages: **a)** greywacke (96-05-SLF); **b)** greywacke (96-05-SL); **c)** volcanic sandstone (96-05-MRF); **d)** feldspathic greywacke (96-02-1004/CB02-5); **e)** quartz-lithic greywacke (96-06-2059). Inset diagrams show the filtered dataset for each sample (analyses $\geq 90\%$ concordant, with 1σ errors ≤ 20 Ma).

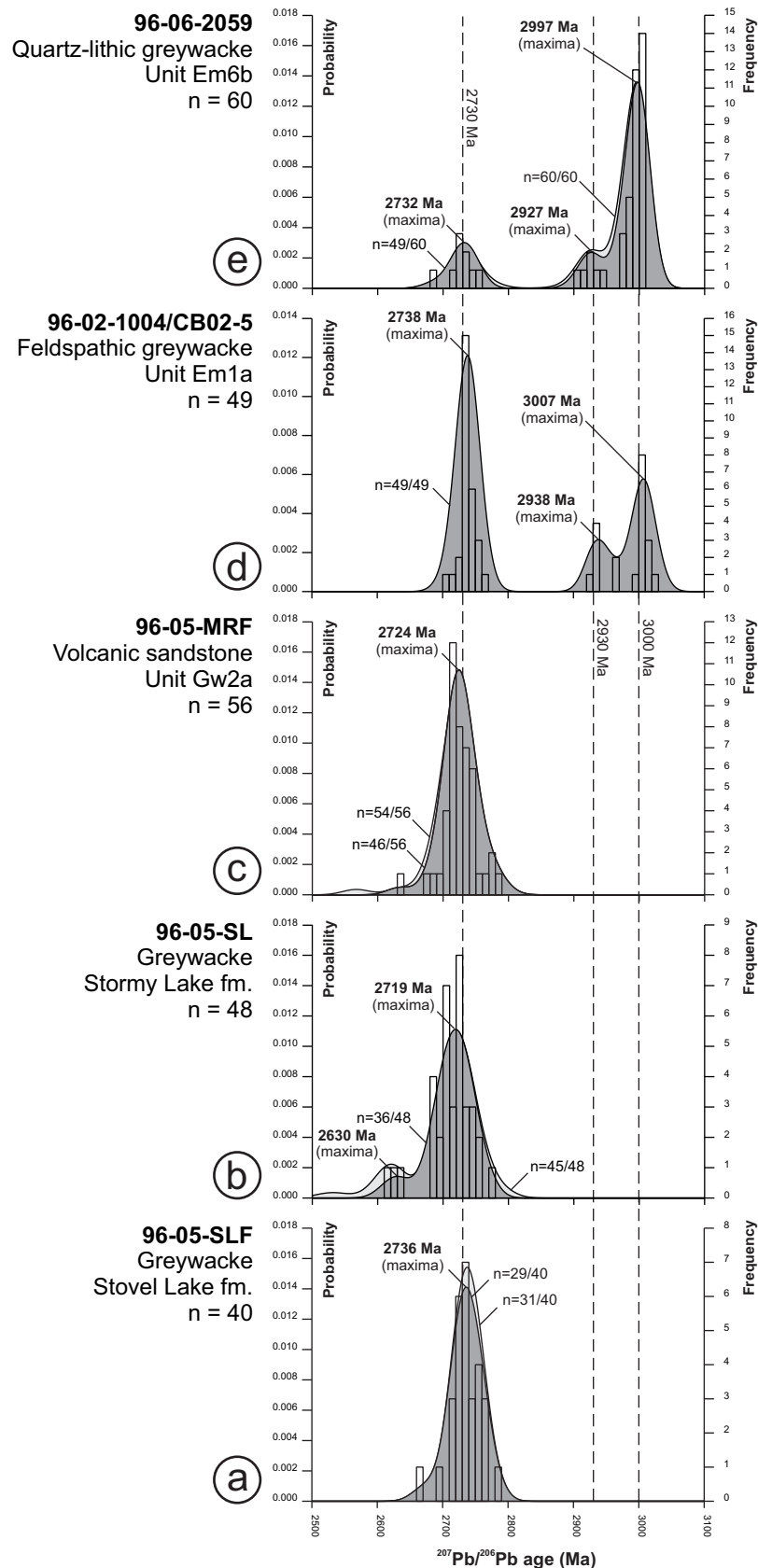


Figure 69: Combined frequency histograms and probability-density distribution (PDD) curves of $^{207}\text{Pb}/^{206}\text{Pb}$ ages (Ma) for detrital zircons from sedimentary rocks in the Bidou, Gem and Edmunds assemblages, in stratigraphic order from oldest (bottom) to youngest (top): **a)** sample 96-05-SLF ($n = 40$); **b)** sample 96-05-SL ($n = 48$); **c)** sample 96-05-MRF ($n = 56$); **d)** sample 96-02-1004/CB02-05 ($n = 49$); **e)** sample 96-06-2059 ($n = 60$). Light shaded curve indicates PDD for the unfiltered datasets, excluding outlier analyses ($^{207}\text{Pb}/^{206}\text{Pb}$ ages < 2600 Ma). Dark shaded curve indicates PDD for the filtered datasets (analyses $\geq 90\%$ concordant, with 1σ errors ≤ 20 Ma). Bin width on the histograms is 10 Ma. See text for discussion.

1050/CB02-02) in the upper succession may be inherited, and may thus provide an approximate age constraint for the lower succession.

Davis (1994) also reported a U-Pb zircon age of 2871 ± 2 Ma for detrital zircons in the arkosic sandstone that unconformably overlies the GLIC, which represents the maximum age of the upper succession. Uranium-lead isotopic data from the dacitic crystal tuff or massive flow from unit Gn5c (sample 96-02-1050/CB02-02) indicate very complex zircon systematics and thus preclude unambiguous interpretation. Nevertheless, the multigrain fraction with an essentially concordant $^{207}\text{Pb}/^{206}\text{Pb}$ age of ca. 2851 Ma is interpreted to represent the best estimate of the emplacement age. By this constraint, the komatiitic basalt flows in the upper succession would be at least 20 m.y. younger than the GLIC.

The remainder of the data points from this sample show significant discordance that may be related to a Pb-loss event at ca. 1100–1000 Ma; the single-grain fraction with a near-concordant $^{207}\text{Pb}/^{206}\text{Pb}$ age of 1012 Ma indicates that this event may locally have resulted in new zircon growth. Similar lower-intercept ages were described by Corfu and Stott (1993) from rocks on strike to the east along the south margin of the NCT, and were tentatively attributed to low-grade hydrothermal activity associated with fault reactivation. Similarly, Corfu and Stone (1998) reported upper- and lower-intercept ages of 2736 ± 3 –2 Ma and ca. 1045 Ma, respectively, for a sample (C64) of hornblende tonalite at Donald Lake, Ontario, which is located 27 km east of Wallace Lake along the north margin of the Wanipigow fault (Figure 1). Coupled with the results of this study, these anomalously young lower-intercept ages may indicate reactivation and localized hydrothermal activity along crustal-scale faults at the south margin of the NCT in Manitoba.

Bidou assemblage

Age constraints indicate that the Bidou assemblage was deposited during a relatively narrow time interval, between approximately 2745 and 2730 Ma. Detrital zircons from a sample of greywacke in the Stovel Lake formation (sample 96-05-SLF), near the bottom of the exposed portion of the lower (back-arc) succession, define an essentially unimodal distribution with a probability maximum at 2736 Ma. They include a single grain with a near-concordant $^{207}\text{Pb}/^{206}\text{Pb}$ age of ca. 2745 Ma, which is taken to indicate the maximum depositional age. The assemblage is capped by ca. 2730 Ma (Turek et al., 1989) dacitic volcanoclastic rocks of The Narrows formation and is intruded by ca. 2730–2720 Ma (Turek et al., 1989; Anderson, 2008) tonalite and granodiorite of the Ross River plutonic suite. The sample of greywacke from the Stovel Lake formation includes a younger population of zircons with $^{207}\text{Pb}/^{206}\text{Pb}$ ages of ca. 560–1110 Ma ($n = 7$) and yielded an analysis with a near-concordant $^{207}\text{Pb}/^{206}\text{Pb}$ age of 1016 Ma, which is comparable to the results from the Garner assemblage.

Gem assemblage

Age constraints indicate that the Gem assemblage was also deposited during a relatively narrow time interval, between approximately 2730 and 2720 Ma. Rhyolitic ignimbrite (unit

Gw4d) of the West association of the assemblage yielded a U-Pb zircon age of 2722 ± 2 Ma (Davis, 1994) from an exposure on the central peninsula in Gem Lake. This age overlaps within error the probable age of the East association of the assemblage, based on a reported age of 2718 ± 3 –2 Ma for a felsic tuff located along strike to the east in Ontario (Rogers and McNicoll, unpublished, cited by Lemkow et al., 2006). New results from this study provide broadly similar constraints. On the western limb of the Beresford Lake anticline at Gem Lake, the top of the West association is defined by crystal-lithic lapilli tuff, tuff and tuff breccia of unit Gw7, which are interpreted to represent a subaqueously emplaced felsic ignimbrite. Dacitic crystal-lithic lapilli tuff from near the top of this unit (sample 96-06-1845) yielded a U-Pb zircon age of 2727 ± 2 Ma, which is interpreted to approximate the age of volcanic emplacement. Along strike to the northwest, lateral equivalent rocks of unit Gw2a consist of felsic volcanoclastic turbidites and mass-flow deposits, and contain detrital zircons that define an essentially unimodal population with a probability maximum at ca. 2724 Ma (sample 96-05-MRF), consistent with a local source dominated by ca. 2730–2720 Ma detritus.

Wanipigow River plutonic complex

The Garner assemblage is intruded from the east by granitoid rocks of the Wanipigow River plutonic complex (WRPC), and two of these intrusions were selected for U-Pb geochronology. Biotite granite (sample 96-03-1116) from the small pluton at the southeast end of Garner Lake has a best-estimate emplacement age of 2726 ± 1 Ma but yielded data that show significant discordance and a wide range of $^{207}\text{Pb}/^{206}\text{Pb}$ ages (2743–2719 Ma). Feldspar-quartz porphyry (sample 96-03-1261/CB02-01) from a dike cutting komatiitic flows north of Garner Lake likewise yielded significantly discordant data, with $^{207}\text{Pb}/^{206}\text{Pb}$ ages of 2747 Ma (two analyses) and 2716 Ma, the former of which is interpreted to represent the maximum age of emplacement. The range of $^{207}\text{Pb}/^{206}\text{Pb}$ ages (2747–2716 Ma) obtained from these two samples is similar to that obtained by Corfu and Stone (1998) from their regional reconnaissance of tonalite-granodiorite plutons in the North Caribou terrane.

Edmunds assemblage

Regional constraints indicate that the Edmunds assemblage was also deposited during a relatively narrow time interval, between approximately 2710 and 2700 Ma. Previously reported ID-TIMS analyses of single detrital zircons in two samples of greywacke collected near the base of the lower facies association (LFA) indicate a maximum depositional age of 2725 Ma (Davis, 1996). New U-Pb analyses of detrital zircons from a greywacke bed slightly higher in the stratigraphy of the LFA (sample 96-02-1004/CB02-05) define a distribution profile that includes a prominent mode at 2738 Ma, with subsidiary modes at 2938 Ma and 3007 Ma, indicating a mostly local source dominated by ca. 2740–2730 Ma detritus (e.g., the Bidou assemblage and/or the Wanipigow River plutonic complex). The older modes signal the arrival of ‘exotic’ detritus from a presumably more distant source.

Previously published ID-TIMS analyses of single detrital zircons from a sample of coarse quartz greywacke of the upper facies association (UFA) indicate a maximum depositional age of 2705 Ma (Davis, 1996). New U-Pb analyses of detrital zircons from a quartz-lithic greywacke bed slightly higher in the stratigraphy of the UFA (sample 96-06-2059) define a distribution profile that is distinctly different from that of the LFA and includes a prominent mode at 2997 Ma, with subsidiary modes at 2927 Ma and 2732 Ma, indicating an extrabasinal provenance for most of the detritus. Quartz porphyry in the UFA (sample 96-07-2150) yielded a poorly constrained maximum emplacement age of ca. 2727 Ma.

Post-tectonic dikes

The post-tectonic diorite dike in the Beresford Lake shear zone (sample 96-02-1056) yielded a poorly constrained U-Pb age of ca. 2665 Ma for metamorphic rutile, which is interpreted to provide an approximate minimum age for dike emplacement and penetrative ductile deformation in the host shear zone. As described in the ‘Summary and regional implications’ section, this age appears to record the waning stages of thermotectonism at the present level of exposure.

Structural geology

Deformation structures throughout the Garner–Gem lakes area were examined in detail to gain a better understanding of the structural evolution of the southeast portion of the Rice Lake belt. In the field, emphasis was placed on reconstructing the sequence of deformations by documenting overprinting relationships between various generations of mesoscopic deformation fabric. In the laboratory, these data were augmented by microstructural examinations of oriented thin sections. Previous descriptions of structural geology for the southeastern

Rice Lake belt were provided by Stockwell and Lord (1939), McRitchie and Weber (1971b), Weber (1971a), Zwanzig (1971) and Brommecker (1991, 1996).

Deformation structures

Map patterns in the Garner–Gem lakes area indicate a complex structural geometry. The prominent northwest structural grain of the area is defined by a series of lenticular structural panels, bounded by an anastomosed network of ductile shear zones. Deformation structures within the panels generally record comparatively low finite strains, and overprinting relationships between the various generations of deformation fabric tend to be well preserved, thus forming the basis for the structural analysis presented below. Map patterns in the largest panels define an early generation of upright macroscopic folds, the limbs of which are transposed into the adjacent shear zones. The most prominent of these folds, the Beresford Lake anticline, is defined by the regional-scale map pattern of the Bidou, Gem and Edmunds assemblages (Figure 2). Deformation structures in the intervening shear zones record comparatively high finite strains and locally preserve evidence of at least two episodes of movement. The most prominent of these structures, the Beresford Lake shear zone (BLSZ), sharply truncates stratigraphy and juxtaposes assemblages of significantly different age and tectonic affinity, suggesting that the cumulative displacement may have been substantial.

Ductile and brittle-ductile deformation structures in the study area are divided into five generations on the basis of overprinting relationships (G_1 – G_5 ; Table 7). In areas of discontinuous exposure or ambiguous overprinting, similarities in style and kinematics of deformation structures and their patterns of orientation were used for correlation. For the purposes of this report, these similarities are inferred to indicate a broadly

Table 7: Summary of deformation structures and episodes in the Garner–Gem lakes area.

Generation	Shortening direction ¹	Mesoscopic structure	Macroscopic structure	Deformation episode and inferred tectonic significance	Age (Ma)	Regional correlation ²
G_1	?	Local layer-parallel S_1 foliation	?	D_1 : initial crustal thickening?	<2705	G_2
G_2	NE-SW	Regional NW-trending S_2 foliation and flattening fabric; steep L_2 stretching lineation; tight to isoclinal, doubly-plunging, similar-style F_2 folds	Regional-scale folds (e.g., BLA); early high-strain zones with sinistral-oblique (NE-side-up) kinematics (e.g., SGSZ)	D_2 : collisional tectonics; crustal thickening; peak of metamorphism	2690–2680	G_3
G_3	NNE-SSW	S_3 crenulation cleavage; minor F_3 Z-folds	?	Early- D_3 : onset of terminal collision		G_4
G_4	NW-SE	S_4 shear-band cleavage; mylonitic S_4 in NW-trending high-strain zones; shallow L_4 lineation; open to tight parallel-style F_4 Z-folds with axial plane cleavage	Dextral transcurrent shear in major high strain zones (e.g., BLSZ; LL-GLSZ; MLSZ); open NE-trending Z-folds	Main- D_3 : terminal (oblique-dextral) collision; transcurrent shear deformation with progressive folding; retrogression	2670–2640	$G_5 - G_6$
G_5	N-S	Discrete brittle-ductile faults	NW and NE-trending faults	D_4 : late block faulting	?	?

¹ Based on *present* orientations of associated fabric elements

² Refers to structural generations in the Rice Lake area, as described by Anderson (2008)

Abbreviations: BLA, Beresford Lake anticline; BLSZ, Beresford Lake shear zone; LL-GLSZ, Long Lake–Gem Lake shear zone; MLSZ, Moore Lake shear zone; SGSZ, South Garner shear zone

synchronous relative timing of each generation of structures throughout the study area. However, owing to the fact that the absolute age of structures is poorly constrained, it is possible that similar structures were formed at different times in different locations.

The study area is divided for descriptive purposes into six structural domains (A–F), based on the prevailing orientations and styles of the constituent deformation structures. The boundaries of these domains mostly coincide with major shear zones, as indicated on Figure 70. The deformation structures include planar fabrics (e.g., foliations, cleavages, shear bands, fractures), linear fabrics (e.g., mineral, stretching, slickenline and intersection lineations) and folds, which are denoted in the text and figures by S_x , L_x and F_x , respectively, where ‘X’ indicates the assigned generation. Intersection lineations are denoted by L^x_y , where ‘X’ and ‘Y’ refer to the generations of intersecting planar fabrics. Structural descriptions are accompanied by lower-hemisphere equal-area projections of structural data, subdivided according to generation and domain. As shown in Figure 71a–d, primary layering and bedding throughout the study area are typically subvertical and generally trend north-west. Poles to bedding define partial to complete girdles on stereographic projections owing to the presence of upright folds of at least two generations, which plunge at steep to moderate angles toward the northwest (see below).

G₁ structures

The G₁ structures consist of an early planar shape-fabric (S_1) that is only readily identified in the hinges of F_2 folds in domains B, E and F. In domain B, the S_1 fabric is defined by biotite and white mica, and consists of a finely spaced to penetrative foliation that is oriented roughly parallel to the local primary layering. In this domain, garnet porphyroblasts locally contain sigmoidal inclusion trails that are interpreted to result from dynamic overgrowth of either the S_1 fabric or an early increment of the S_2 fabric (Figure 72a). Interestingly, inclusion trails are lacking in garnet porphyroblasts in the contact metamorphic aureole of the Garner Lake intrusive complex along the north shore of Garner Lake (Figure 72b; Weber, 1971a), perhaps indicating that garnet growth occurred prior to development of the S_1 fabric. However, it is equally possible that the S_1 fabric predated these porphyroblasts but was obliterated by intense recrystallization within the metamorphic aureole shortly prior to their growth. Hence, the relative age of the S_1 fabric in domain B with respect to the Garner Lake intrusive complex remains unconstrained, as does its relative age with respect to the S_1 fabric in domains E and F (i.e., the ‘ S_1 ’ fabric in the various domains may be unrelated).

In domains E and F, the S_1 fabric is a variably developed, weak to moderate foliation that parallels bedding and is defined by fine-grained chlorite and white mica. This fabric appears to correspond to the ‘ S_1 cleavage’ described by Brommecker (1991) and is best observed in the hinges of mesoscopic F_2 folds near the hinge of the Beresford Lake anticline. Here, the S_1 fabric locally consists of a moderate to strong, penetrative foliation within narrow, bedding parallel, high-strain zones that contain fault-fill-type quartz veins and are overprinted by F_2 folds and

S_3 cleavage (Figure 72c); these zones correspond to the ‘D_{1b} shear zones’ of Brommecker (1991).

Near the southeast end of domain E, at the outlet of the Manigotagan River, younging reversals in turbiditic sedimentary rocks of the Gem and Edmunds assemblages indicate the presence of an isoclinal anticline-syncline fold pair (the East Gem Lake anticline and syncline, respectively; Figure 70). Bedding-cleavage relationships indicate that these folds are transected by S_3 and S_4 planar fabrics, and locally also an earlier generation of fabric that is slightly discordant to bedding and appears to correspond to the S_2 foliation. On the basis of these relationships, these folds are tentatively assigned to the G₁ generation of structures.

G₂ structures

The G₂ structures are pervasive in the Garner–Gem lakes area and characteristically constitute a prominent S–L shape-fabric defined by deformed primary features and aligned peak-metamorphic minerals. This G₂ shape-fabric is well preserved east of the BLSZ, where it is the dominant fabric observed in most outcrops. West of the BLSZ, this fabric is only consistently well preserved outside the major northwest-trending shear zones in the interior portions of the major structural panels.

In domain A, the G₂ fabric includes a penetrative S_2 foliation that trends northwest, dips subvertically and is defined by aligned biotite, hornblende and elongate feldspar aggregates (Figures 73a, 74a). The L_2 lineation is defined by a weak alignment of hornblende porphyroblasts, recrystallized quartz ribbons and elongate feldspar aggregates in the S_2 plane, and varies in orientation from subvertical to moderately northwest plunging (Figure 75a). Multicomponent orthogneiss along the west margin of the Wanipigow River plutonic complex contains a moderate to strong gneissosity that parallels the S_2 foliation (Figure 73b); this zone is referred to as the East Garner shear zone (EGSZ). The S_2 foliation is axial planar to minor rootless isoclinal folds of the gneissic layering. Ductile asymmetric fabrics (e.g., shear bands, boudins, transposed layering) on horizontal outcrop surfaces variably indicate sinistral or dextral shear, perhaps indicating that the zone accommodated a significant component of zone-normal shortening. Vertical outcrop surfaces are not well exposed; however, shear bands and σ -porphyroclasts in a vertical exposure of quartz-ribbon mylonite in granitic orthogneiss of the EGSZ indicate north-east-side-up shear in one location.

The G₂ shape-fabric is particularly pervasive and intense in domain B. Here, the S_2 foliation is defined by aligned amphiboles in mafic and ultramafic volcanic rocks, and by aligned biotite (\pm muscovite \pm amphibole) in intermediate–felsic volcanic rocks. In general, hornblende is the dominant amphibole in the eastern portion of the domain, whereas actinolite increases in abundance toward the west. This relationship was also observed by Brommecker (1991) in the area east of Beresford Lake, near the northern boundary of the study area. The S_2 foliation includes a prominent planar shape-fabric defined by strongly flattened primary features, such as pillows and clasts (Figures 10d, 74b). The S_2 fabric generally trends toward the southeast and is subvertical. However, it is strongly overprinted

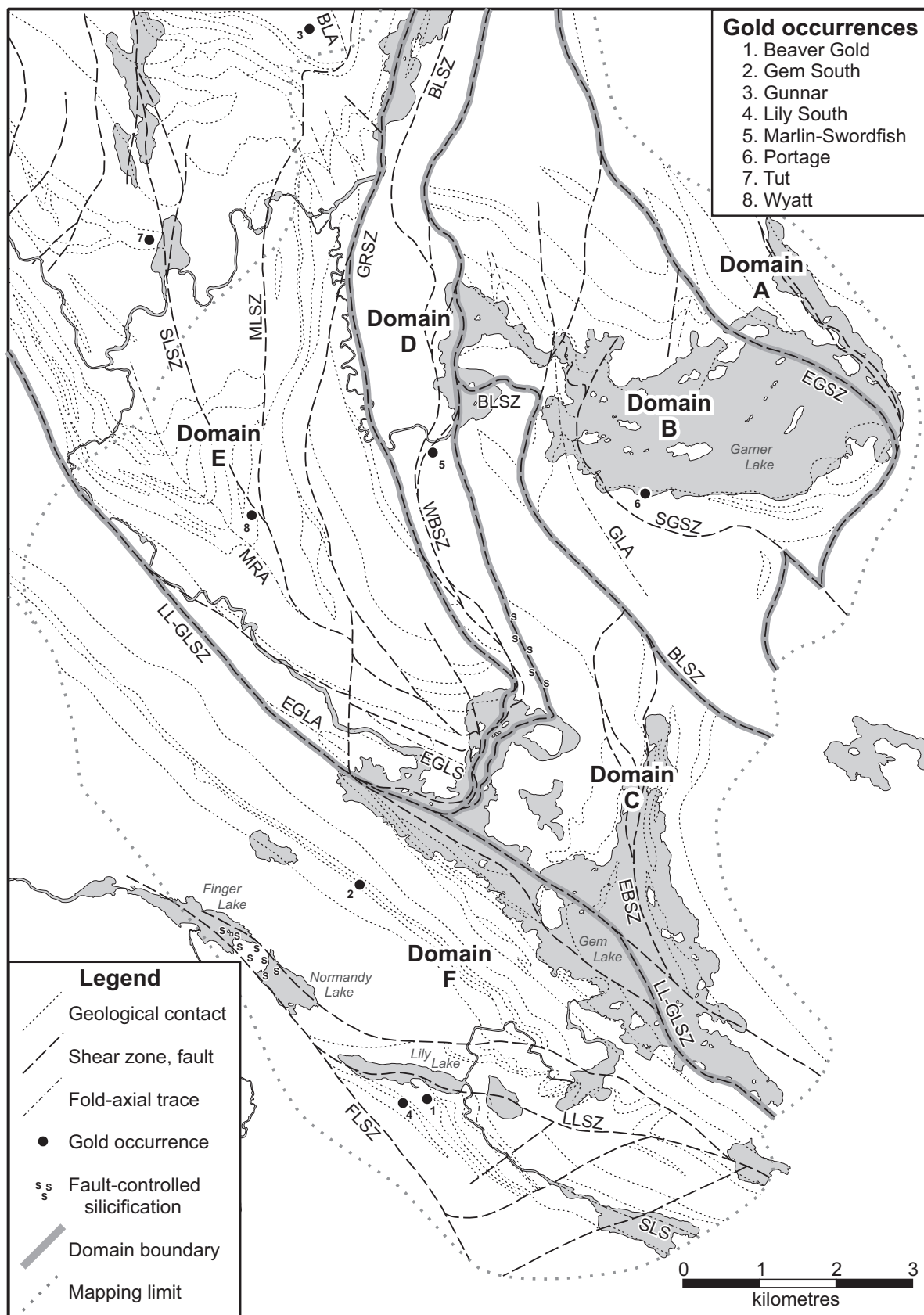


Figure 70: Simplified geology of the Garner-Gem lakes area, showing major structures, geological contacts, Au occurrences (1–8) and structural domains (A–F). Abbreviations: BLA, Beresford Lake anticline; BLSZ, Beresford Lake shear zone; EBSZ, East Bay shear zone; EGSZ, East Garner shear zone; EGLA, East Gem Lake anticline; EGLS, East Gem Lake syncline; FLSZ, Finger Lake shear zone; GLA, Garner Lake anticline; GRSZ, Garner River shear zone; LLSZ, Lily Lake shear zone; LL-GLSZ, Long Lake-Gem Lake shear zone; MRA, Manigotagan River anticline; MLSZ, Moore Lake shear zone; SLSZ, Slate Lake syncline; SLSZ, Stormy Lake shear zone; WBSZ, West Bay shear zone.

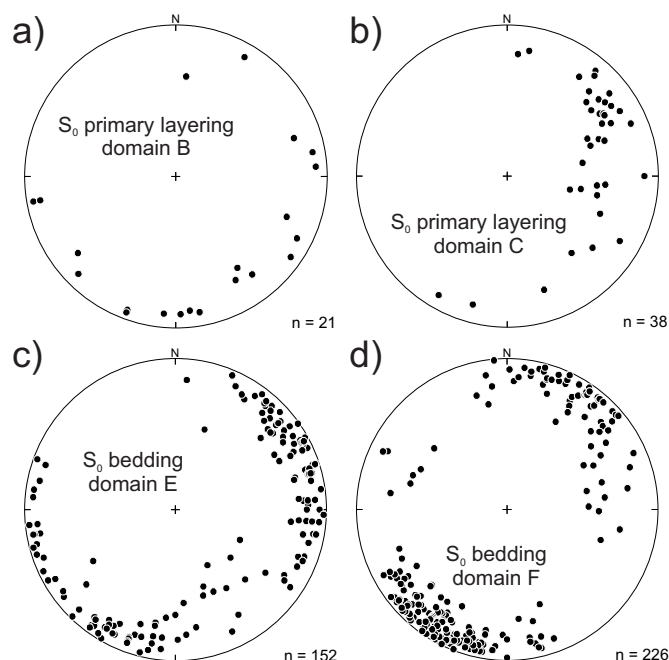


Figure 71: Lower-hemisphere, equal-area stereographic projections of the poles to primary layering and bedding in the Garner–Gem lakes area: **a)** domain B; **b)** domain C; **c)** domain E; **d)** domain F. The number of data points (*n*) plotted is indicated to the lower right of each diagram.

by younger folds, as indicated by the subhorizontal great-circle distribution of poles in Figure 73c. The L_2 lineation is moderate to strong throughout domain B and is defined by aligned hornblende porphyroblasts and elongated primary features (Figure 74c), which generally plunge at steep angles toward the west (Figure 75b). In places, the L-fabric dominates and approaches that of a pure L-tectonite (Figure 74d). The S_2 foliation is axial planar to minor F_2 folds that are generally tight to isoclinal, S asymmetric and similar style, and plunge steeply to moderately northwest (Figure 76a, b), subparallel to the local L_2 lineation.

In domain B, the G_2 fabrics intensify into several discrete high-strain zones, the best examples of which occur south of Garner Lake and include the South Garner shear zone (SGSZ) and the southeast segment of the BLSZ. These zones lack evidence of significant reactivation or retrogression during later deformation and thus contain well-preserved G_2 fabric elements. Although somewhat disrupted by later faults and folds, the SGSZ trends in a general northwesterly direction, parallel to the south shoreline of Garner Lake, and defines the west margin of the Garner Lake intrusive complex. The BLSZ trends in a northwest direction through the poorly exposed area farther south of Garner Lake, and defines the southwest boundary of domain B.

The G_2 high-strain zones in domain B are defined by zones of cohesive quartzofeldspathic or amphibolitic mylonite that range up to several tens of metres wide and are characterized by intense planar-linear shape-fabrics, which are concordant to, and thus correlated with, the S_2 - L_2 fabrics in the wallrocks. The mylonitic foliation is defined by aligned metamorphic minerals,

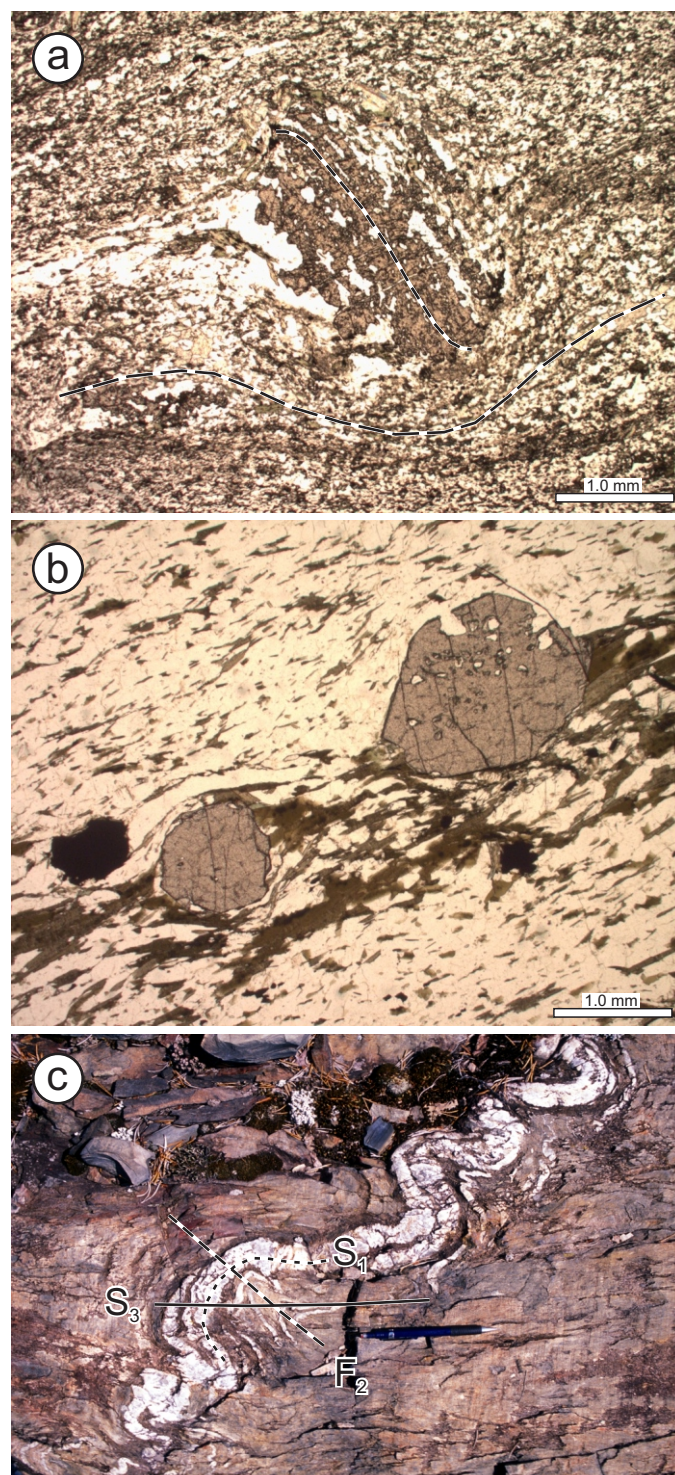


Figure 72: Outcrop and thin-section photographs of G_1 structures: **a)** sigmoidal inclusion trails, representing S_1 (or possibly early S_2 fabric) in syn- G_2 garnet porphyroblast in the South Garner shear zone (plane-polarized light), southwest shoreline of Garner Lake; **b)** garnet porphyroblasts from the contact metamorphic aureole along the north margin of the Garner Lake intrusion, showing absence of inclusion trails (plane-polarized light), eastern Garner Lake; **c)** bedding-parallel shear with penetrative S_1 foliation and fault-fill quartz veins in The Narrows formation near the hinge of the Beresford Lake anticline, west shoreline of Beresford Creek; S_1 foliation is overprinted by F_2 folds and spaced S_3 cleavage.

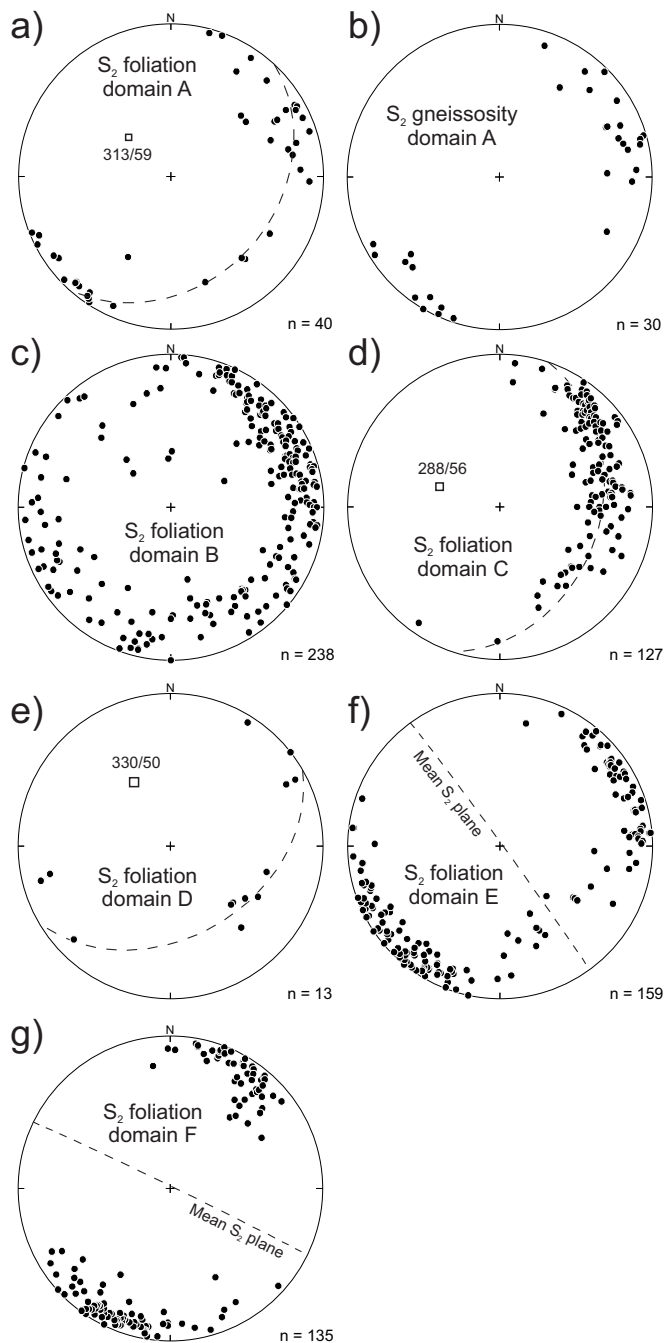


Figure 73: Lower-hemisphere, equal-area stereographic projections of the poles to G_2 planar fabrics in the Garner-Gem lakes area: **a)** foliation, domain A; **b)** gneissosity, domain A; **c)** foliation, domain B; **d)** foliation, domain C; **e)** foliation, domain D; **f)** foliation, domain E; **g)** foliation, domain F. The number of data points (n) plotted is indicated to the lower right of each diagram. Open squares in Figures 73a, d and e indicate the poles to the corresponding girdles (trend and plunge shown).

recrystallized quartz ribbons and highly attenuated primary features. In the most intense zones of mylonite in the SGSZ, the S_2 foliation also includes a very fine compositional banding defined by alternating quartzofeldspathic and micaceous domains; in two locations, this banding clearly constitutes a differentiated crenulation cleavage formed by heterogeneous transposition of a pre-existing (S_1 or early S_2) foliation. Garnet and hornblende porphyroblasts show evidence of synkinematic growth in the

form of sigmoidal inclusion trails and well-developed pressure fringes (Figure 72a) and also locally overgrow the S_2 - L_2 fabric (Figure 77a), suggesting that the deformation occurred under amphibolite-facies metamorphic conditions. The associated L -fabric is defined by aligned metamorphic minerals, elongated primary features and quartz ribbons. Tight to isoclinal, similar-style folds overprint the mylonitic foliation and are commonly rootless and intrafolial. The fold axes plunge steeply and are mostly subparallel to the local L_2 stretching lineation. S -folds predominate over Z -folds, but both are present in individual outcrops, with some showing complex sheath geometries (Figure 77b). Asymmetric fabrics on horizontal outcrop surfaces generally indicate sinistral shear (Figure 77c), whereas those on vertical exposures consistently indicate reverse (northeast-side-up) shear (Figure 77d). Based on their structural geometry and kinematics, the G_2 high-strain zones are interpreted to represent zones of sinistral-oblique transpression.

As noted above, the G_2 fabrics are also pervasive west of the BLSZ (domains C–F), but they are consistently well preserved only in the interior portions of the major structural panels, in areas outside the influence of the major north-west-trending shear zones (see below). In these areas, the S_2 planar fabric generally trends northwest and is subvertical (Figure 73d–g), except where overprinted by later folds. The S_2 foliation is defined by an alignment of fine-grained chlorite (\pm white mica \pm biotite \pm actinolite) and also includes a planar shape-fabric defined by flattened clasts in coarse sedimentary and volcanoclastic rocks (Figures 16c, d, 78a). These clasts are also prominently elongated in the S_2 plane, and define an L_2 stretching lineation that plunges at steep to moderate angles to the northwest in most locations (Figure 75c–f). Map patterns and changes in S_0 - S_2 vergence clearly indicate the presence of macroscopic F_2 folds, although mesoscopic examples of these folds are somewhat rare. The F_2 folds vary from open to isoclinal and plunge at moderate to steep angles toward the northwest (Figure 76c–f), subparallel to the local L_2 lineation. Tight to isoclinal F_2 folds tend to be curved and nonparallel in profile (Figure 78b), with axial planes that parallel the S_2 shape-fabric and are thus distinguished from younger (F_3 or F_4) folds, which overprint the S_2 shape-fabric and are typically angular-parallel in profile. In F_2 fold hinges, the S_2 fabric overprints the S_1 foliation and defines an axial-planar crenulation cleavage, which is strongly differentiated in places (Figure 78c).

The Beresford Lake anticline (BLA) is the most prominent F_2 fold in the southeast portion of the Rice Lake belt, and is clearly defined by younging directions and regional-scale map patterns in the Neoproterozoic succession east of the Ross River pluton. Other major F_2 folds are identified by younging directions northwest and south of Gem Lake, and are referred to as the Manigotagan River anticline and Slate Lake syncline, respectively (Figure 70). The BLA is an upright, doubly plunging structure that is truncated to the east by the BLSZ and its subsidiary structures. The northeast limb is comparatively thin and strongly attenuated along the BLSZ, whereas the southwest limb is substantially thicker, with several subsidiary F_2 fold closures, and appears intact. From northwest to southeast along the axial trace of the BLA, the axes of minor F_2 folds show a continuous change in orientation from moderately northwest plunging at Halfway Lake to steeply southeast plunging at Beresford

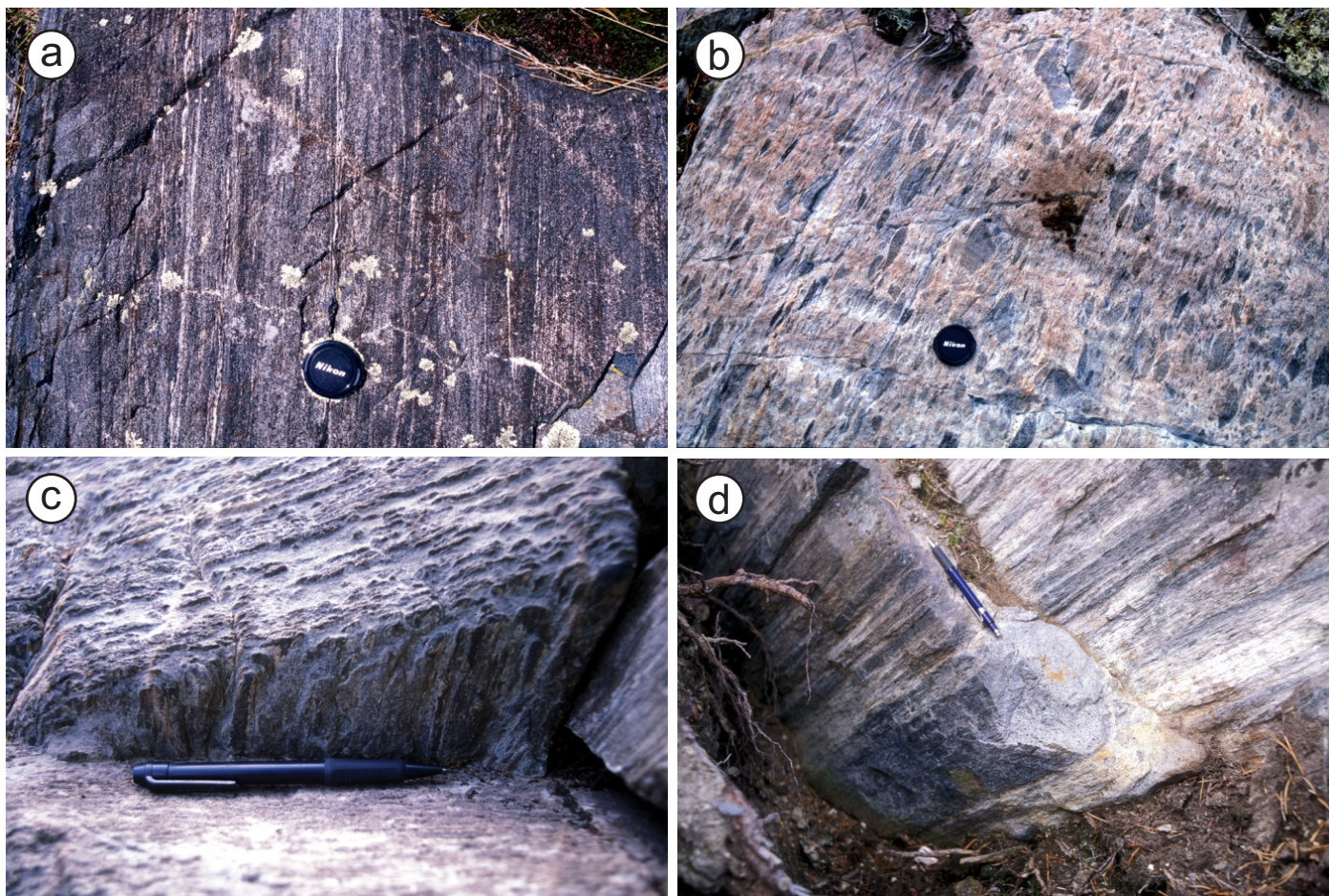


Figure 74: Outcrop photographs of G_2 fabrics in the Garner Lake area: **a)** penetrative foliation and weak gneissosity in gabbroic orthogneiss, domain A, eastern Garner Lake; **b)** planar shape-fabric defined by flattened clasts, domain B, south of Garner Lake; **c)** strong S-L shape-fabric defined by flattened and stretched clasts, domain B, south shore of Garner Lake at the eastern end of the narrows; **d)** intense L-fabric defined by stretched clasts, domain B, south of Garner Lake.

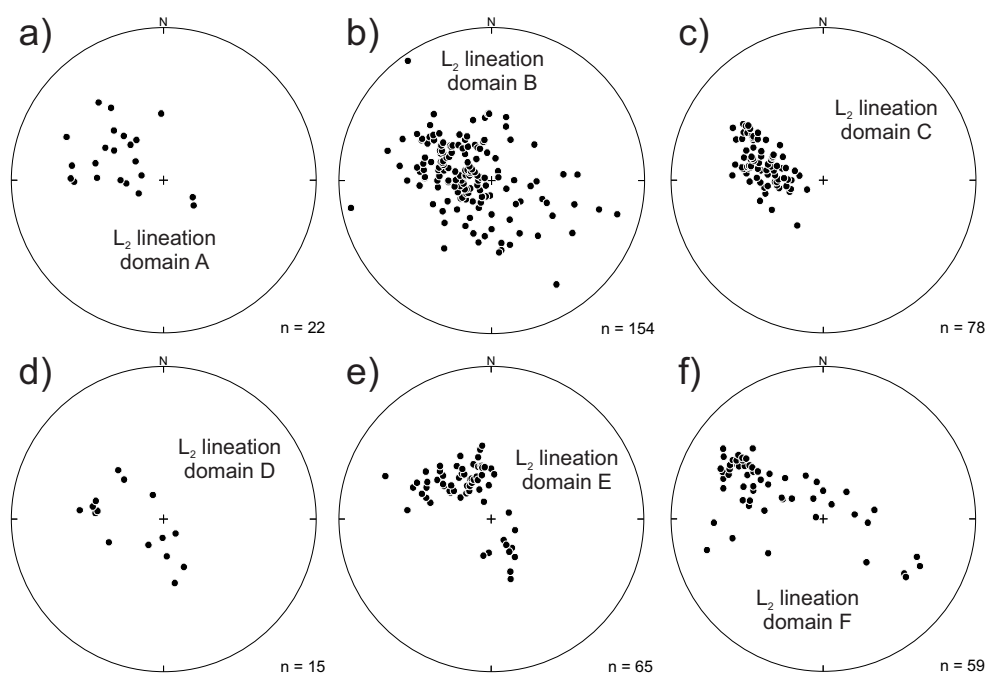


Figure 75: Lower-hemisphere, equal-area stereographic projections of G_2 linear fabrics in the Garner–Gem lakes area: **a)** domain A; **b)** domain B; **c)** domain C; **d)** domain D; **e)** domain E; **f)** domain F. The number of data points (n) plotted is indicated to the lower right of each diagram.

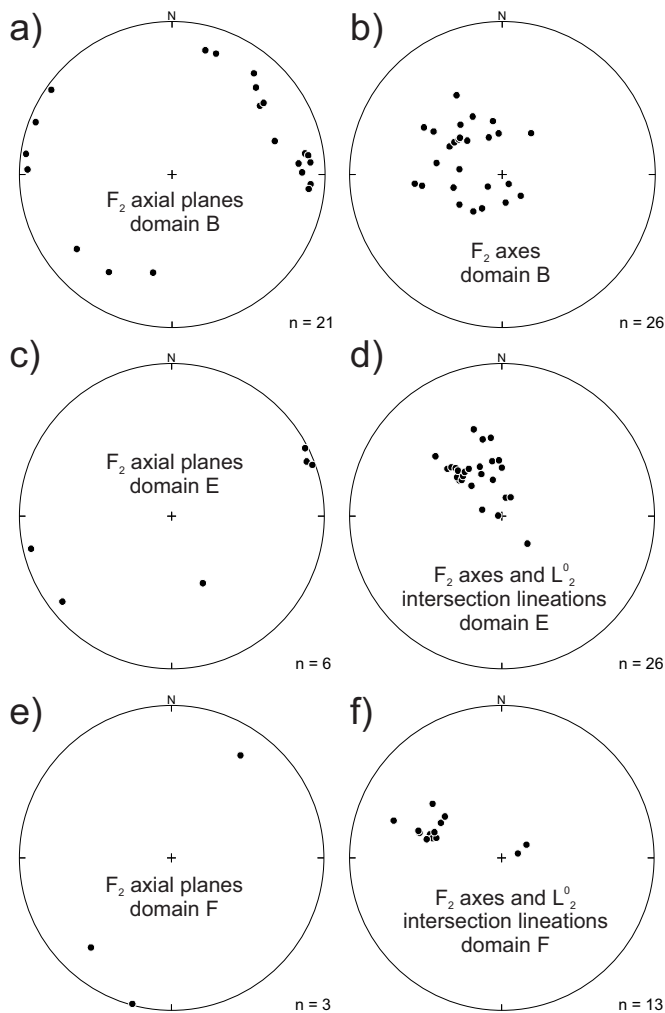


Figure 76: Lower-hemisphere, equal-area stereographic projections of F_2 axial planes and axes in the Garner–Gem lakes area: **a)** poles to axial planes, domain B; **b)** axes, domain B; **c)** poles to axial planes, domain E; **d)** axes, domain E; includes L_2^0 intersection lineations; **e)** poles to axial planes, domain F; **f)** axes, domain F, including L_2^0 intersection lineations. The number of data points (n) plotted is indicated to the lower right of each diagram.

Lake, with a complex culmination between Cliff Lake and Tinney Lake (Stockwell and Lord, 1939; Brommecker, 1991, 1996). South of Beresford Lake in domain E, minor F_2 fold axes plunge at steep to moderate angles back toward the northwest (Figure 76d), thus indicating that the BLA has a sheath-like geometry on a macroscopic scale. Unambiguous younging criteria in turbidites of the Edmunds assemblage indicate the presence of facing reversals (i.e., beds locally face northwest on the S_2 foliation, in opposition to the dominant southeast facing direction; Figure 79), which is compatible with the presence of doubly plunging F_2 folds (alternatively, this could be explained by refolding of F_1 isoclinal). Despite this, no examples of mesoscopic sheath-like F_2 folds were observed in domain E. Facing reversals in the Edmunds assemblage south of Long Lake have also been attributed to doubly plunging folds (Zwanig, 1971). The axes of these folds plunge to the east at steep to moderate angles and are subparallel to the local mineral and stretching lineation, and the L_2^0 intersection lineation. Similar geometric

relationships were described by Brommecker (1991) for G_2 structures in the northwest portion of the study area.

G_3 structures

The G_3 structures are only consistently observed west of the BLSZ, in the areas of relatively low finite strain in the interiors of domains E and F. Possible examples of G_3 structures are also observed in one location east of the BLSZ, near the west margin of domain B, and are described in detail below.

In domains E and F, the characteristic G_3 structure is a variably developed cleavage that trends west-northwest, dips subvertically and crosscuts the S_2 foliation at a small counter-clockwise angle (Figure 80a, b). This cleavage varies in style from a weak, widely spaced fracture cleavage to a penetrative, closely spaced crenulation cleavage defined by fine-grained chlorite (\pm white mica). These characteristics indicate a possible correlation to the S_3 cleavage described from the area east of Beresford Lake by Brommecker (1991), although his S_3 fabric trends west-southwest and thus transects the S_2 foliation at a much higher angle. In thin-bedded turbidites, the S_3 cleavage is locally developed preferentially in mudstone beds, where it overprints the S_2 foliation to form a differentiated crenulation cleavage (Figure 81a). Adjacent sandstone beds preserve the S_2 foliation, which is only weakly crenulated, presumably owing to their higher competence. The S_3 cleavage transects F_2 folds (Figure 81b) and maintains a consistent angular relationship to northwest-trending beds, regardless of younging direction, on both limbs of the BLA. The S_3 cleavage is axial planar to minor, kink-like Z-folds of the S_2 fabric and locally contains strongly boudinaged quartz veins.

East of the BLSZ, possible examples of G_3 structures are observed near the western margin of structural domain B, in coarse volcanoclastic rocks (map unit Gn3b) exposed on the south shoreline of the narrows in Garner Lake, near their eastern end. Deformation structures in this locality are particularly well exposed and complex, and were mapped in detail to elucidate their geometry and overprinting relationships (Figure 82). Flattened and elongated clasts in the volcanoclastic rocks define a penetrative and pervasive planar-linear shape-fabric that corresponds to the S_2 - L_2 fabric described previously; this is the oldest structure observed in this locality. On a stereographic projection, the poles to the S_2 planar fabric define a great-circle girdle, with a β -axis that plunges moderately to the south-southeast ($42^\circ \rightarrow 148^\circ$), whereas most (15 of 17) of the L_2 lineations fall on a small-circle girdle, with a cone axis that has a similar orientation to the β -axis (Figure 82a).

In this outcrop, the G_2 shape-fabric is overprinted by two generations of upright folds and crosscut by a series of steeply dipping quartz veins and strike-slip faults. The early generation of folds is associated with a tight, large-amplitude synform that trends northwest, plunges moderately to the south-southeast (Figure 82b) and thus appears to account for the girdle distributions of G_2 fabric elements. The late generation of folds comprises minor open structures that trend southwest, plunge steeply to the northeast (Figure 82d) and do not significantly disrupt the girdle distributions. Neither fold generation is associated with a well-developed axial-planar fabric. Quartz veins on the southwest limb of the early synform crosscut the G_2

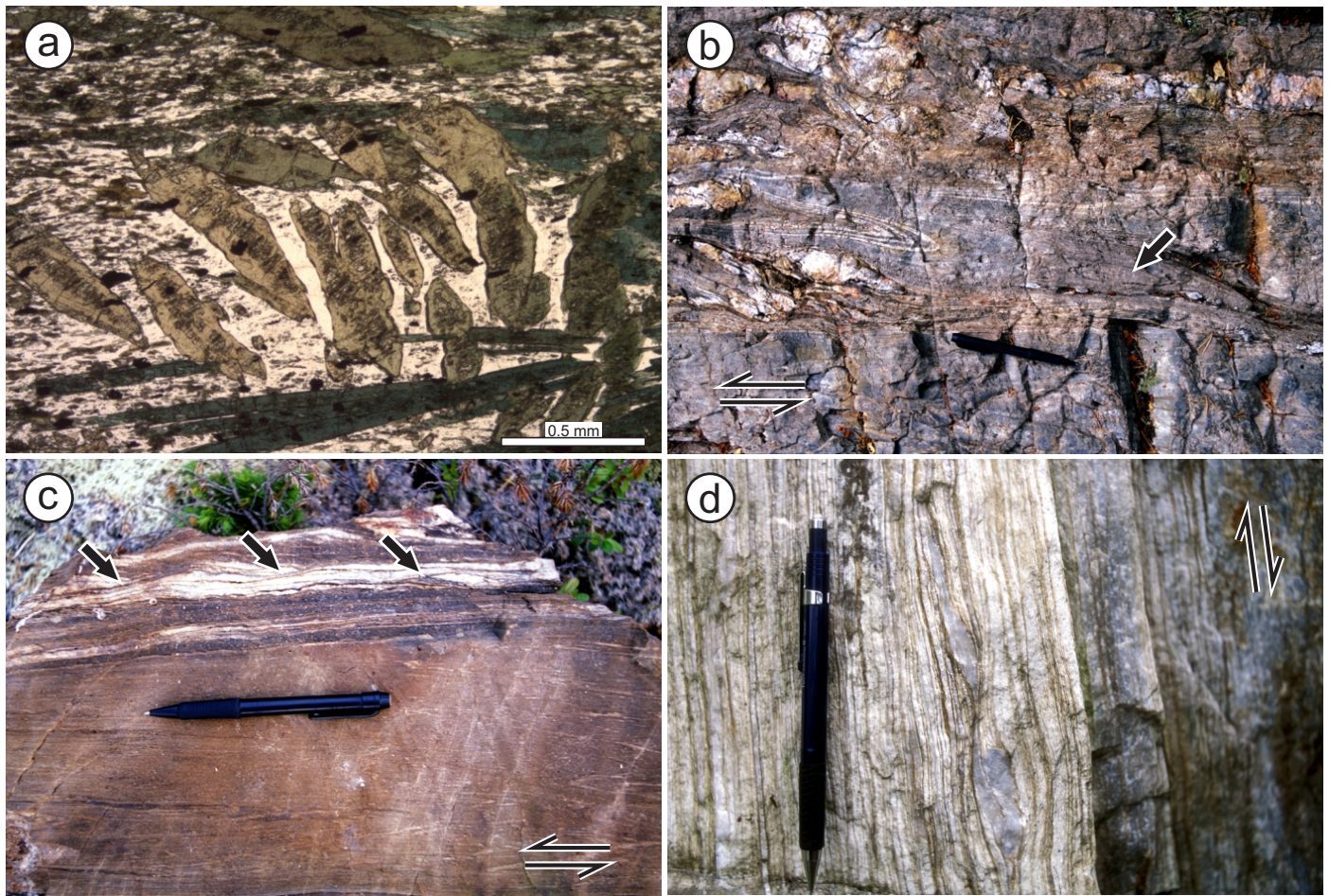


Figure 77: Outcrop and thin-section photographs of deformation structures in G_2 high-strain zones, domain B: **a)** photomicrograph (plane-polarized light) showing mylonitic foliation overgrown by hornblende porphyroblasts in the BLSZ, south of Garner Lake; **b)** mylonitic S_2 foliation overprinted by isoclinal S -folds, BLSZ, western shoreline of Garner Lake; note doubly plunging closure of a sheath-like fold (arrow); **c)** mylonitic S_2 foliation, BLSZ, western shoreline of Garner Lake; asymmetric boudins and shear bands indicate sinistral shear; **d)** mylonitic S_2 foliation, BLSZ, south of Garner Lake; asymmetric boudins and shear bands indicate north-east-side-up shear.

shape-fabric at a high angle (Figure 82c), and pinch and swell in both the horizontal and vertical planes as a result of biaxial (i.e., chocolate-tablet) boudinage subsequent to emplacement. Late brittle-ductile faults crosscut the quartz veins and contain subhorizontal slickenline lineations (Figure 82e); offsets of markers indicate sinistral movement. Taken together, these structural relationships are interpreted to record two episodes of subhorizontal shortening subsequent to development of the G_2 shape-fabric. In this scenario, the early folds and discordant quartz veins are interpreted to represent G_3 structures, which accommodated northeast–southwest shortening (based on *present* structural orientations), whereas the late crossfolds, chocolate-tablet boudins and faults are interpreted to represent G_4 structures (see below), which accommodated northwest–south-east shortening.

G_4 structures

The G_4 structures are developed throughout the Garner–Gem lakes area, but are markedly heterogeneous in terms of style, orientation and intensity. These structures are pervasive

in the major, north- to northwest-trending, high-strain zones that dominate the structural grain west of the BLSZ, but are comparatively poorly developed in high-strain zones east of the BLSZ, which contain well-preserved G_2 structures. East of the BLSZ, the dominant G_4 structures are northeast-trending folds of G_2 fabrics. Folds assigned to the G_4 generation are also ubiquitous west of the BLSZ, where they include map-scale open flexures that trend northeast or east and significantly reorient earlier deformation structures. As described below, the heterogeneous character of the G_4 structures is interpreted to relate to their progressive development during dextral transcurrent-shear deformation. These structures likely correspond to the ‘ D_3 – D_6 deformations’ in the scheme of Weber (1971a).

Deformation structures assigned to the G_4 generation are pervasive and penetrative in zones of chlorite±sericite mylonite that delineate the major, north- to northwest-trending, high-strain zones in the study area. The G_4 mylonite zones range up to several tens of metres wide and anastomose around low-strain structural lozenges of variable size that contain relatively ‘intact’ primary features or G_2 – G_3 fabrics. In general, the G_4 mylonite tends to be more micaceous and fissile than

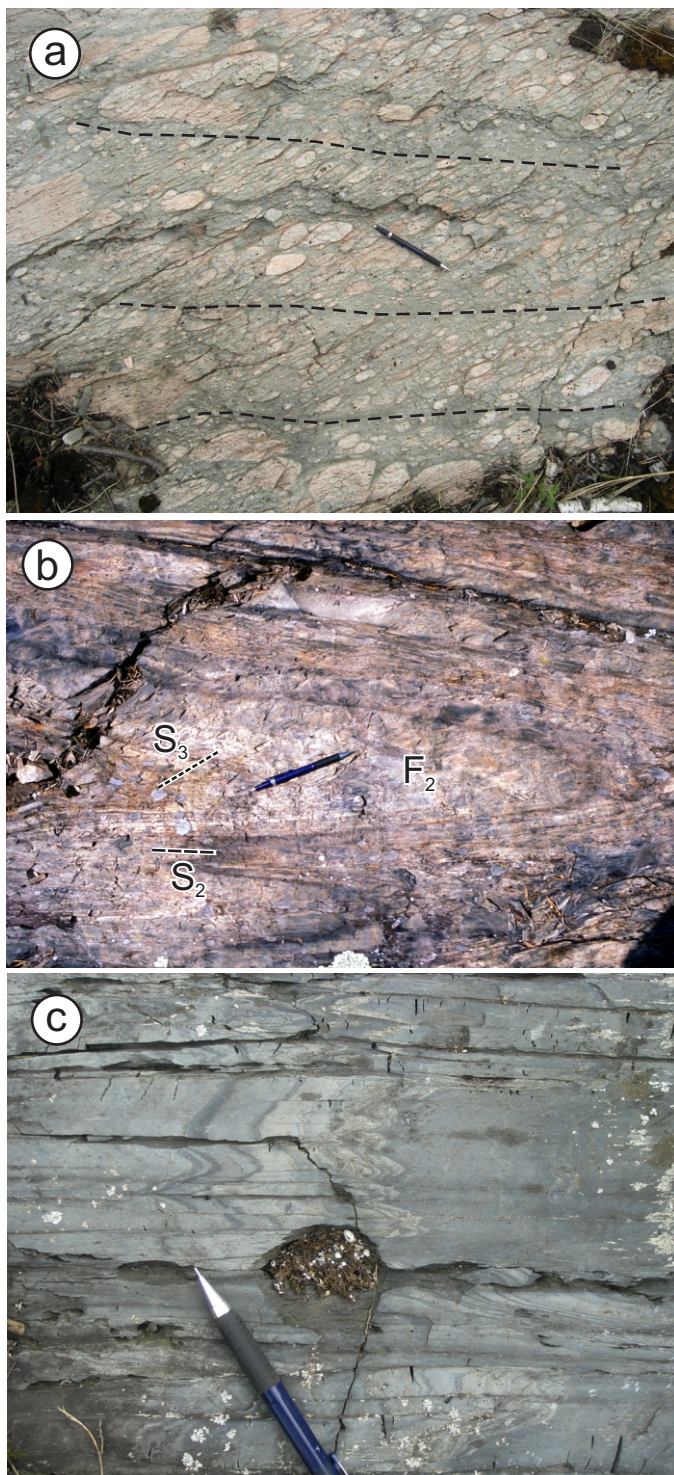


Figure 78: Outcrop photographs of G_2 structures, west of the Beresford Lake shear zone: **a)** S_2 shape-fabric defined by flattened clasts in volcanic conglomerate, domain C, eastern Gem Lake; crude stratification, oblique to S_2 , indicated by dashed lines; **b)** tight, similar-style F_2 folds near the hinge of the Beresford Lake anticline, domain E, southwest of Beresford Lake; **c)** differentiated S_2 crenulation cleavage in the hinge of the Slate Lake syncline, domain F, Slate Lake.

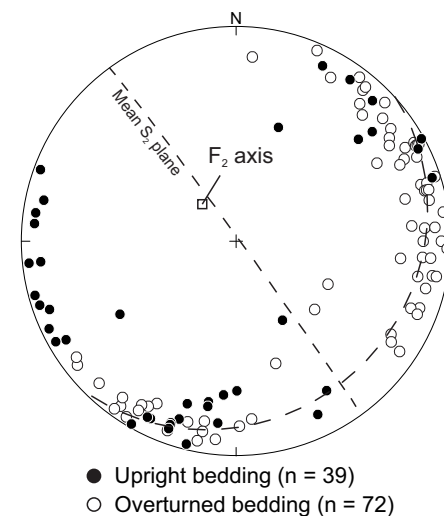


Figure 79: Lower-hemisphere, equal-area stereographic projection of poles to bedding in domain E. Overturned beds (open circles) generally face southeast on the S_2 foliation, whereas upright beds (filled circles) face either southeast or northwest, indicating the presence of F_1 isoclinal or doubly plunging F_2 folds.

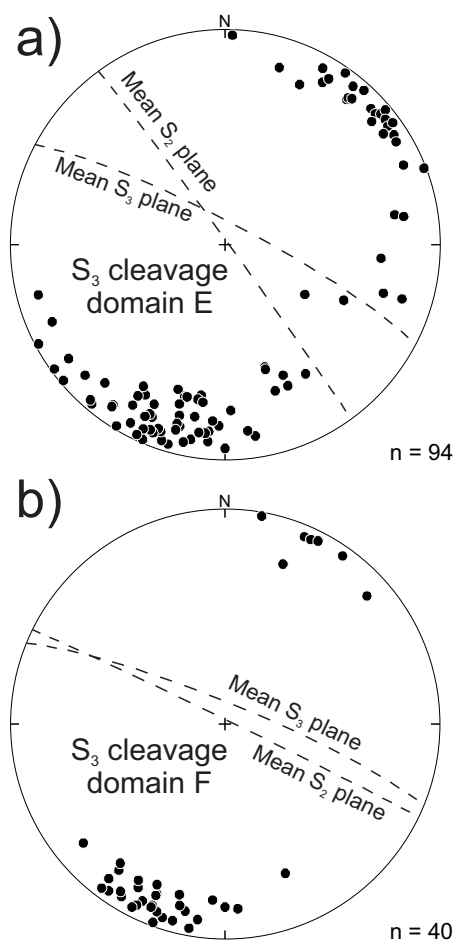


Figure 80: Lower-hemisphere, equal-area stereographic projections of poles to the S_3 cleavage: **a)** domain E; **b)** domain F. Mean orientations of the S_2 and S_3 planar fabrics in each domain are indicated by the dashed great circles. The number of data points (n) plotted is indicated to the lower right of each diagram.

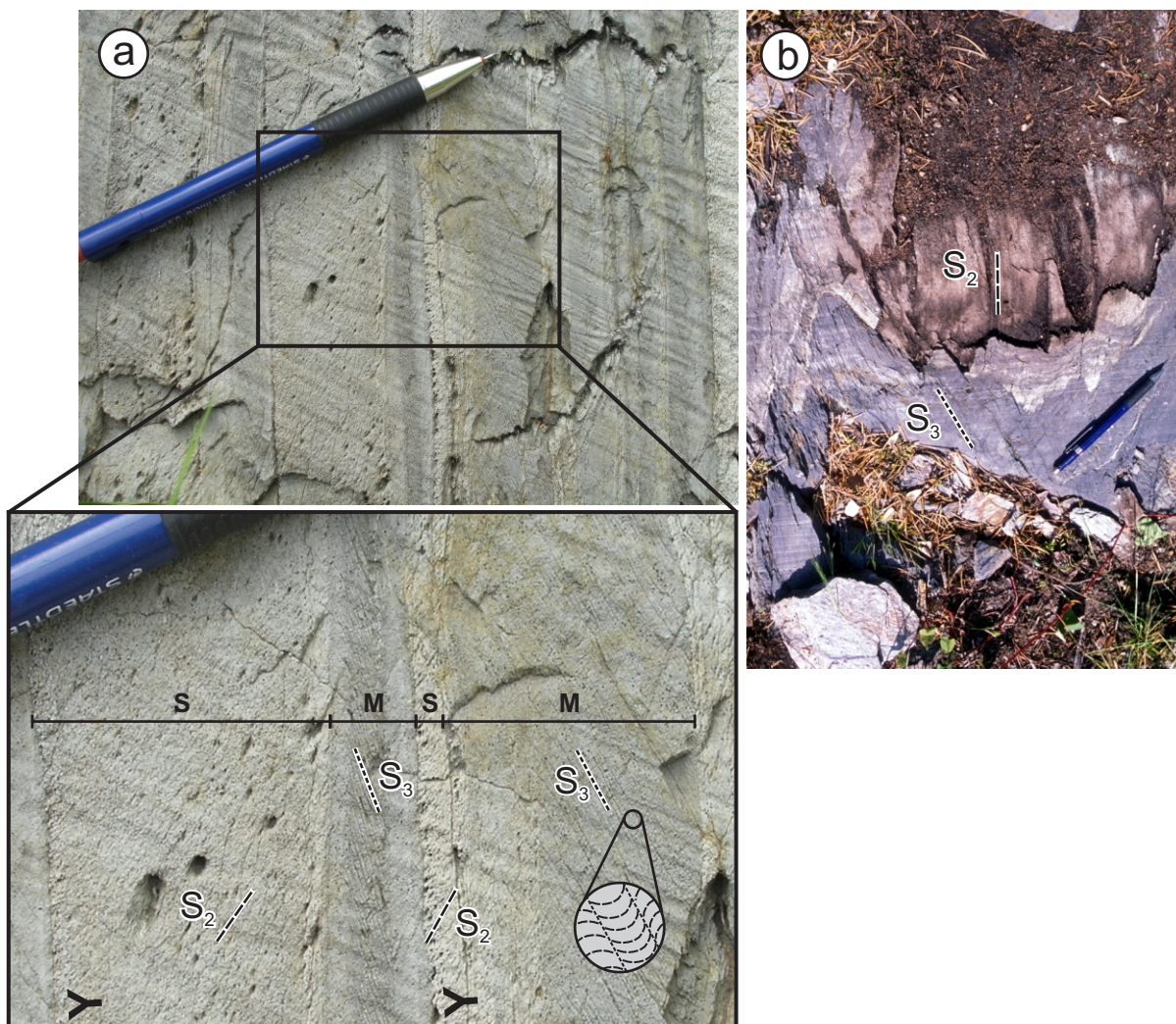


Figure 81: Outcrop photographs of G_3 structures in domain E (pencil points north): **a)** thin-bedded turbidites near the base of the Edmunds assemblage, southwest limb of the F_2 Beresford Lake anticline, northwest of Gem Lake; inset shows spaced S_3 crenulation cleavage in mudstone beds (M) and penetrative S_2 foliation in sandstone beds (S), interpreted to be the result of preferential development of the S_3 cleavage in the less competent mudstone beds; graded beds face northwest on the S_2 foliation in this locality, indicating that this outcrop is situated on the short limb of a parasitic, doubly plunging F_2 fold or F_1 isocline; **b)** minor F_2 fold and axial-planar S_2 fabric transected by S_3 crenulation cleavage, northeast limb of the F_2 Beresford Lake anticline, west of Garner Lake.

the quartzofeldspathic G_2 mylonite and is typically characterized by moderate to strong carbonatization. As a result, the G_4 mylonite tends to be poorly exposed in comparison to the G_2 mylonite. Discrete zones of G_4 mylonite are also developed in the interior portions of the relatively low-strain structural panels, where they are generally less than 10 m wide. The margins of these zones typically show well-developed strain gradients over several metres, but are also locally abrupt and sharp. A particularly good example of a thick strain gradient is exposed in continuous outcrop along the south shoreline of Garner Lake at the mouth of the Garner River. Here, basaltic volcanoclastic rocks (map unit Gw1b) exhibit a fairly continuous westward increase in fabric intensity and finite strain over a distance of approximately 100 m into the east margin of the West Bay shear zone.

The mylonitic S_4 foliation trends northwest or north through most of the study area, with a subvertical dip (Figure 83a–f). This foliation is penetrative to finely spaced and is defined by

an alignment of fine-grained chlorite and sericite, quartz ribbons and flattened primary features. In domains A and B, the S_4 foliation is associated with retrograde recrystallization of the peak-metamorphic mineral assemblage (biotite±garnet±hornblende), and is locally manifest as a cataclastic fabric in granitic orthogneiss of domain A. In the unseparated tectonite of domain D and the major high-strain zones in other domains, the S_4 foliation parallels an intense centimetre- to metre-scale compositional layering defined by strongly attenuated and transposed primary features and/or alternating domains of chlorite-sericite phyllonite and quartzofeldspathic mylonite. Kinematic indicators, including S-C fabrics, shear bands, porphyroclast systems and asymmetric boudins and Z-folds (Figure 84a–c), are well developed on horizontal outcrop surfaces and indicate a dextral sense of movement in all but a few locations, as described below. The S_4 foliation plane contains a weak to moderate L_4 lineation defined by aligned chlorite and sericite, quartz ribbons and ductile slickenline striations (Figure 84d). This lineation

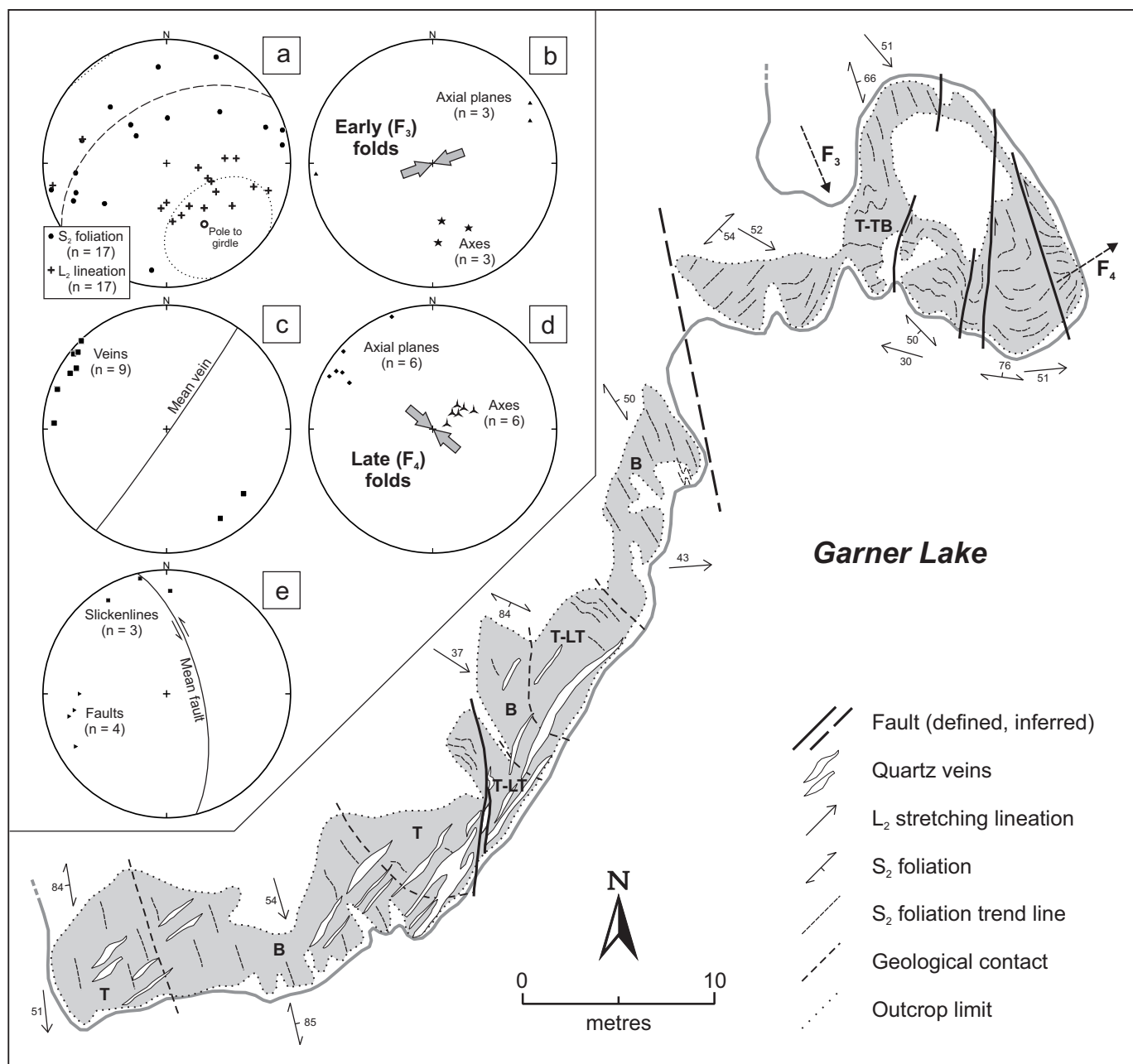


Figure 82: Detailed map of outcrops on the south shoreline of the narrows in Garner Lake, near its eastern end. The rocks consist of crudely stratified tuff (T), lapilli tuff (LT), tuff breccia (TB) and breccia (B) of unit Gn3b of the Garner assemblage (grey fill), crosscut by veins of massive quartz (white fill). Orientation data for the various structures are presented on lower-hemisphere equal-area projections (insets A–E), with the number of data (n) points indicated; planar data are plotted as poles. Thick grey arrows (insets B and D) indicate the approximate shortening direction inferred from the geometry and present orientations of the corresponding deformation structures. See text for discussion.

typically plunges at shallow angles to the northwest or south-east (Figure 85a–d); the comparatively weak L-fabric of the G₄ mylonite also serves to distinguish it from G₂ mylonite. The structural geometry of the G₄ mylonite zones indicates that they accommodated dextral transcurrent-shear deformation.

Shear bands are an intrinsic component of the planar fabric in G₄ mylonite (e.g., Figure 84a–c) and are oriented at a shallow clockwise angle to the S₄ foliation. In domains C, E and F, these shear bands are also well developed along the margins of the G₄ mylonite zones, and constitute a spaced shear-band

or fracture cleavage (Figure 86a, b) that is developed for significant distances outward into the relatively low-strain country rocks. The shear bands are oriented at a shallow clockwise angle to the local mylonitic S₄ foliation (Figure 87a–c; compare to orientation of corresponding S₄ foliation in Figure 83) and their sense of asymmetry is consistently dextral. This fabric is particularly well developed and widespread in domain E, which is bounded by major G₄ shear zones, and locally intensifies into narrow subsidiary shear zones that transect the domain. Overprinting of the regional S₂ shape-fabric and S₃ cleavage by these

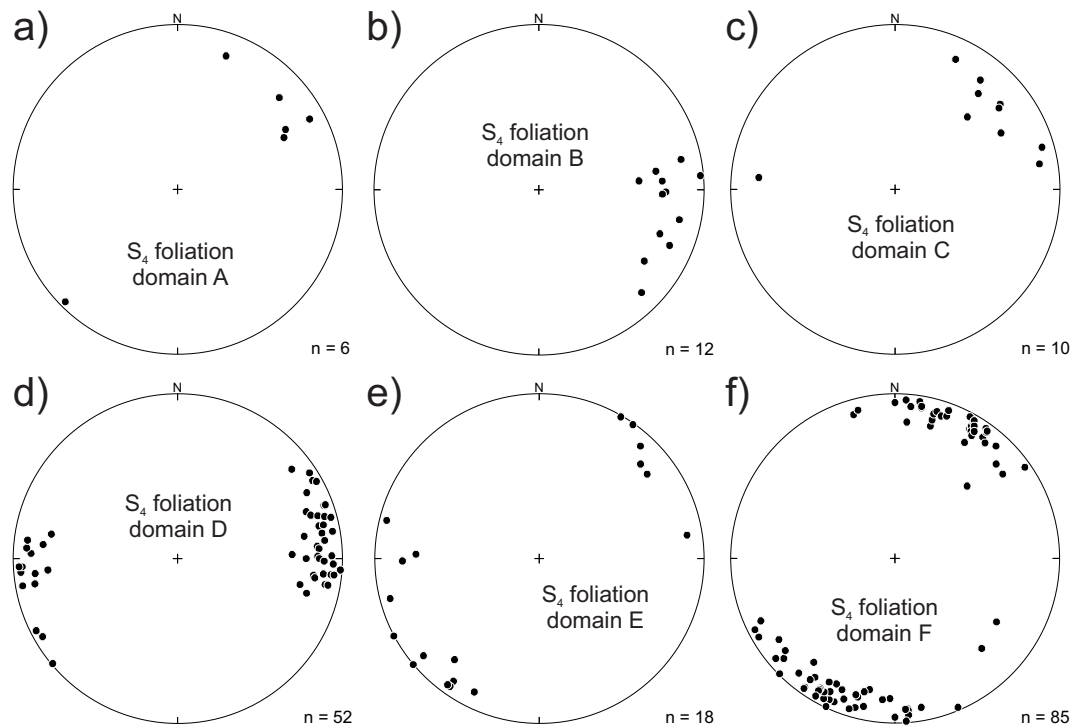


Figure 83: Lower-hemisphere, equal-area stereographic projections of poles to the mylonitic S_4 foliation: **a)** domain A; **b)** domain B; **c)** domain C; **d)** domain D; **e)** domain E; **f)** domain F. The number of data points (n) plotted is indicated to the lower right of each diagram.

shear bands along the margins of the G_4 mylonite zones locally results in a composite fabric that resembles the S-C-C' fabric in the mylonite (e.g., Figure 86a).

With the exception of domain A, folds assigned to G_4 are developed throughout the Garner–Gem lakes area (Figure 88a–j). Generation F_4 folds are particularly prominent in domains B and F, likely due to the fact that both contain a very strong anisotropy, as represented by the G_2 shape-fabric and bedding, respectively. The local anisotropy also exerts a strong influence on the orientations of the folds: the anisotropy in domains B, E and F generally trends northwest and the axial planes of the F_4 folds typically trend northeast, whereas the main anisotropy in domains C and D trends in a northerly direction and the F_4 folds show more variable trends, with a well-developed conjugate geometry apparent in the orientation data from domain D (Figure 88e). Hence, the F_4 folds appear to have accommodated north-northwest–south-southeast shortening of the study area. The fold axes typically plunge steeply, but show significant variability in some domains (e.g., domains D and F; Figure 88f, j). As noted previously, F_4 folds are commonly angular and parallel in profile, in contrast to the typically curved and nonparallel profiles of F_2 folds, which implicates buckling as the main mechanism for F_4 folding.

In domain B, the F_4 folds are typically open and symmetric to slightly S-asymmetric, overprinting the penetrative G_2 fabric and isoclinal F_2 folds at a high angle (Figure 89a, b). These folds are locally associated with a weak, subvertical, axial-planar crenulation cleavage that trends northeast (Figure 90a). In domain C, the F_4 folds are open to tight, mostly

Z-asymmetric and commonly associated with a subvertical crenulation cleavage that trends northwest (Figure 90b). The F_4 folds in domain D show considerable variation in orientation and geometry, and are thus described separately below. In domains E and F, the F_4 folds are open to tight (or rarely isoclinal), prominently Z-asymmetric and commonly parallel and somewhat angular in profile (Figure 91a). S-asymmetric folds are rare. The axial planes of the Z-folds are subvertical and trend toward the east-northeast (Figure 88g, i). In domain F, they are locally associated with an axial-planar crenulation cleavage that trends east-northeast (Figure 90d) and overprints pre-existing fabrics at a shallow counter-clockwise angle. This cleavage is not apparent in domain E, where the S_4 shear bands represent the dominant G_4 fabric. The F_4 fold axes generally plunge at steep angles to the north in domain E and to the east in domain F, although they define a prominent girdle in the S_4 foliation plane in the latter.

South of Gem Lake, F_4 folds are developed on a variety of scales and locally dominate the structural grain. Micro- to mesoscopic Z-folds are an important component of the deformation fabric in G_4 mylonite zones, and are locally penetrative within discrete tabular domains of intensely crenulated mylonite (Figure 91b). Macroscopic F_4 Z-folds were mapped in the area of Banksian Lake, where they range up to several hundred metres in amplitude. Mutual overprinting relationships between the mylonitic foliation, shear bands and axial-planar cleavage indicate development of F_4 folds and S_4 fabrics during progressive shear. The girdle distribution of F_4 fold axes in domain F is interpreted to result from progressive rotation of initially steep

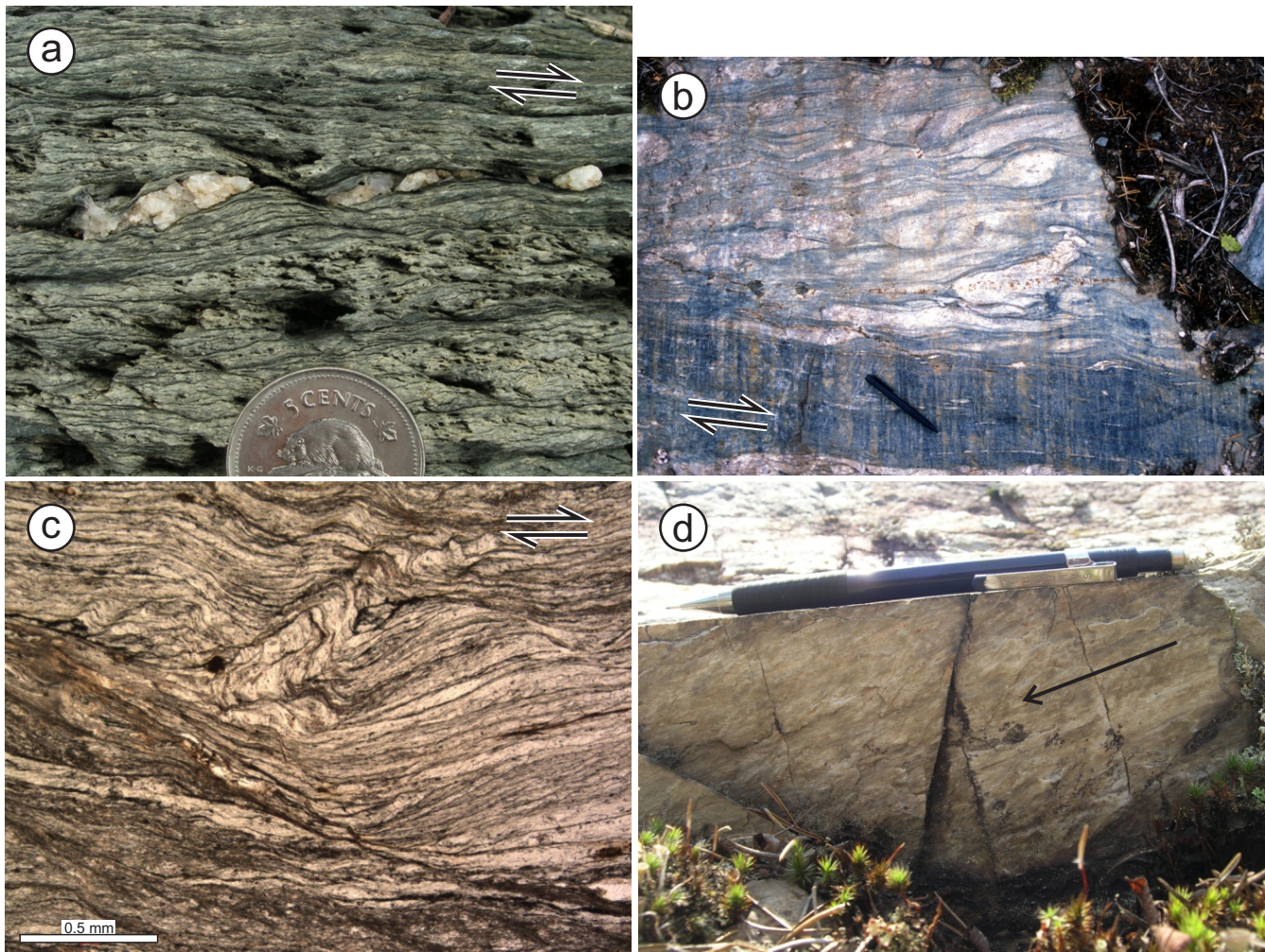


Figure 84: Outcrop and thin-section photographs of deformation structures in G_4 mylonite zones: **a)** S-C fabric, shear bands and asymmetric quartz boudins in sericitic mylonite, domain F, south shoreline of Gem Lake; **b)** asymmetric quartz boudins and shear bands associated with a narrow zone of chloritic mylonite (bottom edge of photo), central portion of domain E, northwest of Gem Lake; **c)** photomicrograph of chloritic mylonite, domain F, south of Gem Lake, showing S-C fabric, shear bands and Z-folds; **d)** shallow L_4 slickenline lineation in sericitic mylonite, domain F, north of Lily Lake.

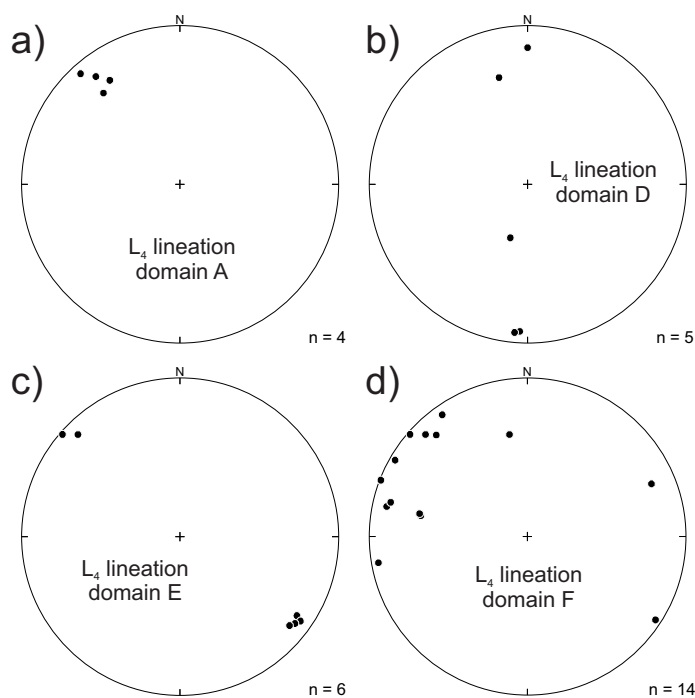


Figure 85: Lower-hemisphere, equal-area stereographic projections of the L_4 lineation in G_4 mylonite zones: **a)** domain A; **b)** domain D; **c)** domain E; **d)** domain F. The number of data points (n) plotted is indicated to the lower right of each diagram.

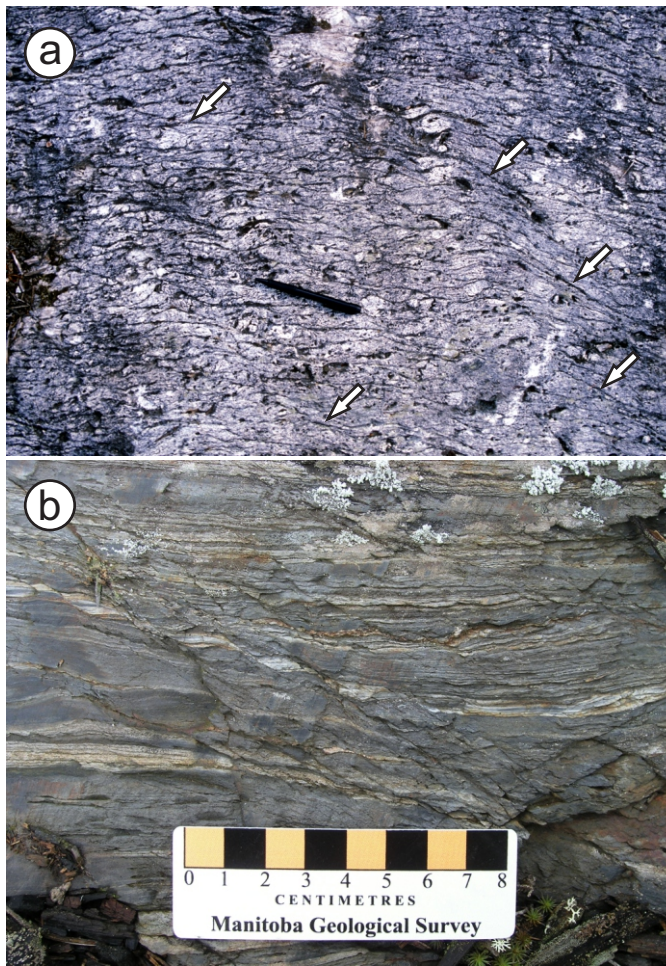


Figure 86: Outcrop photographs of G_4 shear bands: **a)** example of a composite fabric that includes the penetrative S_2 shape-fabric (defined by flattened clasts), S_3 fracture cleavage and spaced S_4 shear bands (arrows), eastern margin of domain E, south of the Garner River; **b)** spaced shear-band cleavage in thin-bedded greywacke and mudstone, north margin of domain F, west of Gem Lake.

fold axes toward the shear direction during transcurrent shear; the sense of fold and fabric asymmetry consistently indicates dextral movement. Hence, the overall structural geometry and kinematics (Figure 92) are consistent with dextral transcurrent shear, as illustrated schematically in Figure 93.

As noted above, the F_4 folds in domain D are somewhat distinct from those in the other structural domains in that they exhibit much greater variability in orientation and geometry, and are thus taken to indicate a more complex kinematic scenario for the associated G_4 shear zones. In domain D, millimetre- to centimetre-scale F_4 folds overprint the mylonitic S_4 foliation and tectonite layering. They vary from angular kinks to gentle warps to tight folds (Figure 94a–c); isoclinal folds are rare. Close to tight F_4 folds are strongly asymmetric and are commonly confined to discrete structural ‘panels’ that range up to several metres thick. In some locations, it is apparent that the folds preferentially nucleated in more competent (i.e., quartzofeldspathic) layers in the mylonite. The sense of fold asymmetry is variable from one panel to the next, but tends to be internally consistent. S-asymmetric folds are abundant

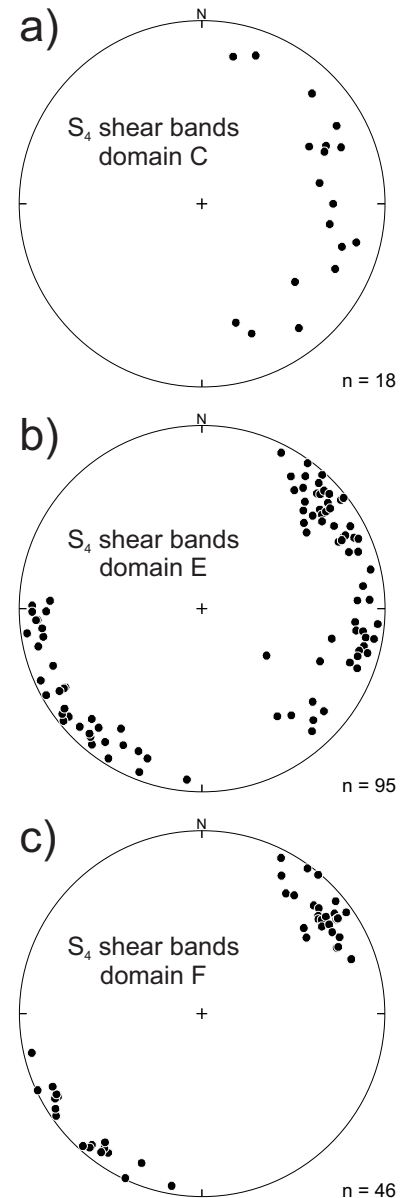


Figure 87: Lower-hemisphere, equal-area stereographic projections of poles to S_4 shear bands: **a)** domain C; **b)** domain E; **c)** domain F. The number of data points (n) plotted is indicated to the lower right of each diagram.

(Figure 94b, c), in contrast to domains E and F. The folds die out toward the margins of the panels, which are either gradational or abrupt, with the latter defined by discrete planar (i.e., non-folded) slip surfaces (Figure 94b, c). Associated kinematic indicators (e.g., shear bands, foliation fish, asymmetric boudins) are consistent with the sense of fold asymmetry.

Some panels exhibit systematic across-strike variations in fold amplitude, intralimb angle and axial-plane orientation, and locally contain folds with curved axial surfaces (Figure 94b), consistent with progressive folding during heterogeneous shear. Axial-planar crenulation cleavages (Figure 90c) are variably developed and locally show evidence of having been transposed into parallelism with the mylonitic foliation (Figure 94d). Both sinistral and dextral sense of transposition is observed in

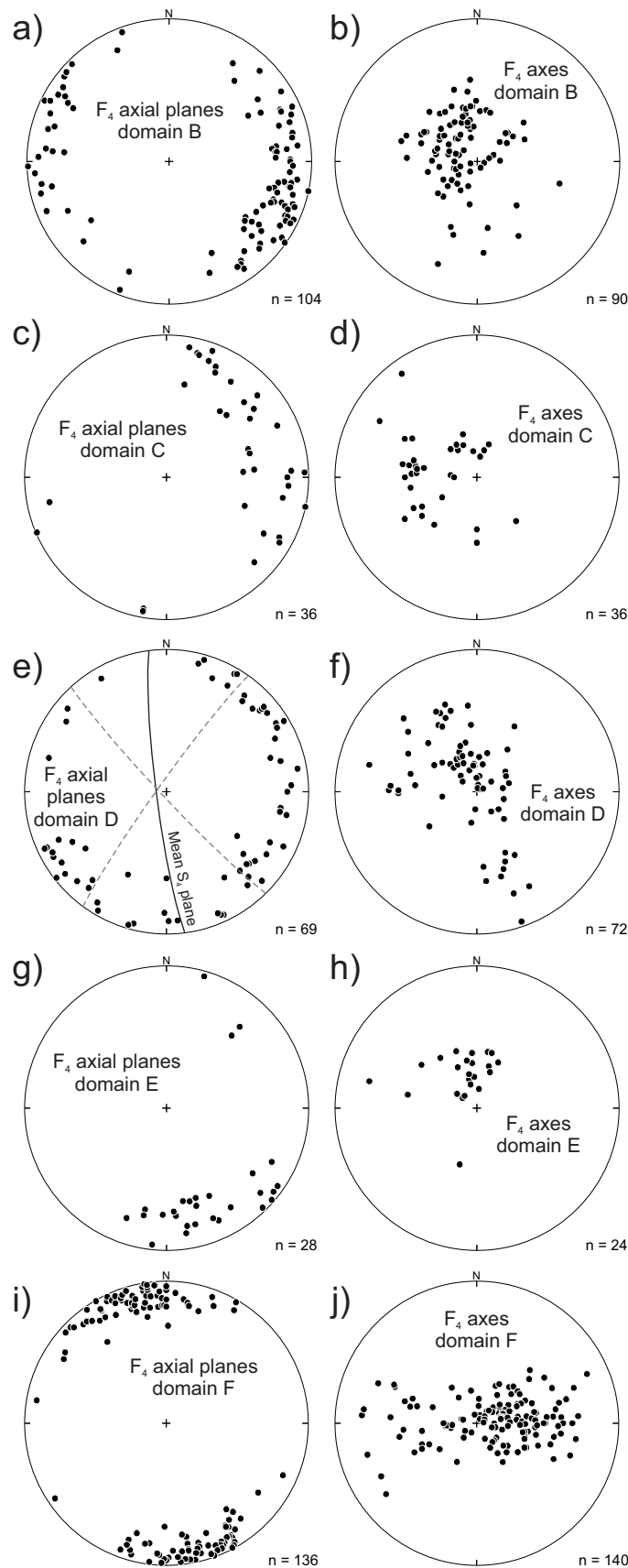


Figure 88: Lower-hemisphere, equal-area stereographic projections of F_4 axial planes and axes: **a)** poles to axial planes, domain B; **b)** axes, domain B; **c)** poles to axial planes, domain C; **d)** axes, domain C; **e)** poles to axial planes, domain D; dashed lines schematically illustrate the conjugate geometry of F_4 fold-axial planes with respect to the mean orientation of the S_4 foliation (solid line); **f)** axes, domain D; **g)** poles to axial planes, domain E; **h)** axes, domain E; **i)** poles to axial planes, domain F; **j)** axes, domain F. The number of data points (n) plotted is indicated to the lower right of each diagram.

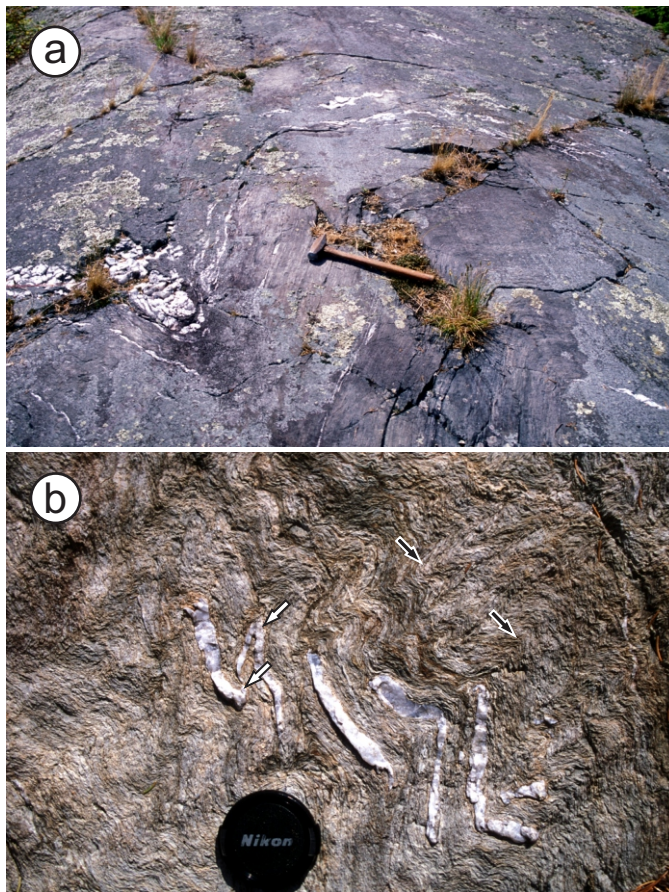


Figure 89: Outcrop photographs of F_4 folds in domain B: **a)** open, S-asymmetric, F_4 folds of the S_2 foliation and strongly attenuated quartz veins, shoreline outcrop, north-central Garner Lake; **b)** detail of open to tight, S-asymmetric F_4 folds (black arrows) that overprint the S_2 foliation and tight to isoclinal F_2 folds (white arrows; defined by quartz vein), north shoreline of the narrows in Garner Lake.

horizontal outcrop surfaces. The fold axes typically plunge to the northwest at steep to moderate angles; however, their orientations are quite variable and define a partial girdle in stereographic projections (Figure 88f). No curvilinear fold hinges were observed in outcrop, and orientation data do not indicate any systematic relationship between plunge direction and sense of asymmetry. In one location, open to close S-folds with a well-developed axial-planar crenulation cleavage are clearly overprinted by open Z-folds that lack an associated cleavage (Figure 94e), indicating that S-folds are older than Z-folds. In other locations, the S-folds and Z-folds display mutual overprinting relationships indicative of a conjugate set (Figure 94f). A conjugate geometry is also apparent in the orientation data for F_4 axial planes in domain D (Figure 88e).

Taken together, the variable geometry and kinematics of F_4 folds suggest that G_4 strain was markedly heterogeneous and strongly partitioned in domain D. Similar associations of variably asymmetric folds in high-strain zones elsewhere have generally been interpreted in terms of noncylindrical folding and sheath-fold development during progressive shear (e.g., Lin, 2005; Kuiper et al., 2011) or overprinting deformations. In the present case, however, the apparent absence of curvilinear

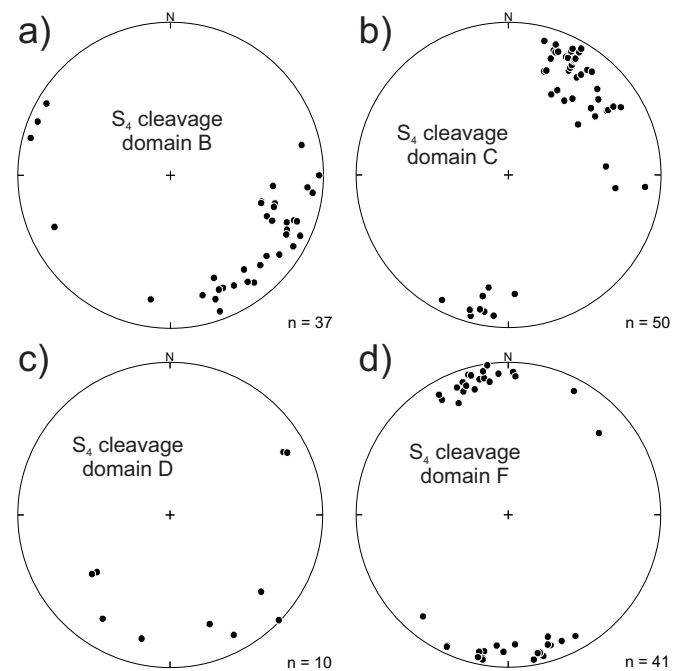


Figure 90: Lower-hemisphere, equal-area stereographic projections of the poles to S_4 axial-planar crenulation cleavage: **a)** domain B; **b)** domain C; **c)** domain D; **d)** domain F. The number of data points (n) plotted is indicated to the lower right of each diagram.

fold hinges and the relative scarcity of isoclinal folds appear to be incompatible with noncylindrical folding. The possibility of two separate deformation episodes is also considered unlikely, as overprinting relationships suggest that the S-folds and Z-folds mostly likely developed synchronously. Hence, the overall geometry of F_4 folds in domain D appears to indicate that G_4 strain was partitioned into discrete panels of broadly coeval dextral or sinistral transcurrent shear. Similarly complex kinematics were also described by Brommecker (1991) for shear zones in the Beresford Lake area. The causative mechanism for this complexity remains unknown, but may relate to the atypical trend of the tectonite fabric in domain D (i.e., north versus northwest), coupled with the pronounced nature of the strength anisotropy in the tectonite, and perhaps local variations in boundary conditions.

G_5 structures

The youngest deformation structures in the study area consist of brittle-ductile and brittle faults and shear fractures that crosscut the ductile deformation fabrics of the G_1 – G_4 generations; these appear to correspond to the ‘ D_3 faults’ of Brommecker (1991). The G_5 structures are developed at least locally throughout the study area, but are particularly abundant in the areas around Lily Lake and Slate Lake. They are characterized by discrete, planar slip-surfaces (Figure 95a) that dip subvertically and typically strike to the north-northwest, with a subordinate set that strikes to the southwest (Figure 96). The slip surfaces are commonly associated with thin (<10 cm) seams of cohesive cataclasite and/or veinlets of dark purple-grey

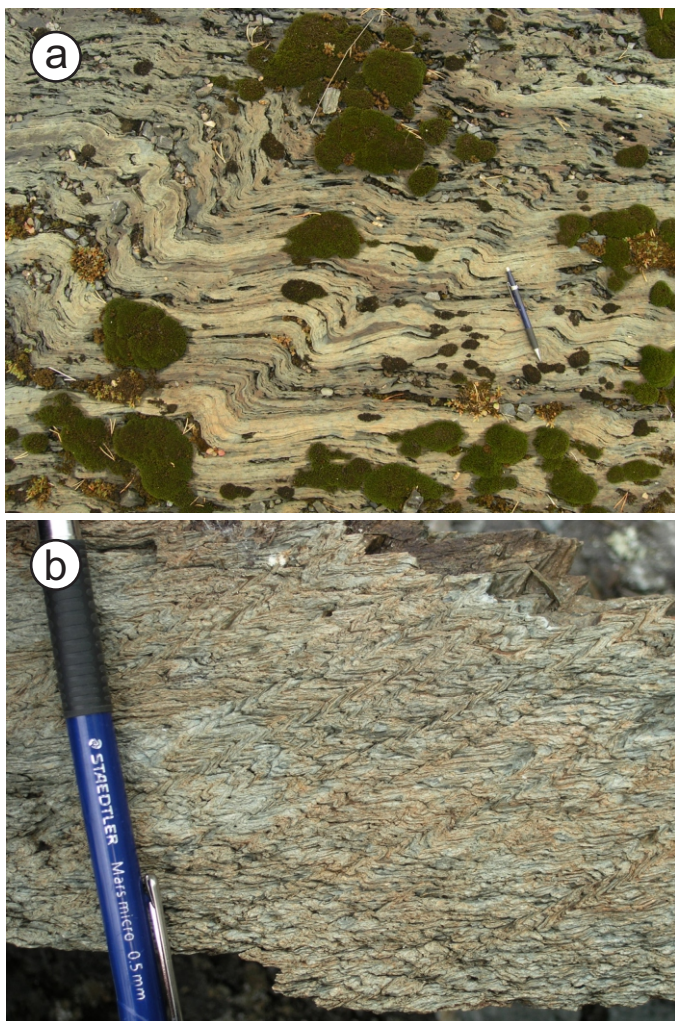


Figure 91: Outcrop photographs of F_4 folds in domain F: **a)** open Z-asymmetric folds in strongly deformed pillowed basalt, south shoreline of Lily Lake; **b)** close to tight, Z-asymmetric, chevron-style crenulations of the mylonitic S_4 foliation, east of Banksian Lake.

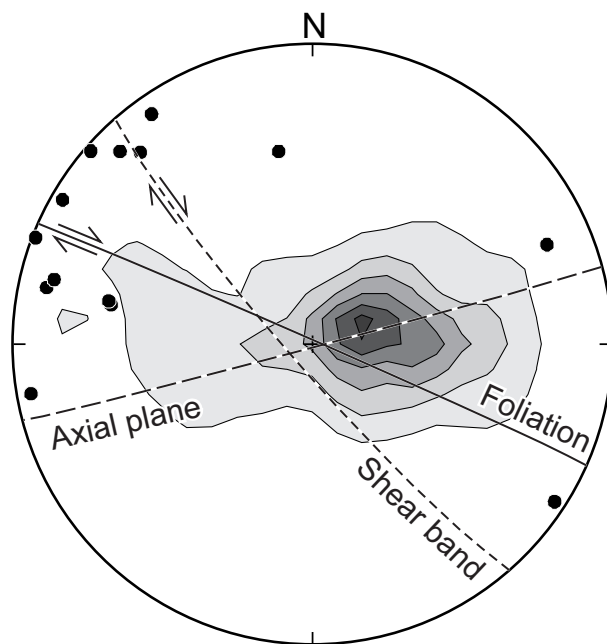


Figure 92: Stereographic projection (lower-hemisphere, equal-area) of orientation data for G_4 structures in domain F, which illustrates the geometric relationships and kinematics of the various fabric elements. Great circles indicate the mean orientations of the mylonitic foliation ($n = 85$), shear-band cleavage ($n = 46$) and axial planes ($n = 136$). Black dots indicate the L_4 lineations measured in the plane of the mylonitic foliation ($n = 14$), whereas the grey-scale contours indicate the distribution of the fold axes ($n = 140$). The overall structural geometry is interpreted to result from progressive folding and fabric development during dextral transcurrent shear.

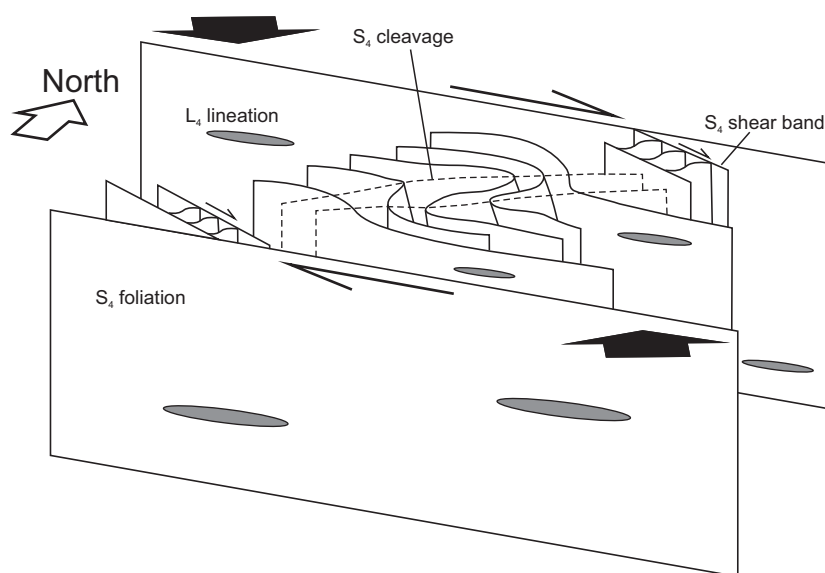


Figure 93: Schematic diagram showing the geometry and kinematics of G_4 structures in domain F. Large black arrows indicate the inferred far-field stress regime of northwest-southeast compression.

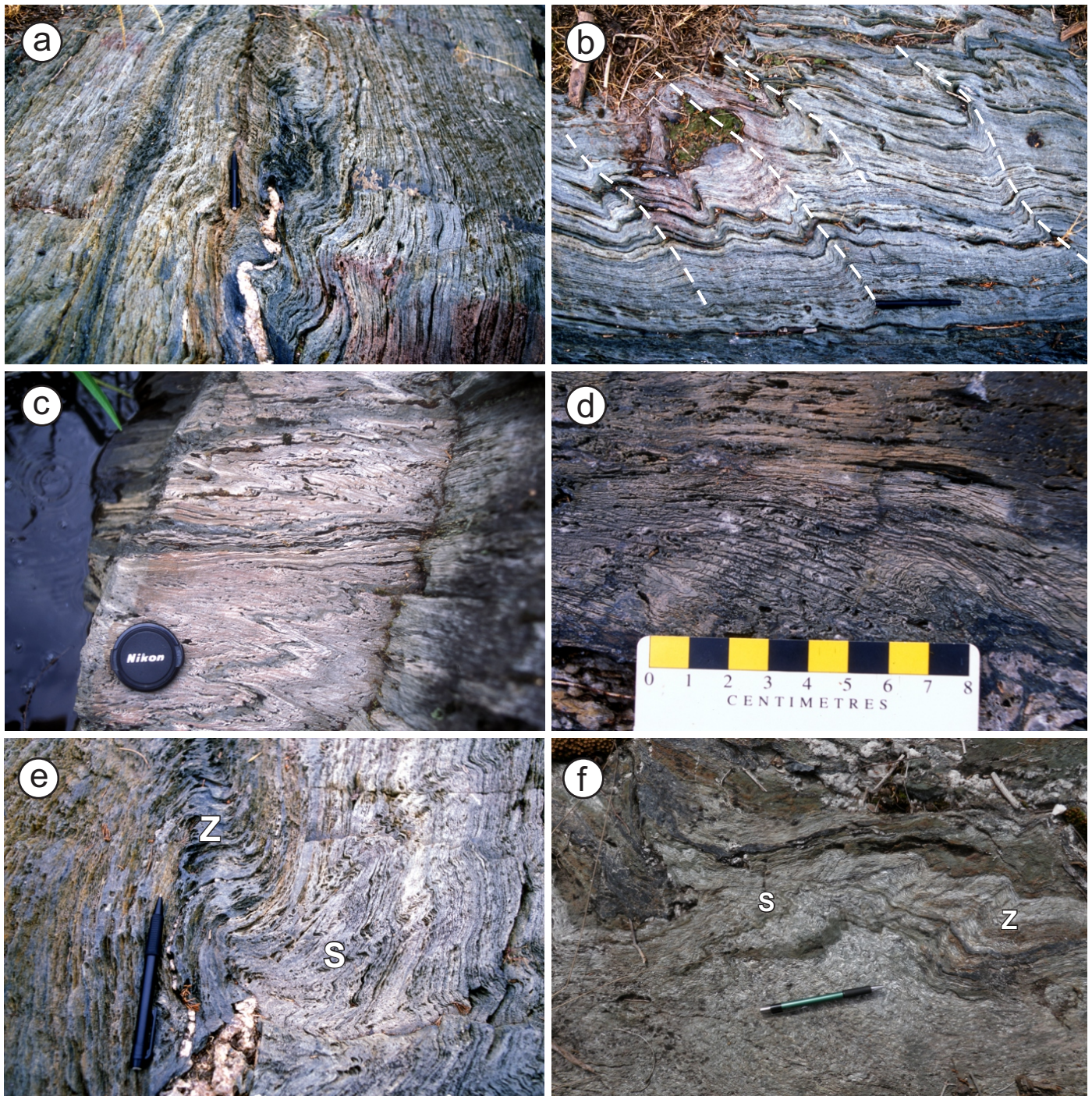


Figure 94: Outcrop photographs of F_4 folds in exposures of chloritic G_4 mylonite along the Garner River, near the eastern margin of domain D: **a)** thin 'panel' of Z-asymmetric folds with weak axial-planar crenulation cleavage; fold nucleation in this location may relate to the presence of the quartz vein; **b)** eastern margin of a thick panel of S-asymmetric folds, showing discrete slip-surface (bottom edge of photo); note systematic increase in fold amplitude and tightness toward the centre of the domain (top of photograph); fold-axial planes exhibit a sympathetic change in orientation toward parallelism with the panel margin, resulting in local preservation of curved axial planes (dashed lines); **c)** discrete panels of S-asymmetric folds; **d)** spaced crenulation cleavage associated with S-asymmetric folds; cleavage is transposed into parallelism with the mylonitic foliation along the top edge of the photograph; sense of asymmetry is sinistral; **e)** open to close S-folds with a well-developed axial-planar crenulation cleavage overprinted by open Z-folds that lack an associated cleavage; S-folds preceded Z-folds in this location; **f)** example of conjugate S-folds and Z-folds.

pseudotachylite (Figure 95b). Offset stratigraphic markers and discordant topographic linears in the Slate Lake area indicate the presence of several significant G_5 faults of the southwest set that were not observed in outcrop. Both sets of structures are locally observed in single exposures and display mutual cross-cutting relationships indicative of a conjugate set (Figure 95c). The sense of offset is right-lateral for the northwest set and left-lateral for the southwest set (e.g., Brommecker, 1991), thereby indicating that they accommodated north–south shortening. In places, the wallrocks within 1–2 m of the G_5 faults are brecciated and strongly silicified, and contain abundant quartz veins. Local open-space-filling textures indicate high-level emplacement (Figure 95d). In two locations, the G_5 faults are associated with, and are interpreted to control, zones of intense SiO_2 flooding (Figure 70), which are described in the ‘Economic considerations’ section.

Structural evolution

The orientation and style of the deformation structures, coupled with inferences drawn from associated kinematic indi-

cators and macroscopic map patterns, indicate that the structural evolution of the Garner–Gem lakes area involved at least four episodes of deformation (Figure 97). The G_1 structures are defined to include early, bedding-parallel S_1 foliations in rocks on both sides of the BLSZ; however, the relative ages of the S_1 fabrics on either side of the shear zone are unknown. The fact that the S_1 foliations are bedding parallel may indicate that they are associated with the development of low-angle structures, perhaps during early crustal shortening and localized thrust imbrication of the various supracrustal assemblages in the initial increments of crustal thickening associated with collisional orogenesis. If these fabrics formed contemporaneously, this would require that thrusting occurred after deposition of the Edmunds assemblage, which contains an S_1 foliation and has a maximum depositional age of ca. 2705 Ma.

The G_2 structures record sinistral-oblique (northeast-side-up) non-coaxial shearing, bulk flattening, subvertical stretching and the development of upright, tight to isoclinal, doubly plunging folds on a macroscopic scale (Figure 97). The G_2 shape-fabrics are pervasive in each of the four supracrustal assemblages

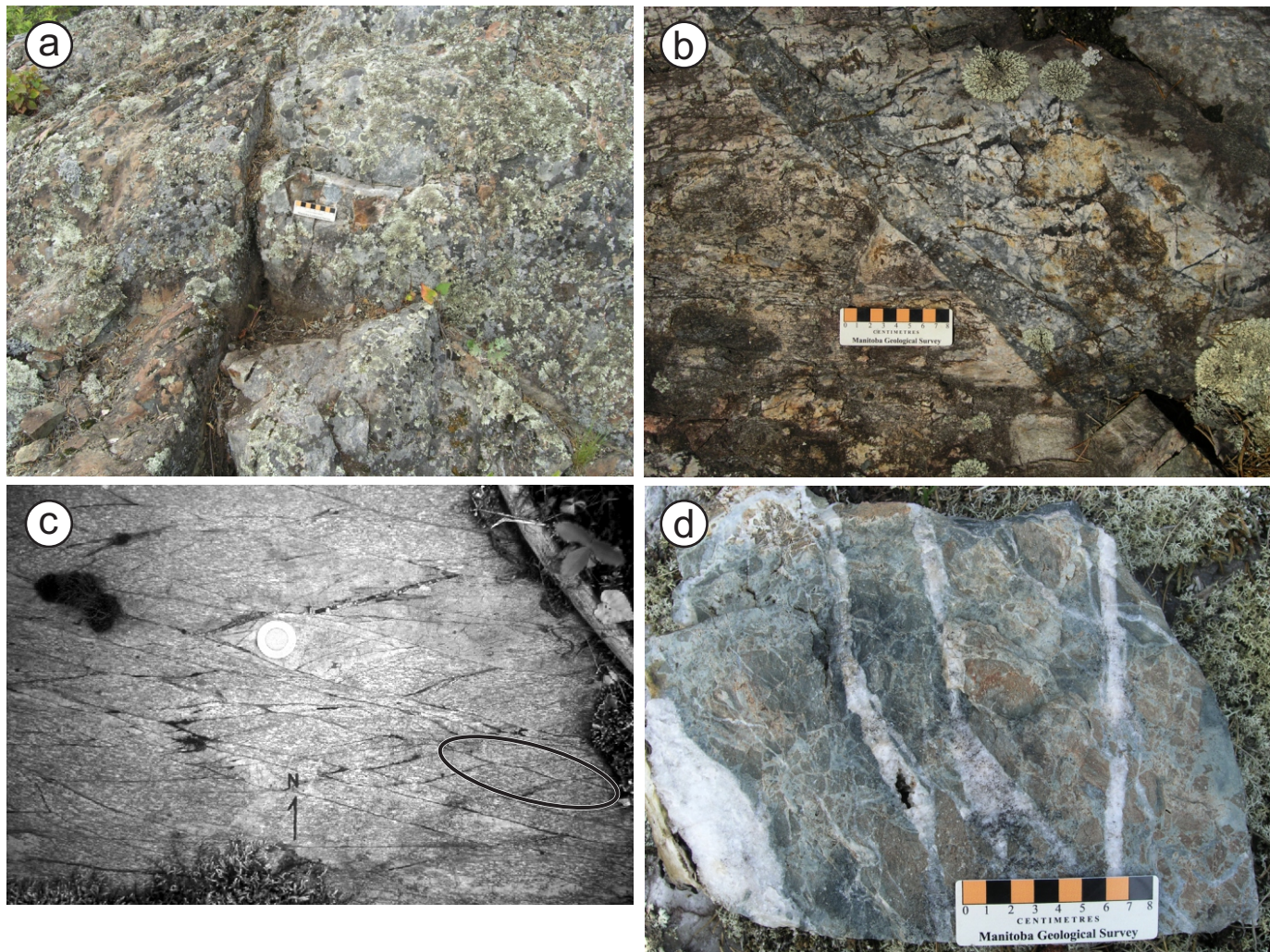


Figure 95: Outcrop photographs of G_5 faults: **a)** discrete planar fault separating weakly altered rocks (left) from brecciated and silicified rocks (right), domain C, north of Gem Lake; **b)** thin seam of pseudotachylite hosted by a fault, domain F, south of Gem Lake; **c)** conjugate array of brittle shear fractures, showing mutual crosscutting relationships (the ellipse indicates a particularly good example; coin is 2 cm in diameter), domain E, northwest of Gem Lake; the geometry and kinematics of these fractures are compatible with north–south shortening; **d)** detail of fault rock showing brecciated texture, pale green cataclasite matrix and stockwork quartz veins with local open-space-filling textures, domain C, north of Gem Lake.

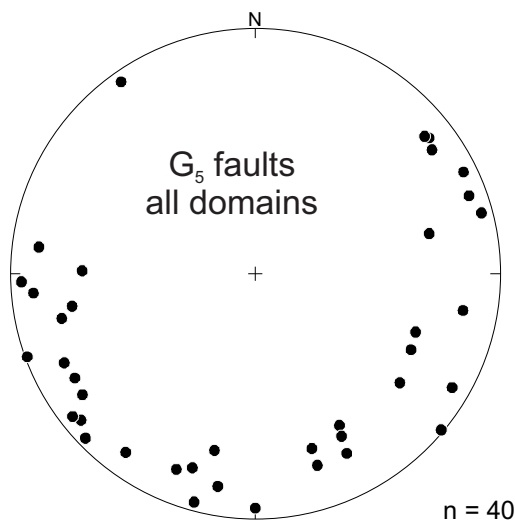


Figure 96: Lower-hemisphere, equal-area stereographic projection of the poles to G_5 faults in all structural domains.

and are also variably developed in granitoid intrusions of the Wanipigow River plutonic complex. Overprinting relationships with metamorphic mineral assemblages indicate that the G_2 structures were contemporaneous with the metamorphic peak on both sides of the BLSZ. The geometry and kinematics of the structures are compatible with northeast–southwest shortening (present co-ordinates) within a broad zone of bulk sinistral transpression (Figure 97). Similar fabrics and kinematics define a zone of sinistral transpression along the north margin of the belt in the Rice Lake area (Anderson, 2008). Hence, deformation is interpreted to represent a belt-scale event, which accompanied major crustal thickening along the interface between the NCT and Uchi subprovince during regional collisional orogenesis.

The G_3 and G_4 structures formed during transcurrent-shear deformation in a distinctly different kinematic frame than that of the G_2 structures (Figure 97). The G_3 structures consist of a penetrative to finely spaced S_3 crenulation cleavage that transects the macroscopic F_2 folds west of BLSZ and appears to have accommodated weak north-northeast–south-southwest shortening (present co-ordinates) during an early increment of this deformation. The G_4 structures include a series of ductile>brittle shear zones and an associated S_4 shear-band cleavage that generally trend northwest. The G_4 shear zones are characterized by penetrative, greenschist-grade mylonitic foliations, shallowly plunging lineations and packets of Z-asymmetric folds, and contain dextral kinematic indicators on horizontal outcrop surfaces. In the southern portion of the study area, the G_4 shear zones are associated with meso- to macro-scale, northeast-trending F_4 folds that are also strongly Z-asymmetric. The geometry and kinematics of these structures are compatible with northwest–southeast shortening (present co-ordinates), thereby implying an approximately 90° switch in the orientation of the principal shortening direction from that which prevailed during the G_2 deformation episode. Collectively, the G_3 – G_4 structures are interpreted to record progressive, partitioned, transcurrent-shear deformation in a regional regime of dextral transpression during the terminal stages of orogenesis (Figure 97).

The G_5 structures formed during the latest episode of deformation in the Garner–Gem lakes area. They consist mainly of northeast- or northwest-trending brittle faults; mutual overprinting relationships are consistent with a conjugate set that accommodated north–south shortening. As described below, some of these faults evidently served as conduits for the focused discharge of hydrothermal fluids, which were perhaps sourced from dehydration reactions at depth.

Economic considerations

Since the discovery of Au at Rice Lake in 1911, the Rice Lake greenstone belt has been the focus of considerable exploration and mining activity. The belt hosts hundreds of mineral occurrences and several Au deposits, most notably the Rice Lake mine complex of San Gold Corporation, located at Bissett, Manitoba. The metallogeny of the belt has been described by several workers, culminating with the belt-scale overview by Poulsen et al. (1996). Intermittent prospecting and exploration in the Garner–Gem lakes area from the early 1920s onward has resulted in the discovery of two significant Au deposits (the past-producing Gunnar and Diana mines) and numerous Au (\pm base-metal) occurrences. Theyer and Ferreira (1990) and Theyer (1994) described the geological setting, nature and exploration history of the most significant of these. Coupled with the results of this study, this work indicates potential for several types of mineral deposit, which are here divided into four groups on the basis of geological characteristics and commodities of interest: 1) magmatic nickel–copper–platinum group elements (Ni–Cu–PGEs); 2) volcanic-associated base metals; 3) magmatic-hydrothermal copper–gold–rare-earth elements (Cu–Au–REEs); and 4) lode gold.

Magmatic Ni–Cu–PGEs

Although there are no significant occurrences of magmatic Ni, Cu or PGE sulphides in the study area, the Garner assemblage nevertheless shows potential for two subtypes of magmatic sulphide deposit: komatiite-hosted Ni and reef-type PGEs.

Komatiite-hosted Ni

Komatiite-hosted Ni deposits consist of stratiform lenses of disseminated to massive sulphides (pyrrhotite–pentlandite \pm chalcopyrite) that occur at or near the base of komatiitic or komatiitic basalt flows (e.g., Naldrett, 2004; Eckstrand and Hulbert, 2007). Ore-bearing flows are typically found near the base of marine rift sequences, in trough-like structures underlain by sulphidic sedimentary rocks. The preferred genetic model for these deposits involves 1) contamination of komatiitic lavas with sulphur from crustal rocks (possibly via thermal erosion, melting and assimilation of interflow sulphidic sedimentary rocks); 2) sulphur saturation and generation of an immiscible sulphide liquid; 3) partitioning of Ni (\pm Cu \pm PGE) from the parent lava into the sulphide liquid; and 4) segregation/accumulation of Ni-sulphides by gravitational settling in lava channels at or near the base of the host flow. Key guides to ore on a district to deposit scale are komatiitic flows with geochemical indications of crustal contamination (e.g., Th–LREE

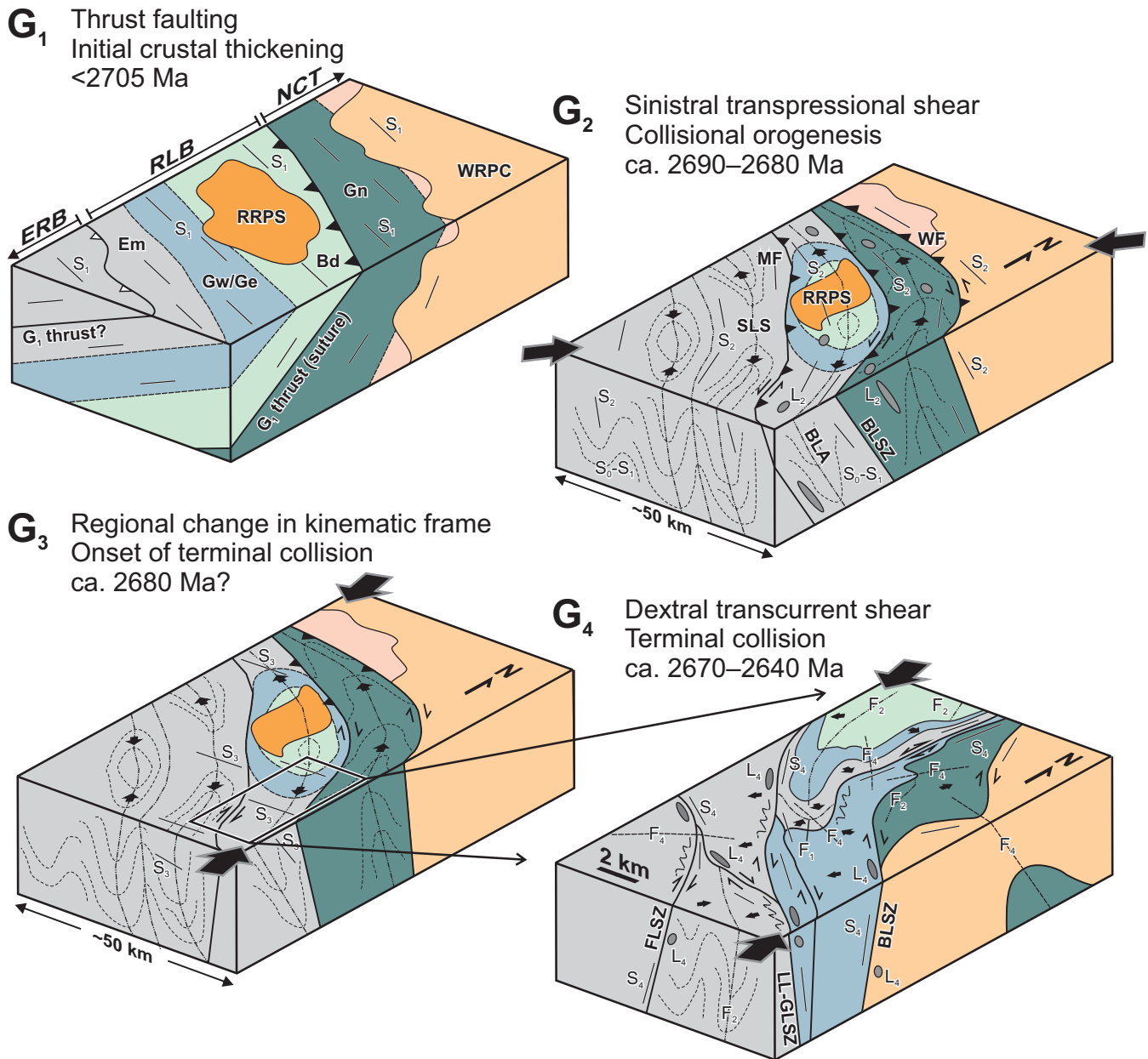


Figure 97: Schematic block diagrams illustrating the structural evolution (G_1 – G_4) of the Garner–Gem lakes area and the surrounding region. Abbreviations: Bd, Bidou assemblage; BLA, Beresford Lake anticline; BLSZ, Beresford Lake shear zone; Em, Edmunds assemblage; ERB, English River basin; FLSZ, Finger Lake shear zone; Gn, Garner assemblage; Gw/Ge, Gem west/Gem east assemblage; LL-GLSZ, Long Lake–Gem Lake shear zone; MF, Manigotagan fault; NCT, North Caribou terrane; RLB, Rice Lake belt; RRP, Ross River pluton; RRPS, Ross River plutonic suite; SLS, Slate Lake syncline; WF, Wanipigow fault; WRPC, Wanipigow River plutonic complex.

enrichment, Nb depletion) or sulphide segregation (e.g., Ni–Cu–PGE depletion), or both (Leshner et al., 2001). In the case of the Garner assemblage, the best potential for this deposit type is thought to exist near the base of unit Gn6, where subaqueous komatiitic flows with thin interflow sedimentary layers (unit Gn6) are underlain by iron formation (subunit Gn5d). Several of these flows contain evidence of crustal contamination in the form of strong Th–LREE enrichments and Nb depletions (Figure 54c). Variable Ni contents (151–1780 ppm) may relate to sulphide segregation during emplacement of some of these flows, or may simply result from ‘normal’ magmatic processes

such as olivine fractionation (Leshner et al., 2001). There are no records of exploration drilling on this target.

Reef-type PGE

Reef-type PGE deposits consist of stratiform layers of cumulate silicate, sulphide and PGE minerals in large layered intrusions of mafic and ultramafic composition. The preferred genetic model for these deposits involves a complex interplay between magma mixing, generation of an immiscible sulphide liquid, partitioning of PGEs (\pm Ni \pm Cu) from the silicate

magma into the sulphide liquid, and crystal accumulation by gravitational settling (\pm density inversion) in a stratified magma chamber (e.g., Naldrett, 2004; Eckstrand and Hulbert, 2007). Potential for this type of deposit exists in the Garner Lake intrusive complex (GLIC), which is poorly exposed on islands in the main basin of Garner Lake. As described previously, the GLIC consists of a lower section of interlayered peridotite and pyroxenite, and an upper section of heterogeneous pyroxenite and gabbro, with abundant dikes and segregation pods of pegmatitic tonalite. Despite the layered aspect of the complex, there are no reports of cumulate layering. Two occurrences of disseminated or fracture-controlled pyrrhotite-chalcopyrite mineralization were described by Scoates (1971) from pyroxenite in the northwest portion of the complex, but there are no reports of PGE values. Several magnetic and electromagnetic anomalies have been detected in the GLIC and were tested by several short drillholes, with no significant results (Assessment Files 91111, 92070, 93003, 93920).

Volcanic-associated Zn-Pb-Cu (Ag-Au)

Volcanic-associated base-metal sulphide or volcanogenic massive-sulphide (VMS) deposits are stratiform accumulations of massive to semimassive polymetallic sulphide that precipitate on or just below the seafloor by rapid cooling of hydrothermal fluids. These deposits form contemporaneously with their submarine volcanic and sedimentary hostrocks via focused discharge of hot metalliferous fluids from fault- or fracture-controlled seafloor vents above subvolcanic magma chambers. They represent the downstream ends of large-scale hydrothermal circulation systems that are induced by heat flux from high-level intrusions and produce distinctive patterns of discordant and semiconformable alteration in stratigraphic footwall rocks. Extensional settings, such as arc-rift or back-arc basins, or localized grabens or calderas in volcanic arcs, are the most common sites for VMS deposition. Subaqueous felsic volcanic rocks associated with major VMS deposits in the Superior province are generally characterized by distinctive geochemical signatures (e.g., low Zr/Y, $(La/Yb)_n$; high Y, Yb_n ; pronounced negative Eu anomalies) that are attributed to late-stage fractionation in high-level magma chambers and are utilized to distinguish prospective from nonprospective areas (Leshner et al., 1986; Barrie et al., 1993; Hart et al., 2004; Gaboury and Pearson, 2008). In the classification scheme of Leshner et al. (1986), these rocks are referred to as 'FII' and 'FIII' felsic metavolcanic rocks.

Given the subaqueous depositional settings inferred for nearly all volcanic rocks in the Garner–Gem lakes area, each of the major lithostratigraphic assemblages is considered to have at least notional potential for VMS mineralization. However, only the Gem assemblage preserves evidence of each of the key components of a seafloor hydrothermal-circulation system, and is therefore considered to possess the best potential for VMS deposits. Franklin (1996) and Galley et al. (2007) described key exploration guides or criteria for VMS systems, with emphasis on Canadian examples. The following list summarizes these criteria and their potential analogues in the Gem assemblage:

1) ***Submarine bimodal volcanic successions:*** Effusive flows and primary volcanoclastic rocks indicate deposition in

shallow-submarine to locally subaerial settings, and vary in composition from primitive basalt to high-SiO₂ rhyolite, with a well-defined Daly gap between 64 and 69 wt. % SiO₂ indicative of a bimodal distribution (Figure 59).

- 2) ***Extensional geodynamic setting:*** The lithological diversity, complex stratigraphy and distinctive geochemical attributes of bimodal volcanic rocks indicate a very dynamic depositional setting in a volcanic-arc environment, and are interpreted to record extension and incipient rifting of a mature back-arc–arc complex (Bidou assemblage) to form a regionally extensive intra-arc basin (Edmunds assemblage and English River basin).
- 3) ***Large subvolcanic magma chambers:*** Quartz-feldspar porphyry granite (unit Ge4) in the East association displays several characteristics of high-level (i.e., subvolcanic) intrusions in major VMS districts elsewhere, including porphyritic texture; laterally extensive sill-like shape; narrow or nonexistent metamorphic halo; oxidized (magnetite-series) mineralogy; compositional similarity to overlying volcanic rocks; and highly fractionated composition (FIII-type; Figure 56d).
- 4) ***Extension-related (FII and FIII-type) felsic volcanic rocks:*** Effusive flows, primary pyroclastic rocks and associated hypabyssal intrusions of rhyolite and high-SiO₂ rhyolite (units Gw4, Gw6, Ge4) display the key chemical attributes of FII- and FIII-type felsic volcanic rocks (Figure 56d), as defined by various authors (e.g., Leshner et al., 1986; Hart et al., 2004).
- 5) ***High-temperature reaction zones (semiconformable alteration or discordant alteration pipes):*** Evidence of synvolcanic high-temperature reaction zones is preserved in both the East and West associations. Felsic volcanoclastic rocks overlying the quartz-feldspar porphyry intrusion in the East association contain semiconformable alteration (Figure 98a) and stringer-style (discordant?) chlorite \pm garnet alteration (Figure 98b), and overlying epiclastic rocks contain angular clasts of intense epidote-SiO₂ alteration (Figure 98c). In the West association, rhyolitic volcanoclastic rocks and effusive flows of unit Gw4 contain semiconformable sericite alteration (Figures 20e, 98d) and sericite-pyrite alteration (Figure 98e), and clasts of the latter are also present in overlying epiclastic rocks (Figure 98f). As described below, the intrusion breccia on the central peninsula in Gem Lake (unit Gw5) is also associated with high-temperature alteration assemblages, which may likewise be related to seafloor hydrothermal circulation.

Based on the above criteria, three stratigraphic horizons in the Gem assemblage stand out as particularly favourable targets for VMS exploration:

- 1) ***Unit Ge1:*** This unit overlies the subvolcanic quartz-feldspar porphyry intrusion and contains both semiconformable (SiO₂ \pm epidote) and discordant (chlorite \pm garnet) alteration.
- 2) ***Subunit Gw4f:*** This subunit overlies sericite-pyrite-altered flows of FII-FIII rhyolite and coarse volcanoclastic rocks (unit Gw4a, b), and contains layers of black siliceous

mudstone (exhalite?) that are interpreted to record deposition in a relatively quiescent marine setting during a hiatus in rhyolitic volcanism.

- 3) **Units Gw2 and Gw4 (northwest of Gem Lake along the Manigotagan River):** These units are intercalated with, or include flows of, FII-FIII rhyolite and dacite, and contain zones of semiconformable sericite±pyrite alteration.

Although the VMS potential of these rocks has been recognized and evaluated in the past (e.g., Assessment File 93616), there is no record of exploration drilling on any of the targets listed above.

Magmatic-hydrothermal Cu-Au-REEs (La, Ce, Nd)

This style of mineralization is hosted by biotite leucogranite and aphanitic rhyolite of the felsic intrusion breccia (unit Gw5) on the central peninsula in Gem Lake. This unit is traceable along strike for 3 km and ranges up to approximately 400 m thick; discordant external contacts indicate its intrusive nature. Both components of the intrusion breccia contain irregular veinlets of opalescent blue quartz and patchy zones of weak to moderate sericite-pyrite, K-feldspar or biotite-magnetite±epidote alteration, with or without sheeted quartz±magnetite±actinolite±epidote±K-feldspar±chlorite±pyrite±chalcopyrite veins (Figures 26d, 99a, b), which are unique to this unit. The alteration and veins are best developed in the central portion of the southern lobe of the intrusion breccia, where they are controlled by closely spaced northeast-trending fractures (Figure 26d).

Trace-element profiles for representative samples of unit Gw5 vary from relatively flat to markedly concave upward, and show evidence of significant decoupling of the MREE (Figure 57e). As described previously, this decoupling is interpreted to result from selective mobilization of LREE, MREE and Y in relation to HREE and HFSE during a transient episode of high-temperature fluid-rock interaction, which most likely accompanied emplacement of the intrusion breccia. Similar chemical signatures are documented from alteration zones beneath VMS deposits (Campbell et al., 1984) and from highly evolved magmatic systems that are transitional between silicate melts and aqueous fluids (Bau, 1996; Irber, 1999; Jahn et al., 2001). Either setting would be compatible with the high-temperature alteration assemblages, although the opalescent blue quartz might be more compatible with the latter. Grab samples of stockwork veins from the southern lobe of the intrusion breccia returned anomalous values of Cu (126–789 ppm), Au (13–20 ppb) and LREE (363–389 ppm La, 820–848 ppm Ce, 328–391 ppm Nd). Taken together, these features are indicative of a high-level transitional magmatic–hydrothermal system of the sort known to be associated with several types of mineral deposits, including Fe-oxide–Cu–Au (IOCG), Cu–Au porphyry, high-sulphidization epithermal or VMS. This mineral system is only weakly developed at the present level of exposure but may intensify with depth; there is no record to indicate that it has been tested by drilling.

Lode Au

Significant lode Au occurrences are documented in each of the four supracrustal assemblages in the Garner–Gem lakes area, and are also found in the granitoid intrusions of the Wanipigow River plutonic complex and Ross River plutonic suite. Three distinct styles of lode Au mineralization are recognized: 1) laminated quartz-carbonate veins hosted by ductile shear zones; 2) stratabound disseminations in sulphidized iron formations; and 3) stockwork-breccia quartz veins and SiO₂ replacements associated with brittle faults. In the classification scheme of Poulsen et al. (2000), each of these styles falls within the broad clan of ‘greenstone’ Au deposits.

Shear-hosted quartz-carbonate veins

This style of mineralization consists of auriferous quartz-carbonate vein systems in ductile>brittle shear zones and associated arrays of shear and tensile fractures. It is the most common style of mineralization in the study area and accounts for most of the major Au occurrences, including the Gunnar and Diana deposits (Stockwell and Lord, 1939; Russell, 1952), and the Portage (Assessment File 93330), Tut (Assessment File 93358), Marlin-Swordfish (Assessment File 74298), Wyatt (Assessment File 4436) and Beaver Gold (Assessment File 94589) prospects (Figure 70). The host rocks include a wide variety of rock types, but the largest deposits occur in tholeiitic basalt (Gunnar) and gabbro (Diana). Significant prospects are hosted by volcanic conglomerate (Portage), tholeiitic gabbro (Tut), intermediate and felsic volcanoclastic rocks (Marlin-Swordfish and Wyatt, respectively), and turbiditic sedimentary rocks (Beaver Gold). The host shears consist of discrete zones of quartzofeldspathic, chloritic or sericitic mylonite that vary from parallel to transverse to the local hostrock anisotropy and are steeply dipping. Shear-hosted veins (Figure 100a, b) are massive, laminated and/or brecciated, and typically pinch and swell along strike. Vein textures are indicative of synkinematic emplacement under brittle-ductile rheological conditions.

Auriferous veins hosted by G₂ structures (e.g., Portage vein; Figure 100a) tend to be relatively intact, whereas those hosted by G₄ structures (e.g., Marlin-Swordfish veins; Figure 100c) tend to be strongly attenuated and folded, indicating that ductile deformation outlasted vein emplacement in the younger shear zones. Shear-hosted veins in tholeiitic basalt north of Garner Lake locally contain cockade or crustiform-banded carbonate, indicative of open-space filling and relatively high-level emplacement (Figure 100d). These veins are not known to be auriferous but are texturally similar to early colloform-crustiform carbonate veins in the Red Lake deposit (e.g., Dubé et al., 2004). All significant occurrences of this style of mineralization in the study area are situated in the proximal portions of secondary shears that splay off the principal (named) shear zones (Figure 70).

Auriferous veins consist of quartz, with subordinate carbonate (ankerite>calcite); minor albite, chlorite, sericite or biotite; and rare tourmaline or fuchsite. Vein quartz in several showings is mottled and dark grey with a microcrystalline (‘cherty’) texture (Figure 100b); according to Stockwell and Lord (1939), this type of quartz was associated with the highest Au grades in the Gunnar mine. Quartz veins in the Banksian Lake area

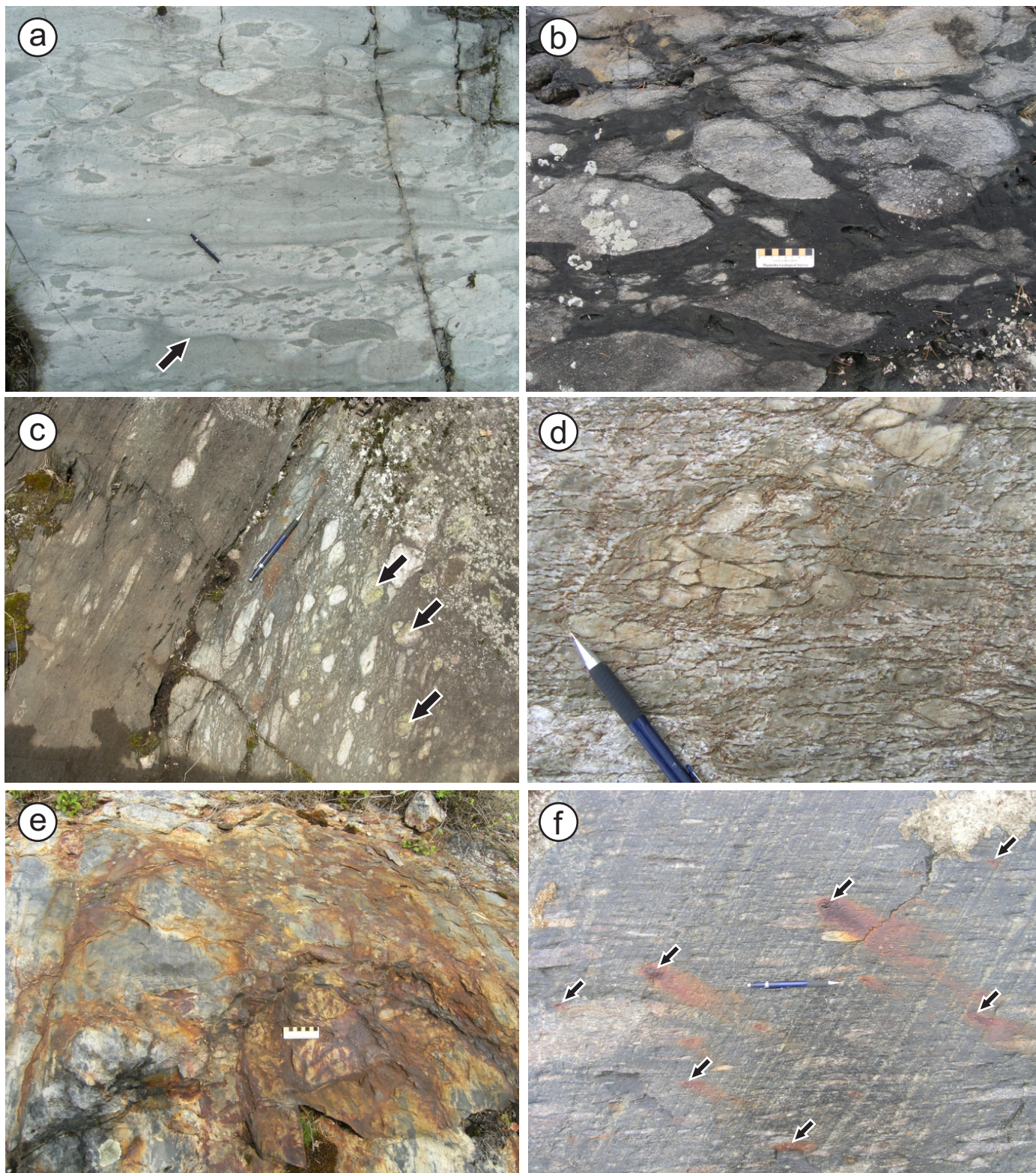


Figure 98: Outcrop photographs of alteration and mineralization indicative of seafloor hydrothermal circulation, which may have generated volcanic-associated base-metal sulphide deposits in the Gem assemblage: **a)** semiconformable alteration (SiO_2 ?) in epiclastic rocks of unit Ge1b, east shoreline of Gem Lake; arrow indicates a stratiform alteration boundary; **b)** stringer-style chlorite-garnet alteration in porphyritic dacite breccia of unit Ge1a, east shoreline of Gem Lake; **c)** clasts of epidote- SiO_2 -altered rock (arrows) in bedded epiclastic rocks of unit Ge1b, east shoreline of Gem Lake; **d)** intense sericite alteration in rhyolitic volcaniclastic rocks of unit Gw4a, northwest of Gem Lake; **e)** sericite-pyrite alteration and gossan in aphyric rhyolite flow of unit Gw4b, southeast shoreline of Gem Lake; **f)** clasts of sericite-pyrite-altered rock (arrows) in volcanic conglomerate of unit Gw2b, northwest of Gem Lake.

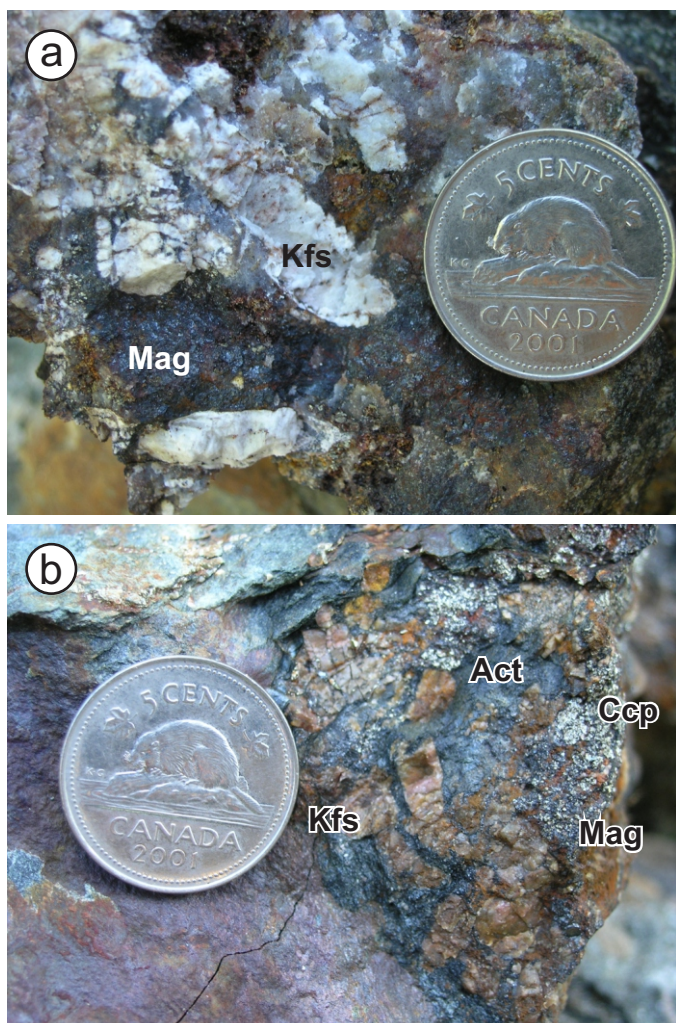


Figure 99: Hand-specimen photographs of mineralization hosted by sheeted veins in the southern lobe of the intrusion breccia (unit Gw5) on the central peninsula in Gem Lake: **a)** K-feldspar–magnetite–quartz vein; K-feldspar in this specimen is completely replaced by clay minerals; **b)** K-feldspar–actinolite–magnetite–chalcopyrite vein. This style of vein mineralization is typical of high-temperature fluid-interaction zones associated with several types of magmatic-hydrothermal ore deposits (see text for discussion). Abbreviations: Act, actinolite; Ccp, chalcopyrite; Kfs, K-feldspar; Mag, magnetite.

are commonly black and glassy, with an unusual iridescent lustre; many of these veins have been prospected by trenching but apparently did not contain sufficient values to warrant further work. Associated sulphide minerals consist mostly of pyrite, with subordinate arsenopyrite or pyrrhotite, and rare chalcopyrite, sphalerite and galena. Arsenopyrite is only abundant in veins hosted by the Edmunds assemblage or the adjacent portions of the Gem assemblage. Sulphides generally account for less than 5 vol. % of individual veins and occur as scattered crystals and blebs in vein quartz, or are concentrated along vein margins or planar slip surfaces. Gold commonly occurs as free grains; grades are highly erratic. Auriferous veins are characterized by high Au:Ag ratios (>5:1) and low concentrations of base metals (Cu, Pb, Zn) and pathfinder elements (B, Bi, Sb, Te, W), with the exception of local strong As enrichments (up to 19 400 ppm). Wallrock-alteration haloes are typically

narrow (<0.5 m) and zoned outward from proximal ankeritic assemblages (\pm chlorite \pm SiO₂ \pm sericite \pm albite \pm biotite \pm fuchsite; Figure 100e, f) to distal calcitic assemblages; this alteration overprints the regional metamorphic assemblages. Most veins exhibit evidence of wallrock sulphidization in the form of distinct haloes of euhedral pyrite or arsenopyrite crystals.

The above characteristics identify these as ‘greenstone-hosted vein’ or ‘mesothermal’ deposits (e.g., Poulsen et al., 2000), which have also been termed ‘orogenic’ (Groves et al., 1998) to emphasize their spatial association with accretionary orogens and the synkinematic and synmetamorphic timing of lode emplacement (e.g., Kerrich and Wyman, 1990; Hodgson, 1993; Kerrich and Cassidy, 1994). The preferred model for this deposit type involves fluids generated by thermal equilibration of accreted sediments during the clockwise P-T-t evolution of accretionary orogens (e.g., Kerrich and Cassidy, 1994; McCuaig and Kerrich, 1998). The resulting fluids are thought to migrate upward along transcrustal fault systems into subsidiary brittle-ductile shear and fracture arrays in the mid to upper crust, where Au is deposited in synkinematic and synmetamorphic quartz-carbonate veins due to physical and/or chemical changes in the ore fluid brought about by pressure fluctuations, wallrock sulphidization reactions, phase separation and/or fluid mixing.

In keeping with lode Au districts elsewhere, the most important district- to prospect-scale exploration guides include 1) chemically and/or rheologically favourable rock types (e.g., Fe-rich gabbro, basalt or iron formation); 2) structural preparation, in the form of brittle-ductile shear zones or fracture arrays; and 3) hydrothermal alteration (particularly Fe-carbonate). Detailed exploration for shear-hosted Au deposits in the Garner–Gem lakes area should focus on extensional or compressional bends in the principal shear zones, and the proximal portions of any secondary splay structures.

Iron formation–hosted stratabound Au

This style of mineralization consists of stratabound, disseminated sulphide replacements of Fe-rich layers in oxide-facies iron formation. As described by Poulsen et al. (2000), deposits of this type are generally regarded as members of the ‘greenstone’ or ‘orogenic’ clan of deposits, and are interpreted to form by similar processes. Based on the style, distribution and geometry of the mineralized zones, two end-member varieties have been described in the literature: stratiform and nonstratiform (Kerswill, 1996). Gold in the former occurs in laterally continuous units of sulphidized iron formation, whereas, in the latter, it is mostly restricted to late structures or veins that cross-cut the iron formation. Both varieties have been identified in the Edmunds assemblage south of Gem Lake; the most significant of these are referred to as the Gem South and Lily South occurrences (Figure 70). Iron formation in the upper succession of the Garner assemblage (units Gn5, Gn6, Gn7) is also considered to have good potential for this style of mineralization. As with iron formation–hosted deposits elsewhere, the most useful guides for exploration are 1) structural complexity (i.e., shear zones, folds and/or quartz veins); and 2) high concentrations of iron sulphides (i.e., pyrrhotite and/or pyrite).

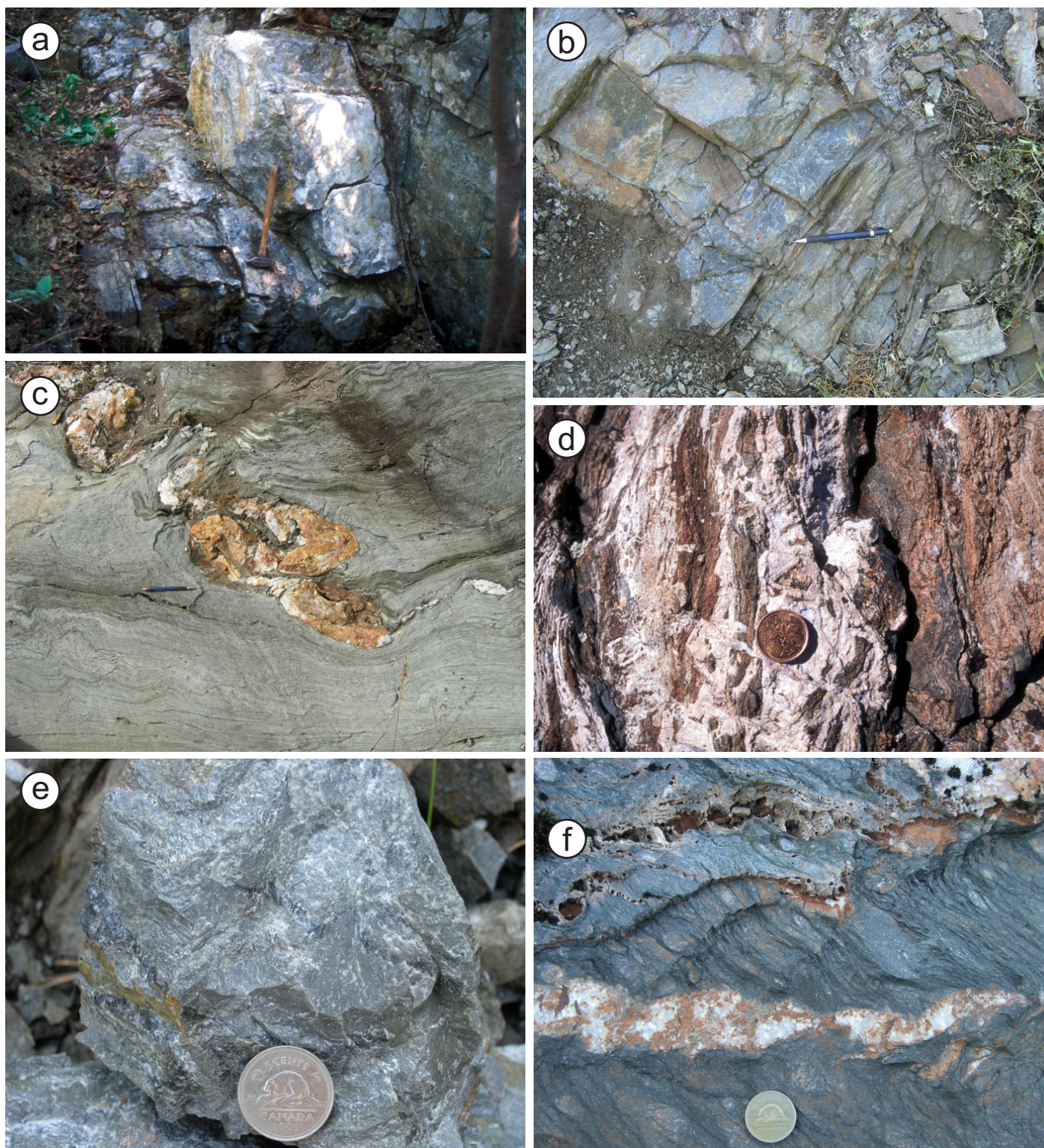


Figure 100: Outcrop photographs of mineralization and alteration associated with shear-hosted quartz-carbonate veins: **a)** thick laminated vein at the Portage occurrence, south shoreline of Garner Lake; vein contains abundant visible Au in this location; note sharp planar contacts with strongly foliated wallrock; **b)** massive, dark grey, microcrystalline vein at the Beaver Gold occurrence, south of Lily Lake; note sharp planar contacts with strongly foliated wallrock; **c)** attenuated and folded vein in chloritic mylonite at the Marlin-Swordfish occurrence, south of the mouth of the Garner River at Garner Lake; veins in this location contain visible Au and are crosscut by post-tectonic dikes (Figure 46d); **d)** laminated, brecciated and crustiform textures in carbonate vein, north of Garner Lake; **e)** intense, proximal, SiO_2 -ankerite-sericite-arsenopyrite alteration in quartz greywacke, Beaver Gold occurrence, south of Lily Lake (same locality as Figure 100b); **f)** quartz-ankerite extension vein and proximal, strong, ankerite-chlorite alteration in felsic volcaniclastic rocks, north tip of the large island in central Gem Lake.

The Gem South occurrence is situated roughly midway between Gem Lake and Finger Lake (Figure 70), and was identified in 1984 by a reconnaissance rock-chip geochemical survey completed by Nelson Baker Geological Services Ltd., which returned values as high as 630 ppb Au and 10 000 ppm As over the occurrence. In 1984–1985, Amalgamated Mining Development Corporation Ltd. investigated this occurrence through prospecting and rock-chip geochemistry, as well as ground magnetometer and VLF-EM surveys. This work outlined a northwest-trending zone of stratabound, disseminated arsenopyrite mineralization and sparse quartz-arsenopyrite veins associated with interbedded turbidites and magnetite iron formation (unit Em4). This zone was traced by prospecting for 900 m along strike and returned values up to 710 ppb Au from surface samples. Two diamond-drill holes (84-1 and 85-1) were completed to test a 90 m strike length of the anomalous zone. The best results were obtained from DDH84-1, which intersected 13.1 m of disseminated arsenopyrite mineralization that contained several narrow zones with values up to 24 406 ppm As and 2560 ppb Au (Assessment File 93616). Based on these characteristics, the Gem South occurrence is interpreted to represent an example of stratiform-type mineralization.

The Lily South occurrence (identified by the MGS in 2007) is located approximately 300 m west of the Beaver Gold occurrence (Figure 70). The occurrence is hosted by interstratified quartz greywacke, polymictic conglomerate and oxide-facies iron formation of subunit Em6b, approximately 10 m stratigraphically below the contact with pillowed basalt flows of unit Em8. The hostrock consists of a 3–4 m thick layer of banded magnetite-chert iron formation, which is discontinuously exposed along strike for 80 m. At the occurrence, the iron formation appears to abruptly terminate, perhaps indicating the presence of a crosscutting fault. Here, the iron formation is strongly silicified and chloritized, and contains up to 30% pyrite and arsenopyrite; quartz veins are absent (Figure 101). The pyrite is coarsely crystalline and occurs as irregular veinlets and disseminations, whereas the arsenopyrite is very fine grained and forms near-solid blebs and disseminations. Hand specimens are nonmagnetic, suggesting that the primary

magnetite was completely replaced by sulphide minerals. A grab sample of this material returned 3550 ppb Au and 20 200 ppm As, with negligible Ag and base metals. Based on these characteristics, the Lily South occurrence is interpreted to represent an example of nonstratiform-type mineralization.

In terms of the geological setting and styles of mineralization, the Gem South and Lily South occurrences are closely analogous to lode Au deposits hosted by Neoproterozoic iron formations in the Beardmore-Geraldton greenstone belt of the Superior province (e.g., Lafrance et al., 2004) and the Rankin Inlet greenstone belt of the western Churchill province (e.g., Carpenter and Duke, 2004). In both belts, significant Au occurrences are situated along or adjacent to structurally modified contacts between mafic metavolcanic rocks and turbiditic metasedimentary rocks, and are hosted by chemically favourable rock types (principally iron formation) in areas of structural complexity resulting from heterogeneous deformation. Fruitful exploration strategies for these types of Au deposits employ detailed geological mapping and high-resolution geophysical surveys to delineate areas of structural complexity and/or sulphide enrichment, with emphasis on iron formations associated with major lithological contacts or structural ‘breaks’.

Fault-controlled quartz veins and SiO₂ replacements

This style of mineralization consists of quartz-vein stockworks and SiO₂ (±sulphide) replacements controlled by brittle-ductile faults of the G₅ generation. It defines extensive zones of intense, pervasive, SiO₂ flooding along major faults in two localities (Figure 70; described below) and is also exposed in several locations in the area between Gem Lake and Lily Lake, where it is developed on a much smaller scale in association with relatively minor faults.

The thickest and most extensive zone of SiO₂ flooding is exposed on the neck of land between Finger Lake and Normandy Lake (Figure 70), and on several small islands in Finger Lake. This zone is traceable along strike for approximately 800 m and is up to 200 m thick in continuous exposure. It is one of three “giant quartz zones” described by Russell (1952, Sheet 50-3a, Map 8), the others being located along major faults west of Flintstone Lake beyond the limits of the study area. Nearly the entire thickness of the Finger Lake zone consists of intensely silicified fault or hydrothermal breccia that contains multiple generations of stockwork-breccia quartz veins and large areas of pervasive SiO₂ replacement (Figure 102a, b). It is situated in the immediate hangingwall of the faulted contact between pillowed basalt of unit Em8 on the south and greywacke-mudstone turbidite of unit Em1 on the north. The second zone of SiO₂ flooding is located north of Gem Lake (Figure 70), where it is traceable for 1.2 km along strike at the faulted contact between basaltic andesite of unit Gw1 on the west and dacite of unit Gw4 on the east. Here, the controlling fault is marked by a discrete slip surface (Figure 95a) and locally contains a quartz-breccia vein up to 2.5 m thick. The fault is bounded on one or both sides by brecciated and intensely silicified wall-rock that grades outward into marginal zones of stockwork or sheeted quartz veins; the entire zone ranges up to 7 m thick (Figure 102c). Local open-space-filling textures in quartz veins are indicative of high-level emplacement (Figure 95d, 102d).



Figure 101: Hand specimen of disseminated-replacement-style mineralization hosted by magnetite-chert iron formation at the Lily South occurrence, south of Lily Lake.

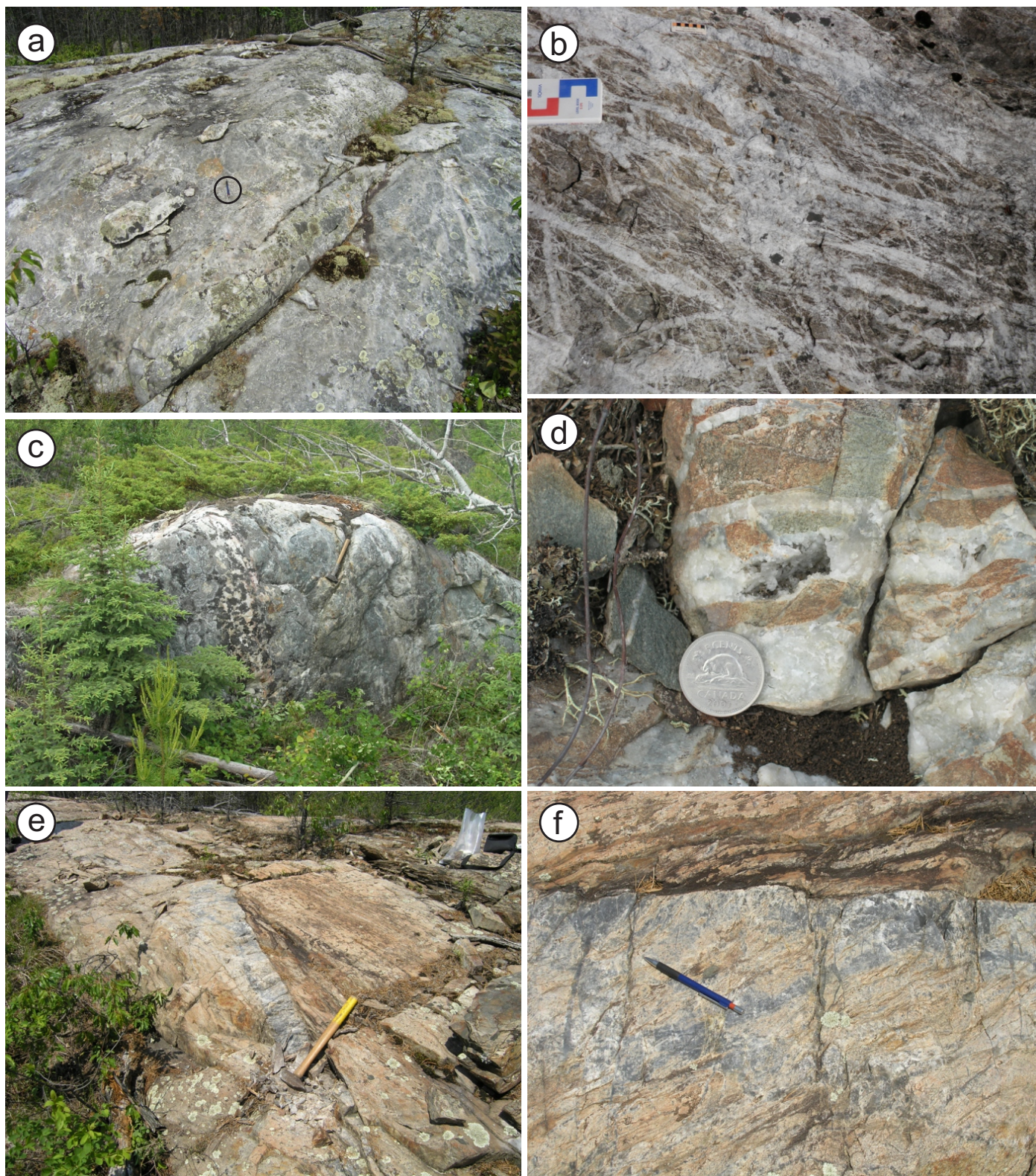


Figure 102: Outcrop photographs of quartz veins and alteration associated with G_5 faults in the Gem Lake area: **a)** intensely silicified fault or hydrothermal breccia, east shoreline of Finger Lake; pencil for scale (circled); **b)** stockwork-breccia quartz vein, island outcrop in Finger Lake; **c)** fault-controlled quartz-breccia vein and marginal zones of intense silicification, north of Gem Lake (hammer for scale is 45 cm in length); **d)** drusy vug in quartz vein, indicative of open-space filling, north of Gem Lake; **e)** narrow zone of SiO_2 -sericite-pyrite-arsenopyrite alteration associated with discordant minor fault, north of Lily Lake; **f)** detail of previous photo, showing fracture-controlled SiO_2 -sericite-pyrite-arsenopyrite alteration (grey), sharply truncated by a planar slip-surface.

Quartz veins in both zones contain minor (<2%) disseminated to blebby sulphides (pyrite±chalcopyrite±arsenopyrite) and are associated with thin haloes of weak to moderate chlorite alteration in the wallrocks.

Both zones of intense SiO₂ flooding are associated with large-scale faults that evidently served as conduits for the focused discharge of large volumes of siliceous hydrothermal fluid. They record brittle deformation and fluid migration during the latest stages of thermotectonism at the present level of exposure. The textural and structural characteristics of the veins indicate emplacement in a transitional mesozonal–epizonal regime in the middle to upper crust. These zones likely represent the downstream (epizonal) segments of large-scale hydrothermal flow systems sourced from late-orogenic dehydration reactions (e.g., Colvine et al., 1988; Hagemann and Cassidy, 2000; Cox, 2005); as such, they may have been associated with the development of quartz-carbonate vein systems at deeper levels of the orogen and thus indicate potential for late-orogenic lode Au deposits. Neither zone is known to be auriferous; however, previous exploration has been limited to surface prospecting and geophysics (Assessment Files 92860, 92915). As described below, smaller scale occurrences of fault-controlled mineralization are locally auriferous and thus indicate significant exploration potential.

In the Gem Lake–Lily Lake area, occurrences of fault-controlled mineralization are associated with relatively minor (low-displacement) faults and appear to be best developed in the relatively thick-bedded turbidites of unit Em6. Of particular significance is an occurrence of auriferous fault breccia located approximately 450 m southeast of the Gem South occurrence. The occurrence is hosted by thick-bedded quartz greywacke of unit Em6a, approximately 100 m stratigraphically above the oxide-facies iron formation of unit Em4. Younging reversals over distances of 50–100 m across strike indicate the presence of tight to isoclinal fold closures that predate faulting. At the occurrence, diffuse zones of moderate to intense SiO₂–sericite–pyrite–arsenopyrite alteration are associated with discordant faults (Figure 102e, f) and stratabound arrays or stockworks of quartz extension veins. The most intense alteration zones, which rarely exceed 1.0 m in width, are associated with narrow seams of SiO₂–cemented fault breccia and cataclasite that contain ghost-like fragments of altered wallrock and 2–5% disseminated pyrite and arsenopyrite. Wallrock alteration is zoned outward from proximal silicification and sulphidization to distal sericitization over 0.5–1 m. In some cases, the alteration is sharply bounded by slip surfaces, indicating that it preceded the latest increment of faulting. A grab sample of SiO₂–cemented fault breccia and strongly altered wallrock returned 350 ppb Au and 3270 ppm As, indicating that the hydrothermal fluid was auriferous in at least this portion of the system.

Summary and regional implications

Uranium–lead zircon ages from the Rice Lake greenstone belt and adjacent portions of neighbouring domains span approximately 360 m.y. and indicate two major phases of crustal growth, separated by nearly 100 m.y. of apparent quiescence (data sources: Krogh et al., 1974; Ermanovics and Wanless, 1983; Turek et al., 1989; Turek and Weber, 1991, 1994;

Davis, 1994; Corfu et al., 1995; Corfu and Stone, 1998; Whalen et al., 2003; Percival et al., 2006a; Sasseville et al., 2006; Anderson, 2008; this study). This two-phase growth history is also indicated by the distinctly bimodal distribution of U–Pb ages obtained from detrital zircons in sedimentary rocks of various ages across the region, based on a dataset that includes close to 600 single-grain analyses from 18 samples (data sources: Davis, 1994, 1996; Percival et al., 2006a; Sasseville et al., 2006; Anderson, 2008; this study). Progressive younging of supracrustal assemblages from north to south across the region strongly implicates an accretionary tectonic process. A ‘time gap’ of comparable duration (60–100 m.y.) and ending at about 2.75 Ga is apparent in greenstone belts at the south margin of the NCT over at least 500 km of strike length (e.g., Stott and Corfu, 1991; Percival et al., 2006b), indicating that this process operated at a regional scale.

The older phase of crustal growth (ca. 3.01–2.85 Ga) is recorded by volcano–plutonic rocks of the North Caribou terrane (NCT) and by detrital zircons of the same age in much younger (ca. 2.7 Ga), synorogenic sedimentary rocks in adjacent domains. Crustal growth during this phase was characterized by complex interactions between arc and mantle–plume magmatism (e.g., Hollings et al., 1999; Whalen et al., 2003) and coeval deposition of supracrustal assemblages in mostly continental settings. In contrast, the younger phase (ca. 2.75–2.65 Ga) is well represented by granitoid rocks across all domains and is interpreted to reflect crustal growth at a dynamic convergent margin associated with northward subduction beneath the NCT (e.g., Stott and Corfu, 1991). Accretion, driven by northward subduction of oceanic crust, is thought to have terminated at ca. 2.71 Ga and was closely followed by collisional orogenesis related to convergence and final amalgamation of the North Caribou and Winnipeg River continental terranes (e.g., Stott and Corfu, 1991; Corfu et al., 1995; Sanborn–Barrie et al., 2001; Percival et al., 2006a, b). Field relationships, litho–geochemistry and U–Pb age constraints indicate that this phase of crustal growth involved a systematic progression from early continental–arc and oceanic arc–back–arc magmatism to synorogenic sedimentation, regional thermotectonism and late-orogenic emplacement of peraluminous granite plutons (e.g., Stott and Corfu, 1991; Corfu et al., 1995; Poulsen et al., 1996; Corfu and Stone, 1998; Bailes et al., 2003; Percival et al., 2006a; Anderson, 2008).

The geodynamic evolution of the region is herein divided for descriptive purposes into six time intervals, each of which was associated with accumulation of distinct supracrustal assemblages and/or significant additions of new crust.

ca. 3.01–2.92 Ga

The 3.01–2.92 Ga time interval is mostly recorded by granitoid rocks of the NCT, widely regarded as the Mesoarchean protocraton around which Mesoarchean and Neoarchean terranes were accreted during the protracted assembly of the western Superior province (e.g., Thurston et al., 1991; Percival et al., 2006b). This time interval is thought to include the initial development and stabilization of NCT continental crust, and subsequent plume-influenced extension and rifting of this crust to form a south-facing (present configuration) continental

margin and long-lived oceanic basin. Vestiges of early continental crust are uniquely well preserved along the south margin of the NCT in Manitoba and consist of juvenile, ca. 3.01–2.99 Ga, tonalite–diorite–gabbro–anorthosite suites, interpreted to have formed via fluid-fluxed partial melting of mantle-wedge peridotite in a primitive oceanic arc (Whalen et al., 2003). Platform quartz arenite and pebble conglomerate exposed at Wallace Lake and along the east shore of Lake Winnipeg record uplift, erosion and stabilization of this continental mass by ca. 2.98 Ga and are conformably overlain by ca. 2.98–2.92 Ga komatiite, tholeiitic basalt and iron formation (Davis, 1994; Percival et al., 2006a; Sasseville et al., 2006) that are interpreted to signal plume-influenced extension and subsequent rifting of the proto-craton (e.g., Percival et al., 2006b).

The platform-rift cover sequence (i.e., the Wallace assemblage and local equivalents; Table 1) is likely correlative with komatiite-bearing assemblages in the Red Lake greenstone belt in Ontario, including the ca. 2.99–2.96 Ga Balmer and ca. 2.94–2.92 Ga Ball assemblages (Stott and Corfu, 1991; Sanborn-Barrie et al., 2001). The Balmer assemblage is interpreted to record plume-influenced extension and rifting of the proto-craton, whereas the Ball assemblage is interpreted to represent a primitive arc to intra-arc rift built on extended continental crust of the NCT (Stott and Corfu, 1991; Tomlinson et al., 1998; Sanborn-Barrie et al., 2001; Percival et al., 2006b). Minor dikes and plutons of ca. 2.94–2.92 Ga tonalite and granodiorite along the NCT margin in Manitoba (Turek et al., 1989; Davis, 1994; Percival et al., 2006a; Sasseville et al., 2006) likely represent local manifestations of this continental arc. Percival et al. (2006a) and Sasseville et al. (2006) described cryptic evidence of Mesoarchean (>2.92 Ga) ductile deformation of basement and cover at the south margin of the NCT; the significance of this deformation is unknown.

ca. 2.89–2.85 Ga

This time interval includes the construction and subsequent plume-influenced rifting of a volcanic arc situated on, or marginal to, the NCT (Figure 103a). It is represented by two distinct successions of supracrustal rocks east of the Beresford Lake shear zone, which are defined in this report as the Garner assemblage. Intermediate–felsic volcanoclastic and derived epiclastic rocks of the lower succession, deposited in a shallow-marine setting on the proximal flank of a subaerially exposed volcanic edifice, show geochemical affinity to continental-arc rocks. The age of this arc remains poorly constrained, but it was intruded by the mafic–ultramafic Garner Lake intrusive complex at ca. 2.87 Ga (Davis, 1994; this study), indicating that it had achieved significant thickness by that time. Distinctly older (ca. 2.89 Ga) zircons in overlying volcanic rocks may be inherited from this arc; similar ages have been obtained from granodiorite plutons at the south margin of the NCT (Turek et al., 1989).

The pronounced erosional unconformity at the base of the upper succession requires uplift and erosion of the arc, perhaps in response to accretionary tectonics or thermal doming above an upwelling mantle plume. Arkosic sandstone and tonalite-pebble conglomerate above the unconformity contain 2.87 Ga detrital zircons (Davis, 1994) and are overlain by ca. 2.85 Ga

intermediate–felsic volcanic rocks with minor interlayers of chert, carbonate and argillite, and a thick unit of magnetite–chert iron formation, all of which were deposited in a relatively quiescent marine basin. This basin was subsequently infilled by subaqueous komatiitic and tholeiitic basalt derived from a strongly depleted, probably mantle-plume, source. Thermal doming above an ascending plume may account for uplift of the arc, with subsequent extension and rifting to form the marine basin, which became sediment starved during eruption of the komatiite–basalt succession. In this regard, the upper succession is thought to be analogous to Archean rift sequences documented elsewhere (e.g., Thurston and Chivers, 1990; Hunter et al., 1998; Bleeker et al., 1999; Thurston and Kozhevnikov, 2000; Hartlaub et al., 2004; Percival et al., 2006a; Sasseville et al., 2006).

Stratigraphic, geochemical and age constraints for the Garner assemblage suggest possible correlations to the Bruce Channel and Trout Bay assemblages in the central and western portions of the Red Lake belt, respectively. As described by Sanborn-Barrie et al. (2001), the Bruce Channel assemblage consists of 2.89 Ga intermediate–felsic volcanoclastic rocks, locally overlain by a fining-upward clastic sedimentary sequence capped by magnetite iron formation; it is interpreted to represent a continental-arc succession. The Trout Bay assemblage includes clastic sedimentary rocks, ca. 2.85 Ga intermediate volcanoclastic rocks and magnetite iron formation, overlain by a thick sequence of strongly depleted tholeiitic basalt flows that are thought to represent a back-arc or oceanic-plateau succession (Sanborn-Barrie et al., 2001). Although neither is known to contain komatiite, they are otherwise similar to the Garner assemblage in terms of facies associations, general stratigraphy and apparent ages, suggesting they may represent portions of a single tectonostratigraphic entity that was tectonically segmented at Red Lake but preserved as an intact section at Garner Lake.

In this model, the upper succession of the Garner assemblage, with its distinctive association of clastic sedimentary rocks, ca. 2.85 Ga volcanic rocks, iron formation and depleted tholeiitic basalt, would be a lateral equivalent to the Trout Bay assemblage and upper Bruce Channel assemblage, whereas the lower succession would correlate with the lower Bruce Channel assemblage. The Trout Bay and Garner assemblages occur on opposite flanks of the composite batholith that separates the Red Lake and Rice Lake belts, suggesting they may well have been contiguous prior to its emplacement; both contain mafic–ultramafic intrusions with potential for Ni–Cu–PGE deposits. Farther north in the NCT, continental-arc magmatism of comparable age is evidenced by ca. 2.89 Ga granitoid plutons and ca. 2.85 Ga felsic volcanic rocks in the Island Lake greenstone belt (e.g., Parks et al., 2006).

ca. 2.75–2.73 Ga

The time interval from about 2.75 Ga to 2.73 Ga is interpreted to include renewed northward subduction of oceanic crust beneath the south margin of the NCT (Figure 103b), following a magmatic hiatus that appears to have lasted close to 100 m.y. In the study area, this interval is represented by two major lithotectonic components: 1) tonalite–granodiorite

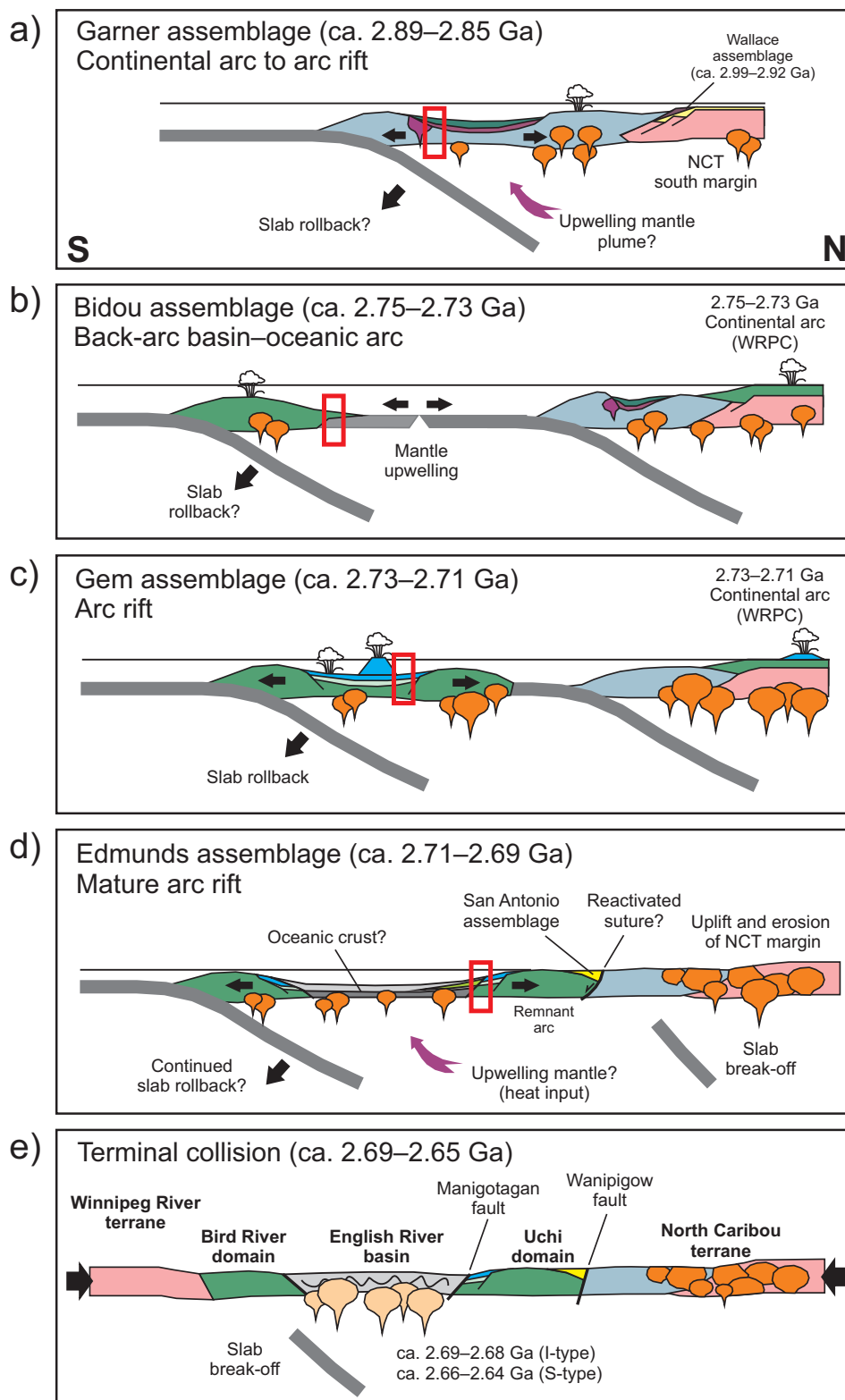


Figure 103: Schematic sections illustrating the postulated tectonic evolution of the south margin of the North Caribou terrane through 250 m.y. of geological time. Red rectangles indicate the inferred geodynamic settings of supracrustal assemblages in the Garner–Gem lakes area: **a)** ca. 2.89–2.85 Ga deposition of the Garner assemblage in a continental-arc to arc-rift setting; **b)** ca. 2.75–2.73 Ga deposition of the Bidou assemblage in an oceanic arc–back-arc complex outboard of the NCT margin, with coeval continental-arc magmatism inboard of the margin; **c)** ca. 2.73–2.71 Ga deposition of the Gem assemblage in an intra-arc rift setting, with continued continental-arc magmatism inboard of the NCT margin; **d)** ca. 2.71–2.69 Ga deposition of the Edmunds assemblage in a mature arc-rift basin after cessation of major arc magmatism and coeval with synorogenic fluvial-alluvial sedimentation in fault-bounded, probably extensional basins along the NCT margin; **e)** ca. 2.69–2.65 Ga terminal collision of the North Caribou and Winnipeg River terranes, resulting in tectonic burial, regional thermotectonism, crustal-scale faulting (with an evolution from early sinistral to late dextral kinematics) and voluminous granitoid magmatism. Abbreviation: WRPC, Wanipigow River plutonic complex. See text for discussion.

batholiths of the Wanipigow River plutonic complex; and 2) bimodal subaqueous volcanic and subvolcanic intrusive rocks and basinal marine sedimentary rocks of the Bidou assemblage.

The Wanipigow River plutonic complex represents the southwest portion of a vast domain of composite granitoid batholiths that extends north and east of the Rice Lake belt for several hundred kilometres and is thought to represent a magmatic arc built on continental crust of the NCT. It includes several distinct suites of calcalkalic tonalite, granodiorite and granite that were emplaced during an essentially continuous pulse of magmatism between 2.75 and 2.69 Ga (Corfu and Stone, 1998). Early suites exhibit close chemical affinity to the products of Cenozoic magmatic arcs and consist mostly of hornblende tonalite and granodiorite emplaced between 2.75 and 2.72 Ga. Contemporaneous mafic–felsic volcanic rocks of calcalkalic and tholeiitic affinity in the ca. 2.75–2.73 Ga Confederation assemblage of the Red Lake and Birch-Uchi belts in Ontario are thought to record construction and localized rifting of a continental arc on the south margin of the NCT (Stott and Corfu, 1991; Hollings and Kerrich, 2000; Sanborn-Barrie et al., 2001; Percival et al., 2006b). In the Birch-Uchi belt, these rocks are locally associated with volcanic-hosted massive-sulphide mineralization (Stott and Corfu, 1991). A regional angular unconformity marked by polymictic conglomerate at the base of this assemblage at Red Lake indicates early (pre–2.74 Ga) nonpenetrative deformation of underlying autochthonous assemblages, perhaps related to early accretionary events (Sanborn-Barrie et al., 2001).

At the type locality in the eastern Rice Lake belt, the Bidou assemblage is thought to record a transition from back-arc to arc volcanism, within a bimodal oceanic arc–back-arc complex that formed in a marginal-marine setting outboard of the NCT (Figure 103b). Percival et al. (2006a) attributed the initiation of this arc complex to subduction-zone step-back, possibly in response to early accretion events along the NCT margin, as suggested by evidence of ca. 2.74–2.73 Ga deformation in the Red Lake belt (Sanborn-Barrie et al., 2001). Deposition of the Bidou assemblage was confined to a relatively narrow time interval between ca. 2.75 and 2.73 Ga, broadly coeval with major continental-arc magmatism inboard of the terrane margin. Subaqueous tholeiitic basalt flows and subvolcanic gabbro sills in the lower succession are chemically similar to MORB erupted at steady-state spreading centres in relatively mature (>100 km wide) back-arc basins and alternate with intervals of basinal-marine turbidite with a maximum depositional age of ca. 2.75 Ga. Juvenile isotopic signatures and the absence of older (>2.75 Ga) inherited or detrital zircons are interpreted to indicate an intraoceanic setting; the basal contact of this assemblage is nowhere exposed. The absence of Mesoarchean detrital zircons further suggests a depositional setting that was isolated from the NCT margin, perhaps on the opposite (south) side of a back-arc spreading centre (Figure 103b).

The appearance of tonalite boulders in volcanic conglomerate, and significant detrital quartz in proximal turbidites, signal a transition from back-arc to arc volcanism toward the top of the lower succession. Overlying coarse volcanoclastic rocks of the upper succession were derived from ca. 2.73 Ga (Turek et al., 1989) porphyritic dacite and were likely deposited as subaqueous debris and grain flows proximal to an active volcanic

centre, perhaps on the north flank of the oceanic arc. Possible local correlatives include intermediate–felsic volcanoclastic rocks west of the Ross River pluton (i.e., the Independence Lake unit of Anderson, 2008) and at Black Island on Lake Winnipeg (i.e., the Black Island rhyolite of Bailes and Percival, 2005a).

ca. 2.73–2.71 Ga

The Gem assemblage conformably overlies the Bidou assemblage and is interpreted to mark the onset of extension and incipient rifting of the Bidou arc–back-arc complex during the waning stages of magmatism (Figure 103c; Bailes and Percival, 2005a), eventually leading to the development of an intra-arc basin of regional extent along the south margin of the NCT. Volcanic flows and primary volcanoclastic rocks, varying in composition from primitive basalt to high-SiO₂ rhyolite, were deposited between approximately 2.73 and 2.72 Ga in shallow-subaqueous to subaerial settings. The wide diversity in eruptive settings and styles, coupled with abrupt lateral and vertical facies changes, and the presence of high-SiO₂ rhyolite flows, indicate proximal deposition in a volcanic complex comprising multiple eruptive centres. Age-equivalent rocks at Rice Lake (i.e., the Rainy Lake Road, Townsite and Round Lake units of Anderson, 2008) and at Black Island on Lake Winnipeg (the Gray Point and Drumming Point sequences of Bailes and Percival, 2005a) were deposited in submarine settings and include geochemical analogues of rocks at the Gem Lake type locality. Associated epiclastic rocks either lack detrital zircons or are exclusively of Neoarchean provenance, suggesting deposition in sites remote from the NCT. At Rice Lake, extension and incipient rifting of the ‘Bidou’ volcanic arc is tightly constrained to ca. 2.725 Ga and was associated with deposition of exhalative base-metal sulphides in a restricted marine basin controlled by a synvolcanic growth fault (Anderson, 2008).

Intermediate–felsic volcanic rocks of the FI suite of the Gem assemblage are chemically similar to adakite formed by relatively deep partial melting of basaltic sources in supra-subduction settings. Broadly coeval (ca. 2.73–2.72 Ga) tonalite–granodiorite–granite plutons and hypabyssal porphyry intrusions of the Ross River plutonic suite and Wanipigow River plutonic complex exhibit similar geochemical attributes (Corfu and Stone, 1998; Anderson, 2008) and likely formed by similar processes. Rhyolitic rocks of the FII–FIII suite show evidence of a trend toward highly evolved compositions via late-stage fractionation and are comparable to felsic volcanic rocks in modern and ancient rifts, where high heat flows associated with upwelling basaltic magmas are thought to facilitate partial melting at shallow crustal depths. In keeping with the common association of FII–FIII-type rhyolite with volcanic-hosted massive-sulphide deposits (e.g., Leshner et al., 1986; Barrie et al., 1993; Lentz, 1998; Syme, 1998; Hart et al., 2004; Gaboury and Pearson, 2008), the widespread distribution of syngenetic alteration in the Gem assemblage indicates large-scale hydrothermal circulation during rifting and therefore good potential for exhalative base-metal sulphide deposits. Age-equivalent rocks along strike in Ontario include the Anderson formation of the Bee Lake belt (ca. 2.72 Ga; Rogers and McNicoll, unpublished, cited by Lemkow et al., 2006) and the St. Joseph assemblage (ca. 2.72–2.71 Ga; Stott and Corfu, 1991; Corfu

and Stott, 1993) of the Lake St. Joseph belt, the latter of which is interpreted to represent a continental- or marginal-arc setting (Stott and Corfu, 1991).

At Red Lake, penetrative regional deformation and main-stage Au mineralization are constrained between ca. 2.72 and 2.71 Ga (Dubé et al., 2004), indicating that orogenic activity was at least locally ongoing during the latest stages of arc volcanism (e.g., Sanborn-Barrie et al., 2001). Regional uplift and tilting of the ca. 2.725–2.715 Ga arc-rift succession at Rice Lake (Anderson, 2008), as indicated by the pronounced angular unconformity at the base of the synorogenic San Antonio assemblage ($<2705 \pm 5$ Ma; Percival et al., 2006a), may also have occurred during this time interval. Hence, synorogenic sedimentation and collisional orogenesis (see below) were likely preceded by a short-lived tectonic event, perhaps associated with accretion of the 2.75–2.72 Ga arc complex to the NCT margin.

ca. 2.71–2.69 Ga

This time interval is marked by the cessation of major arc volcanism in the Uchi domain, followed in rapid succession by renewed extension, major erosional denudation of the NCT, synorogenic sedimentation and the onset of regional thermotectonism related to terminal collision with the Winnipeg River Terrane. The latest arc volcanism in the Rice Lake belt is represented by hypabyssal rhyolite porphyry near the top of the arc-rift succession north of Rice Lake, which yielded an age of 2715 ± 2 Ma (Anderson, 2008). Synorogenic coarse-clastic sedimentary rocks unconformably overlie this porphyry and define a series of areally restricted fluvial-alluvial basins at the NCT-Uchi interface. Examples include the San Antonio assemblage at Rice Lake ($<2705 \pm 5$ Ma; Percival et al., 2006a) and the Hole River assemblage at Lake Winnipeg ($<2708 \pm 12$ Ma; Percival et al., 2006a). At least one margin of each basin is bounded by the crustal-scale Wanipigow fault. Also deposited during this time interval was the regionally extensive English River basin (<2.71 Ga; Corfu et al., 1995; Davis, 1996), which conformably onlaps the arc-rift succession along the south boundary of the Uchi domain.

Submarine turbiditic sedimentary rocks and basaltic flows of the Edmunds assemblage define the north margin of the English River basin (Figure 103d) and provide a key record of the complex geodynamic evolution of the region in the 2.71–2.69 Ga time interval. Distinctive lower and upper facies associations record deposition below wave base in a coarsening-upward (progradational) submarine fan. Major sedimentation was preceded by a brief period of depositional quiescence, as indicated by a locally thick basal unit of laminated mudstone. Distal greywacke-mudstone turbidite, polymictic conglomerate, massive quartz-lithic greywacke and turbiditic iron formation of the lower facies association (LFA) were deposited in a channelized lower- to mid-fan setting. Uranium-lead ages of detrital zircons in greywacke near the base of the LFA define a distribution profile that includes a prominent mode at ca. 2.74 Ga and subsidiary modes at 2.94 and 3.01 Ga, and indicates a maximum depositional age of ca. 2.71 Ga. Volcanic clasts in conglomerate are mostly representative of the underlying arc and arc-rift succession; however, the older detrital

zircon modes signal the first arrival of ‘exotic’ detritus, which was most likely sourced from the NCT (e.g., Davis, 1996).

Distribution profiles of detrital zircon U-Pb ages from fluvial-alluvial sedimentary rocks of the San Antonio and Hole River assemblages are similar to that of the LFA, consistent with the interpretation that they represent proximal facies of the same depositional system. The localization of the proximal facies of this system in fault-bounded basins at the NCT-Uchi interface (Figures 2, 103d) indicates an important tectonic control on basin subsidence, probably by reactivation of early accretionary faults or sutures. Along the south margin of the basin at the Rice Lake type locality, the San Antonio assemblage includes a ‘landslide facies’ (Weber, 1971c) tonalite-boulder conglomerate that perhaps indicates the presence of a basin-margin fault. Considered in the context of coeval uplift of the NCT margin and subsidence of the orogen-scale English River basin, extensional (as opposed to strike-slip; e.g., Corcoran and Mueller, 2007) fault reactivation is considered the most likely scenario and thus implicates a synorogenic phase of crustal extension, as has been proposed to explain the formation of ‘Timiskaming-type’ sedimentary basins in the Abitibi greenstone belt of Ontario (Bleeker, 2012).

Channel-fill polymictic conglomerate at the base of the upper facies association (UFA) contains abundant ‘exotic’ clasts and thus appears to signal a profound shift in sediment source and supply rate, likely related to a change in base level in response to regional uplift. Proximal greywacke-mudstone turbidites of the UFA were deposited after 2705 ± 2 Ma (Davis, 1996) in a channelized, upper-fan to feeder-channel setting. Detrital zircons in coarse quartz-lithic greywacke of the UFA include a prominent mode at ca. 3.0 Ga, with subsidiary modes at 2.93 and 2.73 Ga, thus defining a distinctly different distribution profile from that of the LFA. As suggested by the high abundance of tonalite and quartzite clasts in the UFA, much of the older detritus was likely sourced from tonalitic crust of the NCT (3.01–2.99 Ga; Whalen et al., 2003) or was recycled from its cover sequence (2.98–2.92 Ga; Davis, 1994; Percival et al., 2006a; Sasseville et al., 2006). Although the maximum depositional age of the UFA is the same as that documented for the San Antonio assemblage at Rice Lake ($<2705 \pm 5$ Ma; Percival et al., 2006a), the dominance of Mesoarchean detrital zircons indicates that it was likely deposited during a later stage of uplift, after the source area had become more deeply and extensively exhumed.

Thick units of very coarse dacitic volcanic conglomerate (deposited from debris flows) indicate erosional denudation of the adjacent volcanic arc and were accompanied by voluminous basalt flows, suggesting proximity to a basin-margin structure that served as a conduit for basaltic magmas and the venting of hydrothermal fluids to form iron formations. Coeval eruption of N-MORB-, E-MORB- and CAB-like basaltic lavas suggests an analogy to complex rift settings in Cenozoic back-arc basins (e.g., Hochstaedter et al., 1990; Gribble et al., 1998). Similar chemical diversity is apparent in basaltic flows of the St. Joseph assemblage (ca. 2.72–2.71 Ga; Stott and Corfu, 1991) of the Lake St. Joseph greenstone belt in Ontario, where it is attributed to variable degrees and depths of partial melting of metasomatized mantle wedge (Hollings and Kerrich, 2006).

Similarly diverse, though slightly older, geochemical suites also characterize the Confederation assemblage in the Birch-Uchi and Meen-Dempster greenstone belts in Ontario, and are likewise attributed to a back-arc eruptive setting (e.g., Hollings et al., 2000; Hollings and Kerrich, 2000).

In the Garner–Gem lakes area, the geochemical attributes of basaltic volcanism in the Edmunds assemblage are interpreted to reflect continued extension, perhaps due to slab roll-back, and a geodynamic evolution from incipient arc rift (Gem assemblage) to a more mature intra-arc basin (Figure 103d). Mantle upwelling in response to this extension and slab roll-back may account for rare sills of komatiitic basalt in the Edmunds assemblage. Pan et al. (1998) similarly proposed an extensional (back-arc) geodynamic setting for the English River basin, based on the depleted MORB-like compositions of amphibolite layers within the south margin at Werner Lake, Ontario. These authors noted a close association with ultramafic intrusions and Co–Cu–Au mineralization, the latter postulated to be of exhalative origin (Pan and Therens, 2000), and thus suggested an analogy to sites of active extension in continental-rift settings. The presence of ultramafic rocks along both margins of the English River basin is compatible with localized emplacement of mantle-derived melts during the earliest stages of sedimentation, and lends strong support to an extensional geodynamic scenario.

Taken together with the data reported by Davis (1996), new U–Pb data for detrital zircons in the Edmunds assemblage define three distinct age populations at 3.01–3.0 Ga, 2.94–2.93 Ga and 2.74–2.73 Ga. Although the detrital sources for both the LFA and UFA appear to have remained fairly constant, the proportion of older detritus increases upsection, consistent with progressive uplift and erosion of the NCT during continued extension. In Ontario, rocks correlative with the UFA contain tonalite boulders dated at 2703 ± 2 Ma and are intruded by the 2696 ± 3 – 2 Ma Wingiskis Lake pluton (Rogers and McNicoll, unpublished, cited by Lemkow et al., 2006). Farther south, the English River basin was intruded by a voluminous suite of calcalkalic tonalite–diorite–granodiorite plutons at 2698 Ma (Corfu et al., 1995), which constrains the latest stages of marine sedimentation to ca. 2.7 Ga and requires rapid burial to mid-crustal depths in the early stages of regional orogenesis.

ca. 2.69–2.64 Ga

Regional orogenesis, considered to be related to terminal collision of the North Caribou and Winnipeg River terranes (Figure 103e), is manifest in the Rice Lake belt as multiple generations of ductile and brittle-ductile deformation structures, formed under greenschist- to (local) amphibolite-facies metamorphic conditions. Most, if not all, penetrative ductile deformation postdates the Edmunds assemblage and must therefore have occurred after 2.7 Ga, the maximum depositional age of the UFA. Earlier structures, perhaps related to initial accretion of the arc–back-arc assemblages to the NCT margin, may well be present in the study area but could not be reliably identified due to an intense tectonic overprint. The earliest structures on both sides of the Beresford Lake shear zone are bedding-parallel foliations, the absolute and relative ages of which are unknown. Similar low-angle fabrics at Rice Lake were developed

during thrust imbrication of ca. 2.72 Ga arc-rift volcanic rocks and ca. 2.7 Ga synorogenic sedimentary rocks, and are interpreted to record crustal thickening in the earliest increments of collisional orogenesis (Anderson, 2008).

Regionally pervasive G_2 structures record sinistral-oblique (northeast-side-up) noncoaxial shearing, bulk flattening, sub-vertical stretching and development of upright, doubly plunging folds on a macroscopic scale. The structural geometry and kinematics indicate northeast–southwest shortening (present co-ordinates) within a broad zone of bulk sinistral transpression. Sinistral transpression is also recorded within the Wanipigow fault north of Rice Lake (Anderson, 2008). Metamorphic mineral assemblages indicate that this deformation was contemporaneous with peak greenschist- to amphibolite-facies metamorphism on both sides of the Beresford Lake shear zone, requiring significant burial, perhaps by overthrusting, prior to G_2 shortening. Overprinting relationships with shear-hosted quartz–carbonate veins indicate that the late increments of this transpressive deformation were coeval with Au mineralization along the Rice Lake mine trend (Anderson, 2011a, b) and a similar kinematic framework was proposed for auriferous vein systems southeast of the Ross River pluton (Brommecker, 1991, 1996). These deposits correspond to typical ‘greenstone’ or ‘orogenic’ Au deposits, which are thought to form during the clockwise P–T–t evolution of their host orogens from upward-migrating auriferous fluids generated by thermal equilibration of accreted sedimentary or volcanic rocks (e.g., Groves et al., 1998).

Regional constraints indicate that G_2 transpressive deformation was probably coeval with major orogenesis in the English River basin, which also involved penetrative, multi-phase, ductile deformation; high-T–low-P metamorphism; and the development of crustal-scale sinistral-oblique shear zones (e.g., Breaks, 1991; Corfu et al., 1995; Bethune et al., 2006). Regional orogenesis culminated at 2.69 Ga in the English River basin with local granulite-grade metamorphism, crustal anatexis and coeval emplacement of peraluminous granitoid plutons; widespread growth of metamorphic zircon, monazite and titanite continued to 2.68–2.66 Ga (Corfu et al., 1995). The very short time interval between sedimentation (<2705 Ma) and the orogenic peak (2691 Ma; Corfu et al., 1995) requires some combination of rapid crustal thickening, perhaps by internal imbrication (Corfu et al., 1995) or thick-skinned overthrusting by the NCT margin (Percival et al., 2006a), coupled with accelerated heat input from upwelling mantle, possibly in response to slab break-off (Corfu et al., 1995) or crustal extension (Pan et al., 1998; this report).

The G_3 and G_4 structures in the study area record a transition to a distinctly different kinematic frame, under conditions of waning temperature and pressure. An early episode of weak, north-northeast–south-southwest shortening (present co-ordinates) is recorded by the S_3 crenulation cleavage west of the Beresford Lake shear zone. Regionally developed G_4 structures are associated with a complex network of brittle-ductile shear zones that contain penetrative, greenschist-grade mylonitic foliations; shallowly plunging lineations; Z-asymmetric folds; and dextral kinematic indicators on horizontal outcrop surfaces. These fabrics are penetrative and pervasive within the

Wanipigow and Manigotagan faults, and their subsidiary structures, along both margins of the Rice Lake belt (Percival et al., 2006a; Sasseville et al., 2006; Anderson, 2008). The geometry and kinematics of these structures indicate northwest–southeast shortening (present co-ordinates) and are interpreted in the context of a progressive, partitioned, transcurrent-shear deformation in a regional regime of dextral transpression during the later stages of orogenesis. This style of retrograde deformation also characterizes both margins of the English River basin, where it is attributed to the strike-slip component of strongly partitioned dextral-transpressive deformation that took place between ca. 2.67 and 2.64 Ga (e.g., Bethune et al., 2006; Hrabí and Cruden, 2006; Duguet et al., 2009).

At Garner Lake, an estimate of the minimum age of the G_4 deformation is provided by metamorphic rutile (ca. 2665 Ma) in the post-tectonic diorite dike that cuts greenschist-facies mylonite of the Beresford Lake shear zone. This poorly constrained age corresponds to the waning stages of thermotectonism at the present level of exposure in the English River basin, as recorded by ‘post-tectonic’ granite at Black Lake, Manitoba (2663 \pm 7 Ma; Turek et al., 1989) and metamorphic titanite in amphibolite at Miniss Lake, Ontario (2662 \pm 2 Ma; Corfu et al., 1995). Widespread late-tectonic leucogranite plutons and pegmatite dikes in the English River basin and adjacent Bird River belt were mostly emplaced between 2.65 and 2.64 Ga (e.g., Larbi et al., 1999; Gilbert et al., 2008; Duguet et al., 2009) and appear to represent the youngest phase of Archean magmatism in the region. Granitic pegmatite dikes are not observed north of the Manigotagan fault, suggesting they predate the latest increments of faulting.

The latest deformation in the study area was associated with conjugate sets of northeast- or northwest-trending brittle faults (G_5 structures) that accommodated weak north–south shortening. Some of these faults are associated with extensive zones of intense silicification and quartz veining, and evidently served as conduits for the focused discharge of very large volumes of siliceous hydrothermal fluid, which may have been sourced from late-orogenic dehydration reactions at depth in the English River basin.

References

- Allen, R.L. 1988: False pyroclastic textures in altered silicic lavas, with implications for volcanic-associated mineralization; *Economic Geology*, v. 83, p. 1424–1446.
- Anderson, S.D. 2002: Preliminary report on the geology and structure of the Garner Lake area, southeast Rice Lake greenstone belt (NTS 52L14), Manitoba; *in* Report of Activities 2002, Manitoba Industry, Trade and Mines, Manitoba Geological Survey, p. 234–249.
- Anderson, S.D. 2003a: Geology and structure of the Garner Lake area, southeast Rice Lake greenstone belt, Manitoba (NTS 52L14); *in* Report of Activities 2003, Manitoba Industry, Economic Development and Mines, Manitoba Geological Survey, p. 178–195.
- Anderson, S.D. 2003b: Geology and structure of the Garner Lake area, southeast Rice Lake greenstone belt, Manitoba (part of NTS 52L14); Manitoba Industry, Economic Development and Mines, Manitoba Geological Survey, Preliminary Map PMAP2003-1, scale 1:20 000.
- Anderson, S.D. 2004: Preliminary results and economic significance of geological mapping and structural analysis in the Rice Lake area, central Rice Lake greenstone belt, Manitoba (NTS 52M4 and 52L13); *in* Report of Activities 2004, Manitoba Industry, Economic Development and Mines, Manitoba Geological Survey, p. 216–231.
- Anderson, S.D. 2005a: Geology and structure of the Rice Lake area, Rice Lake greenstone belt, Manitoba (part of NTS 52M04 and 52L13); Manitoba Industry, Economic Development and Mines, Manitoba Geological Survey, Preliminary Map PMAP2005-1, scale 1:20 000.
- Anderson, S.D. 2005b: Preliminary results and economic significance of geological mapping in the Gem Lake area, southeastern Rice Lake belt, Manitoba (NTS 52L11 and 14), with emphasis on the Neoproterozoic Gem assemblage; *in* Report of Activities 2005, Manitoba Industry, Economic Development and Mines, Manitoba Geological Survey, p. 104–116.
- Anderson, S.D. 2006a: Geology and structure of the Garner–Gem lakes area, Rice Lake greenstone belt, Manitoba (NTS 52L11 and 14); Manitoba Science, Technology, Energy and Mines, Manitoba Geological Survey, Preliminary Map PMAP2006-7, scale 1:20 000.
- Anderson, S.D. 2006b: Update and economic significance of geological mapping in the Garner–Gem lakes area, Rice Lake greenstone belt, southeastern Manitoba (NTS 52L11 and 14); *in* Report of Activities 2006, Manitoba Science, Technology, Energy and Mines, Manitoba Geological Survey, p. 155–169.
- Anderson, S.D. 2007: Stratigraphic and structural setting of gold mineralization in the Lily Lake area, Rice Lake greenstone belt, Manitoba (NTS 52L11, 14); *in* Report of Activities 2007, Manitoba Science, Technology, Energy and Mines, Manitoba Geological Survey, p. 114–128.
- Anderson, S.D. 2008: Geology of the Rice Lake area, Rice Lake greenstone belt, southeastern Manitoba (parts of NTS 52L13, 52M4); Manitoba Science, Technology, Energy and Mines, Manitoba Geological Survey, Geoscientific Report GR2008-1, 97 p.
- Anderson, S.D. 2011a: Detailed geological mapping of the Rice Lake mine trend, southeastern Manitoba (part of NTS 52M4): stratigraphic setting of gold mineralization; *in* Report of Activities 2011, Manitoba Innovation, Energy and Mines, Manitoba Geological Survey, p. 94–110.
- Anderson, S.D. 2011b: Detailed geological mapping of the Rice Lake mine trend, southeastern Manitoba (part of NTS 52M4): structural geology of hostrocks and auriferous quartz-vein systems; *in* Report of Activities 2011, Manitoba Innovation, Energy and Mines, Manitoba Geological Survey, p. 111–126.
- Ayres, L.D. and Peloquin, A.S. 2000: Subaqueous, Paleoproterozoic, metarhyolite dome-flow-cone complex, Flin Flon greenstone belt, Manitoba, Canada; *Precambrian Research*, v. 101, p. 211–235.
- Bachmann, O. and Bergantz, G.W. 2008: Rhyolites and their source mushes across tectonic settings; *Journal of Petrology*, v. 49, p. 2277–2285.
- Bailes, A.H. 1998: Geochemical sampling of the Bidou Lake subgroup of the Rice Lake greenstone belt; *in* Report of Activities 1998, Manitoba Energy and Mines, Geological Services, p. 144–150.
- Bailes, A.H. and Percival, J.A. 2000: Geology and structure of the North Caribou Terrane–Uchi Subprovince boundary in eastern Manitoba, with emphasis on volcanic and volcanoclastic rocks of the Black Island assemblage; *in* Report of Activities 2000, Manitoba Industry, Trade and Mines, Manitoba Geological Survey, p. 161–174.

- Bailes, A.H. and Percival, J.A. 2005a: Geology of the Black Island area, Lake Winnipeg, Manitoba (parts of NTS 62P1, 7 and 8); Manitoba Industry, Economic Development and Mines, Manitoba Geological Survey, Geoscientific Report GR2005-2, 33 p.
- Bailes, A.H. and Percival, J.A. 2005b: Litho-geochemical and lithological data, Sm-Nd isotopic data and geochronological data for the Black Island area, Lake Winnipeg, Manitoba (parts of NTS 62P1, 7 and 8) and the Rice Lake greenstone belt (parts of NTS 62P, 52M and 52L); Manitoba Industry, Economic Development and Mines, Manitoba Geological Survey, Data Repository Item DRI2005004, Microsoft® Excel® file, URL <<http://www.gov.mb.ca/stem/mrd/info/libmin/DRI2005004.xls>> [April 4, 2013].
- Bailes, A.H., Percival, J.A., Corkery, M.T., McNicoll, V.J., Tomlinson, K.Y., Sasseville, C., Rogers, N., Whalen, J.B. and Stone, D. 2003: Geology and tectonostratigraphic assemblages, West Uchi map area, Manitoba and Ontario; Manitoba Geological Survey, Open File OF2003-1, 1:250 000 scale with marginal notes.
- Barrett, T.J. and Fralick, P.W. 1989: Turbidites and iron formations, Beardmore-Geraldton, Ontario: application of a combined ramp/fan model to Archaean clastic and chemical sedimentation; *Sedimentology*, v. 36, p. 221–234.
- Barrie, C.T., Ludden, J.M. and Green, T.H. 1993: Geochemistry of volcanic rocks associated with Cu-Zn and Ni-Cu deposits in the Abitibi Subprovince; *Economic Geology*, v. 88, p. 1341–1358.
- Bau, M. 1991: Rare-earth element mobility during hydrothermal and metamorphic fluid-rock interaction and the significance of the oxidation state of europium; *Chemical Geology*, v. 93, p. 219–230.
- Bau, M. 1996: Controls on the fractionation of isovalent trace elements in magmatic and aqueous systems: evidence from Y/Ho, Zr/Hf, and lanthanide tetrad effect; *Contributions to Mineralogy and Petrology*, v. 123, p. 323–333.
- Bau, M. 1997: The lanthanide tetrad effect in highly evolved felsic igneous rocks—a reply to the comment by Y. Pan; *Contributions to Mineralogy and Petrology*, v. 128, p. 409–412.
- Bédard, J.H., Brouillette, P., Madore, L. and Berclaz, A. 2003: Archaean cratonization and deformation in the northern Superior Province, Canada: an evaluation of plate tectonic versus vertical tectonic models; *Precambrian Research*, v. 127, p. 61–87.
- Bédard, J.H., Harris, L.B. and Thurston, P.C. 2013: The hunting of the snArc; *Precambrian Research*, v. 229, p. 20–48.
- Bethune, K.M., Helmstaedt, H.H. and McNicoll, V.J. 2006: Structural analysis of the Miniss River and related faults, western Superior Province: post-collisional displacement initiated at terrane boundaries; *Canadian Journal of Earth Sciences*, v. 43, p. 1031–1054.
- Blackburn, C.E. 1980: Towards a mobilist tectonic model for part of the Archaean of northwestern Ontario; *Geoscience Canada*, v. 7, p. 64–72.
- Bleeker, W. 2012: Targeted Geoscience Initiative 4. Lode gold deposits in ancient deformed and metamorphosed terranes: the role of extension in the formation of Timiskaming basins and large gold deposits, Abitibi greenstone belt—a discussion; in Ontario Geological Survey, Summary of Field Work and Other Activities 2012, Open File Report 6280, p. 47-1–47-12.
- Bleeker, W., Ketchum, J.W.F., Jackson, V.A. and Villeneuve, M.E. 1999: The Central Slave Basement Complex, part I: its structural topology and autochthonous cover; *Canadian Journal of Earth Sciences*, v. 36, p. 1083–1109.
- Breaks, F.W. 1991: English River Subprovince; in *Geology of Ontario*, P.C. Thurston, H.R. Williams, R.H. Sutcliffe and G.M. Stott (ed.), Ontario Geological Survey, Special Volume 4, Part 1, p. 239–277.
- Brommecker, R. 1991: The structural setting of gold occurrences in the southeast Rice Lake greenstone belt, southeast Manitoba; M.Sc. thesis, Queen's University, Kingston, Ontario, 267 p.
- Brommecker, R. 1996: Geology of the Beresford Lake area, southeast Manitoba; Geological Survey of Canada, Open File 3318, 127 p.
- Brommecker, R., Poulsen, K.H. and Hodgson, C.J. 1989: Preliminary report on the structural setting of gold at the Gunnar mine in the Beresford Lake area, Uchi Subprovince, southeastern Manitoba; in *Current Research, Part C*, Geological Survey of Canada, Paper 89-1C, p. 325–332.
- Brommecker, R., Scoates, R.F.J. and Poulsen, K.H. 1993: Komatiites in the Garner Lake–Beresford Lake area: implications for tectonics and gold metallogeny of the Rice Lake greenstone belt, southeast Manitoba; in *Current Research, Part C*, Geological Survey of Canada, Paper 93-1C, p. 259–264.
- Brown, M. 2006: Duality of thermal regimes is the distinctive characteristic of plate tectonics since the Neoproterozoic; *Geology*, v. 34, p. 961–964.
- Burwash, E.M. 1923: Geology of Ontario–Manitoba boundary, Winnipeg River to Bloodvein River, 1921; Ontario Department of Mines, Annual Report, v. 32, pt. 2, p. 1–48.
- Cabanis, B. and Lecolle, M. 1989: Le diagramme La/10–Y/15–Nb/8: un outil pour la discrimination des séries volcaniques et la mise en évidence des processus de mélange et/ou de contamination crustale; *Comptes Rendus de l'Académie des Sciences*, v. 309, p. 2023–2029.
- Campbell, F.H.A. 1971: Stratigraphy and sedimentation of part of the Rice Lake Group, Manitoba; in *Geology and Geophysics of the Rice Lake Region, Southeastern Manitoba (Project Pioneer)*, W.D. McRitchie and W. Weber (ed.), Manitoba Department of Mines and Natural Resources, Mines Branch, Publication 71-1, p. 135–188.
- Campbell, I.H., Griffiths, R.W. and Hill, R.I. 1989: Melting in an Archaean mantle plume; heads it's basalts, tails it's komatiites; *Nature*, v. 339, p. 697–699.
- Campbell, I.H., Leshner, C.M., Coad, P., Franklin, J.M., Gorton, M.P. and Thurston, P.C. 1984: Rare-earth element mobility in alteration pipes below massive Cu-Zn-sulfide deposits; *Chemical Geology*, v. 45, p. 181–202.
- Card, K.D. 1990: A review of the Superior Province of the Canadian Shield, a product of Archean accretion; *Precambrian Research*, v. 48, p. 99–156.
- Card, K.D. and Ciesielski, A. 1986: Subdivisions of the Superior Province of the Canadian Shield; *Geoscience Canada*, v. 13, p. 5–13.
- Carpenter, R.L. and Duke, N.A. 2004: Geological setting of the West Meliadine gold deposits, western Churchill Province, Nunavut, Canada; *Exploration and Mining Geology*, v. 13, p. 49–65.
- Cas, R.A.F. and Wright, J.V. 1987: Volcanic successions, modern and ancient: a geological approach to processes, products and successions; Unwin Hyman Ltd., London, United Kingdom, 528 p.
- Castillo, P.R., Janney, P.E. and Solidum, R.U. 1999: Petrology and geochemistry of Camiguin Island, southern Philippines: insights to the source of adakites and other lavas in a complex arc setting; *Contributions to Mineralogy and Petrology*, v. 134, p. 33–51.
- Cawood, P.A., Kröner, A. and Pisarevsky, S. 2006: Precambrian plate tectonics: criteria and evidence; *GSA Today*, v. 16, p. 4–11.
- Chardon, D., Choukroune, P. and Jayananda, M. 1998: Sinking of the Dharwar Basin (South India): implications for Archaean tectonics; *Precambrian Research*, v. 91, p. 15–39.
- Chiaradia, M., Müntener, O., Beate, B. and Fontignie, D. 2009: Adakite-like volcanism of Ecuador: lower crust magmatic evolution and recycling; *Contributions to Mineralogy and Petrology*, v. 158, p. 563–588.
- Colvine, A.C., Fyon, J.A., Heather, K.B., Marmont, S., Smith, P.M. and Troop, D.G. 1988: Archean lode gold deposits in Ontario: Part I. A depositional model; Part II. A genetic model; Ontario Geological Survey, Miscellaneous Paper 139, 136 p.
- Condie, K.C. and Pease, V. 2008: When did plate tectonics begin on planet Earth?; K.C. Condie and V. Pease (ed.), Geological Society of America, Special Paper 440, 294 p.

- Corcoran, P.L. and Mueller, W.U. 2007: Time-transgressive Archean unconformities underlying molasse basin-fill successions of dissected oceanic arcs, Superior Province, Canada; *The Journal of Geology*, v. 115, p. 655–674.
- Corfu, F. and Stone, D. 1998: Age structure and orogenic significance of the Berens River composite batholiths, western Superior Province; *Canadian Journal of Earth Sciences*, v. 35, p. 1089–1109.
- Corfu, F. and Stott, G.M. 1993: U-Pb geochronology of the central Uchi Subprovince, Superior Province; *Canadian Journal of Earth Sciences*, v. 30, p. 1179–1196.
- Corfu, F., Davis, D.W., Stone, D. and Moore, M.L. 1998: Chronostratigraphic constraints on the genesis of Archean greenstone belts, northwestern Superior Province, Ontario, Canada; *Precambrian Research*, v. 92, p. 277–295.
- Corfu, F., Stott, G.M. and Breaks, F.W. 1995: U-Pb geochronology and evolution of the English River Subprovince, an Archean low P–high T metasedimentary belt in the Superior Province; *Tectonics*, v. 14, p. 1220–1233.
- Corkery, M.T. 1995: Geologic mapping in the Garner Lake–Beresford Lake area of the Rice Lake greenstone belt; *in* Report of Activities 1995, Manitoba Energy and Mines, Geological Services, p. 136–139.
- Corkery, M.T. 1999: Reassessment of major geologic boundaries in the southeast Rice Lake greenstone belt; *in* Report of Activities 1999, Manitoba Industry, Trade and Mines, Geological Services, p. 111–113.
- Cox, S.F. 2005: Coupling between deformation, fluid pressures, and fluid flow in ore-producing hydrothermal systems at depth in the crust; *Economic Geology*, 100th Anniversary Volume, p. 39–75.
- Davidson, J., Turner, S., Handley, H., Macpherson, C. and Dosseto, A. 2007: Amphibole “sponge” in arc crust?; *Geology*, v. 35, p. 787–790.
- Davis, D.W. 1994: Report on the geochronology of rocks from the Rice Lake belt, Manitoba; Royal Ontario Museum, Geology Department, Toronto, Ontario, unpublished report.
- Davis, D.W. 1996: Provenance and depositional age constraints on sedimentation in the Western Superior Transect area from U-Pb ages of zircons; *in* LITHOPROBE Western Superior Transect, Second Annual Workshop, R.M. Harrap and H. Helmstaedt (ed.), LITHOPROBE Secretariat, University of British Columbia, LITHOPROBE Report 53, p. 18–23.
- Davis, D.W. 1998: Speculations on the formation and crustal structure of the Superior Province from U-Pb geochronology; *in* Western Superior LITHOPROBE Transect, Fourth Annual Workshop, R.M. Harrap and H.H. Helmstaedt (ed.), LITHOPROBE Secretariat, University of British Columbia, LITHOPROBE Report 65, p. 21–28.
- Defant, M.J. and Drummond, M.S. 1990: Derivation of some modern arc magmas by melting of young subducted lithosphere; *Nature*, v. 347, p. 662–665.
- De Lury, J.S. 1927: The mineral resources of southeastern Manitoba, Rice Lake District, Oiseau River District, Boundary District; Industrial Development Board of Manitoba, Winnipeg, Manitoba, 55 p.
- DePaolo, D.J. 1981: Neodymium isotopes in the Colorado Front Range and crust-mantle evolution in the Proterozoic; *Nature*, v. 291, p. 193–196.
- de Rosen-Spence, A.F., Provost, G., Dimroth, E., Gochner, K. and Owen, V. 1980: Archean subaqueous felsic flows, Rouyn-Noranda, Quebec, Canada, and their Quaternary equivalents; *Precambrian Research*, v. 12, p. 43–77.
- de Wit, M.J. 1998: On Archean granites, greenstones, cratons and tectonics: does the evidence demand a verdict?; *Precambrian Research*, v. 91, p. 181–226.
- Dilek, Y. and Furnes, H. 2011: Ophiolite genesis and global tectonics: geochemical and tectonic fingerprinting of ancient oceanic lithosphere; *Geological Society of America Bulletin*, v. 123, p. 387–411.
- Dostal, J. and Mueller, W.U. 1997: Komatiite flooding of a rifted Archean rhyolitic arc complex: geochemical signature and tectonic significance of the Stoughton-Roquemaure Group, Abitibi greenstone belt, Canada; *Journal of Geology*, v. 105, p. 545–563.
- Dowling, D.B. 1900: Report on the east shore of Lake Winnipeg and adjacent parts of Manitoba and Keewatin, from notes and surveys by J. Burr Tyrrell; Geological Survey of Canada, Annual Report, Volume XI, 1898, Report G, p. 1G–98G.
- Dubé, B., Williamson, K., McNicoll, V., Malo, M., Skulski, T., Twomey, T. and Sanborn-Barrie, M. 2004: Timing of gold mineralization at Red lake, northwestern Ontario, Canada: new constraints from U-Pb geochronology at the Goldcorp high-grade zone, Red Lake mine, and the Madsen mine; *Economic Geology*, v. 99, p. 1611–1641.
- Duguet, M., Lin, S., Davis, D.W., Corkery, M.T. and McDonald, J. 2009: Long-lived transpression in the Archean Bird River greenstone belt, western Superior Province, southeastern Manitoba; *Precambrian Research*, v. 174, p. 381–407.
- Eckstrand, O.R. and Hulbert, L.J. 2007: Magmatic nickel-copper-platinum group element deposits; *in* Mineral Deposits of Canada: A Synthesis of Major Deposit Types, District Metallogeny, the Evolution of Geological Provinces, and Exploration Methods; W.D. Goodfellow (ed.), Geological Association of Canada, Mineral Deposits Division, Special Publication 5, p. 205–222.
- Eichelberger, J.C., Izbekov, P.E. and Browne, B.L. 2006: Bulk chemical trends at arc volcanoes are not liquid lines of descent; *Lithos*, v. 87, p. 135–154.
- Ermanovics, I.F. and Wanless, R.K. 1983: Isotopic age studies and tectonic interpretation of Superior Province in Manitoba; Geological Survey of Canada, Paper 82-12, 22 p.
- Ewart, A., Bryan, W.B., Chappell, B.W. and Rudnick, R.L. 1994: Regional geochemistry of the Lau-Tonga arc and back-arc systems; *Proceedings of the Ocean Drilling Program, Scientific Results*, v. 135, p. 385–425.
- Falloon, T.J., Malahoff, A., Zonenshaina, L.P. and Bogdanova, Y. 1992: Petrology and geochemistry of back-arc basin basalts from Lau Basin spreading ridges at 15°, 18° and 19°S; *Mineralogy and Petrology*, v. 47, p. 1–35.
- Fisher, R.V. 1966: Rocks composed of volcanic fragments and their classification; *Earth-Science Reviews*, v. 1, p. 287–298.
- Franklin, J.M. 1996: Volcanic-associated massive sulphide base metals; *in* Geology of Canadian Mineral Deposit Types; O.R. Eckstrand, W.D. Sinclair and R.I. Thorpe (ed.), Geological Survey of Canada, Geology of Canada, no. 8, p. 158–183.
- Fretzdorff, S., Livermore, R.A., Devey, C.W., Leat, P.T. and Stoffers, P. 2002: Petrogenesis of the back-arc East Scotia Ridge, South Atlantic Ocean; *Journal of Petrology*, v. 43, p. 1435–1467.
- Furnes, H., de Wit, M., Staudigel, H., Rosing, M. and Muehlenbachs, K. 2007: A vestige of Earth’s oldest ophiolite; *Science*, v. 315, p. 1704–1707.
- Gaboury, D. and Pearson, V. 2008: Rhyolite geochemical signatures and association with volcanogenic massive sulphide deposits: examples from the Abitibi Belt, Canada; *Economic Geology*, v. 103, p. 1531–1562.
- Galley, A.G., Hannington, M.D. and Jonasson, I.R. 2007: Volcanogenic massive sulphide deposits; *in* Mineral Deposits of Canada: A Synthesis of Major Deposit Types, District Metallogeny, the Evolution of Geological Provinces, and Exploration Methods; W.D. Goodfellow (ed.), Geological Association of Canada, Mineral Deposits Division, Special Publication 5, p. 141–161.
- Garrison, J.M. and Davidson, J.P. 2003: Dubious case for slab melting in the Northern volcanic zone of the Andes; *Geology*, v. 31, p. 565–568.

- Geist, D., Howard, K.A. and Larson, P. 1995: The generation of oceanic rhyolites by crystal fractionation: the basalt-rhyolite association at Volcán Alcedo, Galápagos Archipelago; *Journal of Petrology*, v. 36, p. 965–982.
- Gibson, H.L., Morton, R.L. and Hudak, G.J. 1999: Submarine volcanic processes, deposits, and environments favourable for the location of volcanic-associated massive sulphide deposits; *in* Volcanic Associated Massive Sulphide Deposits: Processes and Examples in Modern and Ancient Settings; C.T. Barrie and M.D. Hannington (ed.), *Reviews in Economic Geology*, v. 8, p. 13–51.
- Gilbert, G. 1927: Gammon River area and Rickaby Lake schist belt, District of Kenora (Patricia Portion); Ontario Department of Mines, Annual Report, v. 36, pt. 3, p. 73–84.
- Gilbert, H.P., Davis, D.W., Duguet, M., Kremer, P.D., Mealin, C.A. and MacDonald, J. 2008: Geology of the Bird River Belt, south-eastern Manitoba (parts of NTS 52L5, 6); Manitoba Science, Technology, Energy and Mines, Manitoba Geological Survey, Geoscientific Map MAP2008-1, scale 1:50 000 (plus notes and appendix).
- Goldstein, S.L., O’Nions, R.K. and Hamilton, P.J. 1984: A Sm-Nd study of atmospheric dusts and particulates from major river systems; *Earth and Planetary Science Letters*, v. 70, p. 221–236.
- Gribble, R.F., Stern, R.J., Newman, S., Bloomer, S.H. and O’Hearn, T. 1998: Chemical and isotopic composition of lavas from the northern Mariana Trough: implications for magma genesis in back-arc basins; *Journal of Petrology*, v. 39, p. 125–154.
- Groves, D.I., Goldfarb, R.J., Gebre-Mariam, M., Hagemann, S.G. and Robert, F. 1998: Orogenic gold deposits: a proposed classification in the context of their crustal distribution and relationship to other gold deposit types; *Ore Geology Reviews*, v. 13, p. 7–27.
- Hagemann, S.G. and Cassidy, K.F. 2000: Archean orogenic lode gold deposits; *Society of Economic Geology Reviews*, v. 13, p. 9–68.
- Hamilton, W.B. 1988: Plate tectonics and island arcs; *Geological Society of America Bulletin*, v. 100, p. 1503–1527.
- Hamilton, W.B. 1998: Archean magmatism and deformation were not products of plate tectonics; *Precambrian Research*, v. 91, p. 143–179.
- Hamilton, W.B. 2003: An alternative Earth; *GSA Today*, v. 13, no. 11, p. 4–12.
- Hamilton, W.B. 2007: Earth’s first two billion years—the era of internally mobile crust; *in* 4-D Framework of Continental Crust, R.D. Hatcher, Jr., M.P. Carlson, J.H. McBride and J.R. Martínez Catalán (ed.), *Geological Society of America, Memoir* 200, p. 233–296.
- Hart, T.R., Gibson, H.L. and Lesher, C.M. 2004: Trace element geochemistry and petrogenesis of felsic volcanic rocks associated with volcanogenic massive Cu-Zn-Pb sulfide deposits; *Economic Geology*, v. 99, p. 1003–1013.
- Hartlaub, R.P., Heaman, L.M., Ashton, K.E. and Chacko, T. 2004: The Archean Murmac Bay Group: evidence for a giant Archean rift in the Rae Province, Canada; *Precambrian Research*, v. 131, p. 345–372.
- Hawkesworth, C.J., Gallagher, K., Hergt, J.M. and McDermott, F. 1993: Mantle and slab contributions in arc magmas; *Annual Review of Earth and Planetary Sciences*, v. 21, p. 175–204.
- Heaman, L.M., Erdmer, E. and Owen, J.V. 2002: U-Pb geochronologic constraints on the crustal evolution of the Long Range Inlier, Newfoundland; *Canadian Journal of Earth Sciences*, v. 39, p. 845–865.
- Henry, P., Stevenson, R.K. and Gariépy, C. 1998: Late Archean mantle composition and crustal growth in the western Superior Province of Canada: neodymium and lead isotopic evidence from the Wawa, Quetico, and Wabigoon subprovinces; *Geochimica et Cosmochimica Acta*, v. 62, p. 143–157.
- Henry, P., Stevenson, R.K., Larbi, Y. and Gariépy, C. 2000: Nd isotopic evidence for Early to Late Archean (3.4–2.7 Ga) crustal growth in the western Superior Province (Ontario, Canada); *Tectonophysics*, v. 322, p. 135–151.
- Hildreth, W. and Moorbath, S. 1988: Crustal contributions to arc magmatism in the Andes of central Chile; *Contributions to Mineralogy and Petrology*, v. 98, p. 455–489.
- Hochstaedter, A.G., Gill, J.B. and Morris, J.D. 1990: Volcanism in the Sumisu Rift, II. Subduction and non-subduction related components; *Earth and Planetary Science Letters*, v. 100, p. 195–209.
- Hodgson, C.J. 1993: Mesothermal lode-gold deposits; *in* Mineral Deposit Modelling, R.V. Kirkham, W.D. Sinclair, R.I. Thorpe and J.M. Duke (ed.), *Geological Association of Canada, Special Paper* 40, p. 635–678.
- Hoffman, P.F. 1989: Precambrian geology and tectonic history of North America; *in* The Geology of North America—an overview, A.W. Bally and A.R. Palmer (ed.), *Geological Society of America, The Geology of North America*, v. A, p. 447–512.
- Hollings, P. and Kerrich, R. 2000: An Archean arc basalt–Nb-enriched basalt–adakite association: the 2.7 Ga Confederation assemblage of the Birch-Uchi greenstone belt, Superior Province; *Contributions to Mineralogy and Petrology*, v. 139, p. 208–226.
- Hollings, P. and Kerrich, R. 2006: Light rare earth element depleted to enriched basaltic flows from 2.8 to 2.7 Ga greenstone belts of the Uchi Subprovince, Ontario, Canada; *Chemical Geology*, v. 227, p. 133–153.
- Hollings, P., Stott, G. and Wyman, D. 2000: Trace element geochemistry of the Meen-Dempster greenstone belt, Uchi subprovince, Superior Province, Canada: back-arc development on the margins of an Archean protocontinent; *Canadian Journal of Earth Sciences*, v. 37, p. 1021–1038.
- Hollings, P., Wyman, D. and Kerrich, R. 1999: Komatiite-basalt-rhyolite volcanic associations in northern Superior Province greenstone belts: significance of plume-arc interaction in the generation of the proto continental Superior Province; *Lithos*, v. 46, p. 137–161.
- Hrabi, R.B. and Cruden, A.R. 2006: Structure of the Archean English River Subprovince: implications for the tectonic evolution of the western Superior Province, Canada; *Canadian Journal of Earth Sciences*, v. 43, p. 947–966.
- Hunter, A.G. 1998: Intracrustal controls on the coexistence of tholeiitic and calc-alkaline magma series at Aso volcano, SW Japan; *Journal of Petrology*, v. 39, p. 1255–1284.
- Hunter, M.A., Bickle, M.J., Nisbet, E.G., Martin, A. and Chapman, H.J. 1998: Continental extensional setting for the Archean Belingwe Greenstone Belt, Zimbabwe; *Geology*, v. 26, p. 883–886.
- Irber, W. 1999: The lanthanide tetrad effect and its correlation with K/Rb, Eu/Eu*, Sr/Eu, Y/Ho and Zr/Hf of evolving peraluminous granite suites; *Geochimica et Cosmochimica Acta*, v. 63, p. 489–508.
- Jacobsen, S.B. 1980: Sm-Nd isotopic evolution of chondrites; *Earth and Planetary Science Letters*, v. 50, p. 139–155.
- Jahn, B., Wu, F., Capdevila, R., Martineau, F., Zhao, Z. and Wang, Y. 2001: Highly evolved juvenile granites with tetrad REE patterns: the Woduhe and Baerzhe granites from the Great Xing’an Mountains in NE China; *Lithos*, v. 59, p. 171–198.
- Jensen, L.S. 1976: A new cation plot for classifying subalkaline volcanic rocks; Ontario Geological Survey, Miscellaneous Paper 66, 22 p.
- Jicha, B.R., Hart, G.L., Johnson, C.M., Hildreth, W., Beard, B.L., Shirey, S.B. and Valley, J.W. 2009: Isotopic and trace element constraints on the petrogenesis of lavas from the Mount Adams volcanic field, Washington; *Contributions to Mineralogy and Petrology*, v. 157, p. 189–207.
- Kelemen, P.B., Johnson, K.T.M., Kinzler, R.J. and Irving, A.J. 1990: High-field-strength element depletions in arc basalts due to mantle-magma interaction; *Nature*, v. 345, p. 521–524.
- Kerrich, R. and Cassidy, K.F. 1994: Temporal relationships of lode gold mineralization to accretion, magmatism, metamorphism and deformation — Archean to present: a review; *Ore Geology Reviews*, v. 9, p. 263–310.

- Kerrick, R. and Wyman, D. 1990: Geodynamic setting of mesothermal gold deposits: an association with accretionary tectonic regimes; *Geology*, v. 18, p. 882–885.
- Kerrick, R. and Polat, A. 2006: Archean greenstone-tonalite duality: thermochemical mantle convection models or plate tectonics in the early Earth global dynamics?; *Tectonophysics*, v. 415, p. 141–165.
- Kerswill, J.A. 1996: Iron-formation-hosted stratabound gold; in O.R. Eckstrand, W.D. Sinclair and R.I. Thorpe (ed.), *Geology of Canadian Mineral Deposit Types*, Geological Survey of Canada, *Geology of Canada*, no. 8, p. 367–382.
- Krogh, T.E., Ermanovics, I.F. and Davis, G.L. 1974: Two episodes of metamorphism and deformation in the Archean rocks of the Canadian Shield; *Carnegie Institution of Washington, Geophysical Laboratory Yearbook*, 1974, v. 73, p. 573–575.
- Kuiper, Y.D., Lin, S. and Jiang, D. 2011: Deformation partitioning in transpressional shear zones with an along-strike stretch component: an example from the Superior Boundary Zone, Manitoba, Canada; *Journal of Structural Geology*, v. 33, p. 192–202.
- Lafrance, B., DeWolfe, J.C. and Stott, G.M. 2004: A structural reappraisal of the Beardmore-Geraldton Belt at the southern boundary of the Wabigoon Subprovince, Ontario, and implications for gold mineralization; *Canadian Journal of Earth Sciences*, v. 41, p. 217–235.
- Lafrance, B., Mueller, W.U., Daigneault, R. and Dupras, N. 2000: Evolution of a submerged composite arc volcano: volcanology and geochemistry of the Normétal volcanic complex, Abitibi greenstone belt, Québec, Canada; *Precambrian Research*, v. 101, p. 277–311.
- Langford, F.F. and Morin, J.A. 1976: The development of the Superior Province of northwestern Ontario by merging island arcs; *American Journal of Science*, v. 276, p. 1023–1034.
- Larbi, Y., Stevenson, R., Breaks, F., Machado, N. and Gariépy, C. 1999: Age and isotopic composition of late Archean leucogranites: implications for continental collision in the western Superior Province; *Canadian Journal of Earth Sciences*, v. 36, p. 495–510.
- Le Bas, M.J., Le Maitre, R.W., Streckeisen, A. and Zanettin, B. 1986: A chemical classification of volcanic rocks based on the total alkali-silica diagram; *Journal of Petrology*, v. 27, p. 745–750.
- Lemkow, D.R., Sanborn-Barrie, M., Bailes, A.H., Percival, J.A., Rogers, N., Skulski, T., Anderson, S.D., Tomlinson, K.Y., McNicoll, V., Parker, J.R., Whalen, J.B., Hollings, P. and Young, M. 2006: GIS compilation of geology and tectonostratigraphic assemblages, western Uchi Subprovince, western Superior Province, Ontario and Manitoba; *Manitoba Geological Survey, Open File OF2006-30*, CD-ROM.
- Lentz, D.R. 1998: Petrogenetic evolution of felsic volcanic sequences associated with Phanerozoic volcanic-hosted massive sulphide systems: the role of extensional geodynamics; *Ore Geology Reviews*, v. 12, p. 289–327.
- Leshner, C.M., Burnham, O.M., Keays, R.R., Barnes, S.J. and Hulbert, L. 2001: Trace-element geochemistry and petrogenesis of barren and ore-associated komatiites; *The Canadian Mineralogist*, v. 39, p. 673–696.
- Leshner, C.M., Goodwin, A.M., Campbell, I.H. and Gorton, M.P. 1986: Trace-element geochemistry of ore-associated and barren, felsic metavolcanic rocks in the Superior Province, Canada; *Canadian Journal of Earth Sciences*, v. 23, p. 222–237.
- Lin, S. 2005: Synchronous vertical and horizontal tectonism in the Neoproterozoic: kinematic evidence from a synclinal keel in the northwestern Superior craton, Canada; *Precambrian Research*, v. 139, p. 181–194.
- Ludwig, K.R. 2003: *Isoplot 3.00: a geochronological toolkit for Microsoft® Excel®*; Berkeley Geochronological Center, Special Publication 4, 71 p.
- Macpherson, C.G., Dreher, S.T. and Thirlwall, M.F. 2006: Adakites without slab melting: high pressure differentiation of island arc magma, Mindanao, the Philippines; *Earth and Planetary Science Letters*, v. 243, p. 581–593.
- Marshall, J.R. 1918: Gold-bearing district of southeastern Manitoba; *Geological Survey of Canada, Summary Report*, 1917, Part D, p. 17–21.
- Martin, H. 1999: Adakitic magmas: modern analogues of Archean granitoids; *Lithos*, v. 46, p. 411–429.
- Martin, H., Smithies, R.H., Rapp, R., Moyen, J-F. and Champion, D. 2005: An overview of adakite, tonalite-trondhjemite-granodiorite (TTG), and sanukitoid: relationships and some implications for crustal evolution; *Lithos*, v. 79, p. 1–24.
- Mattinson, J.M. 2005: Zircon U-Pb chemical abrasion ('CA-TIMS') method: combined annealing and multi-step partial dissolution analysis for improved precision and accuracy of zircon ages; *Chemical Geology*, v. 220, p. 47–66.
- McBirney, A.R. 1984: *Igneous petrology*; Freeman, Cooper and Co., San Francisco, 504 p.
- McCall, G.J.H. 2003: A critique of the analogy between Archean and Phanerozoic tectonics based on regional mapping of the Mesozoic-Cenozoic plate convergent zone in the Makran, Iran; *Precambrian Research*, v. 127, p. 5–17.
- McCuaig, T.C. and Kerrich, R. 1998: P-T-t-deformation fluid characteristics of lode gold deposits: evidence from alteration systematics; *Ore Geology Reviews*, v. 12, p. 381–453.
- McPhie, J. and Allen, R.L. 1992: Facies architecture of mineralized submarine volcanic sequences: Cambrian Mount Read Volcanics, western Tasmania; *Economic Geology*, v. 87, p. 587–596.
- McPhie, J., Doyle, M. and Allen, R. 1993: *Volcanic Textures: A Guide to the Interpretation of Textures in Volcanic Rocks*; Centre for Ore Deposit and Exploration Studies, University of Tasmania, 198 p.
- McRitchie, W.D. 1971: Geology of the Wallace Lake-Siderock Lake area: a reappraisal; in *Geology and Geophysics of the Rice Lake Region, Southeastern Manitoba (Project Pioneer)*, W.D. McRitchie and W. Weber (ed.), Manitoba Department of Mines and Natural Resources, Mines Branch, Publication 71-1, p. 107–125.
- McRitchie, W.D. and Weber, W., ed. 1971a: *Geology and geophysics of the Rice Lake region, southeastern Manitoba (Project Pioneer)*, Manitoba Department of Mines and Natural Resources, Mines Branch, Publication 71-1, 430 p.
- McRitchie, W.D. and Weber, W. 1971b: Metamorphism and deformation in the Manigotagan Gneissic Belt, south-eastern Manitoba; in *Geology and Geophysics of the Rice Lake Region, Southeastern Manitoba (Project Pioneer)*, W.D. McRitchie and W. Weber (ed.), Manitoba Department of Mines and Natural Resources, Mines Branch, Publication 71-1, p. 235–284 (and accompanying Maps 69-1 to -4).
- Miller, C.F. and Mittlefehldt, D.W. 1982: Depletion of light rare-earth elements in felsic magmas; *Geology*, v. 10, p. 129–133.
- Moore, E.S. 1913: Wanipigow, Manigotagan and Oiseau rivers, Manitoba; *Geological Survey of Canada, Map 96A*, 1:253 440 scale.
- Moore, E.S. 1914: Region east of the south end of Lake Winnipeg; in *Summary Report of the Geological Survey, Department of Mines, for the calendar year 1912*, Geological Survey of Canada, Sessional Paper 26, p. 262–270.
- Moyen, J-F. 2009: High Sr/Y and La/Yb ratios: the meaning of the "adakitic signature"; *Lithos*, v. 112, p. 556–574.
- Naldrett, A.J. 2004: *Magmatic sulfide deposits: geology, geochemistry and exploration*; Springer-Verlag, Berlin Heidelberg, Germany, 728 p.

- Nesbitt, R.W., Sun, S.-s. and Purvis, A.C. 1979: Komatiites: geochemistry and genesis; *The Canadian Mineralogist*, v. 17, p. 165–186.
- Owens, D.J. 1986a: Stormy Lake (part of 52L/14SW); Manitoba Energy and Mines, Geological Services, Preliminary Map 1986R-1, scale 1:1000.
- Owens, D.J. 1986b: Stratigraphy and structure of the upper Stormy Lake Formation, Rice Lake greenstone belt; *in* Report of Field Activities 1986, Manitoba Energy and Mines, Minerals Division, p. 115–119.
- Owens, D.J. and Seneshen, D.M. 1985: Stormy Lake (part of 52L/14SW); Manitoba Energy and Mines, Geological Services, Preliminary Map 1985R-1, scale 1:10 000.
- Pan, Y. 1997: Controls on the fractionation of isovalent trace elements in magmatic and aqueous systems: evidence from Y/Ho, Zr/Hf, and lanthanide tetrad effect—a discussion of the article by M. Bau (1996); *Contributions to Mineralogy and Petrology*, v. 128, p. 405–408.
- Pan, Y. and Therens, C. 2000: The Werner Lake Co-Cu-Au deposit of the English River Subprovince, Ontario, Canada: evidence for an exhalative origin and effects of granulite facies metamorphism; *Economic Geology*, v. 95, p. 1635–1656.
- Pan, Y., Therens, C. and Ansdell, K. 1998: Geochemistry of mafic-ultramafic rocks from the Werner–Gordon Lake area: back-arc origin for the English River Subprovince?; *in* Western Superior LITHOPROBE Transect, Annual Meeting, R.M. Harrap and H.H. Helmstaedt (ed.), LITHOPROBE Secretariat, University of British Columbia, LITHOPROBE Report 65, p. 29–34.
- Parks, J., Lin, S., Davis, D. and Corkery, T. 2006: New high-precision U-Pb ages for the Island Lake greenstone belt, northwestern Superior Province: implications for regional stratigraphy and the extent of the North Caribou terrane; *Canadian Journal of Earth Sciences*, v. 43, p. 789–803.
- Pearce, J.A. 1996: A user's guide to basalt discrimination diagrams; *in* Trace Element Geochemistry of Volcanic Rocks: Applications for Massive Sulphide Exploration, D.A. Wyman (ed.), Geological Association of Canada, Short Course Notes, v. 12, p. 79–113.
- Pearce, J.A. 2008: Geochemical fingerprinting of oceanic basalts with applications to ophiolite classification and the search for Archean oceanic crust; *Lithos*, v. 100, p. 14–48.
- Pearce, J.A. and Peate, D.W. 1995: Tectonic implications of the composition of volcanic arc magmas; *Annual Review of Earth and Planetary Sciences*, v. 23, p. 251–285.
- Pearce, J.A. and Stern, R.J. 2006: Origin of back-arc basin magmas: trace element and isotope perspectives; *in* Back-Arc Spreading Systems: Geological, Biological, Chemical, and Physical Interactions, D.M. Christie, C.R. Fisher, S.-M. Lee and S. Givens (ed.), American Geophysical Union, Geophysical Monograph Series, v. 166, p. 63–86.
- Percival, J.A. and Helmstaedt, H., ed. 2006: The Western Superior Province LITHOPROBE and NATMAP transects; *Canadian Journal of Earth Sciences*, Special Issue, v. 43, no. 6, p. 743–1117.
- Percival, J.A. and Williams, H.R. 1989: Late Archean Quetico accretionary complex, Superior province, Canada; *Geology*, v. 17, p. 23–25.
- Percival, J.A., Bailes, A. and McNicoll, V. 2002: Mesoarchean breakup, Neorarchean accretion in the western Superior craton, Lake Winnipeg, Canada; Geological Association of Canada–Mineralogical Association of Canada, Joint Annual Meeting, May 30–June 2, 2002, Saskatoon, Saskatchewan, Field Trip B3 Guidebook, 42 p.
- Percival, J.A., McNicoll, V. and Bailes, A.H. 2006a: Strike-slip juxtaposition of ca. 2.72 Ga juvenile arc and >2.98 Ga continent margin sequences and its implications for Archean terrane accretion, western Superior Province, Canada; *Canadian Journal of Earth Sciences*, v. 43, p. 895–927.
- Percival, J.A., Sanborn-Barrie, M., Skulski, T., Stott, G.M., Helmsstaedt, H. and White, D.J. 2006b: Tectonic evolution of the western Superior Province from NATMAP and LITHOPROBE studies; *Canadian Journal of Earth Sciences*, v. 43, p. 1085–1117.
- Perfit, M.R., Gust, D.A., Bence, A.E., Arculus, R.J. and Taylor, S.R. 1980: Chemical characteristics of island-arc basalts: implications for mantle sources; *Chemical Geology*, v. 30, p. 227–256.
- Plank, T. and Langmuir, C.H. 1988: An evaluation of the global variations in the major element chemistry of arc basalts; *Earth and Planetary Science Letters*, v. 90, p. 349–370.
- Polat, A., Kerrich, R. and Wyman, D.A. 1999: Geochemical diversity in oceanic komatiites and basalts from the late Archean Wawa greenstone belts, Superior Province, Canada: trace element and Nd isotope evidence for a heterogeneous mantle; *Precambrian Research*, v. 94, p. 139–173.
- Poulsen, K.H., Davis, D.W., Weber, W. and Scoates, R.F.J. 1993: Geological and geochronological studies in the Rice Lake Belt; *in* Report of Activities 1993, Manitoba Energy and Mines, Geological Services, p. 152.
- Poulsen, K.H., Robert, F. and Dubé, B. 2000: Geological classification of Canadian gold deposits; Geological Survey of Canada, Bulletin 540, 106 p.
- Poulsen, K.H., Weber, W., Brommecker, R. and Seneshen, D.N. 1996: Lithostratigraphic assembly and structural setting of gold mineralization in the eastern Rice Lake greenstone belt, Manitoba; Geological Association of Canada–Mineralogical Association of Canada, Joint Annual Meeting, May 27–29, 1996, Winnipeg, Manitoba, Field Trip A4 Guidebook, 106 p.
- Poulsen, K.H., Weber, W., Garson, D.F. and Scoates, R.F.J. 1994: New geological observations in the Rice Lake belt, southeastern Manitoba; *in* Report of Activities 1994, Manitoba Energy and Mines, Geological Services, p. 163–166.
- Price, R.C., Johnson, L.E. and Crawford, A.J. 1990: Basalts of the North Fiji Basin: the generation of back arc basin magmas by mixing of depleted and enriched mantle sources; *Contributions to Mineralogy and Petrology*, v. 105, p. 106–121.
- Rapp, R.P. and Watson, E.B. 1986: Monazite solubility and dissolution kinetics: implications for the thorium and light rare earth chemistry of felsic magmas; *Contributions to Mineralogy and Petrology*, v. 94, p. 304–316.
- Richards, J.P. and Kerrich, R. 2007: Adakite-like rocks: their diverse origins and questionable role in metallogenesis; *Economic Geology*, v. 102, p. 537–576.
- Rogers, N. 2001: Preliminary report on the stratigraphy and structure of the Bee Lake greenstone belt, Superior Province, northwestern Ontario; Geological Survey of Canada, Current Research 2001-C17, 17 p.
- Rogers, N. 2003: Geology, Bee Lake greenstone belt, Ontario-Manitoba; Geological Survey of Canada, Open File 4315, scale 1:50 000.
- Rollinson, H. 2007: When did plate tectonics begin?; *Geology Today*, v. 23, p. 186–191.
- Ross, P.-S. and Bédard, J.H. 2009: Magmatic affinity of modern and ancient subalkaline volcanic rocks determined from trace-element discriminant diagrams; *Canadian Journal of Earth Sciences*, v. 46, p. 823–839.
- Russell, G.A. 1952: Geology of the Lily Lake–Kickley Lake area; Manitoba Department of Mines and Natural Resources, Mines Branch, Publication 50-3, 17 p.
- Sanborn-Barrie, M., Skulski, T. and Parker, J. 2001: Three hundred million years of tectonic history recorded by the Red Lake greenstone belt, Ontario; Geological Survey of Canada, Current Research 2001-C19, 14 p.

- Sasseville, C., Tomlinson, K.Y., Hynes, A. and McNicoll, V. 2006: Stratigraphy, structure, and geochronology of the 3.0–2.7 Ga Wallace Lake greenstone belt, western Superior Province, south-east Manitoba, Canada; *Canadian Journal of Earth Sciences*, v. 43, p. 929–945.
- Saunders, A.D. and Tarney, J. 1984: Geochemical characteristics of basaltic volcanism within back-arc basins; Geological Society, London, Special Publication 16, p. 59–76.
- Saunders, A.D., Norry, M.J. and Tarney, J. 1991: Fluid influence on the trace element compositions of subduction zone magmas; *Philosophical Transactions of the Royal Society of London*, v. 335, p. 377–392.
- Schmidberger, S.S., Heaman, L.M., Simonetti, A., Creaser, R.A. and Whiteford, S. 2007: Lu-Hf, in-situ Sr and Pb isotope and trace element systematics for mantle eclogites from the Diavik diamond mine: evidence for Paleoproterozoic subduction beneath the Slave craton, Canada; *Earth and Planetary Science Letters*, v. 254, p. 55–68.
- Scoates, R.F.J. 1971: Ultramafic rocks of the Rice Lake greenstone belt; in *Geology and Geophysics of the Rice Lake Region, Southeastern Manitoba (Project Pioneer)*, W.D. McRitchie and W. Weber, (ed.), Manitoba Department of Mines and Natural Resources, Mines Branch, Publication 71-1, p. 189–201.
- Seneshen, D.M. 1986: Stratigraphy of the Manigotagan River Formation, Rice Lake greenstone belt; in *Report of Field Activities 1986*, Manitoba Energy and Mines, Minerals Division, p. 109–114.
- Seneshen, D.M. 1990: The genesis of Archean pyroclastic rocks of the Manigotagan River Formation, southeastern Manitoba; M.Sc. thesis, University of Manitoba, Winnipeg, Manitoba, 173 p.
- Seneshen, D.M. and Owens, D.J. 1985: Geological investigations in the Stormy Lake area; in *Report of Field Activities 1985*, Manitoba Energy and Mines, Geological Services/Mines Branch, p. 112–119.
- Shklanka, R. 1967: Geology of the Bee Lake area; Ontario Department of Mines, Geological Report 47, 42 p., and accompanying Map 2097, 1:31 680 scale.
- Simonetti, A., Heaman, L.M., Hartlaub, R.P., Creaser, R.A., MacHattie, T.G. and Böhm, C. 2005: U-Pb zircon dating by laser ablation-MC-ICP-MS using a new multiple ion counting Faraday collector array; *Journal of Analytical Atomic Spectrometry*, v. 20, p. 677–686.
- Sinton, J.M. and Fryer, P. 1987: Mariana Trough lavas from 18°N: implications for the origin of back arc basin basalts; *Journal of Geophysical Research*, v. 92, no. B12, p. 12782–12802.
- Sinton, J.M., Ford, L.L., Chappell, B. and McCulloch, M.T. 2003: Magma genesis and mantle heterogeneity in the Manus back-arc basin, Papua New Guinea; *Journal of Petrology*, v. 44, p. 159–195.
- Sircombe, K.N. 2004: AGE DISPLAY: an EXCEL workbook to evaluate and display univariate geochronological data using binned frequency histograms and probability density distributions; *Computers and Geosciences*, v. 30, p. 21–31.
- Skulski, T., Corkery, M.T., Stone, D., Whalen, J.B. and Stern, R.A. 2000: Geological and geochronological investigations in the Stull Lake–Edmund Lake greenstone belt and granitoid rocks of the northwestern Superior Province; in *Report of Activities 2000*, Manitoba Industry, Trade and Mines, Manitoba Geological Survey, p. 117–128.
- Spitz, G. and Darling, R. 1978: Major and minor element litho-geochemical anomalies surrounding the Louvem copper deposit, Val d'Or, Quebec; *Canadian Journal of Earth Sciences*, v. 15, p. 1161–1169.
- Sproule, R.A., Leshner, C.M., Ayer, J.A., Thurston, P.C. and Herzberg, C.T. 2002: Spatial and temporal variations in the geochemistry of komatiites and komatiitic basalts in the Abitibi greenstone belt; *Precambrian Research*, v. 115, p. 153–186.
- Stacey, J.S. and Kramers, J.D. 1975: Approximation of terrestrial lead isotope evolution by a two-stage model; *Earth and Planetary Science Letters*, v. 26, p. 207–221.
- Stern, R.J. 2005: Evidence from ophiolites, blueschists, and ultrahigh-pressure metamorphic terranes that the modern episode of subduction tectonics began in Neoproterozoic time; *Geology*, v. 33, p. 557–560.
- Stern, R.J., Lin, P.-N., Morris, J.D., Jackson, M.C., Fryer, P., Bloomer, S.H. and Ito, E. 1990: Enriched back-arc basin basalts from the northern Mariana Trough: implications for the magmatic evolution of back-arc basins; *Earth and Planetary Science Letters*, v. 100, p. 210–225.
- Stewart, A.L. and McPhie, J. 2006: Facies architecture and late Pliocene–Pleistocene evolution of a felsic volcanic island, Milos, Greece; *Bulletin of Volcanology*, v. 68, p. 703–726.
- Stockwell, C.H. 1940: Gold mines and prospects in Rice Lake–Beresford Lake area, Manitoba; *Transactions of the Canadian Institute of Mining and Metallurgy*, v. 43, p. 613–626.
- Stockwell, C.H. 1945a: Beresford Lake; Geological Survey of Canada, Map 809A, scale 1:63 360.
- Stockwell, C.H. 1945b: Gem Lake; Geological Survey of Canada, Map 811A, scale 1:63 360.
- Stockwell, C.H. and Lord, C.S. 1939: Halfway Lake–Beresford Lake area, Manitoba; Geological Survey of Canada, Memoir 219, 67 p., and accompanying Maps 535A, 536A and 537A, scale 1:12 000.
- Stott, G.M. and Corfu, F. 1991: Uchi Subprovince; in *Geology of Ontario*, P.C. Thurston, H.R. Williams, R.H. Sutcliffe and G.M. Stott, (ed.), Ontario Geological Survey, Special Volume 4, Part 1, p. 145–236.
- Stott, G.M., Corkery, M.T., Percival, J.A., Simard, M. and Goutier, J. 2010: Project units 98-006 and 98-007: a revised terrane subdivision of the Superior Province; in *Summary of Field Work and Other Activities 2010*, Ontario Geological Survey, Open File Report 6260, p. 20-1–20-10.
- Sun, S.-s. and McDonough, W.F. 1989: Chemical and isotopic systematics of oceanic basalts: implications for mantle composition and processes; in *Magmatism in the Ocean Basins*, A.D. Saunders and M.J. Norry, (ed.), Geological Society, Special Publication 42, p. 313–345.
- Syme, E.C. 1998: Ore-associated and barren rhyolites in the central Flin Flon belt: case study of the Flin Flon mine sequence; Manitoba Energy and Mines, Geological Services, Open File OF98-9, 26 p.
- Tatsumi, Y. 1986: Formation of the volcanic front in subduction zones; *Geophysical Research Letters*, v. 13, p. 717–720.
- Terakado, Y. and Fujitani, T. 1998: Behavior of the rare earth elements and other trace elements during interactions between acidic hydrothermal solutions and silicic volcanic rocks, southwestern Japan; *Geochimica et Cosmochimica Acta*, v. 62, p. 1903–1917.
- Theyer, P. 1987: Mineral deposit investigations in the Rice Lake greenstone belt; in *Report of Field Activities 1987*, Manitoba Energy and Mines, Minerals Division, p. 113–114.
- Theyer, P. 1994: Mineral deposits and occurrences in the Flintstone Lake area, NTS 52L/11; Manitoba Energy and Mines, Geological Services, Mineral Deposit Series Report 22, 60 p.
- Theyer, P. and Ferreira, K.J. 1990: Mineral deposits and occurrences in the Garner Lake area, NTS 52L/14; Manitoba Energy and Mines, Geological Services, Mineral Deposit Series Report 10, 173 p.
- Theyer, P. and Gaba, R.G. 1986: Mineral occurrence investigations in the Rice Lake greenstone belt; in *Report of Field Activities 1986*, Manitoba Energy and Mines, Minerals Division, p. 120–124.
- Thurston, P.C. and Chivers, K.M. 1990: Secular variation in greenstone sequence development emphasizing Superior Province, Canada; *Precambrian Research*, v. 46, p. 21–58.

- Thurston, P.C. and Kozhevnikov, V.N. 2000: An Archean quartz arenite-andesite association in the eastern Baltic Shield, Russia: implications for assemblage types and shield history; *Precambrian Research*, v. 101, p. 313–340.
- Thurston, P.C., Ayer, J.A., Goutier, J. and Hamilton, M.A. 2008: Depositional gaps in Abitibi greenstone belt stratigraphy: a key to exploration for syngenetic mineralization; *Economic Geology*, v. 103, p. 1097–1134.
- Thurston, P.C., Osmani, I.A. and Stone, D. 1991: Northwestern Superior Province: review and terrane analysis; *in* *Geology of Ontario*, P.C. Thurston, H.R. Williams, R.H. Sutcliffe and G.M. Stott (ed.), Ontario Geological Survey, Special Volume 4, Part 1, p. 81–142.
- Tomlinson, K.Y., Stevenson, R.K., Hughes, D.J., Hall, R.P., Thurston, P.C. and Henry, P. 1998: The Red Lake greenstone belt, Superior Province: evidence of plume-related magmatism at 3 Ga and evidence of an older enriched source; *Precambrian Research*, v. 89, p. 59–76.
- Turek, A. and Weber, W. 1991: New U-Pb zircon ages from the Rice Lake area: evidence for 3 Ga crust; *in* *Report of Activities 1991*, Manitoba Energy and Mines, Minerals Division, p. 53–55.
- Turek, A. and Weber, W. 1994: The 3 Ga granitoid basement to the Rice Lake supracrustal rocks, southeast Manitoba; *in* *Report of Activities 1994*, Manitoba Energy and Mines, Minerals Division, p. 167–169.
- Turek, A., Keller, R., Van Schmus, W.R. and Weber, W. 1989: U-Pb zircon ages for the Rice Lake area, southeastern Manitoba; *Canadian Journal of Earth Sciences*, v. 26, p. 23–30.
- Unterschutz, J.L.E., Creaser, R.A., Erdmer, P., Thompson, R.I. and Daughtry, K.L. 2002: North American margin origin of Quesnel terrane strata in the southern Canadian Cordillera: inferences from geochemical and Nd isotopic characteristics of Triassic metasedimentary rocks; *Geological Society of America Bulletin*, v. 114, p. 462–475.
- Volpe, A.M., Macdougall, J.D. and Hawkins, J.W. 1987: Mariana Trough basalts (MTB): trace element and Sr-Nd isotopic evidence for mixing between MORB-like and arc-like melts; *Earth and Planetary Science Letters*, v. 82, p. 241–254.
- Volpe, A.M., Macdougall, J.D. and Hawkins, J.W. 1988: Lau Basin basalts (LBB): trace element and Sr-Nd isotopic evidence for heterogeneity in backarc basin mantle; *Earth and Planetary Science Letters*, v. 90, p. 174–186.
- Walker, R.G. 1978: Deep-water sandstone facies and ancient submarine fans: models for exploration for stratigraphic traps; *American Association of Petroleum Geologists Bulletin*, v. 62, p. 932–966.
- Walker, R.G. 1984: Turbidites and associated coarse clastic deposits; *in* *Facies Models*, Second Edition, R.G. Walker (ed.), Geoscience Canada, Reprint Series 1, p. 171–188.
- Watson, E.B. and Capobianco, C.J. 1981: Phosphorus and the rare earth elements in felsic magmas: an assessment of the role of apatite; *Geochimica et Cosmochimica Acta*, v. 45, p. 2349–2358.
- Weber, W. 1971a: Geology of the Long Lake–Gem Lake area, southeastern Manitoba; *in* *Geology and Geophysics of the Rice Lake Region*, Southeastern Manitoba (Project Pioneer), W.D. McRitchie and W. Weber (ed.), Manitoba Department of Mines and Natural Resources, Mines Branch, Publication 71-1, p. 63–106, and accompanying Map 71-1/5, scale 1:31 680.
- Weber, W. 1971b: Geology of the Wanipigow River–Manigotagan River region; *in* *Geology and Geophysics of the Rice Lake Region*, Southeastern Manitoba (Project Pioneer), W.D. McRitchie and W. Weber (ed.), Manitoba Department of Mines and Natural Resources, Mines Branch, Publication 71-1, and accompanying map Map 71-1/4, scale 1:63 360.
- Weber, W. 1971c: The evolution of the Rice Lake–Gem Lake greenstone belt, southeastern Manitoba; *in* *Geoscience Studies in Manitoba*, A.C. Turnock (ed.), Geological Association of Canada, Special Paper 9, p. 97–103.
- Weber, W. 1987: Geological investigations in the Lily Lake area; *in* *Report of Field Activities 1987*, Manitoba Energy and Mines, Minerals Division, p. 108–109.
- Wentworth, C.K. 1922: A scale of grade and class terms for clastic sediments; *The Journal of Geology*, v. 30, p. 377–392.
- Whalen, J.B., Percival, J.A., McNicoll, V.J. and Longstaffe, F.J. 2003: Intra-oceanic production of continental crust in a Th-depleted ca. 3.0 Ga arc complex, western Superior Province, Canada; *Contributions to Mineralogy and Petrology*, v. 146, p. 78–99.
- White, D.J., Musacchio, G., Helmstaedt, H.H., Harrap, R.M., Thurston, P.C., van der Velden, A. and Hall, K. 2003: Images of a lower-crustal oceanic slab: direct evidence for tectonic accretion in the Archean western Superior province; *Geology*, v. 31, p. 997–1000.
- White, J.D.L. and Houghton, B.F. 2006: Primary volcanoclastic rocks; *Geology*, v. 34, p. 677–680.
- Williams, H.R. 1990: Subprovince accretion tectonics in the south-central Superior Province; *Canadian Journal of Earth Sciences*, v. 27, p. 570–581.
- Williams, H.R., Stott, G.M., Thurston, P.C., Sutcliffe, R.H., Bennett, G., Easton, R.M. and Armstrong, D.K. 1992: Tectonic evolution of Ontario: summary and synthesis; *in* *Geology of Ontario*, P.C. Thurston, H.R. Williams, R.H. Sutcliffe and G.M. Stott (ed.), Ontario Geological Survey, Special Volume 4, Part 2, p. 1255–1332.
- Winchester, J.A. and Floyd, P.A. 1977: Geochemical discrimination of different magma series and their differentiation products using immobile elements; *Chemical Geology*, v. 20, p. 325–343.
- Wood, D.A. 1980: The application of a Th-Hf-Ta diagram to problems of tectonomagmatic classification and to establishing the nature of crustal contamination of basaltic lavas of the British Tertiary Volcanic Province; *Earth and Planetary Science Letters*, v. 50, p. 11–30.
- Wright, J.F. 1924: Geology and mineral prospects of the northern part of Beresford Lake map-area, southeast Manitoba; *Geological Survey of Canada, Summary Report*, 1923, Part B, p. 86–104.
- Wright, J.F. 1927: Beresford and Rice Lakes area, east of Principal Meridian, Manitoba; *Geological Survey of Canada, Map 195A*, 1:63 360 scale.
- Wright, J.F. 1930: Gold, copper-nickel, and tin deposits of southeast Manitoba; *Geological Survey of Canada, Summary Report*, 1929, Part B, p. 136–171.
- Wright, J.F. 1932a: Geology and mineral deposits of a part of southeastern Manitoba; *Geological Survey of Canada, Memoir 169*, 150 p.
- Wright, J.F. 1932b: Wadhope area, Township 22, Range 16, east of Principal Meridian, Manitoba; *Geological Survey of Canada, Map 280A*, scale 1:24 000.
- Wyman, D.A. 2013: A critical assessment of Neoproterozoic ‘plume only’ geodynamics: evidence from the Superior Province; *Precambrian Research*, v. 229, p. 3–19.
- Zwanig, H.V. 1971: Structural geology at Long Lake, Manitoba; *in* *Geology and Geophysics of the Rice Lake Region*, Southeastern Manitoba (Project Pioneer), W.D. McRitchie and W. Weber (ed.), Manitoba Department of Mines and Natural Resources, Mines Branch, Publication 71-1, p. 285–298.